Copyrighted Materials
Copyright © 2009 American Society of Civil Engineers (ASCE)
Retrieved from www.knovel.com

GEOTECHNICAL SPECIAL PUBLICATION NO. 185

CONTEMPORARY TOPICS IN DEEP FOUNDATIONS

SELECTED PAPERS FROM THE 2009 INTERNATIONAL FOUNDATION CONGRESS AND EQUIPMENT EXPO

March 15–19, 2009
Orlando, Florida

SPONSORED BY
The Geo-Institute of the American Society of Civil Engineers

International Association of Foundation Drilling (ADSC)

Pile Driving Contractors Association (PDCA)

EDITED BY
Magued Iskander, Ph.D., P.E.
Debra F. Laefer, Ph.D.
Mohamad H. Hussein, P.E.

ASCE
Published by the American Society of Civil Engineers

Library of Congress Cataloging-in-Publication Data

International Foundation Congress and Equipment Expo (2009 : Orlando, Fla.)
Contemporary topics in deep foundations : selected papers from the 2009 International Foundation Congress and Equipment Expo, March 15-19, 2009, Orlando, Florida / sponsored by the Geo-Institute of the American Society of Civil Engineers [and] International Association of Foundation Drilling [and] Pile Driving Contractors Association ; edited by Magued Iskander, Debra F. Laefer, Mohamad H. Hussein.
p. cm. -- (Geotechnical special publication ; no. 185)
Includes bibliographical references and indexes.
ISBN 978-0-7844-1021-9
1. Foundations--Congresses. 2. Piling (Civil engineering)--Congresses. 3. Offshore structures--Foundations--Congresses. I. Iskander, Magued. II. Laefer, Debra F. III. Hussein, Mohamad H. IV. American Society of Civil Engineers. Geo-Institute. V. Association of Drilled Shaft Contractors (U.S.) VI. Pile Driving Contractors Association (U.S.) VII. Title.

TA775.I6522 2009
624.1'5--dc22 2009004037

American Society of Civil Engineers
1801 Alexander Bell Drive
Reston, Virginia, 20191-4400

www.pubs.asce.org

Any statements expressed in these materials are those of the individual authors and do not necessarily represent the views of ASCE, which takes no responsibility for any statement made herein. No reference made in this publication to any specific method, product, process, or service constitutes or implies an endorsement, recommendation, or warranty thereof by ASCE. The materials are for general information only and do not represent a standard of ASCE, nor are they intended as a reference in purchase specifications, contracts, regulations, statutes, or any other legal document. ASCE makes no representation or warranty of any kind, whether express or implied, concerning the accuracy, completeness, suitability, or utility of any information, apparatus, product, or process discussed in this publication, and assumes no liability therefore. This information should not be used without first securing competent advice with respect to its suitability for any general or specific application. Anyone utilizing this information assumes all liability arising from such use, including but not limited to infringement of any patent or patents.

ASCE and American Society of Civil Engineers—Registered in U.S. Patent and Trademark Office.

Photocopies and reprints.
You can obtain instant permission to photocopy ASCE publications by using ASCE's online permission service (http://pubs.asce.org/permissions/requests/). Requests for 100 copies or more should be submitted to the Reprints Department, Publications Division, ASCE, (address above); email: permissions@asce.org. A reprint order form can be found at http://pubs.asce.org/support/reprints/.

Copyright © 2009 by the American Society of Civil Engineers. All Rights Reserved.
ISBN 978-0-7844-1021-9 Manufactured in the United States of America.

Copyrighted Materials
Copyright © 2009 American Society of Civil Engineers (ASCE)
Retrieved from www.knovel.com

Preface

This Geotechnical Special Publication (GSP), along with its two companion volumes contain selected papers from the International Foundations Congress and Equipment Expo (IFCEE09) held in Orlando, Florida on March 15–19, 2009. This unprecedented Congress combined the 2009 annual meetings of the Geo-Institute of ASCE, the International Association of Foundation Drilling (ADSC), and the Pile Driving Contractors Association (PDCA). IFCEE09 provided an international forum to discuss technological advances, case histories, and present challenges related to foundations, ground support, and earth retention. The congress was heavily attended by a wide range of geo-professionals including engineers, contractors, academicians, equipment manufacturers, geo-technologists, researchers, and suppliers of tools and services.

An international call for papers and a rigorous peer review process yielded 242 accepted technical papers that were presented in 44 sessions, in addition to invited keynote presentations and 12 panel discussions. These contributions are organized by theme in three GSPs, as follows:

- GSP **185**: Contemporary Topics in Deep Foundations
- GSP **186**: Contemporary Topics in In Situ Testing, Analysis, and Reliability of Foundations
- GSP **187**: Contemporary Topics in Ground Modification, Problem Soils, and Geo-Support

The editors would like to express their appreciation for having been provided the opportunity to be a part of this Congress' organization, and hope that these proceedings will be of use to the geotechnical engineering community, for many decades to come.

The Editors

Magued Iskander, PhD, PE
Polytechnic Institute of
New York University
New York, NY, USA
Iskander@poly.edu

Debra F. Laefer, PhD
University College
Dublin, Ireland
debra.laefer@ucd.ie

Mohamad H. Hussein, PE
GRL Engineers, Inc.
Orlando, Florida, USA
MHGRL@pile.com

Copyrighted Materials
Copyright © 2009 American Society of Civil Engineers (ASCE)
Retrieved from www.knovel.com

Contents

Keynote Lectures

Management of Risk in Deep Foundations with Design-Build 1
Dan Brown

Ultimate Micropile Bond Stresses Observed during Load Testing in Clays and Sands 12
John R. Wolosick

Drilled Shafts

Load Transfer Mechanisms of Tip Post-Grouted Drilled Shafts in Sand 23
Miguel E. Ruiz and Miguel A. Pando

Post Grouted Drilled Shafts—A Comprehensive Case History from Texas 31
Phil King, Americo Fernandez, and Miguel A. Pando

Large-Scale Laboratory Study on the Innovative Use of Compaction Grout for Drilled Shaft Tip Post Grouting 39
Jeyasuthan Pooranampillai, Sherif Elfass, Walt Vanderpool, and Gary Norris

Tip Post-Grouting of Slurry-Drilled Shafts in Soil: Chinese Experiences 47
Xinsheng Duan and Fred H. Kulhawy

Designing and Characterizing the LEED Concrete for Drilled Shaft Applications 55
C. Vipulanandan and Emrah Demircan

Evaluation of Compression Tip Capacity for Drilled Shafts 63
Yit-Jin Chen, Yi-Chung Fang, and Tsu-Hung Chu

Evaluation of Side Resistance of Drilled Shafts in Multilayered Soils 71
Yit-Jin Chen, Hsin-Wen Chang, and Ting-Jui Chiu

Prediction and Measurement of Pile Loads and Settlement at the Thames River Bridge 79
Frederick C. Rhyner, Ira Beer, T. C. Michael Law, and Asher Peltz

Issues Related to Use of OD vs. ID Casing in Drilled Shaft Construction 87
William M. Isenhower and M. D. "Bo" Walker

Analysis of Anchor Foundation with Root-Caisson in Non-Homogeneous Soils 95
Chenrong Zhang, Maosong Huang, and Linlong Mu

Lesson from Instrumented Slope Stabilization Project Using Drilled Shafts 103
Robert Y. Liang, Mohammad Yamin, and Wassel M. Al Bodour

Load Tests Help Optimize Design of Deep Foundations 111
James C. Pegues, Wade Anundson, and Ayoade Adeyefa

Drilled Shaft Performance in Cemented Calcareous Formations in the Southeast US 119
Dan Brown and W. Robert Thompson III

Interpreted Failure Load for Drilled Shafts via Davisson and L_1-L_2 127
Fred H. Kulhawy and Anwar Hirany

A Case Study on the Overturning of Drill Rigs on Construction Sites 135
Satoshi Tamate and Tomohito Hori

Old Drilling Elements Combined with Some New Tricks for Secant Pile Construction: A Full Scale Test Program 143
Allen Cadden, Ralph Capelli, and Javier Rodriguez

Drilled Shafts Socketed in Uncemented Clay Shale 151
C. Vipulanandan and Moon S. Nam

Effects of Rock Anisotropy on Lateral Response of Drilled Shaft 159
Robert Y. Liang and Ehab S. Shatnawi

Willis Avenue Swing Bridge: Design and Construction of Drilled Shaft Foundations 167
Vedrana Krstic, Raymond Mankbadi, and Aravinda Ramakrishna

Axial Load Transfer Behavior of Rock-Socketed Shafts 175
Lianyang Zhang and Jinming Xu

Drilled Shaft Foundations for the James River Crossing in Richmond, Virginia 183
Jan J. Hartman and Raymond J. Castelli

Driven Piles

Effective Use of Steel Piles for a Large Transportation Project in Central Florida 191
Mohamad H. Hussein, Loreen Choate, Robert Mangogna, and Kathy Gray

The Effect of Installation Technique on Capacity of Cylinder Piles in the Yorktown Formation 199
Mike Muchard, Rick Palmer, and Michael Simpson

Case History: Value Engineering of Driven H-Piles for Slope Stability on the Missouri River 207
W. Robert Thompson III, Jeffrey R. Hill, and J. Erik Loehr

Foundation Engineering of Offshore "Jacket" Structures 215
Ioannis Chatzigiannelis, Khaled Elsayed, and Kostas Loukakis

Geotechnical Design of a Partially Piled Raft Foundation 223
Ron Xia, Vladimir Dolezel, L. Rak, H. Qian, and B. Rao

Axial Load Capacity of Un-Tapered Piles in Cohesionless Soils 231
Roy E. Olson and Magued G. Iskander

Analyses of Pile Capacity for Offshore Structures in Hurricane Katrina 239
Jiun-Yih Chen, Britain A. Materek, Justin F. Carpenter, Robert B. Gilbert, and Frank J. Puskar

H-Piles Selected for New Power Plant Based on Pre-Award Testing Program and Cost Comparison 247
Kenneth Bell, Scott Newhouse, and Jeff O'Neal

Driven Pile Foundation in the Offshore Fields of Qatar: Installation Problems, Challenges, and Potential Solutions 255
Waddah Akili

Driven Pile Capacity in Intermediate Geomaterial Formations 263
Robert L. Mokwa and Heather Brooks

Use of Dynamic Measurements to Drive High Capacity Concrete Piles in Washington's Potomac Formation 271
John E. Regan and Karl A. Higgins III

Measured versus Predicted Shaft Resistance of H- and Closed Ended Pipe Piles in Sands 279
Scott M. Mackiewicz

Intelligent Pile-Driving with a Diesel Impact Hammer 287
Michael D. Justason

Driven Ductile Iron Pipe Piles: Design, Installation, and Performance 295
Frank Schmidt and Thomas N. Dobras

Characterization of Precast UHPC Pile Drivability 303
Thomas Vande Voort, Muhannad Suleiman, and Sri Sritharan

The Vibro-Jetting Driving Method 311
Hermann Zeilinger

Centrifuge Model Tests on Instability of Automotive Pile Drivers 319
Tomohito Hori and Satoshi Tamate

Seismic Hazards and Construction Vibrations 327
Justin Moderie and Arlan H. Rippe

Monitoring Pile Driving Vibrations—Problem Avoidance and Case Studies 335
David Harrison

An Overview of Relevant Guidelines for Deep Foundation Generated Ground Vibrations 343
Edward L. Hajduk, Les R. Chernauskas, Stephanie van der Horst, and Elizabeth Penn-Sanders

Development of a Driven Pile Ground Vibration Case History Database 351
Edward L. Hajduk, Kevin C. Bower, Timothy W. Mays, David A. Falatok, and Timothy S. Perkins

Micropiles

High Capacity Micropiles in Wissahickon Schist Bedrock 359
Terence P. Holman

Influence of Confining Micro Piles on the Bearing Capacity of Sand 367
N. Unnikrishnan and P. Sachin

Micropile Foundations for ESSROC Cement Plant Expansion **375**
Paul D. Martin

Micropiles for Re-Support and Lifting of Two Buildings under Construction **383**
Brent Byford and Mark Hampton

Use of Multiple Techniques to Support Construction of a New Hospital Addition **390**
James B. Pease

Banjo Bill Rock Catchment Basins **398**
Paul B. Groneck and Tom Armour

Seismic Analysis of Inclined Micropiles Using Numerical Method **406**
Reza Noorzad and G. Reza Saghaee

Continuous Flight Auger (CFA) Piles

Design, Testing, and Automated Monitoring of ACIP Piles in Residual Soils **414**
Stephen W. Lacz and Richard C. Wells

Load Displacement Behavior of ACIP Piles in Cohesive Soils **422**
C. Vipulanandan, Kalaiarasi Vembu, and Tracy Brettmann

Load Tests on Small Diameter Augered Cast-in-Place Piles through Fill **430**
W. Ken Beck and Patrick J. Harrison

Practical Considerations for Design and Installation of Drilled Displacement Piles **438**
W. Morgan NeSmith and J. Fox

Advancements in Data Acquisition-Based Design for Drilled Displacement Piles **447**
W. Morgan NeSmith and Willie M. NeSmith

Helical Piles and Anchors

Cylindrical Shear or Plate Bearing?—Uplift Behavior of Multi-Helix Screw Anchors in Clay **456**
Alan J. Lutenegger

Lateral Resistance of Helical Piles in Oil Sands **464**
Mohammed Sakr

Load Transfer Behavior of Full-Scale Instrumented Screw Anchors **472**
Kristen Tappenden, David Sego, and Peter Robertson

LRFD for Helical Anchors: An Overview **480**
Donald Deardorff and Ronaldo Luna

Load Test Results—Large Diameter Helical Pipe Piles **488**
Kelly Hawkins and Richard Thorsten

Performance-Based Design for Helical Piles **496**
Mamdouh Nasr

Wind Energy Converter (Turbine) Foundations

Design and Construction of Intermediate Foundation Solutions for Wind Turbines 504
Brendan FitzPatrick, Richard Gernant, and Jeromy Miceli

Design of Monopile Foundations for Offshore Wind Energy Converters 512
Kerstin Lesny and Peter Hinz

Offshore Wind Energy in Germany Compared to Other European Areas—Challenges and Recent Developments 520
Kerstin Lesny

Foundation Testing

Analysis Collateral: Information Needed for Foundation Integrity Test Data Analysis 528
Bernard H. Hertlein

Capabilities and Limitations of Cross Hole Ultrasonic Testing of Piles 536
J. M. Amir and E. I. Amir

Combined Parallel Seismic and Cone Penetrometer Testing of Existing Foundations for Foundation Length and Evaluation 544
Dennis A. Sack and Larry D. Olson

A Case History Evaluation of CSL Access Tube Debonding 552
Joshua C. Adams, Edward L. Hajduk, Peo Halvarsson, and Al Neumann, Jr.

The Use of Crosshole Tomography to Evaluate Drilled Shaft Repairs 560
Les R. Chernauskas and Edward L. Hajduk

Shortcomings of the Davisson Offset Limit Applied to Axial Compressive Load Tests on Cast-in-Place Piles 568
W. Morgan NeSmith and Timothy C. Siegel

Experimental Investigation of the Effect of Shearing Rate on the Capacity of Piles in Soft Silt 575
Paul Doherty and Kenneth Gavin

Impedance Logs for Drilled Shafts at the Northwestern NGES 583
Sarah L. Gassman and Hongfen Li

Advances in Dynamic Foundation Testing Technology 591
Garland Likins, Ingemar Hermansson, Mike Kightley, Jon Cannon, and David Klingberg

Dynamic Pile Testing—Construction Control and Design Verification 599
Benjamin Smith

Dynamic Pile Testing of Three Drilled Shafts on the Bridge over the Changuinola River in Panama 607
Jorge W. Beim and Cesar A. de Gracia G.

Evaluating Uplift Capacity of Driven Steel H-Piles, Comparing PDA and Load Test Results 615
Scott Newhouse, Kenneth Bell, and John Davie

Driven Concrete Pile Foundation Monitoring with Embedded Data Collector System 621
Rodrigo Herrera, Lawrence E. Jones, and Peter Lai

Improved Methods for Rapid Load Tests of Deep Foundations 629
Takaaki Miyasaka, Garland Likins, Fumio Kuwabara, Frank Rausche, and Masayuki Hyodo

Dynamic Verification of Static Load Testing of Pin-Piles in Seattle 637
G. Mann, R. D. Holtz, and D. Maloney

Indexes

Author Index 645

Subject Index 649

Copyrighted Materials
Copyright © 2009 American Society of Civil Engineers (ASCE)
Retrieved from www.knovel.com

Management of Risk in Deep Foundations with Design-Build

Dan Brown[1], M.ASCE, Ph.D., P.E.

[1]President, Dan Brown and Associates, PLLC, 300 Woodland Road, Sequatchie, TN 37374; Phone: 423-942-8681; dbrown@danbrownandassociates.com

ABSTRACT: The design-build delivery system is receiving increased use on large infrastructure projects, and deep foundations often represent a significant component of the risks to project costs and schedule. This paper presents a discussion of the management of the risk elements associated with the design and construction of deep foundations, along with some strategies that have been employed to help mitigate these risks. The effective management of risks with deep foundation design and construction is seen to require cooperative effort, particularly between the constructors and designers, and an ability to evaluate the problem from a broad perspective. Test programs can be utilized to develop mitigation strategies and reduce risks relative to both performance and productivity.

INTRODUCTION

Design-build has become a preferred method of project delivery for many large construction projects. There may be numerous factors leading to the choice of design-build by the owner, but perceived advantages with respect to schedule and costs are often major considerations. With respect to deep foundation design and construction, the design-build team must take on the responsibility to deliver foundations which satisfy the performance criteria set by the owner and meet other requirements for support of the structure.

Inherent to this responsibility, are the risks the design-builder takes with respect to the design, construction, and performance of deep foundations. These risks must be assessed and managed effectively in order to develop a winning proposal and achieve a successful project. A successful project would be one which is financially rewarding to the design-builder, achieves the performance required, and is delivered on-time to the owner.

This paper outlines some of the risk components and possible mitigation strategies associated with design and construction of deep foundations in the design-build environment. The paper is presented from the point of view of the design-builder and with emphasis on infrastructure projects. The risks inherent in design-build with large infrastructure projects can be substantial with respect to both direct

costs and schedule. Failure to adequately address risks can lead to increased costs, schedule impacts, poor performance, and financial losses.

The issue of risk must be confronted by all stakeholders in the design-build project, including the constructors, the design professionals, and the owners. Constructors are confronted with risks inherent to the nature of their work with conventional construction, but the design element presents new challenges unique to the design-build delivery system. Most geotechnical design professionals have traditionally been very "risk-averse" (i.e., cautious and conservative) in the design of deep foundations, and with good reason; the conventional design-bid-build system offers little incentive for efficiency compared to the penalty for failure. However, the competitive nature of the bidding process with major public works projects represents an unusual environment for most geotechnical engineers, and an overly conservative assessment of risks on the part of the design-build team can result in an unsuccessful proposal/bid. Project owners have a stake in the management of risk by the design-builder because of the possible negative impact of schedule delays or costs associated with litigation and/or claims related to differing site conditions. Thorough pre-bid geotechnical investigations and/or foundation testing by the owner can reduce risk to the design-builder during bidding and therefore reduce contingency costs and lower bid prices.

In order to manage risks effectively, significant risks must be identified and their potential impact assessed, a plan for possible mitigation of the risks developed, and an appropriate allocation for the costs associated with the risks included in the bid.

IDENTIFICATION AND ASSESSMENT OF RISKS

During the design-build proposal process, a preliminary deep foundation design must be completed in order to develop a technical proposal, a work plan and tentative schedule, and cost estimate. The proposal stage is the most critical time to develop an initial assessment of risks, and this task often must be completed in a short time with limited subsurface information. Some of the more significant risk items are included in the following categories.

Stratigraphy. Variability in stratigraphy across the site may affect deep foundation length requirements and costs. Variability may be difficult to accommodate with some types of deep foundations. A potential for unusual depth in some locations may preclude some foundation types from consideration. Variability increases the need for additional borings or soundings, and this work can affect the project schedule. Examples include variable depth to top of rock, voids due to weathering or solution activity, or variable depth to bearing stratum due to alluvial-filled channels. One method to assess the impact of stratigraphy is to estimate the potential range of variations in stratigraphy across the project site, along with the likely numbers of foundation units falling within the spectrum of possibilities. Another approach might be to develop a design for the range of possible conditions and then assign probabilistic values to the most likely, most unfavorable, and most favorable conditions. When the available geotechnical data are sparse, these approaches generally include a fair amount of engineering judgment combined with a dose of guessing (do you feel lucky?).

As an example, a design-build project for a bridge along the Gulf Coast consisted of several miles of elevated roadway extending between the mainland and a barrier island beachfront community. A design-build team composed of a regional engineering firm, a regional bridge contractor, and a regional pile driving contractor was assembled and "short-listed" to bid the work. Each of these firms was a well-run organization and highly respected in their field. The project was a relatively straightforward job, to consist of repetitive spans with precast concrete girders supported on prestressed piles; however, there were only a few borings across several miles of distance. The depth to good bearing soils was variable and therefore the anticipated pile length could not be predicted except within a broad range. Because of the size of the project and the magnitude of the downside risk, this design-build team elected not to tender a bid. The project was awarded to a much larger contractor with greater resources. Because the project owner left most of the site investigation work to the post-award effort of the design-builder, the resulting risk eliminated a team of local engineers and constructors who were very well qualified to perform the work at a competitive price. The cost of borings can be estimated fairly easily; the cost of a lack of borings is more difficult to quantify in this case.

Foundation Performance. Uncertainties in material behavior of soil or rock can affect anticipated foundation performance and construction techniques or productivity. Examples include uncertainties relating to measurements of performance as required by contract or as proposed with a value-engineering cost proposal. Besides conventional static load tests, dynamic tests are often required for verification on driven pile projects, and unanticipated results such as large setup or unusually low indicated resistance can lead to production delays and/or additional testing requirements. Measurements require interpretation to evaluate foundation performance, and foundation performance risks to the design-builder are increased by an owner or owner's representative who insists on extremely narrow or inappropriate interpretations of measurements. Where foundation performance risks are identified as significant, it is helpful to assess the range of potential behavior and the potential impact on the project costs or schedule.

Construction Productivity. Effects of material behavior on construction techniques or productivity can have a huge impact on costs and time. Examples include drivability of driven piles, difficulties in rock excavation or boulders with drilled shafts, effects of artesian groundwater or caving soils, potential ground subsidence with continuous flight auger piles, and impacts of solution cavities on construction of all types of deep foundations. Productivity is most often estimated on the basis of experience in similar geology or circumstances. The assessment of the possible range of productivity with different construction techniques and the risk elements in this category is most effectively performed by a team of constructors, estimators, and geotechnical/structural engineers. By working cooperatively in brainstorming sessions, a group can bring the broadest possible perspectives to the problem and intelligently assess risk components with each potential foundation type or installation method.

Construction Defects. Defects which must be corrected can lead to significant costs and delays in some instances. Issues such as broken or out-of-position piles, or

concrete defects in drilled shafts represent potential risks to the design-builder. Excessive inspection and quality assurance requirements from the owner can greatly increase the risks to the design-builder, such as low tolerances on drilled shaft bottom cleanliness, inappropriate interpretation of integrity test results, or excessive demands for restrike measurements on driven piles. As with productivity, an assessment of risks of defects, probability of occurrence, and the potential impact should be included with each foundation alternative.

MITIGATION STRATEGIES

Once the most significant risks are identified and the magnitude assessed, mitigation strategies may be developed to reduce the negative consequences of risk to the design-builder. Strategies can include transfer of the risk to some other party or reduction of risk with a different approach. Engineered solutions may be developed to reduce risk with better or more reliable information or with a more robust foundation design or construction approach that will reduce the impact.

Risk Transfer. Transfer of risk from the design-builder to an outside party can be accomplished with the purchase of insurance, but this approach is not typically employed for the deep foundation component of a construction project. A more common approach is to seek to transfer some level of risk back to the project owner through negotiated exception clauses included in the bid or through claims. Exception clauses may be negotiated between the design-builder and the project owner, both of whom must agree with contract stipulations. Exceptions can cause a cost proposal to be considered "non-responsive" on many competitively bid public works projects and therefore may not be possible in many instances. Claims for differing site conditions or other changes provide a means of mitigating unusual variations in conditions.

Differing site conditions clauses (FHWA, 1996) are intended to provide a means for constructors to recover costs associated with conditions that could not reasonably have been anticipated at the time of bidding, and therefore eliminate the need for the bidder to include contingency costs for items which presumably could not have been anticipated anyway. However, claims for differing site conditions (DSC) or other changes can be expensive to pursue and can result in lengthy delays of reimbursement for costs or even risks of non-reimbursement for costs if the owner disagrees. With design-build, it is generally expected that DSC or other changes are truly "unanticipated" and therefore represent risks or deviations beyond the range of conditions that reasonable and responsible bidders would anticipate. To this end, it is desirable that the geotechnical professionals document the anticipated range of conditions as described in the previous section so that a claim can be more effectively be presented should the need arise. A pre-bid design based on an unreasonably narrow range of conditions does not provide an effective mitigation strategy.

Mitigation of Stratigraphy Risks. The owner can often provide the most effective measures to mitigate risks of subsurface variability by executing a more extensive pre-bid site investigation. The design-builder may decide to conduct additional site investigation pre-bid to mitigate risk of uncertainty, but the time available to do so is limited and the costs must be weighed against the uncertain

prospects of winning the job. A relatively modest investment in site exploration on the part of the owner can pay great dividends in terms of reduced contingency costs in the bids and reduced risk of claims for differing site conditions.

The geotechnical baseline report (GBR) as a basis for bidding has been used successfully for tunnel projects, which have a high degree of risk with respect to subsurface conditions. The GBR does not eliminate risk, but defines the extent of the risk to the constructor so that it can be more effectively quantified and budgeted. The use of this approach for deep foundations is encouraged by ASCE (2007), but to date the concept has been rarely used for deep foundations.

Post-award mitigation of stratigraphy risks may include additional site investigation, development of an adaptive foundation construction plan that allows adjustment to actual conditions encountered, or a combination of both.

After a design has been developed based on the overall geotechnical investigation, additional exploration might be performed solely for a specific purpose related to the foundation construction. Given that design-build projects are often executed with an aggressive schedule, the foundation design may be finalized as construction proceeds based on the actual conditions encountered. Examples of investigations that might be conducted concurrent with construction include:

- Exploratory borings at the location of each drilled shaft, drilled without sampling to determine depth to rock and then cored into rock to determine rock conditions and establish fnal tip elevation.
- Extensive coverage with CPT soundings or borings with SPT only to determine pile or shaft tip elevations at each foundation location.
- A test pile driven at each foundation location to more reliably define pile length requirements

The strategy employed must be consistent with the geology and the nature of the anticipated variations. For instance, drilled shafts constructed in karst formations typically require more extensive investigation at each shaft location to depths below the anticipated tip elevation to finalize each specific shaft design. Drilled shafts in rock from geologic conditions with less inherent variability might require only an evaluation of the depth of weathered rock at each specific shaft location.

The recently completed I-35W St. Anthony Falls bridge in Minneapolis was constructed with a very aggressive schedule in order to rebuild the structure which collapsed in 2007. The new bridge was founded on groups of drilled shafts constructed into the St. Peter Sandstone formation, a friable (poorly cemented) sandstone. Most of the axial resistance of the shafts is derived from side resistance in the sandstone, but the uppermost 3 to 8 m was typically weathered and soft. The measured side resistance and performance of the drill rig during the test shaft construction was used to develop a construction plan to accommodate variations. This plan included one or two borings at each shaft group location along with monitoring of the drill rig penetration rate during construction of each individual shaft. By careful observation of the drill rig performance during excavation of the sandstone, the depth of the soft, weathered sandstone could be readily distinguished

from the relatively unweathered sandstone below. The final tip elevation of each shaft was then determined during construction on the basis of these observations.

A transmission line project in the western United States traversed a broad range of geology including relatively soft alluvial soils, as well as stronger cemented soils and rock. Design of the deep foundations was controlled by lateral and overturning loads. Foundations in the soft soils were designed for the worst case soil conditions anticipated within the soft alluvial soils based on the several borings made, and no additional exploration was performed in these areas. This approach was optimal for the alluvial soil conditions because: a) the schedule was very aggressive and the soft soil areas were on the critical path, b) the foundation design was sufficiently robust to accommodate variability, and c) no significant cost savings could be realized by trying to adjust the foundation length on a case-by-case basis. The construction equipment and installation methods were sized to handle the worst case conditions.

The foundations in the stronger soil and rock areas were designed for a baseline case representative of each geologic area from the pre-design borings. The specific shaft tip elevation at each foundation location was developed from a boring at each location, performed concurrent with the ongoing construction operation. The boring at each location is a fast and simple probe with SPT and visual classification only, and besides the design information this boring provides a means to identify rock or obstructions such as boulders.

Mitigation of Foundation Performance and Productivity Risk. Mitigation of foundation performance and productivity risks are discussed together, because the strategies employed usually can be directed toward both. The most effective means to reduce risks associated with productivity and performance is to conduct full-scale tests in representative ground conditions. When the owner conducts a pre-bid testing program, these risks can be minimized and bidders can eliminate much of the contingency costs associated with these risks. An example is the pre-bid program of axial and lateral load tests of drilled shafts into the Cooper Marl and overlying alluvium for the Cooper River Bridge in Charleston, SC (Brown et al, 2002; Camp et al, 2002). This project was subsequently awarded as a design-build contract, and the final selection of foundation type could be changed by the design-builder; however, the foundation type to be used (drilled shafts into the marl) was fairly obvious for this site. The potential savings to the project owner from pre-bid deep foundation test programs are difficult to quantify, and if a variety of deep foundation types or construction techniques are viable for the project then it may be preferable to leave the test shafts or piles for the design-builder to perform in a manner specific to their foundation design.

A design-builder may conduct their own pre-bid tests to evaluate foundation performance and productivity. At the pre-bid stage, the results are used not only to reduce risks and refine cost estimates, but also to gain competitive advantage. Drilled foundations in rock represent one type of deep foundations where there may be large potential variations in construction productivity and foundation performance, and where significant competitive advantage may be realized from pre-bid tests. Pre-bid tests may sometimes be conducted off-site in similar geology, or research to find test data from other projects in similar conditions may serve a similar purpose. In any

case, the constructor and the geotechnical design professionals in a design-build environment should explore the possible benefits as a joint effort to develop the most cost-effective and efficient foundation solution.

A post-award testing program is often mandatory for verification of performance to the owner on major projects, but with careful planning, test foundations can be highly beneficial in mitigating risks. Foundation testing is affected by both the compressed schedule associated with design-build and the shared interest of the geotechnical designer and constructor to mitigate risks associated with performance and productivity. The test pile program must usually be initiated concurrent with the final site investigation and geotechnical design efforts, and therefore it is desirable that a plan be developed during the pre-bid stage so that implementation can proceed soon after notice to proceed.

The recently completed Biloxi Bay Bridge provides an example of an extensive test pile program which was used to mitigate risks of performance and productivity. The bridge across Biloxi Bay, destroyed by Hurricane Katrina, was to be replaced with a new structure constructed on driven prestressed concrete piles. The schedule was very aggressive, and included both early completion bonuses and liquidated damages for late delivery. In this case, the greatest risk factor was that variable pile lengths requiring extensive restrike measurements or pile splices might affect the schedule. A relatively few borings were available pre-bid and the debris from the old bridge impacted the schedule of completion of new borings.

A testing program consisting of 20 test piles (approximately every 4^{th} pier) spread across the bay was initiated as the site exploration was ongoing. Early borings were concentrated at the planned locations of test piles so that estimated tip elevations for these piles could be developed and piles cast as quickly as possible. Because of the storm damage, the local prestressing plant was not yet operating a full capacity and there was great demand for their product for reconstruction elsewhere in the area (notably the local casinos); therefore it was imperative to start casting piles quickly and continue to cast piles for the bridge at a steady pace. Soil conditions consisted of a highly variable mix of interbedded sands and clays.

The test piles were completed with dynamic measurements, and restrike measurements were performed for dynamic load tests over a period of up to two months after the initial pile installation. One static axial load test and two rapid load tests (using the Statnamic device) were also performed to validate the static axial resistance indicated by the dynamic load tests. Two lateral load tests were performed to verify lateral soil resistance for design. A key component of the test measurements were the verification of the increase in axial resistance as a function of time across the broad range of conditions across the bay. The test piles also verified that the pile installation equipment selected for the project could install the piles without damage for a wide range of conditions and even install the piles through soils with an axial resistance significantly greater than the design requirements.

Because the end bearing resistance was highly variable, a foundation design reliant upon this component of resistance would have resulted in significant variations in pile length and challenges in achieving required driving resistance

during installation without splices or cutoffs. Therefore, the foundation design and target pile tip elevation at each pier was based on the resistance of those piles which did not have large end bearing resistance. Where substantial base resistance was indicated from the signal matching of restrike blows (based on analyses from CAPWAP), the resistance was discounted to that measured by piles without high end bearing. In almost all cases, the pile driving system was able to achieve penetration without refusal and the need for cutoffs. Based on the setup indicated by extensive restrike measurements available from the test pile program, driving criteria for production piles were easily achieved and even relatively low driving resistance observed during installation did not require restrike measurements. The need to restrike production piles was largely avoided; restrikes would require repositioning of barges, disrupt productivity, and adversely affect the schedule.

The design-build contract for the Biloxi Bay Bridge was awarded in June, 2006 and the bridge opened to traffic in October, 2007, 2 weeks ahead of schedule. The State of Mississippi was pleased, the people of Biloxi were pleased and the constructor was pleased (translation: incentive bonus was achieved). The test pile program for this project was instrumental in maintaining productivity and completing the bridge on schedule.

Mitigation of Construction Defect Risks. There will always be some risks of construction defects related to equipment failures, acts of nature, and fallible human beings. From a geotechnical design and construction perspective, the most effective means of reducing risks from construction defects is to develop a robust design and construction plan with an emphasis on "design for constructability". The best foundation design is one which is easy to construct, and the best installation plan is one which does not push the limits of equipment capabilities. In many instances, a test installation or load test program can be used to improve both the design for constructability and the methods used for installation.

An example of the use of a test shaft to mitigate the risk of construction defects is provided by the drilled shaft load tests for the new Christopher Bond Memorial Bridge across the Missouri River in Kansas City. The main pylon for this cable stayed bridge was founded on a group of 8 drilled shafts, each 3.2 m (10.5 ft) diameter and extending through approximately 30 m (100 ft) of overburden to penetrate 8 m (26 ft) into shale. A permanent casing was installed through the river and overburden to the shale. This shale, like many shales, is prone to decompose rapidly when exposed in the shaft excavation. For this reason, the standard MoDOT specification includes a restrictive time limit on the period for which the shaft rock socket excavation may be open if the design relies on side resistance for axial capacity. The time required to complete the hole cleanout, install the reinforcement, and start concrete placement in the large diameter and deep shafts on this project would exceed the time allowed by specification and result in a constructed shaft which was considered not in conformance with the project requirements.

Slake durability tests were performed on shale taken from core samples using both water and a solution of polymer drilling slurry. These tests suggested that the use of polymer slurry reduced the tendency of the shale to quickly decompose compared to the use of water alone. Although the permanent casing to rock would

allow the shafts to be constructed with water rather than slurry, the polymer appeared to provide advantages with respect to decomposition of the shale. Therefore the test shaft was designed to be constructed using polymer slurry and, pending favorable results, polymer slurry was planned for production shafts.

A 1.8 m (6 ft) diameter prototype load test shaft was constructed to measure axial resistance in the shale in side shear and base resistance using an embedded bi-directional load cell (O-cell). In order to establish a basis for construction of production shafts, the test shaft was drilled with polymer slurry and left open for a period of four days prior to completion and concrete placement. The load test results indicated side and base resistance of this test shaft slightly higher than the design parameters estimated pre-bid, and the special provisions for production shafts were modified to allow up to four days to start concrete placement in the shaft after completion of the rock excavation. This modification to the specification subsequently proved to be very valuable when a drilling tool malfunctioned during construction of one of the production shafts. The 1.5 days of delay associated with extraction of this tool and repair of the equipment was accommodated by the revised specification, thanks to the demonstrated performance of the load test shaft.

Another example of a robust design of a drilled shaft which can reduce the risk of defects is the use of base grouting at the toe of a shaft (Dapp, et al, 2006). Although often used as a means to improve the base resistance of a shaft in granular soil, the use of base grouting has been demonstrated to mitigate the effects of imperfect bottom cleaning operations. Many agencies have specifications with tolerance on loose material at the base of the shaft which can be difficult or impossible to achieve in large diameter and very deep drilled shafts under slurry. The delivery of grout under pressure at the toe of the shaft has been demonstrated by load tests to mitigate the effects of imperfect cleaning and justify a relaxation of the tolerances on bottom cleanout.

The use of full length segmental casing for drilled shaft construction installed with a rotator or oscillator system can reduce the risk of construction defects in certain conditions. Where the risk of hole collapse is high and the consequences are especially severe (such as near an existing structure), the full length casing helps mitigate the risk of instability. Risks associated with delays or difficulties with alignment and excavation stability posed by obstructions such as boulders or buried logs can be reduced because the casing is used like a coring tool to cut through such obstructions. One contractor's internal documentation of integrity test measurements indicates that the incidence of "anomalies" in drilled shaft concrete is reduced in shafts constructed with this method. The full length casing typically allows concrete to be placed in the dry or in a water-filled excavation as opposed to a slurry excavation which may have a greater quantity of suspended particles.

On a recent project in the southeast, the constructor was placing concrete with a tremie in a shaft which was 2.4 m (8 ft) diameter and over 60 m (200 ft) deep. A failure of the tremie occurred when the shaft was approximately one third completed. Because the shaft was constructed using the oscillator method with full length casing, the casing was re-advanced to the bottom of the original excavation, the concrete removed with an air-lift, the reinforcement recovered, and the shaft reconstructed in

the same excavation a few days later. Although the removal of concrete and re-do of the shaft was expensive, the problem of the repair of a shaft with a structural defect was avoided thanks to the excavation stability provided by the segmental casing method.

COSTS ALLOCATED TO RISKS

As a final part of the pre-bid management of risks, a cost must be included in the bid to allow for some magnitude of adverse conditions encountered in the design and construction of deep foundations. In order to manage these costs effectively, a typical strategy is that the individual risk components are estimated, along with a cost impact and an estimated probability of occurrence so that the estimators can make an appropriate allowance. For example, if there are 10 elements of risk, each of which might have a $1million impact, and the probability of each is estimated at 30%, it would be appropriate to include a $3million contingency cost in the bid. If these probabilities are estimated realistically, it is unlikely that all 10 elements would be realized on the project. A single large risk item would not be treated in such a simplified manner.

Because the pre-bid design is typically completed with incomplete information, the estimates of variability and the assessment of costs are imperfect; these facts must be acknowledged and accepted by all parts of the design-build team. It is important that the constructor not harbor unrealistic expectations of the geotechnical designers to "peer into their crystal ball" and see into the unknown. It is also not appropriate for the geotechnical design professionals to take the most pessimistic view of each possible aspect and therefore add conservatism on top of conservatism.

A bridge was planned across a waterway in a northern location, with foundations to be constructed of drilled shafts constructed through the water and socketed into the underlying hard rock. The design of the shafts was controlled by lateral and uplift resistance because of lateral forces from ice. The rock was extremely hard and abrasive, but the site included several old faults in which extensive fractures could be anticipated. The locations where fractures might be encountered were not known.

Two designs were developed, one for conditions where sound rock might be encountered and another (plan "B") for conditions where highly fractured rock might be encountered. The latter condition would require significantly deeper sockets as well as additional effort and time for installation. The geotechnical professionals (engineers and geologists) developed an estimate that 20% of piers (at unknown locations) might encounter the "plan B" conditions and the design-build constructor prepared a bid with the appropriate costs.

SUMMARY AND CONCLUSIONS

The design-build method of project delivery has seen increasing use on large infrastructure projects with extensive deep foundation components. The management of risk related to deep foundation design and construction is a key component of a successful project, and one which affects all of the stakeholders including the constructors, geotechnical professionals, and project owners. The effective management of risks with deep foundation design and construction requires

cooperative effort, particularly between the constructors and designers, and an ability to see the problem from a perspective beyond one's own traditional perspective. Mitigation strategies can be developed with proactive thinking and particularly with utilization of testing programs which are designed with both performance and productivity risks in mind.

ACKNOWLEDGMENTS

The author wishes to acknowledge the helpful dialog and thoughtful discussions of the issues described in this paper by the following individuals: Mr. Steve Saye, Kiewit Engineering; Mr. Heinrich Majewski and Mr. Terry Tucker, Malcolm Drilling; Mr. Pat Byrne, Massman Construction; Mr. Frank Daams and Mr. Terry Poole, Flatiron Constructors; Mr. Brian Christenson, Black & Veatch; Mr. Rich Lamb, Minnesota DOT; and Mr. Jeff Gebhard, Braun Intertec.

REFERENCES

American Society of Civil Engineers (2007). "Geotechnical Baseline Reports for Construction: Suggested Guidelines." R. Essex, editor, 72 p.

Brown, D. A. and Camp, W.M., 2002. "Lateral Load Testing Program for the Cooper River Bridge, Charleston, SC" Geotechnical Special Publication No. 116, ASCE, pp. 95-109.

Camp, W.M., Mayne, P.W., and Brown, D.A. 2002. "Drilled Shaft Axial Design Values: Predicted Versus Measured Response In A Calcareous Clay" Geotechnical Special Publication No. 116, ASCE, pp. 1518-1532.

Dapp, S., M. Muchard, and D. Brown, 2006. "Experiences with Base-Grouted Drilled Shafts in the Southeastern United States" Proceedings of the 10th International Conf. on Piling and Deep Foundations, Amsterdam, June, 2006.

Federal Highway Administration (FHWA) (1996). "Geotechnical Differing Site Conditions." *Geotechnical Engineering Notebook Issuance GT-15,* Washington D.C., 37 p.

Copyrighted Materials
Copyright © 2009 American Society of Civil Engineers (ASCE)
Retrieved from www.knovel.com

Ultimate Micropile Bond Stresses Observed during Load Testing in Clays and Sands

John R. Wolosick, PE, MASCE [1]

(1) Director, Hayward Baker Inc., 515 Nine North Court, Alpharetta, GA 30004: jrwolosick@haywardbaker.com

ABSTRACT: Micropile designers must use their experience and best judgment when sizing bond zones for the piles. Rock socketed micropiles offer a certain level of forgiveness in design since high capacities are often available. However, in soft or loose soil deposits, enhanced grouting techniques such as pressure grouting through casing or post-grouting may often be required to provide a reasonable bond length to make the micropile installation affordable. This paper presents several load tests where these grouting methods were employed. The ultimate bond stresses observed are reported and compared with reported values in Table 5-2 of the FHWA Micropile Design and Construction Implementation Manual which lists ultimate bond stresses for preliminary design.

INTRODUCTION

Prior to the advent of specialty pressure grouting techniques, it was difficult or impossible to achieve reasonable bond values for micropiles installed in weak soil deposits. In particular, problematic soils included soft clays or loose sands with blow counts less than about 7. Soft clay deposits with unconfined compression strengths of less than 500 psf (24 kPa) and water contents higher than about 30 percent also presented challenges to micropile contractors. The required theoretical bond lengths to achieve reasonable micropile design loads were excessive or uneconomical. In addition, it was found that much longer bond lengths did not necessarily provide additional capacity due to the phenomenon of progressive de-bonding between the grout and the steel reinforcement within the bond zone of the micropiles. The weak soils were unable to provide enough confinement to keep the grout bonded to the steel under load.

This paper presents the results from several projects where reasonable bond lengths for the micropiles were installed. Enhanced grouting techniques including pressure grouting through casing in loose sands and post-grouting using sleeve-port pipes in soft clays enabled the projects to be completed successfully, with reasonable costs.

Also, the ultimate bond stresses observed from several load tests are compared with published values by the FHWA. In addition, the bond enhancement from post-grouting soft clay on a representative project is presented.

MICROPILE ULTIMATE CAPACITIES IN VERY STIFF CLAY

Jackson, MS International Airport Parking Garage Expansion:

A need for additional parking spaces at the two-level parking garage at the Jackson Airport called for adding additional levels to the existing garage in 2005. The increase in foundation loads required the installation of deep foundation support in low-headroom conditions within the existing garage structure. Micropiles were utilized to accommodate the increased loadings. See Figure 1 for a view of the structure.

Figure 1 – Jackson Airport Parking Garage

The soil conditions at the site consist of Yazoo clay, a high plasticity clay with expansive characteristics. The Yazoo clay in the Jackson area consists of an upper weathered zone above a lower unweathered zone. Unconfined compressive strengths for the lower unweathered Yazoo clay were reported in the geotechnical report as averaging 6600 psf (316 kPa) and cohesion of 3300 psf (158 kPa). These values were obtained from unconfined compression tests and UU triaxial tests.

The micropiles were designed for capacities of 55 tons (489 kN) working load. The micropile consisted of an upper 3 foot (1 m) cased length of 7 inch (178 mm) OD, thin walled standard steel pipe. The pile was reinforced with a full-length Grade 75 ksi (517 MPa) No. 14 (45 mm) all-thread bar. They were installed using augers and included post-grout tubes. See Figure 2 for a cross-section of the micropile.

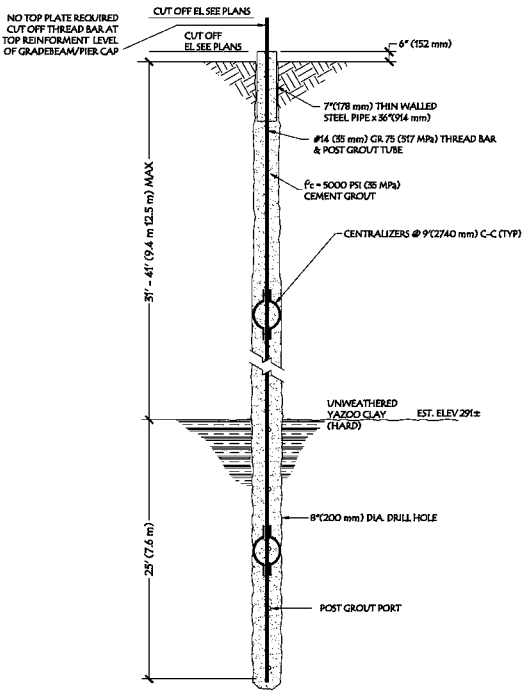

Figure 2 – Cross-Section of Test Pile, Jackson Airport Project

The test program consisted of first testing a non-post-grouted micropile with a 25 foot (8 m) bond zone. After the initial test, the same pile was post-grouted using a sleeve-port pipe and tested again. Next, another pile was installed with a 30 foot (9 m) bond zone and post-grouted prior to any testing. The piles were tested in compression. Figure 3 shows the pile load test set-up.

The post-grouting was performed globally from the ground surface, using about 5 cubic feet (85 liters) of neat cement grout, with a 0.5 water/cement ratio. The post-grouting was generally applied the next day after installation with a high pressure piston pump. Typical fracture pressures were 450-500 psi (3100-3450 kPa). Grout was pumped at 100-150 psi (689-1030 kPa) initially and then stopped when pressures reached 300 psi (2068 kPa). Figure 4 shows the results from the load test program.

Figure 3 – Compression Load Test Set-Up

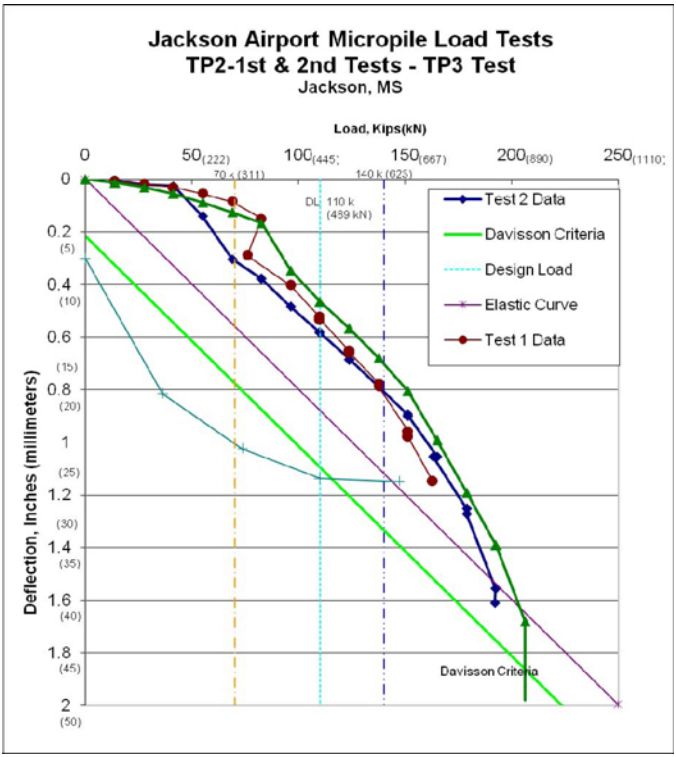

Figure 4 – Results from Test Piles

Analyses of the testing results provided the ultimate bond stresses for the test pile program. The ultimate bond stress value measured for the initial gravity grouted micropile was 22 psi (149 kPa). The ultimate bond stress measured for the same pile after post-grouting was 25 psi (176 kPa), which indicated an increase in ultimate capacity of about 18 percent by post-grouting. Note that these results are very close to the reported cohesion of 23 psi (158 kPa) for the soils. The effect of the initial loading on the pile to the subsequent result from the second test is unknown.

The third pile load test on the micropile with a 30 foot (9 m) bond length indicated an ultimate bond stress of 23 psi (158 kPa). This pile held a higher total load of 206 kips (916 kN) versus 192 kips (854 kN) for the second test.

For the production piles, 30 foot (9 m) bond zones were installed. All of the production piles were globally post-grouted using the same methods as the test piles. The results from these three tests are compared with the ultimate bond stress values from the FHWA Micropile Manual at the conclusion of the paper.

MICROPILE ULTIMATE CAPACITIES IN MEDIUM STIFF CLAY

Arts and Sciences Museum, University of Puerto Rico, Mayaguez:

In 2005, the Arts and Sciences Museum at the University of Puerto Rico in Mayaguez underwent a major repair and renovation project after the roof was destroyed during Hurricane Georges in 1998. Micropiles were installed in confined access and limited headroom to support a new roof structure for the historic structure.

The micropiles were installed in high moisture content silts (w = 45%) and post-grouted using sleeve-port pipes within a few days after installation. Reported shear strength of the silt was 14 psi (96 kPa) when tested with a pocket penetrometer. The specifications required that the 50 kip (222 kN) design load pile be tested to a factor of safety of 2.5, maximum test load of 125 kips (556 kN). The micropile consisted of an upper 10 foot (3 m) cased length of 6 inch (152 mm) OD, thin walled standard steel pipe. The micropile was reinforced with a full-length epoxy-coated Grade 95 ksi (655 MPa) No. 11 (35 mm) all-thread bar. See Figure 5 for the design micropile cross-section.

The piles were globally post-grouted from the ground surface, using about 3-4 cubic feet (113-142 liters) of neat cement grout, with a 0.5 water/cement ratio. The post-grouting was applied the next day after installation with a high pressure piston pump. Typical fracture pressures were 450-500 psi (3100-3450 kPa). Grout was pumped at 100-150 psi (689-1030 kPa) initially and then stopped when pressures reached 300 psi (2068 kPa). See Figure 6 for an illustration of the post-grout tubes. They are the white tubes with black rubber sleeves on the ground in the background. The sleeves are spaced on 24 inch (610 mm) centers.

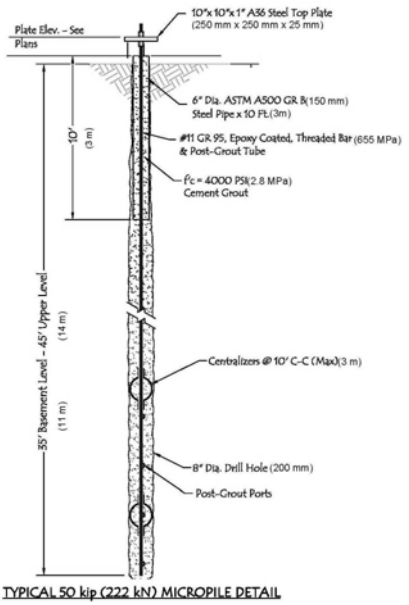

Figure 5 – Pile Cross-Section

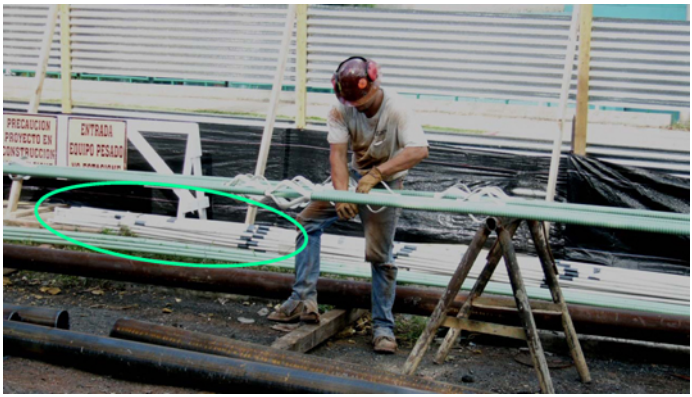

Figure 6 – Post-Grout Tubes in Background

A sacrificial pile was tested on the first level of the structure to 120 kips (534 kN). The pile load test set-up is shown on Figure 7. The pile load test result is illustrated on Figure 8. The pile successfully held the required test load. The micropile reached a modified Davisson Criteria at a deflection of 0.44 inches (11 mm) at 120 kips (534 kN), indicating failure by this criterion.

Figure 7 – Micropile Load Test, University of Puerto Rico

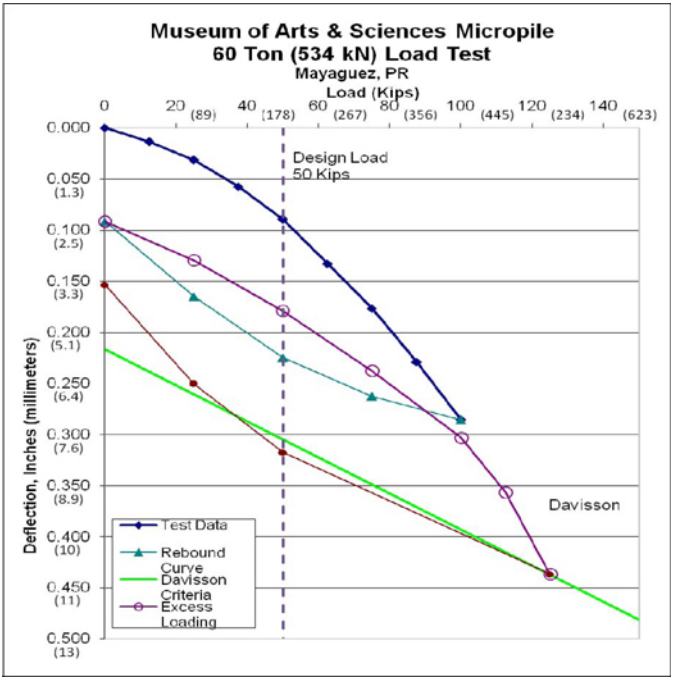

Figure 8 – Load Test Results

Analyses of the load test results indicate an ultimate bond stress of 16 psi (110 kPa) for the post-grouted pile with a 25 foot (8 m) long bond length. Note that this value is very close to the reported cohesion of 14 psi (96 kPa) for the soils.

MICROPILE ULTIMATE CAPACITIES IN DENSE SAND

Kimberly Clark Paper Mill, Mobile Alabama:

Using concepts originally put forward by Littlejohn (1970) for pressure grouted tiebacks in cohesionless soils, micropiles have been installed in clean sands and pressure grouted during installation to provide high capacities. Pressure grouted micropiles were installed in 2001-2002 at a Kimberly Clark plant in Mobile, Alabama. The piles were installed in limited access and headroom in the basement of the plant to support new machinery independently from an existing 4 foot (1.2 m) thick mat foundation. The engineer required that the 80 kip (356 kN) design load pile be tested to a factor of safety of three (240 kips, 1,070 kN). The micropile consisted of an upper 35 foot (11 m) cased length of 7 inch (178 mm) OD, 0.498 inch (12.6 mm) wall thickness N80 (80 ksi, 550 MPa yield) steel pipe. The pile was also reinforced with a full-length No. 11 (35 mm) Grade 75 ksi (517 MPa) all-thread bar.

Figure 9 – Drilling Micropiles with Water Flush

The piles were installed using open end casing with water flush to a depth of 55 feet (17 m) in dense sands. See Figure 9 for a photograph of the drilling process. The full-length reinforcing bar was then lowered into the hole in coupled sections along with a flexible tremie tube. After the casing was pumped full with cement grout, the casing was extracted in sections while pressure grout, averaging 60 psi (414 kPa), was applied to the end of the pipe through the drill head. The pressure grouting was applied for 20 feet (6 m), establishing the bond zone for the pile. The bond zones for the micropiles on this site were founded in fairly clean fine sands with Standard Penetration blow counts that averaged 35.

Figure 10 – Kimberly Clark Load Test Assembly

A sacrificial test pile was tested in compression nearby in the basement to 240 kips (1070 kN). The load test assembly is shown on Figure 10. The pile load test results are shown on Figure 11. The pile successfully held the required test load. However, the slope of the load-deflection curve at the last loading increment became very steep, indicating impending failure.

Analysis of the test results shows an ultimate bond value of 40 psi (274 kPa).

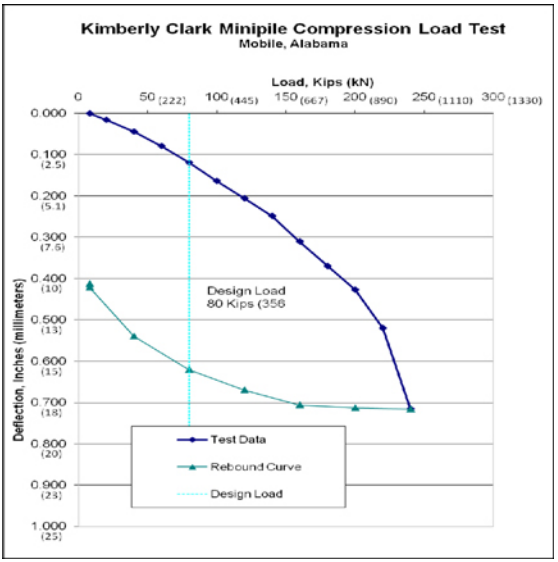

Figure 11 – Pile Test Results, Kimberly Clark

Comparison of the Pile Load Test Results with FHWA Manual: Table 5-2 from the FHWA Micropile Design and Construction Implementation Manual is shown below for Clays and Sands. Values from the load test programs described in this paper are added to the Table for comparison. The test results are identified using the following letters:

I) Jackson Airport, gravity grouted pile, 25 foot (8 m) bond length
II) Jackson Airport, post-grouted pile, 25 foot (8 m) bond length
III) Jackson Airport, post-grouted pile, 30 foot (9 m) bond length
IV) Univ. of Puerto Rico, post-grouted pile, 25 foot (8 m) bond length
V) Kimberly Clark, pressure grouted pile, 20 foot (6 m) bond length

Table 5-2. FHWA Micropile Implementation Manual, 2000

	Typical Range of Grout-to-Ground Bond Nominal Strengths, psi(kPa)			
Soil / Rock Description	Type A	Type B	Type C	Type D
Silt & Clay (some sand) (soft, medium plastic) **[Test Program Results]**	5-10 (35-70)	5-14 (35-95)	7-17 (50-120)	7-21 (50-145) **IV) 16 (110)**
Silt & Clay (some sand) (stiff, dense to very dense) **[Test Program Results]**	7-17 (50-120) **I) 22 (152)**	10-28 (70-190)	14-28 (95-190)	14-28 (95-190) **II) 23 (159)** **III) 25 (172)**
Sand (some silt) (fine, loose-medium dense)	10-21 (70-145)	10-28 (70-190)	14-28 (95-190)	14-35 (95-240)
Sand (some slit, gravel) (fine-course, med.-very dense) **[Test Program Results]**	14-31 (95-215)	17-52 (120-360) **V) 40 (276)**	21-52 (145-360)	21-56 (145-385)

[Bold values refer to the load test programs described in this paper]

Type A- Gravity grout only
Type B- Pressure grouted through the casing during casing withdrawal
Type C- Primary grout placed under gravity head, then one phase of secondary "global" pressure grouting
Type D- Primary grout placed under gravity head, then one or more phases of secondary "global" pressure grouting

CONCLUSIONS:

Post-grouting of a previously tested micropile in stiff clay resulted in an 18 percent increase in the ultimate capacity of a micropile.

The results of micropile load tests in clay indicated that the observed ultimate bond stresses were very close to the values of cohesion reported for the clays.

The results of the test pile programs show that the FHWA Micropile Implementation Manual recommendations for preliminary design match well with real test results from these projects.

ACKNOWLEDGEMENTS:

Peter Nufer at Hayward Baker was the Project Manager for these micropile projects. Shane Truesdell was the Superintendent for the clay projects and Jim Jones was the Superintendent for the sand project.

REFERENCES:

ARMOUR, T. A., GRONECK, P., KEELEY, J., and SHARMA, S., (2000). *Micropile Design and Construction Guidelines Implementation Manual.* Priority Technologies Program Project, Publication Number FHWA-SA-97-070, 356 p.

Davisson, M.T. (1973), "High Capacity Piles" in *Innovations in Foundations Construction,* proceedings of a lecture series, Illinois Section ASCE, Chicago

Littlejohn, G. S., (1970). "Soil Anchors." *Symposium on Ground Engineering, Institution of Civil Engineers*, London.

Wolosick, John R., (2008). "Micropile Design and Construction Considerations in Various Types of Ground." 23rd *Central Pennsylvania Geotechnical Conference*, Hershey, PA, 17 p.

Wolosick, John R., Bonar, Eduardo and Nufer, Peter J., (2007). "Micropile Foundation Repair and Underpinning, Arts and Sciences Museum, University of Puerto Rico, Mayaguez." *International Workshop on Micropiles*, Toronto, Ontario, Canada, 13 p.

Copyrighted Materials
Copyright © 2009 American Society of Civil Engineers (ASCE)
Retrieved from www.knovel.com

Load Transfer Mechanisms of Tip Post-Grouted Drilled Shafts in Sand

Miguel E. Ruiz[1] and Miguel A. Pando[2], M. ASCE

[1]Full Professor, Department of Structures, National University of Cordoba, Cordoba, Argentina, mruiz@efn.uncor.edu
[2]Associate Professor, Department of Civil and Environmental Engineering, University of Puerto Rico, Mayaguez, Puerto Rico, mpando@uprm.edu

ABSTRACT: Post-Grouted Drilled Shafts (PGDS) are a deep foundation system in which grout is injected at high pressure through the tip after the drilled shaft has been installed. Available field load tests show significant load and stiffness improvements of PGDS due to tip pressure grouting. The improved ultimate load capacity and stiffness of PGDS compared to conventional drilled shafts are believed to be related to the pre-stressing effect which the tip post grouting has on the shaft side friction due to the generated upward movement. It also is related to the grout bulb formed at the PGDS tip. This grout bulb pre-compresses the soil beneath the tip as well as any disturbed material generated during construction, and results in an enlarged tip area. This paper investigates the contribution of these factors through a series of T-Z analyses applied to a well-documented, full-scale load testing case history.

INTRODUCTION

The deep foundation industry is continuously being challenged with higher loading demands which often promote development of new deep foundation systems with improved performance, i.e., higher capacities and lower settlements. In this regard, post grouted drilled shafts (PGDS) have emerged, for quite some time, as a competitive deep foundation system which has been reported to have an increased performance compared to conventional drilled shaft foundations installed under similar geotechnical conditions and dimensions (e.g., Bolognesi and Moretto, 1973; Brusey, 2000; and Mullins et al., 2001). This evidence is particularly abundant and strong for test sites with sandy soils.

Despite the existing field evidence, PGDS foundations at present (2008) are not extensively used in North America. In recent years this system has become more popular and has been used considerably in several US states such as FL, TX, NC, among others (King, 2008). However, some impediments which have been argued against a wider use of PGDS include: insufficient case histories of full-scale, well-instrumented load tests on diverse soil conditions and the lack of a well established rational design methodology (although recently an empirical design methodology has been proposed for PGDS in sands by Mullins et al., 2006).

This paper presents research carried out to investigate the load transfer mechanisms involved in PGDS foundations installed in sandy soils. The goal was to assess the main factors contributing to the observed increased performance of PGDS compared to conventional drilled shafts installed under similar conditions. Three factors were identified: 1) The ground improvement of the soil below the tip associated primarily to densification during tip grouting; 2) a stiffer load-deflection response due to side shear stress reversal along the shaft that can be locked-in due to upward movement of the PGDS during tip grouting (applicable only if the final grouting pressure is locked in and no relaxation of the underlying soils is observed); and 3) An equivalent enlarged tip area due to the formation of a grout bulb at the base of the PGDS. The relative contribution of each of these three factors is investigated using T-Z analyses applied to available full-scale load test case histories of PGDS in sands.

PGDS CONSTRUCTION PROCEDURE IN NORTH AMERICA

As background information, this section presents a brief description of the typical procedure used in North America for PGDS construction. This procedure involves first the construction of a conventional drilled shaft. However, the difference in PGDS is that it requires installation of a proprietary grouting system consisting of grout pipes attached to the reinforcement cage and a steel grouting base plate that is fixed to the end of the drilled shaft and is connected to the grouting pipes. This grouting system will be used for tip post-grouting after the concrete has set and the design compressive strength is reached. The second stage of PGDS construction involves tip post-grouting. This stage requires use of the special grout system which allows injecting grout at high pressure under a controlled manner. The grout flows down through the grouting pipes left inside the shaft until it reaches the steel grouting base plate. The grout then goes through the base plate and expands a flexible control membrane that is fixed to the bottom end of the steel base plate. The initial volume of injected grout expands this flexible membrane which has the purpose to aid the formation of a grout bulb under the pile tip and also ensure the initial separation between the grout and the soil below the shaft tip. However, this separation is only for the first stages of grouting since it is common that the membrane breaks or separates from the steel base plate after a certain grout volume has been injected. The injected grout is usually designed to ensure compaction grouting. However, permeation grouting may occur in some instances where the grout is too fluid or the soil is too porous. For this situation usually it is difficult to build up pressure during tip grouting. If this is the case, the problem may be resolved by using two stage grouting, with the second grouting applied after the initial grout stage sets (King, 2008). Most case histories studied in this research were reported to have tip compaction grouting. The tip grouting stage is usually finished when a certain sustained grout pressure and grout volume is reached. The preferred procedure (King, 2008) is to lock-in the grout pressure and let the grout bulb set.

As a result of the tip post-grouting procedure, a grout bulb is formed at the base of the shaft which is believed to improve the ground below the tip and effectively enlarge the tip area. The grouting also induces a small upwards movement of the PGDS which may generate shear stress reversal if the movement is sufficient. Axial load distributions for different stages of a PGDS are shown schematically in FIG. 1.

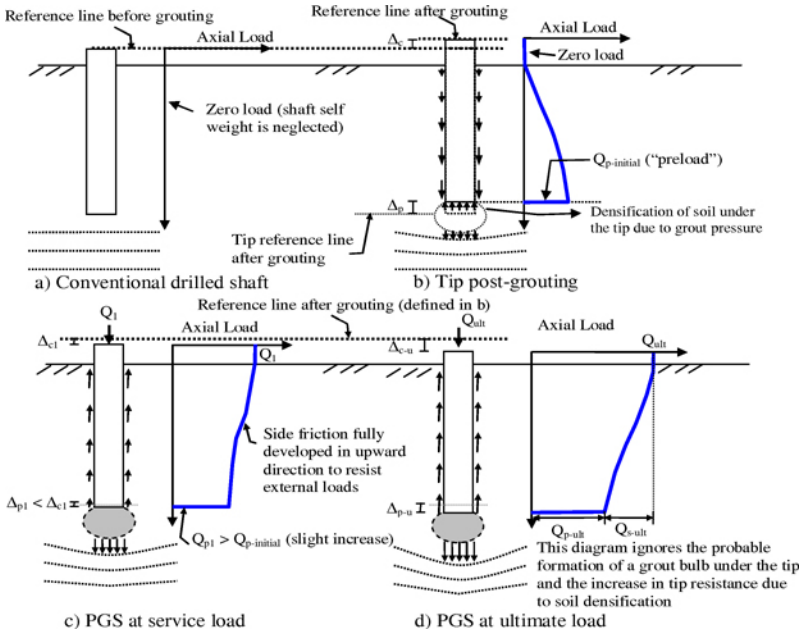

FIG. 1. Transferred axial load for a PGDS at different stages.

FIG. 1(a) shows the condition of a conventional drilled shaft. The axial load distribution after tip post-grouting is shown in FIG. 1(b). For this case the tip post-grouting process has improved the soil below the tip and has lifted the PGDS foundation a certain amount (Δ_c). The resulting axial normal load distribution along the PGDS reflects a reversal of skin friction along the shaft of the PGDS expected if sufficient upward movement occurs and tip-post grouting pressure is locked-in (should not be considered if pressure not locked-in or if the soil beneath the tip shows creep or relaxation). Figure 1(b) also shows an initial mobilization of tip capacity. Figure 1(c) shows a PGDS under service load. For this service loading condition, part of the applied load is used to reverse back the side friction. No additional tip resistance will be mobilized until side shear is reversed back along the full length of the shaft. As discussed later, the shear stress reversal is believed to result in a stiffer load-deflection response for a PGDS, compared to a conventional drilled shaft. In other words, a higher head deflection will be required before further axial load starts to be carried by the tip. Figure 1(d) shows the PGDS under ultimate axial load capacity. For this load condition, the axial load distribution is in essence similar to the conventional drilled shaft case. The higher PGDS ultimate load capacity is related to a higher tip resistance due to ground improvement (i.e., densification and sometime possible improvements due to permeation grouting) and also the application of the tip load over a larger area due to the presence of a grout bulb (this would be equivalent to having some sort of belled drilled shaft). In common practice, the effective tip area enlargement is usually ignored and not included in design. To be

able to include this in practice one would need to have a reliable way to ensure grout bulb formation in a repeatable and predictable way. It should also be noted that the axial load distributions in Figure 1 are only shown up to the elevation of the steel base plate, i.e., the grout bulb effect is only included in terms of ground improvement below the tip. This will be discussed in more detail later in this paper.

LOAD TRANSFER METHODOLOGY

As mentioned before, this paper presents T-Z analyses of full-scale load tests carried out on PGDS foundations installed in sands. The T-Z analyses used the modified hyperbolic T-Z and Q-Z load transfer curves proposed by Pando et al. (2004). These load transfer curves are theoretically derived non-linear load transfer curves defined using as initial reference the maximum or initial shear modulus for very low deformations, (G_0). A detailed description of the load transfer methodology and the expression of load transfer curves used in this paper can be found in Pando et al. (2004) or Ruiz (2005).

CONTRIBUTING FACTORS FOR IMPROVED PERFORMANCE OF PGDS

The actual contributing factors for the observed improvement of tip post-grouting PGDS foundations have not been defined precisely and are still subject to some debate. For this research the following three factors were considered as being responsible for contributing to the observed improved PGDS axial load-deflection performance: (1) Ground improvement (mainly in the form of compression) of the soil under the pile tip, (2) generation of negative (i.e., pointing downwards) residual stresses along the shaft due to the upward movement of the PGDS foundation during grouting, and (3) increase of the pile tip area due to the formation of the grout bulb. These three factors are discussed further in the following paragraphs.

(a) Ground improvement under the PGDS tip (Factor 1)

Tip post-grouting is expected to pre-compress the soil beneath the tip as well as compensate for any disturbance at the bottom due to construction. If the grouting is permeation type, then ground improvement will also result from soil cementation. Based on current North American construction practice, compaction grouting is the only type assumed to occur during tip grouting. To account for this pre-compression effect on the soil under the tip the T-Z analyses used a modified Q_b-Z load transfer curve. The modification was mainly in the form of a stiffer curve obtained by arbitrarily increasing the shear modulus, G of the tip soil.

(b) Stress reversal and residual stresses along the shaft (Factor 2)

During grouting of the pile tip, the PGDS moves upward, thus mobilizing shaft resistance in negative skin friction. This is possible assuming sufficient upward movement and that the grout pressure is locked in (also no creep of relaxation of the soil underlying the tip). This factor was analyzed by assuming that the skin friction development followed the Masing rule (Masing, 1926) with a symmetric backbone curve as shown schematically in FIG. 2.

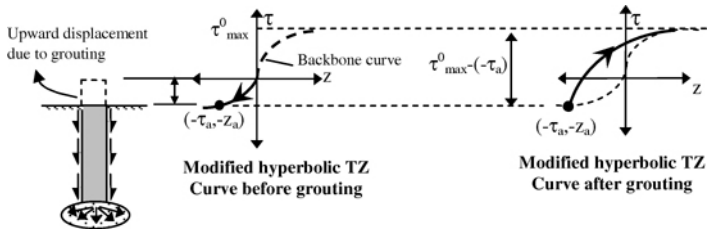

FIG. 2. Effect of stress reversal in the TZ curve of the soil along the shaft.

Incorporating the Masing rule in the T-Z formulation is equivalent to shifting the origin of the T-Z curve to a point with coordinates $(-\tau_a,-Z_a)$, as is shown in FIG. 2.

Since the soil under the pile tip does not experience a load-reversal after grouting, the Q_b-Z curve does not need to be modified by applying the Masing rule. An important point, as illustrated in FIG. 2, is that the resulting TZ-curve will have the same asymptotic value as the original curve but will present a stiffer response since a higher shaft capacity may be developed at smaller displacement. Evidence of a stiffer response of interface shear stresses under reversal cycles was reported by Gomez (2001). Therefore shear stress reversal primarily stiffens the axial load-head deflection response of PGDS. For head deflections below ultimate it does translate into higher load capacities (which are the range expected under service loads). At very high head deflections, ultimate load is reached, and the stiffening effects of shear stress reversal vanish. For modeling purposes, the modified T-Z curves can be defined using field measurements of shaft uplift typically recorded during tip grouting. Using T-Z analysis to model this process and the recorded upward deflections one can estimate the negative side shear stresses mobilized along the shaft.

(c) Increased Tip Area (Factor 3)

Laboratory tests by Mullins et al. (2001) provide evidence of grout bulb formation after pile tip post-grouting. In full scale field tests it has been more difficult to confirm and quantify the extent of grout bulb formation. Assuming a grout bulb is formed, it is reasonable to assume an increased tip load carrying capacity due to the associated increased tip bearing area. This factor of an augmented tip area was modeled by modifying the Q_b-Z load transfer curve by entering an increased radius for the shaft tip in Eq.2. The increase in pile tip radius was estimated using cavity expansion theory and the laboratory data reported by Mullins et al. (2001). Further details of this approach are described by Ruiz (2005).

LOAD TRANSFER ANALYSES OF PGDS FOUNDATIONS IN SAND

Following the methodology described above several case histories were analyzed by Ruiz (2005). However, due to space limitations this paper only presents results of load transfer analyses for a well documented PGDS load test by Mullins et al. (2001).

The case history by Mullins et al. (2001) corresponds to a 0.61 m (2 ft) diameter drilled shaft with a 4.57 m (15 ft) length constructed in the equipment yard of the Coastal Caisson Corporation located in Clearwater, Florida. The general soil conditions at the site consisted of a 1 m thick medium dense sand fill underlain by very loose to loose sand with shell fragments that extended to the final depth investigated of 8 m. An ungrouted drilled shaft (control shaft) was load-tested in the

same site in order to quantify the improvement of shaft capacity after tip grouting. A Flat-Jack grouting apparatus was used to inject a grout volume of 0.107 m3 (3.79 ft3) with a maximum sustained pressure of 462 kPa (67 psi). The maximum measured uplift at the pile tip was 4.83 mm (0.19 in). Practically no relative difference between the head and tip shaft upward displacements was reported by the authors for this relatively short PGDS.

Load transfer analyses were first carried out for the ungrouted drilled shaft (control model). Small initial calibrations were made in order to obtain a good prediction of the load-settlement curve of the control shaft. The shaft head load-settlement curve for the control shaft is shown in Figures 3 through 6, and is labeled as ungrouted baseline. The parameters obtained from the control shaft model were used as baseline values for the T-Z analyses performed for the PGDS. Load-settlement curves for the PGDS were predicted considering the 3 factors mentioned previously.

The contribution of each of the three factors discussed in the previous section was investigated by performing several load transfer analyzes. Systematically, each set of analyses modified only one factor at a time, while keeping the other parameters constant. The first set of analyses consisted of T-Z runs carried out assuming that post grouting only resulted in an increased of shear modulus for the soil under the pile tip (i.e., Factor 1: tip ground improvement). Figure 3 shows the predicted curve using a T-Z analysis with a shear stiffness increase of 100%. As can be seen, this figure shows the predicted curve has good agreement with the PGDS field data primarily in the initial part of the curve. Therefore this factor alone, even considering a large ground improvement of 100% shear modulus improvement, was insufficient to capture the measured ultimate axial load capacity of the PGDS.

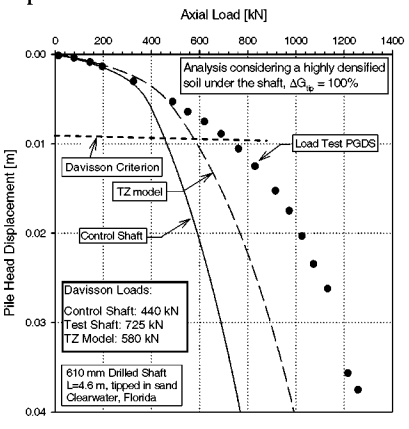

FIG. 3. Analysis assuming ground improvement below the tip (Factor 1).

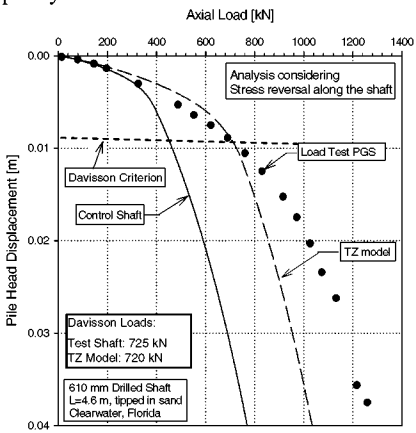

FIG. 4. Analysis assuming shear stress reversal (Factor 2).

The second factor investigated was the development of negative shaft residual stresses due to PGDS uplift during grouting. This factor was modeled using the uplift deflections measured during tip grouting. The results of the T-Z analyses for this second factor are summarized in FIG. 4. This figure shows that the PGDS load settlement curve obtained considering shaft negative residual stresses only has a

reasonable agreement in a small portion of the curve (initial part of the curve), when compared with the measured PGDS load deflection response. Therefore, this factor alone is not sufficient as it under-predicts the PGDS ultimate axial capacity.

The third factor studied was the enlarged tip area due to the formation of a grout bulb at the pile tip. T-Z results for this third factor, assuming a 50% radius increase, are presented in Figure 5. This figure shows a reasonable agreement between the T-Z prediction and the initial portion of the PGDS field curve (up to an axial load of about 550 kN). However this prediction still slightly under-predicts the measured capacity for the PGDS and the portion of the curve for axial loads above 550 kN. Predictions with larger grout bulb radius would probably improve the level of agreement, but it is difficult to reliably ensure that such large sizes of grout bulbs would develop in the field. This is a key factor that requires further research. For this research analyses were limited to grout bulb radii equal to 1.5 times the original shaft radius.

Since none of the three hypothesized factors alone could adequately predict the measured response of the PGDS, additional analyses were performed assuming some sort of combination of all three factors actually occurs. T-Z analysis that assumed that different proportions of the three factors are present resulted in improved PGDS load-settlement predictions. The best prediction, for this case history, was obtained by combining stress reversal (Factor 2) and an augmented tip area due to the formation of a grout bulb (Factor 3). This best prediction is shown in Figure 6. For this particular prediction, the enlarged tip radius of the PGDS was assumed to be 1.35 times that of the ungrouted drilled shaft and no ground improvement in the form of an increased soil shear modulus was considered. Even this best prediction slightly over predicts the portion of the curve between axial loads of 200 and 900 kN.

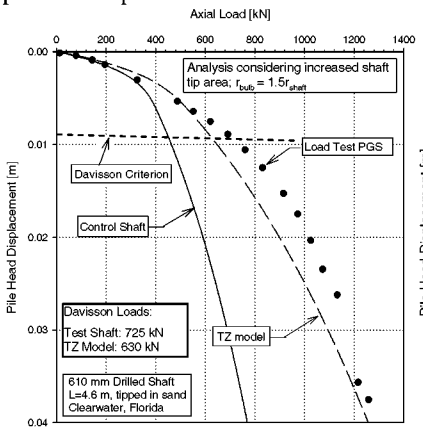

FIG. 5. Analysis assuming an increased shaft tip diameter (Factor 3).

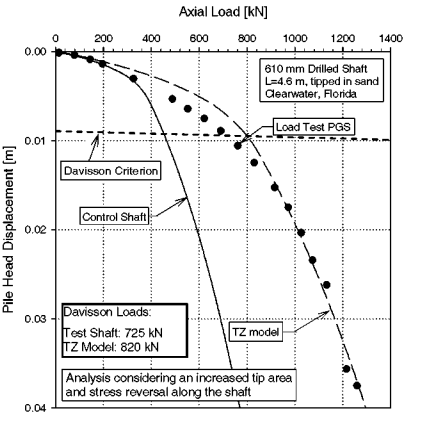

FIG. 6. Best fit of the measured load-settlement curve of the PGDS.

CONCLUSIONS

The load settlement behavior for a case history involving a PGDS was analyzed using the load transfer method. The load transfer method was based on theoretically derived load transfer curves that incorporate the low strain initial shear stiffness of the soil,

and the soil nonlinearity through the use of a modified hyperbola.

The load transfer method was applied systematically to a case history to study the influence of three different factors that are believed to be the main contributing factors for the observed improved axial capacity and stiffness of PGDS compared to conventional drilled shafts installed under similar soil conditions and dimensions. These three main factors are: (a) Ground improvement of the soil under the pile tip (mainly compression was assumed), (b) Shear stress reversal along the shaft due to uplift movement due to tip grouting, and (c) An augmented tip area due to the formation of a grout bulb. T-Z Analyses showed that incorporating any of these three factors individually or alone is not sufficient to predict the PGDS load deflection response measured in the field. On the other hand, a very good agreement was found when all three factors were included in the T-Z analyses suggesting a certain degree of the different three factors must be occurring. For the case history presented the best, the best match was obtained by combining the shear stress reversal along the shaft (Factor 2) and an increased pile tip area (Factor 3).

Although only one case history was presented in this paper, other case histories analyzed by Ruiz (2005) confirm the findings presented in this paper. Nevertheless, more well-documented case histories are needed to understand better the mechanics of PGDS foundations and help shed more light on this issue.

ACKNOWLEDGEMENTS

This research was partially funded through a graduate research assistantship for the first author by the Dept. of Civil Engineering of the University of Puerto Rico at Mayaguez and a research grant from the Beck Foundation Company. The authors gratefully acknowledge and thank this financial assistance.

REFERENCES

Bolognesi, A. J. L. and Moretto, O., 1973. "Stage Grouting Preloading of Large Piles on Sand." *Proceedings of the 8th ICSMFE, Moscow*. pp. 19-25.

Brusey, W. G.. 2000. "Post-Grouted Test Shafts at JFK International Airport." *New Technological & Design Developments in Deep Foundations* (GSP 100), ASCE, Reston/VA, CD-Rom.

Gomez, J. E., 2001. "Development of an Extended Hyperbolic Model for Concrete-to-soil Interfaces." Ph.D. Thesis, Virginia Tech, 429p.

King, P. (2008). Personal communication. Synchropile, Inc., San Antonio, TX.

Masing, G., 1926. "Eigenspannungen und Verfurigung beim Messing." *Proceedings of the 2nd International Congress on Applied Mechanics*, Zurich.

Mullins, G., Dapp, S., Frederick, E., and Wagner, R. (2001). "Post grouting Drilled Shafts Tips – Phase I." *Research Report*, Florida DoT, 306 p.

Mullins, G., Winters, D., and Dapps, S. (2006). "Predicting End Bearing Capacity of Post-Grouted Drilled Shaft in Cohesionless Soils." *J. Geotechnical and Geoenvir. Engrg.*, Vol. 132(4): 478-487.

Pando, M. A., Fernandez, A., and Filz, G., 2004. "Pile Settlement Predictions Using Theoretical Load Transfer Curves and Seismic CPT Data." *Proc. of the ISC-2 Symp. on Geotechnical & Geophysical Site Characterization,* Vol. II: 1525-1531.

Ruiz, M. E., (2005). "Study of axially loaded post grouted drilled shafts using CPT based load transfer curves." MS Thesis, Civil Engrg., U. of Puerto Rico, 284 p.

Copyrighted Materials
Copyright © 2009 American Society of Civil Engineers (ASCE)
Retrieved from www.knovel.com

Post Grouted Drilled Shafts – A Comprehensive Case History from Texas

Phil King[1], M. ASCE, P.E., Americo Fernandez[1] and Miguel A. Pando[2], M. ASCE

[1]SynchroPile, Inc., San Antonio, TX 78213; phil.king@synchropile.com
[2]Department of Civil Engineering, University of Puerto Rico, Mayaguez, PR 00681

ABSTRACT: Post-Grouted Drilled Shafts (PGDS) are a deep proprietary foundation system in which grout is injected at high pressure through the tip after the drilled shaft has been installed. The improved ultimate load capacity and stiffness of PGDS compared to conventional drilled shafts are believed to be related to the pre-stressing effect which the tip post grouting has on the shaft side friction due to the generated upward movement, and the grout bulb formed at the PGDS tip which results in an enlarged tip area and also pre-compresses the soil beneath the tip as well as any disturbed material generated during construction. This paper presents results of a comprehensive full-scale load test program at the clay and sand sites of the well characterized Texas A&M NGES. The test program involved conventional static load tests as well as O-cell tests on PGDS foundations and conventional drilled shafts installed and tested under similar conditions.

INTRODUCTION

Post grouted drilled shafts (PGDS) are modified drilled shafts that use proprietary post construction controlled tip grouting to increase the axial bearing capacity of the drilled shaft. This technique has been reported as successful for quite some time (e.g., Mullins et al., 2001). Several grouting options have been proposed and tried elsewhere and in the past. In North America current PGDS construction involves a post-grouting process that uses several embodiments of injection systems that allows injection of grout below the drilled shaft tip in a controlled manner. This grouting process increases axial load capacity and stiffness of the PGDS compared to a conventional drilled shaft installed under similar conditions. In the U.S., PGDS has been used in several states including: Florida, Texas, South Carolina, Minnesota, Arkansas, among others. PGDS design is based on empirical methods. For example, Mullins et al. (2006) recently proposed an empirical methodology for PGDS installed in sands that is based on several existing Statnamic load tests carried out on PGDS foundations. Today, despite these advances in the grouting system and design procedures there still is a need for additional well-documented case histories and research. The case history presented in this paper hopes to contribute in this regard. First it presents a full scale static load test which is rare due to the high axial loads

required to test these foundations. As mentioned before, to date most reported case histories involved equivalent static load test results derived from Statnamic testing. Although this is commonly done in practice some level of uncertainty may still remain when the dynamic effects due to damping have to be removed. This paper also contributes through the dissemination of results of full scale static load tests carried out at well characterized geotechnical experimental sites of sand and clay.

LOAD TEST PROGRAM AT THE TEXAS A&M NGES

A comprehensive load test program involving PGDS and conventional drilled shafts of similar dimensions and installation conditions was recently carried out at the Sand and Clay sites of the National Geotechnical Experimental Sites (NGES) at Texas A&M. These sites were chosen because their geotechnical conditions are well characterized (e.g., Briaud, 2000). The main events or components of this comprehensive load test program are summarized in Table 1.

Table 1. Main components of PGDS test program at Texas A&M NGES.

Event	Date	Comment
Installation of test shafts in Clay site	11/15/06	3 test shafts: conventional drilled shaft, PGDS, and PGDS with O-Cell (all instrumented)
Installation of test shafts in Sand site	11/17/06	3 test shafts: conventional drilled shaft, PGDS, and PGDS with O-Cell (all instrumented)
First O-cell testing at Sand site	11/27/06	PGDS with O-Cell prior to tip post grouting
First O-cell testing at Clay site	11/29/06	PGDS with O-Cell prior to tip post grouting
Tip post-grouting at Sand site	11/27/06 11/28/06	PGDS with O-Cell PGDS without O-Cell
Tip post-grouting at Clay site	11/29/06 11/29/06	PGDS with O-Cell PGDS without O-Cell
Second O-cell testing at Sand site	11/27/06	PGDS with O-Cell after tip post grouting
Second O-cell testing at Clay site	11/29/06	PGDS with O-Cell after to tip post grouting
Static Load Tests at Clay site (conventional top load test)	12/12/06	Conventional drilled shaft
	12/12/06	PGDS without O-Cell
	12/13/06	PGDS with O-Cell
Static Load Tests at Sand site (conventional top load test)	12/12/06	Conventional drilled shaft
	12/12/06	PGDS without O-Cell
	12/13/06	PGDS with O-Cell

GEOTECHNICAL CONDITIONS

A generalized geotechnical stratigraphy for both test sites is presented in Figure 1. As shown in Fig 1(a), the sand site consists of a deposit of medium dense silty sand

that extends to a depth of about 12.5 m and is underlain by a hard clay shale. Similarly, the clay site, shown in Fig. 1(b), consists of very stiff, high plastic clay that extends to about 12.5 m depth and is underlain by a hard clay shale.

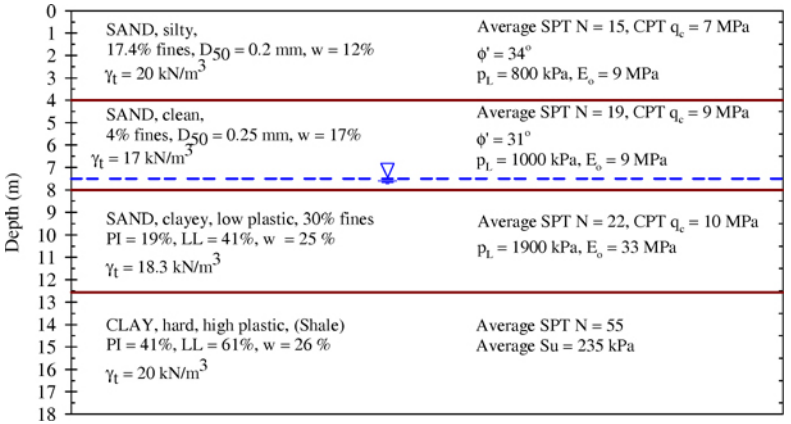

a) Generalized stratigraphy at Texas A&M NGES Sand site

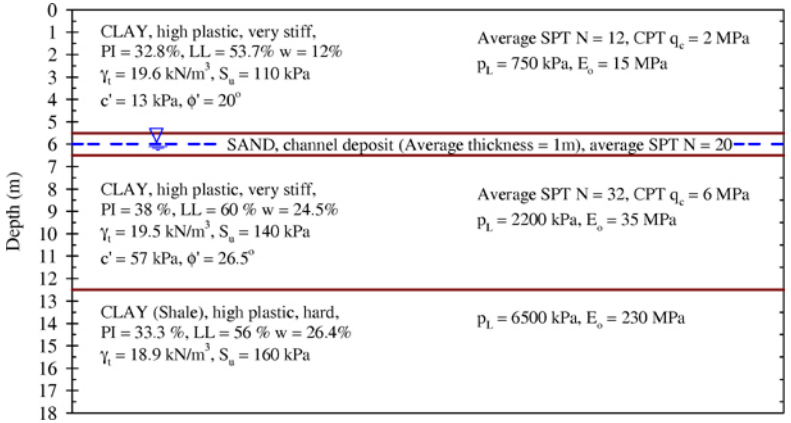

b) Generalized stratigraphy at Texas A&M NGES Clay site

FIG. 1. Generalized soil conditions at the test sites (data from Briaud, 2000).

TEST PILE INFORMATION

At each test site, i.e. the sand and clay sites, three test shafts were installed for a total of six test shafts. Each test site included a conventional drilled shaft as a reference, a PGDS, and a PGDS with an O-Cell device installed near the tip of the foundation. The three types of test shafts are shown schematically in Figure 2. As shown, all test shafts had a 0.76 m (30 in) nominal diameter and an embedded shaft length of about 10 m (33 ft). All test shafts had three levels of sisterbar strain gages

installed in pairs except at the tip level where three sisterbars were installed for redundancy. The PGDS/O-Cell hybrid shaft had to use a special O-Cell configuration to allow passage of the grouting pipes. The design concrete strength for all test shafts was 27.58 MPa (4000 psi).

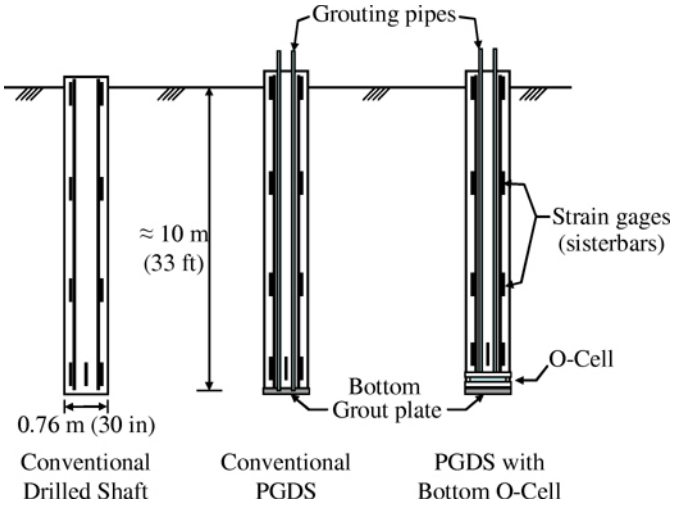

FIG. 2. Types of test shafts.

The grouting of the PGDS foundations was carried out until one of the following conditions occurred: the design grout pressure was reached, or a maximum head deflection of 12 mm (0.5 inches) was reached. At the sand site, the maximum grout pressure achieved, for the two PGDS foundations, was about 2 MPa (300 psi). The measured upward head movements of the PGDS foundations were 4.6 mm (0.18 inches) and 15.5 mm (0.61 inches) for the PGDS with O-Cell and without O-Cell, respectively. For the PGDS at the clay site, the grouting pressures could not be built to as high levels reaching pressures values of only about 0.4 MPa (55 psi). The corresponding upward movement of the PGDS heads at the clay site was 4 mm (0.16 inches) for the one with O-Cell and 7.6 mm (0.3 inches) for the one without an O-Cell. For this load testing program all PGDS installations had the tip grout pressure locked-in at the end of the tip grouting process.

LOAD TEST RESULTS AT THE SAND SITE

At the sand site a conventional static load test was carried out on the reference conventional drilled shaft first. This test was carried out using a 13.34 MN (1500 Ton) reaction beam and in general followed the quick load test procedure described in ASTM Standard D1143 (ASTM, 2007). This reference or baseline load test is shown in Figure 3. As shown in this figure, the maximum load applied was approximately 2937 kN (660 kips) for a pile head displacement of about 100 mm (4 inches). A conventional PGDS foundation was also tested at the sand site using the same testing

procedure and setup. The results for PGDS load test are also shown in Figure 3. For the PGDS foundation the maximum load applied was about 4116 kN (925 kips) which corresponded to a pile head deflection of about 122 mm (4.8 inches). Thus, the PGDS had a total axial load capacity (i.e., including shaft and tip contributions) about 40 % higher than the conventional drilled shaft.

Figure 3 also highlights the much stiffer initial response of the PGDS load deflection curve compared to the conventional drilled shaft curve. For example, by comparing the axial loads at an arbitrary head deflection of 25 mm (1 inch) we observe axial loads for the conventional drilled shaft and the PGDS of 2090 kN (470 kips) and 3380 kN (760 kips), respectively. This shows that the PGDS installed at the sand site, would require an axial load about 62 % higher than the conventional drilled shaft to reach this predefined 25 mm (1 inch) pile head deflection.

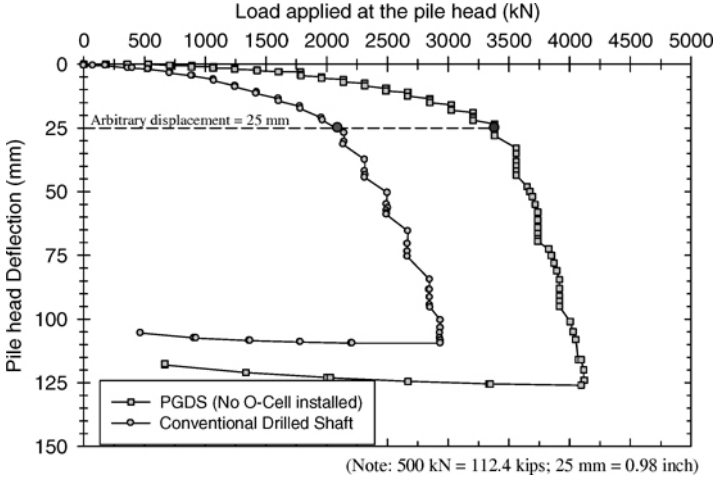

FIG. 3. Comparison of conventional load test results at the Sand site.

In addition to these conventional load tests, two O-cell tests were also carried out on the PGDS/O-Cell hybrid foundation installed at the sand site. An initial O-Cell test was carried out prior to tip post-grouting attempting to calibrate soil moduli and the other test was carried after tip post-grouting to assess any attained soil improvement. The applied tip load versus tip deflection (i.e., at the bottom of O-cell displacement) obtained from the O-cell test prior to tip post-grouting is presented in Figure 4. This figure shows that the axial capacity of the tip, prior to tip grouting, is about 2625 kN (590 kips) and requires a tip displacement of about 75 mm (3 inches) to mobilize this capacity. This displacement is about 10% of the tip diameter. O-Cell results for the PGDS after tip post-grouting are being processed and are not currently available. According to Figure 3, the conventional drilled shaft, installed at the sand site, had an axial load capacity of 2937 kN (660 kips). Assuming the tip resistance results of Figure 4 apply to the conventional drilled shaft we can estimate an ultimate skin friction capacity for this deep foundation of almost 450 kN (100 kips). Assuming the tip post grouting process applied to the PGDS foundation has little effect on the

ultimate skin friction capacity one can estimate the ultimate tip capacity of the PGDS foundation. A summary of the axial load capacities for both the conventional drilled shaft and post grouted drilled shaft at the sand site is provided in Table 2.

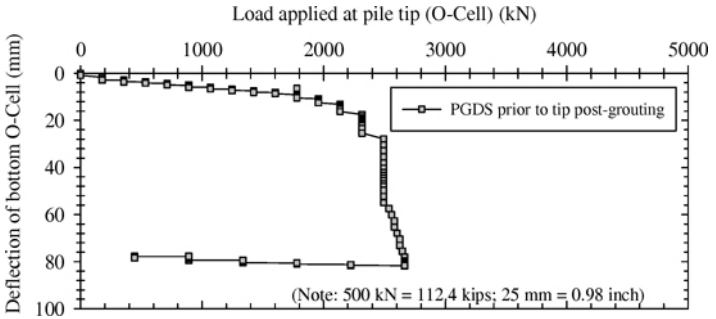

FIG. 4. Tip load resistance measured at the Sand site prior to tip post-grouting.

Table 2. Summary of ultimate capacities from load tests at the sand site.

Load capacity	Conventional	PGDS	% Increase
Ultimate axial	2937 kN	4116 kN	40.1 %
Ultimate tip	2625 kN	3666 kN[2]	39.7 %
Ultimate skin friction	450 kN[1]	450 kN[2]	0 %
At 25 mm head displacement	2090 kN	3380 kN	61.7 %

Notes: ([1]): Estimated from O-Cell results in Fig. 4 (tip resistance)
([2]): Estimated from O-Cell results and assuming no skin friction capacity improvement.

LOAD TEST RESULTS AT THE CLAY SITE

A similar test program was carried out at the clay site of the NGES of Texas A&M. The results of the conventional load tests, also carried out in general accordance with the quick load procedure of ASTM D1143, for the conventional drilled shaft and the PGDS foundation are shown in Figure 5. For the clay site the axial capacity and axial stiffness improvements were not as significant as for the sand site. However, as pointed out before, the tip post-grouting at the clay site did not reach as high grouting pressures as in the sand site since it only reached pressures of about 0.4 MPa (55 psi).

The load-deflection curves of Figure 5 show that the ultimate axial load capacities for the PGDS and the conventional drilled shaft are about 2323 kN (522 kips) and 2033 kN (457 kips), respectively. This represents an axial load capacity increase of about 14.3 % for the PGDS with respect to the conventional drilled shaft at the clay site where both shafts were installed under similar conditions. Similarly, from Figure 5 we can compare the axial loads required to produce a 25 mm (1 inch) head deflection for each foundation type. This head deflection level was reached at the PGDS and conventional drilled shaft at axial loads of 2217 kN (498 kips) and 1928 kN (433 kips), respectively. This shows that an axial load about 15 % higher would be required for the PGDS compared to the conventional drilled shaft to impose a 25 mm head deflection.

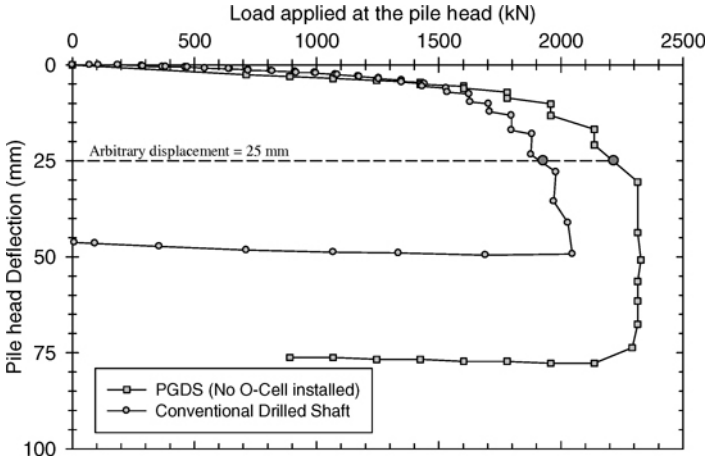

FIG. 5. Comparison of conventional load test results at the Clay site.

O-cell tests were also carried out at the clay site for one of the PGDS foundations. The applied tip load versus tip deflection obtained from the O-cell test prior to tip post-grouting is presented in Figure 6. This figure shows that the tip axial capacity prior to tip grouting is about 992 kN (223 kips) and requires a tip displacement of about 50 mm (2 inches) to be mobilized. This displacement is about 7% of the tip diameter.

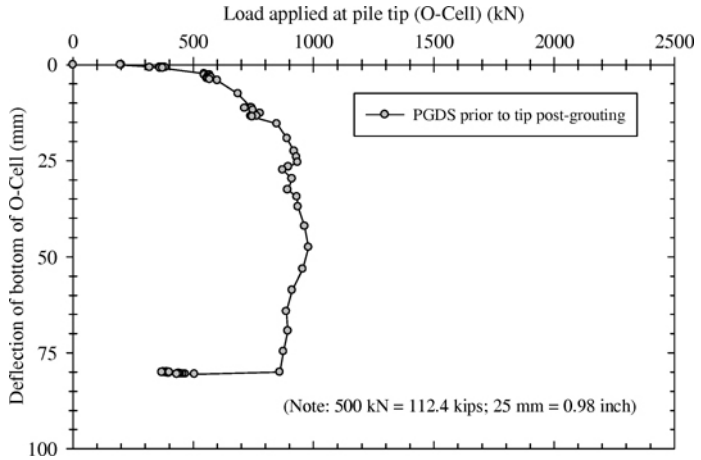

FIG. 6. Tip load resistance measured at the Clay site prior to tip post-grouting.

Axial load capacities, based on the conventional load tests and O-cell test at the clay site, are presented in Table 3 for both the conventional drilled shaft and the PGDS.

Table 3. Summary of ultimate capacities from load tests at the clay site.

Load capacity	Conventional	PGDS	% Increase
Ultimate axial	2033 kN	2323 kN	14.3 %
Ultimate tip	992 kN	1282 kN[2]	29.2 %
Ultimate skin friction	1041 kN[1]	1041 kN[2]	0 %
At 25 mm head displacement	1928 kN	2217 kN	15 %

Notes: ([1]): Estimated from O-Cell results in Fig. 6 (tip resistance)
([2]): Estimated from O-Cell results and assuming no skin friction capacity improvement.

SUMMARY AND CONCLUSIONS

This paper describes and presents results of a comprehensive full-scale load test program of PGDS foundations installed at the clay and sand sites of the well characterized Texas A&M NGES. The test program involved conventional static load tests as well as O-cell tests on PGDS foundations and conventional drilled shafts installed and tested under similar conditions. All foundations had a 10 m embedment and 0.76 m diameter. A very large reaction beam of 13.34 MN had to be used for the static load tests. This is believed to be the first full scale PGDS case history in North America that uses static load tests instead of equivalent static load tests derived from Statnamic testing. The O-Cell tests were also a valuable addition to the test program.

The test results at the sand site showed the PGDS had improved stiffness and about a 40% improvement in terms of axial compressive load capacity compared to the conventional drilled shaft installed under similar conditions. At the clay site the PGDS had about 14 % axial load capacity improvement with respect to the conventional drilled shaft. The less pronounced improvement at the clay site is believed to be related to the lower tip post-grouting pressures obtained at this site.

ACKNOWLEDGMENTS

The authors would like to thank Dr. J.-L. Briaud of Texas A&M for facilitating use of the NGES experimental sites as well as access to testing devices, and information. The authors also acknowledge the contributions of AH Beck Foundation Company Inc., LOADTEST, and AFT, Inc.

REFERENCES

ASTM (2007), "ASTM Standard D 1143: Standard test methods for deep foundations under static axial compressive load", ASTM International, Vol. 04.08, 15 p.

Briaud, J.-L. (2000). "The national geotechnical experimentation sites at Texas A&M University: clay and sand." *National Geotechnical Experimentation Sites* (GSP 93), ASCE, Reston/VA: 26-51.

Mullins, G., Dapp, S., Frederick, E., and Wagner, V. (2001). "Post grouting Drilled Shafts Tips – Phase I." *Research Report*, Florida DoT, 306 p.

Mullins, G., Winters, D., and Dapps, S. (2006). "Predicting end bearing capacity of post-grouted drilled shafts in cohesionless soils", *J. Geotechnical and Geoenvir. Engrg.*, Vol. 132(4): 478-487.

Copyrighted Materials
Copyright © 2009 American Society of Civil Engineers (ASCE)
Retrieved from www.knovel.com

LARGE-SCALE LABORATORY STUDY ON THE INNOVATIVE USE OF COMPACTION GROUT FOR DRILLED SHAFT TIP POST GROUTING

Jeyasuthan Pooranampillai[1], Sherif Elfass[2], P.E., M.ASCE, Walt Vanderpool[3], P.E., M.ASCE, Gary Norris[4], P.E., M.ASCE.

[1]Graduate Research Assistant, Department of Civil & Environmental Engineering, University of Nevada, Reno, 1664, N Virginia St, MS 258, Reno, NV 89557, dhiv_2002@yahoo.com.
[2]Research Assistant Professor, Department of Civil and Environmental Engineering, University of Nevada, Reno, 1664, N Virginia St, MS 258, Reno, NV 89557, elfass@unr.edu
[3]Senior Engineer, Terracon Consultants, Inc., 750 Pilot Road, Suite F, Las Vegas, NV, 89119, wevanderpool@terracon.com
[4]Professor of Civil Engineering, Department of Civil and Environmental Engineering, University of Nevada, Reno, 1664, N Virginia St, MS 258, Reno, NV 89557, norris@unr.edu

ABSTRACT

This paper presents the results of a comparative analysis carried out on the behavior of two 32.4 cm (12.75 inch) diameter model shafts load tested at the Large Structures Laboratory of the University of Nevada, Reno. While one of these shafts was grouted with a low mobility compaction grout at its tip prior to vertical loading, the other was not. Both model shafts were tested within a soil tank containing the same non-cohesive soil prepared to a similar target relative density. Evaluation of the load – displacement response of both shafts undergoing similar load-unload-reload cycles showed the tip capacity at a top displacement of 5% of the shaft diameter for the grouted shaft to be eight times that of the ungrouted shaft. This increased end bearing was found to be due to two reasons: 1) The effect of preloading of the soil caused by the grout induced tip pressures that effectively eliminate a great deal of plastic deformation of the supporting soil mass (as in strain hardening of steel); and 2) The increased tip bearing area, caused by the compaction post grout that, because of its very viscous but unconfined nature, forms an intact mass or bulb that is larger than the shaft area.

INTRODUCTION

Deep foundations such as cast-in-drilled-hole (CIDH) concrete shafts generally show stiffer load-displacement response during reloading than they do under virgin loading. This aspect of shaft response is more noticeable in the tip given the

prevalence of slough left during the drilling operation. Indeed, the necessity for excessive displacement of the shaft tip to mobilize design level base resistance is the major reason many engineers choose to completely disregard tip capacity in design. On the other hand, it is accepted that post grouting of the shaft tip subsequent to hardening of the shaft concrete could be likened to preloading of the soil at the shaft tip against the negative skin friction and self weight of the shaft. Thereafter, as the grout hardens the stresses within the tip and skin will mutually relax or remain locked in (dependent on soil creep and time dependent soil deformation). Subsequently, the axial load applied on the shaft, due to the superstructure, could be likened to reloading of the shaft. This would result in a stiffer load-displacement response. This process would negate the initial "soft" response of the ungrouted shaft tip under virgin loading, therefore allowing engineers to incorporate higher tip capacities into their designs resulting either in shorter and/or smaller diameter shafts or fewer numbers of shafts.

Commonly, post grouting of a CIDH shaft tip involves using a suitable grout delivery system at the tip to allow controlled injection of fluid or permeation grout in an initially confined area or cavity. If, on the other hand, a low mobility compaction grout was utilized, it would be possible to avoid the flow of a more fluid grout into the surrounding soil mass once confinement is broken and instead allow possible build up of a viscous bulb below the shaft tip that might exceed the shaft diameter. Low mobility compaction grout is defined as grout having a slump in the region of 1 inch and whose aggregate gradation falls within the envelope for particle distribution shown in the diagram below (Figure 1).

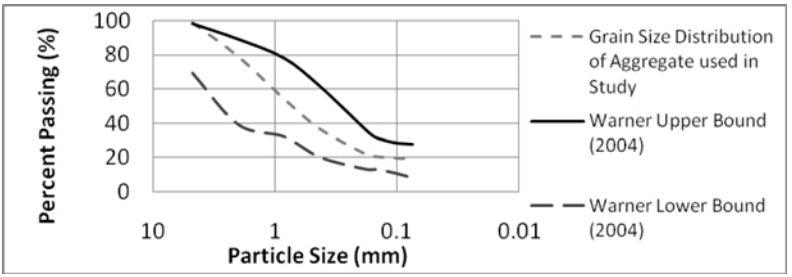

FIG. 1. Aggregate grain size distribution.

Compaction grout, when pumped through the shaft tip, would compact the soil within the tip vicinity, thereby increasing the soil density by taking out a substantial amount of plastic deformation. The pressure with which the grout is pumped will on one hand displace the soil and conversely push the shaft upwards. This upward force on the shaft caused by the grout pressure will be resisted by the shaft self-weight and the negative skin friction from the surrounding soil. Therefore the maximum grouting

pressure attainable is limited to the sum of the shaft self-weight and the negative skin friction that can be mobilized by the soil surrounding the shaft.

Providing a bell at the tip of bored shafts by using an under-reaming cutting tool is an effective technique to increase the tip bearing area and thus the tip capacity of these shafts. If a bulb of grout forms at the tip of a CIDH shaft, with its area greater than that of the shaft, it would increase the tip capacity solely by virtue of its increased bearing area. It becomes evident, therefore, that there exists another potential advantage in the unconfined compaction grout system in that it would allow the grout bulb to form by expanding in all directions. This would result in not only a downward displacement of soil but also a radial displacement from the shaft longitudinal axis. This could potentially be accomplished by strategic placement of grouting tubes within the shaft, and a planned sequence of grouting steps. When the bulb's radial area becomes greater than the base of the shaft, it would result in an increased tip capacity as in the case of the under-reamed/belled shaft leading to possible increased overall capacity. Based on volume measurements it becomes possible to estimate the size of the grout bulb that has formed at the shaft tip. Dependent on the area of the grout bulb in the direction orthogonal to the shaft's longitudinal axis (assuming that the grout pressures cause the bulb to form fairly uniformly), estimates can be developed for the tip capacity. Conversely, there are issues regarding quality control in an unconfined post grouting operation. A confined system allows the grouter to control the volume pumped so as not to cause fracture within the soil at the tip until confinement fails. In a poorly conducted unconfined compaction grouting operation, fracture might occur (e.g. at the interface of differing soil layers), and would be noted by the substantial amount of grout being pumped into the tip without any significant increase in pressure within the grout. In addition, unless the grouting contractor is experienced and employs grout that meets specifications, grout may not be successfully pumped past the tip as described by Vanderpool et al. (2008).

METHODOLOGY

General

Tests at the Large Structures Laboratory were carried out to ascertain the benefits of compaction post grouting. These tests were carried out within a steel tank 244 cm (96 in.) in diameter and 274 cm (108 in.) high. Figure 2 shows a sectional view of the test tank. The model shaft used for these tests is a steel circular steel section 32.4 cm (12.75 in.) outer diameter and 12.7 mm (0.5 in.) thick. The size of the tank is based on predictive equations developed by Yang (2006) for a plastic zone surrounding the shaft tip in different soils (sands, silts) of differing relative densities. As a means of simulating the overburden pressure commonly encountered at the shaft tip, a steel

plate reinforced with steel beams is placed on top of the sand and post tensioned on to the sand through four dywidag rods that run through the height of the sand sample and are anchored to the bottom of the prestressed slab on which the tank rests. This overburden platen is post-tensioned onto the sand using four rams centrally controlled. The rams are set to provide a uniform, constant pressure on the sand. Should sand within the tank be displaced in any manner due to compaction grouting and/or shaft displacement, this plate will move in an upward or downward manner to permit soil displacement at constant confining pressure within the tank. A load frame, with attached large capacity hydraulic ram is used to push the shaft downward.

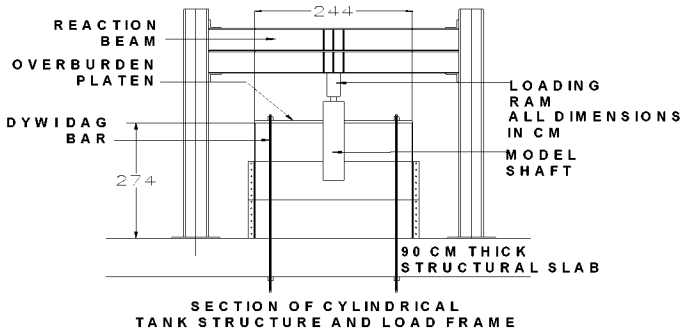

FIG. 2. Sectioned view of test tank and loading frame.

The model shaft used in these tests has a starter void known as a post grout tip module (UNR tip module), to enhance formation of the grout bulb as described by Pooranampillai et al. (2008). The tank was filled with sub-angular fine sand (SP) having a D_{50} of 0.24 mm and C_u of 1.64 with minimum and maximum dry densities of 1355 kg/m^3 (84.5 lb/ft^3) and 1600 kg/m^3 (99.7 lb/ft^3) respectively.

Sample Preparation

The soil within the tank is prepared to a target relative density designated for each test. For the tests under discussion in this paper the target relative density was 50%. Sample preparation occurs in one foot segments. To attain the target relative density, a specially designed vibrating grid is used (see Figure 3). This vibrating grid is made up of 4.83 cm (1.9 in.) outer diameter steel pipes of 30 cm length, placed at approximately 30 cm spacing. These pipes are connected together by welded steel reinforcement. Four turbine vibrators (air powered) are placed on the steel grid. The vibrators are connected to a centralized air supply, and can be operated simultaneously. Once the apparatus is lowered into the tank, and rests on the previously placed lift, sand is poured through the grid using super sack bags. Subsequently the sand is leveled.

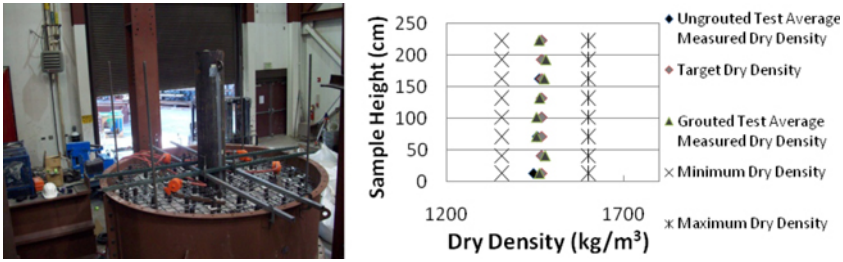

FIG. 3. Densification apparatus with model shaft within tank and sand density data for both ungrouted and grouted tests.

The vibrating grid is operated for 20 seconds to obtain 50% relative density (or 1467.6 kg/m^3 dry unit weight) for the sand employed. This operation time can be adjusted to attain different relative densities. Subsequent to vibration the apparatus is taken out, and the density of the soil within the tank measured using a nuclear density gage. This same process is repeated for the subsequent layers. Upon filling of the tank with soil to an elevation of 137 cm (54 in.) from its base the model shaft is placed in the tank and vertically aligned (Figure 3). The tank is then filled with soil, to an elevation of 244 cm (96 in.) above the base. Once filling is complete the overburden plate is placed on top of the soil, and post tensioned. Subsequently the load frame is assembled.

The Grouting Operation

Though specialized pumps are available for compaction grouting purposes, due to their associated costs and the need to pump only small volumes of grout per lab test (0.085 – 0.113 m^3 of grout per test in the lab as compared to more than 3 m^3 per shaft in the field) the researchers designed and fabricated a specialized unit.

The aggregate used in the grout mix for this test is as shown in Figure 1. The aggregate was mixed with water to obtain a saturated and surface dry condition and left overnight in this state. Mixing was carried out in a traditional concrete mixer and slump checked at regular intervals. At a slump of 14 cm (5 ½ in.) pumping was commenced. As the grout was pumped through the lines, the slump was again measured at its entry point into the shaft. At this location the grout was found to have reduced to 3.8 cm (1 ½ in.) and therefore deemed to be "compaction grout" as per definition. This reduction in slump is due to the absorption of water into the aggregate during pumping. The grouting was carried out using five strokes of the pump. This involved pumping in a total of approximately 0.0816 m^3 (2.88 cu ft) just past the tip. In between each stroke, while recharge was taking place, a gate valve located at the grout entry point into the shaft was closed so as not to allow pressure in the grout to dissipate. Grouting was terminated when it was observed that there was

no appreciable increase in the pressures induced at the tip with successive pumping cycles. A total earth pressure cell was placed at the tip of the model shaft to measure pressures induced on the shaft tip during the compaction grouting operation and during subsequent loading. While tip grouting was in progress, the hydraulic ram positioned for use during the load testing phase was used to provide resistance to the upward movement to the shaft. The ram was set to provide ever increasing downward force on the shaft, together with zero shaft displacement as grout pressures developed at the tip.

Load Testing

Load testing of both the grouted and ungrouted model shafts was carried out in the same manner with load testing of the grouted shaft done 3 days after grouting. The load was increased until shaft top displacement reached 1.62 cm (0.6375 inch), which is equivalent to 5% of the shaft diameter. Thereafter, the shaft was unloaded, and subsequently reloaded. Unloading and reloading was carried out to top displacements of 5.08 cm (2 in.), 10.16 cm (4 in.), 15.24 cm (6 in.) and 25.4 cm (10 in.).

RESULTS AND DISCUSSION

Figure 4 shows how the grout pressure at the tip of the shaft increased with the progression in pumping cycles/strokes. Subsequent to the completion of each cycle of pumping the dissipation in grout pressure with time was observed. This occurred in spite of the grout lines being closed after completion of the pumping cycle. This indicated that there will be relaxation of grout induced tip loads in this system. In addition, it must be noted that the residual pressures to which the tip pressures dropped increased with each successive cycle of pumping until a value of 145 kPa (21 psi) resulted subsequent to the final stroke. The flow rates were 0.049, 0.005, 0.001, 0.017 and 0.001 in m^3/min for pumping cycles 1 – 5 respectively.

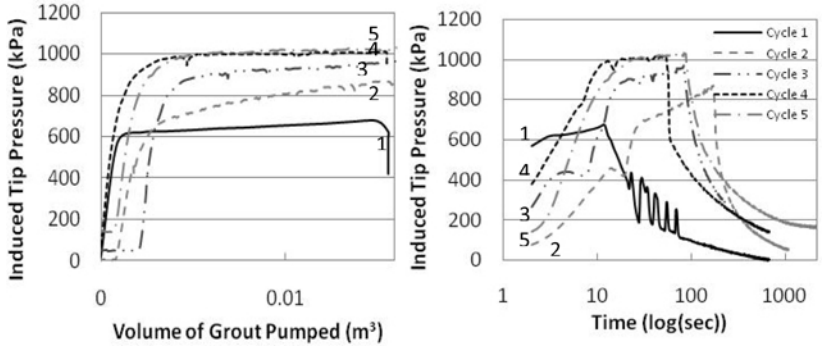

FIG. 4. Measurements during the tip compaction grouting phase.

Load – displacement behavior observed during the two tests are given in Figure 5. The shaft tip loads were calculated by assuming that the tip pressure measured in the total earth pressure cell at the shaft base acts uniformly over the base area of the shaft. If shaft top displacement equal to 5% of shaft diameter is considered as a criterion for shaft capacity, the ungrouted shaft gives a total resistance of 120.4 kN (27 kips) and a base resistance of 31.2 kN (7 kips). By contrast, the grouted shaft yields 468.2 kN (105 kips) and 254.2 kN (57 kips) for the same resistances at the identical value of displacement. This corresponds to an almost four-fold increase in total capacity and an eight-fold increase in tip capacity. The increase in tip capacity cannot be explained solely by considering the post grouting as the removal of plastic strain in the surrounding soil by loading unloading and reloading elastically. The substantial increase is in part due to such unload reload behavior and in part due to the resulting size of the grout bulb at the tip being larger than the shaft area.

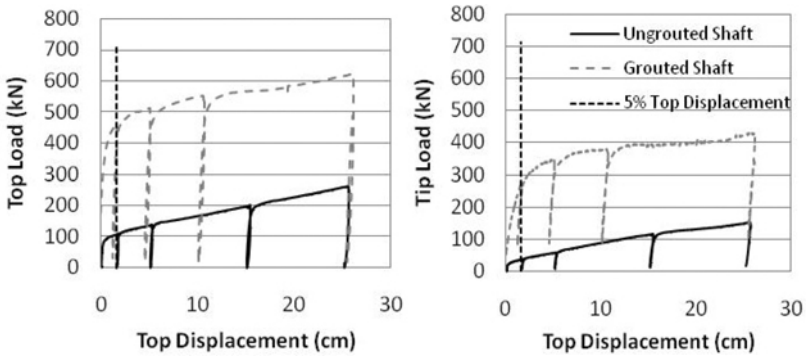

FIG. 5. Measurements during the load testing phase.

The maximum grout pressure induced at the tip was 1030 kPa (149 psi). If it is assumed that the entire tip grout/soil interface was exposed to this pressure, then it can be safely taken that the soil was pre-loaded to this value. Based on the total volume that was pumped beyond the tip of the model shaft, it was anticipated that a grout bulb of spherical shape of 27 cm (0.88 ft) radius would develop. The dimensions of the observed bulb, shown in Figure 6, though not spherical in shape, gave an average radius which compared well with the calculated value. This grout bulb plan area multiplied by the grout pressure is the preload to which the soil at the tip had been exposed. This preload value is 232.8 kN (52.2 kips) which compares well with the 254.2 kN (57 kips) experienced at 5% displacement during the load phase (which was essentially reloading the soil).

FIG. 6. Grout bulb at shaft tip as observed during soil excavation.

CONCLUSIONS

This test has proven the ability of compaction post grouting of a shaft tip to increase its capacity by ridding the soil of a good portion of its plastic deformation and also by increasing the tip bearing area, which is a particular advantage of an unconfined compaction grouting operation. This testing procedure will need to be repeated for different relative densities and different soils with possible field testing for validation.

ACKNOWLEDGEMENTS

The authors would like to thank Dr Saad El-Azazy, Dr Jinxing Zha and Dr Mohammed Islam of Caltrans and Dr Mohammad Sheikhizadeh of WSDOT for their unreserved support and advice. In addition we appreciate the help of Daniel Bell of UNR and the staff of the Large Structures Laboratory in conducting these tests.

REFERENCES

1) Pooranampillai, J.D., Elfass, S., Vanderpool, W., Norris, G., (2008), "Development and Assessment of Post Grouting Methods to Increase the Load Carrying Capacity of Deep Foundations", *41st Symposium on Engineering Geology and Geotechnical Engineering*, Paul Link, Department of Geosciences, Idaho State University, Pocatello ID 83209, 77 – 92.
2) Vanderpool, W, Norris, G, Elfass, S, (2008), "Warning: Low Mobility Grout (LMG) May Not Equal compaction Grout (CG), *Geotechnical News,* March 2008, Volume 26, Number 1, BiTech, Vancouver, British Columbia, Canada, 44-50.
3) Warner J., (2004), "Chapter 6: Cementitous Grout Mixes", *Practical Handbook of Grouting,* John Wiley & Sons, Hoboken, NJ, 113.
4) Yang, J., "Influence Zone for End Bearing of Piles in Sand", (2006), *Journal of Geotechnical and Geoenvironmental Engineering*, ASCE, Vol. 132(9), 1229-1237.

Copyrighted Materials
Copyright © 2009 American Society of Civil Engineers (ASCE)
Retrieved from www.knovel.com

Tip Post-Grouting of Slurry-Drilled Shafts in Soil: Chinese Experiences

Xinsheng Duan[1] and Fred H. Kulhawy[2], Dist.M.ASCE

[1]Professor, Department of Engineering, China University of Geosciences, Wuhan, China 430074; duanxinsheng@hotmail.com, duanxinsheng@163.com
[2]Professor, School of Civil & Environmental Engineering, Hollister Hall, Cornell University, Ithaca, NY 14853-3501; fhk1@cornell.edu

ABSTRACT: Some Chinese experiences are summarized and evaluated for tip post-grouting of drilled shafts constructed in soil using mud slurry. The factors that affect tip post-grouting are discussed, including many grout issues. Capacity increase is discussed, and some empirical Chinese criteria are cited for increasing the capacity.

INTRODUCTION

Drilled shafts are used widely around the world. In caving soil, slurry can be used to maintain the stability of the excavation. In China, slurry is used for stability and for removal of drill cuttings. Generally, water or mud slurry (water mixed with clay or clayey cuttings) is used instead of bentonite.

Where mud slurry is used, a smear can develop along the shaft wall. In Chinese experience, a smear zone thicker than 5 mm will detrimentally affect the shaft side resistance (Wang et al. 2002), and incomplete or poor cleanout of the excavation will increase the settlement needed to mobilize the tip resistance. Most drilled shafts in China are constructed by mud slurry circulation and, more often than not, complete cleanout is impossible. A load test database of 73 slurry-drilled shafts from across China suggests that the mobilized tip resistance is only about 25% of that for driven and jacked piles in the same bearing stratum, on average. The side resistance is about 90 to 95% of that for driven and jacked piles, on average (China Academy of Building Research 1995).

To mitigate these issues, tip post-grouting has been used widely in China. In sand, the tip resistance can increase by up to 220%, and the side resistance, up to 10 to 20 m above the tip, can increase by up to 50 to 90% (Hu et al. 2001). However, these effects vary greatly in practice. This paper describes some experiences and achievements in tip post-grouting, primarily in China, and presents some Chinese design and construction methods for evaluating tip post-grouting in mud slurry-drilled shafts in soil.

OVERVIEW OF CHINESE PRACTICES FOR TIP POST-GROUTING IN SLURRY-DRILLED SHAFTS

Tip post-grouting is conducted as follows. (1) Grout distributors, each connected to the bottom of one grouting pipe or to the bottoms of one grouting pipe and one return pipe, are placed at the base of the shaft excavation with the reinforcing cage. (2) The shaft is concreted using tremie. The concrete strength is assessed so that it is at least 80% of its design value, is not less than 20 MN/m^2, and can withstand the grouting pressure (Chen & Lin 1999). (3) A cement grout is pumped to the distributors one by one, through grouting pipes, to the shaft tip to compact, permeate, and split any debris and the surrounding soil to strengthen them. The grout also penetrates upward a certain distance along the shaft side, splitting and mixing any mud smear, and compacting, permeating, and splitting the surrounding soils to strengthen them.

Conceptually, the shaft capacity is increased because of the following: (a) any debris and the surrounding soil are strengthened by the grout, (b) the grouted tip of the shaft enlarges the shaft bearing area, (c) the grouting stiffens the tip to improve the load-displacement behavior, and (d) the grouting can increase the side resistance and perhaps the "operative" shaft diameter.

GROUT DISTRIBUTOR AND ARRANGEMENT

As shown in Figure 1, the grout distributor is a segment of pipe with two screw ends. The delivery holes, 8 mm diameter at 90° intervals circumferentially and at 100 mm intervals longitudinally, are wrapped with rubber belts (short sleeves) in rows to act as one-way valves. Figure 2 shows the basic vertical and horizontal arrangements at the shaft tip.

Figure 2a shows the bottom of the vertical distributor blocked with a threaded plug, while the top is connected to a grouting pipe, which is bound, or spot-welded, to the reinforcing cage and projects above the ground to be connected to the grout pump. The spot-welded steel bar rings prevent the rubber belts from rolling up during installation. The vertical distributors penetrate the soil under the reinforcing cage. The number of distributors depends on the shaft diameter (B), typically two to three for B = 700-1500 mm and four for B > 1500 mm. When gravel and cobbles are encountered, the grout penetration can be excessive. In this case, multi-stage grouting is done, in which grout is injected into the tip and several hours elapse before the process is repeated, once or more times (He 2002b; Tao 2001).

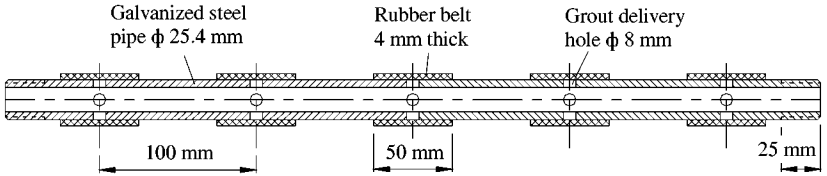

FIG. 1. Grout Distributor

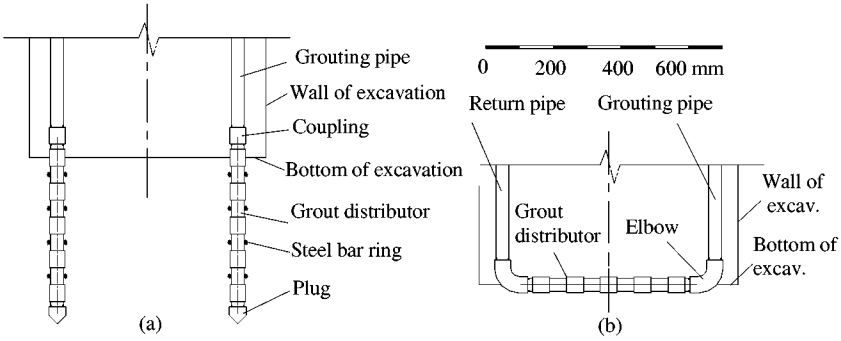

FIG. 2. Grout Distributor Arrangements: (a) Vertical (b) Horizontal

Figure 2b shows a horizontal grout distributor arrangement, which is connected to a grouting pipe at one end and a return pipe at the other end through two 90° elbows. The grouting pipe is attached to the grout pump while the return pipe is attached to the grout sump. The grout penetrates the soil via the distributor, depending on the soil take, while the excess flows through the return pipe for re-circulation. In this way, the grout is kept moving until the grouting is completed, with little possibility for blockage. Horizontal distributors are useful for drilled shafts in gravel or fractured rock. The number of horizontal distributors ranges from two to six, often depending on the shaft diameter (e.g., Dapp & Mullins 2002; Wu & Huang 2003).

GROUT

In tip post-grouting, cement grouts are used widely, including ordinary cement grout and ultra-fine cement grout. Ordinary cement grout is the least expensive and generally is most suitable for use in permeating coarse soils with a relatively high permeability coefficient greater than 10^{-1} cm/s (Shen 2001b). In China, ordinary cement grout also is used in medium sand, fine sand, silt, and silty clay where the grout splits or fractures the surrounding soils and mixes with them to strengthen them.

Ultra-fine cement has an average grain size of three to four microns and can permeate fine sand with a coefficient of permeability of 10^{-3} to 10^{-4} cm/s. Ultra-fine cement grout has been used in tip post-grouting in silty clay in Shanghai (Shen 2001a). The water-cement ratio is usually between 0.5 and 0.7 (Wu & Huang 2003).

Water reducers generally are added to increase the pumpability of grout mixtures by increasing their fluidity or to increase their strength by reducing the water content of the mixtures while at the same time maintaining the same degree of fluidity. Sometimes, aluminum powder is added for shrinkage compensation or a slight to moderate amount of controlled expansion during the plastic stage of the grout. About one teaspoonful of powder per sack of cement is common (US Army Corps of Engineers 1984).

GROUTING PRESSURE

When the grouting pressure is less than that required to split or fracture the soil (herein called soil split pressure), the grout permeates the soil and the grout take increases with the grouting pressure. However, when the grouting pressure is equal to the soil split pressure, the grout splits the soil, and the grout take increases. Clearly, the soil split pressure is an important parameter for grouting control and can be estimated as follows.

For granular soils, assume that the vertical effective stress before grouting = σ_v' and the horizontal effective stress $\sigma_h' = K_o \sigma_v'$, in which K_o = coefficient of horizontal soil stress. Assume also that the grouting pressure p at the shaft tip will decrease both the vertical and horizontal effective stresses by p. When $p = p_o$ (p_o = soil split pressure), splitting occurs.

If $K_o < 1$, then the major principal stress $\sigma_1' = \sigma_v' - p_o$, and the minor principal stress $\sigma_3' = K_o \sigma_v' - p_o$. Using a linear Coulomb-Mohr equation (ϕ' = effective friction angle), substituting these principal stresses, and re-arranging gives:

$$p_o = [K_o (1 + \sin \phi') - (1 - \sin \phi')] (\sigma_v' / 2 \sin \phi') \quad (1)$$

If $K_o > 1$, then the major principal stress $\sigma_1' = K_o \sigma_v' - p_o$, and the minor principal stress $\sigma_3' = \sigma_v' - p_o$. Using a linear Coulomb-Mohr equation (ϕ' = effective friction angle), sub-stituting these principal stresses, and re-arranging gives:

$$p_o = [(1 + \sin \phi') - K_o (1 - \sin \phi')] (\sigma_v' / 2 \sin \phi') \quad (2)$$

For undrained loading in cohesive soils (Essler et al. 2000), the soil split pressure would equal the summation of the overburden stress and the undrained shear strength (s_u), given as $p_o = \gamma D + s_u$, in which γ = soil total unit weight and D = shaft depth.

There are three issues in controlling the grouting pressure. (1) To avoid heaving, the grouting pressure p should be less than the sum of the side resistance and the shaft weight, divided by its tip area, as given below:

$$p \leq (\pi B \sum q_{si} d_i + \pi B D \gamma_c) / (0.25 \pi B^2) \quad (3)$$

in which d_i = depth of shaft in layer i, q_{si}= average side resistance in layer i, and γ_c= effective unit weight of concrete. (2) In permeable soils, the grouting pressure should be kept less than the soil split pressure (p_o) to permeate grout into the soil instead of splitting it. (3) When the grouting pressure must equal the soil split pressure to ensure grouting in "impermeable" soil, the duration when these pressures are equal should be limited to five to ten minutes to limit the grout spread (Xie & Wang 2002). Permeation grouting usually is more effective than split grouting.

It should be noted that the grouting pressure above is that at the shaft tip. However, current practice measures the grouting pressure at the outlet of the grout pump. The pressure difference between the shaft tip and pump outlet is hard to assess because it is affected by many factors including the rate of grout flow, grout viscosity, length and diameter of the grouting pipes, and pipe inner wall roughness, for example.

GROUT (OR CEMENT) AMOUNT FOR TIP POST-GROUTING

In principle, the capacity of a drilled shaft increases with the grout amount injected into the tip, but the relationship between capacity increment and grout amount is not linear. Model experimental studies show that the capacity increases with the grout amount to a certain extent, beyond which it increases very slowly (Gao 1998).

There are many factors affecting the actual grout amount for a particular shaft at a specific project, including the local geological conditions, shaft geometry, boring method, thickness of mud smear, debris remaining after cleanout, and expected increment of capacity. No specific criteria are available to determine the grout amount, even though many post-grouted shafts have been constructed. One practical way is to consider the results from other projects in similar conditions.

Based on statistical analysis of more than 20 tip post-grouted drilled shaft projects in Wuhan, China, reference values of the grout amount have been suggested, as given in Table 1. Observations also have shown that cement grout penetrates upward along the sides of the drilled shaft 10 to 20 m (Liu et al. 1997, He 2002a, Wu & Huang 2003). Occasionally, the grout can penetrate upward more than 40 m to the ground surface (Hu et al. 2001, Huang & Cao 2002).

CAPACITY OF TIP POST-GROUTED SLURRY-DRILLED SHAFTS

To illustrate the effects of tip post-grouting, results were analyzed from two slurry-drilled shafts that were constructed at the same site in Zhenzhou, China. Shaft 1 was normal, while shaft 2 was grouted at its tip with 2000 kg cement. The shafts had B = 800 mm and D = 47.6 m, and stress gages were installed at depths of 9.15, 12.45, 17.25, 27.65, 35.5, and 47.6 m in both shafts (where the soil changes from one layer to another or the shaft tip is located). The soil strata are given in Table 2.

Load tests were conducted on both shafts in accordance with the Chinese slow maintained load procedure (China Academy for Building Research 1995), which is similar to the ASTM standard loading procedure. The load increment for shaft 1 was 600 kN and that for shaft 2 was 700 kN, and the load was increased when the rate of settlement of the shaft butt was less than 0.1 mm per hour. The load-settlement curves for both shafts are shown in Figure 3. Using Chinese recommended procedures, the interpreted capacity of shaft 1 = 6000 kN at a butt settlement = 27.7 mm. For shaft 2, the values are 8400 kN and 25.4 mm, respectively. Based on the instrumentation, for shaft 1, the side capacity = 5539 kN, the tip capacity = 461 kN, and the ratio of tip to total capacity = 7.7%. For shaft 2, the values are 7068 kN, 1332 kN, and 15.8%, respectively.

Table 1. Cement Amount for Tip Post-Grouting (after Zhang et al. 2004)

Shaft Diameter (m)	Cement Amount (kg) for Shaft Depth ≤ 35 m	Cement Amount (kg) for Shaft Depth > 35 m
0.6 - 0.7	1000 - 1500	1500 - 2000
0.8 - 0.9	1500 - 2000	2500 - 3000
1.0 - 1.2	2500 - 3000	3000 - 4000
> 1.2	3000 - 4000	4000 - 5000

Table 2. Soil Strata and Average Side Resistance at Zhenzhou (after He 2002a)

Soil	Depth (m)	q_{s1}[a] (kN/m^2)	q_{s2}[a] (kN/m^2)
Silty Clay	0 - 9.15	37	39
Silty Clay	9.15 - 12.45	53	59
Silt	12.45 - 17.25	47	50
Fine Sand	17.25 - 27.65	62	64
Silt	27.65 - 35.50	42	64
Silt	35.50 - 47.60	40	69

q_{s1}, q_{s2} - average side resistance per soil layer for shaft 1, 2

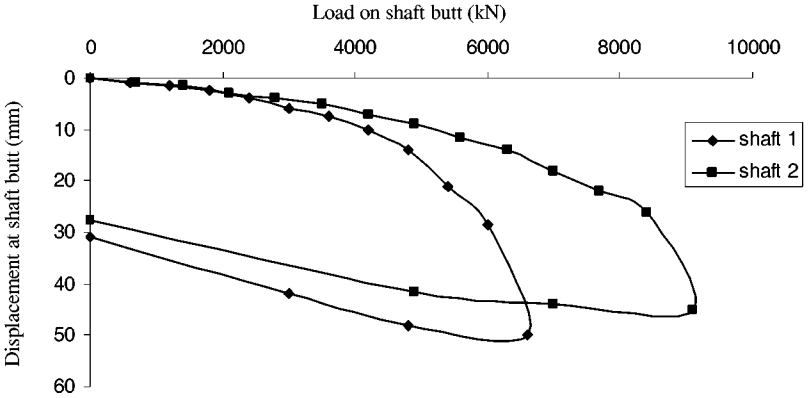

FIG. 3. Load-Displacement Curves (after He 2002a)

Because of tip post-grouting, the total capacity of shaft 2 is 40% larger than shaft 1. The side and tip capacities, and the ratio of tip to total capacity, all increase. The average side resistances in the different soil layers for shafts 1 and 2 are given in Table 2, which shows that, because of tip post-grouting, the average side resistances of the lower silts, 12.10 and 7.85 m up from the tip of shaft 2, increased 73% and 52%, respectively, over shaft 1. For the other soil layers, there are no apparent differences between shafts 1 and 2.

Load tests such as these demonstrate the value of tip post-grouting, but there are many factors influencing the capacity increase, and it is difficult to quantify them accurately. Alternatively, with the accumulation of load test data, statistical evaluations can be established for preliminary design.

For Wuhan, China, based on load test data, Hu et al. (2001) suggested the following to estimate the capacity of post-grouted drilled shafts for preliminary design:

$$Q_{ult} = \pi B \sum \lambda_{si} q_{si} d_i + 0.25 \pi B^2 \lambda_p q_p \quad (4)$$

in which q_{si}= average side resistance in layer i before tip post-grouting, q_p = tip resistance before tip post-grouting, λ_{si} = side resistance increase coefficient in layer i, and

λ_p = tip resistance increase coefficient. Hu et al. (2001) compared the results from 186 post-grouted drilled shafts (B = 0.7-1.0 m, D = 25-49 m, injected at the tip with an average 2400 kg of cement) with that of conventional drilled shafts in the Hankou district in Wuhan, and they found that λ_p ranged between 1.3 and 5.1 and that λ_{si} ranged between 1.3 and 2.2. Their histogram showed λ_p to be normally distributed with a mean = 3.21 and standard deviation = 0.79. Comparable data for λ_{si} were not given. Based on their interpretation of the test data, they recommended the λ_{si} and λ_p ranges in Table 3 for preliminary design in the Hankou district.

Table 3. Recommended Increase Coefficients in Hankou (after Hu et al. 2001)

Increase Coefficient	Clay	Silt	Silty & Fine Sand	Medium Sand	Coarse Sand	Gravel & Cobble
λ_{si} (side)	1.2 - 1.5	1.3 - 1.5	1.5 - 1.9	1.6 - 1.9	1.7 - 2.2	1.7 - 2.2
λ_p (tip)	1.2 - 1.7	1.4 - 1.8	1.8 - 2.5	2.0 - 2.8	2.2 - 2.8	2.2 - 3.0

Note: λ_{si} = 1 for soil layers > 20 m away from tip

SUMMARY AND CONCLUSIONS

Debris can remain at the tip of a slurry-drilled shaft after clean out, which would lead to decreased capacity and increased settlement. To mitigate these problems, tip post-grouting can be used. The original purpose of this process was to strengthen the debris to increase the shaft tip resistance. However, tip post-grouting also can increase the side resistance substantially. This process has been used widely in China, and some Chinese experiences are summarized herein.

Illustrative grout distributors are shown that can be used for shafts in soil and in gravel or fractured rock. A simple procedure is described to estimate the soil split pressure, which is used to distinguish between permeation and split grouting. The strengthening effect of split grouting usually is less than that of permeation grouting. One of the most important construction parameters for tip post-grouting is the cement amount, which is estimated using case history data.

Finally, a simple empirical relationship used in China is given to estimate the capacity of tip post-grouted drilled shafts using tip and side resistance increase coefficients. Illustrative values are shown based on analysis of 186 load tests in Hankou, Wuhan, China.

REFERENCES

Chen, X.-M. & Lin, S. (1999). "Post pressure-grouting technique for bored pile." *Exploration Eng.*, 26 (3), 17-20 (Chinese).

China Academy of Building Research (1995). "Technical code for building pile foundations JGJ94-94." China Architecture & Building Press, Beijing (Chinese).

Dapp, S.D. & Mullins, G. (2002). "Pressure grouting drilled shaft tips." *Deep Foundations (GSP 116)*, Ed. M.W. O'Neill & F.C. Townsend, ASCE, Reston, 335-50.

Essler, R.D., Drooff, E.R. & Falk, E. (2000). "Compensation grouting." *Advances in Grouting (GSP 104)*, Ed. L.K. Krizek & S. Kevan, ASCE, Reston, 1-15.

Gao, W.-S. (1998). "Study on model testing of single post-grouting slurry drilled pile." *Building Science*, 15 (5), 23-26, 36 (Chinese).

He, J. (2002a). "Experimental research on bearing properties of base-grouting bored cast-in-place pile." *Chinese J. Geotech. Eng.*, 24 (6), 743-746 (Chinese).

He, K. (2002b). "Technology analyzing of filling pile with post-pressure grouting." *J. Nanchang Inst. Aeronautical Technology,* 16 (1), 59-61 (Chinese).

Hu, C.-L., Li, X.-D. & Wu, Z.-H. (2001). "Study of bearing capacity for postgrouting bored pile." *Chinese J. Rock Mech. & Eng.,* 20 (4), 546-550 (Chinese).

Huang, S.-G. & Cao, H. (2002). "Mechanism study on post-grouting technology applied in soft soil." *Geotech. Eng. Technique,* 16 (1), 36-39 (Chinese).

Liu J.-L., Zhu, Z.-C. & Zhang, Y. (1997). "Technology of post-grouting for slurry-drilled piles." *Proc. 14th Intl. Conf. Soil Mech. Fndn. Eng.*, Hamburg, 831-834.

Shen, B.-H. (2001a). "Effect analysis on tip post-grouting of drilled piles." *J. Geotech. Eng. World*, 4 (8), 60-64 (Chinese).

Shen, B.-H. (2001b). "Technique of post-grouting piles (6): factors affecting compressive bearing capacity." *Industrial Const.*, 31(10), 62-65 (Chinese).

Tao, X.-W. (2001). "Design & construction of tip post-grouting drilled shafts in Shanghai." *Exploration Eng.,* 28 (4): 35-36, 38 (Chinese).

U. S. Army Corps of Engineers (1984). "Chapter 5: grout materials." *Engineer Manual 1110-2-3506.*

Wang, P., Li, Z.-G. & Sun, H. (2002). "Construction design & application of post-grouting shaft technology in Taiyuan." *Exploration Eng.,* 29 (1), 21-25 (Chinese).

Wu, H.-B. & Huang, Z.-J. (2003). "Application of pile base grouting techniques to Paksey Bridge." *World Bridges,* 2003(4), 10-13 (Chinese).

Xie, Y.-F. & Wang, Y.-Q. (2002). "Research on improving post-grouting effect of drilled shafts." *Port & Waterway Eng.*, 340(5), 47-51 (Chinese).

Zhang, M.-Y., Zhu, L., Zhang, X., Jiang, Z.-X. & Lu, Z.-A. (2004). "Bearing capacity strengthen of postgrouted piles." *J. Wuhan Univ. Tech.*, 26(2), 47-49 (Chinese).

Copyrighted Materials
Copyright © 2009 American Society of Civil Engineers (ASCE)
Retrieved from www.knovel.com

Designing and Characterizing the LEED Concrete for Drilled Shaft Applications

C. Vipulanandan[1], Ph.D., M. ASCE and Emrah Demircan [2]

[1] Chairman, Professor and Director of Center for Innovative Grouting Materials and Technology (CIGMAT), Director of Texas Hurricane Center for Innovative Technology, Department of Civil and Environmental Engineering, University of Houston, Houston, Texas 77204-4003 (Phone: (713) 743-4278; FAX (713) 743-4260; email: cvipulanandan@uh.edu;

[2] Graduate Student, Department of Civil and Environmental Engineering, University of Houston, Houston, Texas 77204-4003; email: edemircan2@uh.edu

ABSTRACT In order to meet Leadership in Energy and Environmental Design (LEED) guidelines, research is underway to produce concrete (LEED concrete) with alternative binders. LEED concepts provide for environmentally sustainable construction. Since its inception in 1998, LEED has grown to encompass projects in 50 US States and over 30 other countries.

In this study, a LEED concrete mix with 70% Class C fly ash as replacement for cement, with appropriate chemical admixture was designed and tested. The behavior of LEED concrete mixture was compared to a conventional Portland cement control mix. The LEED concrete mixture reached similar to higher strength as Portland cement concrete with time due to the pozzolanic properties of Class C fly ash. Internal curing temperature of the LEED concrete mixture was reduced with the addition of fly ash and the setting time of the LEED concrete mixture was increased, which is generally achived by using a retarder in the conventional concrete mix. In addition, volume changes due to shrinkage, and the water absorptions by the LEED concrete mixture were lower than the conventional Portland cement concrete mixture at all ages, indicating that durability of the LEED concrete mixture was comparable or even better than the conventional Portland cement concrete mixture. By using appropriate chemical admixture, highly workable LEED concrete mixture with up to 200 mm (8 in) slump was developed for drilled shaft and/or other pile foundation applications.

INTRODUCTION

In addition to hardened properties required to meet structural design requirements; concrete performance, in terms of workability for duration of the pour and compatibility with congested rebar, plays a significant role in quality of drilled

shafts (Brown 2005). Workability is the ability of a fresh (plastic) concrete mix to flow and fill the form properly with the desired work without reducing the concrete's quality, and slump is the measured property associated with concrete workability. Many state DOT's use specifications which routinely call for a slump of at least 4 inches to be maintained for a period of 4 hours after batching (Brown 2005). In order to maintain workability for the desired period, retarder admixtures are being used commonly.

Fly ash, one of the most commonly used pozzolanic material for cement replacement, gained popularity because of its contribution to durability, strength and eco-system. It is known that approximately one ton of CO_2 is released into the atmosphere as a result of producing each ton of Portland cement (Camoes et al 2003). In contrast to Portland cement, fly ash is a by product and more economical to use in concrete if the needed proportions are achieved. Fly ash also contributes to performance of concrete in terms of improved workability via ball bearing action of spherical particles, higher long-term strength, lower heat of hydration, lower shrinkage characteristics, lower porosity and improved impermeability (Klieger and Lamond 1994). Based on calcium oxide content, ASTM C 618 has classified fly ash as Class C (10-30% calcium oxide content) and Class F (less than 10% calcium oxide content). In contrast to Class F, almost all minerals of Class C fly ash are reactive, giving it both pozzolanic and cementitious properties (Vargas 2007).

OBJECTIVE

The overall objective of this research was to develop a concrete mix with 70% Class C fly ash that will satisfy both slump and strength requirements and meet or exceed the LEED concrete standards.

MATERIALS

Locally available crushed stone with a maximum coarse aggregate size of 25 mm (1 in) and locally available sand were used as aggregates. The mix proportions are summarized in Table 1. Type 1 Portland cement (ASTM C 150) and Class C fly (ASTM C 618) were used as cementitious materials. Tap water was used for the two mixtures. A commercially available admixture was used to adjust the workability of LEED concrete mixture to the desired level.

Table 1. Mixture Proportions

	Coarse Aggregate (kg/m^3)	Fine Aggregate (kg/m^3)	Cement (kg/m^3)	Fly Ash (kg/m^3)	Cement Replacement Percentage	Admixture (ml/100 kg cementitious)	Water (kg/m^3)	W/C %	Slump (mm)	Unit Weight (kg/m^3)
Control mix	1127	756	334.5	-	-	-	177.3	53	150	2303
70% Fly ash mix	1180	783	100.3	234.2	70%	390	133.8	40	200	2299

METHODS

All batches were mixed in a 0.08 m^3 (3 ft^3) nominal capacity electric concrete mixer. A commercially available admixture was used to get the desired workability and the amount of admixture was determined as per total cementitious material (cement + fly ash). The slump for each batch was measured according to ASTM C 143 and unit weight was measured according to ASTM C 138. For each batch, sixteen 100 X 200 mm (4 x 8 in.), one 150 X 300 mm (6 x 12 in.) and five 75 X150 mm (3 x 6 in) were cast in accordance with ASTM C 192. The 150 X 300 mm (6 x 12 in.) cylinder specimen was used to monitor internal temperature change of the mixture with a commercially available thermocouple which was sensitive to response time less than 0.15 seconds. The 75 X 150 mm (3 x 6 in) cylinder specimens were used to determine the time of setting for each mixture as per ASTM C 403. Fifteen of the 100 X 200 mm (4 x 8 in.) cylinder specimens were used for compression test as per ASTM C 39 at 1, 3, 7, 14 and 28 days. Specimens were air-cured until the day of testing. Three specimens were tested at each day of testing and their average was taken as the compressive strength at that testing age. Test for pulse velocity through concrete was measured for each specimen before compression test in accordance with ASTM C 597-02. One 100 X 200 mm (4 x 8 in.) specimen was used to measure the water absorption and voids in hardened concrete after 28 days air curing period as per ASTM C642-06. For each mixture, a 75 X 150 mm (3 x 6 in.) steel mold was filled with concrete to measure the changes in height of the cylindrical specimens as per ASTM C 1090-01. Changes in height were measured at 1, 3, 7, 14 and 28 days.

ANALYSIS OF RESULTS

Plastic Properties of High Volume Fly Ash Concrete

The plastic properties of each mixture are summarized in Table 2. The results of slump test showed that with appropriate amount of the admixture used in the LEED concrete mix, water to binder ratio (w/b) could be cut by 13 percent compared to no use of admixture in the control mix and even higher slump values (200 mm) could be achieved. Even by using little amount (6 oz per 100 pounds of cementitious) of the admixture enables to get the desired slump as well low water-to-binder (w/b) ratio. The unit weights of the mixtures were very close to each other (Table 2).

Table 2. The Plastic Properties of the Concrete Mixtures

	Control Mix		**70% Fly Ash Mix**	
Slump mm (in)	150 (6)		200 (8)	
Unit weight (kg/m^3)	2303		2299	
Time of setting (hr.)	*Initial*	*Final*	*Initial*	*Final*
	3.5	4.2	9.5	10.8

The internal curing temperature changes for the concrete mixtures were monitored during the first 24 hours after casting in 150 X 300 mm (6 x 12 in.) plastic molds. Temperature changes with time for the two mixtures were shown in Fig. 1. Replacement of cement with fly ash caused to lower heat gain that makes the LEED concrete suitable for hot weather applications. Internal curing temperature of concrete mixtures reduced with fly ash replacement. Hydration of cement is an exothermic reaction; therefore the internal temperature monitoring revealed that hydration of cement reaction was delayed with fly ash replacement. Hence, there is no need to use retarder admixture to maintain the workability for longer periods of time including the time to place the concrete in drilled shafts.

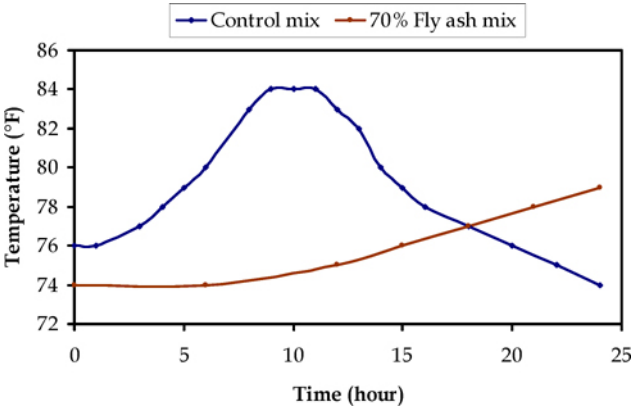

Figure 1 – Internal curing temperature change of mixtures

As a consequence of delay in hydration of cement, replacement of Portland cement with fly ash prolonged the setting time of concrete as shown in Figure 2. Prolonged setting time could also help with more time for finishing operations.

Compressive Strength

In accordance with ASTM C 39/C 39M-01, compressive strength for each mixture was determined at 1, 3, 7, 14 and 28 days by testing three specimens after each curing time and taking average. The results of compression tests were plotted in Figure 3. The control mix (without fly ash) showed higher early strength than the 70% fly ash mixture. However, the 70% fly ash mixture reached the same strength with the control mix at 28 day age. Compressive strength ratios at 7 day to 28 day (σ_7/σ_{28}) for the control mix and the LEED concrete mix were 0.76 and 0.43 respectively. Compressive strength ratios at 1 day to 7 day (σ_1/σ_7) for the control mix and the LEED concrete mix were 0.55 and 0.19 respectively. The results revealed that the LEED concrete mixture exhibited faster strength gain than control mix after 1 day because of fly ash's pozzolanic activity. However, 1 day strength of the LEED mixture was very low compared to the control cement concrete mix.

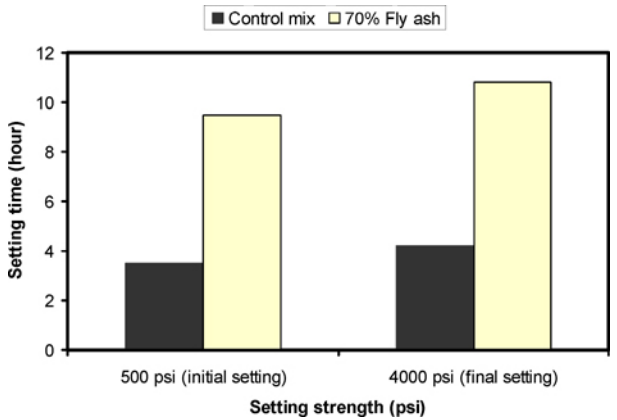

Figure 2 – Effect of fly ash replacement on setting time (1 psi = 6.9 kPa)

The compressive strength results obtained from this study were comparable to the references from literature and past research projects. The data for percent cement replacement with total binder of 400 kg/m^3 (675 lb/yd^3) was compared to current study with 334.5 kg/m^3 (564 lb/yd^3) total binder in Fig. 4 (Kumar et al 2007). By using the formula of the trend line for the data, compressive strength for 70% replacement was predicted (20.5 MPa) for the mixture from literature (400 kg/m^3 total binder). The strength from the current study (37 MPa) was 45% higher than the other study from literature (20.5 MPa) despite lesser amount of total binder (334.5 kg/m^3) was used in the current study mix.

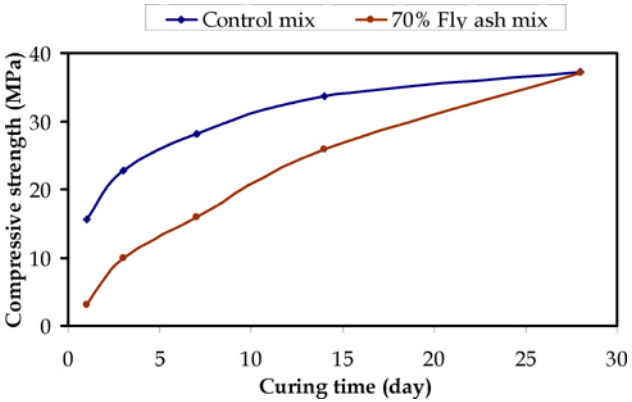

Figure 3 – Strength development with age

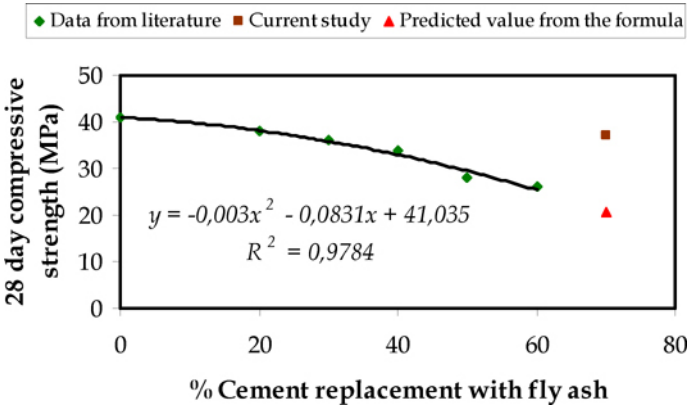

Figure 4 - Comparison of current study with other studies from literature

Pulse Velocity Test

In accordance with ASTM C 597-02 "Standard Test Method for Pulse Velocity through Concrete", pulse velocity for each mixture was determined at 1, 3, 7, 14 and 28 days. The results were plotted in Fig. 5. As shown in the Fig. 5, trends observed in the pulse velocity test results exhibited similar trend with compression test results. Pulse velocity through concrete has a direct relation with stiffness of the specimen. If so, pulse velocity test (which is a non-destructive test) results could be used to predict compressive strength of the specimens.

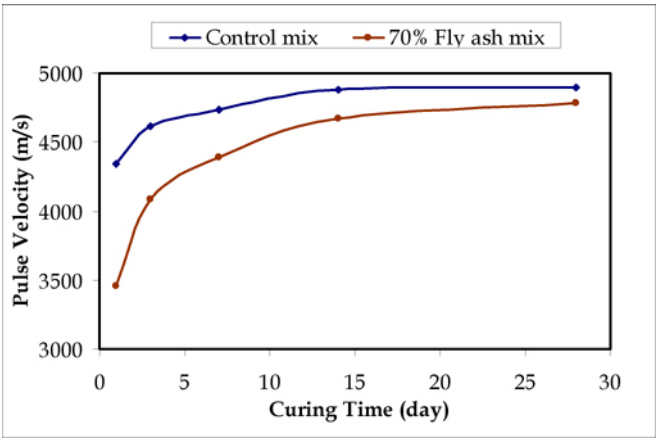

Figure 5 –Pulse Velocity Test through Concrete vs. Time

Shrinkage Test

In accordance with ASTM C 1090-01 "Standard Test Method for Measuring Changes in Height of Cylindrical Specimens of Hydraulic-Cement Grout", volume changes due to shrinkage for the mixtures were measured at 1, 3, 7, 14 and 28 days. The results are compared in Fig. 6. As shown in the Fig. 6, the LEED concrete mixture exhibited lower shrinkage than the ordinary Portland cement concrete mix at all ages, and experienced approximately half of the shrinkage that the control mix experienced after 28 days. Hence, addition of fly ash resulted in reduced shrinkage as shown in the Fig. 6.

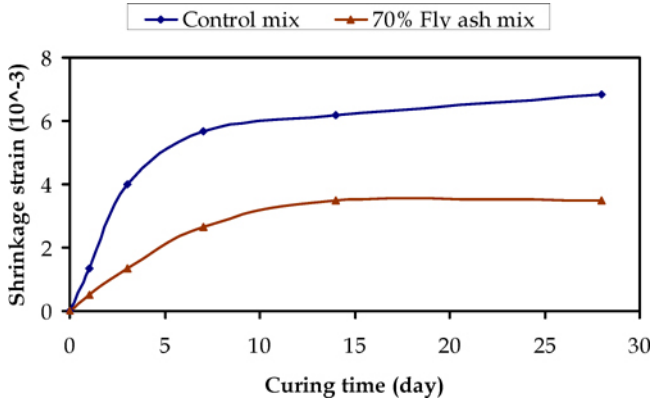

Figure 6 –Shrinkage Test Results

Voids in Hardened Concrete

In accordance with ASTM C 642-06 "Standard Test Method for Density, Absorption, and Voids in Hardened Concrete", void ratios in hardened concrete specimens were measured after 28 days of curing period. Based on the test results, the LEED concrete mixture exhibited lesser void content (0.10 percent) than the conventional Portland cement concrete mix (0.12 percent). Smaller sized and spherical particles of fly ash may have been effective in filling the voids in concrete matrix; as a consequence, the LEED concrete mixture exhibited lower void ratios than the control mix.

CONCLUSION

By using appropriate amount of a commercially available admixture with Class C fly ash, a LEED concrete mixture was designed with 70% fly ash, Based on this study following can be concluded:

(1) The LEED concrete mix with 70% fly ash was more flowable than the control concrete mix. Increased workability, delayed setting time and reduced internal curing temperature properties of the LEED concrete mix makes it a promising material for drilled shaft applications.
(2) The LEED concrete mixture exhibited similar long term strength (28 day) and lower shrinkage values compared to the control concrete mixture.
(3). The LEED concrete strength was about 45% higher than the comparable cement concrete mixtures reported in the literature.
(4) Pulse velocity test results for the LEED and control concrete mixtures showed a similar trend with the compression strength test results. Due to smaller particle size and spherical shape of fly ash particles, the LEED concrete mixture had lesser voids than the ordinary Portland cement concrete mix.

ACKNOWLEDGEMENT

This study was supported by the Center for Innovative Grouting Materials and Technology (CIGMAT) with funding from various industries.

REFERENCES

Brown, D. A. (2005). "Recipe for Success with Drilled Shaft Concrete." Foundation Drilling Magazine, Nov. 2004, pp. 16-24.

Camoes, A., Aguiar B., Jalali S. (2003). "Durability of Low Cost High Performance Fly Ash Concrete." International Ash Utilization Symposia and the World of Coal Ash conference, Covington, Kentucky.

Klieger, P., Lamond, Joseph F. (1994). Significance of Tests and Properties of Concrete and Concrete-Making Materials, 4th Ed., ASTM, pp. 501, Fredericksburg, Virginia.

Kumar, B., Tike, G.K., Nanda, P.K. (2007). "Evaluation of Properties of High-Volume Fly-Ash Concrete for Pavements." Journal of Materials in Civil Engineering, Oct. 2007, pp. 906-911.

Vargas, J.A., (2007). "A Designer's View of Fly Ash Concrete." Concrete International, Feb. 2007, pp. 43-46.

Copyrighted Materials
Copyright © 2009 American Society of Civil Engineers (ASCE)
Retrieved from www.knovel.com

Evaluation of Compression Tip Capacity for Drilled Shafts

Yit-Jin Chen[1], Yi-Chung Fang [2] and Tsu-Hung Chu[3]

[1] Associate Professor, Department of Civil Engineering, Chung Yuan Christian University, Chung-Li 32023, Taiwan; yjc@cycu.edu.tw
[2,3] Graduate Student, Department of Civil Engineering, Chung Yuan Christian University, Chung-Li 32023, Taiwan; g1023024@hotmail.com; 9672008@cycu.edu.tw

ABSTRACT

This study examines representative analytical models to evaluate the tip capacity of drilled shaft foundations under axial compression loading. To ensure a reliable analysis, a wide variety of compression load test data were used for this purpose. Thereafter, these data were divided into drained and undrained databases based on the soil conditions along the shaft tip. For the evaluation of the bearing capacity theory, the predicted and measured results for undrained soils are reasonably consistent. However, the results showed that the predicted model greatly overestimates the tip capacity for drained soils. On the average, the measured capacity of the drained soils is about 10-20% of the predicted theory model under tolerable settlement. The possible influence factors are discussed and a simple suggested correction factor for shaft length is proposed. For the empirical method, the relationships between tip capacity and standard penetration test are directly developed from the measured results.

INTRODUCTION

The tip resistance is an important source of drilled shaft capacity under axial compression loading. Tip resistance is provided by the bearing capacity of the soil beneath the tip. The general solution for ultimate soil bearing capacity (q_{ult}) has been provided and improved by a number of researchers (e.g., Hansen 1970, Vesic 1975, Kulhawy et al. 1983). Later, some authors (e.g., Chen and Kulhawy 2002, Kulhawy and Chen 2003) also examined the effectiveness of general solution of soil bearing capacity using field load test case histories.

In the practice of engineering, the empirical equations related to the results of field tests are also often used to calculate tip resistance. Among these field tests, the N value of standard penetration test (SPT-N) is the most commonly used (e.g., Meyerhof 1976, Reese and O'Neill 1988) in the geotechnical community, owing to its simple and popular geotechnical field test. In general, the design tip resistance is

related to the average SPT-N value by an empirical coefficient.

In this study, a reassessment of the axial tip resistance of drilled shafts was done based on a large amount of field load test data. The possible influence factors are discussed. Furthermore, the suggested correction factor to obtain a more precise prediction of the tip resistance is presented. The empirical correlations of tip resistance and SPT-N value are also established. Specific design recommendations for the use of general solution and empirical equations are then presented.

ANALYSES OF TIP RESISTANCE

Tip resistance in compression is provided by the bearing capacity of the soil beneath the tip and is given by:

$$Q_{tcp} = A_{tip} \cdot q_{ult} \tag{1}$$

in which Q_{tcp} = predicted tip resistance, A_{tip} = shaft tip area and q_{ult} = ultimate bearing capacity. The Terzaghi-Buisman equation was also used for the general solution of q_{ult} (Vesic 1975). The equation is presented below:

$$q_{ult} = cN_c + qN_q + 0.5\gamma BN_\gamma \tag{2}$$

in which c = soil cohesion, γ = soil unit weight, B = shaft diameter, q = vertical stress at shaft tip, and N_c, N_γ, N_q = bearing capacity factors.

Further studies have extended Eq. 2 to actual field conditions, and additional modifiers that include foundation shape (s), depth (d), and rigidity (r) have been introduced by a number of authors (e.g., Hansen 1970, Vesic 1975, Kulhawy et al. 1983). Considering these modifiers for circular shafts, the general form of the bearing capacity equation for undrained compression tip resistance is as follows:

$$q_{ult} = 6.17 s_u \zeta_{cd} \zeta_{cr} + q \tag{3}$$

in which s_u = soil undrained shear strength, ζ_{cd} = modifier of N_c for foundation depth, ζ_{cr} = modifier of N_c for soil rigidity, and q = total vertical stress.

The bearing capacity of drained compression tip resistance is given by:

$$q_{ult} = \bar{q} N_q \zeta_{qs} \zeta_{qd} \zeta_{q\gamma} + 0.3 \bar{\gamma} B N_\gamma \zeta_{\gamma r} \tag{4}$$

in which ζ_{qs}, ζ_{qd}, ζ_{qr} = modifier of N_q for foundation shape, depth, and soil rigidity, respectively, $\zeta_{\gamma r}$ = modifier of N_γ for soil rigidity, and $\bar{q}$ and $\bar{\gamma}$ = effective vertical stress and soil unit weight, respectively. The detailed values of N_γ, N_q, and modifiers are presented elsewhere (Kulhawy 1991).

DATABASE

This study developed a database which included 97 sites with 170 field load tests conducted in a wide variety of soils around the world. Thereafter, these load test data were further divided into drained and undrained soils based on the soil conditions below shaft tip. Among these load test data, 41 sites with 70 tests were undrained soils (cohesive soils), while 56 sites with 100 tests were for drained soils (cohesionless soils). The analysis details for these tests are far too lengthy to list down in this paper. However, they are summarized elsewhere (Fang 2007). All of the selected load tests had almost complete geological data and load-displacement curves, and all tests were conducted on straight-sided drilled shafts.

The L_1-L_2 method, which is a graphical construction method, was adopted to interpret the compression capacity. The related research works (Hirany and Kulhawy 1988, 1989, 2002; Fang 2007) defined that Q_{L2} happens, on average, at 4%B for both drained and undrained soils under compression loading. With the interpreted compression capacity, the measured tip resistance (Q_{tcm}) can be given from the load-distribution curve along shaft length. However, the statistical results (Fang 2007) of tip resistance versus side friction resistance (22% versus 78% at L_2) were also used to infer the Q_{tcm} if the load test report did not present the load-distribution curve. In addition, some load tests were terminated prematurely. For these cases, the research results (Fang 2007) between L_2 and other interpretation criteria from the lower bound to the higher bound were used to infer the required L_2.

The load tests were divided into two groups based on the overall data quality. Group 1 included those cases in which the complete information was reported. Group 2 consisted of all the remaining cases, such as the load-displacement curve, geotechnical parameters, or GWT that were inferred from other sources. For convenience, Table 1 provides a summary of the ranges of foundation geometry, capacity of tip resistance and their coefficient of variation (COV), which is the standard deviation (SD) divided by the mean value. Table 2 lists the statistical data of predicted tip resistance (Q_{tcp}) and measured tip resistance (Q_{tcm}).

Table 1 Range of Axial Compression Load Test Data for Drilled Shafts

Soil type	No. test	Statistical data	Depth, D (m)	Dia., B (m)	D/B	Tip resistance (kN)
Drained	100	Range	4.7~68.5	0.35~2.00	5.1~62.5	36~6100
		Mean	28.4	1.01	28.05	1498
		COV	0.64	0.38	0.51	0.80
Undrained	70	Range	1.8~60.0	0.18~1.80	4.4~60.5	14~4680
		Mean	13.2	0.78	15.24	892
		COV	0.83	0.46	0.31	1.03

Table 2 Statistics of Compression Tip Resistance

Soil type	Statistical data	Group 1	Group 2	All data
Drained	No. test	30	70	100
	Mean Q_{tcm}/Q_{tcp}	0.081	0.098	0.093
	COV	0.52	0.49	0.50
Undrained	No. test	23	47	70
	Mean Q_{tcm}/Q_{tcp}	1.03	0.96	0.99
	COV	0.23	0.28	0.26

COMPARISONS OF BEARING CAPACITY THEORY

Undrained Soils

The undrained Q_{tcp} was calculated using Eqs. 1 and 3, while Q_{tcm} was interpreted using the L_1-L_2 method, as described previously. The statistics in Table 2 show that the predicted and measured tip resistances are reasonably consistent. The mean undrained Q_{tcm}/Q_{tcp} = 0.99 with n = 70 and COV = 0.26. Fig. 1 shows the comparison between Q_{tcm} and Q_{tcp}. The results of the regression analyses are also presented in Fig. 1. It can be seen that, on the overall average, both the predicted and measured results are close to one another. Figs. 2(a) and 2(b) show the relations of Q_{tcm}/Q_{tcp} and shaft tip depth (D) and depth/diameter (D/B), respectively. Based on these available data, the results show a larger scatter of data and larger coefficient of variation if the shaft is shorter. The ratio of Q_{tcm}/Q_{tcp} presents a more consistent value with increasing shaft tip depth. Therefore, Eq. 3 can reasonably predict the undrained tip resistance. However, the prediction uncertainty and COV is larger for shorter shaft or smaller depth/diameter.

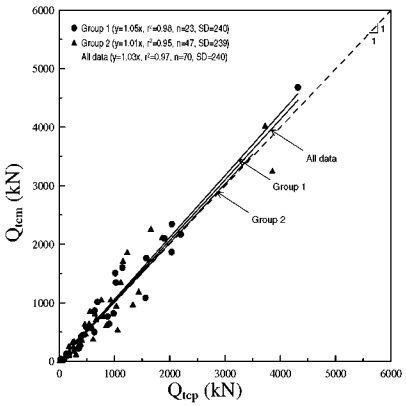

FIG. 1 Comparisons of undrained predicted and measured tip resistances

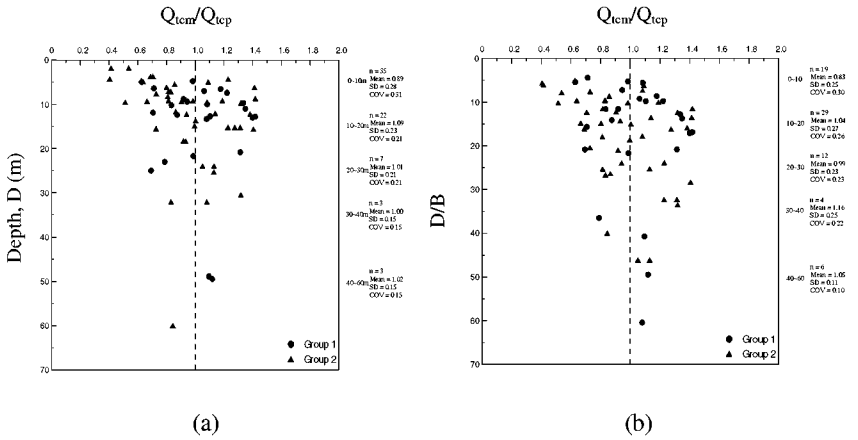

FIG. 2 Undrained Q_{tcm}/Q_{tcp} versus depth and depth/diameter

Drained Soils

Fig. 3 shows the comparisons of predicted and measured tip resistances for drained soils. The drained Q_{tcp} was calculated using Eqs. 1 and 4, while Q_{tcm} was interpreted using the L_1-L_2 method. The statistical results are also listed in Table 2. It can be seen that the measured results are only about 10% of the predicted results. Therefore, the tip resistance of drained soils provides limited resistance under allowable design settlement and the use of Eq. 4 for tip resistance prediction is obviously overestimated. These phenomena indicate that large deformations are needed to mobilize the tip resistance for drained soils, while the undrained soils can fully approach the tip resistance at settlement of L_2 (or 4%B), as described previously.

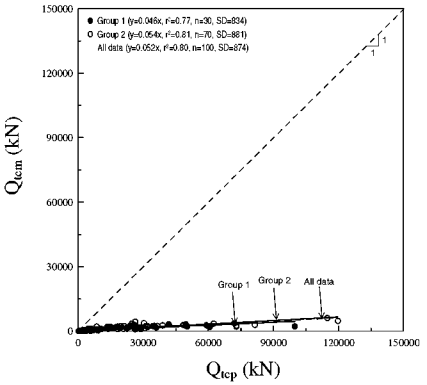

FIG. 3 Comparisons of drained predicted and measured tip resistances

Further analyses were done to observe the possible reasons that may explain the overestimation for the drained prediction model. Table 3 lists the results which consider various conditions of modifiers. These include only individual modifier of shape, depth, and soil rigidity. Neglect of all modifiers was also included in the analysis of Table 3. Based on these analyses, the mean values were between 0.068 and 0.214 for various modifier considerations. These results indicate that no modifier can greatly affect the obvious overestimation of Eq. 4. Therefore, it is highly probable that the basic equation, such as value of $\bar{q}$ and/or N_q, should be improved if the predicted and measured results are to be comparable.

Table 3 Comparisons of Considering Different Modifiers for Drained Soils

Statistical data	Modifier			Neglect all modifiers
	d	s	r	
No. test	100	100	100	100
Mean Q_{tcm}/Q_{tcp}	0.087	0.068	0.214	0.114
COV	0.70	0.76	0.51	0.72

Note: d, s and r express modifier of depth, shape and soil rigidity, respectively.

Fig. 4 demonstrates the relation of Q_{tcm}/Q_{tcp} and depth when the values of Q_{tcp} were calculated only by taking into account the modifiers of shape and rigidity. Although the relation does not present a high coefficient of determination (r^2), it can be seen that the Q_{tcm}/Q_{tcp} appears to be related to depth. The regression relation is given as below:

$$Q_{tcm} / Q_{tcp} = 0.13 - 0.0013D \tag{5}$$

Fig. 5 shows the comparison between Q_{tcm} and Q'_{tcp} after considering the factor of Eq. 5. Four very large values were removed for regression analysis because they greatly impact the results. The data points are scattered although the overall mean value of Q_{tcm}/Q'_{tcp} is close to 1 (n = 100, Mean Q_{tcm}/Q'_{tcp} = 1.00, COV = 0.42).

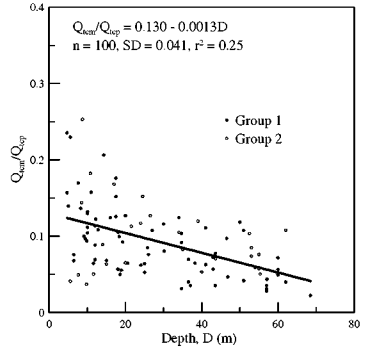

FIG. 4 Q_{tcm}/Q_{tcp} versus shaft depth

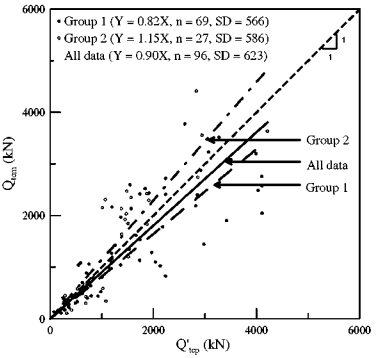

FIG. 5 Comparisons of Q_{tcm} and Q'_{tcp}

SPT-N EMPIRICAL RELATION

Figs. 6(a) and 6(b) show the relationships between measured bearing capacity and SPT-N value. The measured bearing capacity is denoted as q_N, which is back-calculated from Q_{tcm} divided by the tip area (A_{tip}). The average SPT-N value

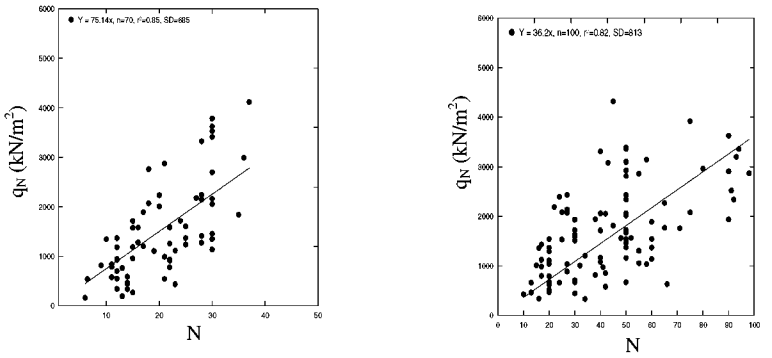

(a) Undrained (b) Drained

FIG. 6 Relations of measured bearing capacity and SPT-N value

was taken below one diameter of the shaft tip. The regression equations are given as follows:

$$q_N = 75.1\text{N kN/m}^2 \quad \text{(for undrained soils)} \quad (6)$$

$$q_N = 36.2\,\text{N kN/m}^2 \quad \text{(for drained soils)} \quad (7)$$

Figs. 6(a) and 6(b) show that the undrained bearing capacity is higher than the drained condition at the same SPT-N value and displacement (4%B). For convenience, the relations can be simplified as $q_N = 75N$ (kN/m^2) or $\fallingdotseq 7.5N$ (t/m^2) for undrained soils and $q_N = 36N$ (kN/m^2) or $\fallingdotseq 3.6N$ (t/m^2) for drained soils. Although the use of an empirical equation is much easier for engineering practice, it is warranted that the standard deviations of these relations are large.

CONCLUSIONS AND RECOMMENDATIONS

Axial field compression load test data were used to evaluate tip resistance. The study used a wide variety of compression load test data and subsequently divided them into the drained and undrained databases. Both bearing capacity theory and SPT-N empirical equation were examined with measured tip resistance. Based on these analyses, the following conclusions were reached for the field compression load test data that were studied.

1. The bearing capacity theory can reasonably predict the undrained tip resistance. The analysis results show that a larger coefficient of variation results if the shaft is shorter.

2. The basic bearing capacity equation cannot be reliably applied to prediction of tip resistance for drained soils under tolerable design settlement.
3. The relations between measured bearing capacity and SPT-N can be simplified as $q_N = 75N$ (kN/m^2) or $\fallingdotseq$ 7.5N (t/m^2) for undrained soils and $q_N = 36N$ (kN/m^2) or $\fallingdotseq$ 3.6N (t/m^2) for drained soils.

ACKNOWLEDGEMENTS

This study was supported by the National Science Council, Taiwan, under contract number: NSC 97-2221-E-033-044-MY2.

REFERENCES

Chen, Y.J. and Kulhawy, F.H. (2002). "Evaluation of Drained Axial Capacity of Drilled Shafts", *Deep Foundations 2002 (GSP 116)*, Ed. MW O'Neill and FC Townsend, ASCE, Reston, 2, 1200-1214.

Fang, Y.C. (2007). "Evaluation of Tip Resistance and Compression Interpretation Criteria for Drilled Shafts", *M.S. Thesis*, Chung Yuan Christian Univ., Taiwan.

Hansen, J.B. (1970). "Revised and Extended Formula for Bearing Capacity", *Bulletin 28*, Danish Geotechnical Institute, Copenhagen, 5-11.

Hirany, A. and Kulhawy, F.H. (1988). "Conduct and Interpretation of Load Tests on Drilled Shaft Foundations: Detailed Guidelines", *Rpt. EL-5915(1)*, Electric Power Research Institute, Palo Alto.

Hirany, A. and Kulhawy, F.H. (1989). "Interpretation of Load Test on Drilled Shafts (1): Axial Compression", *Foundation Engineering: Current Principles and Practices (GSP 22)*, Ed. F.H. Kulhawy, ASCE, New York, 1132-1149.

Hirany, A. and Kulhawy, F.H. (2002). "On the Interpretation of Drilled Foundation Load Test Results", *Deep Foundations (GSP 116)*, Ed. M.W. O'Neill and F.C. Townsend, ASCE, Reston, 2, 1018-1028.

Kulhawy, F.H. and Chen, Y.J. (2003). "Evaluation of Undrained Side and Tip Resistances for Drilled Shafts", *Soil & Rock America 2003, Proc.*, 12th Pan-Am Conf. Soil Mech. & Geotech. Eng. / 39th US Rock Mech. Symp.), Ed. P.J. Culligan, H.H. Einstein & A.J. Whittle, Cambridge (MA), 1963-1968.

Kulhawy, F.H., O'Rourke, T.D., Stewart, J.P., and Beech, J.F. (1983). "Transmission Line Structure Foundations for Uplift-Compression Loading", *Rpt. EL-3160*, Electric Power Research Institute, Palo Alto.

Meyerhof, G.G. (1976). "Bearing Capacity and Settlement of Pile Foundation", *Journal of the Geotechnical Eng. Div.*, ASCE, 102(GT3), 195~227.

Reese, L.C. and O'Neill, M.W. (1988). Drilled Shafts: Construction Procedures and Design Methods, *Report FHWA-HI-88-042*, Federal Highway Administration, McLean.

Vesic, A.S. (1975). "Bearing Capacity of Shallow Foundation", *Chap. 3 in Foundation Engineering Handbook*, Van Nostrand Reinhold, New York, 121-147.

Copyrighted Materials
Copyright © 2009 American Society of Civil Engineers (ASCE)
Retrieved from www.knovel.com

Evaluation of Side Resistance of Drilled Shafts in Multilayered Soils

Yit-Jin Chen[1], Hsin-Wen Chang[2] and Ting-Jui Chiu[3]

[1] Associate Professor, Department of Civil Engineering, Chung Yuan Christian University, Chung-Li 32023, Taiwan; yjc@cycu.edu.tw
[2] Senior Engineer, Asia World Engineering & Construction Co., 7F-1, No. 81, Sec. 1, Shin Tai Wu Rd., Hsichih, Taipei County 22101, Taiwan; swen@awec.com.tw
[3] Graduate Student, Department of Civil Engineering, Chung Yuan Christian University, Chung-Li 32023, Taiwan; g9672006@cycu.edu.tw

ABSTRACT

This paper evaluates the behavior of the side resistance of drilled shafts constructed on the interlayer of drained and undrained soils. A wide variety of uplift and compression load test data are used for evaluation and all data have multilayered soils along shaft length. Two analysis models, including complete β method (β model) and hybrid of α and β method (α-β model), are applied to these load test data to compare the side resistance from the measurement results. Based on these analyses, the results show that the prediction of α-β model presents better statistical results than the β model. Moreover, the mean ratio of measured side resistance/predicted side resistance of uplift loading is smaller than that of compression loading for both models and the difference is about 10-20 percents. Both analysis models also become less reliable at the shorter shafts.

INTRODUCTION

Side resistance is an important source of drilled shaft capacity under axial loading, especially when the shaft is under the condition of longer or uplift loading. Based on soil conditions, the analysis methods for side resistance consist of total stress analysis and effective stress analysis. These analysis methods can be further briefly specified into the alpha (α), beta (β), and lambda (λ) methods. In general, the α method is suitable for undrained soils (or cohesive soils) and the β method is more suitable for drained soils (or cohesionless soils), while the λ method may obtain less reliable results (Kulhawy et al. 1983; Chang 2007).

The α method is a conventional total stress analysis for the side resistance of drilled shaft foundations with cohesive soils. The design side resistance is related to the average soil undrained shear strength (s_u) by an empirical coefficient denoted as α, the adhesion factor, as given by:

$$Q_s(\alpha) = \alpha \pi B \int_0^D s_u(z)\, dz \tag{1}$$

in which Q_s = side resistance, B = shaft diameter, D = shaft length, and z = depth. The original α (Tomlinson 1957) was based on empirical correlations with mean s_u over the foundation depth, using primarily driven pile data. The research by Stas and Kulhawy (1984) showed that the α method is meaningful for drilled shafts. They developed the correlation of α versus s_u for the drilled shaft design, but the s_u value in their analysis was taken from any test type. Later, Chen and Kulhawy (1994, 2003) improved the correlation using more consistent undrained shear strength tests. They adopted the consolidated-isotropically undrained triaxial compression (CIUC) test as a "unique" s_u test type for analysis. The more consistent results of α versus s_u [denoted as α_{CIUC}-s_u(CIUC)] for drilled shafts are shown in Fig. 1 and given as below for all data:

$$\alpha_{CIUC} = 0.30 + 0.17/[s_u(CIUC)/p_a] \tag{2}$$

in which p_a is one atmospheric stress (= 101.3 kN/m^2). As shown in Fig. 1, the difference among all data, uplift, and compression is relatively small, so Eq. 2. can be also applicable to both uplift and compression loading.

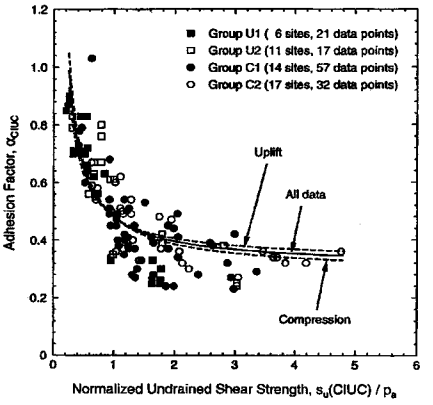

FIG. 1 α_{CIUC}-s_u(CIUC) correlation (Chen and Kulhawy 1994, 2003)

The β method is a representative effective stress analysis which considers the frictional resistance for the soil-shaft interface. The design side resistance is a function of horizontal effective stress ($\bar{\sigma}_{ho} = K\bar{\sigma}_{vo}$, $\bar{\sigma}_{vo}$ = vertical effective stress), effective stress friction angle (δ) for the soil-shaft interface, and shaft geometry, as given by:

$$Q_s(\beta) = \pi B \int_0^D \bar{\sigma}_{ho}(z) \tan\delta(z) dz = \pi B \left(\frac{K}{K_o}\right) \int_0^D \bar{\sigma}_v(z)\, K_o(z) \tan\left[\bar{\phi}(z) \cdot \frac{\delta}{\bar{\phi}}\right] dz \tag{3}$$

Kulhawy et al. (1983) examined the operative horizontal stress coefficient (K) using

field load test data and showed that the stress factor (K/K_o) is generally less than 1 and is dependent on the construction method and its influence on the in-situ stress. They also suggested that the ratio of interface friction angle (δ) to soil friction angle ($\bar{\phi}$) is equal to 1 for drilled shafts. Subsequent examinations by Chen and Kulhawy (1994, 2002) showed that the stress factor by Kulhawy et al. was underestimated and they proposed that the stress factor should essentially be 1 for properly constructed shafts regardless of construction methods. Recently, Chang (2007) back-calculated a large amount of load test data and further suggested that the values of K/K_o are 0.73, 0.97, and 1.03 for slurry, casing, and dry construction, respectively for drained soils, while the suggested values are 0.79, 0.88, and 1.12 for slurry, casing, and dry construction, respectively, for undrained soils. Moreover, the results of Chang's study also showed that the ratio of measured β/predicted β (β_m/β_p) is less reliable when the shaft is short, as shown in Fig. 2.

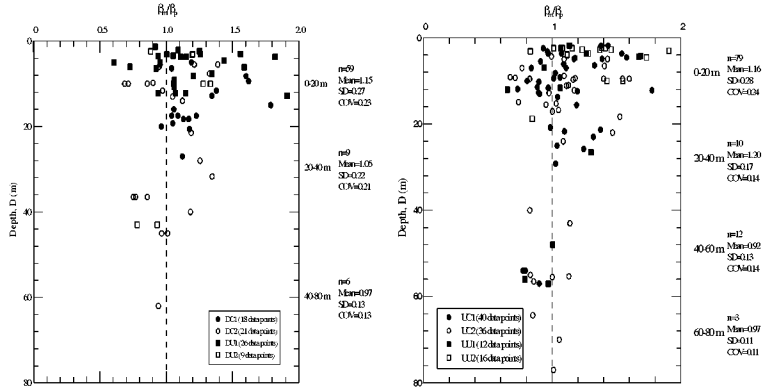

(a) Drained soils (b) Undrained soils

FIG. 2 Comparisons of β_m/β_p versus shaft depth (Chang 2007)

Although various research efforts on the behavior of drained and undrained side resistances have substantially progressed in the previous decades, it is worth discussing the subject for shafts constructed on the interlayer of drained and undrained soils. In this paper, the analysis methods were examined using a large amount of load test data. Thereafter, the relative merits and reliability of these methods are established. Likewise, specific drilled shaft design recommendations for the analysis of side resistance with multilayered soils are given in this paper.

DATABASE

The database developed for this study included 27 sites with 64 field load tests conducted in a wide variety of multilayered soil profiles. Among these load test data, 8 sites with 9 tests were for uplift loading, while 19 sites with 55 tests were for compression loading. These load tests were not sufficient to identify the dominant soil types because the contents of both soil types occupy between 30 and 70

percentages. All of the selected load tests had almost complete geological data and load-displacement curves. In addition, all tests were conducted on straight-sided drilled shafts.

The L_1-L_2 method (Hirany and Kulhawy 1988, 1989a, 1989b, 2002), which is a graphical construction method, was adopted to define the capacity in both uplift and compression. The updated research works by Chen and colleagues (Chang 2007; Fang 2007; Chen et al. 2008) defined that Q_{L2} happens, on the average, at 10.6 mm (for drained soils) and 12.1 mm (for undrained soils) under uplift loading, while it occurs at 4%B for both drained and undrained soils under compression loading. They also developed the relationships between L_2 and other interpretation criteria from the lower bound to the higher bound. Therefore, these interrelationships among interpretation criteria were also used to infer the required L_2 if the load test data were insufficient or were terminated prematurely.

The load test database mainly covers Asia (Taiwan, Thailand, and Singapore) and the USA at different time periods. Analysis details for these tests are far lengthy to list down in this paper. Nonetheless, they are summarized elsewhere (Chang 2007). For convenience, the ranges of foundation geometry, capacity of side resistance, and their coefficient of variation (COV), which is the standard deviation (SD) divided by the mean value, are summarized in Table 1. Evidently, the range of geometry is broad. However, the shaft dimension and capacity for the compression load test data are larger than the uplift load test data.

Table 1 Range of Geometry and Capacity of Drilled Shafts for Analysis

Loading type[a]	No. test		Shaft geometry (m)		D/B	Capacity of side resistance[b] (kN)
			Depth, D	Dia, B		
U	9	Range	3.1 – 47	0.46 - 1.80	3.3 – 53.3	463 – 10052
		Mean	29.82	0.96	34.10	4025
		COV	0.48	0.49	0.49	0.95
C	55	Range	4.7 – 72	0.46 – 1.8	5.1 – 62.5	1120–32200
		Mean	35.54	1.07	32.82	8383
		COV	0.55	0.29	0.52	0.68

a– u : uplift; c : compression

b– Capacity of side resistance was interpreted from L_2 method.

COMPARISONS OF ANALYSIS RESULTS

Two analytical models can be used for the analysis of side resistance of multilayered soils. One is the hybrid of the α and the β method (denoted as α-β model), that is the α method (Eqs. 1 and 2) for undrained soils and the β method (Eq. 3. and Chang's conclusions) for drained soils. The other model uses a complete β method (denoted as β model) for both drained and undrained soils. Table 2 lists the

analysis results for α-β and β models under uplift and compression loading. The mean ratio of measured side resistance/predicted side resistance (Q_{sm}/Q_{sp}) and their statistics data are all presented herein to describe the quality of these comparisons.

Table 2 Analysis Results of α-β and β Models

Model	Loading type[a]	Statistics[b] of Q_{sm}/Q_{sp}				Regression analysis[c]			
		Mean	n	SD	COV	Equation	n	r^2	SD (kN)
α–β	U	0.91	9	0.25	0.28	$Q_{sm} = 0.79\ Q_{sp}$	9	0.92	1400
	C	1.10	55	0.42	0.38	$Q_{sm} = 0.90\ Q_{sp}$	55	0.90	3376
	U+C	1.07	64	0.41	0.38	$Q_{sm} = 0.90\ Q_{sp}$	64	0.90	3178
β	U	1.27	9	0.50	0.39	$Q_{sm} = 0.79\ Q_{sp}$	9	0.89	1867
	C	1.38	55	0.55	0.40	$Q_{sm} = 0.94 Q_{sp}$	55	0.83	4914
	U+C	1.36	64	0.54	0.40	$Q_{sm} = 0.93\ Q_{sp}$	64	0.84	4519

a– u : uplift, c : compression
b– n = data points, SD = standard deviation, COV = coef. of variation.
c– n = data points, r^2 = coef. of determination, SD = standard deviation.

Analytical Model Factor

Table 2 shows that the mean Q_{sm}/Q_{sp} = 1.07 with n = 64, SD = 0.41, and COV = 0.38 for α-β model, while the mean Q_{sm}/Q_{sp} = 1.36 with n =64, SD = 0.54, and COV = 0.40 for β model. It can be seen that the α-β model presents better results for both prediction and reliability. On the average, the predicted results of the hybrid method are reasonably close to the measured results, while the predicted capacity of complete β method has about 40% underestimation. The possible reason behind the abovementioned results may be due to the reliability of the original analysis equations. A comparison of Figs. 1 and 2 shows that the use of the α method (Fig. 1) presents more reliable results than the β method (Fig. 2). Therefore, the use of the α-β model for multilayered soils can obtain better results than the use of the complete β model.

In addition, the predicted capacity for both analysis models is all underestimation. This can also be observed from Fig. 2, which shows that the measured β (β_m), on average, is larger than the predicted β (β_p). Therefore, this results in the underestimation of both models for multilayered soils because the analysis results of Fig. 2 was used for this study.

Figs. 3 and 4 show the comparisons of measured and predicted results for α-β model and β model, respectively. The regression analysis data are listed in Table 2. It seems like that both analytical models are less reliable when the capacity is larger than 10,000 kN.

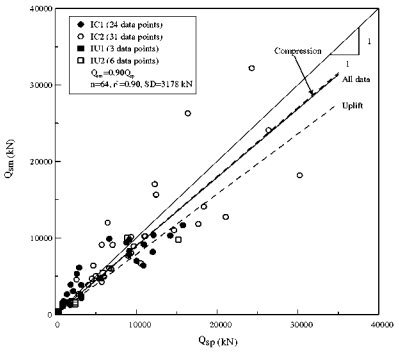

FIG. 3 Comparisons of measured and predicted results (α-β model)

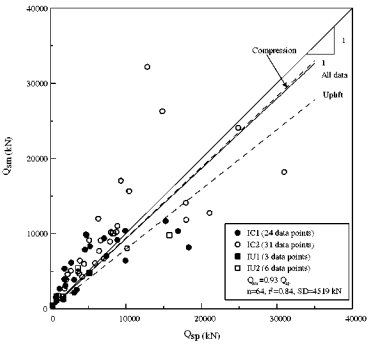

FIG. 4 Comparisons of measured and predicted results (β model)

Loading Factor

Table 2 also lists both mathematical statistics and regression analysis data for different loading types. Based on the data analyses, it is obvious that the mean Q_{sm}/Q_{sp} of uplift loading is smaller than that of compression loading for both α-β and β models. They have a difference of about 10-20 percents. There are some possible reasons that may explain this difference, such as the factors of the shaft capacity interpretation, Poisson's effect, and so on. However, the difference is relatively small and more load test data may be needed for further verification because this study only used a few uplift load test data.

Depth Factor

Figs. 5 and 6 demonstrate the relationship between the ratio of Q_{sm}/Q_{sp} and depth for α-β model and β model, respectively. The statistical data for various depth intervals is also shown in figures. First, the statistical results show that a larger coefficient of variation if the shaft is shorter. The ratio of Q_{sm}/Q_{sp} presents a more consistent value as the shaft depth increases. For the α-β model, the ratio is between 0.6-2.2 for shaft less than 20 m. The mean ratio is 1.34 with SD = 0.51 and COV = 0.37. The mean measured result is larger than the mean predicted result about one third. The mean ratio becomes between 0.5-1.8 with mean = 0.97, SD = 0.32, and COV = 0.33 for shaft longer than 20 m. It is obvious that, on the average, the measured capacity is similar to the predicted capacity. These results are consistent with previous studies (Chang 2007) for dominant drained or undrained soils, which showed that the longer of the shaft, the measured and predicted results becomes more consistent.

A same trend can be found in the β model. The mean ratio is between 0.7-3.0 for shafts less than 20 m. The mean Q_{sm}/Q_{sp} ratio is 1.67 with SD = 0.64 and COV = 0.38. The mean measured result is larger than the mean predicted result about two

thirds. The mean ratio becomes between 0.5-2.2 with mean = 1.26, SD = 0.47, and COV = 0.38 for shaft longer than 20 m. It is obvious that, on average, the measured capacity is still larger than the predicted capacity.

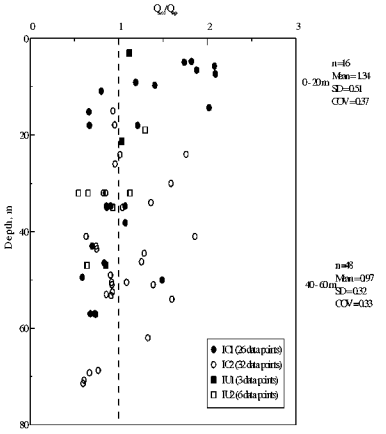

FIG. 5 Q_{sm}/Q_{sp} versus shaft depth for α-β model

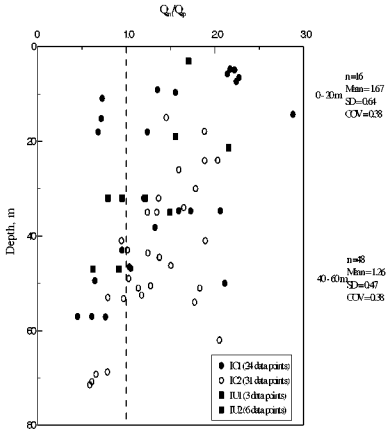

FIG. 6 Q_{sm}/Q_{sp} versus shaft depth for β model

A comparison of Figs. 5 and 6 also indicates that the overall data consistence of α-β model is somehow superior to the β model. The phenomenon is consistent with the statistical results.

CONCLUSIONS AND RECOMMENDATIONS

Axial field load test data were used to evaluate side resistance for straight-sided drilled shafts. They were constructed on the interlayer of drained and undrained soils. The database was wide for shaft geometry, and representative analysis models were used for evaluation. Based on these analyses, the following preliminary conclusions were obtained.

1. The α-β model presents better results for both prediction and reliability than the β model. On the average, the predicted results of hybrid method are reasonably close to the measured results.
2. The predicted capacity for both the α-β and the β models is underestimated.
3. The mean Q_{sm}/Q_{sp} of uplift loading is smaller than that of compression loading for both α-β and β models. The difference is about 10-20 percents.
4. The analyses show that the shorter of the shaft, the larger of the coefficient of variation. The ratio of Q_{sm}/Q_{sp} presents a more consistent value as the shaft depth increases.
5. It is suggested that further analysis can be performed based on localized database, specific size, length, or capacity of drilled shafts, etc. when more load test data are established.

ACKNOWLEDGEMENTS

This study was supported by the National Science Council, Taiwan, under contract number: NSC 97-2221-E-033-044-MY2.

REFERENCES

Chang, H.W. (2007). "Evaluation of Side Resistance and Uplift Interpretation Criteria for Drilled Shafts", *M.S. Thesis*, Chung Yuan Christian Univ., Taiwan.

Chen, Y.J., Chang, H.W., and Kulhawy, F.H. (2008). "Evaluation of Uplift Interpretation Criteria for Drilled Shaft Capacity", *J. of Geotech. and Geoenvironmental Eng.*, ASCE, 134, 10, 1459-1468.

Chen, Y.J. and Kulhawy, F.H. (1994). "Case History Evaluation of Behavior of Drilled Shafts under Axial and Lateral Loading", *Rpt. TR-104601,* Electric Power Research Institute, Palo Alto.

Chen, Y.J. and Kulhawy, F.H. (2002). "Evaluation of Drained Axial Capacity of Drilled Shafts", *Deep Foundations 2002 (GSP 116)*, Ed. M.W. O'Neill and F.C. Townsend, ASCE, Reston, 2, 1200-1214.

Fang, Y.C. (2007). "Evaluation of Tip Resistance and Compression Interpretation Criteria for Drilled Shafts", *M.S. Thesis*, Chung Yuan Christian Univ., Taiwan.

Hirany, A and Kulhawy, F.H. (1988). "Conduct and Interpretation of Load Tests on Drilled Shaft Foundations: Detailed Guidelines", *Rpt. EL-5915(1),* Electric Power Research Institute, Palo Alto.

Hirany, A. and Kulhawy, F.H. (1989a). "Interpretation of Load Test on Drilled Shafts (2): Axial Uplift", *Foundation. Engineering: Current Principles & Practices (GSP 22),* Ed. FH Kulhawy, ASCE, New York, 1150-1159.

Hirany, A and Kulhawy, FH (1989b). "Interpretation of Load Test on Drilled Shafts (1): Axial Compression", *Foundation. Engineering: Current Principles & Practices (GSP 22),* Ed. FH Kulhawy, ASCE, New York, 1132-1149.

Hirany, A and Kulhawy, FH (2002). "On the Interpretation of Drilled Foundation Load Test Results", *Deep Foundations (GSP 116)*, Ed. MW O'Neill and FC Townsend, ASCE, Reston, 2, 1018-1028.

Kulhawy, FH and Chen, Y.J. (2003). "Evaluation of Undrained Side and Tip Resistances for Drilled Shafts", *Soil & Rock America 2003, Proc.,* 12th Pan-Am Conf. Soil Mech. & Geotech. Eng. / 39th US Rock Mech. Symp.), Ed. PJ Culligan, HH Einstein & AJ Whittle, Cambridge (MA), 1963-1968.

Kulhawy, FH, O'Rourke, TD, Stewart, JP, and Beech, JF (1983). "Transmission Line Structure Foundations for Uplift-Compression Loading", *Rpt. EL-3160,* Electric Power Research Institute, Palo Alto.

Copyrighted Materials
Copyright © 2009 American Society of Civil Engineers (ASCE)
Retrieved from www.knovel.com

Prediction and Measurement of Pile Loads and Settlement at the Thames River Bridge

By Frederick C. Rhyner[1], P.E., M. ASCE, Ira Beer[1], P.E., M. ASCE, T. C. Michael Law[1], P.E. and Asher Peltz[1], E.I.T., A.M. ASCE

[1]Mueser Rutledge Consulting Engineers, 225 W. 34th Street, New York, NY 10122; f.rhyner@mrce.com; ibeer@mrce.com; mlaw@mrce.com; apeltz@mrce.com

ABSTRACT

During retrofit construction, an unexpected settlement and creep problem prompted a prediction of the estimated settlements and pile loads for the Amtrak railroad bridge over the Thames River in Connecticut. When the piles for the retrofit were installed, one pier abruptly settled and tilted 1.5 inches (38 mm) and then continued to creep month after month. These settlements were of great concern to the safe operation of the existing bascule span, which remained in service during construction. The instrumentation program consisted of optical surveying, tiltmeters, and inclinometers. These instrumentation systems provided remarkably consistent data and proved invaluable to understanding the nature of movement of this complex structure. The writers used 2-D and 3-D finite element models to predict the settlement and tilt of the caisson and the pile reactions. Remedial grouting arrested the creep movement. This paper describes the analysis of these unusual foundation conditions, compares the predicted settlements and loads to the observed values, and describes the effects of ambient air and water temperatures.

INTRODUCTION

The moveable bridge carrying the Amtrak railroad over the Thames River in Connecticut was constructed in 1918. It is a five span bridge, approximately 1,387 feet long (423 m) and carries two tracks, although the substructure was made wide enough to carry four tracks. The center span was a 188 ft. long (57 m) Strauss bascule. The clever design for the retrofit replaced the bascule with a lift span using a strategy to widen the piers and construct the lift-span towers while the tracks and bascule remained in full service. The towers supporting the new lift span were constructed outboard of the existing truss. (See Figure 1.)

The 1918 foundations were timber crib caissons filled with tremie concrete. The Pier 2 caisson supported the pivot works and was 40 feet wide by 99 feet long (12.2 x 30.2 m). Pier 3 supported the rest pier. Because only two of the four tracks had been

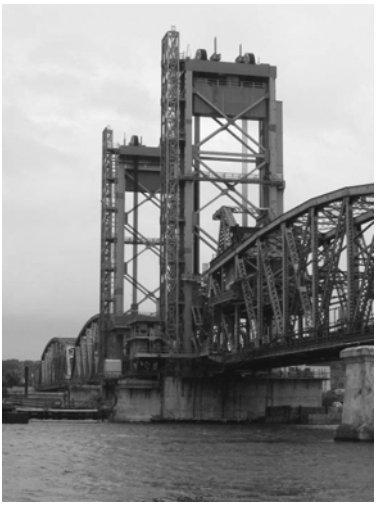

FIG. 1 New lift span towers were constructed outboard of existing truss structure.

FIG.2 Rendering showing arrangement of new piles, the 1918 caisson and stratigraphy (courtesy HNTB Corp.)

constructed, both piers had large load eccentricities toward the south. The caissons extended approximately 130 feet (40 m) below water, through organic silt and were founded on coarse to fine sand and gravel with trace silt, cobbles and boulders. The sand and gravel was 30 to 40 feet (9 to 12 m) thick and erratic in density, from loose to very dense. Underlying this stratum was a 10 foot (3 m) thick layer of boulders and cobbles, in turn underlain by gneissic-schist bedrock. The new design called for extending Piers 2 and 3 to the south by 24 feet (7.3 m). (See Figure 2.)

INITIAL PILE INSTALLATION & SETTLEMENT PROBLEM

The four piles supporting the extension were approximately 180 feet long by 36 inch diameter (55 m by 914 mm) open-end steel pipe piles. The piles were drilled into place to minimize vibrations because they were only 20 feet (6 m) from the existing caisson. When the piles advanced below the bearing level of the caisson, Pier 2 began to settle and tilt. After drilling the piles to the top of rock, the top of the caisson had tipped approximately one-half inch to the south. The piles were driven home using a 300,000 foot-pound drop hammer (407 kN-m). PDA testing verified an ultimate pile capacity of 1,000 tons (8,900 kN). During the two days of PDA testing, it moved an additional inch to the south and continued creeping thereafter, but at a slower rate. Once the rapid movement was realized, construction immediately stopped. The tilting of the caisson impeded the opening and closing of the bascule span. Amtrak was concerned that the subsequent construction activities would cause further settlement and tilt; not only preventing the operation of the bascule span, but

also jeopardizing the new lift span. Amtrak engaged the writers at this time to: first, design an instrumentation system to better understand the pier movements; second, predict the settlement, tilt and pile reactions for the remaining construction; and finally, design a remedial permeation grouting program of the subsoils to arrest the movement.

INSTRUMENTATION SYSTEMS

Prior to the settlement problem, instrumentation consisted of eight optical prisms and two benchmarks on opposite shorelines. Surveyors took multiple readings throughout each day on each prism in order to establish baseline conditions prior to construction work. The resolution of the surveying data was 0.1 inch (2.5 mm).

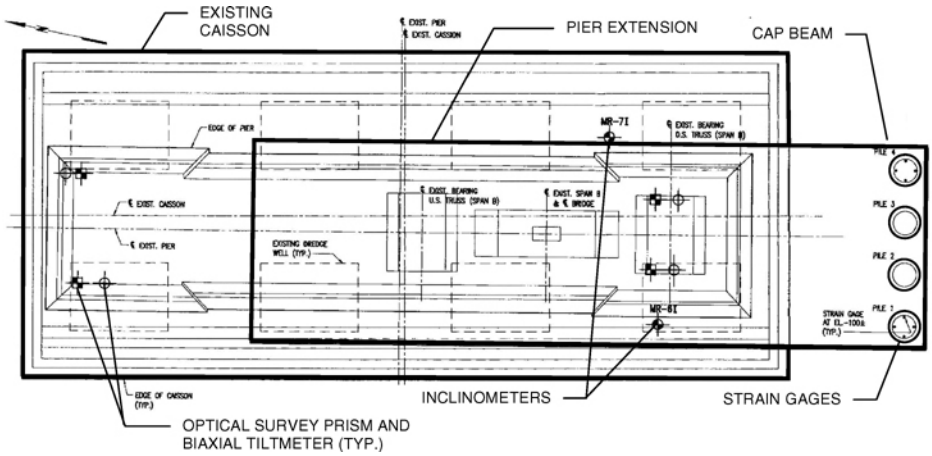

FIG. 3 Instrument Location Plan for Pier 2 (Plan View)

After the settlement problem, two other systems were installed: tiltmeters and inclinometers. (See Fig. 3.) Eight bi-axial tiltmeters were installed to provide a check on the surveying data and obtain better accuracy. A data logger automatically obtained a reading every 15 minutes, which was necessary because there tended to be many unexplained spikes in the data. Only by having a large data set did the unusual spikes become apparent and they were set aside as bad data points, rather than real movement of the structure. Fig. 4 shows a plot of tiltmeter data with relevant construction activities. Two slope inclinometers were installed in Pier 2 and extended to rock. The inclinometers showed that the pier was tilting as a rigid body. (See Figure 5.) The inclinometers also showed that the seat of the movement was in the sand and gravel stratum. After a month of inclinometer data, an apparent bowl-shaped failure surface was evident extending nearly the full depth of the sand and gravel stratum. This information confirmed the need for the grouting program and

targeted the required improvement to the sand and gravel stratum at the south ends of the two piers.

ANALYSES OF PILE LOADS AND SETTLEMENT PREDICTIONS

The writers used 3-D RISA and 2-D PLAXIS models to predict the foundation movements and pile reactions. The foundation is complex in that the distribution of load between the caisson and piles depends to a great degree on the stiffness of the sand and gravel stratum beneath the caisson. (See Fig. 6.) If this stratum were infinitely stiff, the piles would support the weight of half the cap beam and no load from the towers. The sand, however, is compressible and some portion of the load

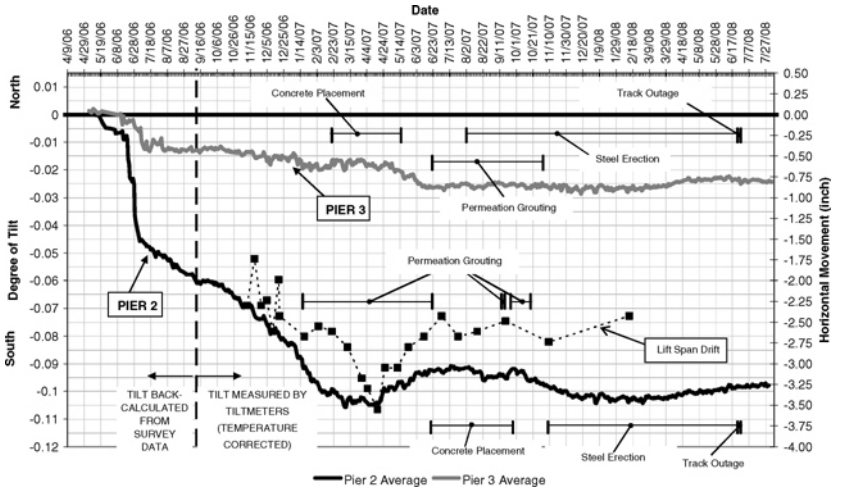

FIG. 4 Piers 2 and 3 Movement Measured by Tiltmeters

from the towers transfers through the cap beam to the piles. At Pier 2 we were concerned that if the creep could not be arrested, that not only the new loads, but also the weight of the existing caisson (approximately 70,000 kips or 311,000 kN) would transfer to the piles, because they would be propping up the end of the pier.

We assumed a range of modulus for the sand and gravel stratum from 850 to 1,700 kips per square foot (40,000 to 80,000 kPa), representing medium-dense to very-dense sand. We even conducted a full-scale load test to measure the modulus by arranging for a fully-loaded quarry train to stop on the bridge while surveyors measured the prisms and tiltmeter readings were obtained. However, no discernable change in settlement or tilt occurred, indicating that the sands had long-since been pre-compressed and were not cycling with the live load each time a train crossed the bridge. The writers also analyzed the post-grouted sands.

The new concrete extension weighed 4,600 kips (20,500 kN) and the lift span towers weighed 4,900 kips (21,800 kN) at Pier 2. Because no new concrete was

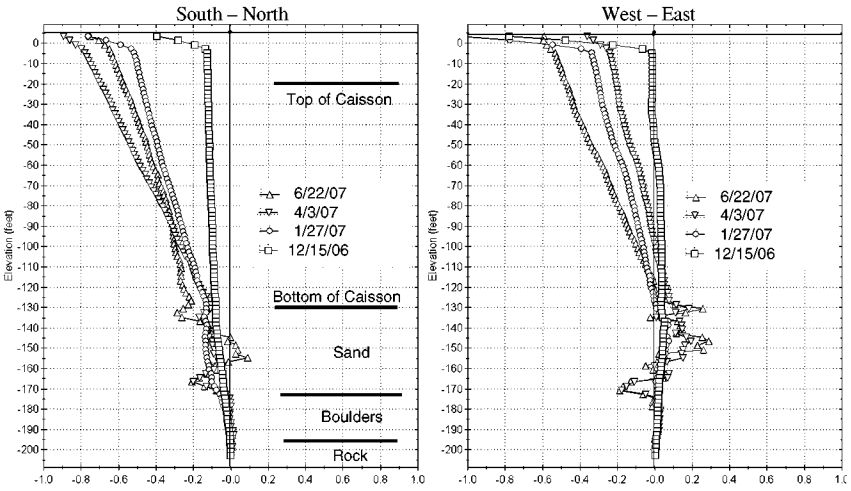

FIG. 5 Pier 2 Cumulative Displacement in Inches Measured by Inclinometer (Boring No. MR-6I)

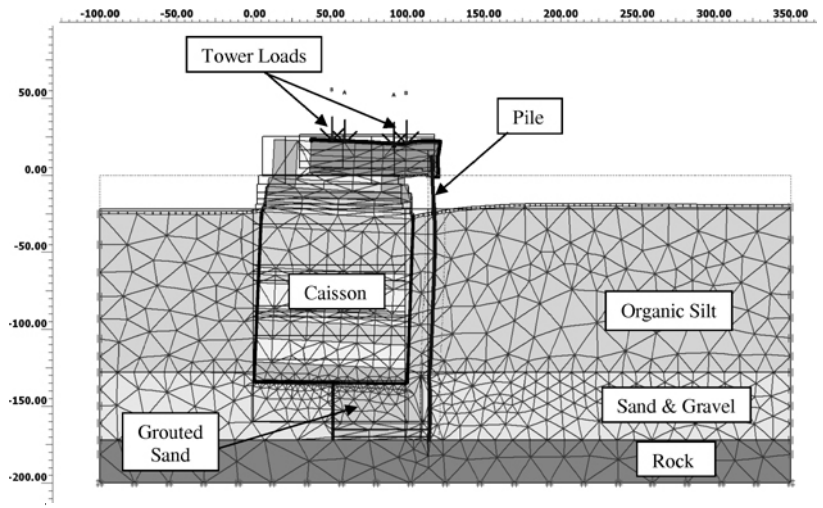

FIG. 6 Finite Element Analysis Result for Pier 2 Showing Typical Deformed Shape (Exaggerated 100 times)

added at the northern end of the piers, the new loads further contributed to the eccentric loading. The new loads increased the foundation bearing stress by 14 percent, from 7 to 8 tons per square foot (670 to 770 kPa), which is a high bearing

pressure for medium dense sand even considering the embedment depth and large size of footing. The writers suspected that the high bearing pressure contributed to the creep problem. The estimated movement and pile reactions were predicted at each of 11 stages of construction, so that the monitoring could be compared to the predicted values as construction proceeded. The predicted pile reactions ranged from 1,100 kips (4,890 kN) for the medium-dense sand model to 800 kips (3,560 kN) for the dense sand model to 500 kips (2,230 kN) for the grouted sand model.

GROUTING

The third task authorized by Amtrak was a remedial grouting program, described in detail by Kaeck, et al (2009). Briefly, the permeation grouting program utilized microfine cement grout, at water to cement ratios ranging from 2:1 to 4:1 (by weight) and targeted the 40 feet (12 m) thick sand and gravel stratum. Grouting was performed with tube-a-manchettes and gage pressures of a few hundred psi to overcome the large line losses. Grout takes were generally high, even on the secondary holes, and the total grout pumped under Pier 2 was more than 600,000 gallons (2,271,000 liters). Microfine cement grout has a long set time, about one month. Consequently, Pier 2 continued to creep for almost two months after the start of the grouting program. Eventually, enough grout was placed and enough time elapsed for the grout to gain strength and the pier stopped moving.

COMPARISON OF PREDICTED AND ACTUAL MOVEMENTS

The writers maintained daily plots for the tiltmeters and prisms and weekly plots for the inclinometers. Day to day, the data showed small movement in sometimes unexplained, haphazard fashion. By studying the data over long periods of time, trends in the data became apparent and led to interpretations of the movement of the pier. Also, comparing the data to the ambient air and water temperature led to new insights about the movement of pier.

Figure 7 shows the actual and predicted movement at Pier 2. The horizontal movement was calculated from the tiltmeter data assuming that the caisson tilted as a rigid body and did not translate at the base. The 1.5 inches (38 mm) of movement during pile installation is obvious in June 2006 (See Fig. 4). Afterwards, the pier moved at an average rate of ¼ inch (6 mm) per month for 7-1/2 months. As a result of grouting, the creep slowed beginning in mid-February 2007 and essentially stopped by April 18, 2007. From then until April 26, 2007, the tiltmeters showed an unexpected reversal of movement with the pier tilting to the north. The writers believe that the northward tilt was due to high grout pressures acting on the base of the south end of the caisson, which caused it to move upwards.

In June 2007, the contractor began placing concrete, thus adding new load for the first time. In response, Pier 2 again began tilting to the south. The observed tilt generally followed the prediction for the grouted sand model, but was less than the predicted tilt for the dense sand case. The predicted horizontal tilt to the south was 0.25 inches (6 mm) for the grouted sand case. The actual measured value was 0.2 inches (5 mm).

COMPARISON OF PREDICTED AND ACTUAL PILE LOADS

Four strain gages were installed in Pile 4 at Pier 2 (see Fig. 3). All four gages were placed at the same elevation on sister bars and the pile was grouted. The elastic modulus of the pile grout (not the same as the microfine cement grout) was measured in the laboratory during the testing of the grout specimens. The tested specimens showed a modulus between 2,400 and 2,600 ksi (16,600 and 17,900 MPa) at 28 days. We used the measured modulus as a lower bound and assumed a value 50% higher for the upper bound.

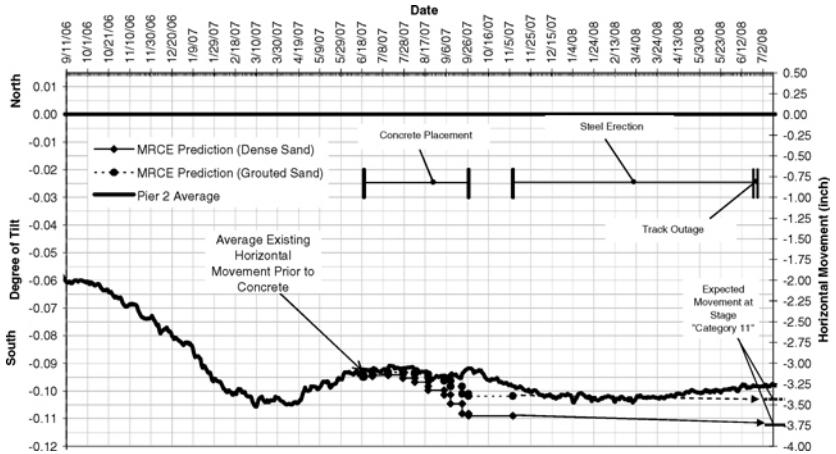

FIG. 7 Comparison of Predicted and Measured Tilt at Pier 2

Figure 8 shows the measured load in Pile 4 and compares it to the predicted load at each stage of construction. Initially, the measured load corresponded well with the predictions. Later, the strain gage readings in Pile 4 began to drop indicating that the load in the pile was decreasing with time. By the end of the 2007, the load in the pile had bled away to almost nothing. When a plot of the strain readings were overlaid with the change in daily water temperature, it became clear that the strain readings were being affected by the change in the water temperature. But, the location of the gages, 85 feet (26 m) below the river bottom, ruled out the possibility that the gage itself was experiencing these changes in temperature.

The writers reasoned that the temperature of the top 20 feet (6 m) of the piles (the portion above the mudline) changes with the water temperature. Due to its massive size, only the exterior faces of the caisson fluctuate in temperature, the majority of its volume remaining unchanged at the temperature of the soil below the river. The cooling of the piles above the waterline causes the piles to contract as the temperature drops. The contraction of the pile causes the pile to shrink away from the giant concrete cap beam. The stiffness of the grouted sand beneath the caisson prevents the bridge pier and cap beam from settling as the pile contracts. Thus the load transfers from the piles back to the caisson. As the water heats up and the pile expands again

and it picks up the load once again, as shown during the spring and summer months. The thermal effect reduced the actual loads in the piles and increased the bearing stresses under the caisson. Fortunately, the magnitude of the bearing stress increase was well within the capacity of the grouted sands.

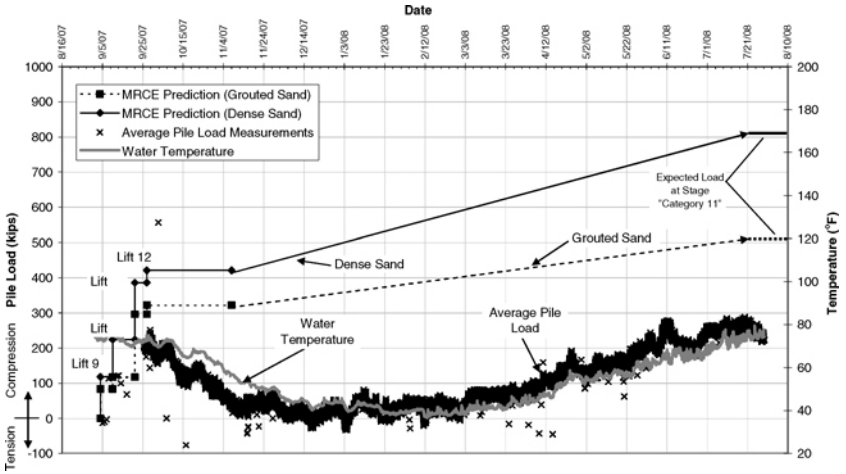

FIG. 8 Comparison of Predicted and Measured Loads in Pile 4

CONCLUSIONS

Installation of piles near existing foundations has risks. Although the contractor used adequate safeguards, it is believed that loss of ground during drilling and vibrations during the PDA tests contributed to the initial settlement at Pier 2. The relatively high bearing pressures at the base of the caisson probably contributed to the long creep thereafter. Permeation grouting halted the creep. Multiple instrumentation systems were necessary to understand the behavior of the structure. Although surveying prisms were helpful, tiltmeters provided better resolution. Inclinometers provided the only means to confirm that the caisson itself had not ruptured and that the seat of the movement was a deep, creep-like failure in the sand and gravel stratum. Finite element methods were useful to diagnose the indeterminate foundation reactions and load sharing between the caisson and the piles. Two different programs and soil models were used to provide a check on each other. Ambient air and water temperatures affected the interpretation of data and actual movement of the structure, in unanticipated ways.

REFERENCE

Kaeck, W.E., Rhyner, F.C., Lacy, H.S., and Quasarano, M. (2009). "Grouting of Deep Foundations at the Thames River Bridge." *IFCEE 2009*, GSP No. pending, ASCE, Reston, VA: pp pending.

Copyrighted Materials
Copyright © 2009 American Society of Civil Engineers (ASCE)
Retrieved from www.knovel.com

Issues Related to Use of OD vs. ID Casing in Drilled Shaft Construction

William M. Isenhower, M. ASCE, P.E., and M. D. "Bo" Walker

[1] Project Manager, Ensoft, Inc./Lymon C. Reese & Associates, 3003 Howard Lane, Austin, Texas 78728, wmi@ensoftinc.com
[2] Vice-President, Texas Shafts, Inc. P.O. Box 79218, Fort Worth, TX. 76179, bwalker@texashafts.com.

ABSTRACT: Drilled shafts are commonly designed in the United States using diameter increments of six inches. Usually, the choice of means and methods to be used to construct the shafts to these standard sizes is left to the contractor. Frequently, a contractor may elect to use the casing method of construction, in which temporary casing is used to support the borehole until concrete placement is completed, after which the casing is extracted. It is common for overbreak to occur during drilling. Overbreak results in a borehole that is larger in diameter than the auger used to drill the borehole. Overbreak occurs due to multiple causes, including breaking of soil along natural planes of weakness as the auger rips the soil and raveling of the borehole sidewalls as the auger moves vertically during the drilling process. This paper discusses the typical amount of overbreak that occurs during drilling and will show that required use of ID casing is rarely needed.

INTRODUCTION

This paper discusses issues that can arise from the confusion that can result from the use of temporary casing that is dimensioned by its outside diameter (OD) or its inside diameter (ID). This confusion arises from erroneous assumptions by different members of the design and construction teams. This paper describes one such case.

In the United States, drilled shafts are commonly designed and constructed using diameter increments of six inches. The length of shafts may be specified either as a specified length or length of penetration into a bearing strata. Other common design practices include use of axial steel bars of No. 8 and larger, and a minimum percentage of axial steel of one percent (O'Neill and Reese, 1999).

Contractors usually review their installation plan in a preconstruction meeting in which they describe their proposed time schedule, construction sequencing, and means and methods of construction (ADSC and DFI, 2004). The term "means and methods" includes the choice of tools and methods of construction. Once the contract is awarded, choice of means and methods used to construct the shafts is (by contract) left to the contractor. This type of arrangement usually results in the shortest time of

construction because the contractor may vary the methods of construction as needed for differing soil conditions and to obtain the most efficient use of drilling equipment and tools.

USE OF TEMPORARY CASING

Typically, a contractor will select either the dry method, the casing method, the wet method, or combinations of the above to construct the drilled shaft foundations (O'Neill and Reese, 1999, Reese, et al., 2006). If a contractor elects to use the casing method of construction, temporary casing may be used to support the borehole until concrete placement is completed, after which the casing is extracted. The temporary casing is installed using different methods that depend on the soil conditions present at the site.

Temporary casing is one of the drilling contractor's tools and is not covered by the construction specifications. Casing is sized by the outside diameter and a specified wall thickness by manufacturers in the United States. Minimum casing wall thickness is typically 3/8 inches (9.5 mm).

Often, it is necessary for a contractor to weld casing sections together at the job site if lengths over 40 feet are needed. Usually, casings with lengths up to 40 feet can be mobilized to the site. This maximum length is usually dictated by state roadway regulations governing maximum length of trailers.

REASONS FOR OVERBREAK

It is common for "overbreak" to occur during drilling. Overbreak results in a borehole that is larger in diameter than the auger used to drill the borehole. The causes for overbreak may be due to a number of different causes, including breaking of soil along natural planes of weakness as the auger rips the soil and raveling of the borehole sidewalls as the auger moves vertically during the drilling process. The amount of overbreak depends on the type of soil, the type of drilling tool, and the power of the drill rig.

MEASUREMENTS OF OVERBREAK

Borehole Caliper

Borehole caliper measurements often find that the borehole is larger near the ground surface due to the raveling effect and that borehole is somewhat oval shaped near the ground surface because swinging of the drill rig may cause the auger to hit the side of the borehole during insertion of the auger.

Concrete Volumes Utilized

The occurrence of overbreak causes an overrun in the volume of concrete needed to fill the borehole. Cost accounting data reveal that the typical percentage of overrun in concrete volume on projects in Texas varies. The typical range for shafts drilling with

temporary casing ranges from 25 to 35 percent. Occasionally, overrun may be as low as ten percent for favorable conditions that rarely occur. This amount of concrete overrun is less that what might be reasonably expected by slight over-drilling of shaft depth by a few feet.

COMMON TOOLING DIMENSIONS

Casing is dimensioned by the manufacturer by the outside diameter. Standard relationships between casing OD, opening auger size, and through auger size is summarized in ADSC (1999, Item 2, page 1). Opening auger size is generally 2 inches larger than the casing OD and through auger dimension is generally 2 inches smaller than the casing OD.

A survey was made of contractor members in the Southwest Section of ADSC to determine the common combinations of tooling and casing dimensions used to construct drilled shafts using the casing method. The results of this survey are presented in Table 1 for OD-size casing and in Table 2 for ID-size casing.

Table 1. Tooling for Standard Outside Diameter Casing (OD Casing)[1]

Design Diameter, inches	Opening Auger, inches[2]	Casing Dimensions			Auger Diam. In.	Theoretical Increase in Volume
		OD, in.	ID, in.	2t, in.		
18	22	20	19 ¼	¾	18	23.5%
24	26	24	23 ¼	¾	22 ½	33.5%
30	32	30	29 ¼	¾	28 ½	26.1%
36	38	36	35 ¼	¾	34 ½	21.3%
42	44	42	41 ¼	¾	40 ½	18.0%
48	50	48	47 ¼	¾	46 ½	15.6%
54	56	54	53 ¼	¾	52 ½	13.8%
60	62	60	59 ¼	¾	58 ½	12.3%
66	68	66	65 ¼	¾	64 ½	11.1%
72	74	72	71	1	70	11.8%
78	80	78	77	1	76	10.8%
84	86	84	83	1	82	10.0%
90	na	na	na	na	na	na
96	98	96	94 ½	1 ½	94	8.7%

[1]All dimensions shown in inches because metric sizes are not used. 1 inch = 25.4 mm.
[2]Note - Outside over-cutters are used in standard augers to enlarge the hole by an extra 2 inches.

Note that the dimensions in Table 1 differ from those described by ADSC (1999). In general, the through auger dimension is ¾ to 1 ¼ inch smaller than the ID of the temporary casing, whereas ADSC (1999) describes the diameter of the through auger as 2 inches smaller than the OD of the temporary casing.

For shaft sizes larger than those shown in Tables 1 and 2, temporary casing is usually ordered to fit the large diameter augers used. The large diameter auger must have over-cutters installed to permit installation of the casing. Once the casing is

installed, the over-cutters are removed to permit passage of the auger. Thus, all casing used for tools larger than those shown in the tables are ID casing.

Table 2. Tooling for Specially Rolled Inside-Diameter Casing (ID Casing)

Design Diameter, inches	Opening Auger, inches[2]	Casing Dimensions			Inside Auger, in.	Theoretical Increase Over Nominal Volume	Volume Difference of ID vs. OD
		OD, in.	ID, in.	2t, in.			
18	22	20	19 ¼	¾	18	49.4%	49.4%
24	28	26	25 ¼	¾	24	36.1%	54.9%
30	34	32	31 ¼	¾	30	28.4%	42.3%
36	40	38	37 ¼	¾	36	23.5%	34.4%
42	46	44	43 ¼	¾	42	20.0%	29.0%
48	52	50	49 ¼	¾	48	17.4%	25.1%
54	58	56	55 ¼	¾	54	15.4%	22.0%
60	64	62	61 ¼	¾	60	13.8%	19.7%
66	72	68	67 ¼	¾	66	19.0%	24.6%
72	78	74 ½	73 ½	1	72	17.4%	24.2%
78	84	80 ½	79 ½	1	78	16.0%	22.2%
84	90	86 ½	85 ½	1	84	14.8%	20.5%
90	na	na	na	na	na	na	an
96	102	99 ½	98	1	96	12.9%	17.7%

[1]All dimensions shown in inches because metric sizes are not used. 1 inch = 25.4 mm.
[2]Note - All opening augers are specially purchased to install ID casing.

Some designers may exercise conservatism by prohibiting use of OD-dimension casing due to their belief that the borehole diameter is always equal to the drilling tool diameter. This leaves the contractor facing the choice of drilling six inches oversize or of purchasing custom-rolled casing that is dimensioned by inside diameter. Unless a client can assure the contractor of sufficient future work requiring ID casing, the cost of purchasing casing is prohibitive.

The theoretical increase in shaft volume shown in Tables 1 and 2 is based on the volume of a borehole with a diameter equaling the opening auger size versus one with an auger diameter equal to the drilling auger size. No overbreak is considered in this table.

Table 2 shows the increase of shaft volume for an ID casing borehole over that for a borehole drilling with OD-sized casing for the same design diameter. The increase in volume for boreholes drilled using ID casing ranges from 17.7% to 54.9% over that required by boreholes drilled using OD casing, and the increase in nominal shaft volume ranges from 12.9% to 49.4%. As with Table 1, no overbreak is considered in the computation of values for this table.

The increases in shaft volume when using ID-sized casing are well known to many drilling contractors and their associated higher costs are considered when preparing bids for construction. However, some foundation designers are not aware of this issue

and unwittingly increase the cost of construction if they specify the use of ID-sized casing.

EXPERIENCE WITH BOREHOLE CALIPER MEASUREMENTS

Several systems for making borehole caliper measurements have been developed. Usually, borehole caliper measurements are made for demonstration shafts or for load test shafts. Caliper measurements are rarely performed on production shafts. Some systems are based on direct measurement of the borehole diameter. One such system was developed by Lymon C. Reese & Associates and is shown in Figure 1.

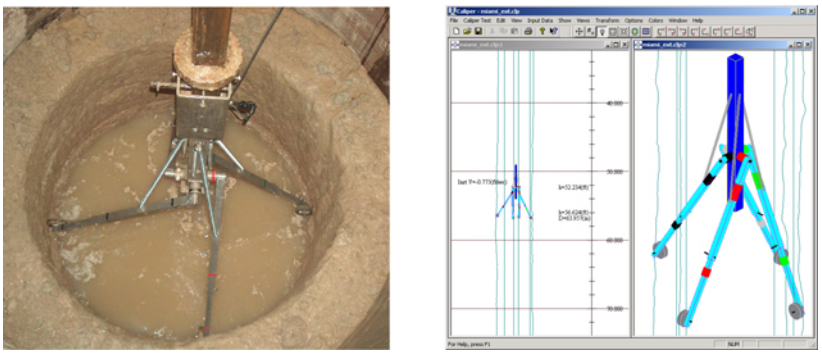

(a) (b)

Figure 1. Borehole Caliper System, (a) Measuring 8-ft, Slurry-filled Borehole, (b) Computer Display of Real-time Measurements of Borehole Caliper

The caliper system shown in Figure 1 consists of four spring-loaded arms to track the borehole sides. The angles of the four arms relative to the caliper body are measured with rotational sensors. A biaxial tilt sensor is encased inside the caliper body so that corrections can be made for any tilt of the caliper body. Resolution of the diameter measurement depends on the angle of the arms, but is typically less than 1 mm. Depth is measured using depth encoder pulley system actuated by the instrumentation cable. All sensors and the depth encoder are read using an analog to digital data acquisition system. A real-time display of caliper arm position and processed data are displayed on laptop computer.

The borehole caliper system shown in Figure 1 is usually used three times to make 12 diagonal measurement of diameter, spaced at 30-degree intervals, with vertical measurements taken every one-half inch (12 mm). The real-time readings are shown on a laptop computer and volume of the borehole versus depth is automatically computed. In this particular case, the caliper was attached to the kelly of the drill rig, but it may be lowered on a cable system in lieu of using the drilling kelly

Borehole caliper measurements often find that for uncased boreholes, the borehole is larger near the ground surface due to vertical movement of the auger during

drilling. In addition, an uncased borehole is usually somewhat oval shaped near the ground surface because swinging of the drill rig may cause the auger to hit the side of the borehole during removal and insertion of the auger during drilling. Both of these effects typically cause the borehole to be larger near the surface and closer to the diameter of the auger at depth. In all cases, the diameter of the borehole at depth is larger in diameter than is the diameter of the auger. For boreholes in clay soils, the borehole diameter is typically more than two inches (50 mm) larger than the auger diameter near the ground surface and is typically at least one inch (25 mm) larger than the auger diameter near the pile tip.

The smoothness of the borehole wall depends on many factors and cannot be predicted with certainty, but can be learned based on local experience. Existence of fissuring in the soil or rock being drilling has an effect on borehole smoothness and overbreak. The combination of drilling torque, vertical crowd force on the auger, and the characteristics of the drilling are also very important factors. The authors speculate that rigs capable of higher torque and crowd force are more likely to produce rougher boreholes using augers, but we have no firm data on which to base this opinion.

In summary, one may state with certainty on the basis of experience with borehole caliper measurements that the diameter of a drilled borehole is always larger than diameter of the auger. Usually, a borehole is at least one inch larger than the auger diameter and may be over two inches larger in some cases.

RECENT CASE HISTORY

Drilled shafts were designed to use six-inch increments for a large public works project in Texas. Several contractors submitted bids in which common methods of construction and toolings were described. Presumably, the construction methods and tooling schedules were considered by the designers when the bids were reviewed. The contract was awarded to several contractors and work commenced.

The typical soil profile for the project consisted of very stiff to hard clays overlying a hard clay shale. Some of the upper clay strata are known to be expansive near the ground surface, but no special effort was made in the geotechnical investigation to determine their expansive properties nor the depth of seasonal moisture change. In much of the area of the project, the thickness of the soil strata overlying the shale ranged from zero to less than ten feet in thickness. Since this range of thicknesses was within the depth range of seasonal moisture change and because some of the clays were known to be expansive, the geotechnical consultants recommended ignoring the contribution of soils above the clay shale. No special action was needed to address the swelling of the upper clays because the shafts supported an elevated structure (i.e. there was no pile cap or floor slab) and the axial loading were high. The recommendation to ignore side resistance soils above the shale was partly based on consideration of desiccation cracking of the cohesive soils and the relatively short length of shafts in the clays compared to the much longer lengths of penetration into the shale at depth

It was later learned that several unusual design practices were used by the foundation designers when conditions differed from the usual conditions. In some

large areas, the depth to shale was deep and the thickness of the overburden soils exceeded 60 feet. The original geotechnical recommendations did not include the contribution to axial capacity of the soils above the shale because the depth of shale was expected to be shallow. The contribution of the upper soils to axial capacity in side resistance of the upper soils in such a situation would be substantial. A reasonable request from the foundation designers to the geotechical consultant would be for recommendations for axial load-transfer capacity in side resistance for these soils (which had been investigated and tested by the geotechical consultant). Instead, the original recommendations were followed and a substantial amount of axial capacity was left unaccounted for by the foundation designer.

After the start of construction, the design engineers notified the drilling contractor that use of the wet method was prohibited. This prohibition was made in spite of the submission and approval of the wet method in the contractor's installation plan and the fact that the wet method was used fairly extensively for shafts drilled into the same strata for other projects. The reason cited for disallowing the wet method was the result of a single axial load test from the mid-1970's that found reduced axial side resistance for a drilled shaft drilled with mineral drilling slurry. This prohibition was also extended to use of polymer drilling slurry. No consideration was made for use of polymer drilling slurry that prevent water loss from the borehole into the formation. For polymer drilling slurries, the water-loss prevention properties enable the elevation head of the slurry to be raised above the natural water table to stabilize the borehole.

In addition, axial side resistance was disallowed in any strata in which temporary casing was used, in spite of the casing being pulled after concrete placement.

Later, the foundation designer discovered that the contractor was constructing the shafts using the casing method, installing OD casing as was agreed prior to the bid. At this time, the foundation designer changed the requirements of the job to require use of ID casing. When this change in requirements was made, a claim was made because of the change in requirements. A third party engineering analysis proved little or no change in the axial load capacity of the design shafts versus shafts installed using OD casing and standard tooling. It was decided by the foundation designer to deepen the penetration depths of the shafts to allow for continued use of OD casing and standard tooling diameters. Typically, the extension depth was two feet (0.6 m) or less. It was argued that concrete volume data of prior shafts was confirming the overbreak of soils and shale during drilling and that the omission of side resistance for the soils above the shale was unneeded conservatism. It was not possible to change the mind of the foundation designer. This resulted in an increase of cost for the owner.

As part of the discussion with the geotechnical consultant, foundation designer and owner, a load test program was proposed. The geotechnical consultant had also proposed a load test program at the time of the original geotechnical investigation (several years past). It was decided by the owner not to perform the load test program in spite of the potential savings in order avoid delay to the project.

CONCLUSIONS

Standard casing sizes of 96 inches and smaller are dimensioned by manufacturers by the outside diameter and casing wall thickness. Casing is typically sized equal to the shaft diameter and the opening auger is usually 2 inches larger than the casing.

A review of borehole dimension data obtained by caliper measurements finds that boreholes are always larger in diameter than the augers used to drill the boreholes. The argument that a borehole is equal in size to the drilling auger cannot be supported by caliper measurements. In addition, typical concrete volumes utilized for boreholes drilled using the casing methods are typically 25 to 35 percent higher than the theoretical volume of the shaft, thereby providing additional evidence that overbreak occurs during drilling.

Any casing sized by the inside diameter is non-standard and is an added expense to the contractor. This increases the cost of building the foundations and this added cost is passed on to the owner.

REFERENCES

ADSC – The International Association of Foundation Drilling, (1999). *Standards and Specifications of the Foundation Drilling Industry*, 33 p.

ADSC – The International Association of Foundation Drilling and DFI: Deep Foundations Institute (2004). *Drilled Shaft Inspector's Manual*, 2nd Edition, 72 p.

O'Neill, M. W., and Reese, L. C. (1999). "Drilled Shafts: Construction Procedures and Design Methods," FHWA Report FHWA-IF-99-025, 790 p.

Reese, L. C., Isenhower, W. M., and Wang, S.-T. (2006). *Analysis and Design of Shallow and Deep Foundations*, Wiley, 574 p.

Copyrighted Materials
Copyright © 2009 American Society of Civil Engineers (ASCE)
Retrieved from www.knovel.com

Analysis of Anchor Foundation with Root-Caisson in Non-homogeneous Soils

Chenrong Zhang[1], Maosong Huang[2], Linlong Mu[3]

1. PhD Student, Department of Geotechnical Engineering, Tongji University, Shanghai 200092, China
2. Professor, Department of Geotechnical Engineering, Tongji University, Shanghai 200092, China
3. PhD Student, Department of Geotechnical Engineering, Tongji University, Shanghai 200092, China

ABSTRACT: This paper describes a novel type of deep foundation-anchor foundation with root-caisson. A simplified analysis procedure based on Winkler subgrade model is proposed to compute responses of anchor foundation in layered soils subjected to vertical and horizontal loads, considering the root as stretching beam. The method incorporates limiting soil stress to represent soil nonlinear reaction and passive caisson to explain group effect. The suitability of the analysis method is checked by comparison with in-situ tests and finite-element solution.

INTRODUCTION

Anchor foundation with root-caisson is a new structural foundation for anchorage of suspension bridges. With prefab roots pushing into soils through reserved holes in installed caisson as shown is Fig. 1, root-caisson gives better a load-displacement performance by enhancing structure-soil interaction with penetrating roots. As root-caisson is a relatively new technology, little work has been performed either in field experiments or theoretical analysis. Investigation is necessary so as to disseminate among practitioners to establish the knowledge in engineering practice.

In this paper, a simplified analysis method is presented to analyze the behavior of anchor foundation with root-caisson embedded in non-homogeneous soils.

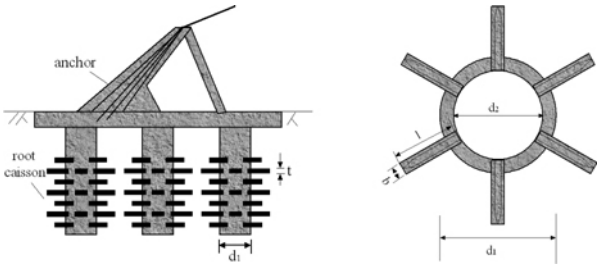

FIG. 1. Schematic figure for anchor foundation with root-caisson

METHOD OF ANALYSIS

No couple effect of vertical and lateral load is considered. The improved caisson is modeled as elastic beams and the soil is treated as distributed springs. Nonlinear behavior of loaded caisson is obtained by considering limiting soil pressures around the caisson and transfer matrix is adopted to analyze soil layer effects.

Behavior of a single root-caisson

As a particular structure of root-caisson, the analysis of a root-caisson involves two parts: (1) usual section without roots and (2) section with penetrating roots.

Axial Response

A theoretical load transfer model proposed by Randolph & Wroth (1979) is employed here to calculate vertical soil-caisson interaction in usual section, which gives a stiffness of the vertical distributed soil spring as follows:

$$k_{z1} = 2\pi G_s / \ln(2r_m / d_1) \tag{1.}$$

where r_m is the limiting radius of influence of the caisson, $r_m = L(1 - v_s)$, L is the length of the caisson, G_s, v_s is the shear modulus and Possion's ration of the surrounding soil, d_1 is the outer diameter of the usual caisson.

The caisson base settlement can be estimated through the model for a rigid punch on a half-space by the Boussinesq solution and corresponding vertical soil spring is

$$k_{b1} = d_1 E_b / (1 - v_b^2) \tag{2.}$$

where E_b and v_b are the Young's modulus and Poisson's ratio of the soil at the pile base.

The penetrating roots improve the vertical mechanical behavior of the caisson by enhancing soil-caisson interaction. The soil resistance along the side and at the base of roots supplies additional capacity for bearing the applied load.

A configuration of section with m roots is considered here, each of which is l in length, b in width and t in height, as shown in Fig. 1. The equivalent stiffness of the distributed soil spring for the caisson section with roots can then be calculated by

$$k_{z2} = 2\pi G_s / \ln(2r_m / d_3) \tag{3.}$$

where d_3 is the equivalent diameter for calculation, which satisfies $\pi(d_3^2 - d_2^2)/4 = A_2$ with A_2 being the cross-sectional area of the section with roots $A_2 = \pi(d_1^2 - d_2^2)/4 + mlb$, d_2 is the inner diameter of the usual caisson.

With the same model for rigid punch acting on soils, the vertical soil spring at the bottom of roots can be expressed as

$$k_{b2} = d_4 E_s / (1 - v_s^2) \tag{4.}$$

where E_s is the corresponding Young's modulus of the soil. d_4 is the corresponding calculation diameter, which satisfies $\pi d_4^2/4 = A_3$ with A_3 being the cross-sectional area of the roots $A_3 = mlb$.

For n cells of the caisson, repeating the equation of motion for each cell, while imposing the continuity of force N and displacement w at each interface, we take

$$\begin{Bmatrix} w(L) \\ N(L) \end{Bmatrix} = [R] \begin{Bmatrix} w(0) \\ N(0) \end{Bmatrix} \tag{5.}$$

where $[R]=\prod_{i=1}^{n}[R_i]$, and $[R_i]$ is the load transfer matrix for cell i

$$[R_i]=\begin{bmatrix}\cosh(\eta_i) & -(E_pA^*\eta_i)^{-1}\sinh(\eta_i)/h_i\\ -E_pA^*\eta_i\sinh(\eta_i)/h_i & \cosh(\eta_i)\end{bmatrix} \tag{6.}$$

where h_i is the length of cell i, E_p is the Young's modulus of the cassion, $\eta_i=h_i\sqrt{\frac{(k_{s1})_i}{E_pA^*}}$ with $A^*=A_1$ and $\eta_i=h_i\sqrt{\frac{(k_{s2})_i+(k_{b2})_i/t}{E_pA^*}}$ with $A^*=A_2$ are for section without and with roots respectively, and A_1 is the cross-sectional area of the usual section $A_1=\pi(d_1^2-d_2^2)/4$.

When the base stiffness is taken into account, we take the vertical flexibility stiffness of the caisson f as

$$f=\frac{R_{22}-k_{b1}R_{12}}{k_{b1}R_{11}-R_{21}} \tag{7.}$$

With increasing load, certain soil cell will reach limiting soil stress first. The yielding cell will then transfer load to neighboring cell in elastic state, and in this case the incremental transfer matrix is then expressed as

$$\begin{Bmatrix}\Delta w_i\\ \Delta N_i\end{Bmatrix}_b=\begin{bmatrix}1 & -(E_pA^*)^{-1}h_i\\ 0 & 0\end{bmatrix}\begin{Bmatrix}\Delta w_i\\ \Delta N_i\end{Bmatrix}_t=[R_i]\begin{Bmatrix}\Delta w_i\\ \Delta N_i\end{Bmatrix}_t \tag{8.}$$

As the load-displacement relationship is nonlinear, the governing equation has to be solved incrementally. In each increment, the calculated shaft friction stress should be updated by comparing with the limiting stress. The response of a single caisson is the sum of the calculated value in each increment.

Lateral Response

With subgrade-reaction theory, Vesic(1961) expressed the modulus of subgrade reaction k_x, as follows

$$k_x=\frac{0.65E_s}{(1-\nu_s^2)}\sqrt[12]{\frac{d^4E_s}{E_pI_p}} \tag{9.}$$

where I_p is the moment inertia of the usual caisson section. For n cells of the caisson, with parameter $\lambda_i=h_i\sqrt[4]{\frac{k_{si}}{4E_pI_p}}$, $k_{1i}=\frac{h_i}{\lambda_i}$, $k_{2i}=\left(\frac{h_i}{\lambda_i}\right)^2\frac{1}{E_pI_p}$, $k_{3i}=\left(\frac{h_i}{\lambda_i}\right)^3\frac{1}{E_pI_p}$, $A(x)=\sinh(x)\cos(x)$, $B(x)=\cosh(x)\sin(x)$, $C(x)=\sinh(x)\sin(x)$, $D(x)=\cosh(x)\cos(x)$, the transfer matrix for cell i in the usual section of the caission is represented as

$$[T_i]=\begin{bmatrix}D(\lambda_i) & -\frac{k_{1i}}{2}[A(\lambda_i)+B(\lambda_i)] & k_{3i}[B(\lambda_i)-A(\lambda_i)] & \frac{k_{2i}}{2}C(\lambda_i)\\ \frac{1}{k_{1i}}[B(\lambda_i)-A(\lambda_i)] & D(\lambda_i) & -\frac{k_{3i}}{2k_{1i}}C(\lambda_i) & -\frac{k_{2i}}{2k_{1i}}[A(\lambda_i)+B(\lambda_i)]\\ -\frac{2}{k_{3i}}[A(\lambda_i)+B(\lambda_i)] & \frac{2k_{1i}}{k_{3i}}C(\lambda_i) & D(\lambda_i) & \frac{k_{2i}}{k_{3i}}[A(\lambda_i)-B(\lambda_i)]\\ -\frac{2}{k_{2i}}C(\lambda_i) & \frac{k_{1i}}{k_{2i}}[B(\lambda_i)-A(\lambda_i)] & -\frac{k_{3i}}{2k_{2i}}[A(\lambda_i)+B(\lambda_i)] & D(\lambda_i)\end{bmatrix}^i=\begin{bmatrix}T_1\\ T_2\\ T_3\\ T_4\end{bmatrix}^i \tag{10.}$$

In the case of section with roots, it is believed that the presence of roots has impacts

on the behavior of a laterally loaded caisson: (1) the moment inertia of the caisson section with roots is enlarged by stretching roots; and (2) the load induced rotation along caisson imposes additional resisting bending moment with root through mobilized pressure existing between the upside of the root and surrounding soil as well as the downside. The vertical Winkler subgrade modulus at the position of root is now written as

$$k_t = 2\times\frac{0.65E_s}{1-v_s^2}\left[\left(\frac{4bt}{\pi}\right)^2\frac{E_s}{E_pI_p}\right]^{\frac{1}{12}} \tag{11.}$$

Then, the rotation induced bending moment for roots can be obtained by

$$M_i^r == \left[\frac{1}{6}k_n l\left(6d_1 l+3d_1^2+2l^2\right)\sum_{j=1}^{m}\cos^2\alpha_j\right]\theta_i = q_i\theta_i \tag{12.}$$

where α_j is angle between the long axis of root and the direction of horizontal load.

A jumping bending moment at the section with roots leads to a corresponding transfer matrix as

$$\begin{Bmatrix} y \\ \theta \\ H \\ M \end{Bmatrix}_t^i = \begin{Bmatrix} y \\ \theta \\ H \\ M - q_i\theta \end{Bmatrix}_b^{i-1} = \begin{bmatrix} T_1 & & & \\ & T_2 & & \\ & & T_3 & \\ & & T_4 - q_iT_2 & \end{bmatrix}^{i-1}\begin{Bmatrix} y \\ \theta \\ H \\ M \end{Bmatrix}_t^{i-1} = [T_{i-1}]\begin{Bmatrix} y \\ \theta \\ H \\ M \end{Bmatrix}_t^{i-1} \tag{13.}$$

where subscript t and b refer to corresponding values at the top or bottom of the cell. With a similar approach as vertical loaded caisson in which the base acts as a rigid punch on an elastic half-space, we take

$$[K_b] = \begin{bmatrix} k_{bx} & 0 \\ 0 & k_{b\theta} \end{bmatrix} = \begin{bmatrix} \dfrac{8(1-v_b)E_bd_1}{(7-8v_b)(1+v_b)} & 0 \\ 0 & \dfrac{E_bd_1^3}{6(1-v_b^2)} \end{bmatrix} \tag{14.}$$

For n cells of the caisson, the responses of a caisson can be written as

$$\begin{Bmatrix} u(L) \\ \theta(L) \\ H(L) \\ M(L) \end{Bmatrix} = [T]\begin{Bmatrix} u(0) \\ \theta(0) \\ H(0) \\ M(0) \end{Bmatrix} \tag{15.}$$

where $[T] = \prod_{i=1}^{n}[T_i]$ and $[T_i]$ is lateral transfer matrix for cell i. Divide matrix $[T]$ into four parts, i.e. $[T] = \begin{bmatrix} T_{11} & T_{12} \\ T_{21} & T_{22} \end{bmatrix}$, each hybrid matrix is a 2 by 2 matrix. The lateral flexibility matrix of the caisson can then be expressed as

$$[f^s] = \{[K_b][T_{11}]-[T_{21}]\}^{-1}\{[T_{22}]-[K_b][T_{12}]\} \tag{16.}$$

It is well known that the relationship between the internal forces and deflection of laterally loaded caisson is nonlinear, since soils at the top of caisson are likely to yield at relatively low loads. As load increases, the yielding elements with limiting lateral soil stress will then transfer load to neighboring elements in elastic state.

The solution of governing differential equation for yielding element gives

incremental lateral transfer matrix as

$$\begin{Bmatrix}\Delta y\\ \Delta\theta\\ \Delta H\\ \Delta M\end{Bmatrix}_b^i = \begin{bmatrix}1 & -h & \frac{h^3}{6E_pI_p} & \frac{h^2}{2E_pI_p}\\ 0 & 1 & -\frac{h^2}{2E_pI_p} & -\frac{h}{E_pI_p}\\ 0 & 0 & 1 & 0\\ 0 & 0 & h & 1\end{bmatrix}^i \begin{Bmatrix}\Delta y\\ \Delta\theta\\ \Delta H\\ \Delta M\end{Bmatrix}_t^i = [T_i]\begin{Bmatrix}\Delta y\\ \Delta\theta\\ \Delta H\\ \Delta M\end{Bmatrix}_t^i \tag{17.}$$

Interaction between two caissons

Two identical, equally-loaded caissons *i*, *j* are considered. Various interaction factors to describe the interactions between two caissons $\alpha_{wPij}=\frac{w_i(0)}{w_j(0)}$, $\alpha_{uHij}=\frac{u_{Hi}(0)}{u_{Hj}(0)}$, $\alpha_{uMij}=\frac{u_{Mi}(0)}{u_{Mj}(0)}$, $\alpha_{\theta Pij}=\frac{\theta_{Hi}(0)}{\theta_{Hj}(0)}$, $\alpha_{\theta Mij}=\frac{\theta_{Mi}(0)}{\theta_{Mj}(0)}$ are the rates of additional displacement and rotation at the top the free-headed caisson *i* caused by a loaded adjacent caisson *j* and the displacement and rotation at the top the free-headed caisson *j* due to its own load. The influence of roots on the interaction between two caissons is ignored.

With finite-difference method, the vertical and lateral governing differential equations for a loaded caisson give the values of $w_j(0)$, $u_{Hj}(0)$, $\theta_{Hj}(0)$, $u_{Mj}(0)$ and $\theta_{Mj}(0)$. The displacement field around the loaded caisson will induce additional deflection on neighboring unloaded caisson (as a passive caisson). In conventional analysis, it is thought that unloaded caisson follows exactly the free-field displacement, which in fact gives a higher estimation of interaction factor. As a passive caisson, the governing equations for the unloaded caisson *i* are written as

$$\frac{d^2w_i}{dz^2}-\frac{\eta^2}{h^2}(w_i-w_s(s,z))=0 \tag{18.}$$

$$\frac{d^4u_i}{dz^4}+\frac{4\lambda^4}{h^4}(u_i-h_s(s,z))=0 \tag{19.}$$

where $w_s(s,z)$ (Mylonakis and Gazetas (1998)) and $h_s(s,z)$ are the vertical and lateral free displacements at the position of caisson *i* induced by adjacent caisson *j* with corresponding load, s is center-to-center caisson-spacing. Based on plane-strain approximation, $w_s(s,z)$ can be expressed as

$$w_s(s,z)=\begin{cases}\frac{\ln(r_m)-\ln(s)}{\ln(r_m)-\ln(d_1/2)}w_s(d_1/2,z) & d_1/2\le s\le r_m\\ 0 & s>r_m\end{cases} \tag{20.}$$

By the Mindlin equation for the horizontal displacement in stratum and the principle of superposition, $h_s(s,z)$ is obtained and of which the details are not introducted here. Solutions of equations (18) and (19) give the values of $w_i(0)$, $u_{Hi}(0)$, $\theta_{Hi}(0)$, $u_{Mi}(0)$ and $\theta_{Mi}(0)$. With all the calculated values above, various interaction factors are obtained.

Anchor foundation with root-caisson

In anchor foundation with *n*-caissons, it is assumed that a rigid off-ground cap rigidly attaches to caissons, in which the rotations and deflections of all caissons are

equal and the settlement of a caisson is related to its position in group and the rotation.

The resulting equations for vertical and lateral displacement and rotation may be written conveniently in matrix form by Poulos and Davis (1980), as follows:

$$\begin{bmatrix} A_v & B_v & C_v \\ A_h & B_h & C_h \\ A_\theta & B_\theta & C_\theta \end{bmatrix} \begin{Bmatrix} N \\ H \\ M \end{Bmatrix} = \begin{Bmatrix} \delta_w \\ \delta_u \\ \delta_\theta \end{Bmatrix} \tag{21.}$$

where sub-matrices A_v, B_v, C_v, A_h, B_h, C_h, A_θ, B_θ and C_θ are of order $n \times n$. $A_{vij} = \alpha_{wNij} f_j$, $B_{hij} = \alpha_{uHij} f^s_{11,\ j}$, $C_{hij} = \alpha_{uMij} f^s_{12,\ j}$, $B_{\theta ij} = \alpha_{\theta Hij} f^s_{21,\ j}$, $C_{\theta ij} = \alpha_{\theta Mij} f^s_{22,\ j}$, $B_{vij} = 0$, $C_{vij} = 0$, $A_{hij} = 0$, $A_{\theta ij} = 0$

The vectors N, H and M of order n are the unknown vertical and horizontal forces, moment at the top of order, while δ_w, δ_u, δ_θ of order n are the unknown rigid settlement, deflection and rotation at the top of the caisson. Equation (21) together with three load-equilibrium and moment-equilibrium equations may be solved to obtain the unknown loads and displacements at the caisson head, in which incremental steps with updating vertical and lateral flexibility stiffness for a single caisson are used to calculate non-linear responses of a caisson group.

VERIFICATION

In order to investigate the fundamental mechanism for loaded caissons, full-scale field load tests were carried out aiding the design of anchor foundation of Ma-an-shan Yangtze River Bridge in China.

Five field tests named tests 1, 2, 3, 4 and 5 were conducted at the site where the construction of south anchorage foundation has been planned. Tests 1 and 2 are the vertical and lateral static load tests for a single root-caisson. Tests 3, 4 and 5 are lateral static load tests for anchor foundations with 1, 3 and 6 root-caissons respectively, configuration of which are shown in Table 1. Properties of soils obtained from laboratory tests are summarized in Table 2.

Table 1. Schematic plan layout of group configuration

Test 3	Test 4	Test 5
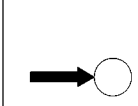	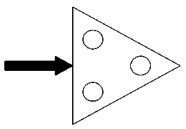	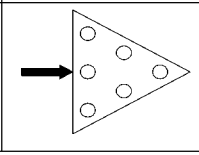

Table 2. Soil layer and soil parameters

Soil layer	Name	Thickness (m)	E_s (MPa)	ν_s
①$_1$	Refilled soil	2.0		0.35
②$_{2\text{-}2}$	Clay	1.7	64.74	0.3
②$_{3\text{-}2}$	Clay	7.3	35.88	0.3
②$_4$	Silt	12.4	60.06	0.3
③$_5$	Sand	15.1	87.62	0.3

For tests 1 and 2, the caisson is 39m in length and 6m in diameter(d_1). Vertical statically load tests were conducted by Osterberg load test method. In horizontal statically load tests, two caissons were loaded by lateral jacking instruments placed between them. The load is measured as the jacking force. The settlement and deflection of the caisson are measured with electronic settlement gauges.

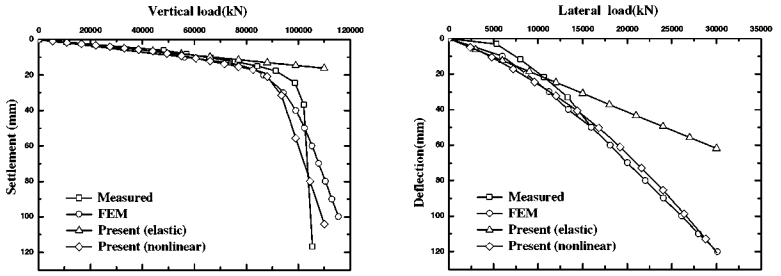

(a)test1 (b)test2

FIG. 2. Comparisons of load-displacement curves for a single root-caisson

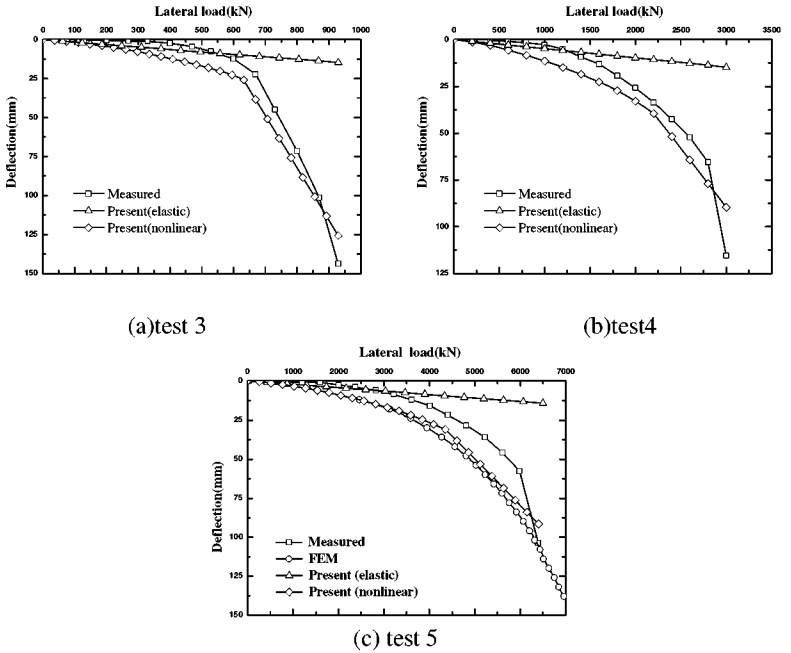

(a)test 3 (b)test4

(c) test 5

FIG. 3. Comparisons of load-deflection curves for caisson groups

Fig. 2(a) shows a comparison of the measured load-displacement curve with predicted profile for a single caisson using the present method and that with FEM

method. The nonlinear analysis procedure gives a fairly good prediction, while substantial discrepancy with increasing load is shown in elastic analysis. Fig. 2(a) shows a sudden increase in settlement with the ultimate load from measured data, but the slope of predicted curve is relatively small. The reason is that in reality all the soils along the shaft and at the base of the caisson are in limiting state, while reduction of base resistance is not considered in the non-linear analysis. In Fig. 2(b), it is thought that the applied load is much less than the ultimate lateral capacity of the caisson. As the main concern of lateral loaded caisson is the maximum deflection, the deflection shown is seen to be a little overestimated in early load step.

For tests 3, 4 and 5, caissons are connected to a rigid concrete cap with 2 m in thickness, such that head is restrained from rotation and deflection, according with the basic assumption in the proposed method. The caisson is 9m in length and 1.3m in diameter(d_1). Predicted results from the analysis of capped caisson groups subjected to horizontal loading and the measured load-deflection curves are shown in Fig. 3, besides the corresponding curve by FEM for six caissons is also shown. Reasonable agreement between the predictions by nonlinear analysis and measurements can be observed for the lateral load-deflection relationships. Similar discrepancy also appears now that non-linear predicted values give a little overestimation on the deflections of caisson groups. With the applied load in the last step, the deflection increment is smaller than the measured values.

CONCLUSION

This paper describes a simplified analysis method for the anchor foundation with root-caisson in layer soils. The effects of penetrating roots in caisson are considered by model the root as a small beam and the nonlinear mechanism behavior of root-caisson is considered with limiting soil stress. The group effect may be assessed by considering the responses of passive caisson in the displacement field induced by an adjacent loaded caisson. With accurate estimation of limiting soil stress, it is generally possible to obtain a satisfactory prediction of the responses of anchor foundation with root-caisson by present method. The writers hope this technical paper may give some advantage for design work of foundation with respect to the construction cost and technique improvement.

REFERENCES

Mylonakis, G. and Gazetas G. (1998). "Settlement and additional internal forces of grouped piles in layered soil." *Geotechnique*, 48 (1): 55-72.

Poulos, H.G. and Davis, E.H. (1980). "Pile foundation analysis and design." *John Wiley & Sons, Inc.* 1980.

Randolph, M.F. and Wroth, C.P. (1979). "An analysis of the vertical deformation of pile groups." *Geotechnique,* 29(4): 423-439.

Vesic, A.S. (1961). "Bending of beam resting on isotropic elastic solid." *Journal of. Engineering Mechanics Division,* ASCE, 87 (2):35-53.

Copyrighted Materials
Copyright © 2009 American Society of Civil Engineers (ASCE)
Retrieved from www.knovel.com

LESSON FROM INSTRUMENTED SLOPE STABILIZATION PROJECT USING DRILLED SHAFTS

Robert Y Liang[1] Member[1], ASCE, Mohammad Yamin[2], Wassel M Al Bodour[3]

[1]Professor, Department of Civil Engineering, The University of Akron, Akron, OH44325, 330-972-7190, rliang@uakron.edu
[2]Graduate Assistant, Department of Civil Engineering, The University of Akron, Akron, OH44325, 330-206-8857, yaminstr@yahoo.com
[3]Graduate Assistant, Department of Civil Engineering, The University of Akron, Akron, OH44325, 330-972-7364, wassel1975@yahoo.com

ABSTRACT: A case study of a slope stabilization project using a single row of rock socketed drilled shafts is presented in this paper. The design method, instrumentation program, and slope/drilled shafts monitoring results are presented. The slope is instrumented with inclinometers to obtain soil movement, piezometers to observe the GWT line, and soil pressure cells to measure earth pressures in different zones. Two drilled shafts are instrumented with an inclinometer in each one to measure the shaft deflection. Furthermore, strain gages and pressure cells were also embedded in the drilled shafts to measure the strain in the longitudinal reinforcement and contact earth pressures at the contact interface between the shaft and the soil. Observations and conclusions regarding the effectiveness of drilled shafts in stabilizing the reconstructed roadway embankment are presented.

INTRODUCTION

The case study presented in this paper is located in Jefferson County, Ohio, along the State Route 152. An approximately 90 m (300 ft) long roadway embankment had experienced substantial subsidence due to the sliding of the embankment slope. As a remediation measure, a single row of rock-socketed drilled shafts were used to enhance the factor of safety of the reconstructed roadway embankment and to arrest the potential slope movements. A brief description is given of the final layout and dimensioning of the drilled shafts for the project, based on the design method presented in Liang and Zeng (2002). A detailed field instrumentation program was planned and carried out to monitor the behavior of the re-constructed slope and the as-built drilled shafts during construction and subsequently during in-service condition. The instrumentation program and the monitoring results are presented in

this paper. Observations and conclusions based on field monitoring results are given at the end of the paper.

GENERAL SITE DESCRIPTION

The embankment slope failure occurred along the west side of State Route 152, approximately 240 m (800 ft) north of the intersection of SR 152 and SR 125 in Jefferson County. The affected slope failure area is approximately 84 m (280 ft) long, from station 54 + 40 to 57 + 20.

Based on detailed geotechnical site investigation and engineering judgment, the failed slope was believed to be due to translational sliding along the interface between overburden soil, which is predominantly consisted of silty clay fill and sometimes mixed with gravel and cobbles, and weathered mudstone bedrock. Fig. 1 presents a schematic plan view of the affected slope area to be reconstructed, while Fig. 2 shows the schematic diagram of the simplified slope cross section. Also shown in Fig. 1 and Fig. 2 are the instrumentation used for monitoring the site. Groundwater is believed to be flowing along the top of and through the bedrock and hydraulically connected to upland abandoned underground mines. Groundwater is clearly a contributing factor to the instability. The area had exhibited instability for many years, and due to sudden mine collapse in the area, an emergency type A repair was made in July 2004 The emergency remediation had been in place for nearly seven years before the final stabilization using the drilled shafts was carried out in the current project. About 3.6 m (12 ft) of soil were cut (starting from the pavement) and replaced in restoring the slope to the original grade of 2:1 grade, after the stabilization drilled shafts were constructed in place.

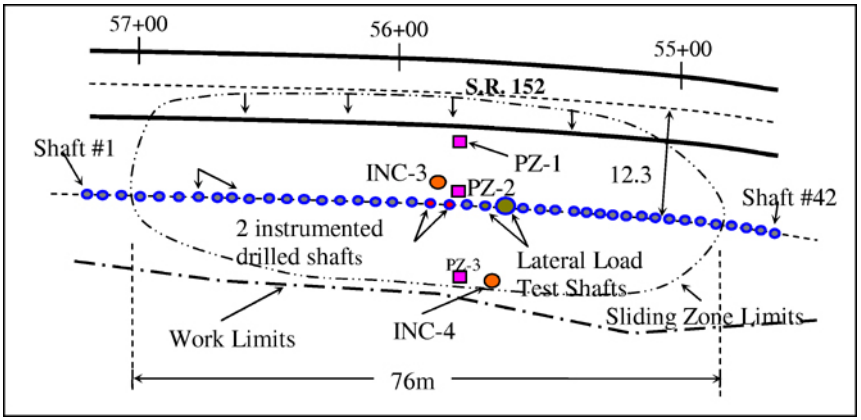

FIG. 1: Schematic general plan view of the failed slope and layout of drilled shafts

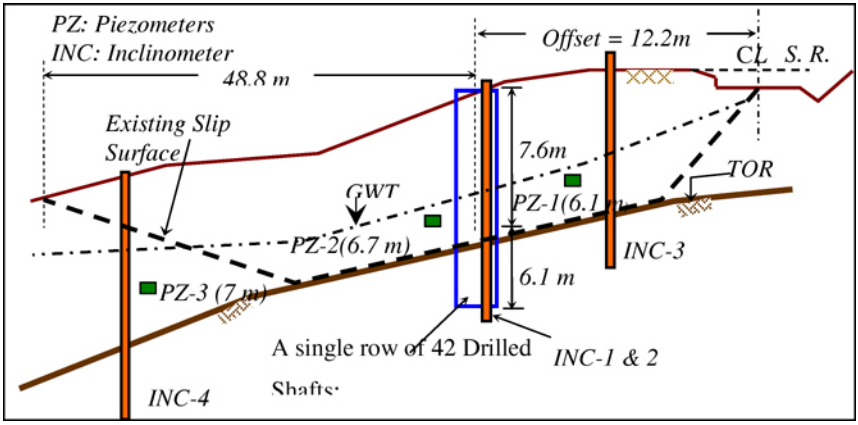

FIG. 2: Schematic cross-section showing slip surface and instrumentation

LABORATORY AND FIELD TESTS

The strength parameters of the slip zone were back-calculated from the known slope geometry and interpreted slip zone location. The back-calculated cohesion was assumed to be zero, while the residual friction angle was determined to be 12 degrees. The properties of mudstone are critical for design of rock socket length; therefore, field pressuremeter tests were conducted. From the pressuremeter test results and using Briaud (1992) method for interpretation, the p-y curves generated for lateral analysis of drilled shaft using LPILE computer program were deduced and they are presented in Fig. 3. The uni-axial compression test results on intact rock core samples are summarized in Table 1, where Q_u is unconfined compressive strength and E_i is initial tangent modulus.

TABLE 1: Laboratory Test Results at JEF-152 Site

Sample	Top (m)	Bottom (m)	Q_u (kN/m^2)	E_i (kN/m^2)	Poisson's Ratio
1	7.95	8.1	268.9	115142.4	N/A
2	8.1	8.25	144.8	28958.0	0.39
3	8.4	8.55	393.0	30750.6	0.43
4	8.7	8.85	386.1	32336.4	N/A
5	9.5	9.6	103.4	3792.1	N/A
6	9.6	9.75	110.3	3998.9	0.38
RQD of the rock = 0.65 and it seems to be IGM					

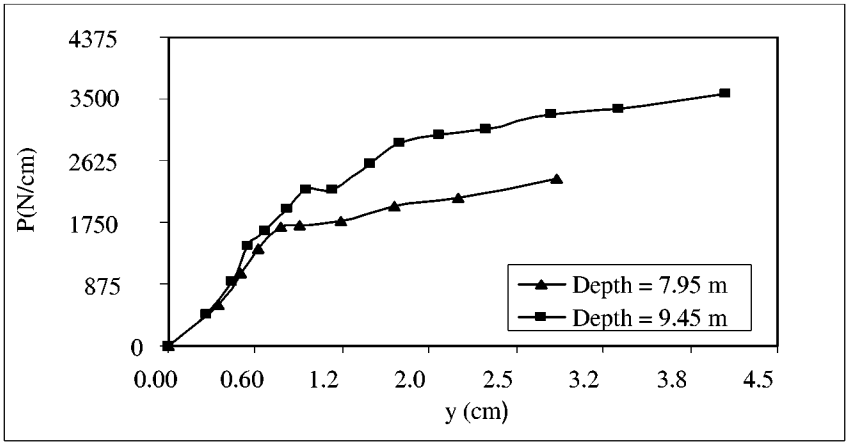

FIG. 3: P-y Curves for JEF-152 Deduced Using Briaud's Method

A full scale shaft loading test was conducted in the field for a shaft of a total length of 12.9 m (43 ft), with diameter 1.05 m (3.5 ft). The concrete compressive strength at 28 days was determined as 3.5 Mpa (5115 psi). The purpose of the lateral load test on the drilled shafts was to obtain the rock response. The maximum load obtained was 73.5 kN (165 kips), and the corresponding deflection was 203 mm at the point of loading.

FINAL DESIGN LAYOUT

Based on Liang and Zeng (2002) method and the accompanying computer program, the design of the drilled shafts for stabilizing the slope was carried out. The essence of this method can be summarized as follows: First, a parametric finite element study was performed to formulate a factor R_p to reflect the effect of soil arching due to the presence of the drilled shafts in slope. It was found that the soil strength parameters and the S/d (the ratio of the clear shaft spacing over the diameter of the shaft) can greatly influence the factor R_p. Next, the limiting equilibrium method of slide approach was used in the computing the factor of safety by incorporating the effect of the reduction factor on the transmitted interslice force on the down-slope side of the shafts as given in Equ (2) and Equ (3).

$$R = \frac{1}{S/d} + \left(1 - \frac{1}{S/d}\right) R_p \qquad \text{Eq. 1}$$

$$P'_{i-1} = \frac{P_{i-1} S - F_{shaft}}{S} \qquad \text{Eq. 2}$$

$$P'_{i-1} = RP_{i-1} \quad \text{Eq. 3}$$

P_{i-1}: The interslice force acting on the slice in front of the shaft
P'_{i-1}: the force transmitted to slice behind the shaft

Finally, starting from the boundary force condition and through an iterative solution procedure, the net forces exerted on the shafts can be calculated along with the FS of the reinforced slope. The final design of the stabilizing drilled shafts for this project is as follows. A total of 42 drilled shafts will be used in the roughly 90 m (300 ft) long roadway section. The diameter of each shaft is 1.05 m (3.5 ft) and the clear spacing (S) to shaft diameter (d) ratio is 2. In general, the drilled shaft socket length is about 6 m (20 ft), while the total length of the drilled shaft is about 13.5 m (45 ft). The reinforcement in the shaft consists of 26 #11 rebars, which provides a nominal moment capacity (Mn) of 3768 m-kN (2,824 ft-kip). The net earth thrust force acting on each drilled shaft was estimated as 445 kN (100 kips) applied at about 2.4 m (8 ft) above the elevation of the top of the mudstone. Furthermore, based on Liang and Zeng (2002) method, the factor of safety of the reinforced slope was calculated to be 1.36.

INSTRUMENTATION

An extensive instrumentation program was planned and carried out to monitor the behavior of the reconstructed embankment slope and the response of the installed drilled shafts. Within the drilled shafts, sensors such as vibrating wire sister bars, inclinometer casings, and Jackout pressure cells were installed to monitor the strain, the deflection and the contact pressure between the shaft and the soil, respectively. In the reconstructed embankment slope, inclinometer casings and piezometers were installed to monitor movements of the slope and ground water tables. A schematic diagram depicting the deployment of the instrumentation inside and outside the drilled shafts is given in Fig. 4. It should be noted that Shaft #20 and shaft #21 are the two shafts installed with instrumentation. Specifically, sixteen (16) vibrating wire strain gages were installed in each shaft at 8 different levels (i.e., depth from shaft top = 3.9 m (13 ft), 4.8 m (16 ft), 5.7 m (19 ft), 6.6 m (22 ft), 7.5 m (25 ft), 8.1 m (27 ft), 8.7 m (29 ft), and 9.3 m (31 ft)), with two strain gages at each level (i.e., upslope side and downslope side). Also, two inclinometer casings were installed inside each drilled shaft.

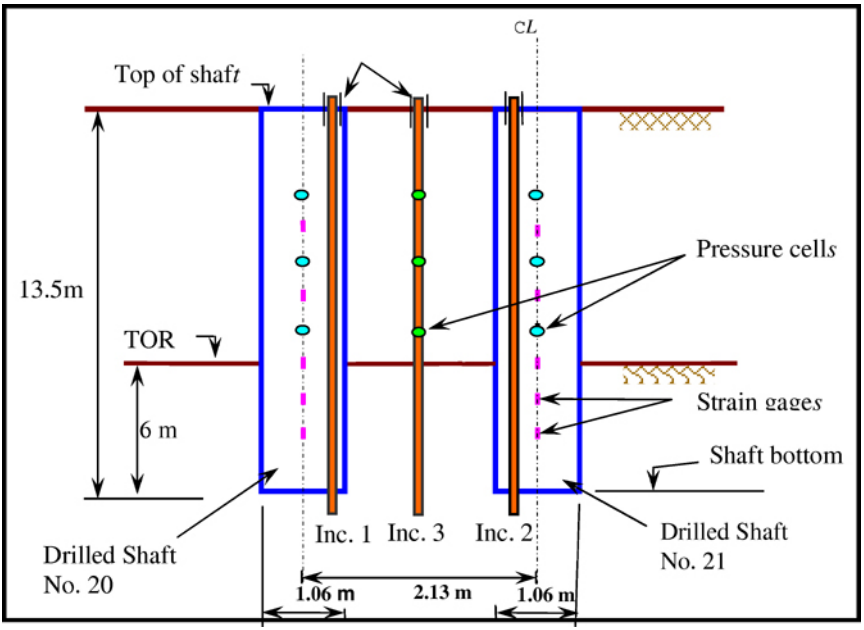

FIG. 4: Instrumentation Plans for Two Drilled Shafts (Cross-section) – JEF-152

FIELD DATA MONITORING RESULTS

The construction at the site occurred between March 2006 and May 2006. Representative inclinometer readings of drilled shaft deflections are presented in Fig. 5(a) while representative readings for soil movements are shown in Fig. 5(b). As can be seen, about 50% of the deflection of the shaft occurred during construction (i.e., back filling, re-grading, etc.) due to the movement of heavy construction equipment. The rate of movements for both drilled shafts and soils on the slope, since the completion of the construction (end of May 2006), has been relatively small. For example, the drilled shaft deflection rate at depth 2 m (6.5 ft) from the top is about 14 mm (0.55 inch) per year, while the slope movement rate at depth 2.0 m (6.5 ft) from the top of the ground is about 18 mm (0.7 inch) per year. Those two inclinometers readings represent the maximum movement ether in the soil or the shafts, among all the inclinometer readings on site.

Measured strain readings were used to calculate the bending moments by multiplying the curvature (strain reading/gage distance at the same depth) by the flexural rigidity of the shaft (EI). A representative moment versus depth plot is presented in Fig. 6. The maximum moment registered is about 1068 m-KN (800 ft-kips). The recorded maximum moment in the drilled shafts is well below the moment capacity of the constructed shafts.

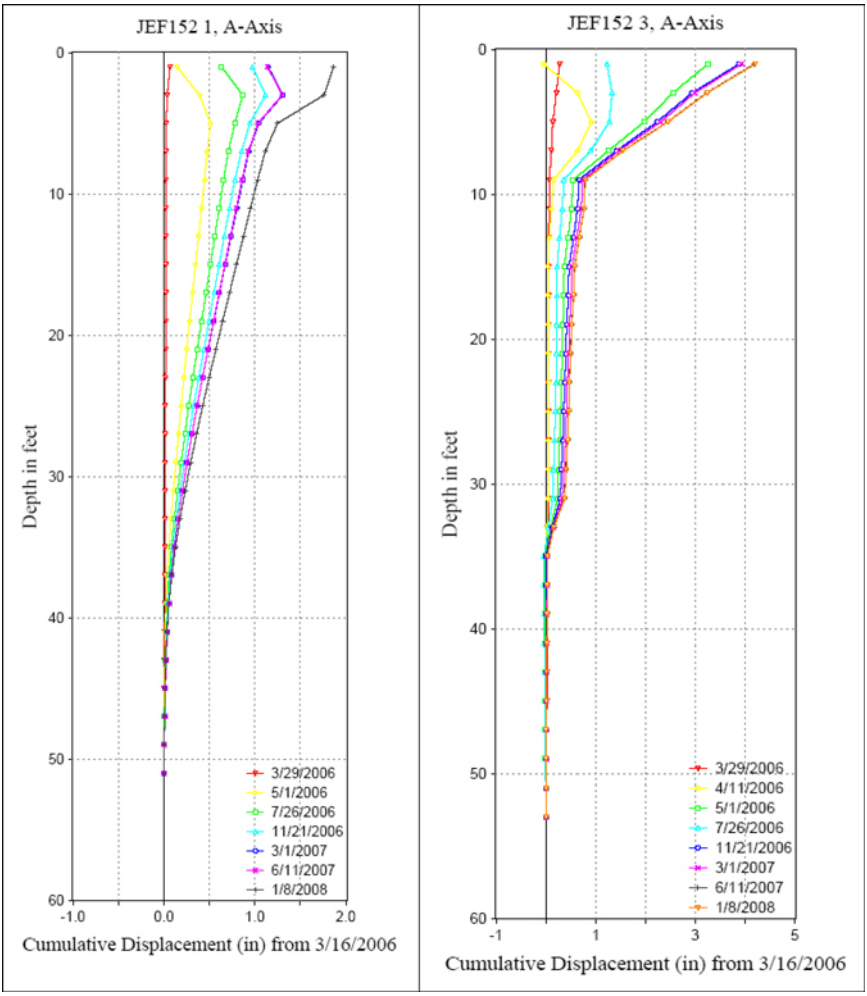

a b

FIG. 5: a) Cumulative Displacement in Inc 1 (Shaft # 21); b) Cumulative Displacement in Inc 3 (Soil)

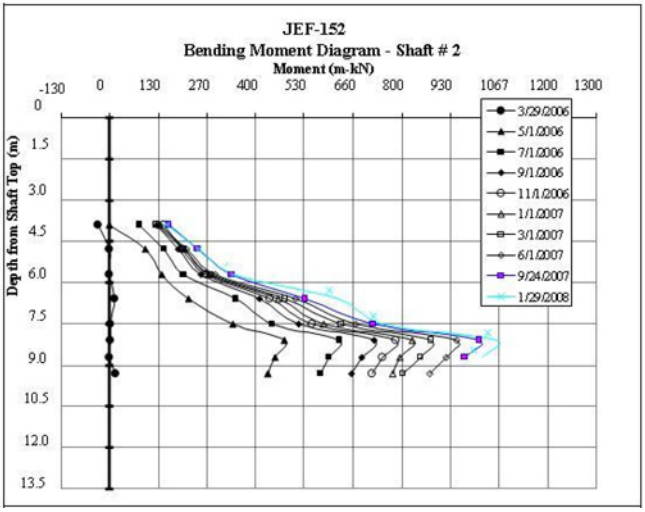

FIG. 6: Bending Moment in Shaft # 22

OBSERVATIONS AND CONCLUSIONS

- The monitoring results of the magnitude of soil movement and the rate of soil movement in the reconstructed and reinforced slope indicate that the drilled shaft reinforced slope is fairly stable even after two years since the completion of the embankment reconstruction.
- The monitoring results of the deflections and moments of the reinforcing drilled shafts suggest that the drilled shafts are safe structurally to resist the earth thrust force from the slope.

REFERENCES

1. Briaud, J. L. (1992). Design of horizontally loaded piles, *The Pressuremeter* published by A. A. Balkema, Rotterdam, Netherlands, pp. 132-160
2. Liang, R., and Zeng, S. (2002). "Numerical study of soil arching mechanism in drilled shafts for slope stabilization." *Soils and Foundations, Japanese Geotechnical Society, 42(2), pp. 83-92.*

Copyrighted Materials
Copyright © 2009 American Society of Civil Engineers (ASCE)
Retrieved from www.knovel.com

Load Tests Help Optimize Design of Deep Foundations

James C. Pegues[1], P.E., M. ASCE, Wade Anundson[2], P.E., Ayoade Adeyefa[3], P.E., M. ASCE

[1]Supervising Principal, Earth Science & Environmental Engineering Department, Southern Company, 42 Inverness Center Parkway, Bin B426, Birmingham, AL 35242;
[2]Principal Geotechnical Engineer, WorleyParsons Group, Inc., 2675 Morgantown Road, Reading, PA 19607;
[3]Geotechnical Engineer, WorleyParsons Group, Inc., 2675 Morgantown Road, Reading, PA 19607

ABSTRACT: Augercast piles and drilled shafts are being used to support environmental control structures and equipment at a Southeast electric generating plant. The plant is located within the Piedmont physiographic province, and is underlain by a typical subsurface profile consisting of upper silty and clayey sands, silts and clays, underlain by a partially weathered rock stratum of varying thickness grading to relatively unweathered rock. Structures with moderate loading were designed to be supported by augercast piles bearing in the partially weathered rock and designed for both side friction and end bearing. Drilled shafts bearing in rock, also designed for both side friction and end bearing, were used to support the more heavily loaded structures. The initially installed augercast piles were subjected to static load tests for compressive, uplift and lateral capacity, indicating higher compressive capacities were available and subsequent phases of the project utilized capacities as much as 50 percent higher than those used originally. Similarly, Osterberg® cell load tests (O-cell) were performed on two drilled shafts at the site, one installed using wet construction methods and the other with dry construction methods (with dewatering and downhole cleaning/inspection.) The load tests evaluated end bearing as well as side friction in the rock, the partially weathered rock and the overburden soils. The results of the drilled shaft load tests allowed for optimization of foundation design with end bearing and rock socket side shear values higher than originally predicted. Furthermore, the O-cell tests revealed similarity between capacities generated from both dry and wet methods of construction. Thus, the decision was made to issue a foundation contract using wet construction methods. Both load test findings resulted in direct cost savings of several million dollars, along with indirect savings due to reductions in the length of the construction schedule.

INTRODUCTION

Plant Robert W. Scherer, located near Macon, Georgia, is an electric generating facility consisting of four coal-fired units having a total capacity of approximately 3,500 megawatts. A large environmental controls initiative at the facility includes the

construction of baghouses, selective catalytic reduction (SCR) facilities, and flue gas desulfurization (FGD) facilities. The geotechnical studies for these projects were performed by in-house Southern Company geotechnical engineers. Design services were performed by WorleyParsons, and their geotechnical engineers worked closely with Southern Company geotechnical engineers to develop the foundation systems.

Plant Scherer is located within the Southern Piedmont Physiographic province. At this site, biotite gneiss is the predominant rock unit. Residual overburden soils in the Piedmont typically consist of silty and clayey fine to medium-grained sands. There is also typically a transition zone of partially weathered rock (PWR) having soil characteristics as well as evidence of relic structure of the parent bedrock. This transition zone is generally characterized by standard penetration test (SPT) N-values greater than 100 blows per 300 mm (or 100 blows per foot, bpf).

SITE INVESTIGATIONS

Four separate geotechnical explorations were performed in 2006 and 2007 to support the environmental control projects. The total geotechnical exploration scopes of work included fifty SPT borings, most including rock coring, five CPT soundings, and two cased boreholes with downhole geophysical testing. In general, the upper residual silty sands (with some clay and silt) exhibited SPT N-values ranging from 0 to 50 bpf. The greatest variability across the site related to the depth and thickness of the PWR, which varied from about 3 m (10 feet) to greater than 12 m (40 feet) before rock was encountered, and in a few select borings, was basically non-existent. The underlying rock varied in quality, with initial core run recoveries as low as 5 to 10 percent, increasing to 90 to 100 percent recovery after penetration below the depth of refusal of 3 m to 6 m (10 to 20 feet).

INITIAL FOUNDATION SELECTION AND RECOMMENDATIONS

Baghouse Foundations

Compressive loads on supports for the baghouse structures ranged from about 2936 KN (660 kips) to as much as 8674 kN (1950 kips), with uplift loads of 534 kN (120 kips) to 2157 kN (485 kips). Lateral loads at the supports were expected to range from about 1068 kN (240 kips) to 2002 kN (450 kips). Augercast piles were selected for the baghouse structures, as the piles had a history of successful application in the Piedmont for moderately loaded structures. The initial design of the augercast piles was based on extension into the PWR a minimum of 3 m (10 feet) (or refusal if shallower), with a minimum pile length of 7.6 m (25 feet). Axial capacity was predicted using the methods recommended by Zelada and Stephenson (2000).

Lateral load capacities for both free-head and fixed-head conditions were predicted using Ensoft's LPILE® software. Lateral capacities of various pile center-to-center spacings were evaluated, using p-multipliers recommended by Rollins, et al (2005). Pile spacings of 6 diameters or greater were assumed to undergo no reduction in capacity due to influence from adjoining piles.

FGD and SCR Structure Foundation Design

High compressive loads were expected for several FGD components, particularly new stacks and absorber vessels. Additionally, high uplift loads were expected for the primary SCR structures due to a combination of wind loads and the height of the structures relative to their foundations. Therefore, augercast piles were recommended for lightly to moderately loaded structures and equipment (such as pumps, fans and tanks), and drilled shafts were recommended for the more heavily loaded structures and where lateral loads were considered a design constraint. Due to limited access considerations, micropiles were given primary consideration for many of the SCR structures. As micropile construction was not yet underway at the time this paper was prepared, they are not addressed further herein.

Historic geotechnical and design documents indicate allowable end-bearing pressures of 1436 kPa (30 ksf) to 2873 kPa (60 ksf) were used on past projects, with limited documentation of capacities as high as 4788 kPa (100 ksf) for some structures. Due to expected high loads in some locations, we recognized that drilled shaft design would need to include both side shear and end bearing components. An allowable end bearing component of 2873 kPa (60 ksf) was recommended. For sockets in competent rock, an allowable side shear value of 239 kPa (5 ksf) was used. Additionally, side shear values of 144 kPa (3 ksf) for the PWR layers and 48 kPa (1 ksf) for the soil above PWR were to be considered. The stack foundations utilized 2438 mm (96-in) diameter shafts while both 1524 mm (60-in) diameter and 1829 mm (72-in) diameter drilled shafts were used for the absorber foundations. Other lightly loaded structures in the absorber area utilized 1219 mm (48-in) diameter shafts.

LOAD TESTS AND FOUNDATION OPTIMIZATION

Construction at the site began in 2007 with the baghouse structures, and static load tests were performed to evaluate compression, uplift and/or lateral loads on the augercast piles. Drilled shaft construction followed in early 2008, and O-cell load tests were performed on two test shafts to help optimize design.

Augercast Piles

For the first baghouse project, both 406 mm (16-in) diameter and 610 mm (24-in) diameter augercast piles were used. Due to variability in thickness in PWR, the decision was made at the time of initial construction to terminate all augercast piles at the initial depth of refusal. The rigs used by Berkel & Co. Contractors for augercast pile installation had a torque rating of almost 50 kN-m (37,000 ft-lbs), and a drill unit on the order of 22 kN (5,000 lbs). Refusal was defined as less than one foot of penetration in one minute at the limiting torque capacity.

Compression, tension and lateral load tests were performed on 406 mm (16-in) diameter and 610 mm (24-in) diameter augercast test piles installed using the aforementioned refusal criteria. Piles were first loaded to twice the design load for each case, with only nominal deflections measured. The piles were then loaded in an attempt to simulate failure conditions. The 406 mm pile (14 m long) was loaded to

about 2224 kN (500 kips), with total deflection on the order of 4 mm (0.16 inches). For the 610 mm pile (9 m long), load was applied incrementally to about 4448 kN (1000 kips), with a total deflection of about 15 mm (0.6 inches). Load-deflection curves for the two "failure" tests are shown in Figure 1.

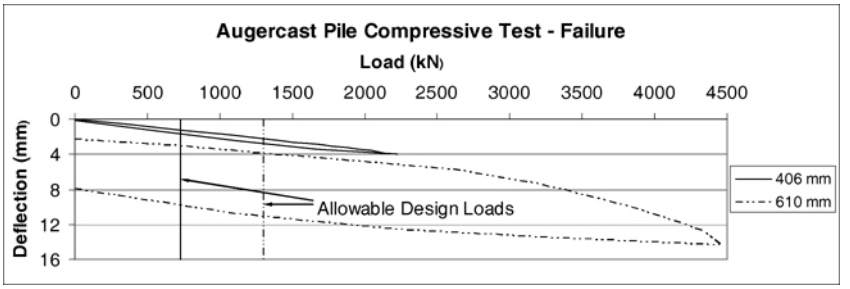

FIG. 1 Compression Load Test Results

Tension tests were performed in a similar manner on 406 mm and 610 mm test piles, again indicating significantly higher than predicted capacities were available. Most notable was the attempt to fail the 610 mm test pile in tension. The pile was loaded to 2224 kN (500 kips) tension with only 5.7 mm (0.225 inch) movement. The 406 mm pile was loaded to about 1580 kN (355 kips), with 3.3 mm (0.13 inch) movement. Both tests were terminated upon reaching the capacity of the test system.

For lateral load tests, only free-head conditions were evaluated to check the design soil model. Initially, each test pile was loaded to twice the design load. Total deflection for the 406 mm pile was 9.1 mm (0.36 inches) at 133 kN (30 kips), with measured deflection of 6.9 mm (0.27 inches)for the 610 mm pile at a loading of 267 kN (60 kips). The lateral tests were then rerun in an effort to achieve a deflection of 25 mm (1-in). A load of 280 kN (63 kips) was achieved for the 406 mm pile, and 680 kN (153 kips) for the 610 mm pile at about 25 mm deflection. Figure 2 presents the load-deflection curves for the 25 mm deflection testing.

Based on the results of the initial load testing, subsequent design of augercast piles utilized allowable axial and lateral design values 50 percent higher than those used for the Unit 3 project. Subsequent load testing on a 457 mm (18-in) diameter augercast pile designed with the revised, higher capacities revealed acceptable results.

Drilled Shafts

Two test shafts were installed within the vicinity of the Units 3 and 4 chimney and absorber foundations. The design diameter for both wet-constructed and dry-constructed test shafts was 1524 mm (60 inches). However, as with typical drilled shaft construction in rock, the shafts were oversized at the top in order to allow for staged casing size reductions. Both test shafts were constructed as 1829 mm (72-in) diameter at the top, with an intermediate diameter of about 1676 mm (66-in),

terminating with the design 1524 mm diameter. Both shafts extended approximately 3 m (10 feet) below the top of relatively unweathered rock, with dry-constructed shaft installed to a depth of approximately 25 m (81 feet) below the existing ground surface and the wet-constructed shaft installed to an approximate depth of 24 m (78 feet). The top of concrete was approximately 0.61 m (2 feet) and 2 m (7 feet) below grade for the dry-constructed and wet-constructed shaft, respectively.

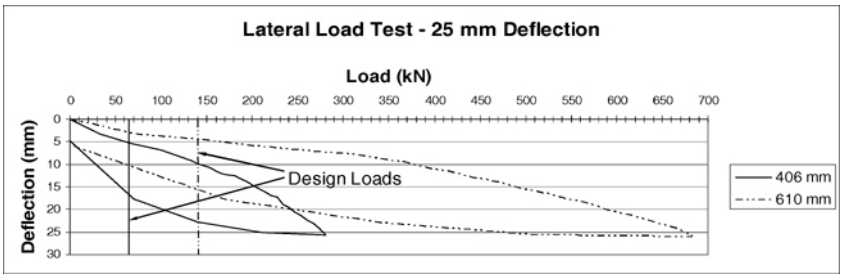

FIG. 2 Lateral Load Test Results

There were two primary objectives with the load test program. The first was to evaluate the feasibility of using "wet" construction techniques as opposed to "dry" methods requiring dewatering of the shaft to allow for downhole cleaning and inspection of the bearing surface and exposed rock socket. The second objective was to evaluate the measured side shear and end bearing values and compare them against the theoretically estimated values with the possibility of revising the estimated values for the final design of the drilled shaft foundations.

Test shafts were installed by Russo Corporation. The wet-constructed shaft was drilled to the top of rock, as indicated by refusal to a rock auger. Coring was then used to extend the shaft approximately 3 m (10 feet) below the top of rock. A cleanout bucket was used to remove sediment and rock fragments from the bottom of the shaft. Concrete was then placed via the tremie method. The dry shaft was installed using "conventional" dry construction techniques. After cleaning with an auger and cleanout bucket, downhole hand cleaning was performed, and a test hole was installed to a depth of 3 m (10 feet) below the bottom of the shaft. An inspector went down the hole, checked the bearing surface, the exposed rock socket and the test hole, and the shaft was judged adequate and the concrete was placed.

Test shaft instrumentation and assembly, carried out by LOADTEST, Inc., was practically identical for both methods of construction. As indicated in Figure 3 for the wet-constructed shaft, the loading assembly consisted of one 660 mm (26-in) diameter O-cell located 0.6 m (1.8 feet) above the tip of the shaft. O-cell testing instrumentation included three Linear Vibrating Wire Displacement Transducers (LVWDTs) positioned between the lower and upper plates of the O-cell assembly to measure expansion. Two telltale casings (nominal 13 mm steel pipe) were attached to the carrying frame, diametrically opposed, extending from the top of the O-cell

assembly to beyond the top of concrete. Strain gages were used to assess the side shear load transfer of the shaft above the O-cell assembly. Two lengths of steel pipe were also installed, extending from the top of the shaft to the top of the bottom plate, to vent the break in the shaft formed by the expansion of the O-cell (see Figure 3). The pipes were filled with water prior to the start of the test.

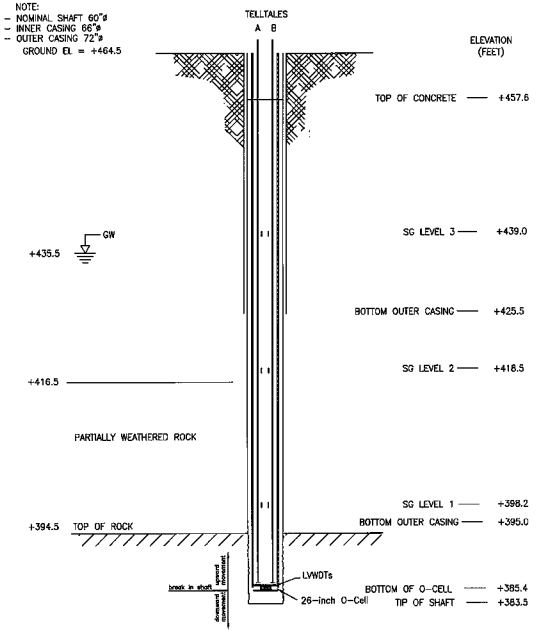

FIG. 3 Schematic Section of the Test Shaft (from LOADTEST)

The loads applied by the O-cell act in two opposing directions. The maximum sustained bi-directional loads applied to the dry-constructed shaft and wet-constructed shaft were 19 MN (4,278 kips) and 18 MN (4,108 kips), respectively. For the dry-constructed shaft (Figure 4), unit shear data calculated from strain gages indicated average unit side shear of 800 kPa (16.7 ksf) in the rock and 177 kPa (3.7 ksf) in the PWR. A maximum applied end bearing pressure of 9260 kPa (193.4 ksf) was also calculated at an approximate displacement of 33 mm (1.3 inches). For the wet-constructed shaft, the average unit side shear was calculated to be 886 kPa (18.5 ksf) in the rock and 115 kPa (2.4 ksf) in the PWR (Figure 5.) At a displacement of approximately 38 mm (1.5 inches), the maximum applied end bearing pressure was calculated to be on the order of 8834 kPa (184.5 ksf).

There was no appreciable difference between the load test results for the wet-constructed shaft and the dry-constructed shaft. Therefore, the decision was made to allow construction of the production drilled shafts using wet construction methods.

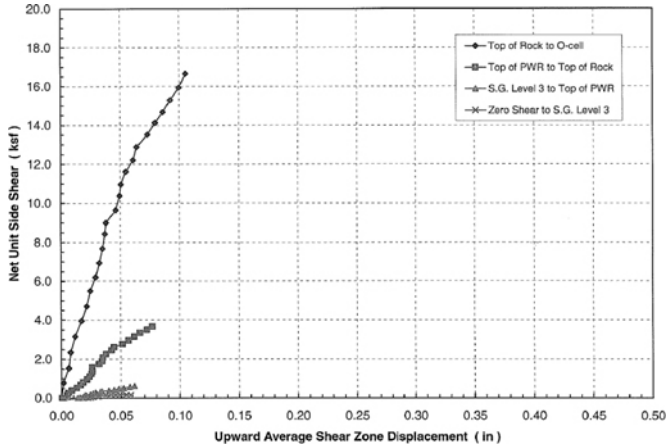

FIG. 4 Mobilized Net Unit Side Shear for Dry Shaft (from LOADTEST)

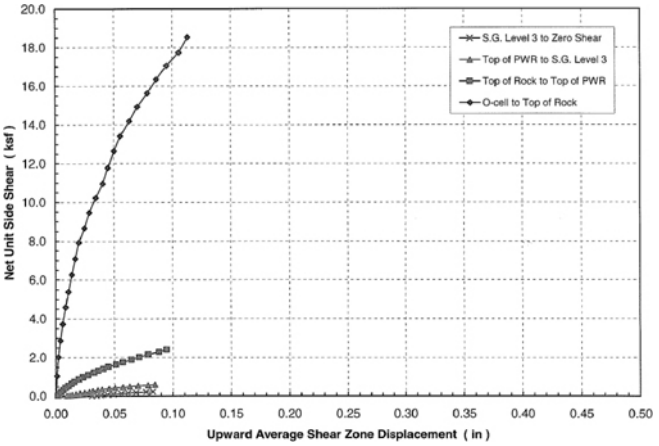

FIG. 5 Mobilized Net Unit Side Shear for Wet Shaft (from LOADTEST)

Furthermore, the end bearing results can be misleading at first glance. The load test reports indicate an ultimate end bearing contribution on the order of 9097 kPa (190 ksf). However, these higher end bearing values occurred at displacements on the order of 33 mm to 38 mm. Thus, lower end bearing values (than indicated by the load tests) were necessitated in order to maintain shaft displacements within acceptable ranges.

A review of the load test results indicate that some increase in the originally recommended design values was warranted. After evaluation of the data, a

modification to the design values was recommended as shown in the Tables 3 and 4. Both an end-bearing along and an end-bearing with side friction options were considered. It should be noted that the recommended values are "allowable" values.

Table 3 Recommended Drilled Shaft Design Values - End Bearing Option

Design Component	Original Recommended Design Values	**Revised Design Values**
Rock Socket Side Friction	240 kPa (5 ksf)	**383 kPa (8 ksf)**
End Bearing	2873 kPa (60 ksf)	**3830 kPa (80 ksf)**

Table 4 Recommended Drilled Shaft Design Values - Side Friction Option

Design Component	Original Recommended Design Values	**Revised Design Values**
Side Friction Above PWR	48 kPa (1 ksf)	**48 kPa (1 ksf)**
Side Friction in PWR	144 kPa (3 ksf)	**144 kPa (3 ksf)**
Rock Socket Side Friction	144 kPa (3 ksf)	**383 kPa (8 ksf)**
End Bearing	1436 kPa (30 ksf)	**2873 kPa (60 ksf)**

CONCLUSIONS

Static load tests on the augercast piles drilled to practical refusal in the PWR revealed capacities much higher than those predicted by published methods and/or typically used in this area, thus allowing for fewer and/or smaller diameter piles. O-cell load tests on both "wet" and "dry" construction drilled shafts raised the comfort level of acceptance for using wet construction methods when dry construction was the typical approach in the region. The O-cell tests also allowed for the use of higher allowable design values for axial capacity in the drilled shafts. The use of the revised design values for drilled shafts significantly reduced the foundation sizes and lengths, thereby reducing both the overall costs associated with drilled shaft construction and the amount of time required for foundation construction. The use of the wet construction method also resulted in a reduction in the required construction schedule, and resulted in significant cost savings as well.

REFERENCES

Zelada, G. A. and Stephenson, R.W., (2000). "An Evaluation of Auger Cast-in-Place Design Methodologies for Compression Loading." *New Technological and Design Developments in Deep Foundations*, Proceedings of Sessions of Geo-Denver 2000, ASCE

Rollins, K.M., Lane, J.D., and Gerber, T.M. (2005). "Measured and Computed Lateral Response of a Pile Group in Sand." *Journal of Geotechnical and Geoenvironmental Engineering*, January 2005, 103-114

Copyrighted Materials
Copyright © 2009 American Society of Civil Engineers (ASCE)
Retrieved from www.knovel.com

Drilled Shaft Performance in Cemented Calcareous Formations In the Southeast US

Dan Brown[1], M.ASCE, Ph.D., P.E., and W. Robert Thompson, III,[2] M.ASCE, P.E.

[1]President, Dan Brown and Associates, PLLC, 300 Woodland Road, Sequatchie, TN 37374; Phone: 423-942-8681; dbrown@danbrownandassociates.com
[2]Principal, Dan Brown and Associates, PLLC, 2400 Old Creek Road, Montgomery, AL 36117; Phone: 334-239-3135; rthompson@danbrownandassociates.com

ABSTRACT: Cemented calcareous formations, typically referred to as chalk or marl, are widespread in the southeastern U.S. and are ideally suited to the use of drilled shaft foundations. Chalk formations are relatively stable in an open borehole and are relatively easy to drill but difficult to penetrate with driven piling. These cohesive intermediate geomaterials are sometimes difficult to characterize for design purposes because of the difficulty in sampling and testing. This paper provides a review of recent instrumented load tests performed in these cemented calcareous materials. A total of 15 tests were selected from southeastern states based on the availability of good quality load test data and geotechnical information. Most of the test data include measurements of compressive strength from cores. Ultimate unit side shear and end bearing resistance is found to show a relationship with unconfined compressive strength using existing published correlations for weak rock materials.

INTRODUCTION

As a part of ongoing research sponsored by the ADSC Industry Advancement Fund, researchers at several universities are performing an evaluation of design methods using drilled shaft load test data from around the U.S. This article provides a review of data from cemented calcareous formations, typically referred to as chalk or marl. Similar studies are ongoing for other types of rock and intermediate geomaterials.

These chalk materials are typically massive and often have the appearance of hard clay or very soft rock. Microfossils are typically abundant, as evident in the scanning electron micrograph of a marl sample from Charleston, SC shown in Figure 1. Sand may be present in varying amounts, as well as phosphate and clay minerals.

Sampling can be difficult, as the chalks are typically too hard to sample with pushed tube samplers. Rock core sampling techniques can sometimes be used, but cores of softer chalks are easily damaged when using rock coring techniques.

Common practices include standard penetration tests (although SPT N-values of greater than 50 blows per 0.3 m (foot) are common) and pitcher-barrel coring samplers as shown in the photos of Figure 2.

Load tests that were selected for inclusion in this study are based on a review of data collected from Loadtest, Inc., the Alabama Department of Transportation, the Mississippi Department of Transportation, and available literature. A total of 15 tests were selected from southeastern states, based on the availability of good quality load test data and geotechnical information. A case history summary of each load test is included in Brown and Thompson (2008) as are the reference citations of the load tests and geotechnical reports for each test.

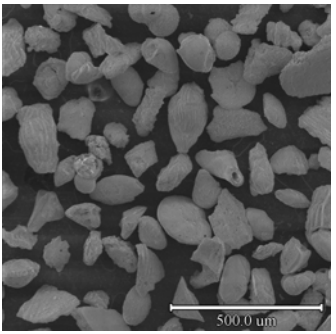

FIG. 1. SEM Photograph of a Cooper Marl Sample (Camp, 2004)

FIG. 2. Pitcher Barrel Sample of Chalk from Alabama

ANALYSIS

Analyses of load test data can be complicated by the lack of consistency of the types of data collected, particularly in strength data used to characterize the geomaterials. The unconfined compressive strength, or q_u, is typically used to describe hard cohesive soils and soft rocks.

The collected load test data listed in Table 1 has values of q_u ranging from 138.9 to 6080 kPa (2.9 to 127 ksf). Some sites had SPT data available. Except for the tests in Cooper Marl, SPTs (where performed) were usually recorded as 100+ blows per 0.3 m (foot), or refusal. The sites in the Cooper Marl tended to have blow counts less than 50 blows per 0.3 m (foot). The US 80 project site in Alabama had only SPT data; an estimated $q_u = 2150$ kPa (45 ksf) was used for analyses based on correlations from nearby projects.

Side Shear

Turner (2006) summarized several basic formulas for estimating ultimate unit side shear resistance utilizing a correlation between ultimate unit side shear, f_s, and the square root of the unconfined compressive strength, q_u. These relationships may be expressed in a dimensionless form by normalizing compressive strength by atmospheric pressure as shown in (1):

Unit Side Resistance:
$$f_s = C \cdot p_a \cdot \sqrt{\frac{q_u}{(p_a)}} \tag{1}$$

where p_a is atmospheric pressure and C is an empirical constant.

Correlations of this type have been applied to rock sockets in shale, mudstone, claystone, limestone, and marl. Horvath and Kenny (1979) first proposed such a relationship, with an empirical constant ranging from 0.65 to 1 for smooth to rough sockets (with their original expression adjusted to the units normalized by p_a as indicated above). Rowe and Armitage (1987) proposed a similar expression with different constants, and Kulhawy and Phoon (1993) evaluated a larger database of rock sockets and proposed values of C ranging from 1 to 3 depending upon sidewall roughness and degree of weathering. An updated evaluation of these test data by Kulhawy et al (2005) suggests that a value of C = 1 represents the mean estimate of design ultimate side shear resistance, based on the most up-to-date analysis of the available data.

Table 1. Summary of Load Test Data (Brown and Thompson, 2008) (bpf = b/0.3m; 1 ksf = 47.88 kPa)

State	*Project*	*Test No.*	*Reference*	*Test Type*	*Material*	*Shaft Dia. (in)*	*SPT N values (bpf)*	*q_u (ksf)*	*Unit Side Shear (ksf)*	*Unit End Bearing (ksf)*
AL	US 80 over Mill Creek	AFT-106058	1	Statnamic	Demopolis/Mooreville Chalk (hard gray, clayey silt)	84	N > 100	---	5.8 – 10.7	41.6
AL	SR 10 Blue Springs	LT-8571	2	O-Cell	Claystone	54	N > 100	---	0.9 - 1.7	27.4
AL	Hyundai Motor Manufacturing	LT-8904	2	O-Cell	Demopolis Chalk	42	42 - 62	18.4	3.4 – 9.4	90.9
AL	Andalusia, AL	WRT-1-1	3	Conventional	Claystone	28	---	17 - 127	7.0 - 9.6	---
MS	US 45 over Town Creek	LT-8194	2	O-cell	Mooreville Chalk (Hard grey, clayey, silt)	48	---	22.9	5.1	36.9
MS	SR 25 over Talking Warrior Creek	LT-8373	2	O-cell	Basal Formation (Hard Clayey Silt and Silty Clay)	42	---	6.1 - 27.9	2.2 - 5.9	67.8
MS	US 82 Oktibbeha County	LT-8461-1	2	O-cell	Demopolis Formation (Hard, Argillaceous Chalk)	48	---	10.9 - 38.6	3.1 - 7.3	214.0
MS	US 82 Oktibbeha County	LT-8461-2	2	O-cell	Prairie Bluff Formation (Hard, Silty, Clay) and Ripley Formation (Hard, Sandy, Silt)	48	---	27.1 - 28.8	2.1 - 3.9	108.0
MS	SR 42 over Thompson Creek	LT-8487	2	O-cell	Very stiff to hard, clayey silt and silty sand	54	---	11.1	1.9 - 5.0	24.8
MS	I-55 at Old Agency Rd.	LT-8788	2	O-cell	Yazoo Formation (Hard, tan, silty clay)	24	---	9.0 - 11.1	0.3 - 1.5	52.3
MS	SR 9 over SR 6	LT-8912-1	2	O-cell	Clayton Formation (Hard, clayey silt and silty clay)	48	N > 100	18.0	7.7 - 8.4	202.8
MS	SR 9 over SR 6	LT-8912-2	2	O-cell	Ripley Formation (Hard, very fossiliferous, sandy silt)	48	N > 100	18.0	8.8 - 12.9	221
MS	Leake County, MS	WRT-4	3	O-cell	Chalk	66		12.1	3.2	46.2
SC	Mt. Pleasant, SC	WRT-5-1	3	Conventional	Cooper Marl	24	9 - 100+	2.9	3.6	28.6
SC	Mt. Pleasant, SC	WRT-5-2	3	Conventional	Cooper Marl	24	9 - 100+	2.9	3.6	---
SC	Cooper River Bridge Charleston/Mt. Pleasant	LT-8650	2,4	O-cell (10 tests)	Cooper Marl (Clayey sand, sandy clay, sandy silt)	72 and 96	15 - 100+	---	2.0 - 6.5	43.5 - 80
SC	Breach inlet Bridge	LT-8661	2	O-cell	Cooper Marl (Clayey sand, sandy clay, sandy silt)	48	15 - 28	4.2 - 5.9	0.2 - 2.8	49.4

Reference:

1. AFT-XXXXXX: Statnamic test report from AFT, Inc. with permission of owning state DOT
2. LT-XXXX: O-Cell test report from Loadtest, Inc. with permission of owning state DOT;;
3. WRT-X: Test data from Thompson, W.R. III (1994) *Axial Capacity of Drilled Shafts Socketed into Soft Rock*, M.S. Thesis, Auburn University, AL
4. Values shown are the ranges from the 10 tests. Seven shafts were 96 inches in diameter, three were 72 inches. Shaft LT-8650-1 is used as representative for Figure 4a.

The Horvath & Kenney relationship is compared with measured unit side resistance from the data evaluated in this study, with the data plotted versus q_u.on Figure 3. Each test site with q_u data is shown as a small open symbol. The averages of the groups of tests (Mississippi (MS) Chalk, South Carolina (SC) Cooper Marl, and Alabama (AL) Claystone) are shown in large shaded symbols. The US 80 test is plotted using an estimated value for q_u. The curve representing the equation derived from the Horvath & Kenney relation for ultimate unit side shear resistance is shown, with the empirical constant ranging from C = 0.65 to 1.0. The data presented in this figure suggest that the relationship provides a reasonably conservative estimate of side shearing resistance with the constant at the lower end of this range (0.65), and a better fit through the mean with C = 0.85.

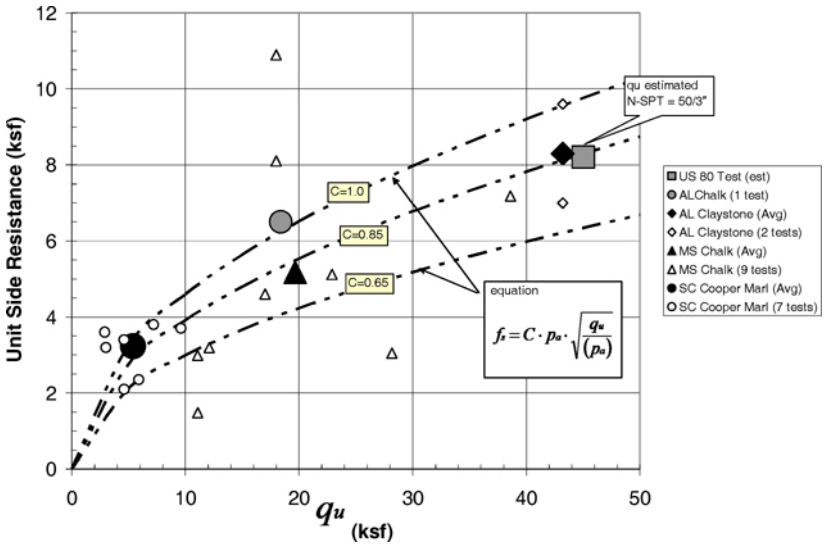

FIG. 3. Unit Side Resistance vs. q_u (100kPa ≈ 2 ksf)

End Bearing

A wide range of expressions are available for relating base resistance to strength parameters of weak rock or marl. The O'Neil and Reese (1999) guidelines for cohesive intermediate geo materials (IGM), which are massive and relatively free of joints, fissures, or weak seams, would suggest a value similar to (2):

Unit Base Resistance: $$q_{ult} = 2.5 q_u \quad (2)$$

Since the mobilization of unit base resistance occurs over a much larger range of deflections than unit side resistance, the base resistance data are evaluated from the

load tests as a function of displacement in terms of the shaft diameter. Figures 4a and 4b illustrate the mobilized unit base resistance from the load tests plotted as a function of displacement. The shaft displacements are normalized by dividing the displacements by the shaft diameter, and thus are expressed as a percent of the shaft diameter. The mobilized unit base resistance was normalized by q_u.

Two figures were used to plot the data for easier reading. Each test is labeled with the Test No. from Table 1. Three of the tests (LT-8571, WRT-1-1, and WRT-5-2) did not have sufficient end bearing data to plot. The curve labeled LT-8560-1 is plotted as representative of the ten load tests included in Table 1 as LT-8650.

For all but two of the remaining tests, the measured end bearing load-displacement curve was available and is included on the plots. Two tests reached the maximum applied load at a shaft deflection of less than 1%. These are shown as single points on the graphs, and may not have fully mobilized the available base resistance.

The data presented on these figures suggest that the use of the O'Neil and Reese (1999) guideline for cohesive IGM would be conservative in most cases. Some of the data indicate that this guideline could be very conservative; it is possible that the q_u data from some of these sites may have been affected by sample disturbance, or that a higher sand content affects the correlation with a simple q_u measure of strength.

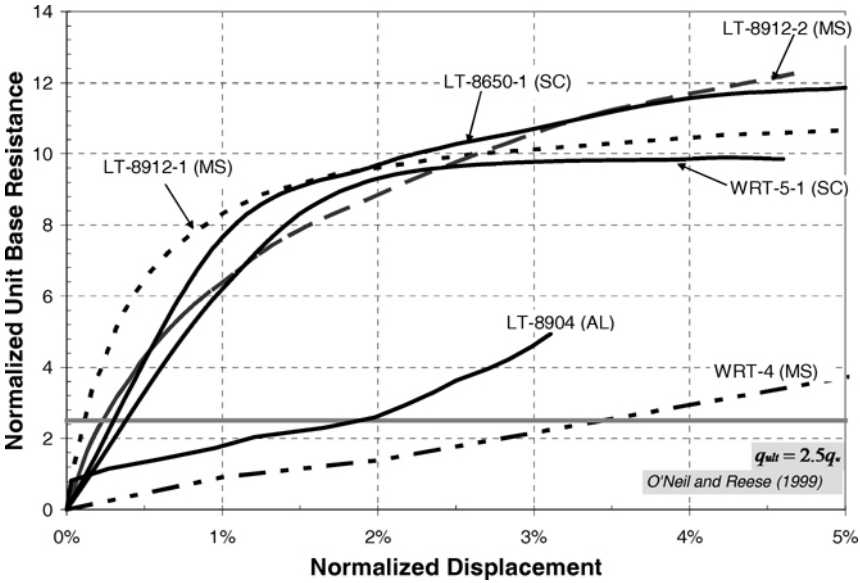

FIG. 4a. Normalized Base Resistance (Resistance/q_u) vs Normalized Displacement (Shaft Deflection/Shaft Diameter in %)

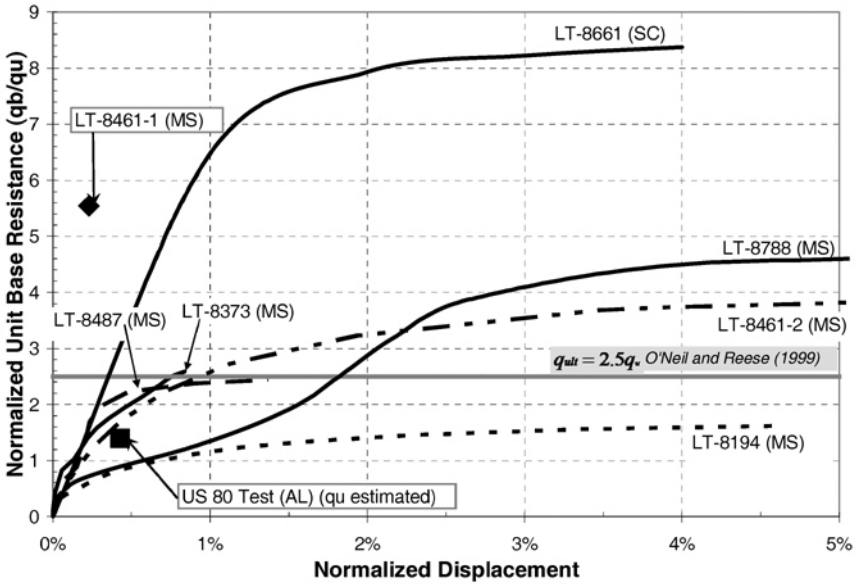

FIG. 4b. Normalized Base Resistance (Resistance/q_u) vs Normalized Displacement (Shaft Deflection/Shaft Diameter in %)

CONCLUSIONS

The load test data from chalk and marl formations suggest that drilled shafts may conservatively be designed based on unconfined compressive strength data using Eq. 1 with C=0.65 for side shear and using Eq. 2 for base resistance. Additional discussion of the design methodology for these geomaterials is included in the final project report and in the forthcoming update to the FHWA Drilled Shaft Manual.

ACKNOWLEDGMENTS

The writers wish to acknowledge the contributions of ADSC: The International Association of Foundation Drilling, Ms. Lyndi Blackburn Davis, P.E. of the Alabama Department of Transportation, Mr. Sean Ferguson, P.E. of the Mississippi Department of Transportation, and Loadtest, Inc.

REFERENCES

Brown, D.A. and Thompson, W.R. (2008). "BRF-0008(536) Drilled Shaft Load Test Assessment, Sumter County", Research Reports for the Alabama Department of Transportation, Montgomery, AL.

Camp, W.M. (2004). "Drilled and Driven Foundation Behavior in a Calcareous Clay", *GeoSupport 2004*, Orlando, FL, ASCE GSP 124, Vol 1, 1-18.

Horvath, R.G. and Kenney, T.C. (1979). "Shaft Resistance of Rock-Socketed Drilled Piers", *Symposium on Deep Foundations*, ASCE National Convention, Atlanta, GA, 182-214.

Kulhawy, F.H. and Phoon, K.-K. (1993). "Drilled Shaft Side Resistance in Clay Soil to Rock", *Geotechnical Special Publication No. 38: Design and Performance of Deep Foundations*, ASCE, Reston, VA, 172-183.

Kulhawy, F.H., Prakoso, W.A., and Akbas, S.O. (2005). "Evaluation of Capacity of Rock Foundation Sockets". *Alaska Rocks 2005, Proceedings, 40th Symposium on Rock Mechanics* (CD-ROM), G. Chen, S. Huang, W. Zhou, and J. Tinucci, Eds., Anchorage, AK, June 2005.

O'Neil, M.W. and Reese, L.C. (1999). *Drilled Shafts: Construction Procedures and Design Methods*, FHWA Publication No. FHWA-IF-99-025, Federal Highway Administration, Washington, D.C.

Rowe, R.K. and Armitage, H.H. (1987). "A Design Method for Drilled Piers in Soft Rock", *Canadian Geotechnical Journal*, Vol. 24, 1987, 126-142.

Turner, J. (2006). *NCHRP Synthesis 360: Rock Socketed Shafts for Highway Structure Foundations*, Transportation Research Board, Washington, D.C.

Copyrighted Materials
Copyright © 2009 American Society of Civil Engineers (ASCE)
Retrieved from www.knovel.com

Interpreted Failure Load for Drilled Shafts via Davisson and L_1-L_2

Fred H. Kulhawy[1], Dist.M.ASCE and Anwar Hirany[2], M.ASCE

[1]Professor, School of Civil and Environmental Engineering, Hollister Hall, Cornell University, Ithaca, NY 14853-3501; fhk1@cornell.edu
[2]Account Executive, Electric Power Research Institute, Dallas, TX 75234; ahirany@epri.com

ABSTRACT: The 1972 Davisson method for load test interpretation was developed for specific driven pile conditions. Because it is simple and easy to use, it has been applied widely and indiscriminately. However, if used as is, it is not appropriate for drilled foundations and will give interpreted capacities that are too low. Modifying it into the slope tangent method improves the results for drilled shafts, but the capacities still are too low. The alternative L_1-L_2 method was developed by the authors in 1989 for drilled shafts, and it gives consistently higher capacities. Subsequently, this method has been found to be applicable for other drilled foundations as well. Case history evaluations show that the slope tangent and L_1-L_2 capacities can be correlated very conveniently for practical use when the load test data are less than optimal.

INTRODUCTION

Load-displacement curves from axial compression tests on deep foundations can exhibit any of the three shapes shown in Figure 1. The peak of A and the asymptote of B define clearly the limit or "failure load" for the foundation. However, for curve C, this limit is not defined clearly. Accordingly, many investigators have proposed procedures to define an "interpreted failure load". In 1972, Davisson proposed one such procedure for specific driven pile conditions. Because it is simple and easy to use, it has been applied widely and, in our opinion, indiscriminately. At the March 2009 joint meeting of the ASCE Geo-Institute, ADSC, and PDCA, a panel discussion entitled "Application of the Davisson Offset Method in Determining the Ultimate Load for Drilled Shafts" is to be held, including the first author as a panelist. This paper was prepared for this discussion and future reference, and it includes the following: (1) a review of Davisson's actual method, (2) various modifications to this method, (3) a preferred alternative to this method, and (4) useful interrelationships among the methods. Practical implications are noted throughout.

DAVISSON METHOD

In 1972, Davisson presented his load test interpretation method with only minimal

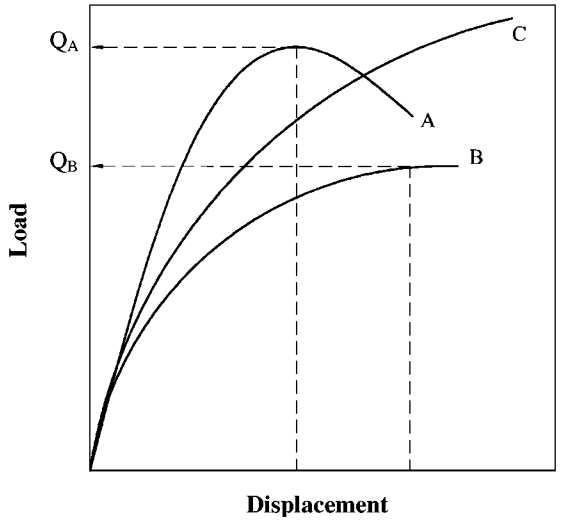

FIG. 1. Typical Load-Displacement Curves for Deep Foundations

explanation. He stated "This method is presented without full background explanation because a separate publication is intended for that purpose." Unfortunately, that publication was not done, to the best of our knowledge. His explanation is given in one figure and less than one page of text in a 32 page paper entitled "High Capacity Piles", in which high capacity is defined as working load capacities exceeding the range of 80 to 100 tons (about 700-900 kN). He described his interpretation method as follows:

> "For piles of normal dimensions, approximately 1 foot wide, ρ_{tip} is approximately 0.10 inch for most soils. It has been found that when the pile settlement is 0.15 inches plus ρ_{tip} below the elastic index line, the ultimate load can be presumed to have been reached." [Note that $\rho_{tip} = Q_{tip}$ (original Davisson notation) = soil quake = displacement required to cause yielding of the soil at the pile tip.]

This method was developed for high capacity piles driven by impact hammer. In the examples in his paper, he uses primarily HP and WF steel piles, 10 to 14 in. (254 to 356 mm), pipe step-tapers, and both an 18 in. (457 mm) steel pipe and an 18 in. octogonal prestressed concrete pile. The depth-to-diameter ratio (D/B) ranged from 50 to 100 and more. There is no mention of drilled foundations or cast-in-place concrete. Furthermore, the method applies to compression tests conducted using a "quick" method or constant-rate-of-penetration (CRP) method. Pile support is assumed from combined tip and side resistance, all the way to the limit cases of tip or side only.

The original Davisson definition was generalized quickly (e.g., Peck et al. 1974) to

a definition that includes: (1) the elastic pile compression (PD/AE), in which P = load on pile, D = pile depth, A = pile cross-sectional area, and E = Young's modulus of pile material, plus (2) an intercept equal to (0.15 + 0.1 B) inches, with B = diameter in feet. The intercept is given now more commonly as (0.15 + B/120) inches, with B = diameter in inches. [In SI units, (3.8 + B/120) mm, with B = diameter in mm.]

This commonly-used Davisson definition includes two key extrapolations from the original: (1) B can be significantly greater than one foot, the "normal dimensions", and (2) ρ_{tip} = B/120, which can be significantly different from 0.1 in. (2.5 mm). The limitations for high capacity, driven piles, or "quick" or CRP load tests are no longer stated. It also seems to be accepted, at least implicitly, that the 0.15 in. (3.8 mm) empirical constant is unique and that the method can be used routinely for any type of soil. Davisson cautioned about indiscriminate use of the method, and even gave an example of a pile in micaceous soil. In this case, ρ_{tip} was measured at 0.3 in. (7.6 mm), which is very different from the commonly-assumed 0.1 in (2.5 mm).

APPLICATIONS DIRECTLY TO DRILLED SHAFTS

O'Rourke and Kulhawy (1985) attempted to use the Davisson method for interpreting uplift tests on drilled shafts. However, they found that it was better to use the initial slope of the actual load-displacement curve instead of the elastic extension of the foundation. Also, they limited the intercept to 0.15 in. (3.8 mm) because the tip displacement normally does not contribute to capacity in uplift tests. This revision was named the slope tangent method.

Later research at Cornell University by various authors, summarized by Kulhawy (2004), confirmed the slope tangent method in uplift (STU) for various drilled foundations. They also confirmed the slope tangent method in compression (STC), which is similar to STU, except that the B/120 term is introduced back into the intercept.

Davisson (1993) also suggested the following for drilled shafts: "the term containing B may need to be multiplied by a factor varying from 2 to 6". This suggestion would result in B/60 to B/20, with B = diameter in inches.

Remember that the Davisson method has three components: elastic compression, empirical offset, and tip displacement. Consider each of these specifically for drilled shafts.

First, Hirany and Kulhawy (1988) confirmed that the initial slope of the load-displacement curve in compression load tests on drilled shafts was significantly less than the elastic shaft compression, especially for shorter (smaller D/B) shafts. For deeper shafts with larger D/B, the initial slope approaches the elastic slope, as shown in Figure 2. This process occurs because a significant load is transferred to the tip at small D/B, and there is greater tip displacement. Both lead to a "softer" initial slope.

Second, Davisson implied that the 0.15 in. (3.8 mm) offset was determined from load tests conducted on "point bearing piles". The piles cited in the paper had B = 10 - 18 in. (254 - 457 mm) and D/B well above 50. However, normal drilled shafts have B much larger than 18 in. and D/B much smaller than 50. Observations show that the Davisson method gives conservative values of the "failure load" for drilled shafts (Hirany & Kulhawy 1988, 1989a; Davisson 1993, Canadian Geotechnical Society 2006). Accordingly, an increase in this empirical offset should be warranted.

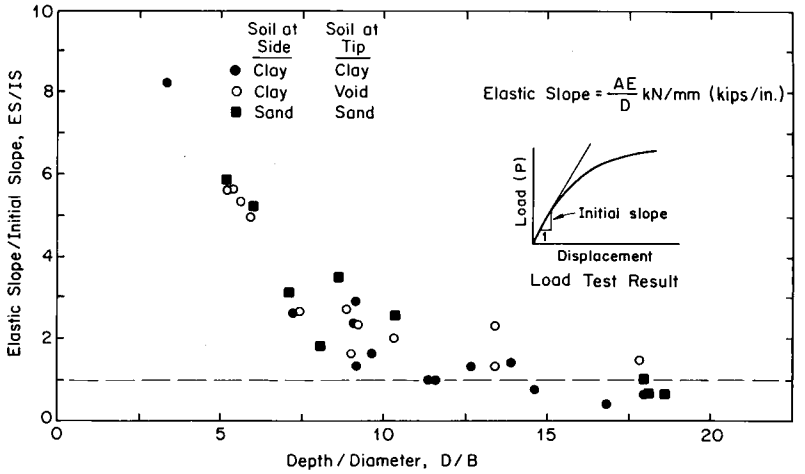

FIG. 2. Effect of Foundation Depth/Diameter on Initial Slope of Load-Displacement Curve (Hirany & Kulhawy 1988)

Third, various studies have shown that the tip displacement required to mobilize the tip resistance for drilled shafts is significantly greater than B/120 (Hirany & Kulhawy 1988, 1989a, Davisson 1993, O'Neill & Reese 1999). Davisson (1993) suggested a multiplier of 2 to 6 for his method. Again, an increase should be warranted.

The original Davisson method gives a very conservative (low) estimate of the "interpreted failure load". As stated above, this difference results largely from the geometric differences between drilled shafts and driven piles, as a minimum. If modifications to the elastic slope, empirical offset, and tip displacement are made, then the Davisson method may give more realistic results for drilled shafts. However, research would be needed to quantify these issues.

L_1-L_2 METHOD FOR DRILLED FOUNDATIONS

In the mid-1980s, as part of a very large research effort, the authors were faced with the problem of establishing consistent criteria for interpreting the results of load tests conducted on drilled shafts under axial loading (Hirany & Kulhawy 1988, 1989a, 1989b). More than forty existing methods were examined in detail, including Davisson, and it was found that none could evaluate the "interpreted failure load" in a consistent manner. Accordingly, we went back to the basics and examined a large amount of field data, ranging from poor to very high quality. What emerged was a clearer picture of foundation behavior.

Careful examination of drilled shaft compression and uplift load-displacement curves showed that they normally can be simplified into three distinct regions: initial linear, transition, and final linear, as shown in Figure 3. The initial region exhibits more-or-less linear response, prior to load levels causing an initial yield along the

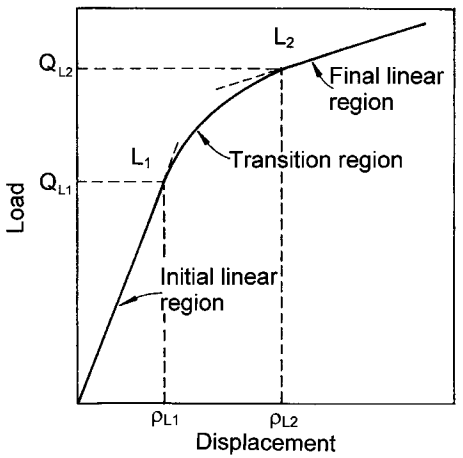

FIG. 3. Regions of Load-Displacement Curve

soil-foundation interface. Once yield begins along the interface, the response becomes nonlinear and continues as yield progresses along the interface. Once full yield has developed along the entire interface, the response returns to more-or-less linear as full slippage occurs along the interface. Point L_1 corresponds to the load (Q_{L1}) and butt displacement (ρ_{L1}) at the end of the initial linear region, while point L_2 corresponds to the load (Q_{L2}) and butt displacement (ρ_{L2}) at the initiation of the final linear region, beyond which a small increase in load produces a significant increase in displacement. Similar behavior has been observed for drilled shafts socketed into rock (Carter & Kulhawy 1988, Kulhawy & Carter 1992).

These L_1 and L_2 points are evaluated from the load-displacement curves by direct graphical interpretation, as shown in Figure 3. However, during some load tests, it is difficult to obtain high quality data beyond L_2 because of logistics issues and creep displacements. Without these large-displacement data, it is sometimes difficult to interpret L_2 reliably. This issue will be discussed later.

The failure loads interpreted by most existing methods lie either in the transition region or in the early portion of the final linear region, or sometimes even above the final linear region (extrapolated failure loads). For drilled shafts, Hirany and Kulhawy (1989a) showed that, for six other common interpretation methods based on various criteria, the ratio of Q_{L2} to the interpreted failure load by the other methods varied, on average, from 0.93 to 1.14. In addition, various studies at Cornell (e.g., Chen & Kulhawy 1994) have shown that Q_{L2} agrees well with the capacity predicted by high-quality analytical models.

Since we presented the L_1-L_2 method, these criteria have been used widely (correctly and incorrectly). Our follow-up paper (Hirany & Kulhawy 2002) re-examined the interpretation criteria, provided additional guidelines and clarifications, and recommended detailed procedures for applying these criteria in a more consistent man-

ner. Since the initial proposal, these criteria also have been applied to other types of drilled foundations, including augercast piles, pressure-injected footings, and micropiles. It appears that, in principle, these interpretation criteria are appropriate across the full range of drilled foundations (Kulhawy 2004). These general interpretation criteria are described below.

COMPARISON OF DAVISSON, SLOPE TANGENT, AND L_1-L_2 METHODS

For compression tests, the load interpreted by the Davisson method (Q_D) is always higher than Q_{L1} and lower than Q_{L2}, and it always occurs within the transition region in Figure 3. This Q_D is conservative (low), but it is a useful predictive method and can be applied to nearly all load test data.

A nearly identical statement can be made about the slope tangent method in compression, except that Q_{STC} is larger than Q_D at smaller D/B. At larger D/B, they are essentially the same. For drilled foundations, Q_{STC} should be preferred.

By contrast, the graphical L_2 interpretation is a back-plotting method that requires relatively high-quality data at larger displacements. Sometimes this is difficult because of logistics issues and creep displacements, as noted above. Therefore, it would be useful to correlate Q_D, or even better Q_{STC}, with Q_{L2} so that Q_{STC} could be used to help estimate Q_{L2} when the large displacement data are poor or non-existent.

For drilled shafts in compression, Hirany and Kulhawy (1989a) found that Q_{L2}/Q_D averaged 1.14 over a range of soil and loading conditions. For their database, Q_{STC} and Q_D are similar. Kulhawy (2004) summarized similar studies at Cornell for compression load tests of augered cast-in-place (ACIP) or augercast piles, pressure-injected footings, and micropiles. These studies showed Q_{L2}/Q_{STC} in the range of 1.18 to 1.20. Therefore, Q_{L2} is about 15 to 20% larger than Q_{STC} over a range of drilled foundations.

For drilled shafts in uplift, Hirany and Kulhawy (1989b) showed that the L_1-L_2 criterion also was applicable. Subsequently this method was used successfully for other drilled foundations in uplift (Kulhawy 2004). Recently, Chen, et al (2008) evaluated uplift tests on drilled shafts using several interpretation methods including L_1-L_2 and the slope tangent method in uplift (STU). As expected, Q_{STU} always occurred within the transition region of Figure 3, and the average Q_{L2}/Q_{STU} was 1.11. Hirany and Kulhawy (1989b) made the same observation previously and noted that the average Q_{L2}/Q_{STU} was 1.13. For pressure-injected footings in uplift, Chen (1998) showed that the average Q_{L2}/Q_{STU} was about 1.18 to 1.20. Therefore, Q_{L2} is about 10 to 20% larger than Q_{STU} over a range of drilled foundations.

SUMMARY AND RECOMMENDATIONS

This paper has focused on estimating the "failure load", or more correctly the "interpreted failure load", from field load tests on drilled shafts using the Davisson method or a more viable alternative. The emphasis has been on the writers' extensive experience with drilled foundations and load test interpretation.

In 1972, Davisson proposed a method for interpreting the "failure load" from field load tests for specific driven pile conditions in compression loading. Because this

method is simple and easy to use, it has been applied widely and indiscriminately. However, in its present form, as described herein, it is not appropriate for drilled shafts and will give an interpreted capacity (Q_D) that is too low, compared with actual load-displacement behavior.

One straightforward modification to the Davisson method is to use the initial slope of the load-displacement curve, not the elastic slope from the test foundation. This modification is known as the slope tangent method. It is just as convenient to use, but it gives a higher and more appropriate failure load than Q_D. Variations of this method can be used in both compression (Q_{STC}) and uplift (Q_{STU}).

A better method, which was developed specifically for drilled shafts, is the L_1-L_2 method that is valid for both uplift and compression load tests (Hirany and Kulhawy 1988, 1989a, 1989b). This method is rational and consistent and is based on analysis of the load-displacement curve. The "interpreted failure load" (Q_{L2}) from this method reflects full soil-shaft yielding, as shown in the load-displacement curve, and is larger than Q_{ST}. However, the Q_{L2} interpretation can be difficult when relatively high-quality data at larger displacements are lacking or are of poor quality. Fortunately, empirical observations show that Q_{L2} can be correlated consistently with Q_{ST}. Results also show that the L_1-L_2 method applies to a wide range of drilled foundations, including drilled shafts, augercast piles, pressure-injected footings, and micropiles.

The L_1-L_2 method is recommended for interpreting the results of compression and uplift load tests on drilled foundations in general. Where there are problems with the large displacement data, the slope tangent method can be used to help estimate Q_{L2} using empirical correlations. This approach gives Q_{L2} that is 10 to 20% larger than Q_{ST} and subsequently Q_D. The Q_{L2} also agrees well with the capacity predicted by high-quality analytical models

REFERENCES

Canadian Geotechnical Society (2006), *Canadian Foundation Eng. Manual, 4th Ed.*, BiTech Publishers, Richmond, BC.

Carter, J.P. & Kulhawy, F.H. (1988). "Analysis & Design of Drilled Shaft Foundations Socketed Into Rock", *Rpt. EL-5918,* Electric Power Research Inst., Palo Alto.

Chen, J-R. (1998) "Case History Evaluation of Axial Behavior of Augered-Cast-In-Place Piles & Pressure-Injected Footings", *MS Thesis*, Cornell Univ., Ithaca, NY.

Chen, Y-J., Chang, H-W. & Kulhawy, F.H. (2008), "Evaluation of Uplift Interpretation Criteria for Drilled Shaft Capacity", *J. Geotech. Eng. (ASCE), 134(10)*, Oct 2008, 1459-1468.

Chen, Y.-J. & Kulhawy, F.H. (1994). "Case History Evaluation of Behavior of Drilled Shafts Under Axial & Lateral Loading", *Rpt. TR-104601,* Electric Power Research Inst., Palo Alto.

Davisson, M.T. (1972). "High Capacity Piles", *Proc. Lecture Series on Innovations in Foundation Construction*, Soil Mech. Div., Illinois Sec.-ASCE, Chicago, 81-112.

Davisson, M.T. (1993). "Negative Skin Friction in Piles and Design Decisions", *Proc. 3rd Intl. Conf. Case Histories in Geotech. Eng.(3),* St. Louis, 1793-1801.

Hirany, A. & Kulhawy, F.H. (1988). "Conduct & Interpretation of Load Tests on

Drilled Shaft Foundations: Detailed Guidelines", *Rpt. EL5915(1)*, Electric Power Research Inst., Palo Alto.

Hirany, A. & Kulhawy, F.H. (1989a). "Interpretation of Load Tests on Drilled Shafts - 1: Axial Compression", *Foundation Eng.: Current Principles & Practices (GSP 22)*, Ed. F.H. Kulhawy, ASCE, New York, 1132-1149.

Hirany, A. & Kulhawy, F.H. (1989b). "Interpretation of Load Tests on Drilled Shafts - 2: Axial Uplift", *Foundation Eng.: Current Principles & Practices (GSP 22)*, Ed. F.H. Kulhawy, ASCE, New York, 1160-1172.

Hirany, A. & Kulhawy, F.H. (2002). "On the Interpretation of Drilled Foundation Load Test Results", *Deep Foundations 2002 (GSP 116)*, Ed. M.W. O'Neill & F.C. Townsend, ASCE, Reston, 1018-1028.

Kulhawy, F.H. (2004). "On the Axial Behavior of Drilled Foundations", *GeoSupport 2004 (GSP 124)*, Ed. J.P. Turner & P.W. Mayne, ASCE, Reston, 34-51.

Kulhawy, F.H. & Carter, J.P. (1992). "Socketed Foundations in Rock Masses", Chap. 25 in *Eng. in Rock Masses,* Ed. F.G. Bell, Butterworth, Oxford, 509-529.

O'Neill, M. W. & Reese, L. C. (1999), "Drilled Shafts: Construction Procedures & Design Methods", *Rpt. FHWA-IF-99-025*, Federal Highway Admin., Washington, DC.

O'Rourke, T.D. & Kulhawy, F.H. (1984). "Observations on Load Tests on Drilled Shafts", *Drilled Piers & Caissons II*, Ed. C.N. Baker, ASCE, New York, 113-128.

Peck, R. B., Hanson, W. E. & Thornburn, T. H. (1974), *Foundation Engineering, 2nd Ed.*, Wiley, New York.

Copyrighted Materials
Copyright © 2009 American Society of Civil Engineers (ASCE)
Retrieved from www.knovel.com

A Case Study on the Overturning of Drill Rigs on Construction Sites

Satoshi Tamate[1] and Tomohito Hori[2]

[1]Senior Researcher, National Institute of Occupational Safety and Health, Japan, 1-4-6 Umezono, Kiyose, Tokyo 204-0024, JAPAN; tamate@s.jniosh.go.jp
[2] Researcher, National Institute of Occupational Safety and Health, Japan, 1-4-6 Umezono, Kiyose, Tokyo 204-0024, JAPAN; horito@s.jniosh.go.jp

ABSTRACT: Drill rigs are large pieces of construction machinery used to build pile foundations and to improve the ground stability. Crawlers comprising the lower base enable the machines to propel themselves. A tall leader given in the upper structure provides top heavy weight distribution. Sufficient bearing capacity and flatness are required in the bearing ground to keep the machinery stable without any tilts while it is propelling itself. Nevertheless, overturning often occurs at constructions. This study focuses on the phenomenon of ground instability causing machines to overturn. A drill rig weighing 372.5kN and with a leader 15.9m tall overturned on a building construction site. This machinery moved within the site to the positions required for building the diaphragm walls. This paper, firstly, summarizes operations prior to the accident. Secondly, the equilibrium condition of the machinery was calculated to clarify the stability, and the pressure acting on the ground through the crawlers was estimated. Ground properties were also investigated to assess the potential risk of failure in bearing ground. Finally, problems with the stability of drill rigs are discussed.

INTRODUCTION

Some drill rigs and similar machinery for piling and ground improvements are propelled by crawlers on both sides of the lower base carrier. Such machinery must be kept near horizontal on the bearing ground when moving if the derrick is raised. Nevertheless, accidents have often occurred due to overturning of drill rigs in Japan as well as in countries throughout the world. Ground penetration by crawlers was observed in many cases where actual overturning occurred as shown in Fig 1.

While the safety regulations for drill rigs worldwide prescribe the stability angle as the allowable tilt in the machinery, the ground is assumed to be sufficiently stiff and firm. The necessary ground conditions for setting up drill rigs are not specifically prescribed in the regulations.

This study examines the phenomenon of ground instability causing the drill rigs to overturn. A case study on an accident was carried out to investigate the problems with stability in terms of the bearing ground. This paper, firstly, summarizes the outline of

operations prior to the accident. Secondly, the equilibrium condition of the machinery was calculated to clarify the stability, and the pressure acting on the ground through the crawlers is estimated in accordance with the regulations (British Standards Institution (1996a and 1996b) and Japanese Standards Association (2007)). The bearing capacity of ground is investigated to make sure the potential risk of overturning. Finally, problems with the stability of drill rigs are discussed.

FIG.1. Overturning of a drill rig in construction site.

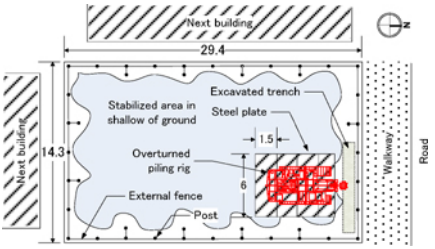

FIG. 2. Schematic view of the site.

FIG.3. Preliminary trench excavation.

SITE CONDITIONS IN THE ACCIDENT

An eight stories apartment house was being constructed at the site as shown in Fig 2. Diaphragm walls were selected as the foundation type in this construction. An external fence supported by posts was installed in the site to protect the adjacent buildings. Fig.1 shows the overturned drill rig discussed in the paper from an incident that occurred in Japan in 2004. The drill rig was comprised of three augers in the leader and hit a car parked beside the site. Two workers were severely injured in this accident. Ground penetration by a crawler was clearly observed.

Soft clay was overlaid by sandy subsoil down to a depth of 0.7m. Shallow soil was stabilized by mixing with cement to increase the bearing capacity in advance. Though preliminary theoretical calculation indicated that thickness of 1.0m of stabilization was required to support heavy machinery, the actual stabilization was only performed to 0.7m due to difficulty mixing in the clay. Therefore, the bearing capacity was lower than the required value. In addition, existences of both the fence and the supporting posts disrupted the stabilization. Consequently, the bearing capacity in this around area was smaller than that of other areas. It seems that insufficient of bearing capacity was one cause of the accident.

A small trench, 0.9m in depth and 0.8m in width, was excavated by a backhoe in the north area prior to building the diaphragm wall as shown Fig 3. This trench excavation was carried out as preliminary preparation to indicate the positions of drilling columns and to prevent the overflow of mixing mud. However, the depth of the trench was deeper than 0.7m of the designed value. The deeper trench reduced the bearing capacity near the walls, and made the drill rig unstable. This was also considered to be another cause of the accident.

PROCESS PRIOR TO THE ACCIDENT

Table 1 shows the process of constructions at the site prior to the accident. Shallow soil stabilization was carried out as one of the preliminary preparations to increase the bearing capacity to ensure the machinery is kept nearly horizontal during self-propelling. The drill rig was assembled the previous day. Placing steel plates at the site was also required to support the heavy machinery.

Preliminary trench excavation started at 9:00 in the morning. Since a buried water pipe was broken at the excavation, however, the trench was submerged at 10:00. A site manager called up the water supply office to inform them of the trouble with water pipes. Running water was stopped by water supply personnel at 11:30. The remaining preparations were resumed soon after completion of the repairs even though the bearing ground softened due to the exposure to water.

Table 1. Process of the constructions prior to accident

Process		Contents of work
Before		Shallow soil stabilization by cement
Previous day		Assembling the drill rig in the site.
Day of the Accident	8:00	Meeting.
	9:00	Started preliminary preparations such as excavation of small trench and placement of the steel plates.
	10:00	A buried water pipe was broken at the trench excavation.
	10:05	Started pumping the water from the submerged trench
	10:45	Water department officials arrived
	11:30	Water leakage stopped
	11:45	Water pipe was repaired. Trench excavations and placing the steel plates were resumed.
	12:15	Completion of the preparations.
	13:00	The Drill rig moved toward to the position for excavation.
	13:10	Overturned near the trench

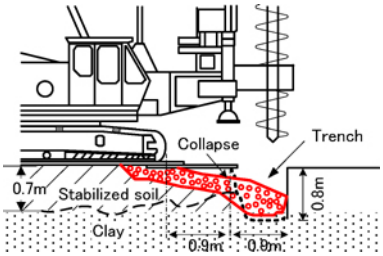

FIG.4. Soil collapse under drill rig.

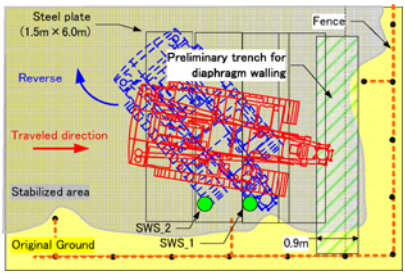

FIG.5. Location of drill rig prior to overturning.

The drill rig moved to the north east position to build the diaphragm walls as shown in Fig 4. However, the machinery was tilting slowly when it had reached a distance of 0.9m offset from the trench. An operator who observed the tilt quickly reversed the travel and turned the upper structure right as shown Fig 5. The increment of tilt in the machinery accelerated due to collapsed soil, and the machinery finally overturned as shown in Fig 1.

STABILITY OF THE DRILL RIG

Stability angle

Fig 6 shows a summary of the drill rig with a leader 15.9m in length and 372.5kN in total weight (W). Since the x axis and the y axis are defined as shown Fig 6, the origin (O) is positioned at the horizontal center of the crawler on the ground surface. Coordination of the center of gravity in horizontal axis (G_x) and vertical axis (G_y) was calculated to investigate the stability of the machinery. Table 2 summarizes the specifications of the drill rig.

Safety regulations prescribe structural requirements in terms of the stability angle as allowable tilt of drill rigs. Table 3 shows comparison of the stability angles between Europe and Japan. The European Norm (British Standard Institution (1996a) and (1996b)) prescribes the stability angles in both EN996 of "Piling equipment - safety requirements" and EN791 of "Drill rigs – safety". EN996 describes that a stability angle of 5 deg must be provided in the drill rigs as minimum requirement. 8 deg is also written for propelling on job sites. EN791 also describes the stability angles which shall not be less than 10 deg in any direction when moving and not be less than 5 deg under any other conditions. The stability angle of 10 deg also includes a margin for the effects of the inertia forces from acceleration, braking and swaying of the drill rigs. The Japanese Ministry of Health, Labor and Welfare prescribes a stability angle of 5 deg in the Ordinance on Occupational Safety and Health as a minimum value. The Society of Materials Science, Japan (2002) recommends two sets of values in connection with the stability angles that are 7 deg when drilling and 9 deg when self-propelling.

Larger values in the stability angle during self-propelling are introduced in both regulations since the inertia forces increase the instability. The stability angles were calculated by giving consideration to the specifications of machinery as shown in Table 4. The stability angle in forward (θ_{sf}) means a tipping angel where the center of gravity turns above the front sprockets due to tilt, and this value is derived by Eq.(1). The stability angle in lateral (θ_{sl}) is also obtained by Eq.(2). Both 18.4 degrees for θ_{sf} and 21.6 degrees for θ_{sl} are greater than 10 deg of the limitation by EN791. Hence, the drill rig overturned even though sufficient stability was provided in the machinery. Accordingly, it was ascertained that a collapse of the bearing ground was the main cause of the accident.

Pressures acting on the ground

EN791 and EN996 define five types of distributions in the pressures acting on the

ground through the crawlers as well as JIS A 8509-1 by the Japanese Standards Association(2007) . These distributions are specified by the position of a single load (e) as shown in Table 5. A value of e is the same as that of G_x introduced above. The maximum pressures acting on the ground (σ_2) are obtained by the equations given.

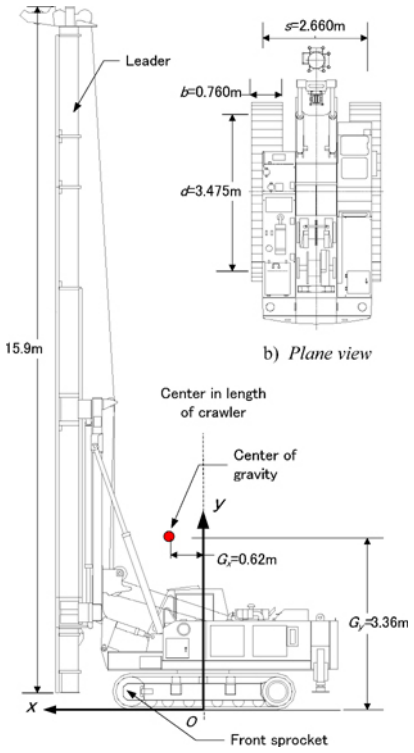

a) *Profile view*

FIG. 6. Summary of the drill rig

Table 2. Specifications of drill rig

Total weight (W)	372.5kN
Horizontal distance of the centre of gravity from the centre of crawler (G_x)	0.62m
Vertical distance of the centre of gravity from ground surface (G_y)	3.36m
Length of contacting area on crawler (d)	3.475m
Width of crawler (b)	0.76m
Tread between crawlers (s)	2.660m

Table 3. Comparison of the stability angle in safety regulations

	Stability angles (deg)
EUR	Usually 5 Either 8 (EN996)or 10 (EN791) at self-propelling
JPN	5*

* 7 (at the drilling) and 9 (at self-propelling) are recommended by the Society of Material Science, Japan (2002).

Table 4. Calculation of the stability angle

	Forward	Lateral
Calculating formula	$\tan\theta_{sf}=\frac{d-2G_x}{2G_y}$ (1)	$\tan\theta_{sl}=\frac{s}{2G_y}$ (2)
Stability angle (deg)	θ_{sf}=18.4	θ_{sl}=21.6

Table 5. Calculation of maximum ground pressure under crawlers

Load and stress diagram	Position of the single load P	Ground pressure
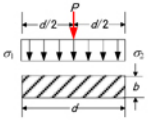	e=0 P in the middle	$\sigma_1=\sigma_2=P/bd$
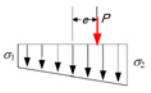	$e<d/6$	$\sigma_1=\frac{P(1-6e/d)}{bd}$ $\sigma_2=\frac{P(1+6e/d)}{bd}$
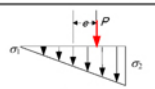	$e=d/6$	σ_1=0 $\sigma_2=2P/bd$
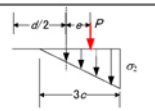	$e>d/6$ $c=d/2-e$	$\sigma_2=2P/3bc$
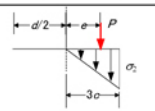	$e=d/3$	$\sigma_2=4P/bd$

A value of e and a value of d were 0.62m and 3.475m in the drill rig, respectively. The relationship between e and $d/6$ is derived as Eq.(3). Consequently, σ_2 is calculated by Eq.(4).

$$e > \frac{d}{6} \qquad (3)$$

$$\sigma_2 = \frac{2P}{3bc} = 146(kPa) \qquad (4)$$

where the single load (P) is substituted by a value of $W/2$.

As the steel plates were sheeted on the ground surface, the actual pressure acting on the ground was smaller than the value of σ_2.

Bearing grounds are assumed to be sufficiently stiff and firm. Safety regulations don't consider the machinery becoming unstable by tilt with an increase of differential settlement in the crawlers. However, this settlement increases the pressure acting on the ground by an increase in the overturning moment due to the machinery tilting. Accordingly, the values of the actual pressure acting on the ground become greater than the values suggested by the regulations where the machinery tilts due to settlement of crawlers.

Supporting ground conditions

Swedish weight sounding tests (SWS) were carried out to investigate the distribution of stiffness at the two positions of SWS_1 and SWS_2 shown in Fig.5. The N value is well known as an index to classify the ground stiffness. N-value means the number of blows in standard penetration tests that are carried out in boreholes during site investigations. The procedure is specified in BS1377. In addition, the interpreted N value (N_i) is also known to be introduced by Eq.(5) and Eq.(6) depending on soil materials.

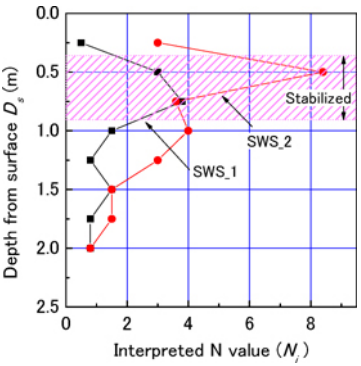

FIG.7. Relationship between the interpreted *N* values (N_i) and depth (D_s)

<Sand> $N_i = 0.002W_{sw} + 0.067N_{sw}$ (5) <Clay> $N_i = 0.003W_{sw} + 0.050N_{sw}$ (6)

where W_{sw} is the value of the loading weight, N_{sw} is the equivalent number of half turns required to penetrate 1m in depth.

Fig 7 shows the relationship between depth (D_s) and N_i. Since SWS_2 shows higher value than SWS_1, the bearing capacity of ground is lower in the northeast corner. Both curves show the existence of a stabilized layer between 0.2m and 0.9m. Soft clay was deposited below 1m so N_i decreased rapidly. A likely difference in measured N_i was the water seepage by the broke water supply line.

DISCUSSIONS ON PROBLEMS WITH STABILITY

Hazards in the ground

Various hazards usually exist in constructions. Since drill rigs are large pieces of machinery, their overturning causes serious damage to the surroundings of the sites as well as inside the site.

Two problems existed in the construction.

1) Existence of both fences and supporting posts disturbed stabilization near their boundaries. Hence, the bearing capacity was lower in this area.
2) Insufficient stabilization thickness reducing the bearing capacity.

In addition, another three problems made the bearing ground unstable.

1) Bearing capacity near the walls was reduced because the depth of the trench was deeper than the designed value.
2) A broken water pipe caused the excavated trench to be submerged. Water seepage made the bearing ground soft.
3) Soon after the completion of repairs, the remaining works were resumed without confirmation of the stability.

Safety requirements for the stability of sites

Safety regulations commonly assume that sufficient bearing capacity is provided in the ground of construction sites. Meanwhile, either pilings or ground improvements were conducted on sites where the bearing capacity is insufficient for supporting facilities. Therefore, various stabilization methods such as deep soil mixing and the installations of pile foundations are used to support the structures. Accordingly, the drill rigs must move over unstable ground on construction sites.

Tamate et al. (2005) investigated the mechanism of the overturning of the mobile cranes. Top heavy distribution in both the mobile cranes and drill rigs induce potential instability. Four outriggers support mobile cranes while hooking the load. Mobile cranes become quite unstable where the outriggers rapidly penetrate the surface due to the brittle failure in the bearing ground.

CIRIA (2003) recommends three sets of safety factors in terms of bearing capacity (F_s) as follows. F_s of 1.5 is the absolute minimum and should only be used where ground conditions have been accurately identified under the guidance of an experienced geotechnical engineers. F_s of 2.0 is adequate for most situations. F_s of 3.0 is more normally used for permanent works for foundations and will give a conservative size of foundation area. It should be used for outrigger foundations where little ground information is available, where soils are variable or where minor settlements could be critical to a precision lifting and placing operation.

Theoretical calculations were carried out by Tamate et al (2006) to learn about the relationship between the probability of safety for overturning (P_{ss}) and F_s. P_{ss}>0.984 at F_s=3 resulted whereas P_{ss}>0.802 at F_s=1.5 in particular ground that induces rapid outrigger penetration. Accordingly, it is ascertained that safety for overturning can be easily ensured by using F_s=3 to prevent any ground penetration by outriggers.

Drill rigs propel by themselves whereas mobile cranes stand still in the positions they perform hooking operations. The potential risk of overturning because of different penetration of the crawlers due to failure in the bearing ground is unclear. In addition, flatness of the surface and variation of the stiffness cause a swaying motion, and thus

inertia forces are generated. Accordingly, drill rigs are considered to be quite unstable because of the inertia forces due to sway during self-propulsion. It was confirmed that further study is needed to specify the safety requirements in terms of the bearing ground.

CONCLUSIONS

A case study on the overturning of drill rigs on construction sites was discussed to address problems with stability. The conclusions are summarized as follows:

1) Drill rigs are top heavy structure during propelling. Sufficient bearing capacity is required to support the machinery safely. The case introduced to illustrate overturning occurred due to penetration by the crawlers because of a failure of the bearing ground. Hence, sufficient capacity must be provided to keep drill rigs stable in the bearing ground.
2) Safety regulations worldwide prescribe the stability angles as allowable tilt by the overturning moment. By contrast, the bearing ground is assumed to be sufficiently stiff and firm. Safety requirements on bearing ground are not prescribed in the regulations.
3) Calculation procedures regarding the pressures acting on the ground are specified in the regulations. Nevertheless, the values obtained are generally lower estimated because the tilts in drill rigs induced by differential settlement in crawlers are not considered.
4) Drill rigs propel themselves in sites while mobile cranes stand still in their positions during hooking operations. Inertia force caused by sway during propelling makes drill rigs more unstable than mobile cranes. Accordingly, the potential risk of the overturning increases for drill rigs.
5) Safety requirements for bearing ground are necessary to prevent the overturning of drill rigs and similar foundation machinery. Clarification of the relationship between characteristics of instability of the drill rigs and properties of the bearing ground needs to be addressed in further studies.

REFERENCES

British Standards Institution. (1996a). "*Piling equipment - Safety requirements*", BS EN 996.

British Standards Institution. (1996b). "*Drill rig -Safety*", BS EN 791.

Japanese Standards Association. (2007). "*Foundation work machinery - Safety – Part 1: Requirements for piling equipment*", JIS A 8509-1.(in Japanese)

Tamate, S., Suemasa, N. & Katada, T. (2005). "*Analyses of Instability in Mobile Cranes due to Ground Penetration by Outriggers*", American Society of Civil Engineers (ASCE), Journal of Construction Engineering and Management Vol.131 (6): pp 689-704.

CIRIA. (2003). "*Crane Stability on Site*", Special publication 131, pp39-56.

Tamate, S., Katada, T. & Suemasa, N. (2006). "*A study on safety requirements of bearing ground for mobile cranes*", Physical Modeling in Geomechanics – 6th ICPMG '06, pp.1297-1303.

The Society of Materials Science, Japan. (2002). "*A guideline for design and construction of diaphragm walls*", pp.77-79.(in.Japanese)

Copyrighted Materials
Copyright © 2009 American Society of Civil Engineers (ASCE)
Retrieved from www.knovel.com

Old Drilling Elements Combined With Some New Tricks for Secant Pile Construction: A Full Scale Test Program

Allen Cadden, P.E. Member[1], Ralph Capelli[2], Javier Rodriguez, P.E.[3]

[1]Principal, Schnabel Engineering, Inc., 510 East Gay Street, West Chester, PA, 19380, acadden@schnabel-eng.com; [2]Manager of Drilling Operations, Posillico Civil, Inc., 131-36A 20th Avenue, College Point, NY 11356, rcapelli@posillicogroup.com; [3]Senior Engineer, Schnabel Engineering, Inc., 510 East Gay Street, West Chester, PA, 19380, crodriguez@schnabel-eng.com

ABSTRACT

Drilled shaft construction and secant or tangent pile wall construction has often experienced challenges with the drilling process as well as placement of the concrete. Often, numerous different methods are attempted to penetrate obstructions and debris in overburden materials. These methods may involve tripping in and out of a hole to change tooling, and on occasion removing protective casing or extending tools below the casing resulting in unsupported ground. Quality control with maintaining locations and verticality of shafts, as well as the placement of the concrete, present further challenges.

A research effort was undertaken to investigate the possibility of utilizing generally existing technologies of duplex drilling systems; however, the inner string had a down-the-hole hammer modified to allow reverse circulation. The casing was advanced with a moving rotator table. This combination effectively created a large diameter double-head duplex system. The research focused not only on the ability to utilize such a system, but also on its ability to maintain location and verticality tolerance and to place the concrete through the ports in the down hole hammer. This paper discusses the drilling system and the results of a full scale test program consisting of a 6x6m secant pile box. Although the focus of this paper is Secant wall construction, the method has proven uses for other medium size deep foundation systems.

INTRODUCTION

Drilling overburden is one of the most challenging endeavors for a foundation contractor. The further challenges associated with tight tolerances needed for a successful secant pile wall to be structurally sound and essentially water tight make

the contractor's work even more difficult. Often, the alignment challenges are dealt with utilizing a scalloped guide wall at the ground surface. Even with this assistance, the process of changing tools and moving in and out of a drill hole location to change tools, set casing, clean the hole, set reinforcement, and tremie place concrete open up numerous opportunities for problems with the final shaft.

BACKGROUND

Secant pile wall construction methods are typically reserved for ground conditions unsuitable for more traditional applications of steel sheeting or soldier pile and lagging. Often, difficult fill conditions such as obstructions, loose sand deposits or high ground water render these traditional systems difficult or impossible to construct. In instances where lateral or vertical movements typically associated with these traditional shoring systems may also be unacceptable, the use of a more rigid system such as secant piles may be the preferred alternative.

Construction of these walls generally follow the these steps:

1. Construction of a guide wall
2. Installation of casing in the primary holes
3. Drilling inside the casing of primary holes
4. Concreting of the primary hole
5. Drilling and installing casing in the secondary hole between two primary holes, cutting into the sides of the primary hole to create an interlock
6. Placing reinforcement and concreting the secondary hole

Numerous papers have been prepared recently on the design and construction of such systems including Burland (1989), Suckling (2005), Trevedi (2006) and Turner (2004). Often these systems are done with double wall casing or more traditional drilled shaft and pile installation techniques.

Foremost, Barber Systems

Early dual rotary drills were manufactured by Barber Industries in the late '70s. These rigs have been legendary for their ability to drill in the worse conditions. The Foremost company acquired this technology in the mid '90s and began producing a line of similar drilling equipment. The Foremost Dual Rotary drills include a unique lower rotary drive that is used to advance steel casing through unconsolidated overburden such as sand, gravel, glacial till and boulders. The added benefit of this lower drive table is its ability to hold the casing securely in place during drilling, similar to the function of a guidewall. The lower drive advances the casing until it is seated at the top of rock, at which point the inner string and conventional top drive drill string or down hole hammer string is independent and can continue to advance the hole into the rock open hole without changing the drill tooling.

The key is that the upper and lower rotary drives feed independently on separate hydraulic cylinders allowing the bit position to be highly variable given the casing

and rod length. Thus the center drill bit (roller bits, down hole hammer, etc.) can be located slightly in front of the casing when hard drilling is encountered to pull back into the casing to maintain stability of the hole in soft soils, loose sands, and high ground water conditions.

Reverse circulation (RC) further enhances these capabilities by controlling the cutting fluid and spoils within the drill string. By maintaining pressure within the casing, the air flush travels down between the inner and outer barrels of the RC rod system and returns up the inner barrel of the drill rod. Thus, no spoils are expelled around the drill bit to come up the casing or forced to come up the outside of the casing. This has the further advantage of allowing smaller volumes of air to maintain an adequate uphole velocity to remove cuttings efficiently.

NEW METHOD OVERVIEW

Utilizing the basic concepts of the Foremost and Barber drills coupled with the reverse circulation system presents a unique opportunity to the secant pile construction industry. By combining a very stable and robust drilling rig with the RC drilling method that controls cutting collection and discharge very efficiently, there was a belief that a traditional secant pile wall could be constructed within normal tolerances without the use of a guide wall, which is a significant cost factor in these projects. Furthermore, the ability to vary the location of the drill string within the temporary casing allows even the most difficult ground to be penetrated without sacrificing hole stability or production rates throughout the entire length.

As the methodology was being developed, there was an added benefit envisioned to allow placement of the concrete into the hole through the RC drill string. This would eliminate the steps needed to remove the drill string and place a tremie pipe to concrete the hole, each of which presents an opportunity for the hole to become unstable and reduces productivity.

TEST PROGRAM

Verification of this concept required a testing program that would evaluate the drills' capabilities, concreting potential through the drill string, and the quality control elements including location and verticality. To confirm this, a full scale secant wall bathtub was designed that could be excavated and filled with water to evaluate the interlock success.

The bathtub consisted of 24 piles creating a 3 x 3 m (10 x 10 ft) box. Piles extended to a depth of 5m (16 ft) below the ground surface. Figure 1 shows the pile layout. Each pile was 600 mm (24 inch) diameter and center to center spacing was 500 mm (20 inch). The soil conditions were fairly uniform and consisted of medium dense poorly graded sand with gravel and cobbles. Ground water was below the depth of drilling.

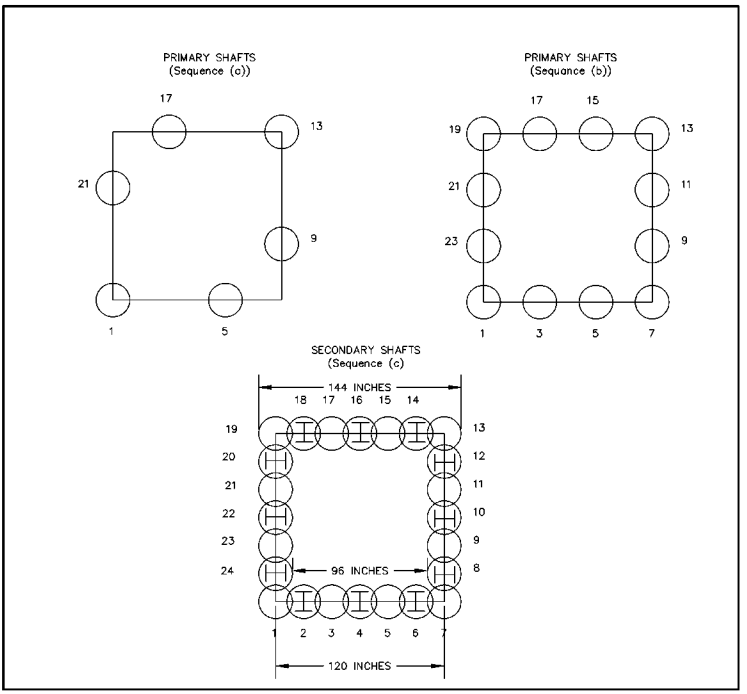

FIG. 1: Pile Layout

The piles were drilled with a truck-mounted Foremost DR24 drill fitted with a rotator and a down hole hammer (Figure 2). Drilling progressed by screwing the casing in with the rotator ahead of the hammer about 0.6-1.2m (2-4 ft). The hammer was then used to clear the casing, maintaining the hammer up inside the casing about 0.6 m (2 ft) (Figure 3). Given the soil conditions, the use of a hammer was not necessary, and this tooling functioned more like an air lift to clean the sandy soil from the casing. Drilling progressed at a rate of about 3 min/m (1 min/ft). Some challenges were experienced where cobbles were caught in the swivel and clogged the return lines, slowing drilling progress.

FIG. 2: Foremost Drill with Reverse Circulation Rotator Attachment

Concrete placement through the drill string and hammer was relatively smooth. Given the hole is fully cased and the hammer is resting on the bottom of the hole after cleaning, the potential for collapse was non-existent. Concrete was pumped into the drill string until back pressure was noticed, indicating that the system was full. At this time, pumping continued and the hammer was lifted slowly. Using the concrete pump pressure to assist with the hammer lifting was a further verification that the hole remained full as the drill string was lifted. Once the drill string was up in the casing at least 3 m (10 ft), lifting of the casing began similar to traditional tremie pours.

FIG. 3: Down Hole Hammer Bit and Casing

Excavation and Observations

Upon completion of the secant wall bathtub, the area was excavated to a depth of about 2.7 m (9 ft) inside and 2 m (6 ft) outside of the bathtub. A 300 mm (1 ft) thick unreinforced concrete mat was poured inside and allowed to set for one day. The bathtub was then filled with water to within about 450 mm (1.5 ft) of the top. Thus, approximately 2 m (6.5 ft) of head was resisted by the secant piles. Water was maintained in the bathtub for about three weeks (Figure 4).

Upon excavation, the secant piles were inspected to evaluate the verticality, overlap and alignment (Figure 5). These elements were well within the allowed tolerances of 1% verticality and 50 mm location established for the program. Given the difficulties of layout within such a small area, and the spoils present at the ground surface, the location accuracy was surprising. Table 1 shows the results of the shaft measurements (Diameter is the measured distance to secant contact points).

FIG. 4: Bathtub with Water

FIG. 5: Observation of Pile Alignment

TABLE No. 1: Alignment and Plumb

Column	Inside Diameter (mm)	Outside Diameter (mm)	Plumb (%)	Location (mm)
1	-	584	-	-
2	-	483	0	0
3	508	470	-	-12
4	508	572	-	-25
5	448	445	-	25
6	-	495	0.2	0
7	-	572	-	-
8	-	495	-	0
9	495	508	-	16
10	508	495	-	-19
11	495	483	-	-12
12	-	508	0.6	0
13	-	521	-	-
14	-	514	-	0
15	483	483	-	16
16	483	521	-	37
17	483	483	-	32
18	-	508	-0.3	0
19	-	521	-	-
20	-	514	0	0
21	457	495	-	35
22	533	483	-	-25
23	432	508	-	50
24	-	483	-	0

Several small horizontal cracks were noted in primary shafts (Figure 6). Although not definitive, these are believed to be the result of one of two conditions. First, the secondary holes in some cases were drilled immediately following the drilling for a secondary hole on the opposite side of the primary in question. Thus, the lateral support may not have been sufficient to resist the resulting lateral forces from drilling, and a bending crack occurred. The second condition may have been a wedging effect during withdrawal of the casing. As the concrete is placed through the drill string, some concrete rises above the hammer and some is likely to have seeped outside of the casing. This aggregate and/or the sand in the parent material may have gotten in the small annular space between the casing and the primary shaft concrete and created a wedge. Where the overburden and lateral resistance was not sufficient, the lifting of the wedged casing may have caused a tension crack to develop in the primary shaft.

FIG. 6: Horizontal Crack

There were also several observed bulges (<10% of the shaft diameter) which did not have an impact on the shaft performance. One interlock of the total 24 interlocks had a 300 mm (1 ft) length that required patching to limit seepage when the tank was full. The remaining inter-locks were either dry or only had limited moisture seepage observed. Figure 7 depicts the conditions of the secant wall when excavated.

Following completion of the three-week hold on the bathtub water level, the western side of the bathtub was excavated to a depth of about 12 ft. No additional anomalous conditions were observed. Figure 8 shows this condition.

CONCLUSIONS

The use of the existing technologies (double-head duplex drilling utilizing a rotator and reverse circulation) combined to provide a robust secant pile construction method. This system was able to maintain the traditional tolerances of secant pile construction while demonstrating potentially significant productivity savings. Productivity improvements included elimination of the guidewall to maintain alignment and tremie placement of concrete through the drill string.

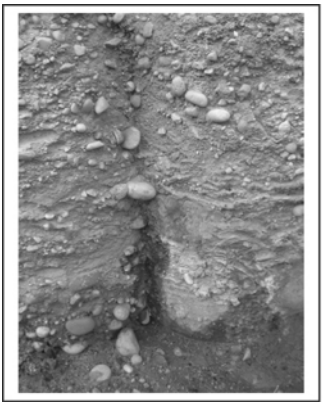

FIG. 7: Joint Leak

FIG. 8: Excavation Along the Western Side of the Bathtub

ACKNOWLEDGEMENTS

We would like to thank Posillico Construction of College Point, New York, and Ziegenfuss Drilling of Ringoes, New Jersey, for their overwhelming support of this test effort, as well as Schnabel Engineering for their assistance during the development of this paper.

BIBLIOGRAPHY/REFERENCES

Burland, J.B., and Mitchell, J.M. (1989). "Piling and Deep Foundations." Deep Foundations Institute 1989: 472 pp.

Suckling, T.P., Wren, C.J., and Troughton, V.M. (2005). "Secant Pile Walls – A Consistent Approach to Risk Management." *30th Annual Conference on Deep Foundations*, Deep Foundations Institute, Chicago, IL: 239-255.

Trivedi, K.H., and Mazzo, A. (2006). "Secant Pile Walls – Design, Construction and Case History." *31st Annual Conference on Deep Foundations*, Deep Foundations Institute, Washington, DC: 121-129.

Turner, J.P., Steele, J.A., Maher, W.F., Zortman, M.R., and Carpenter, J.R. (2004). "Design, Construction, and Performance of an Anchored Tangent Pile Wall for Excavation Support." *GeoSupport 2004,* GSP No. 124, ASCE, Reston, Virginia: 322-333.

Copyrighted Materials
Copyright © 2009 American Society of Civil Engineers (ASCE)
Retrieved from www.knovel.com

Drilled Shafts Socketed in Uncemented Clay Shale

C. Vipulanandan, Ph.D., P.E., M.ASCE[1], and Moon S. Nam, Ph.D.[2]

1 Chairman, Professor, Director of Center for Innovative Grouting Materials and Technology (CIGMAT), Director of Texas Hurricane Center for Innovative Technology (THC-IT), Department of Civil and Environmental Engineering, University of Houston, Houston, Texas 77204-4003 (Phone: (713) 743-4278; FAX (713) 743-4260; email: cvipulanandan@uh.edu;

2 Post Doctoral Fellow, Department of Civil and Environmental Engineering, University of Houston, Houston, Texas 77204-4003; e-mail: nmoon@yahoo.com

ABSTRACT: Rock socketed drilled shafts are being increasingly used in soft rocks such as clay shale to support structures. Due to lack of data and understanding of the drilled shaft behavior in clay shale, in many instances, the design capacity of the rock socket must be verified by performing full-scale load tests on site before installing the production drilled shafts. Hence there is a need to better quantify the performance of drilled shafts in uncemented clay shale.

In this investigation, case studies on testing the performance of rock socketed drilled shafts in soft clay shales in Texas over a period of three decades have been documented. A total of eight case studies have been documented including a recently completed study in Dallas, Texas. The unconfined compressive strength (q_u) for uncemented clay shale was in the range of 6.3 to 14.6 tsf (0.6 to 1.4 MPa) The diameter and length of the rock sockets varied from 2 to 2.9 ft. (0.62 to 0.89 m) and from 4.9 to 20 ft. (1.5 to 6.2 m) respectively. The tests were instrumented to determine or estimate the ultimate unit side friction (f_{max}) and/or ultimate unit end bearing (q_{max}). For the drilled shafts socketed in clay shale and tested to determine the f_{max} only, 50% of the capacity was achieved in the displacement range of 0.013 to 0.42% of the shaft diameter. The f_{max} varied from 1.1 to 7.2 tsf (0.11 to 0.69 MPa). The q_{max} varied from 25 to 64 tsf (2.4 to 6.13 MPa). Simple relationships have been developed to predict the f_{max} and q_{max} based on the unconfined compressive strength (q_u) of the rock and these relationships were verified with the relationships in the literature.

Introduction

Drilled shafts are used increasingly as foundations to support bridges and other transportation structures in many geographical areas, where rock lies near the ground

surface. Drilled shafts are constructed by excavating into the rock, forming a cylindrical socket, and constructing the socket with reinforced concrete. In general, clay shale rocks can be cemented, uncemented and/or with seams of bentonite or calcareous materials. Design of the drilled shafts socketed in uncemented clay shale in Texas is a challenge partly because only limited information is available in the literature on the ultimate unit side resistance and ultimate unit end bearing in uncemented clay shale in various geological formation of marine origin.

In north and central Texas (Dallas, San Antonio and Austin areas), heavier structures are supported using drilled shafts socketed in soft clay shale whose load carrying capacities are largely derived from the skin friction in clay shale rock sockets (O'Neill and Hassan 1993). Since a large amount of capacity is provided through the rock socket in the drilled shafts, it has been a subject of study by number of researchers in various rock types (Reese and O'Neill, 1987; Horvath et. al, 1989; Kulhawy and Phoon, 1993). Many researchers have proposed linear and nonlinear relationships between unconfined compressive strength of rock (q_u) in the socket and the ultimate skin friction in the socket (f_{max}) for various types of rocks (Rowe and Armitage 1987, Carter and Kulhawy 1988 and Reese and O'Neill 1987). O'Neill et al. (1993) and Turner et al. (1993) have reported results on the performance of rock socketed drilled shafts in clay shale rocks in Texas, Colorado and South Dakota. O'Neill et al. (1993) reported test results on rock socket behavior from four test sites in Dallas, Texas. The unconfined compressive strength of the clay shale varied from 7.83 to 31.32 tsf (0.75 to 3 MPa). The adhesion factor for the clay shale varied from 0.1 to 0.26. Turner et al. (1993) reported ultimate unit skin resistance of 0.6 to 2.6 tsf (0.06 to 0.26 MPa) for rocks in Colorado and South Dakota with unconfined compressive strength in the range of 3.92 to 12.82 tsf (0.38 to 1.22 MPa).

From 1976 to the present time, at least a total of eight load tests in the uncemented shale in Texas have been reported in the literature. One of the load test documented was completed recently in Dallas, Texas, where Osterberg Cell was used with vibrating sister bars to determine the load distribution in the test socket. In this study, applicability of some of the relationships in the literature for various types of rocks to the uncemented clay shale was verified.

Objective

The overall objective of this study was to investigate the ultimate unit side resistance and ultimate unit end bearing for drilled shafts socketed in uncemented clay shale.

Site and Load Test Results

A total of eight load tests performed since 1976 on drilled shafts socketed in clay shale in North and Central Texas are documented and investigated in this study. Load tests were performed using conventional static loading system (with reaction frame) in accordance with the ASTM D 1143 method. More details on site characterization, construction and testing procedures are in the references cited.

Texas Cone Penetrometer (TCP)

The Texas cone penetrometer (TCP) penetration per 100 blows is used by the Texas Department of Transportation (TxDOT) to design rock socketed drilled shafts. The TCP test is performed by driving a 3.0-inch diameter, 60-degree solid steel cone affixed to the bottom of a rod and driven by a 170-pound hammer dropped 24 inches onto a flat steel plate at the head of the rod successively for 100 blows. The driving energy per blow is similar to a standard penetration test (SPT). The cone penetration resistance is the distance that the tip of the cone advances in 100 blows (TxDOT Manual, 2000).

For some of the tests that were sponsored by TxDOT, characterization of the clay shale was done using the Texas Cone Pentrometer (TCP). A correlation between unconfined compressive strength (q_u) and TCP was developed using 218 data for uncemented clay shale in Dallas, Texas (Nam, O'Neill and Vipulanandan, 2004). The variation of unconfined compressive strength with TCP is shown in Fig.1. The strength varied from 1 to 30 tsf. and the relationship can be represented as follows:

$$q_u(tsf) = 21.4[TCP(inch)]^{-0.4} \quad (1)$$

For some of the CASES documented in this study, the TCP and unconfined compressive strength of rocks were measured and are indicated in Fig. 1. General information on all the eight load test sites is as follows:

CASES 1 through 3 (1976): The test site was located in Montopolis, Texas, near the intersection of SH 71 and U.S. 183. The main objective of this study was to investigate the effects of various construction methods on the performance of drilled shafts. There were considerable drilling problems at this location due to the presence of loose water-bearing sand, and the clay shale was found at various depths around the site. The shale is from the Austin formation from the Gulf series of the Cretaceous-aged marine deposit. The general soil profile for the site is as follows: Between 14 and 19 ft. (4.2 to 5.7 m)the soil was classified as CH. Below 19 ft. (5.7 m) it was all clay shale also characterized as CH. The TCP blow counts varied from 111 to 300 blows/ft. in the CH soil. In the clay shale the blow count varied from 436 to 800 blows/ft. The 2.5-ft. (0.76 m) diameter shaft constructed using the casing method had an axial capacity of 562 tons (**CASE 1**). The settlement at 50% of the failure load was 0.11 inches. In **CASE 2**, the 2.5-ft. diameter drilled shaft was constructed using the slurry method and had an axial capacity of 551 tons (4.9 MN). The settlement at 50% of the failure load was 0.20 inches (5 mm). In **CASE 3**, the 2.5-ft. diameter drilled shaft was constructed using the dry method for end bearing and had an axial capacity of 538 tons (4.8 MN). The settlement at 50% of the failure load was 0.17 inches. This study was sponsored by the TxDOT (Aurora et al. 1974).

CASE 4 (1976): The test site was located in Dallas, Texas, near the intersection of I-35E and the SH Loop 635 Interchange. The main objective of this study was to investigate the effect of using the casing method on the performance of drilled shafts (similar to CASE 1). The shale is from the Austin formation from the Gulf series of

the Cretaceous-aged marine deposit. The general soil profile for the site is as follows: The top 13 ft. was CL soil. Between 13 and 19 ft., soil was classified as SM-GP. Below 19 ft. (5.7 m) it was all clay shale, also characterized as CH. In the clay shale the TCP blow count varied from 145 to 370 blows/ft. The 3.2-ft. (0.96 m) diameter shaft with 2.9 ft. (0.87 m) socket was constructed using the casing method and had an axial capacity of 440 tons. The settlement at 50% of the failure load was 0.17 inches (4.3 mm). This study was sponsored by the TxDOT (Aurora et al. 1974).

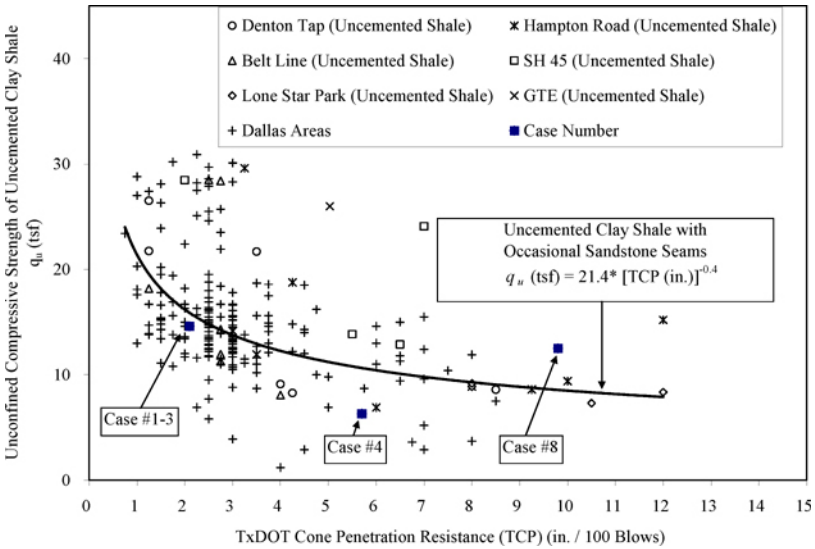

Figure 1. Correlation between TCP (Texas Cone Pentrometer) and q_u (Modified after Nam, O'Neill and Vipulanandan 2004)

CASE 5-7 (1994): The test site was located in Dallas, Texas, near the 2500 block of Lone Star Drive. The main objective of this study was to investigate the effect of expansive concrete on the performance of drilled shafts. The weak clay-shale was from the Eagle Ford formation, which is over 390 ft (120 m). thick and consists of marine sedimentary deposits from the Upper Cretaceous Age. The top part of this formation is known as Arcadia Park shale. The Arcadia Park shale is predominantly dark gray with low carbonate content and thin layers of limestone. Regular concrete was used in one shaft (**CASE 5**), and expansive concrete was used in the other two shafts (**CASES 6 and 7**). The shafts were constructed with 6 in. (0.15 m) of void at the bottom. The general soil profile for the site is as follows: The top 10 ft. (0.3 m)was CL fill. The clay shale was 10 ft. below ground level. The undrained shear strength of the clay shale varied from 40 to 65 psi (300 to 450 kPa). No TCP values were available at the test location. The 2.0-ft. (0.6 m) diameter shaft with 7.3-ft. socket (2.2 m) was constructed using regular concrete and had an axial capacity of 185 tons. The settlement at 50% of the failure load was 0.05 inches (1.25 mm)(**CASE**

5). The two 2.0-ft. (0.6 m) diameter shafts each with 7.3-ft. (2.2 m) socket were constructed using expansive concrete and had axial capacities of 218 tons (1.8 MN)(**CASE 6**) and 242 tons (2.1 MN) (**CASE 7**), respectively. The settlements at 50% of the failure loads for the two shafts were 0.1 inches. This study was sponsored by the FHWA and several industries (Hassan 1994).

CASE 8 (2005): The test site was located near the Hampton Road viaduct over the Trinity River in Dallas, Texas. The site was in the floodplain of the Trinity River, which forms a shallow valley at the location of the site. On the southern flank of this valley are seen outcroppings of the Austin Chalk formation, suggesting that past flooding events may have eroded the overlying rock/soil and caused stress relief in the rock (clay shale) at the site. Based on the measured properties of the rock, this CASE is also shown in Fig. 1. The site consisted of about 20 feet of mixed cohesionless soil overlying the clay shale. The clay shale (Eagle Ford formation) had a dry unit weight of 121 pcf. The TCP decreased (penetration/100 blows) with increasing depth, below 35 feet, an Osterberg Cell with a capacity of 1000 tons was used for the slow load test. Based on the laboratory UU triaxial compression tests, the strength for the rock from 25 to 35 feet varied from 6.3 to 24 tsf with an average strength of 12.5 tsf. The 2.0-ft. diameter test shaft (no end bearing) with 10-ft. socket had an axial capacity of 91 tons. The settlement at 50% of the failure load for the test shaft was 0.003 inches. This study was sponsored by the TxDOT (Vipulanandan et al. 2005).

Analysis and Discussions

The unconfined compressive strength of uncemented clay shale in which the load tests were performed varied from 4 to 15 tsf. The ratio of socket length-to-diameter varied up to 10. The f_{max} varied from 1 to 7.2 tsf. It must be observed that the f_{max} was lowest in the tests where it was determined directly (CASES 5 through 8). In the tests where f_{max} and q_{max} were determined together, f_{max} were much higher with comparable rock strength (CASES 4 and 5). The settlement to reach 50% of f_{max} varied from 0.003 to 0.10 inches (0.076 to 2.54 mm) . The adhesion parameter (α_f) varied from 0.09 to 0.49 with a mean of 0.29 and a coefficient of variation of 44%. The ratio of q_{max}-to-q_u varied from 3.66 to 4.38 with an average of 4.04 and a coefficient of variation of 7.4%.

A number of studies have investigated the relationship between f_{max} or q_{max} with unconfined compressive strength (q_u) of rocks. The relationships can be generalized as follows:

$$f_{max} \text{ or } q_{max} = \alpha_f \text{ or } \alpha_q \, (q_u)^m \qquad (2)$$

Where, the magnitudes of parameters α_f (also known as adhesion coefficient or reduction factor) and α_q depend on the rock type and/or unconfined compressive strength are back calculated from the test data.

(i) Ultimate Unit side Resistance (f_{max})

Studies have suggested using Eqn. (2) with m = 0.5 or 1 for relating the ultimate unit side resistance to the unconfined compression strength. Based on the least square fit of the data (Fig. 2) for the uncemented clay shale the following relationships were obtained:

$$f_{max} = 0.29\, q_u, \qquad (R = 0.64 \text{ and } N = 8) \tag{3}$$

$$f_{max} = 0.30\, q_u^{0.92}, \quad (R = 0.64 \text{ and } N = 8) \tag{4}$$

where f_{max} = ultimate unit side resistance in tsf,
q_u = unconfined compressive strength of rock in tsf.
N = number of data
R = coefficient of correlations

These two relationships (Eqn (3) and (4)) are compared to the experimental results in Fig 2 and both relationships predict the results well. It must be noted that Reese and O'Neill (1987) have suggested a linear relationship with adhesion factor of 0.15 for Midwest clay shale formation with unconfined compressive strength in the range of 18 to 21 tsf. Based on over 200 data, Horvath (1982) suggested a nonlinear relationship (Eqn. (2)) with m = 0.5 and adhesion coefficient of 0.97 (for tsf), and the relationship is compared with the data for the clay shale in Fig. 2. It must be noted that for Pierre Shale in South Dakota and Colorado with an unconfined compressive strength greater than 6.3 tsf (0.6 MPa), the Horvath relationship with adhesion coefficient of 0.65 (in tsf or 0.2 in MPa) well represented the test data (Turner et al, 1993).

(ii) Ultimate Unit End Resistance (q_{max})

Limited studies have suggested using Eqn. (2) with m = 1 for relating the ultimate unit end resistance to the unconfined compression strength. Based on the least square fit of the data(Fig. 4) for the uncemented clay shale in this study, the relationship was as follows:

$$q_{max} = 4.04\, q_u, \qquad (R = 0.97 \text{ and } N = 4) \tag{5}$$

where q_{max} = ultimate unit base resistance in tsf. It must be noted that Rowe and Armitage (1987) previously suggested a linear relationship (Eqn. (5)) with the parameter α_q equal to 2.5.

Conclusions

Since 1976, a total of eight load tests on drilled shafts socketed in uncemented clay shale in Texas have be documented in the literature. All the tests have been performed in the Austin and Eagle Ford formation in the Greater Dallas and Austin areas. Based on the case studies and analysis of the full-scale load tests of eight drilled shafts socketed in clay shale following conclusions can be advanced;

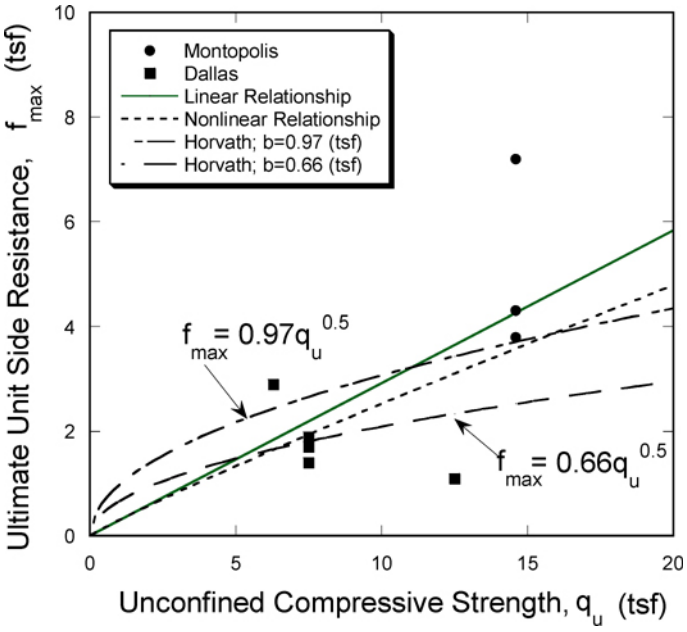

Figure 3 Relationship between f_{max} and q_u for uncemented clay shale

(1) The load tests were performed in uncemented clay shale with unconfined compressive strengths in the range of 6.3 to 14.6 tsf (0.6 to 1.4 MPa). The drilled shaft diameters varied from 2 to 3.2 ft. The socket length-to-diameter ratio varied up to 10.

(2) The f_{max} varied from 1.1 to 7.2 tsf (0.11 to 0.69 MPa). The q_{max} varied from 25 to 64 tsf (2.4 to 6.13 MPa). The settlement at 50% of the ultimate side resistance varied from 0.003 to 0.10 inches (0.076 to 2.54 mm) and was equivalent to 0.013 to 0.42% of the shaft diameter.

(3) The adhesion coefficient (reduction factor) varied from 0.09 to 0.49 with an average of 0.29. The ratio of q_{max} to q_u varied from 3.66 to 4.38 with an average of 4.04.

Acknowledgement

This study was supported by the Center for Innovative Grouting Materials and Technology (CIGMAT) with funding from the Texas Department of Transportation. The funding agency is not responsible for any of the findings or conclusions reported in this study.

References

1. Aurora, R. P. and Reese, L. C. (1976). "Behavior of Axially Loaded Drilled Shafts in Clay-Shales," *Research Report 176-4*, Center for Highway Research, The University of Texas at Austin, March.
2. Carter, J.P. and Kulhawy, F.H. (1988), "Analysis and Design of Drilled Shaft Foundations Socketed into Rock", *EPRI Report El-5919*, Electric Power Research Institute, Palo Alto, California
3. Hassan, K. M. (1994). "Analysis and Design of Drilled Shafts Socketed into Soft Rock," *Ph.D. Thesis*, Department of Civil & Environmental Engineering, University of Houston, Houston, Texas.
4. Horvath, R.G. (1982), "Drilled Shaft Socketed into Weak Shale – Methods of Improving Performance",*Ph.D. Dissertation*, Department of Civil Engineering, Unversity of Toronto, Toronto, Ontario, Canada.
5. Horvath, R.G. and Chae, K-J. (1989), "Long Term Settlement of Rock Socketed Piers", *Canadian Geotechnical Journal*, Vol. 26 No. 3, August, pp.248-358
6. Kulhawy, F.H. and Phoon, K.K. (1993), "Drilled Shaft Side Resistance in Clay Soil to Rock", *Deign and Performance of Deep Foundations: Piles and Piers in Soil and Soft Rock*, GSP No. 38, Ed. by Nelson P., Smith T., Clukey E., ASCE, pp. 173-183.
7. Moon, N.S., O'Neill, M. W. and Vipulanandan, C. (2004), "Correlation between Texas Cone Penetrometer (TCP) Values and the Compressive Strength of Clay Shale in Texas", *Proceeding. CIGMAT 2004 Conference and Exhibition, Houston, Texas (http://www2.egr.uh.edu/-civeb1/CIGMAT/04-poster/12.pdf)*.
8. O'Neill, M.W. and Hassan K.M. (1993), "Perimeter Load Transfer of Drilled Shafts in Eagle Ford Formation", *Design and Performance of Deep Foundations: Piles and Piers in Soil and Soft Rock*, GSP No. 38, ASCE, pp. 227-244.
9. Reese, L.C. and O'Neill, M.W. (1987), "Drilled Shafts: Construction Procedures and Design Methods", *Design Manual*, US Department of Transportation, Federal Highway Administration.
10. Rowe, R.K. and Armitage, H.H. (1987), "A Design Method For Drilled Piers in Soft Rock", *Canadian Geotechnical Journal*, Vol. 24, pp.126-142.
11. Turner, J. P. Sandberg, E. and Chou, N. N. S (1993), "Side Resistance of Drilled Shafts in the Denver and Pierre Formations", *Design and Performance of Deep Foundations: Piles and Piers in Soil and Soft Rock*, GSP No. 38, ASCE, pp. 245-259.
12. TXDOT (2000), "*Geotechnical Manual (online version)*", Texas Dept. of Transportation, Bridge Division, Austin, Texas.
13. Vipulanandan, C. and Kaulgud, S. (2005), "Behavior of ACIP Piles Socketed in Clay Shale", GSP 132, *CD Proceedings, Advances In Deep Foundations, ASCE,* Austin, Texas.
14. Vipulanandan, C. Liu, R. and Moon, N.S., (2005), "Improved Design for Drilled Shafts in Rocks", *Final Report 0-4372,* Texas Department of Transportation, Austin, Texas (*CIGMAT Report 10-2005*).

Copyrighted Materials
Copyright © 2009 American Society of Civil Engineers (ASCE)
Retrieved from www.knovel.com

EFFECTS OF ROCK ANISOTROPY ON LATERAL RESPONSE OF DRILLED SHAFT

Robert Y. Liang, Member, ASCE, PHD, PE
Dept. of Civil Engineering, The University of Akron, Akron, OH 44325-3905, rliang@uakron.edu
Ehab S. Shatnawi, PHD
Technology & Solutions Division, Caterpillar Inc., Mossville, IL 61552 ,
shatnawi_ehab_s@cat.com

ABSTRACT

A p-y curve formulation for a transversely isotropic rock mass is briefly summarized. The results of a sensitivity analysis using this p-y criterion and LPILE program are presented. Both the orientation of the plane of transverse isotropy and the degree of anisotropy (E/E') have shown to exert significant influences on the load deflection response of laterally loaded drilled shafts.

INTRODUCTION

One of the widely used approaches for analysing the response of drilled shafts under lateral loads is the p-y approach. Recently, based on both theoretical derivations and numerical (finite element) parametric analysis results, a p-y criterion has been developed by Shatnawi (2008) for the rock mass that exhibits significant transverse isotropy due to intrinsic mineral grain orientation and influences of parallel sets of joints. In this paper, this p-y curve is succinctly described. Moreover, the proposed p-y criterion is used to exam the effects of anisotropy on the response of laterally loaded drilled shafts in anisotropic rock mass.

A series of parameters defining various transversely isotropic p-y curves are selected in a systematic numerical study using the LPILE computer program with the p-y curves generated from the p-y criterion described in this paper. Based on this set of parametric study, the insights on the influences of rock anisotropy on the predicted response of the rock socketed drilled shaft under the lateral load are discussed. Both the orientation of the plane of transverse isotropy and the degree of anisotropy (E/E') have shown to exert significant influences on drilled shaft responses.

CONSTRUCTION OF P-Y CURVE FOR ANISOTROPIC ROCK MASS

A hyperbolic equation given in Equation (1) is adopted for mathematical modelling of the p-y curves. This equation is based on a study conducted by Yang (2006) who investigated different mathematical representation techniques for field load test derived p-y curves. Note that the subgrade modulus (K_i) and the ultimate resistance (p_u) are two critical parameters in the hyperbolic equation

$$p = \frac{y}{\frac{1}{K_i} + \frac{y}{p_u}} \tag{1}$$

1. Compute K_i

The K_i is computed using Equation (2), in which the values of the η functions can be interpreted from the design charts developed by Shatnawi (2008) and shown in Figure 1.

$$\frac{K_i}{pa} = 1\times10^6 \eta(E,\beta)\eta(E',G')\eta(\nu,\nu')\eta(E_p,\nu_p)\eta(R) \tag{2}$$

2. Compute P_u.

Shatnawi (2008) developed two sets of equations for calculating p_u depending the mode of failure of the rock mass due to the lateral deflection of the shaft. Equations (3) through (6) are used for computing p_u for a sliding failure of a block of rock. Equations (7) through (13) are used for calculating p_u for a failure mode corresponding to strength failure of rock mass with anisotropic strength at a great depth below the ground surface. The value of p_u is the smaller value calculated using these two sets of equations. The design charts shown in Figure 2 together with Equation (6) could be used to to calculate the correction factor CF in Equation (3). Equation (8) could be used to compute P_L, while Equations (11) can be used to estimate τ_{ult}.

$$p_u = CF \times p_u^* \tag{3}$$

$$p_u^* = \frac{dF_{net}}{dH} \tag{4}$$

$$F_{net} = 2F_s \sin\beta + F_{sb} \sin\beta + F_{nb} \cos\beta - F_a \quad (5)$$

$$CF = \eta(\beta, \phi)\, \eta(C_r, C_{joint}, H/D)\, \eta(\sigma_{v0}') \quad (6)$$

$$p_u = \frac{\pi}{4} D p_L + \frac{2}{3} D \tau_{ult} \quad (7)$$

$$P_L = \gamma' Z + \frac{k(\sigma_{c(90°)} - \gamma' Z)}{\cos^4(90-\beta) + k\sin^4(90-\beta) + 2n\sin^2(90-\beta)\cos^2(90-\beta)} \quad (8)$$

$$k = \frac{E}{E'} \quad (9)$$

$$n = \frac{E'}{2G'} - \nu' \quad (10)$$

$$\tau_{ult} = k'(C_{ad} + \sigma_v' \mu) \quad (11)$$

$$k' = 2.39 \times 10^{-6} \eta_{L/D} \left(\frac{E_m}{p_a}\right)\left(\ln\left(\frac{C_r}{p_a}\right) + 2.61\right)\left(\ln\left(\frac{G_s}{p_a}\right) - 3.6\right) \quad (12)$$

$$\eta_{L/D} = \begin{cases} 1 & L/D < 2 \\ 3.43\left(\frac{L}{D}\right)^{-1.55} & Otherwise \end{cases} \quad (13)$$

where,

p_u*	=Ultimate lateral resistance of the straight wedge
τ_{ult}	=Ultimate side shear
P_L	=Frontal compressive strength of rock
E, E', v, v', G'	= Elastic constants of transversely isotropic materials
R	= Shaft radius
E_p	= Young's modulus of shaft
ν_p	= Poisson's ratio of shaft
H	= Height of the failure wedge
Fsb	= Shear force on the bottom face of the failure wedge
Fs	= Shear force on the side faces of the failure wedge
Fnet	= Total net resistance of rock
Fnb	= Normal force on the bottom face of the failure wedge
Fn	= Normal force on the side faces of the failure wedge
p_a	= Atmospheric pressure
CF	= Correction factor
C_r, Φ'	= Cohesion and friction angle of the rock mass
γ'	= Rock unit weight
C_{joint}, μ	= Joint interface strength properties
β	= orientation of plane of transverse isotropy
σ_{v0}'	=Overburden pressure

Em	= Modulus of rock mass
C_{ad}, μ	= Rock-Shaft interface strength parameters
L/D	=Length to Diameter ration

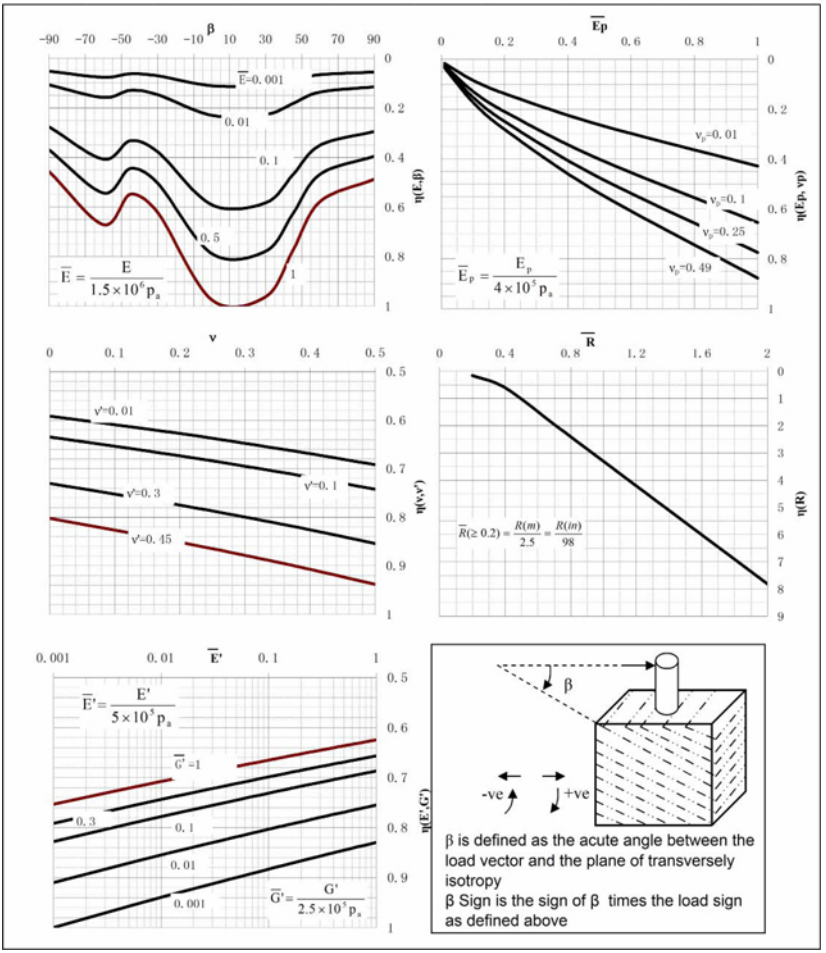

Fig. 1 Design charts for estimating Ki

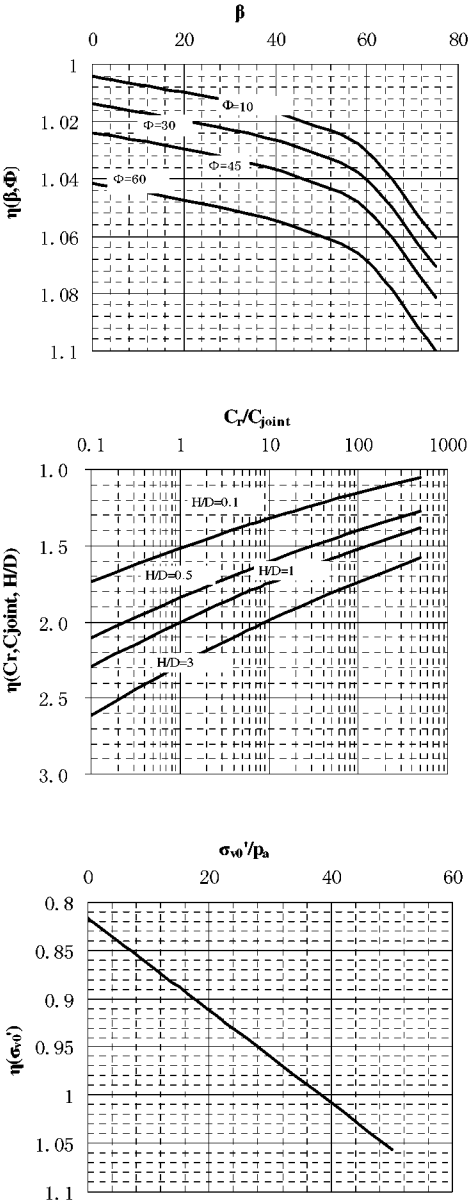

Fig. 2 Design charts to estimate CF

SENSITIVITY ANALYSIS

A series of sensitivity analyses are carried out using the proposed p-y criterion to gain insight on the effects of rock anisotropy on the response of the laterally loaded drilled shaft. The Young modulus of the tested drilled shaft is estimated to be 4000 ksi with Poisson's ratio of 0.25. The test shaft is 6 ft in diameter with 18 ft rock socket length. The rock is classified as Ohio shale with unconfined compressive strength for the intact core shale as 5668 psi. The unit weight of the rock mass is estimated as 0.038 pci. Five different case studies are performed as shown in Table 1. For these analyses, the modulus of elasticity in the plane of transverse isotropy is taken to be equal to the rock mass modulus ($E=E_m$=95 ksi), while a typical value of Poisson's ratio is used (ν = 0.3, ν' = 0.15). The corresponding K_i and p_u computed from these values and the proposed criterion for these cases are also summarized in Table 1.

Table 1 Effect of anisotropy on the p-y curve parameters

Case	β	E/E'	K_i (psi)	Pu (lb/in) at (Depth, in)			
				1	50	100	216
1	30	5	375000	16278	72756	77460	88374
2	45	5	300000	6084	78699	101403	112066
3	80	5	190000	11324	155212	159545	169598
4	30	10	465000	16278	75555	80247	91131
5	30	1	230000	16278	59183	63948	75004

The p-y curves are shown in Figure 3, in which the solid lines represent shallow depth (10 inch below the ground) while the lines with the square marker represent great depth (100 in. below ground surface). As can be seen, the effect of β is significant.

For all the five cases in Table 1, the relevant p-y curves are input into LPILE computer program to compute the response of the test shaft under the applied lateral loads. The predicted load deflection curves are shown in Figure 4 and Figure 5 for different β angle and for different E/E' ratio, respectively. The effect of the orientation of plane of transverse isotropy and the degree of anisotropy on the response of the drilled shaft in terms of deflection is clearly seen in these figures.

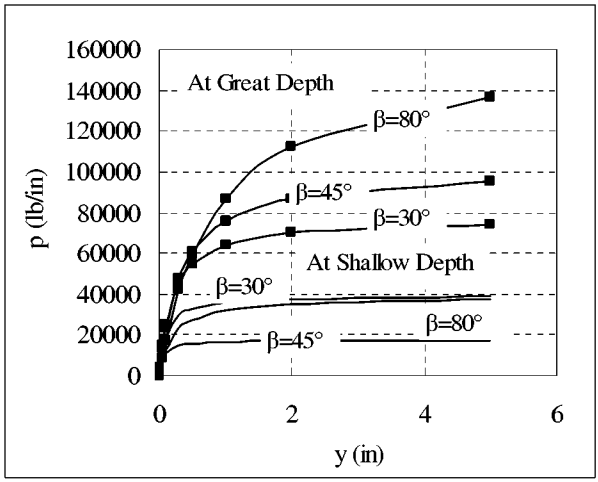

Fig. 3 Effect of β on p-y curves at shallow and great depths

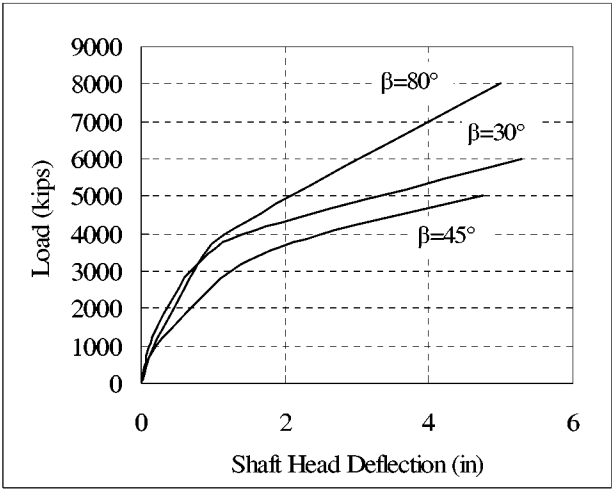

Fig. 4 Load deflection curves for different β

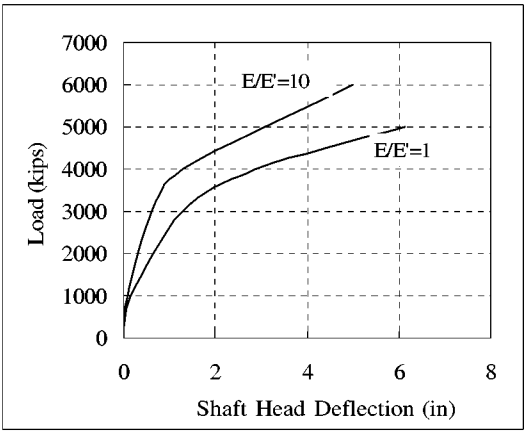

Fig. 5 Load deflection curves for different E/E' ratios

SUMMARY AND CONCLUSIONS

A new hyperbolic p-y criterion for transversely isotropic rock is succinctly summarized in this paper. This criterion can be used to predict the deflection, moment, and shear responses of the drilled shaft in rock under the applied lateral loads. Based on the sensitivity study results presented in this paper, the following conclusions may be drawn.

- At small lateral load, the drilled shaft is found to have its maximal deflection at an orientation angle $\beta = 45°$ and its minimal deflection at an orientation of 30°, while at large lateral loads, the minimal deflection was found at an orientation angle of 80°.

- It can be concluded for the same β that the larger degree of anisotropy, as represented by the ratio E/E', the smaller the drilled shaft head deflection and the smaller the maximum moment would be at a given applied lateral load.

REFERENCES

SHATNAWI E. S. (2008). "Development of p-y Criterion for Anisotropic Rock and Cohesive Intermediate Geomaterials" Ph.D. dissertation, University of Akron, Akron, Ohio, 2008, 222 pp.

Copyrighted Materials
Copyright © 2009 American Society of Civil Engineers (ASCE)
Retrieved from www.knovel.com

Willis Avenue Swing Bridge: Design and Construction of Drilled Shaft Foundations

Vedrana Krstic[1], A.M. ASCE, Raymond Mankbadi[2], M. ASCE, P.E. and Aravinda Ramakrishna[3], M. ASCE, P.E.

[1] Assistant Professor, The College of New Jersey, School of Engineering, Department of Civil Engineering, 2000 Pennington Road, Ewing, NJ 08628; krstic@tcnj.edu
[2] Director of Geotechnical Engineering, Hardesty and Hanover, LLP, 850 Bear Tavern Road, Suite 206, West Trenton, NJ 08628; rmankbadi@hardesty-hanover.com
[3] Geotechnical Engineer, Hardesty and Hanover, LLP, 850 Bear Tavern Road, Suite 206, West Trenton, NJ 08628; aramakrishna@hardesty-hanover.com

ABSTRACT: Drilled shaft foundations are currently being constructed to support selected piers of the new, four lane, 106 meter long Willis Avenue Swing Bridge and approach structures. The Willis Avenue Swing Bridge over the Harlem River is being replaced under a $612 million project which is the largest ever undertaken by the Movable Bridge Group of the New York City Department of Transportation. Drilled shafts vary in diameter from 1220 mm to 1524 mm and extend into bedrock which is composed of Inwood Marble or Fordham Gneiss. The design capacity of the drilled shafts was estimated from the side resistance within the rock socket, discounting any side resistance above the rock socket in accordance to empirically derived methods outlined in the AASHTO Bridge Design Specifications. The design capacity of the drilled shafts is in the process of being verified by means of an Osterberg Cell static load test conducted on four instrumented test shafts representing each drilled shaft size and each type of bedrock on the Bronx side of the project. The load test results suggest that empirical design methods combined with field rock properties data underpredicted the drilled shaft capacity in reported bedrock.

INTRODUCTION

The Willis Avenue Swing Bridge over the Harlem River is being replaced under a $612 million project which is the largest ever undertaken by the Movable Bridge Group of the New York City Department of Transportation. The project is massive in scope as it extends over a mile in length between the Manhattan and Bronx boroughs of the City, passes over the Harlem River and an adjoining railyard and provides connections between FDR Drive and Rt. 87, two major highways in the area. The new alignment not only dramatically improves the alignment from that of the 100

year old existing bridge, but also facilitates maintaining 70,000 vehicles per day of roadway traffic while maintaining navigation on the river.

Due to variations in the depth to suitable bearing material along the project alignment, the construction staging including maintenance of traffic, and the limitations on equipment access due to existing structures, the new proposed bridge and approaches will be founded on a variety of foundation structures including shallow foundations, steel H-piles, steel bored-in pipe piles or mini-piles and drilled shafts. This paper focuses on the design and construction issues related to the drilled shaft foundations for the piers of the new, four lane, 106 meter long swing bridge and approach structures. Drilled shafts vary in diameter from 1220 mm to 1524 mm and extend into bedrock which is composed of Inwood Marble or Fordham Gneiss. The construction of the drilled shaft foundations commenced in January 2008. The design capacity of the drilled shafts is in the process of being verified by means of an Osterberg Cell static load test so far conducted on four instrumented test shafts representing each drilled shaft size and each type of bedrock on the Bronx side of the project. One additional O-cell load test will be conducted on the Manhattan side of the project by the end of 2008.

GEOLOGY OF THE PROJECT SITE

The project site lies within the southernmost terminus of the New England Uplands Physiographic Province, known as the Manhattan Prong, bounded by the Triassic Lowlands Province to the west and the Atlantic Coastal Lowlands Province to the east and south (Schuberth 1968). The bedrock within the project limits is composed of three formations known as the Manhattan Formation, the Inwood Marble, and the Fordham Gneiss, in order of increasing age. The Willis Avenue Bridge twice traverses the boundary of the region underlain by Inwood Marble and a ridge underlain by Fordham Gneiss extending northward along FDR Drive in Manhattan and beneath the Bruckner Ramp alignment in the Bronx. Within the Harlem Lowland and the Harlem River, the Fordham Gneiss is encountered beneath the younger Inwood Marble. The unconsolidated deposits overlying the bedrock within the project site are primarily the remnants of the geologically recent Wisconsin glaciation and post-glaciation events. In general, the bedrock is overlain by the Wisconsin ground moraine deposits, which are overlain by the lacustrine varved silt, sand and clay deposits of the glacial Lakes Hudson and Flushing, which in turn are overlain by the slightly younger post-glacial-uplift fluvial, unconsolidated, stratified sand and gravel deposits ranging from a meter to tens of meters in thickness (Parsons 1976). The depositional sequence is completed by more recent alluvial deposits of organic silts and clays. Peat is encountered in former low-lying wetland areas. Recent manmade fills comprise the surface deposits on both shores of the Harlem River.

ROCK PROPERTIES

The properties specific to rock formations encountered within the limits of the project site were determined through the rock coring exploration program, which included six to nine meters of rock coring at deep foundation locations. According to the field rock coring records, the bedrock underlying the project site generally consists of Inwood Calcitic and Dolomitic Marble overlying Fordham Gneiss within the Harlem Lowland. In the areas overlying the Fordham Ridge, the bedrock consists of Fordham Gneiss.

Ground water observation wells were installed in selected boreholes. Observation well data indicates that the groundwater table is just over Elevation 0.0 meters and increases to 1.4 meters moving away from the waterfront in the Bronx (referencing Borough Works Datum of the Borough of Manhattan as 0.838 meters above Standard U.S. Coast and Geodetic Survey Datum, Mean Sea level at Sandy Hook).

Representative rock cores were tested to verify field classifications and obtain properties for use in foundation design. Estimated design rock properties are summarized in Table 1.

TABLE 1. Estimated Rock Parameters

Rock Description	Unit Weight (kN/m^3)	Unconfined Compressive Strength (MPa)	RQD (%)	Reduction factor (α_E)*
Inwood Calcitic and Dolomitic **Marble**	22	66	0-95 (27 average, 75 required)	0.41
Fordham **Gneiss**	23	88	7-86 (51 average, 75 required)	0.41

* AASHTO 4.4.8.2.2

DRILLED SHAFT FOUNDATIONS

The selection of the foundation types was made considering the variation along the project alignment of the depth to suitable bearing material, the construction staging including maintenance of traffic, the limitations on equipment access due to existing structures, the magnitudes of the pier loads, and the proximity to the bulkhead.

Considering the selection criteria, drilled shaft foundations will be constructed at the following locations within the project limits: FDR Drive approach ramp abutment and piers A1 to A4, Harlem River piers 4 to 8, Bronx piers 9 to 11 and B1 and relieving platforms constructed at Manhattan and Bronx bulkheads.

Drilled shafts of 1220 mm and 1524 mm nominal diameters are being constructed and socketed into the sound bedrock for a minimum length of 2.44 m and 3.35 m respectively. A permanent steel casing was used for the installation of each drilled shaft. The casing was advanced into the top of sound bedrock to seal the construction of the rock socket from overburden and groundwater. The casing was cleaned out and left in place after construction was completed. The rock socket was advanced, typically 90 to 150 mm smaller than the casing diameter (1131 mm and 1372 mm for casing size of 1220 mm and 1524 mm respectively). Reinforcement cages were lowered into the socket and the shaft and the concrete is tremie-placed. Four access tubes were attached to the reinforcement cages and cast into each shaft to permit cross-hole sonic logging integrity verification tests. In order to verify the estimated drilled shaft capacity and to better assess the nature and the quality of the founding rock formations, five production drilled shafts were selected as test shafts with Osterberg cell assembly and required instrumentation attached to the bottom of the reinforcement cages.

Drilled Shaft Design Axial Capacity

The design axial capacity was calculated in accordance with the AASHTO Bridge Design Specifications as required by the New York State Department of Transportation Specifications. The Allowable Stress Design (ASD) method was utilized as per the design specifications however, the LRFD method, used for quality control, yielded identical results. The design capacity of the drilled shafts was estimated in accordance with the empirically derived methods outlined in the AASHTO Bridge Design Specifications Sec. 4.6.5.3., accounting for the estimated rock properties given in Table 1.

The theoretical axial capacity of the drilled shafts was estimated from the side resistance within the rock socket, discounting any side resistance above the rock socket. The design considered that settlement of at least 10 mm is required to mobilize ultimate side resistance and assure load transfer to the tip of the drilled shaft as recommended in the AASHTO Bridge Design Specifications. The rock quality designation (RQD) required for design calculations was determined from the NX Rock Cores taken at each deep foundation pier location. General rock conditions and estimated unit side resistance for the four selected test drilled shafts is presented in Table 2.

In order to achieve design axial capacity, project specifications required drilled shafts to be socketed into sound bedrock having Rock Quality Designation (RQD) of 75% or more. Test borings drilled at several locations within the project limits showed that sound rock was encountered at depths significantly greater than the estimated minimum. For that reason a test program was devised which proposed five Osterberg Cell (O-cell) load tests to be completed on selected production drilled shafts. Four tests on the Bronx side of the project site have been already completed,

while the Manhattan side load test will be completed as installation operations further progress by the end of 2008.

TABLE 2. Estimated Side Resistance of Test Drilled Shafts

Pier-Pile ID	Bedrock (Test Borings)	Shaft/Rock Socket Diameter (mm)	Min. Rock Socket Length (m)	Unit Side Resistance (MN/m)
P10-S4	Highly to moderately fractured calcitic **Marble**	1220/1131	2.44	2.0
P10-S8	Highly to slightly fractured calcitic **Marble**	1220/1131	2.44	2.0
B1-S3	Moderately fractured **Gneiss**	1524/1372	3.35	2.3
Bronx Rel. Platform-S22	Highly to slightly fractured calcitic **Marble**	1220/1131	2.44	2.0

Osterberg Cell Load Test

The drilled shafts selected for load tests were constructed in accordance with the following procedure. After permanent steel casing was installed to the top of bedrock elevation, a rock socket was cored to an estimated tip elevation. Video inspection was used to confirm the rock quality, adjust the tip elevation, and finalize the end of coring operations. The test shaft instrumentation and general properties are shown in Figure 1. Strain gages (SG) were used to assess the side shear load transfer of the shaft above the O-cell assembly. The O-cell was pressurized in 20 loading increments until the loading capacity of the O-cell was reached. The O-cell was then re-pressurized in order to demonstrate that the test shaft is suitable for use as a production shaft. O-cell testing was conducted by LOADTEST, Inc. in accordance with the procedure outlined in ASTM D1143 (Standard Test Method for Piles under Static Axial Load) for Quick Load Test Method.

Field Test Results

Considering the poor RQD estimated from the rock coring records, video inspection was performed after completion of the test shaft excavation. It was noted at that time that rock conditions differ from the ones recorded previously and reflect rock of

better than estimated quality (Table 3). This observation was confirmed through the actual O-cell test by observing axial capacities higher than estimated.

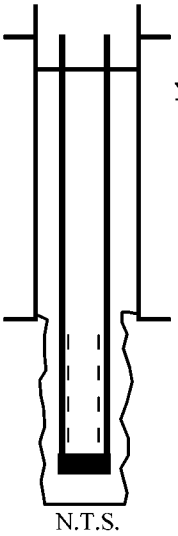

Elevation (m)	P10-S4	P10-S8	B1-S3	BRP-S22
Ground Surface	+2.02	+2.48	+6.43	+2.67
Top of Concrete	+0.31	+1.86	+3.46	+0.03
Ground Water Table	±0.00	+0.74	±0.00	±0.00

	Marble	Marble	Gneiss	Marble
Top of Rock Socket	-24.71	-32.75	-10.61	-25.45
SG-4	---	---	---	-26.40
SG-3	-25.16	---	---	-27.60
SG-2	-25.89	-33.10	-12.30	-28.80
SG-1	-26.62	-34.10	-14.20	-30.00
O-cell (bottom)	-28.62	-36.00	-17.20	-32.00
Tip of Shaft	-31.30	-39.42	-18.13	-33.22

FIG. 1. Drilled Shaft and O-cell Installation Setup

Axial capacity of the test drilled shafts was calculated based on the average unit side shear values recorded between the O-cell and the top strain gauge as shown in Figure 1, accounting for the bi-directional nature of the O-cell test. Observed side resistance per unit length is shown in Table 3. Recorded values were larger than the estimated values reported in Table 2 for all four tested drilled shafts.

Considering the equivalent top load settlement results (LOADTEST 2008), a total settlement of 4 mm to just over 7 mm (about 0.3% to 0.6% of the nominal shaft diameter) was recorded during the tests and resulted in mobilizing unit shaft resistance of the magnitudes reported in Table 3. Since considerably larger settlement is required to mobilize peak strength (AASHTO) it can be concluded that ultimate resistance of the tested drilled shafts has not been reached. This conclusion is in agreement with the linear nature of the O-cell load versus displacement curves shown in Figure 2 (LOADTEST 2008). No apparent creep limit was reached during the tests.

The Crosshole Sonic Logging (CSL) test was used to assess foundation integrity on all production drilled shafts. The results showed that tested shafts are sound with no

significant slower concrete velocities identified. With that in consideration, previously reported capacity and settlement results can be considered reliable.

TABLE 3. Observed Side Resistance of Test Drilled Shafts

Pier-Pile ID	Bedrock (Video Inspection)	Shaft/Rock Socket Diameter (mm)	Actual* Rock Socket Length (m)	Unit Side Resistance (MN/m)
P10-S4	Moderately to slightly fractured calcitic **Marble**	1220/1131	3.37	3.0
P10-S8	Moderately to slightly fractured calcitic **Marble**	1220/1131	2.71	3.6
B1-S3	Moderately to slightly fractured **Gneiss**	1524/1372	5.92	2.8
Bronx Rel. Platform -S22	Moderately to slightly fractured calcitic **Marble**	1220/1131	6.01	2.1

* Extending to the top of the O-cell.

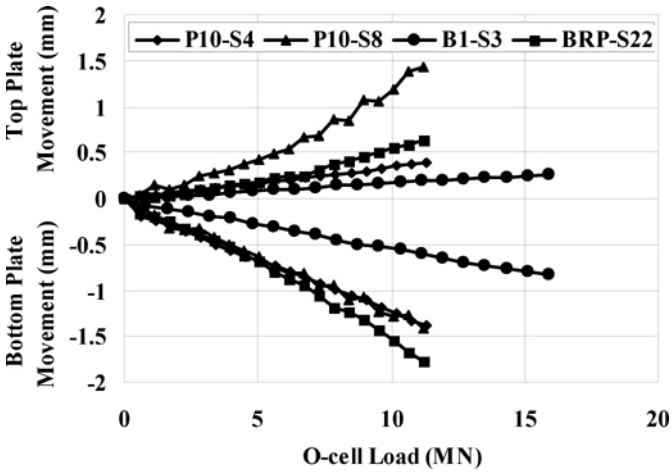

FIG. 2. O-Cell load vs. Displacement Curves

CONCLUSIONS AND RECOMMENDATIONS

This paper outlined a case study of the design and construction of the drilled shaft foundations constructed at various locations of the new Willis Avenue Bridge in NYC. The O-cell load test was conducted on four production drilled shafts. Based on the field test results the following can be concluded:

- The design procedure suggested by AASHTO for estimating axial resistance of drilled shafts socketed into bedrock is greatly sensitive to rock quality. In this case, traditional coring technique used to retrieve rock samples at the Willis Avenue Bridge project site resulted in rock quality being estimated lower than the actual. This subsequently underestimated axial design capacity.
- As per AASHTO design recommendations, settlement of at least 10 mm is required to mobilize ultimate resistance of drilled shafts socketed into bedrock. Significantly smaller settlement was recorded suggesting that the axial compression load applied to the test shaft was below the ultimate resistance of the tested shafts. The linear nature of the load vs. displacement curves supports this conclusion.

It is recommended that engineers cautiously use rock coring data in combination with empirical design procedures outlined in AASHTO Specifications when designing drilled shafts socketed into rock. The use of the Osterberg cell load test is of the most importance for verifying estimated axial capacity. Video inspection is a highly recommended method in cases when the quality of the bedrock is questionable.

References

American Association of State Highway and Transportation Officials (AASHTO), (1997), "*AASHTO Bridge Design Specification*", 16th edition.

The Building Code of The City of New York, Local Law No. 76 Effective Dec, 6, 1968, including Amendments to March 13, 1998.

LOADTEST, Inc. (2008). "Report on Drilled Shaft Load Testing (Osterberg Method)", LT-9320-1, LT-9320-2, LT-9320-3 and LT-9320-4.

Parsons, J.D. (1976). "New York's Glacial Lake Formation of Varved Silt and Clay." *Journal of the Geotechnical Engineering Division,* Vol. 102, American Society of Civil Engineers, 605-638.

Schuberth, C. J. (1968). "*The Geology of New York City and Environs.*" First Edition, The Natural History Press, Garden City, New York, 304 p.

Copyrighted Materials
Copyright © 2009 American Society of Civil Engineers (ASCE)
Retrieved from www.knovel.com

Axial load transfer behavior of rock-socketed shafts

Lianyang Zhang, M.ASCE, P.E.*, and Jinming Xu**

* Assistant Professor, Dept. of Civil Engineering and Engineering Mechanics, University of Arizona, Tucson, AZ, USA

** Associate Professor, Dept. of Civil Engineering, Shanghai University, Shanghai, China

ABSTRACT

In the design of rock-socketed shafts for supporting axial loading, the end bearing resistance is often ignored, resulting in excessive rock-socket lengths and increased cost. This paper investigates the axial load transfer behavior of rock-socketed shafts based on a database of 99 field test rock-socketed shafts. The shafts are 1.4 to 96.3 m long and have a diameter between 0.5 and 1.5 m. The rock-socket lengths are from 0 to 18.8 meters. The database is developed by collecting information on field test rock-socketed shafts from published papers and reports. The results show that it is important to account for the end bearing resistance in the design of rock-socketed shafts because (1) up to 25% of the shaft head load on average can be transmitted to and supported by the shaft base even at relatively small shaft head displacement in the working range of 5–15 mm, and (2) the portion of the shaft head load transmitted to and supported by the shaft base increases with time due to the effect of creep.

INTRODUCTION

Rock-socketed shafts are widely used as foundations of different structures to support large axial loads, including highway bridges and high-rise buildings. For design engineers, a great challenge is the determination of rock-socket length for drilled shafts under axial loading (Zhang 2004; Turner 2006). In current design practice, engineers often neglect the base resistance in their design assuming that the base resistance will not develop without large downward displacement (Crapps and Schmertmann 2002; Turner 2006). The draft Interim 2006 AASHTO *LRFD Bridge Design Specifications* (AASHTO 2006) state that "Design based on side-wall shear alone should be considered for cases in which the drilled hole cannot be cleaned and inspected or where it is determined that large movements of the shaft would be required to mobilize resistance in end bearing." According to Crapps and Schmertmann (2002), the most common reasons cited by designers for neglecting base resistance include settled slurry suspension, reluctance to inspect bottom, concern for underlying cavities, and unknown or uncertain base resistance.

Obviously, neglecting the base resistance in design will result in larger rock-socket lengths. Due to the high cost of shaft construction in rock, an over-design will lead to a great waste of money. For example, according to a North Carolina Department of Transportation construction estimate, the cost of shaft construction in rock is on the order of $1,500 per meter length for a shaft of 1.5 m in diameter; $1.5

million would be wasted for every 1,000 shafts if the socket length were unnecessarily over-designed by 1 m (Cho et al. 2001). Crapps and Schmertmann (2002) suggest that accounting for base resistance in design and using appropriate construction and inspection techniques to ensure quality base conditions is a better approach than neglecting base resistance.

In this paper, the axial load transfer behavior of rock-socketed shafts is investigated based on a database of 99 field test rock-socketed shafts. The database is developed by collecting information on field test rock-socketed shafts from published papers and reports. Using the database, the effect of the shaft length in soil, the rock-socket length, the shaft head displacement and the loading time on the load transfer behavior is investigated. The results show that it is important to consider the end bearing resistance in the design because (1) a large percentage of the shaft head load can be transmitted to and supported by the shaft base even at shaft head displacement that is much smaller than the tolerable displacement of the super structure, and (2) the portion of the shaft head load transmitted to and supported by the shaft base increases with time.

DATABASE OF FIELD TEST ROCK-SOCKETED SHAFTS

The database consists of 99 field test rock-socketed shafts collected from published papers and reports. Information for each test rock-socketed shaft is collected as comprehensively as possible. The parameters considered are defined in Fig. 1. The total shaft lengths (L) range from 1.4 to 96.3 m, the shaft lengths in soil (L_s) from 0.0 to 94.8 m, the socket lengths (L_r) from 0.0 to 18.8 m, and the shaft diameters (B) from 0.5 to 1.5 m, resulting in ratios of L/B from 1.9 to 96.3, L_s/B from 0.0 to 94.8, and L_r/B from 0.0 to 17.7.

In addition to shaft dimensions, the information on the maximum test load Q_t, the shaft head and base displacements s_t and s_b at Q_t, and the total and base resistance of the rock-socket, Q_{rb} and Q_b, corresponding to Q_t is also collected. The total resistance of the rock-socket Q_{rb} is simply the sum of the side shear resistance Q_r and the base resistance Q_b (see Fig. 1). It need be noted that Q_t recorded is the maximum test load which may be much smaller than the ultimate load capacity for some of the test rock-socketed shafts. Four shafts (#96, 97, 98 and 99) were not conventional test shafts but were instrumented construction shafts to measure the time effect on load transfer.

AXIAL LOAD TRANSFER BEHAVIOR OF ROCK-SOCKETED SHAFTS

Based on the developed database, the axial load transfer behavior of rock-socketed shafts is analyzed in the following.

Q_{rb}/Q_t versus L_s/B

Fig. 2 shows the variation of Q_{rb}/Q_t with L_s/B based on the test data in Table 1. As expected, as the shaft length in soil (L_s) increases, the percentage of the total load supported by the rock-socket Q_{rb}/Q_t decreases. It is noted that even when the overburden soil is thick, say $L_s/B > 30$, it is still possible to have more than 40% of the total load transmitted to and supported by the rock-socket, meaning that rock-sockets are still useful even if the overburden soil is thick.

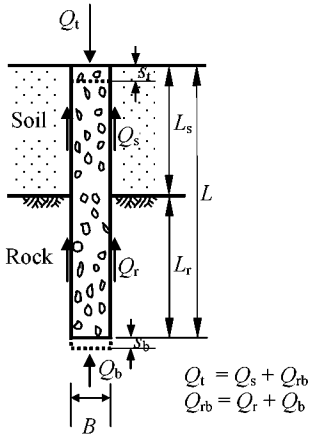

FIG. 1. Parameters considered for a test rock-socketed shaft.

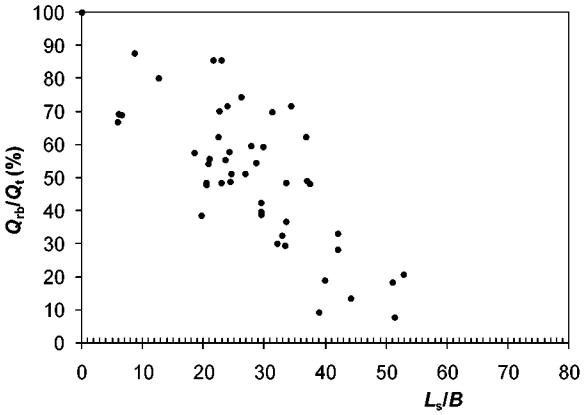

FIG. 2. Variation of Q_{rb}/Q_t with L_s/B.

Q_b/Q_{rb} versus L_r/B

Fig. 3 shows the variation of Q_b/Q_{rb} with L_r/B. As the rock-socket length (L_r) increases, the percentage of the total rock-socket load transmitted to and supported by the socket base Q_b/Q_{rb} decreases. Also shown in the figure are the Q_b/Q_{rb} versus L_r/B curves based on the finite-element elastic analysis by Rowe and Armitage (1987). It can be seen that the elastic results lie in the lower part of the zone defined by the test data and the Q_b/Q_{rb} versus L_r/B curve corresponding to $E_p/E_r = 1$, and $E_b/E_r = 0.5$ can be considered the lower bound of the test Q_b/Q_{rb} versus L_r/B data points, where E_p, E_r and E_b are the elastic modulus, respectively, of the socket, the rock surrounding the socket and the rock below the socket. $E_b/E_r = 0.5$ can be considered for the case that the soft debris is left at the shaft base. This is as expected because, as described in the previous section, the test data correspond to the maximum test load Q_t and at Q_t some

yielding of the socket-rock interface should have taken place for most of the test shafts. As the yielding of the socket-rock interface occurs, a higher percentage of the socket head load will be transmitted to and supported by the socket base.

When the socket-rock interface completely yields, the increased socket head load will be fully supported by the socket base and the corresponding Q_b/Q_{rb} will increase with Q_{rb} until the end bearing capacity is reached. The maximum Q_b/Q_{rb} will be reached when both the ultimate side shear resistance τ_{max} and the end bearing resistance q_{max} are reached. Using the expressions of Kulhawy and Phoon (1993) for τ_{max}:

Lower bound (LB): $$\tau_{max} = 0.225\sigma_c^{0.5} \quad \text{(MPa)} \tag{1a}$$

Upper bound (UB): $$\tau_{max} = 0.675\sigma_c^{0.5} \quad \text{(MPa)} \tag{1b}$$

and the expressions of Zhang and Einstein (1998) for q_{max}:

Lower bound (LB): $$q_{max} = 3.0\sigma_c^{0.5} \quad \text{(MPa)} \tag{2a}$$

Upper bound (UB): $$q_{max} = 6.6\sigma_c^{0.5} \quad \text{(MPa)} \tag{2b}$$

the upper bound Q_b/Q_{rb} curve can be obtained by

$$(Q_b / Q_{rb})_{UB} = \frac{(q_{max})_{UB}(0.25\pi B^2)}{(q_{max})_{UB}(0.25\pi B^2) + (\tau_{max})_{LB}(\pi L_r B)} = \frac{1.65}{1.65 + 0.225(L_r / B)} \tag{3}$$

where σ_c is the unconfined compressive strength of the intact rock, in MPa.

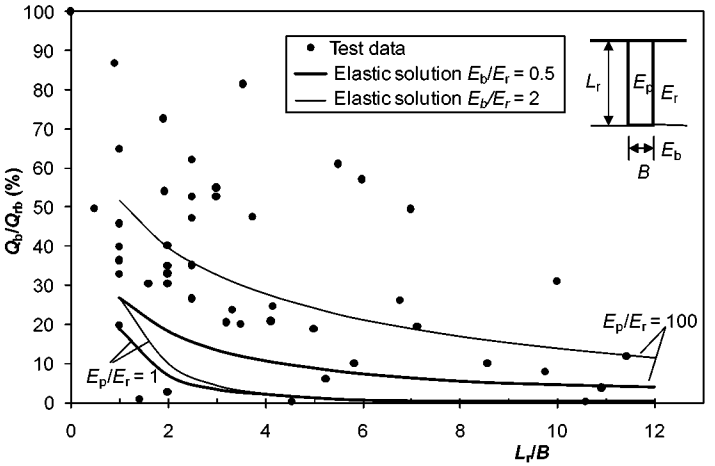

FIG. 3. Variation of Q_b/Q_{rb} with L_r/B – test data and elastic solutions of Rowe and Armitage (1987).

Fig. 4 shows the upper bound Q_b/Q_{rb} curve based on equation (3) and the lower bound Q_b/Q_{rb} curve based on the elastic solution of Rowe and Armitage (1987) at $E_p/E_r = 1$ and $E_b/E_r = 0.5$. It can be seen that most of the test data points are within the band formed by these two bounding curves.

Q_b/Q_{rb} versus s_t

Fig. 5 shows the variation of Q_b/Q_{rb} with the shaft head displacement s_t. Although the test data are widely scattered, the general trend clearly shows that Q_b/Q_{rb} increases with larger s_t. Even at relatively small shaft head displacement, say, in the typical working range of 5–15 mm (Crapps and Schmertmann 2002), a large portion of the total rock-socket load (about 30% on average) is transmitted to and supported by the socket base.

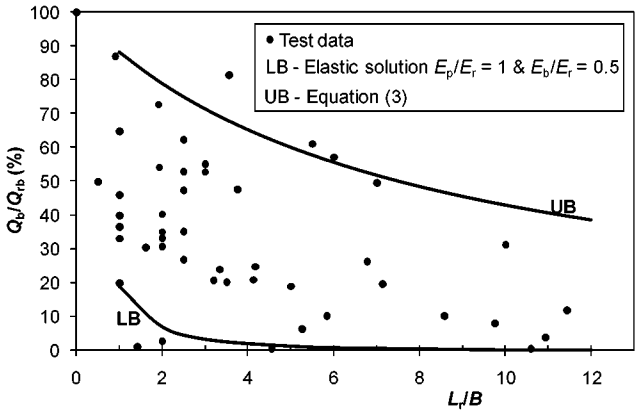

FIG. 4. Variation of Q_b/Q_{rb} with L_r/B – test data and lower and upper bounding curves.

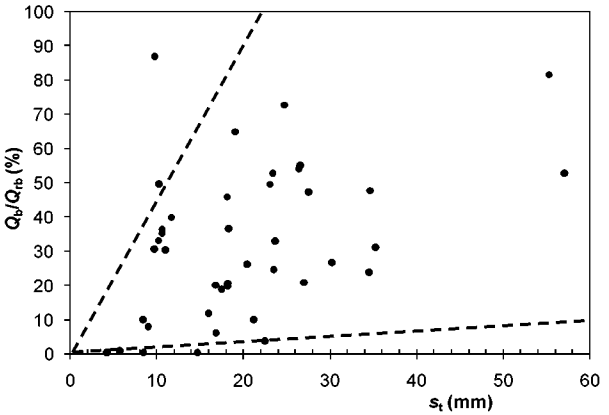

FIG. 5. Variation of Q_b/Q_{rb} with shaft head displacement s_t.

Q_b/Q_t versus s_t

Fig. 6 shows the variation of Q_b/Q_t with the shaft head displacement s_t. The general trend clearly shows that Q_b/Q_t increases with larger s_t. At shaft head displacement in the working range of 5–15 mm, about 25% on average of the total shaft load is transmitted to and supported by the rock-socket base.

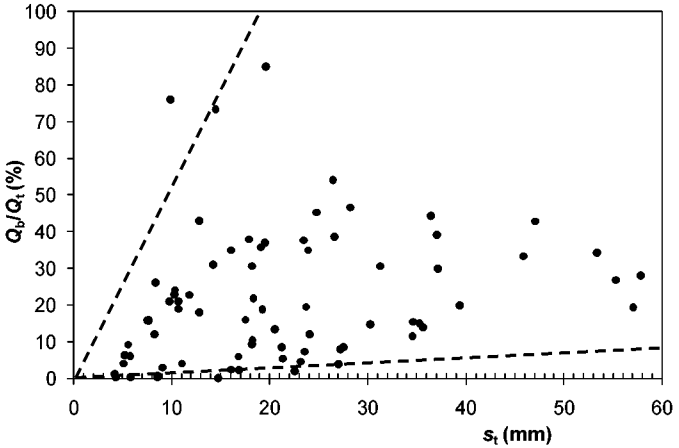

FIG. 6. Variation of Q_b/Q_t with shaft head displacement s_t.

TIME EFFECT ON AXIAL LOAD TRANSFER OF ROCK-SOCKETED SHAFTS

Time effect on axial load transfer of rock-socketed shafts has been studied by several investigators. Tang (1995) used four instrumented in-service rock-socketed shafts in karstic limestone to monitor the relative contribution of side shear resistance and end bearing resistance and their variation throughout the construction and service life of the structure. Fig. 7 shows the variation of Q_{rb}/Q_t with time after the completion of the concrete frame construction for three of them (the fourth shaft was not monitored because its instruments were seriously damaged). The percentage of the total load transmitted to and supported by the rock-socket increased significantly with time, from 92% to 100%, 45% to 80% and 52% to 80% in 300 days, respectively, for shafts 96, 97 and 98.

Not only is the load supported by the side shear resistance in the overlying soil transmitted to the rock-socket, the load supported by the side shear resistance of the rock-socket is also transmitted to the socket base. Ladanyi (1977) reported a case in which the end bearing pressure of an instrumented rock socket increased over a period of four years; although the total applied shaft head load remained essentially constant (see Fig. 8).

Horvath and Chae (1989) conducted long-term tests on model rock-socketed shafts and found that the average increase in base load with time (200 days) was about 10% of the applied loading.

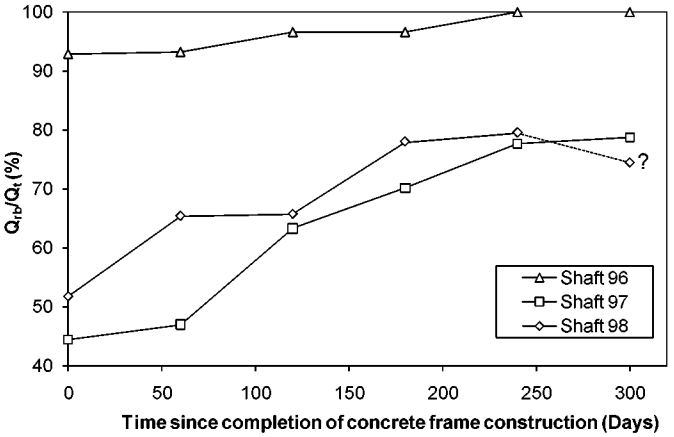

FIG. 7. Increase of rock-socket resistance with time (data from Tang 1995).

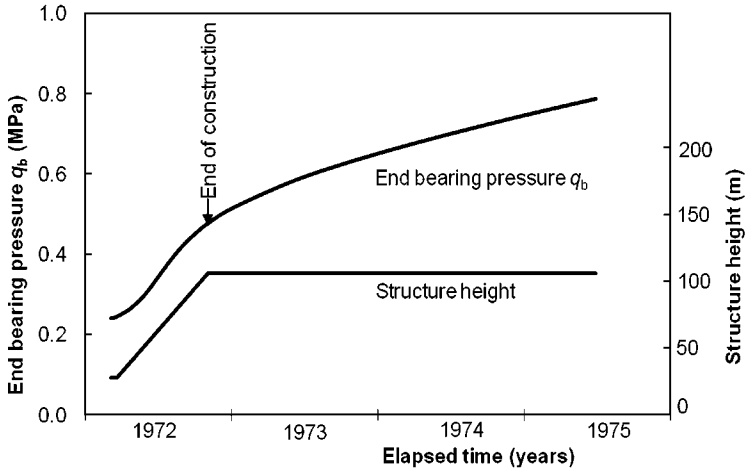

FIG. 8. End bearing resistance increase with time (data from Ladanyi 1977).

SUMMARY AND CONCLUSIONS

This paper has investigated the axial load transfer behavior of rock-socketed shafts using a newly developed database consisting of 99 field tests. The contents and conclusions can be summarized as follows:

1. The portion of the total shaft head load transmitted to and supported by the rock-socket decreases as the shaft length in the soil increases. Even when the overburden soil is thick (say $L_s/B > 30$), however, it is still possible to have more

than 40% of the shaft head load transmitted to and supported by the rock-socket, meaning that rock-sockets are still useful even if the overburden soil is thick.

2. The percentage of the rock-socket load transmitted to and supported by the rock-socket base decreases as the socket length increases. The possible percentage value is within the range between the upper bound Q_b/Q_{rb} curve based on equation (3) and the lower bound Q_b/Q_{rb} curve based on the elastic solution at $E_p/E_r = 1$ and $E_b/E_r = 0.5$.
3. It is important to consider the end bearing resistance when designing rock-socketed shafts because (1) even at shaft head displacement in the working range of 5–15 mm, a large portion of the total shaft head load is transmitted to and supported by the rock-socket base, and (2) the percentage of the total shaft head load transmitted to and supported by the rock-socket base increases with time.

REFERENCES

AASHTO (2006). *Interim Standard Specifications for Highway Bridges.* American Association of State Highway and Transportation Officials, Washington DC.

Cho, K.H., Clark, S.C., Keaney, B.D., Gabr, M.A., and Borden, R.H. (2001). "Laterally loaded drilled shafts embedded in soft rock." *Transportation Research Record* 1772: 3-11.

Crapps, D.K., and Schmertmann, J.H. (2002). "Compression top load reaching shaft bottom – Theory versus tests." *Proc. of International Deep Foundations Congress*, Vol. 2, Orlando, Fla.: 1533-1549.

Horvath, R.G., and Chae, K.-J. (1989). "Long-term settlement of model rock-socketed piers." *Can. Geotech. J.* 26: 348-358.

Kulhawy, F.H., and Phoon, K.K. (1993). "Drilled shaft side resistance in clay soil to rock." *Proc. of Conference on Design and Performance of Deep Found: Piles and Piers in Soil and Soft Rock.* Geotechnical Special Publication No. 38: 172-183.

Ladanyi, B. (1995). "Friction and end bearing tests on bedrock for high capacity socket design: Discussion." *Can. Geotech. J.* 14: 153-155.

Rowe, R.K., and Armitage, H.H. (1987). "Theoretical solutions for the axial deformation of drilled shafts in rock." *Can. Geotech. J.* 24: 114-125.

Tang, Q. (1995). Load transfer mechanisms of drilled shaft foundations in karstic limestone – Behavior under working load. PhD Dissertation, The University of Tennessee, Knoxville.

Turner, J. (2006). *Rock-socketed shafts for highway structure foundations.* A Synthesis of Highway Practice, NCHRP Synthesis 360.

Zhang, L. (2004). *Drilled shafts in rock – Analysis and design.* A. A. Balkema, London, UK.

Zhang, L., and Einstein, H.H. (1998). "End bearing capacity of drilled shafts in rock." *J. Geotech. and Geoenvir. Engrg.* 124(7): 574-584.

Copyrighted Materials
Copyright © 2009 American Society of Civil Engineers (ASCE)
Retrieved from www.knovel.com

Drilled Shaft Foundations for James River Crossing in Richmond Virginia

Jan J. Hartman [1], P.E. and Raymond J. Castelli [2], P.E.

[1] Senior Professional Associate, Supervising Geotechnical Engineer; PB, One Penn Plaza, New York, NY 10119, e-mail: hartmanj@pbworld.com.

[2] Senior Vice President, Principal Geotechnical Engineer, PB, One Penn Plaza, New York, NY 10119, e-mail: castelli@pbworld.com.

ABSTRACT: The Route 895 Connector project provides an informative case history documenting the testing and construction of long, large diameter drilled shaft sockets in very hard rock. The Route 895 bridge over the James River south of Richmond, Virginia has a total length of 1,452.4 m (4,765 ft) and consists of twin segmental concrete bridges with a clear span of 204.8 m (672 ft) at the river crossing. At each of the two main span piers, the twin structures are founded on a single combined footing supported by twenty 2.44 m (96 inch) diameter drilled shafts. These drilled shafts have individual static design load capacities ranging from 40.0 to 47.6 MN (9,000 to 10,700 kips), and are socketed up to 11.9 m (39 ft) into variable quality granite with unconfined compressive strength up to 82.7 MPa (12 ksi).

The paper discusses load tests conducted at four test shafts. For each main river pier these included two Osterberg axial load cell (O-cell) tests conducted on sacrificial test shafts socketed into rock. The sacrificial test shafts had a reduced 1.37 m (54-inch) diameter rock socket - about 56 percent of the diameter of the permanent drilled shafts.

Based on a maximum top-of-shaft settlement criterion of 25.4 mm (1 inch), the allowable unit end bearing capacity for the rock sockets was determined from the load tests to be 8.4 MPa (175 ksf). Allowable side friction values in the rock sockets were determined to be 144 kPa (3.0 ksf) for poor quality rock and 431 kPa (9.0 ksf) for moderate to good quality rock.

INTRODUCTION

A series of drilled shaft load tests were conducted for the Route 895 Connector project in Richmond, Virginia. For the piers supporting the main James River span, a total of four 1.37 m (54 inch) diameter sacrificial (throw-away) test shafts were load tested, with two tests at each of the two main James River span pier foundations. The results of the load tests were then used to estimate the allowable unit side friction resistance and allowable unit end bearing resistance for the larger 2.44 m (96 inch) diameter permanent drilled shaft foundations. The load test results, coupled with a

geotechnical test boring at each production shaft location, were used to adjust original design estimates of the minimum tip penetrations for construction of the permanent shafts.

The location of the Route 895 Connector project is shown in Figure 1.

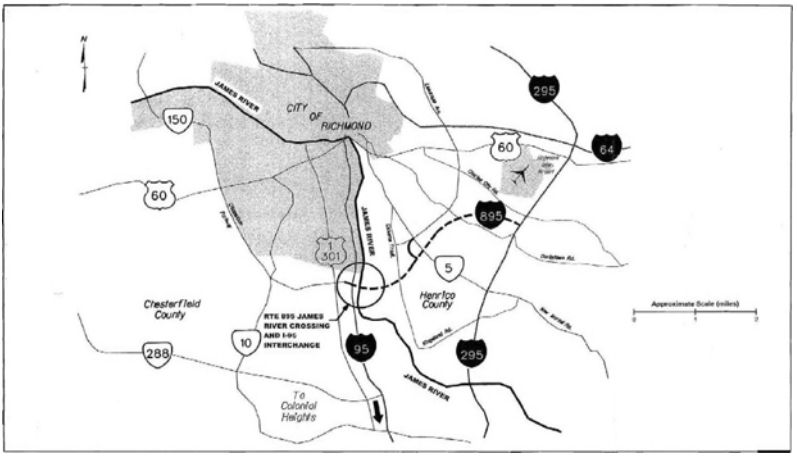

Figure 1. Route 895 Connector Project Location Map

DRILLED SHAFT CONSTRUCTION PROGRAM

Overall, a total of 20 permanent drilled shafts were constructed to support the combined footing for the two west main piers of the twin bridges. An equal number of permanent drilled shafts were constructed to support a similar combined footing for the two east main piers of the bridges. Each of the four test shafts constructed for the main piers were cut off below final grade and abandoned in place. Table 1 summarizes the diameters, socket lengths, and tip elevations for the test shafts. Elevations referred to in this paper are referenced to the 1929 National Geodetic Vertical Datum (NGVD 29).

Table 1 - Summary of Test Shafts in Rock at Main Piers

		Diameter	Rock Socket		Tip	Total
Pier No.	Shaft No.	in Soil	Diameter	Length	Elevation	Length
West Main Piers	TS-1	1.52 m (60 inches)	1.37 m (54 inches)	5.4 m (17.6 ft)	-17.2 m (-56.1 ft)	18.5 m (60.6 ft)
	TS-2	1.52 m (60 inches)	1.37 m (54 inches)	8.1 m (26.6 ft)	-20.5 m (- 67.2 ft)	20.5 m (67.4 ft)
East Main Piers	TS-3	1.52 m (60 inches)	1.37 m (54 inches)	6.5 m (21.3 ft)	-24.0 m (-78.6 ft)	27.2 m (89.2 ft)
	TS-4	1.52 m (60 inches)	1.37 m (54 inches)	11.2 m (36.6 ft)	-23.6 m (-77.3 ft)	26.8 m (87.9 ft)

GEOLOGY AND SUBSURFACE CONDITIONS

On the west side of the James River, river meandering has produced relatively low ground surface levels, ranging from El. +9.1 m (+30 ft) at the western limit of the project to about El. +3.0 m (+10 ft) at the west bank of the river. The mudline in the river dips to approximately El. -10.1 m (–33 ft) in the main channel. In these areas of low ground surface levels, the depth to rock is relatively shallow. The rock profile in the river and to the west consists of a relatively thick mantle of completely weathered to moderately weathered rock over sound granitic bedrock alternating with zones of pegmatite and amphibolite. The overlying soils in these areas are only moderately dense and sometimes soft and compressible, consisting primarily of geologically recent river alluvium.

In contrast, the river's east bank rises steeply above the river forming a bluff reaching approximately El. +20.1 m (+66 ft), or about 10.1 m (33 ft) higher than most bank locations on the west side of the river. The quality of the bedrock on both sides of the river is similar. However, due to the higher ground level and the eastward dipping rock surface, the depth to rock on the east side is greater. Top of bedrock varied considerably from point to point, but ranged from about El. -12 m (-40 ft) on the west to about El. -15 m (–50 ft) on the east.

TEST SHAFT CONSTRUCTION METHODS

For each test shaft at the main pier foundations, construction began with installation of a 1.52 m (60-inch) O.D. steel casing to refusal using a vibratory hammer. Following driving, the casing was excavated by auger or drilling bucket to remove soils inside the casing. After excavating to the bottom of the casing, water was added to the casing to form a natural drilling slurry, and shaft excavation continued to the final shaft tip elevation with rock drilling tools.

The rock sockets were excavated using a full-face reverse-circulation rock cutter head fitted with replaceable 203 mm (8 inch) diameter carbide button-bit rollers. The 1.37 m (54 inch) diameter cutter head used for test shaft rock socket excavation at the main piers utilized 10 rollers. The 2.29 m (90 inch) diameter rock cutter head used for the permanent drilled shaft rock socket excavations used 15 rollers. Figure 2 provides a view of the rock cutter head used for the permanent drilled shaft foundations.

During rock socket drilling operations, the cutter head was ballasted by a stack of solid lead ring castings, providing a combined gross weight of approximately 267 kN (60 kips) to assist in pressing the cutter downward while the cutter head was simultaneously turned by the contractor's drill crane. The contractor used a Soilmec R622 hydraulic drill crane for excavation of the test shafts at the main piers. Figure 3 provides a view of the Soilmec drill crane working at the east main piers.

The contractor's rock socket drilling system included 305 mm (12-inch) OD drill rods providing an interior conduit for upward fluid flow during drilling. Air compressor units forced compressed air through a circumferential array of separate smaller openings in the drill rods down to the cutter head for discharge at the bottom of the shaft creating an air-lift effect. The air-lift drew the drilling fluid and drill cuttings upward through the center of the cutter head and the hollow center of the drill rods to the drill crane's swivel connector at the top of the drill rod assembly above ground. Drilling fluids and cuttings were then routed through flexible hoses

for discharge into nearby slurry sedimentation tanks. The cuttings consisted of gravel, sand, and silt-sized particles of crushed rock.

Figure 2. 2.29 m (90 inch) Diameter Rock Cutter Head for Rock Socket Drilling

Figure 3. Soilmec R622 Hydraulic Drill Crane Working at East Main Piers.

After reaching the final shaft bottom level, the rock cutter head was removed from the shaft excavation, and a separate air-lift pipe was lowered into the shaft and suspended from a crane cable for final shaft bottom cleaning.

As soon as practical after bottom cleaning, a high slump concrete or grout leveling pad was tremied to the bottom of the shaft, followed as soon as practical by lowering a steel reinforcing bar cage into the shaft, followed by placement of the drilled shaft concrete. The leveling pad consisted of approximately 0.75 cubic meters (1 cubic

yard) of high-slump material placed into the bottom of the shaft to assist in providing a firm, uniform bearing for the lower plate of the Osterberg cell (O-Cell). The required instrumentation for the test shafts was fastened to the reinforcing cage, and the load test O-Cell was welded to the bottom of the cage.

LOAD TESTS

The O-Cells had a diameter of 864 mm (34 inches) and a maximum expansion force capacity of 26.7 MN (6,000 kips). The loads applied by an O-Cell act in two opposing directions. Upward displacement of the expanding O-Cell, as well as resulting upward displacement of the overlying portion of the test shaft, is resisted by buoyant weight of the shaft and shear along the side of the shaft above the O-Cell. Downward displacement of the O-Cell as it expands is resisted by the combined end bearing and side shear against the portion of the test shaft underlying the O-Cell. For the Route 895 project, the load tests utilized only a single O-Cell at a single level, set about 0.9 m (3 ft) above of the bottom of shaft. For this arrangement, the magnitude of side shear below the O-Cell was relatively small, requiring only a minor adjustment to the test results to determine the end bearing resistance.

Instrumentation

Typical O-Cell load testing instrumentation for the Route 895 drilled shafts included three or more linear vibrating wire displacement transducers, or LVWDTs, positioned between the lower and upper plates of the O-Cell, arranged around their circumference to measure total expansion of the O-Cell. Compression of the upper portion of the drilled shaft between the top of the O-Cell and the ground was measured by two to three separate sheathed stainless steel telltale rods. One or more additional digital dial gages fixed to a rigidly supported independent reference beam monitored displacement of the top of the shaft reinforcing cage or the shaft casing to determine the absolute upward displacement of the top the shaft relative to the ground and project datum. To determine variation of unit side friction along the embedded length of the shaft, multiple levels of three "sister bar" vibrating wire strain gages were installed on the reinforcing bar cage above the O-Cell.

Loading Procedure

The O-Cell was pressurized and expanded in increments, with each load increment maintained for approximately 5 minutes. In each test, the O-Cell was pressurized in approximately 17 to 26 loading increments until either the upward or downward resistance to O-Cell expansion began to yield, or leakage of the pressurizing water from the O-Cell prevented further increase in load. After holding the maximum test load for approximately 10 minutes, the O-Cell was then unloaded, typically in five decrements. Generally, the O-Cell was then reloaded in 5 to 11 increments back to the maximum test load, or the yield point, in an effort to obtain more data on the end bearing and side shear resistance. The O-Cell was then unloaded again in five decrements, and the tests were concluded after obtaining final displacement readings after a period of about 10 minutes of relaxation under zero load.

LOAD TEST RESULTS

Initial project plans called for one drilled shaft load test at the west main piers and one at the east main piers. However, based on the results of the planned load tests,

the contractor elected to construct a second test shaft at both of the main piers using revised procedures to improve shaft capacity and demonstrate that reduced rock socket lengths could be used for permanent shafts.

Test Shaft No. TS-1

The average ultimate measured side friction resistance for Test Shaft No. TS-1 at the west main piers was 766 kPa (16 ksf) at an upward displacement of approximately 76 mm (3 inches). Measured end bearing resistance was about 9.6 MPa (200 ksf) at a displacement of approximately 25 mm (1.0 inch). The test was terminated when no additional side friction resistance could be mobilized, which occurred before ultimate base resistance could be reached.

Test Shaft No. TS-2

With a considerably longer rock socket, load testing for Test Shaft No. TS-2 at the west main piers was carried out to a maximum net load of almost twice the maximum net test load that had been achieved for Test Shaft No. TS-1. Maximum displacements at the end of the initial loading cycle for Test Shaft No. TS-2 were 40 mm (1.6 inches) upwards, and 18 mm (0.70 inches) downward. Measurements of net load versus upward and downward movement of the O-Cell for Test Shaft TS-2 are illustrated in Figure 4.

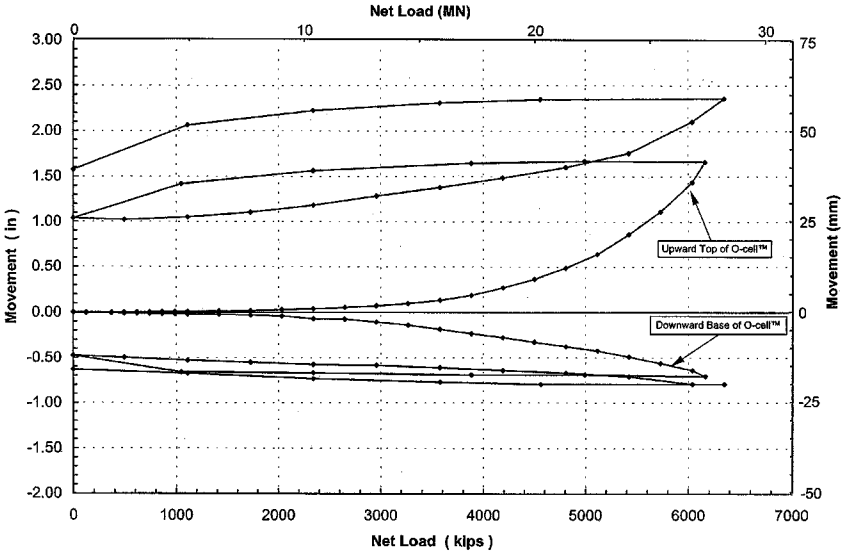

Figure 4. Load Test Measurements for Test Shaft TS-2

Average ultimate unit side friction above El. -17.1 m (–56 ft) was approximately 263 kPa (5.5 ksf) at an upward displacement of 12 mm (0.5 inches). At that same upward displacement, strain gage data showed that below El. -17.1 m (–56 ft), ultimate unit side friction was much greater, averaging approximately 1200 kPa (25 ksf). In analyzing the load test data from Test Shaft No. TS-2, ultimate upward resistance was defined as the condition where upward O-Cell displacement reached

13 mm (0.5 inches). Analysis of the geotechnical test boring's conducted at that test shaft location showed that the quality of rock above El. -17.1 m (–56 ft) was generally very poor to poor (RQD less than 50 percent). Below El. -17.1 m (–56 ft), the rock was generally moderately good to good. Based upon these results, allowable unit side friction values of 3.0 ksf for very poor to poor rock (RQD less than 50 percent) and 9.0 ksf for moderately good to good rock (RQD greater than 50 percent) were established for application to construction of the larger permanent drilled shafts at the west main piers.

The TS-2 test data indicate that the ultimate end bearing capacity of this test shaft was not reached. After adjustment for side friction between the bottom of the O-Cell and the bottom of the test shaft excavation, an end bearing resistance of 17.7 MPa (370 ksf) was calculated for the maximum test load. Based on the Test Shaft TS-2 results, an allowable end bearing resistance of 8.9 MPa (185 ksf) was established. This allowable end bearing value corresponds to a base settlement during initial loading of approximately 2 mm (0.1 inches) at Test Shaft No. TS-2. Considering scale effects for the larger permanent drilled shafts at the west main piers, with 2.29 m (7.5 ft) diameter rock sockets, this allowable end bearing resistance was judged to be equivalent to an allowable end bearing pressure of approximately 8.6 MPa (180 ksf) and a corresponding base settlement estimated to be less than 5 mm (0.2 inches).

Based on the results of the second load test, the minimum required rock socket length for the remaining permanent west main pier drilled shafts was reduced to the minimum 3.67 m (12 ft) value that had been determined during design based on lateral load considerations. This minimum socket length criterion, however, was conditioned upon the dual objectives of obtaining at least 1.22 m (4 ft) of shaft in moderate to good quality rock, and founding the base of the socket on moderate to good quality rock. These recommendations were based upon limiting displacements at the top of the drilled shaft foundations to approximately 25 mm (1.0 inch) under maximum design loads.

Test Shaft No. TS-3

The load test of east main piers Test Shaft No. TS-3 was aborted at an O-Cell load (upward and downward) of only about 3.1 MN (700 kips) when leakage of the pressured O-Cell water prevented further increase in the applied O-Cell load. Based on the LVWDT data and the observed seepage of water from one of the tell-tale pipes, it was concluded that excessive differential expansion of the O-Cell caused by non-uniform bearing resistance at the base of the O-Cell bottom plate led to a rupture of the O-Cell seal. The non-uniform support at the base of the O-Cell was believed to be related to shaft bottom cleaning procedures that were improved for the final test shaft and for production shafts.

Test Shaft No. TS-4

Load testing of east main piers Test Shaft No. TS-4 was carried out to a maximum O-Cell load of approximately 14.2 MN (3200 kips) (upwards and downwards), or about one-half the specified maximum test load. Testing halted prematurely when differential downward displacement (tilting) of the O-Cell bottom plate again caused internal pressure seals of that O-Cell to fail, rapidly depressurizing the O-Cell, and terminating the test. However, sufficient usable information was obtained from the

test before depressurization to develop construction recommendations for the permanent drilled shaft foundations at the east main piers. From these data it was concluded that the allowable unit friction resistance values previously recommended for the west main pier drilled shaft foundations were also applicable to the east main pier foundations.

These recommendations were conditioned upon requirements for thorough cleaning of the bottom of each permanent drilled shaft, and upon maintaining the cleanliness of the bottom of each drilled shaft prior to placement of concrete to avoid non-uniform bearing resistance under the drilled shafts that is believed to be the cause of the differential O-Cell expansion difficulties for the east main pier test shafts.

CONCLUSIONS

Recommended tip elevations and construction procedures for each permanent drilled shaft foundation of the Route 895 bridge were based on the results of the two drilled shaft load tests conducted at each main pier footing, and on the specific quality of rock cores from geotechnical test borings performed at each permanent production shaft location. For some shafts, the recommended tip elevation was governed by providing the minimum rock socket lengths necessary for lateral load resistance. At most of the shafts, however, tip elevations and rock socket lengths were governed by allowable unit side friction and allowable end bearing pressures determined from the load tests, which were established based on the criterion of limiting shaft top compression displacements of the drilled shafts under maximum loading conditions to no more than 25 mm (1.0 inch).

Separate allowable unit side friction values were determined for the portions of rock sockets constructed in poor quality rock versus moderately good to good rock. The rock was categorized primarily based upon the condition of rock cores obtained from the geotechnical test borings drilled at each drilled shaft foundation location. Rock cores with a rock quality designation (RQD) less than 50 percent were generally categorized as poor quality rock. Rock cores with an RQD greater than 50 percent were generally categorized as moderately good to good rock. Importantly, these recommendations were conditioned upon requirements to thoroughly clean the bottom of each drilled shaft foundation.

ACKNOWLEDGMENTS

Drilled shaft load tests were performed by LoadTest, Inc. of Gainesville, Florida. Inspection of drilled shaft construction, plus inspection and logging of design-phase and construction-phase geotechnical test borings was provided by Site-Blauvelt Engineers, Inc. of Richmond, Virginia. The authors wish to acknowledge the Virginia Department of Transportation for its successful management of the project throughout its planning, design, and construction phases, and both design-build general contractor FD/MK, LLC and drilled shaft subcontractor Trevi-Icos of Boston, Massachusetts for the drilled shaft construction.

Copyrighted Materials
Copyright © 2009 American Society of Civil Engineers (ASCE)
Retrieved from www.knovel.com

Effective Use of Steel Piles for a Large Transportation Project in Central Florida

Mohamad H. Hussein[1], P.E., M. ASCE, Loreen Choate[2], P.E., M.ASCE, Robert Mangogna[3], and Kathy Gray[4], P.E.

[1]Vice President, GRL Engineers, Inc., Orlando, Florida; MHGRL@pile.com
[2]Construction Project Manager, FDOT, Orlando, Florida; Loreen.Choate@dot.state.fl.us
[3]Project Administrator, HNTB, Inc., Orlando, Florida; RMangogna@HNTB.com
[4]District 5 Geotechnical Engineer, FDOT, Deland, Florida; Kathy.Gray@dot.state.fl.us

ABSTRACT: A major transportation improvement project in the heart of downtown Orlando, Florida involved twelve structures at the busy junction of Interstate 4 and the East-West Expressway. The deep foundations consisted of 60,000 meters of driven piles, with a distinguishing feature being the extensive use of steel H-piles on such a large scale transportation project in Florida. This paper describes the inherent advantages of steel pile that were used to ensure the success of the foundation work. Special features characteristic of driven steel piles include the ability to bring production pile sections of various lengths to the site prior to driving test piles, ease of transportation and handling, quick welding and cutoff procedures, low ground vibration, partial installation by vibro-hammers, rapid installation for efficient production, compatibility for low-headroom constraints, and drivability characteristics. The paper presents data and discussions on interesting findings from the dynamic pile testing performed, including the demonstration of high load bearing capacity, subsurface variability and soil setup effects, timeliness of field testing and turnaround for production purposes, procedures to expedite construction, and a comparison between the drivability of an H-pile and a prestressed concrete pile in high rebound soil conditions.

INTRODUCTION

The junction of Interstate 4 (I-4) and the East-West Expressway (SR 408) in the heart of downtown Orlando is the most heavily traveled interchange in Central Florida. Through establishment of a joint partnership between the Florida Department of Transportation and the Orlando Orange County Expressway Authority, a $120 million, 900-day, construction project was undertaken to enhance the safety and flow of the increasingly demanding traffic volume that is an inevitable by-product of the area's rapid population growth. The extensive improvements involved twelve structures including the widening of existing, and construction of new bridges, flyover ramps, viaducts and overpasses. Figure 1 shows a general overview of the project and its location in the congested urban setting of downtown Orlando. All

construction was done while maintaining the current number of traffic lanes and capacity during the day on both highways. The twelve structures were supported on a total of 138 foundation units (i.e., bents or piers) consisting of pile groups ranging between 3 and 56 piles per unit. Figure 2 shows a typical driving setup for a large group of bridge pier foundation piles.

Figure 1: General project overview.

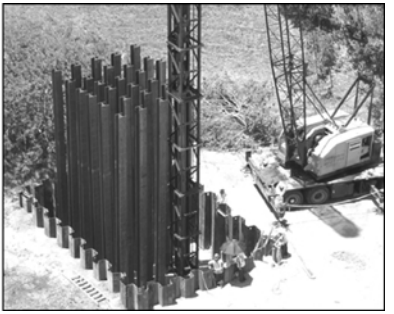

Figure 2: Pile driving at a bridge pier.

Local geologic and geotechnical conditions, structural loading requirements, project and site-specific constraints dictated the use of deep foundations for support of all the structures. A total of 60,000 meters of driven piles were employed, almost all of which were steel piles with minor use of prestressed concrete piles. A distinguishing feature of this project is the extensive use of steel H-piles for a large transportation project in Central Florida. Two steel H-pile sizes were used: HP 12x53 and HP14x89. The inherent advantages of steel piles were utilized to the benefit of the project. This paper describes the engineering, construction and testing practices used that resulted in the effective installation of the driven steel piles, which ensured the success of the foundation work. It also includes data and discussions on interesting findings from the dynamic testing results. Aspects such as high load bearing capacity, soil setup, subsurface variability, timeliness of field testing and related data analysis turnaround for production, effective use of testing to expedite construction, and a comparison between the drivability of an H-pile and a prestressed concrete pile in high rebound soil conditions are demonstrated by examples.

PILING WORK PRACTICES IN FLORIDA

Piling work for transportation projects in Florida typically follows the FDOT Standard Specifications for Road and Bridge Construction (Florida Department of Transportation, 2007). The process in general includes three phases: preliminary evaluation, field testing and data analysis; and recommendations for production pile driving. Initially, information provided by the contractor in the Pile Installation Plan, along with specific project requirements, are used for a preliminary assessment of general adequacy of proposed equipment and methods to install the piles within specifications. This evaluation phase includes Wave Equation Analysis for assessment of the general suitability of the proposed hammer for pile drivability based on the site geotechnical conditions and project structural requirements.

Pile driving activities typically commence with the installation and dynamic testing of a number of test piles at designated production pile locations. Dynamic pile testing is based on the measurement of pile force and velocity records under hammer impacts during initial pile driving and/or restrike. Utilizing Pile Driving Analyzer® (PDA) field equipment, testing results available in-real time on site include information for the assessment of hammer system performance, pile driving stresses and structural integrity, soil/rock resistance and pile static load bearing capacity (Hussein and Likins, 1995). Testing during restrike some time after initial installation is performed to evaluate the time-dependent changes in pile load bearing capacity. Following the field test, representative PDA data is further analyzed with the CAPWAP™ computer program to obtain soil parameters including resistance distribution, damping, and quake for shaft resistance and end bearing. The analysis results also include a simulated static load test relating pile top and tip load-movement relationships.

Results of the dynamic pile testing and related data analyses, including refined Wave Equation Analyses, along with information recorded by the pile driving inspector's installation log, as well as specifics related to the geotechnical conditions in the relevant boring(s), required minimum pile tip elevation, pile top cutoff elevation and other available data are used to issue engineering recommendations regarding production pile lengths and driving criteria. This is done as a cooperative effort between the dynamic pile testing consultant and the project geotechnical design engineer, with input from the FDOT geotechnical engineer. The contractor proceeds by ordering the production piles. For concrete piles, the casting and delivery to the site requires at least one week before production pile driving can start. In the case of steel piles, the contractor typically has the production piles delivered to site in sections of various lengths during, or even before, the Test Pile driving program.

A total of 105 Test Piles and an additional 25 instrumented production piles were dynamically tested for this project. Test Pile data was used for issuing production piles lengths and driving criteria. Production piles were tested for assessment of their static load bearing capacity and structural integrity in cases where the driving criteria was not met or where pile driving exhibited unusual characteristics.

BENIFICIAL FEATURES OF STEEL PILES

The success of the foundation work on this large project depended on the effective use of the beneficial features offered by steel H-piles. The inherent advantages of steel piles were incorporated into a well-planned and coordinated process between the test pile driving, data collection and analysis, and production pile driving. The following presents examples demonstrating the effective use of steel piles on this project.

The ability to bring production piles to the site prior to or at the same time as driving the Test Piles and the ease of splicing by conventional welding made it possible to immediately proceed into production work following driving of the Test

Pile at each pier. The piles were brought to the site in sections with lengths of 9, 12, 15, and 18 m, which allowed for combinations meeting the required production pile lengths. The entire stock of piles needed for the job was stored on site in advance of construction. This feature eliminates construction delays by making it possible to use off-the-shelf pile sections rather than having to wait for custom-made-to-order piles. Production pile driving typically commenced on the same day the Test Pile was driven at a given foundation unit location, and in some cases, the Test Pile and instrumented production piles were installed concurrently.

The relatively light weight and short lengths of the pile sections allowed for ease of transportation to the project and handling on site in the crowded conditions of the urban setting. There was no need for tedious permits or expensive escorts for transporting the piles. Relatively small equipment was adequate for handling and installing the piles at all project locations. The Test Pile for Pier 3 of the Anderson Street over I-4 Bridge was originally designed to be a 610-mm square prestressed concrete pile with a length of 32 m. The location of this pier in a very limited area in the middle of I-4 made it very difficult to mobilize large equipment and safely handle long, heavy piles within extremely close proximity to highway traffic. Using steel H-piles at this pier provided an effective alternative by minimizing the risk that is always present in working close to the traveling public.

A significant portion of the work on this project entailed driving piles within close proximity of in-service bridge foundations. Eighteen residential and commercial high rise buildings were also identified for monitoring. Use of steel H-piles is very suitable for such conditions due to the low level of ground vibration produced by their installation. The project specifications included the standard FDOT requirement of limiting vibration levels to below 12.5 mm/sec. Vibration monitoring was performed using a Safeguard Seismic Unit 2000DK. The monitoring was performed during the driving of over 630 HP 14x89 and HP 12x53 steel H-piles varying in length from 32-40 m at pre-identified locations. The measured vibration levels at all locations were well below the specified Peak Particle Velocity (PPV). No adverse effects were observed on the existing structures due to the nearby pile driving.

Pauses and delays in construction activity normally experienced between the installation of Test Piles and production pile driving were minimized, and in many cases eliminated by the use of steel piles. The construction schedule was expedited by implementing a dynamic pile testing program that was well coordinated with the pile driving activities. In most cases, the piles consisted of two pile sections. The bottom pile sections, mostly 18.3 m long, were installed with a vibro-hammer before splicing on the top sections with the appropriate length for the required pile penetration. For foundation units made up of a few piles, the bottom sections were vibrated and the top sections spliced on and tested during driving. This process typically lasted a total of two days to complete the pile driving for the foundation unit. For large pile groups, the following procedure was typically followed: Test Pile was installed by vibrating the bottom section and impact driving, with PDA testing, of the top section; this process typically took about three hours. While the PDA data

was being analyzed and recommendations for production pile lengths and driving criteria were being developed, the contractor vibrated the bottom sections of the production piles. These concurrent activities typically took a day or two depending on the size of the pile group. By the time the engineering recommendations were issued, the contractor was ready to splice on the top pile sections with lengths that meet the required pile penetrations. The concurrent engineering analysis of Test Pile data and partial installation of production piles contributed to the success of the foundation work on this project. In many cases, the work for very large groups was completed in less than a week, including Test Pile and production pile driving.

The Florida Central Railroad Pier 5 crashwall under the I-4 Robinson Street Bridge presented the usual challenges associated with deep foundation construction in low-headroom conditions. Employing short H-pile sections, welding for quick splicing, and relatively small installation equipment was an effective pile driving solution. HP 14x89 sections with multiple spliced 2 m lengths were installed with a vibro-hammer then dynamically tested under a few blows of an impact hammer for verification of load bearing capacity and structural integrity.

The relative ease in which steel H-piles can be installed by vibro and impact hammers, and the absence of constructability issues typically associated with other pile types contributed significantly to the success of the foundation work. Installation of each steel pile typically took less than an hour, including vibrating the bottom section, splicing, impact driving of the top section, and cutoff. Impact pile driving blow counts were generally less than 40 blows/300 mm. Serious difficulties encountered during the driving of 610-mm square prestressed concrete piles were eliminated with the use of steel H-piles. High elastic rebound experienced by the concrete piles at Ramp E and the Anderson Street Bridge prevented the piles from being driven to desired penetration depths, despite the employment of various means and methods. By comparison, steel H-piles drove to the desired penetration depth and load bearing capacity without any difficulty. More details on the comparison of driving concrete and steel H-piles are presented later in the paper.

The geology of Central Florida often dictates the use of varying length piles for a given project, or even within the same foundation unit. Cases have been documented in the technical literature where the use of steel piles was advantageous due to the ease of adjusting pile lengths to accommodate the varied subsurface conditions (Kuhns et al., 2003). On this project, two neighboring steel piles (HP 12x53, 36 m long) at the Church Street Viaduct East Bound Pier 2 foundation unit drove very differently from each other. Pile 1 had a blow count of 240 blows for 150 mm with a hammer stroke of 2.2 m at a pile tip elevation of –1.2 m. Pile 4, located within 2 m of Pile 1, had a blow count of 33 blows for 300 mm with a hammer stroke of 2.2 m and at pile tip elevation of –1.2 m. Pile 4 was driven 2 m deeper and still did not show marked increase in driving resistance; it was subsequently tested during restrike and showed significant setup effects. In this case, one pile was an end bearing foundation while the one next to it was a friction pile. At other locations, the pile length was conveniently adjusted to accommodate the driving resistance effects and load bearing

requirements. The use of steel piles in varying subsurface conditions is advantageous to any other type of deep foundations.

H-PILE CAPACITY INCREASE DUE TO SOIL SETUP

This project presented an opportunity for evaluation of soil setup effects on the low-displacement H-piles used. There were occasions where dynamic tests were performed during initial driving and restrike to investigate the change in pile capacity over time for further understanding of the long-term pile behavior and comparison with analytical models used in foundation design. Restrike testing was performed to evaluate the in-place condition of production piles that may not have met the driving criteria or experienced unexpected driving behavior. At Ramp D1, Pier 12 the soils from the surface down consist of 11 m of fine sands (SPT N-values 2 to 12); 17 m of layered clayey & silty fine sands (N-values 4 to 30); 4 m of silty & sandy clays (N-values 20 to 30); and highly over-consolidated clay (N-values > 50) extending to depths of 40 m. At this Pier, a 33.5 m long, HP14x89, pile was driven with an ICE I-30 open-ended diesel hammer (29.4 kN ram weight) to a depth of 30 m and a blow count of 41 blows/300 mm at a hammer stroke of 2.5 m. A 30-minute setcheck indicated a blow count of 8 blows/25 mm at a hammer stroke of 2.6 m. Figure 3 presents plots of PDA measured pile top force and velocity records obtained under hammer blows from the end of driving and restrike tests. Also included are plots of CAPWAP simulated static loads tests results. The results indicate an end of driving pile load bearing capacity of 1800 kN, which increased to 2500 kN after 30 minutes. The data confirmed the development of soil setup effects and the marked increase in pile capacity to a high value in a short period of time.

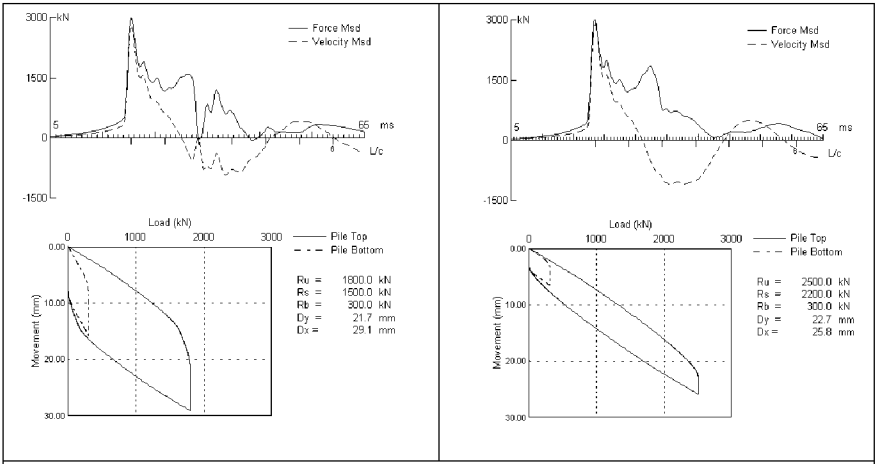

Figure 3: PDA Dynamic pile measurements of pile force and velocity records and CAPWAP analysis generated load-movement relationships for a 33.5 m long HP14x89 pile, from the end of initial driving (left) and beginning of restrike (right).

DRIVEABILITY COMPARISON OF CONCRETE AND STEEL PILES

Deep foundations for the Anderson Street Overpass were originally designed using 610-mm square prestressed concrete piles for an ultimate pile capacity of 2800 kN. From the surface down (elevation at +32 m), the soils consist of 15 m of fine sands (SPT N-values 3 to 27); 12 m of sandy/silty clays & silty/clayey fine sands (N-values 2 to 19); and highly over-consolidated clays & clayey fine sands (N-values > 50) to depth of 42 m. The first concrete Test Pile was 38 m long consisting of two 19 m long sections utilizing a mechanical splice. A Delmag D62 diesel hammer (ram weight of 61 kN) was used to drive the pile. Driving was relatively easy with blow counts between 10 and 20 blows/300 mm to an elevation of +5 m where the blow counts steadily increased to a value of 254 blows/280 mm with a stroke of 2.1 m at an elevation of +2.4 m. At the end of driving, the dynamic pile tension stresses were 6 MPa (exceeding the allowable limit for a spliced concrete pile), ultimate pile capacity was 1600 kN, and elastic pile rebound of 30 mm. Several attempts using redrives over time and changes in driving system failed to advance the pile due to the detrimental high rebound effects on pile driveability.

A renewed attempt to drive a concrete Test Pile was undertaken using a 34 m long, one-piece pile. The pile driving blow counts and capacity for this pile are presented versus elevation in Figure 4. The pile met refusal blow counts at elevation +1 m with an end of driving capacity of 1500 kN; the pile elastic rebound was 25 mm and the dynamic tension stresses reached the limit of allowable value of 8 MPa. The high elastic pile rebound and its detrimental effects on pile driveability (e.g., refusal pile driving blow counts with low pile static bearing capacity, high dynamic driving tension stresses, etc.) frustrated all attempts to drive concrete piles at this location. Means and methods to overcome the difficulties included changes to the pile makeup (one piece instead of splices), changes to the driving system (hammer change, cushion changes, etc.), and pile redrive sequences.

An HP 14x89 steel pile, 40 m long, was driven with an ICE I-30 diesel hammer (ram weight of 29 kN) to assess its driveability characteristics at this pier location and compare it to the nearby concrete piles. The driving blow counts and pile capacity for the ending portion of driving the steel pile are presented in Figure 4. Pile driving was easy for the entire pile penetration depth until the design bearing layer was reached where the blow counts reached 189 blows/300 mm with hammer stroke height of 2.9 m and the pile capacity reached 3000 kN. The difficulties experienced with installation of the concrete piles at this location were not encountered during the driving of the steel piles. The deep foundation for this pier, and others, were redesigned to allow for the use of steel H-piles.

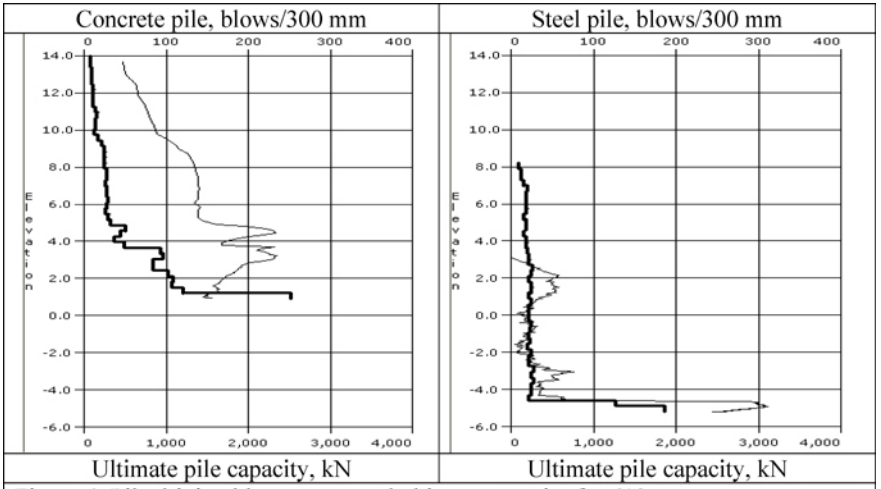

Figure 4: Pile driving blow counts and ultimate capacity for 610 mm square concrete pile driven with Delmag D62 hammer (left), and HP14x89 steel pile driven with an ICE I-30 hammer (right).

CONCLUSIONS

Improvements to the heavily traveled junction of Interstate 4 (I-4) and the East-West Expressway (SR 408) in downtown Orlando, Florida involved twelve structures supported on 60,000 meters of deep foundations. A distinguishing feature of this project was the extensive use of steel H-piles for a large transportation project in Central Florida. Utilizing the many beneficial features of steel H-piles in a well planned and executed construction process allowed for a successful project. The paper contains dynamic pile testing data and discussions highlighting the many advantages of steel H-piles and their effective use on this large project. Some of the practical findings and lessons learned were the high load bearing capacity of H-piles, and the relative ease of their driveability in high-rebound soils.

REFERENCES

Florida Department of Transportation (2007). *"Standard Specifications for Road and Bridge Construction"*, FDOT, Tallahassee, Florida,www.dot.state.fl.us: 490-562.

Hussein, M. and Likins, G. (1995). "Dynamic Testing of Pile Foundations During Construction." Proceedings of the ASCE Structures Congress XIII, held in Boston, Massachusetts, www.asce.org: 1349-1364.

Kuhns, G., Hussein, M, and Gray, K. (2003). "Deep Foundations in the Challenging Geology of Central Florida." Deep Foundations Institute's 28th Annual Conference held in Miami Beach, Florida, www.dfi.org: 33-43.

Copyrighted Materials
Copyright © 2009 American Society of Civil Engineers (ASCE)
Retrieved from www.knovel.com

THE EFFECT OF INSTALLATION TECHNIQUE ON CAPACITY OF CYLINDER PILES IN THE YORKTOWN FORMATION

Mike Muchard, P.E.
Applied Foundation Testing, Tampa, Florida, USA
Rick Palmer
Weeks Marine, Inc., Portsmouth, Virginia
Michael Simpson, P.E.
Applied Foundation Testing, Raleigh, North Carolina

ABSTRACT

Statnamic (Rapid) and dynamic tests were performed on seven (7) 54-inch spun-cast concrete cylinder piles installed with varying methods into the Yorktown Formation bearing stratum and the capacity measured. Four piles were part of an indicator pile program which was performed prior to installation of any production piles. Three additional Statnamic load tests were performed on production piles to assure capacity and verify final installation criteria.

The pile design considered skin and tip resistance in the dominant geologic stratum for the Chesapeake Bay Area known as the "Yorktown Formation." The upper surface of the Yorktown was encountered 30 to 50 feet in depth and extends to depths of 300 feet. It consists of medium dense to dense silty fine sand (SM) with abundant marine shell. It was moderately sensitive to elevated pore pressures from pile driving and was shown to regain most of its strength in about a week. Furthermore these soils were not conducive to plugging during driving or load testing.

The tested cylinder piles were all 54-inch diameter, 6.5-inch wall with lengths of 160 to 164 feet. All of the test piles were cast with four levels of embedded strain gages to measure load transfer characteristics during Statnamic load testing. Statnamic load testing fully mobilized pile capacities ranging from 2,285 kips to 4,014 kips as a result of the various installation techniques. Dynamic testing consistently showed significantly lower pile capacity due to insufficient test energy of the hammer.

An excessively rising soil and water column within the pile core during driving governed the need to predrill. However, the reduction in side shear resistance from predrilling ultimately required an additional 10 feet of pile penetration to obtain the required capacity. Furthermore, the end bearing appeared to act in an unplugged condition.

INTRODUCTION

Spun cast concrete cylinder piles were used as the foundation for a major container terminal wharf project in Portsmouth, Virginia. The pile design considered a combination of side and tip resistance in the dominant geologic stratum for the Chesapeake Bay area known as the "Yorktown Formation." As part of the project, a load test program was performed. The testing included dynamic testing during initial drive and restrike followed by high capacity Statnamic (Rapid) load testing. Piles were installed into the Yorktown with a variety of means and methods and the capacity evaluated. These included varying pre-drill depths, pile tip elevation and using a plywood pile tip insert to limit the internal soil/water column length. A summary of key test pile information is provided in Table 1.

The piles obtained their capacity bearing well within the Yorktown Geologic Formation which is encountered 30 to 50 feet in depth at this site and extends to depths of 300 feet. It consists of medium dense to dense non-plastic silty fine sand (SM) with shell fragments. Generally, SPT "N" values ranged from 11 to 25. It is moderately sensitive to the dynamics of pile driving causing pore pressures to build up thereby decreasing initial drive pile capacities. Testing at this site suggests that most of the strength regain occurred within 7 days. Yorktown soils also exhibited "unplugged" behavior during driving and load testing.

All cylinder piles presented in this paper were spun cast 54-inch outside diameter with a 6.5-inch wall thickness and lengths of 160 feet to 164 feet. Four levels of embedded strain gages were cast in the test piles and monitored during Stanamic load testing. Due to size limitations of this paper, we will not present detailed load distribution results from the strain measurements.

Four of the test piles were part of an indicator pile program performed prior to installation of any production piles. Of these four piles, three had the same tip elevation (-143 feet) with predrill elevations varying from none to -110 feet (60 feet below bay bottom). The fourth indicator pile was held at a tip elevation 10 feet shallower than the rest with no predrilling. It was discovered during pile installation of IP 3 and IP 4 that a soil plug was not forming during driving. To the contrary, the soil and water level inside the pile rose upwards of 50 feet preventing further pile driving until the pile core was cleaned out. It was quickly recognized that this would be devastating to the production pile installation schedule. Predrilling in conjunction with a plywood pile tip plug was a solution, however, at some expense to skin friction capacity. Therefore, various predrilling depths were examined to determine the optimal depth. Although installation methods were somewhat varied for each pile, the predrilling depth seemed to have the greatest effect on pile capacity. It also had the greatest benefit for production as it would replace the need to stop and clean out the pile core.

The indicator piles were dynamically monitored during installation and at various restrike intervals up to as much as three weeks after installation. Statnamic load tests

were performed 13 to 16 days after initial driving. Statnamic load tests showed fully mobilized pile capacities ranging from 2,285 kips to 4,014 kips reflective of the various installation techniques. The dynamic testing consistently showed significantly lower pile capacities of 1,539 kips to 1,809 kips due to insufficient test energy of the hammer. Due to these limitations observed during the indicator pile program, dynamic testing was not used any further on the project to asses pile capacity. Dynamic testing was, however, very useful as a means of monitoring driving stresses, hammer performance and pile integrity.

Based on the test results of the four indicator piles, a driving criteria was developed for production piles. Components of the driving criteria included cushion thickness, stroke heights, predrill elevation, final tip elevation and the use of a plywood pile tip insert to reduce the soil column height in the pile core. To verify production piles were achieving the required capacity according to the installation criteria, three production piles designated 2-A, 77-C, and 127-C were Statnamic load tested.

TABLE No. 1. Indicator and test pile summary information.

Pile	Initial Drive Date	Restrike Date	STATNAMIC Load Test Date	Pile Length (ft)	Predrill Elevation (ft)	Pile Tip Elevation (ft)
IP 3	3/26/05	4/2/05	4/10/05	164	NA	-143.4
IP 4	3/28/05	4/2/05	4/10/05	164	NA	-132.5
IP 7	4/27/05	4/30/05	5/11/05	164	-90	-143.1
IP 8	4/28/05	4/30/05	5/11/05	164	-110	-143.3
2- A	9/28/05	N/A	10/14/05	160	-80	-144.7
77-C	1/23/06	N/A	2/06/06	164	-80	-154.8
127-C	2/02/06	N/A	2/16/06	164	-80	-154.8

FOUNDATION AND SOIL DESCRIPTION

Foundation Description

The piles were constructed by spin casting multiple cylindrical segments and post-tensioning them together to make up the desired length. The pile dimensions were 54 inches O.D. by 6.5 inch wall thickness. Individual segment lengths were 16 feet except the bottom sections which were 4 feet. The pile segments included longitudinal ducts in which strands were threaded and post-tensioned. Shear reinforcement consisted of 3/8 inch diameter wire spirals with a pitch of approximately 3 inches. High strength, low slump concrete was placed in the rotating forms. The centrifugal forces impel the concrete to the walls of the forms which results in a very strong and dense structural element. Concrete compressive strengths for the piles were typically around 10,000 psi. The 54-inch piles were anticipated to achieve an ultimate capacity of 1,630 tons (3,260 kips) at this project.

The cylinder piles were successfully instrumented with four levels of strain gages, which is a major challenge for this pile type. Figures 1, 2, and 3 below provide a view into this pile manufacturing process.

FIG. 1, 2, & 3. Spun cast cylinder pile instrumentation and construction.

Soil Description

Soil conditions can generally be separated into two different strata. The surficial layer consisted of sands with varying amounts of silt and clay. This layer extended to depths of 30 to 50 feet. With the dredge elevation of -54 feet, this layer was completely removed as part of the project. It is noted that the indicator piles were installed prior to dredging and thus used isolation casing to eliminate the capacity contribution from the dredge zone during load testing. The underlying bearing stratum was known as the Yorktown Formation which extends to depths up to 300 feet. This material consists of silty fine sand (SM) materials with abundant marine shell fragments. Relative densities in the upper part of the formation were generally loose to medium dense with SPT "N" values around 10. Below elevation -90 feet, the material graduated to medium dense to dense with SPT "N" values around 11 to 25. The Yorktown is non-plastic with fines contents (% passing #200) around 40 percent above -90 feet elevation. Below -90 feet, the fines content was generally less than 20 percent. During production pile installation, soil conditions showed some variability across the site. It is moderately sensitive to the dynamics of pile driving which cause pore pressures to build up thereby decreasing initial drive pile capacities. Testing at this site suggests that the pore pressures mostly dissipate and the soil regains strength within 7 days.

TEST PILE PROGRAM

Pile Installation

Prior to installing the indicator piles, a 78-inch diameter casing was driven and excavated within to an elevation of -47 to -48 feet to eliminate side shear resistance in the dredge zone. The 54 inch cylinder piles were installed using a Raymond 60X steam hammer with a 7.5 inch plywood pile cushion. Hammer strokes varied from 1.5 feet to 2.5 feet to control driving stresses. It was known that these soil characteristics were not conducive for plugging, but during pile installation of IP 3 it was found that the soil and water level inside the pile actually rose upwards of 50 feet to the pile top. It was therefore necessary to stop driving and cleanout the pile core to prevent pile damage from "water hammer" effects. The next pile IP 4 was fitted with a plywood plug at the pile tip (to reduce the soil and water level inside the pile) and it was held at a tip elevation 10 feet shallower. The soil rise problem still occurred. Recognizing this issue would be devastating to the production pile installation schedule, Predrilling, in conjunction with a complete, sealed (watertight) plywood plug on the tip of the pile, allowed the soil rise in the pile to be controlled. The plug allowed the pile to displace the natural slurry in the predrilled hole as the pile is stabbed, effectively sealing the interior of the pile from water intrusion. The plywood plug typically broke within the first 10 hammer blows. The soil column still rose in the pile, but it started from the bottom of the predrilled hole, not the existing river bottom elevation. Predrill elevations of -90 and -110 feet were utilized for IP 7 and IP 8. Production piles were predrilled to -80 feet with a final tip elevation of -155 feet.

FIG 4. Production Pile Driving.

Dynamic Testing

Dynamic testing was performed on all indicator piles during initial drive and restrikes 2 to 7 days later. Additional restrike tests up to 19 days after initial drive were performed for IP 7 and IP 8. A plot of mobilized capacity over time shown in Figure 5 suggest approximately 7 days were required for the soil to regain the majority of its strength after pile driving. A summary of the ultimate pile capacities based on signal

matching analyses performed on the dynamic test data is shown in Table 2. Also shown is the driving resistance (blows per foot) and hammer transfer energy. Although energy transfer was good, there was very low permanent set per blow on the restrikes. This is a well known cause of underprediction of ultimate pile capacity.

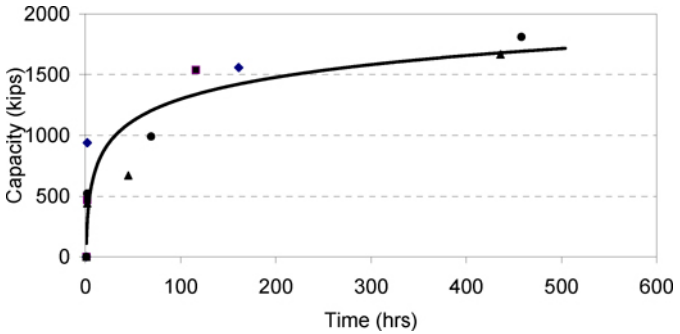

FIG 5. Soil strength gain with time from signal matching.

TABLE No. 2. Summary of signal matching analyses on dynamic test results.

Pile	Blow	Elapsed Time (days)	R_{ult} (kips)	R_{skin} (kips)	R_{toe} (kips)	Blows Per Foot / Energy(kip-ft)
IP 3	EOD	0	939	273	666	58 / 76
IP 3	BOR	7	1558	932	626	184 / 63
IP 4	EOD	0	468	215	253	43 / 87
IP 4	BOR	5	1539	914	625	120 / 90
IP 7	EOD	0	521	257	264	65 / 83
IP 7	BOR	3	990	602	388	108 / 46
IP 7	BOR	19	1809	1185	624	312 / 73
IP 8	EOD	0	439	138	301	33 / 63
IP 8	BOR	2	670	345	325	48 / 64
IP 8	BOR	18	1665	1110	555	288 / 74

STATNAMIC Load Testing

Pile static capacities from the Statnamic load tests were determined utilizing the Segmental Unloading point (SUP) method (Mullins et. al. 2002) in conjunction with a weighted average rate factor of 0.826 (Mullins, 2003). The Statnamic load testing device shown in Figure 6 was used to perform the tests. The ultimate pile capacity was fully mobilized in every pile as seen in Figure 7 with maximum displacements of 2.5 to 4.5 inches during testing. This figure also shows the pile capacity variation of 2,285 kips to 4,014 kips as a result of installation methods and soil conditions. The data in Figure 7 suggests that the pile capacity was generally lower commensurate

with the predrilling depth. IP 7 and IP 8 had a tip of -143 feet and the deepest predrilling at -90 and -110 feet, respectively and had the lowest capacity. IP 4 had no predrilling but a shallower tip elevation of -132 feet and did not meet capacity. IP 3 and 2-A had similar capacity at similar tip elevations of -143 to -144 feet but 2-A was predrilled to -80 feet and IP3 was not predrilled. Both of these piles met the required capacity. Pile 77-C and 127-C with the greatest capacity were predrilled to -80 and driven to a deeper tip elevation of -155 feet Based on strain measurements during Statnamic testing, it appears the end bearing behaved in the unplugged condition.

FIG 6. Statnamic device at project.

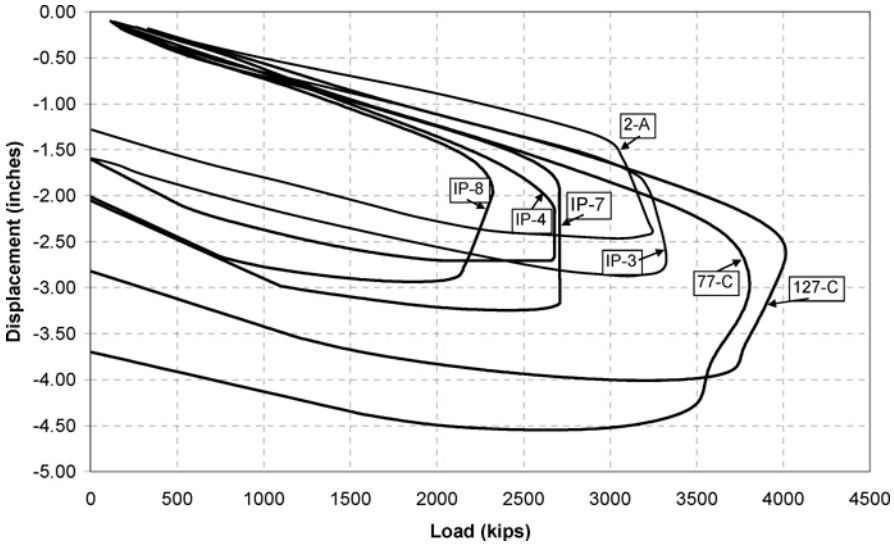

FIG 7. Load vs Displacement curves from Statnamic load tests on 7 piles.

TABLE No. 3. Summary of Statnamic load test results.

Pile	Ultimate Capacity (kips)	Skin Friction (kips)	End Bearing (kips)	Maximum Displacement (inches)	Permanent Displacement (inches)
IP-3	3,315	2,823	492	2.88	1.57
IP-4	2,680	2,213	467	2.67	1.60
IP-7	2,710	2,272	438	3.25	2.04
IP-8	2,285	1,428	857	3.54	2.60
2-A	3,248	3,021	227	2.45	1.25
77-C	3,800	3,599	201	4.55	3.70
127-C	4,014	3,611	403	4.02	2.82

CONCLUSIONS

1) Predrilling, in conjunction with a sealed (watertight) plywood plug on the tip of the pile, successfully allowed the soil rise in the pile to be controlled during installation.
2) The effect of predrilling resulted in the piles requiring an additional 10 feet of embeddement. But additional production costs associated with cleaning out every pile core amid driving eclipsed the extra pile material costs.
3) Statnamic fully mobilized the pile capacity and had reliable load distribution through use of strain measurements.
4) Dynamic testing significantly underpredicted total capacity due to insufficient test energy (low set per blow). Furthermore, as compared to Statnamic end bearing which is based on strain measurements, CAPWAP significantly overpredicted end bearing in three indicator piles and underpredicted in one. Dynamic testing was useful to evaluate driving stresses, hammer energy, integrity and relative soil set up time, but not for assessment of ultimate capacity.
5) The Yorktown soils were moderately sensitive to elevated pore pressures from pile driving and were shown to regain most of the strength in about a week.
6) The data suggests that the Yorktown soils in conjunction with the installation method used resulted in unplugged pile end bearing behavior.

REFERENCES

Mullins, G., Lewis, C., and Justason, M.D., (2002). Advancements in Statnamic data Reduction Techniques. ACSE Geotechnical Special Publication 116, pp. 915-928.

Mullins, G., (2003). NCHRP 21-08 Innovative Load Testing Systems, Critical Evaluation of Statnamic Test Data. National Cooperative Highway Research Program

Copyrighted Materials
Copyright © 2009 American Society of Civil Engineers (ASCE)
Retrieved from www.knovel.com

Case History: Value Engineering of Driven H-Piles for Slope Stability on the Missouri River

W. Robert Thompson, III,[1] M.ASCE, P.E., Jeffrey R. Hill,[2] M.ASCE, P.E., and J. Erik Loehr,[3] M.ASCE, Ph.D., P.E.

[1]Principal, Dan Brown and Associates, PLLC, 2400 Old Creek Road, Montgomery, AL 36117; Phone: 334-239-3135; rthompson@danbrownandassociates.com
[2]Area Manager, Hayward Baker, Inc., 1530 South Second Street, Saint Louis, Missouri 63104; Phone: 314-802-2923; jrhill@haywardbaker.com
[3]Associate Professor, University of Missouri, E2509 Lafferre Hall, University of Missouri, Columbia, MO 65211-2200; Phone: 573-882-6380; eloehr@missouri.edu

ABSTRACT: In order to increase rail traffic capacity, a rail line owner added an additional track adjacent to an existing main line along the Missouri River near Gasconade, MO. The new track was placed on the existing railroad embankment between the existing track and the Missouri River, requiring measures to improve the stability of existing embankment slopes. The initial design included permanent soldier pile retaining walls along portions of the project alignment and jet-grout "shear pins" in other locations to provide the required slope stability. Due to site access issues, the contractor proposed using driven HP 310x79 (HP12x53) piles as an "equal or better" alternate to the jet-grouted columns. This alternate was accepted and constructed with substantial cost and schedule benefits to the overall project.

INTRODUCTION

The subject of this paper is a case history in which driven steel H-piles were utilized as part of a value-engineering effort to replace jet-grout columns for stabilization of an embankment slope. The change from jet-grout columns to driven piles provided substantial benefits to the cost and schedule for the project. The overall project involved adding an additional track adjacent to an existing main line railroad along the Missouri River near Gasconade, MO. The location for the new track is on the existing embankment between the existing track and the river, requiring either the construction of retaining walls or stabilization of the existing embankment slopes.

Initial analysis and design was performed for the owner by others prior to the authors' involvement in the project. Details of the analyses were not made available to the authors. Restrictions on site grading resulted in proposed embankment slopes of 2:1 (H:V) in areas where retaining walls would not be used. The initial analyses

performed by others established that these proposed embankment slopes would have factors of safety in the range of 1.2 to 1.5 when accounting for the proposed grading and loading from the new tracks. A row of jet-grouted columns was therefore designed to act as shear pins to improve the stability of the embankment slopes. The proposed 0.9 m (3 ft) diameter jet-grout columns were to be spaced 1.5 m (5 ft) center-to-center along the crest of the slope, extending from a distance of 1.2 m (4 ft) below grade down to bedrock. The jet-grout shear pins were planned along eight sections of the project alignment, which varied in length from 15 to 305 m (50 to 1000 ft). The height of the slope in these sections varied from 7.6 to 11.3 m (25 to 37 ft). A typical cross-section of the project alignment is shown in Figure 1. A detail of the designed jet-grout column shear pins is shown in Figure 2.

After the project was awarded, it was determined that the available space between the river and the existing rail line was often less than needed to safely operate jet grouting equipment while keeping the rail line open to traffic. Temporary work areas would need to be constructed for staging of the jet grout equipment and providing adequate, safe work space. The specialty contractor determined that driven piles could be safely installed without the need to build temporary work areas, resulting in the proposal of an "equal or better" alternate to the jet-grouted columns. The proposal consisted of driven HP 310x79 (HP12x53) A572 Grade 50 steel pile sections spaced 0.9 m (3 ft) center to center along the crest of the slope, extending from the ground surface down to bedrock. This paper describes the general site conditions and constraints that induced consideration of value-engineered alternatives, evaluations performed to demonstrate equivalency of the driven steel H-piles and jet-grouted columns, and the economic advantages of the value-engineered system.

SUBSURFACE CONDITIONS

Eleven soil borings were drilled along the project alignment for the pre-design site investigation. Standard Penetration Tests (SPT) and field vane shear tests were performed in four of the soil borings. In general, the subsurface conditions observed consisted of fill material overlying alluvial and residual soils overlying bedrock. The fill consisted of various materials, including clay, cinders, sand, gravel, rock fragments, cobbles and boulders. The alluvial soils were typically sandy silts and silty sands. Some deposits of residual clay were encountered immediately above the dolomite/limestone bedrock. The depth to rock was generally 7.6 to 10.7 m (25 to 35 ft). The depth of fill ranged from 1.5 to 9.1 m (5 to 30 ft).

Fourteen additional borings were drilled along the project alignment during development of the "equal or better" proposal to provide additional data as to the depth to rock and to attempt to obtain samples of the soil materials for laboratory shear strength testing. These borings generally confirmed that the depth to rock was relatively consistent at the site. Occasional boulders were encountered at shallower elevations, but the depth to bedrock was on the order of 6.1 to 10.7 m (20 to 35 ft) below existing ground surface. Attempts to obtain quality Shelby tube samples for undrained shear strength testing were generally unsuccessful with only a single suitable sample acquired out of many sampling attempts due to gravel and cobbles

within the embankment soils. The measured undrained shear strength of this lone sample from an unconsolidated-undrained type triaxial compression test was approximately 48 kPa (1000 psf).

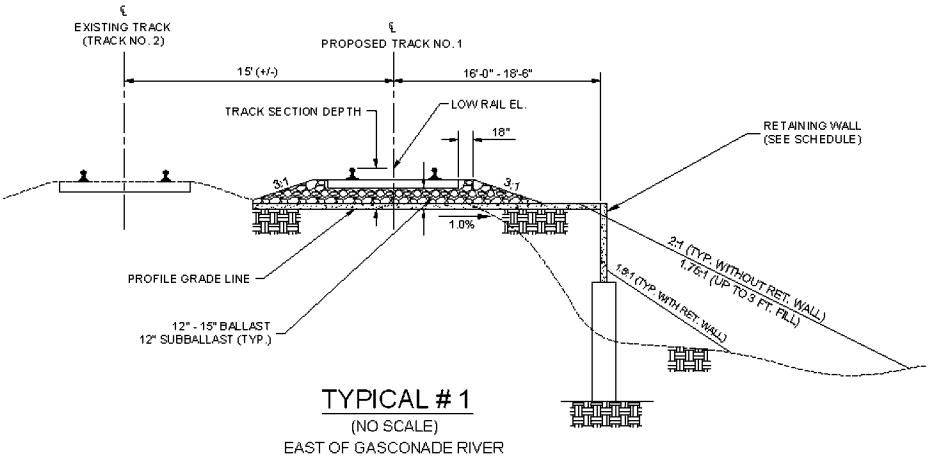

FIG. 1. Typical Cross-Section of Project Alignment (Retaining Wall Shown) (1 ft = 0.305 m)

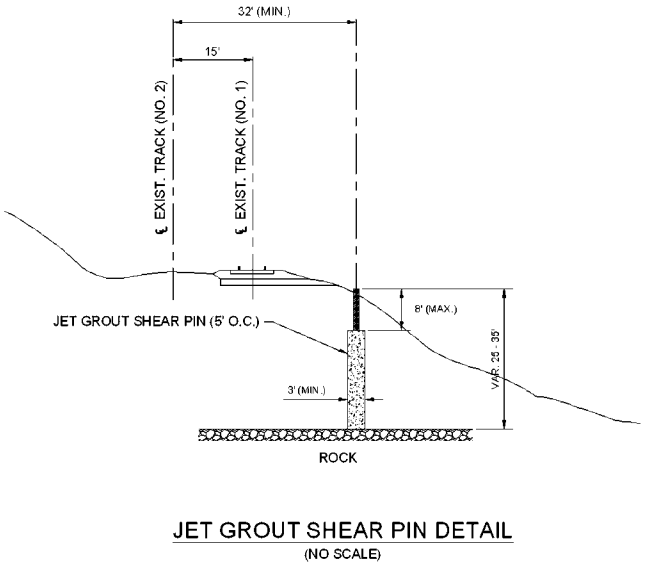

FIG. 2. Proposed Jet-Grout Shear Pin Detail (1 ft = 0.305 m)

ANALYSES

Because the primary objective for the value-engineered design was to demonstrate equivalence with the jet-grout columns, analyses focused on direct comparison of using H-piles for stabilization in lieu of jet-grout columns. Either stabilization technique had to be designed to resist the combination of earth pressure forces and live loads from the railroad lines. Resisting forces to be provided by the piles were predicted using soil-structure interaction analyses with loading induced by moving soil. The predicted resistance forces were then input into limit equilibrium stability analyses for comparison with results of analyses for the jet-grout columns. Analyses were also focused on evaluating stability for potential sliding surfaces that intersected the proposed locations of the new and existing tracks as the owner assumed risk and responsibility for any surficial slides that might occur beyond the rail tracks and timely maintenance of such slides should they occur.

In the original design, the embankment soils were modeled using drained, effective stress shear strength parameters with effective stress cohesion intercepts (c') ranging from 1.2 to 2.4 kPa (25 to 50 psf) and effective stress friction angles (φ') of 32 to 35 degrees. The stability analysis models represented the embankment soils above bedrock in multiple layers using this range of shear strength parameters. These analyses focused on achieving a factor of safety of 1.5 for the embankments.

The slope stability models used for the "equal or better" proposal modeled the soil above bedrock as a single material with the lower bound drained shear strength parameters from the earlier investigations [c'=1.2 kPa (25 psf), φ'=32 deg.]. In addition to comparing the H-piles to the jet-grout columns, these analyses were also focused on evaluating the embankment stability for potential sliding surfaces that intersected the proposed locations of the new and existing tracks.

Four cross-sections representative of the eight sections of the alignment requiring stabilization were selected for analysis. One cross-section, Station 4598+00, was deemed to be representative of most of the project alignment and was the focus of the initial analyses. This cross-section was used to define the slope model and perform sensitivity analyses to evaluate for the effect of variations in soil parameters. Once the model and soil parameters were finalized and the analyses completed for this cross-section, the same parameters were used to evaluate the other representative cross-sections.

In order to evaluate the equivalence of the H-piles as compared to the jet-grouted shear pins, a multi-step approach was used that included the following general steps:

(1) Stability analyses of the existing and proposed conditions for the embankments were performed to replicate results from the original design to ensure consistency among the stability models used for the value engineering evaluations and those used for the initial design. Results of these evaluations demonstrated that the stability models produced similar factors of safety for both the existing and proposed conditions.
(2) Back analyses of the existing embankment were performed to estimate minimum undrained shear strength values for the embankment soils that would result in a factor of safety of 1. Since the embankment is known to

have been stable for many years, thus having a factor of safety greater than 1.0, these analyses produced lower bound estimates of the average undrained shear strength for the embankment soils. These estimates were then used along with results of a limited number of field and laboratory strength tests to estimate undrained shear strengths for use in lateral pile-soil response analyses.

(3) Lateral pile-soil response analyses were performed to predict the shear resistance developed in the piles as the soil moves relative to the piles. Analyses were performed for potential sliding surfaces at various depths in the embankment to develop a shear resistance vs. sliding depth profile for the piles.

(4) Embankment stability analyses were performed to evaluate the embankment stability with the effect of the piles included. The piles were modeled using the computed shear resistance vs. sliding depth profiles from the lateral pile-soil interaction analyses.

(5) Finally, stability analyses were performed for the embankment with the proposed jet-grouted column shear pins for direct comparison with results of analyses performed for the H-piles.

The resisting forces provided by the H-piles were predicted using soil-structure interaction analyses with loading induced by moving soil. Calculations were performed for a soil movement of 127 mm (5 in) at 1.5-meter (5-foot) depth increments to simulate sliding surfaces that would intersect the pile in the slope. The mobilized shear force at the sliding depth (i.e. the predicted resistance force of the pile) was then input into the stability analyses as a user-defined reinforcement element. Figure 3 shows a plot of the predicted shear resistance as a function of sliding depth for one of the slide sections.

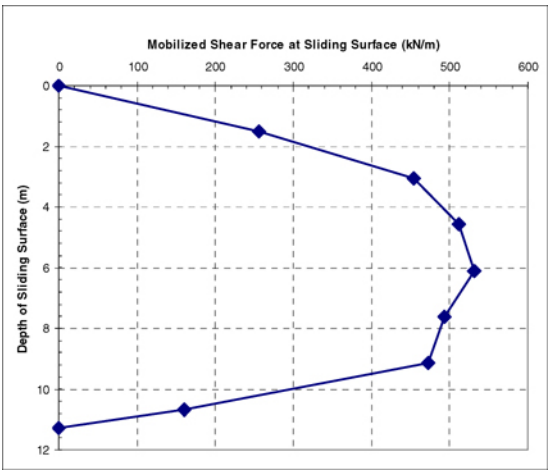

FIG. 3. Predicted Shear Resistance at Sliding Surface for H-Piles subjected to Soil Movement of 127 mm (5 inches)

The jet-grout columns were modeled as a user-defined reinforcement element with constant shear strength. Utilizing a value of f'_c = 3450 kPa (500 psi), a shear capacity of a single 0.9-meter (3-foot) diameter jet-grout column was calculated to be 85.9 kN (19.3 kips). At 1.5-meter (5-foot) center-to-center spacing, the jet-grout columns were modeled with a shear resistance of 56.3 kN/m (3.86 kips/ft).

Drained, effective stress shear strength parameters were used for all slope stability analyses since a drained analysis is appropriate for an existing embankment that has been in place for many years. Analyses of the lateral pile-soil response were generally performed using undrained shear strengths because of the empirical basis for these analyses and because of the potential for the pile-soil loading to be undrained. For the pile-soil response analyses, an undrained shear strength value of 36 kPa (750 psf) was used as a lower bound and 48 kPa (1000 psf) as an upper bound based on results of back-analyses for the existing condition and based on the limited field and laboratory strength tests available. A limited series of analyses considering the lateral pile-soil response to be drained were also performed. Results of these analyses indicated that the undrained lateral response is the critical loading condition with respect to pile-soil response. Thus, lateral pile resistance forces determined from the undrained analyses were used for the slope stability analyses.

SUMMARY OF STABILITY ANALYSIS RESULTS

Table 1 summarizes the results of the stability analyses, listing computed factors of safety for the originally designed stabilization using jet-grout columns and the proposed alternate stabilization using steel H-piles at the representative cross-sections. Figures 4 and 5 show typical results from analyses of the H-pile and jet-grout column stabilization options, respectively. For each stabilization option, computed factors of safety are shown for potential sliding surfaces that encompass both sets of tracks (referred to here as "double track") and for potential sliding surfaces that encompass only the new set of tracks closest to the river (referred to here as "single track").

Table 1. Summary of Calculated Factors of Safety

Cross-Section Station	*Jet Grout Column*		*HP12x53 H-Pile*	
	Double Track[1]	*Single Track*[2]	*Double Track*[1]	*Single Track*[2]
4546+00	1.5	1.4	1.5	1.4
4598+00	1.4	1.3	1.5	1.4
4606+00	1.5	1.4	1.5	1.4
4619+00	1.5	1.3	1.5	1.3

[1]*Double track – potential sliding surfaces encompassing both sets of tracks*
[2]*Single track –potential sliding surfaces encompassing only the new set of tracks (closest to river)*

Comparison of computed factors of safety for the two stabilization options reveals that factors of safety for stabilization with steel H-piles are equal to or greater than those computed for stabilization using jet grout columns for all cases evaluated. This

demonstrates that the proposed steel H-piles would provide stabilization that was "equal or better" than that of the as-bid jet-grouted columns.

The factors of safety shown in Table 1 are based on evaluation of potential sliding surfaces that included the locations of the existing and proposed rail tracks alone and do not reflect the potential for sliding to occur to the river side of the H-piles or jet-grout columns. Computed factors of safety for potential sliding surfaces passing riverward of the jet-grout columns or H-piles were substantially lower than those shown in Table 1 (as low as 1.15), indicating a substantially greater risk of surficial sliding on the embankment slope than for sliding that would impact the rail tracks. The project owner was willing to accept this risk of surficial sliding and accept the responsibility for immediately and appropriately repairing any such slides that do occur to prevent the slides from enlarging and potentially compromising the jet grout columns or H-piles as neither were intended to act as free-standing supports.

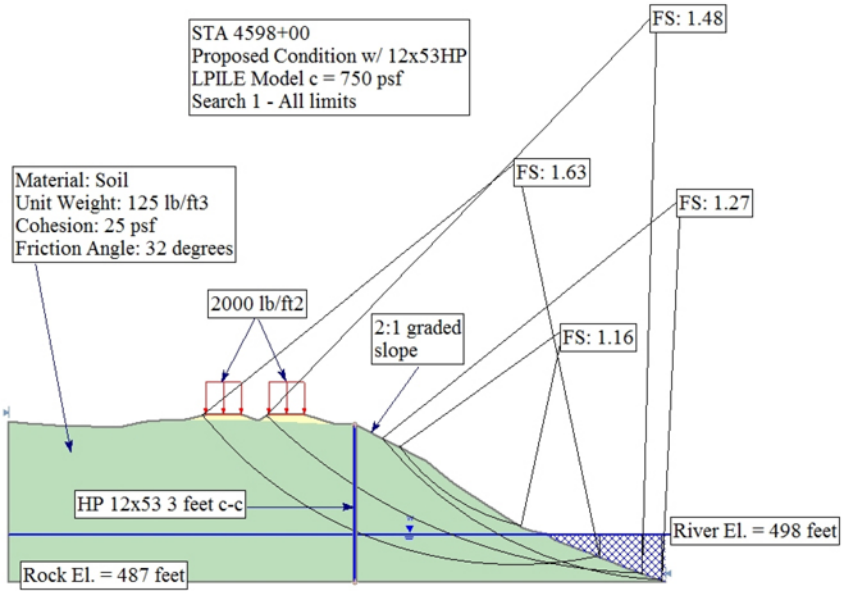

FIG. 4. Typical Result from Analysis of Embankment Stabilized Using H-Piles

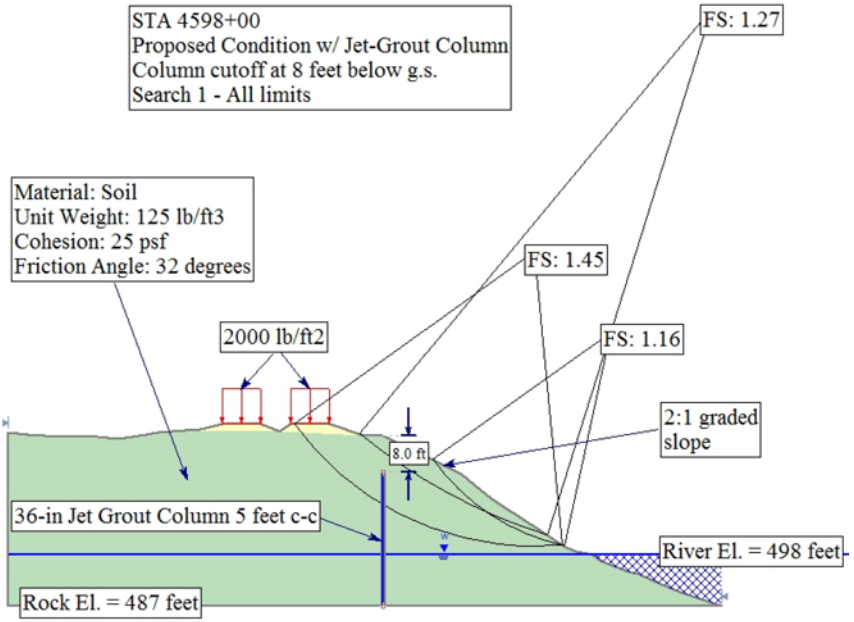

FIG. 5. Typical Result from Analysis of Embankment Stabilized Using Jet-Grout Columns

CONCLUSION AND PROJECT OUTCOME

The analyses performed to compare the proposed use of driven H-piles for slope stabilization in lieu of the as-designed jet-grout columns were described in this paper. The results of the analyses indicated that use of HP 310x79 (HP12x53) A572 Grade 50 steel H-piles placed on 0.9-meter (3-foot) centers near the crest of the embankment and driven to bedrock would provide stabilization similar or superior to use of jet-grouted columns recommended in the original design. The owner elected to accept the driven pile "equal or better" proposal as a substitute for the jet-grout columns. Pile installation began in September 2007 and was completed in late October 2007. Approximately 10,400 m (34,000 ft) of pile was installed at a cost savings of over $275,000 versus the jet-grout shear pin option. The driven piles were installed in approximately half the estimated duration for installation of the jet grout shear pins. Additional cost and schedule savings were provided to the owner by eliminating construction of temporary work areas that would be required for staging of the jet grout equipment.

Copyrighted Materials
Copyright © 2009 American Society of Civil Engineers (ASCE)
Retrieved from www.knovel.com

Foundation Engineering of Offshore "Jacket" Structures

Ioannis Chatzigiannelis[1], Khaled Elsayed[2], and Kostas Loukakis[1], M. ASCE, P.E.

[1]Archirodon NV, Athens Engineering Department, 3 Ag. Andreou Str., Athens, Greece
[2]Archirodon Construction (Overseas) Co. SA

ABSTRACT: "Jackets" are marine structures commonly utilized in civil – offshore construction practice. Foundation engineering of jackets requires exceptional design and construction skills to cope with adverse geotechnical conditions and extreme operational and environmental loads. A synopsis of deep foundation design and practice employed in jacket engineering is summarized in this paper. A case study is presented involving jackets founded on piles, in which the proposed permanent "mudmats" and ground improvement, required for the temporary support of the jackets, were replaced during construction by temporary reusable brackets and piles.

INTRODUCTION

Marine civil engineering encompasses coastal engineering dealing with shoreline processes and protection, and harbor engineering dealing with port development, and berthing, servicing, and navigational requirements of vessels. Offshore engineering has emerged as a result of the ever growing demand for recovery of natural resources (oil and gas) and for conversion of renewable energy sources (winds, waves, and tidal currents). Stationary offshore structures are either secured on the sea bottom through deep foundation systems, or built as gravity type structures. Deep foundations may comprise either pile groups, usually employed in the offshore platform industry, or monopile-type foundations, often encountered in wind turbine offshore practice.

Jacket structures are commonly utilized both in port (e.g., berth facilities and marine terminals) and in offshore engineering practice (e.g., wind turbines and, mainly oil platforms). Difficulties that need to be addressed in the design of jacket structures include engineering against operational and extreme environmental loads (waves, winds, currents, earthquakes).

Jacket structures are commonly assembled on land and transported to their final position, where they are temporarily positioned on the sea floor and then permanently secured in place. Hence, they have to be also designed to sustain temporary loads that are equally adverse to permanent or accidental loads. Piles are employed in unfavourable ground conditions to safely transfer loads from the

superstructure to the foundation layers. If the jacket legs have small diameters, piles are constructed as "skirt piles" through sleeves connected onto the jacket legs (fig. 1a). If the jacket legs can accommodate the required pile diameter, then piles are constructed as "leg or pin" piles through the jacket legs (fig. 1b). A very wide range of pile types and construction methods are employed in offshore engineering foundation practice, e.g. steel driven piles, drilled in situ reinforced concrete piles, or other combinations that better suit project specific ground conditions, such as driven steel piles with rock sockets drilled through the steel casing and filled with concrete.

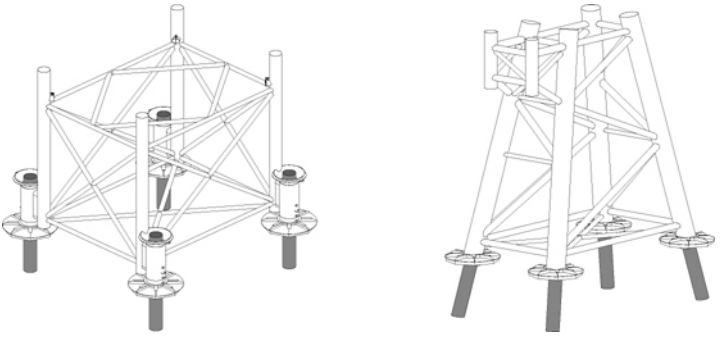

a) skirt piles b) leg piles

FIG. 1. Jacket structure a) with skirt piles and b) with leg piles

A case study dealing with two alternative jacket installation methods is presented, which highlights the importance of engineering innovation in the offshore construction practice. In this application, ground conditions suggested that support of jackets on piles was the only viable foundation solution. In addition, it was envisaged that, for the temporary support of the jackets on the sea floor, each jacket leg would have to be fitted with a permanent steel welded "mudmat". Furthermore, the ground at the locations where the mudmats would be placed would have to be improved. An alternative solution was implemented during construction, which eliminated the need for costly and time consuming ground improvement and mudmats by using temporary reusable brackets and piles.

TYPES OF DEEP FOUNDATIONS IN OFFSHORE JACKET STRUCTURES

The construction sequence of an offshore jacket structure supported on deep foundations includes a series of six high precision steps. According to Gerwick (2000) these are: a) fabrication of steel jacket, b) loading out, tying down and transporting, c) removing from barge, lifting and launching, d) up-ending, e) installation on the sea floor, and f) construction of permanent foundation system. Stationary jacket structures are commonly founded on piles. The type of piles and method of construction depends mainly on ground conditions. Driven steel piles are used, when ground comprises thick soil deposits. Drilled, cast in situ piles are used, when piles are constructed in rock. A combination of drilled cast-in-situ concrete

piles through driven steel casing is employed, when soil deposits overlay bedrock formations.

During the initial temporary placement on the sea floor, the jacket is supported on "mudmats". These are structural steel, or heavily reinforced flat plates, carefully designed to provide proper bearing. Alternatively, the jacket can be supported on temporary piles. It is important that the jacket be level until the permanent foundation piles are installed to avoid introducing high bending stresses in the piles.

Piles are constructed through the jacket legs or the external skirts by either drilling/driving rigs on floating barges or by rigs placed on top of the jacket structure, and connected to the jacket structure usually by grouting the annulus between the pile and the skirt or leg sleeve. The load transfer through grout is enhanced by means of hoops or spiral rebar that are welded onto the perimeter of the jacket leg/skirt to act as shear keys. The load in the permanent situation is transferred as friction between the grout annulus and the shear keys in the jacket to pile connection and as skin friction between the rock and the concrete in the rock socket.

Figures 2 through 5 illustrate various pile construction methods. In fig. 2, steel piles are driven in soil deposits through the jacket leg up to the final depth and are then connected to the jacket legs by grouting and shear keys. Fig. 4 and 5 illustrate two cases where drilled rock sockets are constructed into the bedrock after driving steel casing through the overlying soil layers (fig. 3).

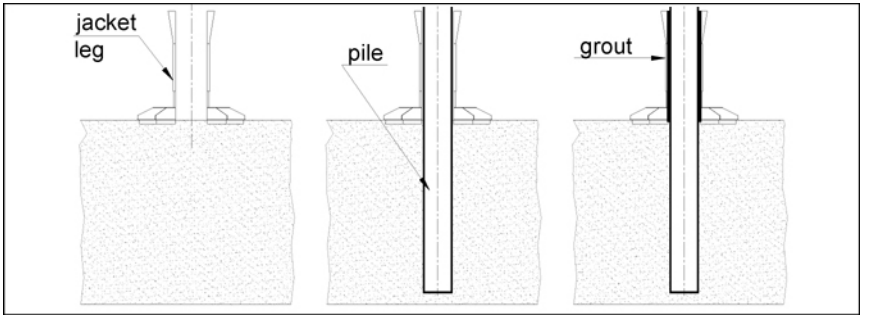

FIG. 2. Driven steel pile through jacket leg into soil deposits

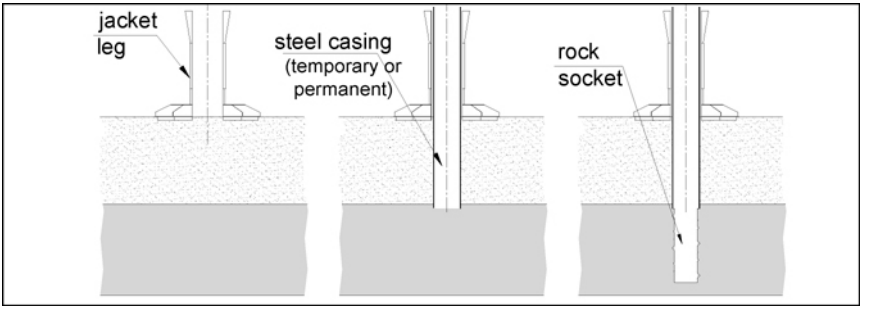

FIG. 3. Construction of rock socket; drilling through jacket leg and steel casing

In fig. 4 the rock socket is filled with concrete, and a steel pile is advanced in the concrete, while it is still fresh. The temporary steel casing is then removed, and the steel pile is connected to the structure by grouting the annulus between the pile and the sleeve. In the case of fig. 5, a cast-in-situ reinforced concrete pile is constructed inside the permanent steel casing used to support the overburden soil while drilling. The permanent steel casing is connected to the jacket leg sleeve by grouting and shear keys.

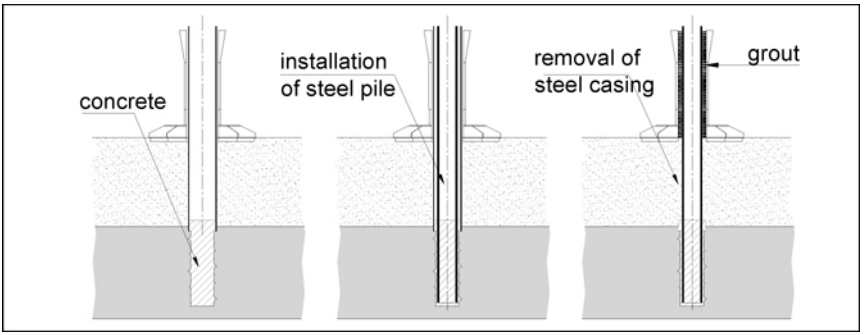

FIG. 4. Installation of steel pile in concrete-filled rock socket.

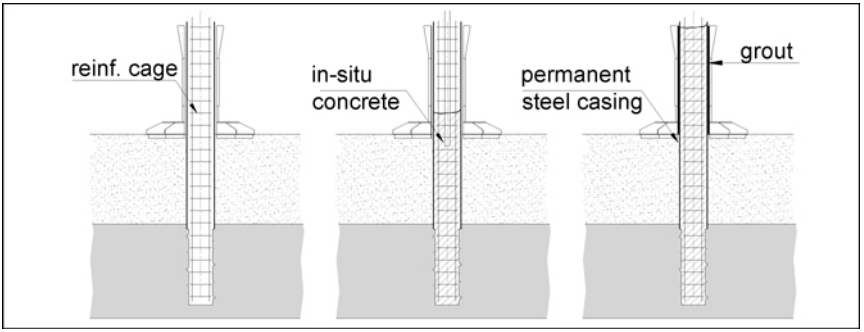

FIG. 5. Construction of R.C. pile connected to permanent steel casing

DESIGN METHODS FOR OFFSHORE JACKET FOUNDATIONS

Foundation design of offshore jacket structures follows the design principles of shallow and deep foundations. Jackets are usually supported on mudmats during initial placement on the sea floor and during construction of the piles through the skirt pile sleeves or jacket legs, whereas they are supported on piles at operation ("in place" condition). The jacket structure during the transient construction stage needs to be firmly supported on the sea floor, to allow for the safe construction of the pile foundation in open sea conditions. Loads exerted on the structure during construction include reduced environmental loads (considering events with a smaller return

period) and loads from construction equipment (e.g., rigs supported on the jacket), which often dictate the design and define the construction procedure.

In addition to the mudmats, it may be required that loose foundation soils are improved to safely sustain the jacket loads. Such methods may include dredging and replacement of unsuitable materials with gravel and preloading of the foundation, vibrocompaction, or vibroreplacement and construction of stone columns, etc.

Foundation design of the jacket on mudmats is carried out with conventional shallow foundation design methods (e.g., bearing capacity equations, settlement calculations). However, potential for differential settlement needs to be thoroughly addressed and considered as a particular loading condition for the modeling of the superstructure.

Jacket foundation design for the "in-place condition" is based on deep foundation design principles. Piles have to be designed to sustain vertical and horizontal loads from the superstructure. The length of the piles is dictated by the applied axial loads. Several methodologies have been proposed in the literature for the determination of rock socket length (e.g., Tomlinson 2001). The skin friction contribution of any loose overburden soil overlying bedrock is usually ignored. The pile tip resistance is also either ignored or scaled down by a large safety factor, since significant displacement is required for its full mobilization. For piles driven in soil deposits, the required embedment depth is determined through driveability analysis. In this case, various design methods based on in-situ testing can also be applied (e.g., API RP-2A). Typical design formulas are presented in table 1.

The lateral resistance of the piles is developed by assuming a depth to "pile fixity" or by the p-y approach (elastic beam supported by non-linear springs). Scour potential needs to be also addressed. The effects of fatigue, corrosion and marine growth are also considered in the structural design of the piles. Design of the foundation includes detailing the connections between steel piles and pile sleeves that transfer the loads from the piles to the superstructure. The grout connections are usually designed after relevant standards (e.g., API RP-2A).

Table 1. Pile design methods – Axial loading

Soil type	Method	Ultimate skin friction
Rock	AASHTO (2002)	$f_{su} = 0.15\ q_u$ for $q_u \leq 1.9$MPa $f_{su} = 0.21\ \sqrt{q_u}$ for $q_u > 1.9$MPa
	Tomlinson (2001)	$f_{su} = \alpha\ \beta\ q_u$, α depends on q_u and β depends on discontinuities in the rock mass
	Fleming et al (1998)	$f_{su} = 1.3\ (p_a\ q_u)^{0.5}$
Clays	API (2000)	$f_{su} = \alpha\ c_u$; α depends on effective stress
Sands	API (2000)	$f_{su} = K\ \sigma'_v \tan\delta$; where K depends on pile type and δ depends on N_{SPT}

CASE STUDY

Several jacket-type platforms were constructed as part of a two-berth expansion of a facility designed to moor and load refrigerated liquefied propane gas carriers, and pentane tankers in the United Arab Emirates. Each new berth comprised a central

loading platform, and several mooring and breasting dolphins. The soil profile in the project area comprises 6.5m ± 1.5m of marine deposits (loose silty sand characterized by 0 ÷ 5 blowcounts at the Standard Penetration Test) underlain by bedrock described as calcarenite, calcareous siltstone with inclusions of gypsum, exhibiting quite high RQD (Rock Quality Designation) values (although the rock mass is termed as weak to very weak based on the unconfined compressive strength determined through laboratory tests).

The initially proposed jacket installation method included dredging level pockets in the sea floor, construction of a gravel pad at the location of each jacket leg and preloading it, fitting each jacket leg with a permanent steel welded "mudmat" (fig. 5a), placing the jacket on the gravel pads, and further preloading at the top of the jacket. The loads during subsequent drilling operations and pile construction are transferred to the foundation layers by the mudmats. A 1,067mm diameter pile steel casing is then driven inside the jacket leg into the top of the bedrock, with a minimal penetration of 0.4m. The annulus between the steel casing and the jacket leg is grouted, thus achieving, in conjunction with shear keys, full collaboration between the two. The rock socket is drilled below the steel casing, the hole is cleaned and the reinforcing cage is lowered into place and concreted through a tremie pipe.

Foundation design included design: a) of the "deep" rock socket for the permanent operation of the jacket and b) of the "shallow" mudmat for the temporary stage of jacket placement on the sea bottom and subsequent pile construction.

The rock socket (900mm diameter and 11m long) was designed using the αβ-method (Tomlinson 2001) along with an average UCS (Unconfined Compression Strength) rock profile (1MPa, 2MPa, and 3MPa at depths 0-3m, 4-7m and >10m, respectively, with linear interpolation in between). Conservatively, the contribution of overburden loose soils and the pile tip bearing resistance were ignored in the calculation of rock socket length.

Foundation design of the jacket for the temporary placement on the sea floor resulted in: a) mudmats of 3.0m diameter, b) dredging 2.8m of the in situ materials (from mudline at -16.0m to -18.8m) and replacement with gravel, and c) preloading of the mudmats. A stepwise preloading scheme was recommended. First the gravel pads should be preloaded with 23ton concrete blocks. Then, after jacket placement on the gravel pads, further preloading would be required via two 40ton blocks on each jacket leg. These measures were required to meet: a) the bearing capacity (calculated according to Brinch-Hansen theory with $\varphi = 36^{\circ}$ for the gravel layer), and b) settlement (due to temporary construction/drilling loads) requirements. After removal of preloading blocks, the temporary platform and the drilling rig would be installed on the jacket for the construction of the foundation piles.

An alternative jacket installation technique was proposed, designed and implemented by the contractor (Archirodon Construction Overseas), in order to eliminate the *permanent* mudmats and ground improvement measures. Such works would be required to deal with the *temporary problems* of jacket stability during jacket placement on the sea floor and of pile construction. The proposed solution involved installation of temporary brackets on the jacket legs to provide support of the jacket on reusable temporary piles (fig. 5b). Brackets included hydraulic jacking devices for accurate level adjustment of the jacket.

Initially, temporary 711mm diameter steel piles were driven in pre-drilled 600mm diameter boreholes, into the seabed by a rig and hammer operating from a jack-up barge. Next, the jacket structure was lowered into the water so that the temporary brackets rested onto the temporary piles, leveled and secured in place by divers. Pile steel casings were then lifted by floating cranes and driven through the jacket legs up to the bedrock. The steel casing was connected to the jacket leg by grouting the annulus between the two. After curing of the grout, a heavy duty platform and drilling rig were installed on the jacket structure and the rock socket was drilled and air-lifted through the steel casing up to the final foundation level (photos in fig. 6 and 7). The reinforcement cage was installed by a floating crane, and the pile was constructed by tremie concreting. The temporary piles and the brackets were then removed to be used for the next jacket.

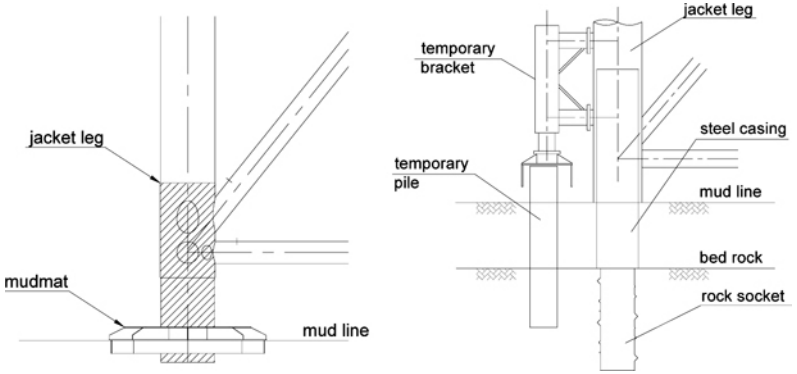

FIG. 5. a) Initial (left) and b) alternative (right) solution for temporary support of steel jacket structure

The alternative installation scheme presented numerous advantages. The costly mudmats were completely eliminated and only reusable brackets with jacking devices and piles were utilized. The installation procedure was accelerated as dredging, placement of gravel and preloading were not required anymore. Safety of the entire operation was greatly enhanced as the time of the unsupported temporary structure in open sea conditions was minimized. Finally, a better control of the construction was achieved through the hydraulic jacks, since deviations up to 300mm could be eliminated by leveling.

CONCLUSIONS

A wide range of piled solutions is available for the foundation of stationary jacket structures. Selection of the proper foundation system depends on ground conditions and requires in depth knowledge of geotechnical engineering and significant construction experience. Adverse ground conditions, extreme design loads, and construction in the open sea require innovative construction, thoroughly engineered solutions. This is highlighted in the case study presented, where a “permanent

solution" involving heavy mudmats and ground improvement to a transient design condition (placement of jackets on the sea floor and construction of foundation piles), was substituted by a "temporary solution" involving temporary reusable brackets and piles.

FIG. 6. Jacket with temporary brackets

FIG. 7. Positioning of drilling rig on temporary platform (left). Drilling rock socket through jacket leg (right)

REFERENCES

AASHTO LRFD (2002). "Standard Specifications for Highways." 17th Ed.

API RP-2A (2000). "Recommended Practice for Planning, Designing and Constructing Fixed Offshore Platforms-Working Stress Design." 21st Ed.

Gerwick, B.C. Jr. (2000). "Construction of Marine and Offshore Structures." 2nd Ed. CRC Press.

Fleming, W.G.K., Weltman, A.J., Randolph, M.F. & Elson, W.K. (1998). "Piling Engineering." 2nd Ed. Taylor & Francis.

Tomlinson, M.J. (2001). "Foundation Design and Construction." 7th Ed. Pearson Education Limited.

Copyrighted Materials
Copyright © 2009 American Society of Civil Engineers (ASCE)
Retrieved from www.knovel.com

Geotechnical Design of a Partially Piled Raft Foundation

Ron Xia[1], Vladimir Dolezel, L. Rak[1], H. Qian[3], B. Rao[1]

[1]McClymont & Rak Engineers, Inc., Markham, Ontario, Canada, L3R 4B5, rxia@mccrak.com
[2]University of Pardubice, Studentska 95, 532 10Pardubice, Czech Republic, Vladimir.Dolezel@upce.cz
[3]Chang-an University, Xi-an, People's Republic of China, qianhui@pub.xaonline.com

ABSTRACT: The paper describes the design of a Partially Piled Raft Foundation (PPRF) adopted under complex geotechnical conditions, in the City of Toronto, Canada. The design of PPRF was governed by lateral soil pressure, unevenly distributed building loads, and non-uniform bearing capacity of foundation soils. Piles were distributed in the area with excessive settlement. Most of the supporting piles were located in the northwest portion of the raft foundation, where high bearing pressure and low soil bearing capacity were encountered. A unit criterion of the proposed settlement has been applied in the design of the raft slab and the piles in order to keep the integrity of the PPRF. Global stability, including sliding and over turning of the PPRF were an integral part of the design. A state of the art computer analysis was utilized.

INTRODUCTION

The High Park project is a medium-density condominium development located in Toronto, Ontario, Canada. Site elevations varied from 101.6 to 102.1 m, along Bloor Street West/Ellis Park Road and step down by approximately 11 m towards the south eastern portion of the site – see Fig. 1.

A three level underground parking was constructed under the entire property. General excavation was about 12 m in depth at the north/west side and about 1 m along southeast boundaries. Since there were no permanent tiebacks/soil anchors allowed to be installed along Bloor Street West and Ellis Park Road, soil pressure of about 140.4 kPa was distributed on the basement wall, along north and west sides.

SUBSURFACE CONDITIONS

Fieldwork for geotechnical investigation consisted of drilling 4 boreholes to maximum depth of 37.4 m. Soil samples were taken using the Standard Penetration

Test (SPT) method. A further examination and characterization of soil samples was carried out in laboratory (Semaan and Rak, 1998). Borehole locations are shown in Figure 1.

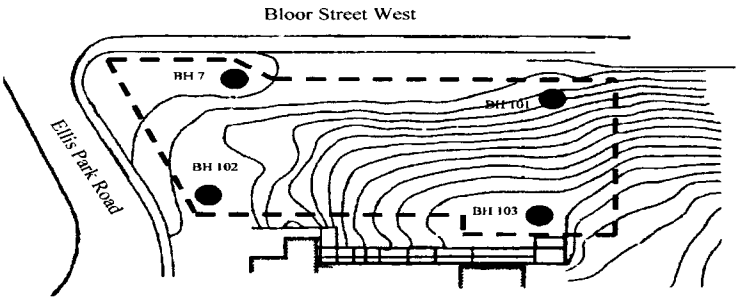

FIG. 1. Site plan and borehole locations

Soil Conditions of the project site can be summarized as follows: *Fill*, about 14 to 14.2 m at north side and 1.7 to 7 m at south side, of dark brown *silty sand to sandy silt* was detected on top of loose to compact fine to medium *sand*. Very stiff, grey *silty clay* extended to depths ranging from 14.6 to 30.0 m. Compact to very dense *sandy silt till*, grey and moist to wet, with inclusions of clayey silt/silty sand and gravelly sand layers, continued to depths ranging from 21.9 to 32.9 m. A lower layer of hard *clayey silt*, grey and moist, was encountered at the top of *weathered shale* at depths ranging from 22.6 to 34.3 m – see Figure 2. The *grey shale* of Georgian Bay Formation, inter-bedded with limestone, extended to the maximum depths of borehole explorations.

Groundwater encountered in open boreholes on completion of drilling, was monitored in observation wells. The depth from surface grade to groundwater, on July 17, 1998, ranged from 10 to 18.3 m (Elev. 80.2 m to 82.4 m).

PARTIAL PILED RAFT FOUNDATION

Based on the encountered subsurface conditions, the partially piled raft foundation was to be constructed on undisturbed native soil and/or on engineered fill, and designed for an allowable bearing capacity of 250 kPa. The strategic use of piles can reduce raft settlements and lead to considerable economy without compromising the safety and performance of the foundation (Poulos, 2000).

The raft slab rests on undisturbed natural sand and lean concrete for an area disturbed during the process of fill removal. The underside of the raft slab elevation varies from 87.90 m at the east end of the raft to 92.00 m at the west end, and has been accomplished by series of steps along the length and width of the raft.

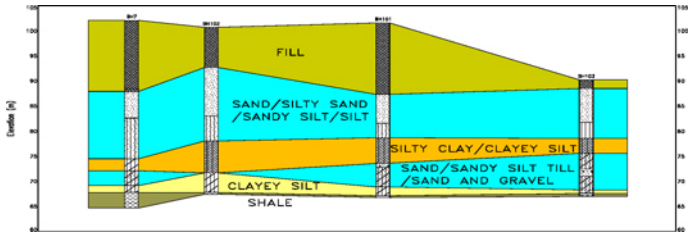

Fig. 2. Stratigraphic profile of subsurface conditions

Footing Pressures q of the raft, during preliminary design, were computed as

$$q = \frac{\sum P}{A} \pm \frac{M_y}{I_x} \pm \frac{M_x}{I_y} \tag{1}$$

Where ΣP is the sum of vertical load combination; A is the area of raft slab; M_x & M_y are the bending moments around x and y axles, respectively; I_x & I_y are the moment of inertias around x and y axles, respectively. To define the total building load P, six load combinations were analyzed for the ultimate and working state of considered dead, live loading and lateral soil pressure.

Potential Settlement of the raft slab (ΔS) was computed as the total of elastic settlement (ΔS_E) and consolidation settlement (ΔS_C) generated from sandy and clayey soils, respectively.

$$\Delta S = \Delta S_E + \Delta S_C \tag{2}$$

$$\Delta S = \frac{1}{E}\int_0^{z1} \sigma_s dz + \int_0^{z2} m_v \Delta\sigma_c dz \tag{3}$$

Here $Z1$ and $Z2$ is the thickness of sandy and clayey soil layers; E and m_v are Young's modulus and the coefficient of volume compressibility; σ_s and σ_c are load bearing stress acting on sandy soil and clayey soil layer, respectively. About 80 nodes were laid out on the proposed raft for footing pressure and settlement analysis. Without piling, the computed settlement for raft foundation was the highest in the northwest corner – about 94.7 mm projected over 20 years. This was due to the footing pressure of about 391 kPa, which was the highest for the entire site.

Piling area was laid out by the comparison of footing pressure and computed potential settlement with the criteria of allowable soil bearing capacity and expected total

settlement. The tolerable magnitude of long term settlement was limited as less than 25 mm for 20 years after completion of construction.

We then back calculated, footing pressure σ_o of the raft foundation, with 25 mm total settlement limit. When comparing the required soil bearing pressure resistance σ with σ_o, the difference $\Delta\sigma = \sigma - \sigma_o$ will need to be supported by piles and the area, where $\Delta\sigma > 0$ will be the anticipated piling area A. In piling area, the total design load Q will be shared by the raft slab and the driven piles $Q = Q_o + Q_P$, and further

$$Q = \int_0^A \sigma_o da + \int_0^A \Delta\sigma da \tag{4}$$

Amount of piles n was defined by total required load Q_P for piles in the piling area, divided by single pile bearing capacity Q_H, and expressed as $n = Q_P / Q_H$.

Here, it has to be noted that the piles have to be designed with tolerable settlement equivalent to the tolerable settlement of raft slab. Ultimate bearing capacity ***R*** of single pile was designed as:

$$R = \sum_{z=0}^{L} C\sigma_{sh}\Delta z + A_t\sigma_t - W_P \tag{5}$$

Where σ_{sh} is the shear stress along the shaft of driven pile; σ_t and A_t are the toe bearing capacity and toe area of the pile, and W_p is the gravity weight of the pile.

GEOTECHNICAL PARAMETERS

Geotechnical parameters for raft foundation design were modulus of subgrade reaction, Young's modulus and coefficient of consolidation settlement (Ulrich, 1988).

The modulus of subgrade reaction is a conceptual relationship between soil pressure and deflection (Bowles, 1996). Considering the encountered consolidation deformation of clayey soils, the modulus of subgrade reaction k_s, was defined as: $k_s = \sigma / \Delta S$ and we have:

$$k_s = \frac{\sigma}{\Delta S_E + \Delta S_C} \tag{6}$$

$$k_s = \frac{k_{sE}\Delta S_E}{\Delta S_E + \Delta S_C} \tag{7}$$

Where k_{sE} is elastic subgrade-reaction.

Young's modulus E is a function of N value of Standard Penetration Test (SPT) data,

and varies with soil type and soil structures. To the same type of soil, Young's modulus' change always follows the N value of SPT. The empirical equation and the correlation with SPT data, for glacial till in the area of Great Toronto Area (GTA), are shown in Figure 3 (Xia et al. 2006).

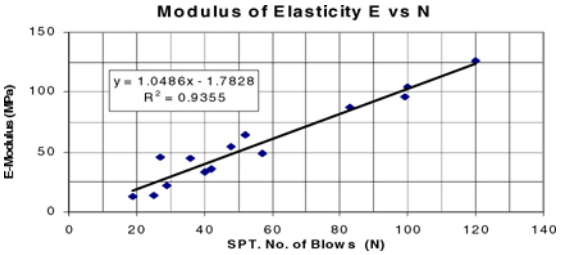

Fig. 3. The Correlation of Young's Modulus vs SPT data (Xia at el. 2006)

Coefficient of consolidation settlement m_v is also defined as coefficient of volume compressibility (Bowles, 1996):

$$m_v = \frac{1}{1+e_o} \cdot \frac{e_o - e_1}{\sigma_1' - \sigma_o'} \tag{8}$$

here e_o and e_1 are void ratios prior to and on completion of settlement; σ_0' and σ_1' are stresses before and on completion of settlement. If m_v and $\Delta\sigma' = \sigma_1' - \sigma_0'$ are assumed to be constant with depth, then consolidation settlement can be calculated as: $s_c = m_v \Delta\sigma' H$, with units of m_v are inverse of pressure (m^2/MN).

FOUNDATION DESIGN

Detailed foundation design was carried out in close cooperation with the project's structural engineers (Fagotto, 2003). Based on the results of preliminary foundation design, a total of 30 H-shaped piles was required in the northwest portion of the raft to reduce potential settlement. The total load shared by piles was 30,000 kN, and was to be spread over 30 piles, each of them with bearing capacity of 1000 kN.

The amount of long-term total settlement, expected to be in the range of 20 to 25 mm with differential settlement to be in the range of 5 to 10 mm, was the focus of the design. It was assumed that approximately, 60% to 80% of the expected settlement would occur within the first 2 years.

A commercial software (SAFE), specifically developed for concrete raft system, was utilized in the PPRF design. Results from the vertical and lateral load analysis were used as input into the SAFE model. Structural foundation and shear walls were incorporated in the Safe analysis.

Since the piles were distributed throughout the area where excessive settlement was expected, settlement of the proposed PPRF varied, along with the various load distribution configurations between piles and raft; hence the modulus of subgrade reaction had to be varied.

Subgrade response was modeled by the variations of footing pressure and settlement distributions. To determination the proper magnitude of the modulus of subgrade reaction, at different locations within the raft footprint, required a very close collaboration of the structural and geotechnical engineers (Ulrich, 1995).

Computer analysis for bearing pressure distribution was conducted by structural engineer through 'SAFE'/Finite Element Method (FEM). Initial modulus of subgrade reaction k_s was supplied by geotechnical engineer according to soil conditions:

$$k_s = k_1 \frac{m + 0.5}{1.5m} \tag{9}$$

Where k_s is desired value of modulus of subgrade reaction for the full-size (or prototype) foundation; k_1 is value obtained from a plate-load test using a 0.3 x 0.3 m or other size of load plate; m is the ratio of length to width (L / B) of a rectangular footing on stiff clay or medium dense sand.

Using computed bearing pressure, soil settlement was calculated without considering the stiffness of raft foundation. Subsequently, the subgrade reaction was updated based on the footing pressure computed by FEM and calculated raft settlement.

By using the updated modulus of subgrade reaction computed for each node, a revised analysis was carried out and a corresponding bearing pressure distribution was laid out. It should be noted that in the updated analysis, the modulus of subgrade reaction variation within the raft foundation, and the effect of piles were coupled – see the simplification in Figure 4.

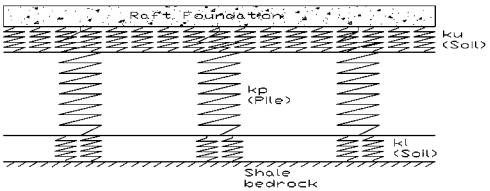

Fig. 4. Plate-on-spring approach of piled raft foundation

Again, using the revised soil bearing pressure, an updated settlement calculation was obtained and new "k_s" value was generated at each node. Using the new modulus of subgrade reaction an updated distribution of bearing pressure was computed – see Figure 5.

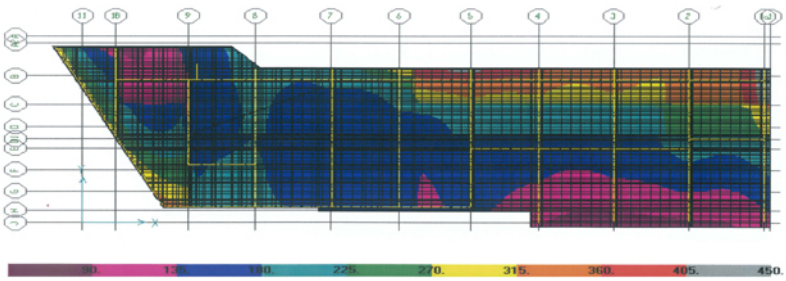

Fig. 5. Computed footing pressure by using FEM program SAFE

In essence, the modus operandi was that by using the soil bearing pressure to compute settlement, and then updating the modulus of subgrade reaction, and repeating the procedure till the computed soil bearing pressure and expected settlement were brought to acceptable range – see Fig. 6.

This convergence was achieved when the soil pressure and displacements, predicted by the finite element analysis, matched the soil bearing capacity and the settlement predicted by geotechnical engineer (Xia and Rak, 2004).

Global stability for the critical sections, incorporating lateral pressure and the proposed structure, was analyzed using the Simplified Bishop Method for circular slip surfaces. A licensed commercial program, SB-Slope, developed by Von Gunten Engineering Software, Inc., Fort Collins, Colorado, was primarily used for the two-dimensional analyses. The minimum Factor of Safety (FS) calculated was about 1.52, which was acceptable according to Canadian Foundation Engineering Manual.

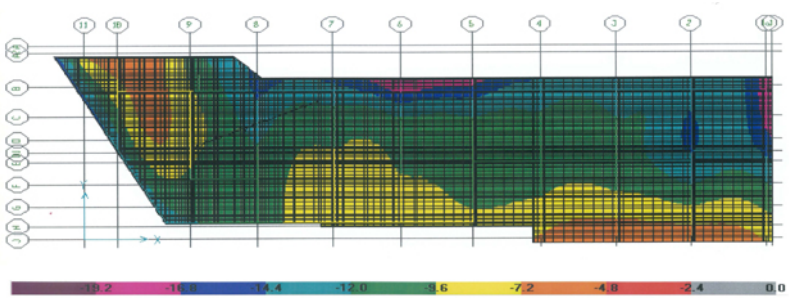

Fig. 6. Computed potential settlement by using FEM program SAFE

DISCUSSION AND CONCLUSION

As soil composition was non uniform and bearing pressure from the structure varied, the computed settlement distribution was also variable. Adding piles, in a critical/heavily loaded area of raft foundation, was an effective way to limit the differential settlement within a tolerable criterion.

Soil conditions, load distribution, quantity and location of piles were important factors in raft foundation design. Subgrade reaction, Young's modulus and coefficient of consolidation settlement prove to be very sensitive parameters in the computer modeling for partial piled raft foundations.

ACKNOWLEDGEMENTS

The authors wish to express their appreciations to Mr. Bill Chiang and Mr. Ossama Yacoub of Urban Development Services of Toronto City and Dr. J. Parslow of McClymont & Rak Engineers, Inc., for their courage and support provided to the research team. Many thanks to Mr. Paul Lildhar for his assistance in the project investigation and field/lab work.

REFERENCES

Bowles, J. E. (1996). "*Foundation Analysis and Design - fifth edition*", The McGraw-Hill Companies, Inc., New York.

Fagotto, D. (2003). "Raft Foundation of Home Condominiums on the Park, 1947 – 1999 Bloor Street West, Toronto, Ontario, Canada." *Report Prepared for the Context High Park Inc.* Read Jones Christoffersen Ltd.

Poulos, H. G. (2000). "Practical Design Procedures for Piled Raft Foundations." *Design Applications of Raft Foundations.* Thomas Telford Ltd, 1 Heron Quay, London, England.

Semaan, G. S. and Rak L. J. (1998). "Supplementary Geotechnical Investigation of a Proposed Residential Development, 1947 – 1999 Bloor Street West, Toronto, Ontario, Canada." *Report Prepared for the First Gulf Development Corporation.* McClyont & Rak Engineers, Inc.

Ulrich E. J. (1995). "*Design and Performance of Mat Foundations.*" American Concrete Institute, P.O. Box 19150, Redford Station, Detroit, Michigan 48219.

Ulrich E. J. (1988). "Geotechnical Considerations in Mat foundation Design", *Soil Structure Interaction*, ASCE, Illinois Section, Chicago 1988, pp 1 – 33.

Xia, Z. J., V. Dolezel, L. J. Rak, B. Rao and J. Chahine (2006). "The Impacts of Construction Dewatering on Surrounding Structures of a Project Site." *Underground Construction and Ground Movement.* ASCE No. 155.

Xia, R. and Rak L. J. (2004). "Geotechnical Design Brief of Home Condominiums on The Park, 1947 – 1999 Bloor Street West, Toronto, Ontario, Canada." *Report Prepared for Context Development Inc.* McClymont & Rak Engineers, Inc.

Copyrighted Materials
Copyright © 2009 American Society of Civil Engineers (ASCE)
Retrieved from www.knovel.com

AXIAL LOAD CAPACITY OF UN-TAPERED PILES IN COHESIONLESS SOILS

Roy E. Olson, PhD, PE, M.ASCE[1] and Magued G. Iskander, PhD, PE, M.ASCE[2]

1 Professor Emeritus, The University of Texas at Austin, Austin, TX 78712
2 Associate Professor, Polytechnic Institute of New York University, Six Metrotech Center, Brooklyn, NY11201, phone: 718-260-3016, e-mail: iskander@poly.edu

ABSTRACT: A method of estimating axial load capacity of driven piles using standard penetration resistances and continuous functions is presented. The accuracy of the method was judged in comparison to predictions made using the API RP-2A method. Space limitations preclude making more extensive comparisons.

INTRODUCTION

Prediction of the axial load capacities of piles driven into cohesionless soils, made prior to driving test piles, utilize static methods. Numerous methods of analysis are in use. Modern methods have often been based on use of quasi static cone tests but the standard penetration test remains widely used and the great bulk of the data in the historical literature utilized standard penetration tests (N values). The continuous function method is based on use of standard penetration tests. For N values to be most useful, the details of the driving system must be standardized. Especially, the hammer energy should be 60% (producing N_{60}) or should be measured and corrected to obtain N_{60}. Unfortunately, the number of published load tests with known values of N_{60} is so small that general fitting for all pile types, load directions, end conditions, soil types, and other parameters is not possible. As a result, we have used the reported N values directly. When values of N_{60} were available (small number of tests), they were used.

It is convenient to compare predictions based on continuous functions and the standard penetration resistances with other methods. Space limitations prevent comparisons with more than one other method. We chose to compare with the American Petroleum Institute method RP-2A in spite of the fact that it was designed for open-end steel pipe piles and in spite of the fact that standard penetration tests are not used offshore, because at least it is a widely known method and because the comparisons can be made using less space than ones based on methods that involve multiple non-linear curves.

Studies of pile load test databases have shown that the margin of error in the

prediction of the static axial load capacities of piles in cohesionless soils is larger than that of comparable piles in cohesive soils (Dennis and Olson, 1983) so we need some way of comparing the accuracy of the continuous function method with some other standard method. We do not propose to deal with questions of whether analyses should use standard penetration or cone data, nor with such questions as how to define the axial capacity of a pile in cohesionless soils, not because such questions are unimportant but rather because of insufficient space.

A serious problem occurs because the parameters used in the continuous function method were derived from a load test data base and then the accuracy of the predictions was determined by comparing predicted capacities with measured values in the same database. However, most of the load tests were also used in development of the API method and thus the comparison of these two methods seems fairer than using some reference method that was based on unknown, and unavailable, load tests.

API RP-2A DESIGN METHOD

The static axial load capacity of a pile in cohesionless soil is the sum of side and tip capacities corrected for the weight of the pile. Side shear is calculated using:

$$Q_S = \sum_{L=1}^{N} f_S C \Delta L = \sum_{L=1}^{N} K \overline{\sigma} \tan(\delta) C \Delta L \qquad (1)$$

where f_s is the local side shear between the pile and the surrounding cohesionless soil, C is pile circumference, ΔL is an increment of pile length, K is the earth pressure coefficient, $\overline{\sigma}$ is the free-field vertical effective stress in the middle of the layer, and δ is the friction angle between the pile and the surrounding soil. Similarly, the tip capacity is calculated using:

$$Q_p = q_p A_p = \overline{\sigma} N_q A_p \qquad (2)$$

where q_p is the net pressure between the pile tip and the subsoil, A_p is the area of the pile tip, $\overline{\sigma}$ is the free field vertical effective stress at the pile tip, and N_q is a dimensionless bearing capacity factor. API RP2A contains upper limits of f_{lim} on f_s and q_{lim} on q_p with the limits imposed to minimize over predicting the capacity of deeply penetrating piles.

The API standard leaves it up to the design engineer to define relative density. We used the standard penetration resistances (N) (ASTM, 2008), reported in source documents, to define relative density. We defined terms for relative density as proposed by Peck et al. (1974). Analyses should use N values corrected for hammer energy but most of the published data have no indication of the actual hammer energy and we chose not to make assumptions about those energies. We used N_{60} if it was available but otherwise used the reported N.

The API (1993) design coefficients (Table 1) are applied with K=1 for closed-end pipes and 0.8 for open-ended pipes, with tension and compression treated as the same.

Table No. 1 – Design Parameters Recommended by the API RP2A

Relative Density	Soil Description	δ deg.	f_{lim} kPa (ksf)	N_q	q_{lim} MPa (ksf)
very loose	sand	15	47.9 (1.0)	8	1.9 (40)
loose	sand-silt				
medium	silt				
loose	sand	20	67 (1.4)	12	2.9 (60)
medium	sand-silt				
dense	silt				
medium	sand	25	81.4 (1.7)	20	4.8 (100)
dense	sand-silt				
dense	sand	30	95.8 (2.0)	40	9.6 (200)
very dense	sand-silt				
dense	gravel	35	114.9 (2.4)	50	12 (250)
very dense	sand				

The API approach, as well as other approaches, have well-known problems which we will not detail here.

DATABASE USED FOR ANALYSIS

A database of about one thousand load tests on piles of a variety of types, and in a variety of soils, was developed for comparison with analytical methods (Dennis and Olson, 1983, Olson 1990). An partially updated version of that database was used for the current study. Although the API method was developed for open-end steel pipe piles, we used it for untapered cast-in-place concrete piles, precast concrete piles, and steel pipe piles, with both open ends and closed ends, and both tension and compression.

STATISTICS

The accuracy of various methods of predicting capacity are reported using the mean ratio of calculated to measured capacity (Q_c/Q_m) and the standard deviations. However, the frequency curves for Q_c/Q_m are log normal so we calculated the mean and standard deviation of $\log_{10}(Q_c/Q_m)$. To put the mean value of Q_c/Q_m into values the profession is more comfortable with, we raised the logarithmic mean to a power of 10 so the desired mean becomes 1.00. Hereafter, "mean" is ten raised to the power of the logarithmic mean, and "standard deviation" is the logarithmic value.

FAILURE CRITERION

Generally, piles in sand do not experience a sudden "plunging" failure, so failure was defined as the peak applied load during the test, but tests were not accepted into the database unless loads reached at least the value defined by Davisson (1973). Displacements at the peak load varied from 15 mm to 250 mm and that wide range doubtless was the source of some amount of scatter in measured capacity, and thus in Q_c/Q_m.

SELECTION OF TESTS

Only load tests where more than 70% of the calculated capacity (based on the API method) came from cohesionless soils were included. For those 132 tests, 98% of calculated side capacity and 100% of calculated tip capacity was from cohesionless soil. No piles that encountered gravel were included. Nineteen tests were in tension and 113 tests were in compression. The breakdown by pile type was: 39 solid precast concrete, 6 solid cast-in-place concrete, 37 open-end steel pipe piles, and 50 closed-end steel pipe piles. The soil profile was entirely cohesionless for 102 tests, and contained clay layers for the other 30 tests. Diameters (widths) ranged from 200 mm to 1 m and penetrations ranged from 3 m to 51 m and averaged 19 m. Fifty one of the tests had reported setup times, which ranged from 2 days to 56 days and averaged 15 days.

The database was subdivided into 75 tests from the United States, 11 tests from Norway, one test from Great Britain, and 46 tests from Japan. The Japanese data were unique in several ways. The source documentation was written in Japanese so there was a degree of uncertainty in extracting the data. Second, Japanese N values came from hammers with higher efficiencies than hammers used elsewhere. Third, some of the Japanese tests probably involved volcanic sands which would have behaved differently from the siliceous sands encountered in the United States and Europe. As a result, the tests from Japan were analyzed separately.

Japanese tests included nine on solid precast concrete piles and 37 tests on closed-end steel pipe piles, all in compression. Their piles ranged in length from 3 to 51 m, and diameters from 200 mm to 1020 mm.

The breakdown of the tests from North America and Europe according to pile types, direction of loading, and end conditions, is included in Table 2 together with the mean and standard deviations for analysis of each data set using the API method.

ANALYSIS USING API METHOD

For the tests in Japan, the mean Q_c/Q_m was 1.00 and the standard deviation was 0.25. Tests with piles from countries other than Japan, with all of the sands assumed to be siliceous and not volcanic, were used in the further analyses (Table 2).

Table No. 2 - Summary of Analyses for Sites in North America and Europe

Pile	Load	End	Number of Tests	Number of Sites	Mean Q_c/Q_m	Std. Dev.
All	Both	Both	87	26	0.74	0.30
CIPC	COMP	CE	6	3	0.39	0.30
CONC	COMP	CE	26	12	0.77	0.22
CONC	TENS	CE	4	2	1.09	0.20
STLP	COMP	CE	33	11	0.73	0.36
STLP	COMP	OE	3	2	0.33	0.12
STLP	TENS	CE	10	4	0.94	0.23
STLP	TENS	OE	5	2	1.03	0.13

Abbreviations used in Table 2 are: All=all options, Both=include both options, CE=closed end, CIPC=cast-in-place concrete (pile driven using a mandrel or on fluted steel casing), CONC=precast concrete, OE=open end, STLP=steel pipe.

There was a significant amount of scatter between measured and computed capacities (Fig. 1) with a range in Q_c/Q_m from 0.15 to 3.19. The logarithmic scale was used to avoid having most of the points in a narrow band of the plot. The lines above and below the middle line show a scatter band with a factor of 2 (Q_c/Q_m=0.5 and 2.0). One source of scatter was the fact that Q_c/Q_m varied with pile penetration (Fig. 2). Further, it was found that multiple load tests on the same site led to small amounts of scatter for that site, but often a wide range in mean Q_c/Q_m between sites, showing that there was an important factor that was held essentially constant for each site but varied between sites. One such factor would be the efficiency of the hammers used in measuring N but numerous other, generally unknown, factors doubtless occurred.

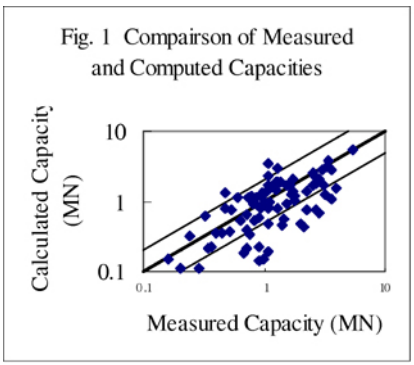

Fig. 1 Compairson of Measured and Computed Capacities

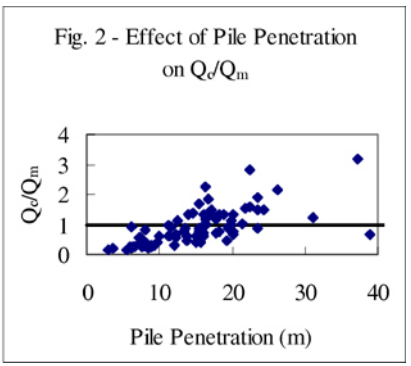

Fig. 2 - Effect of Pile Penetration on Q_c/Q_m

CONCLUSIONS BASED ON THE API METHOD

The API method was intended for use with open-end steel pipe piles so some degree of scatter for other types of piles is expected. The major problem, however, seems to be something fundamental to the method in that Q_c/Q_m varies systematically with pile penetration. In addition, there is scatter because of variations in methods of performing the standard penetration test from site to site.

CONTINUOUS FUNCTION APPROACH

Attempts to obtain estimates of numerical values for δ, K, f_{lim}, N_q, and q_{lim}, from pile load test databases, is difficult because subdividing the database to provide separate analyses based on pile type, soil type, relative density of the soil, direction of loading, end condition (open-end versus closed-end), and a variety of other factors, results in no tests for many categories or, worse yet, multiple tests from a single site, so the researcher can pick parameters that result in $Q_c/Q_m=1$ for that case even if the parameters are illogical, and thus a distorted image of the accuracy of the method results.

An alternative that minimizes such possibilities is to assume some functional relationship, such as:

$$\delta = F_1+F_2 \log_{10}(N) \quad (3)$$

$$f_{lim}= F_3+F_4 \log_{10}(N) \quad (4)$$

$$N_q= F_5+F_6 \log_{10}(N) \quad (5)$$

$$q_{lim}= F_7+F_8 \log_{10}(N) \quad (6)$$

$$K = F_9+F_{10} \log_{10}(N) \quad (7)$$

The assumption of a logarithmic relationship appears to fit the data better than when N is used directly. For lack of a better term we will term this approach the *continuous function* approach.

The parameters are evaluated by first setting up a database of relevant tests and then performing trial analyses to find the best-fit parameters. Generally, it was possible to find hundreds of combinations of parameters that yielded the mean Q_c/Q_m equal to 1.000 and standard deviation less than about 0.02. We had preconceived ideas of reasonable values for the pile/soil friction angle (δ) but we were less certain about values for f_{lim} and q_{lim}. We had ideas for reasonable values of N_q from bearing capacity theory but the theories are generally based on models that do not apply. Similarly, we can estimate values of K from cavity expansion models but such models do not account for the events that happen during pile driving. In the end, we were unable to find a full suite of factors that led to good

predictions with minimal scatter but still yielded what we considered reasonable variations in some parameters with respect to N.

Initially, we split the data into four categories involving tensile and compressive loading, and open ends and closed ends but the number of tests in some categories, e.g., open-ends and compression, was quite small and excellent fits could be obtained but only with unlikely parameters. The result was that we lumped all of the data (132 tests) into a single database and sought parameters that worked best with the whole set of load tests.

Based on our previous studies with a different database (Olson and Shantz, 2004) we assumed that side shear in tension in cohesionless soils was 2/3's of the value in compression, and for open-end piles in compression we assumed that the plug would have perhaps 20% less bearing capacity than a solid tip but the number of tests on open-end piles in compression was too small to allow that factor to be relevant. The resulting equations for the remaining parameters were:

$$\delta^\circ = 10^\circ + 0.12 \log_{10}(N) \quad (8)$$

$$f_{lim}\,(kPa) = 28 + 0.15 \log_{10}(N) \quad (9)$$

$$N_q = 0.1 + 150 \log_{10}(N) \quad (10)$$

$$q_{lim}\,(kPa) = 720 + 75 \log_{10}(N) \quad (11)$$

$$K = 3.1 + 0.15 \log_{10}(N) \quad (12)$$

The mean Q_c/Q_m using the continuous function approach was 1.000 and the standard deviation was 0.17. The scatter was significantly reduced (Fig. 3) compared with scatter for the API method, and Q_c/Q_m did not vary systematically with pile penetration (Fig. 4).

Fig. 3 Compare Measured and Computed Capacities using Fitted Continuous Functions

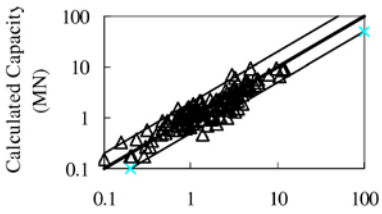

Fig. 4 - Variation of Q_c/Q_m with Pile Penetration

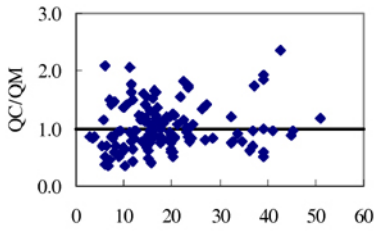

CONCLUSIONS

The following conclusions are drawn from these analyses:

- The number of useful load tests for untapered piles in cohesionless soil is small, especially in certain categories.
- If the parameters in the 1993 API RP-2A are used, the capacities of piles penetrating only a short distance into cohesionless soils are underpredicted whereas the capacities of piles penetrating more than about 20 m tend to be overpredicted.
- A set of properties were found for the continuous function approach which led to mean $(Q_c/Q_m)=1.000$, a small standard deviation, and a Q_c/Q_m ratio that did not vary with pile penetration.
- The continuous function method has the advantage that it is simple to use and the parameters can be adjusted as the database of pile load tests expands.
- The resulting continuous function equations did not fit our pre-conceived ideas, particularly for δ which was lower than expected.

REFERENCES

American Petroleum Institute (1993), "API Recommended Practice for Planning, Designing, and Constructing Fixed Offshore Platforms - Load and Resistance Factor Design RP 2A," API, Production Div., 211 North Ervay, Suite 1700, Dallas, TX 75201

American Society for Testing and Materials (2008), "Standard Test Method for Standard Penetration Test (SPT) and Split Barrel Sampling of Soils", ASTM Designation D1586-2008.

Davisson, M. T. (1973), "High Capacity Piles," *Proc.* Soil Mech. Div., Ill. Section, ASCE, Chicago, pp. 81-112.

Dennis, N. D., Jr., and R. E. Olson (1983), "Axial Capacity of Steel Pipe Piles in Sand," *Proc., Geotechnical Practice in Offshore Engr.*, ASCE Geotechnical Engr. Div. Specialty Conf., Univ. of Texas at Austin, pp. 389-402.

Iskander, M.G. and R.E. Olson (1992), "Review of API Guidelines for Pipe Piles in Sand," *Proceedings*, Civil Engineering in the Oceans V, ASCE, pp. 798-812

Olson, R. E. (1990), "Axial Load Capacity of Steel Pipe Piles in Sand", *Proc.* Offshore Technology Conference, Houston, Paper 6419.

Olson, R. E., and Shantz, T. J. (2004), "Axial Load Capacity of Piles in California in Cohesionless Soils", *Current Practices and Future Trends in Deep Foundations*, ASCE Geotechnical Special Publication No. 125, pp. 1-15.

Peck, R. B., W. E. Hansen, and T. H. Thornburn (1974), *Foundation Engineering,* John Wiley and Sons, NYC.

Copyrighted Materials
Copyright © 2009 American Society of Civil Engineers (ASCE)
Retrieved from www.knovel.com

Analyses of Pile Capacity for Offshore Structures in Hurricane Katrina

Jiun-Yih Chen[1], S.M. ASCE, Britain A. Materek[2], S.M. ASCE, Justin F. Carpenter[3], Robert B. Gilbert[4], M. ASCE, P.E., and Frank J. Puskar[5], P.E.

[1] Graduate Research Assistant, University of Texas at Austin, 1 University Station C1792, Austin, TX 78712-0273; jychen@mail.utexas.edu
[2] Graduate Research Assistant, University of Texas at Austin, 1 University Station C1792, Austin, TX 78712-0273; bmaterek@gmail.com
[3] Graduate Research Assistant, University of Texas at Austin, 1 University Station C1792, Austin, TX 78712-0273; justin_carpenter82@yahoo.com
[4]Hudson Matlock Professor in Civil Engineering, University of Texas at Austin, 1 University Station C1792, Austin, TX 78712-0273; bob_gilbert@mail.utexas.edu
[5]President, Energo Engineering, Inc., 3100 Wilcrest Drive, Suite 240, Houston, TX 77042; fpuskar@energoeng.com

ABSTRACT: This paper presents a case study of pile foundations for two offshore structures that unexpectedly survived in Hurricane Katrina in August 2005. The foundation systems consist of battered, driven steel pipe piles and vertical, driven steel pipes that serve as well conductors. An analysis based on prior exposure (back-analysis) of these structures shows that the actual foundation capacities were significantly greater than the design capacities determined by the American Petroleum Institute (API) design standards for offshore platforms. A parametric analysis of the foundation systems indicates that both axial and lateral capacities had to be increased to explain the survival of these structures. While this work is not fully complete, it does indicate the potential need to update foundation assessment practice, both for offshore and onshore driven pile foundations, based on proof loading of offshore structures during recent hurricanes.

INTRODUCTION

A significant finding from the performance of jacket platforms in major hurricanes, including Andrew (1992), Roxanne (1995), Lili (2002), Ivan (2004), Katrina (2005) and Rita (2005), is that pile foundations perform better than expected (e.g. Aggrawal et al., 1996; Bea et al., 1999, Energo, 2006 and 2007). Jacket platforms are fixed-base offshore structures that are used to produce oil and gas in relatively shallow water, up to a depth of 450 meters (1,500 feet). Driven, open-ended, steel pipe piles are used to support these structures in the Gulf of Mexico.

Assessment of jacket platforms subjected to loads greater than their original design loading has indicated that the capacity of the structural system is sometimes governed by the pile foundation. However, there are no direct observations of foundation damage or failures during these hurricanes and the majority of platform damage and identifiable failures have been observed to occur in the structure above the mudline.

While the lack of foundation failures may be considered acceptable because they are fit for purpose and "conservative," this apparent conservatism is a cause of concern. The conservatism in foundation design can lead to costly construction of new platforms or unnecessary limitations on the manning and production levels of existing platforms. In addition, the engineer might be misled by overlooking more realistic failure modes of the jacket structure above the mudline, if the foundation is unrealistically governing the capacity of the structural system.

PLATFORMS

Two jacket platforms, designated as Platforms A and B, which survived Hurricane Katrina but were expected to fail in the foundation, were chosen for this case study. Platforms A and B are located in 42 meters (137 feet) of water in the Gulf of Mexico and were installed in the mid 1960's. Platforms A and B are eight and six legged jacket structures, respectively, that are connected by a bridge. Jacket platforms consist of a jacket structure with open-ended piles driven into the soil through the jacket legs, which are connected to the platform above the waterline. The 838-mm and 914-mm (33-inch and 36-inch) diameter piles supporting Platforms A and B, respectively, penetrate approximately 43-m (140-ft) into the soil. The wall thicknesses of the piles supporting Platforms A and B are 38 mm (1.5 inches) and 44 mm (1.75 inches), respectively, at the mudline. The piles are battered at 1-horizontal to 8-vertical, with corner piles battered in two directions and edge piles battered in one direction. Platforms A and B are equipped with 18 and 12 well conductors, respectively. The diameters of these conductors range between 508 and 711 mm (20 and 28 inches), with a wall thickness of 13 mm (0.5 inch). They are driven into the soil approximately the same depth as the piles. Both the piles and well conductors are fabricated with A36 steel, which has nominal yield strength of 248 MPa (36 ksi).

SOIL STRATIGRAPHY AND DESIGN PARAMETERS

Geotechnical data for this study were obtained from a boring drilled in 1979 and located 1/2 kilometer (1/3 mile) away from Platforms A and B. It is commonplace in the design of foundations for offshore structures to use soil borings located directly at the platform site. However, when assessing existing platforms, soil borings at the site may not be available and nearby borings may have to be utilized, as is the case for these platforms. The boring was drilled using wire-line percussion methods, and samples of clay layers were obtained by driving thin-walled tubes. The interpreted soil stratigraphy, according to this boring, is presented in Figure 1. The piles supporting Platforms A and B tip in Stratum 5, which is characterized as sandy silt.

The lateral and axial capacities for the pile foundations were estimated for the post-hurricane assessment using the standard of practice for offshore platform design,

API (2000). The relevant design soil parameters developed by the geotechnical engineer are shown in Figure 1. The design undrained shear strength (s_u) profile for clay layers was based primarily on measurements from miniature vane and torvane tests conducted in the sampling tubes. The design parameters for sand layers were developed based on grain size and density estimated from sampler blow counts.

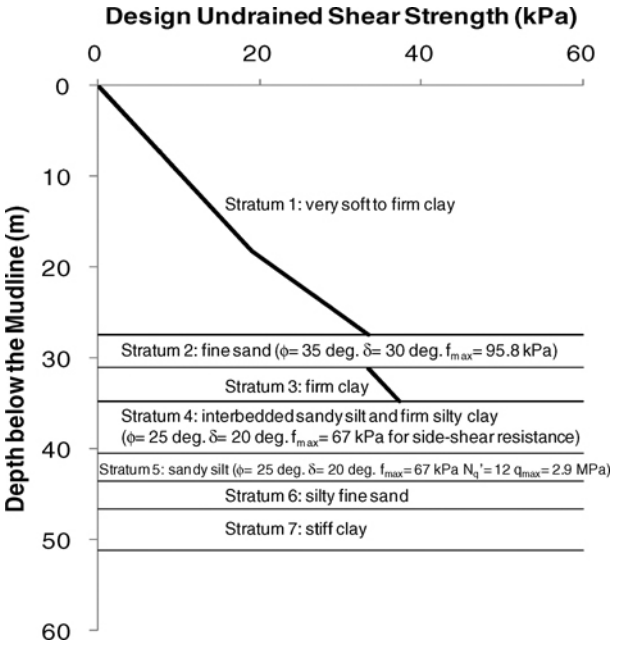

FIG. 1. Soil stratigraphy and design parameters adopted in this study.

MODEL FOR CAPACITY OF FOUNDATION SYSTEM

A simplified plasticity model for pile system collapse, which was originally developed by Murff and Wesselink (1986) and later extended by Tang and Gilbert (1992), was used to predict the capacity of the foundations for Platforms A and B. This model is shown schematically in Figure 2. The jacket structure above the foundation is assumed to be rigid and, thus, can distribute the loads as necessary to develop a full foundation collapse mechanism. The internal work dissipation rate associated with plastic hinges forming in the piles in addition to the piles rotating laterally and moving axially through the soil is calculated. This internal work rate is then compared with the externally applied work rate due to the platform base translating laterally and rotating about a point at the mudline. The difference between

the internal and external work rates is minimized to determine combinations of horizontal force (base shear) and overturning moment that cause a plastic collapse of the foundation system.

This system collapse model was updated for this study to incorporate multiple soil layers and pile wall thicknesses below the mudline. In addition, the contribution of well conductors to the foundation system capacity was included. The wells are modeled as piles that are connected to the structure with rollers (Figure 2) such that the structure can cause the wells to move horizontally but not vertically (that is, the wells contribute lateral resistance but not axial resistance to the foundation system).

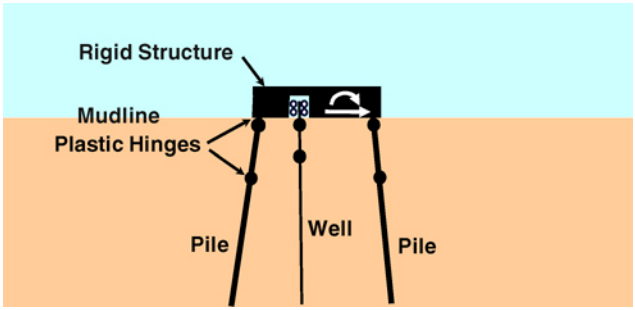

FIG. 2. Schematic of simplified plasticity model for foundation system collapse.

KATRINA PRIOR EXPOSURE (BACK-ANALYSIS)

The maximum wave loading from Hurricane Katrina at the location of Platforms A and B corresponded to approximately 18-m (60-ft) high waves along the long axes of the foundation systems. The maximum load applied to each foundation system is shown in Figure 3 as a horizontal force (base shear) and overturning moment. These loads were established using state-of-the-art methods to estimate waves, winds and currents that occurred during the hurricane at the platform locations and to estimate the resulting forces applied to the jacket structures.

The capacities of the foundation systems for Platforms A and B corresponding to the Katrina wave direction are also shown in Figure 3. The interaction curves show combinations of horizontal force and overturning moment that cause collapse of the foundation systems based on the simplified plasticity model. There are three regions of behavior on the interaction curves. In Region 1, the failure of the foundation system is dominated by shear and piles are failed laterally. The capacity increases with increasing overturning moment in Region 1 due to the batter of piles (Figure 3). In Region 3, overturning is the dominant failure mode and piles are failed axially by pulling out or plunging into the soil. A combined shear and overturning failure mode is characteristic of Region 2. The validity of the results from the simplified plasticity model was evaluated by comparing them to results from a three-dimensional finite element model (3-D FEM), developed using the computer software SACS®, in which the entire structural system was modeled. The results from the simplified model agree

well with those from the more complicated finite element model (Figure 3).

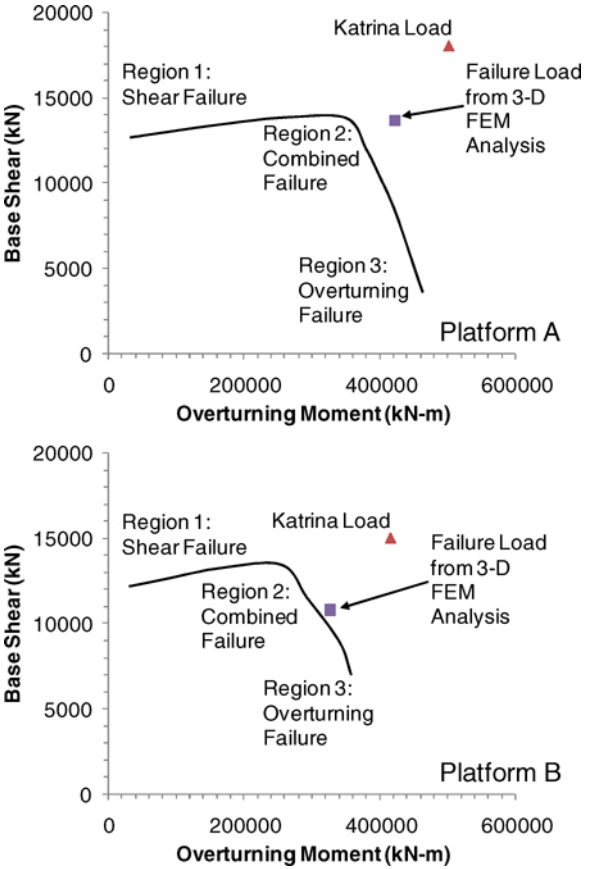

FIG. 3. Foundation system capacity interaction curves.

The Katrina loads exerted on the foundation systems of Platforms A and B were well above the estimated capacities (Figure 3). However, both platforms survived Hurricane Katrina with minimal damage and no indication of movement or failure in the foundation systems. Therefore, the actual capacities for these foundation systems in the hurricane were significantly greater than the capacities estimated using the existing API standard of practice for design.

PARAMETRIC ANALYSIS

In order to investigate the apparent discrepancy between actual and design

(estimated) capacities for these foundation systems, a parametric analysis was conducted. A set of multipliers were used to increase the axial and lateral soil resistance beyond their design values for each pile in the system. The multiplier for the axial soil resistance, NQ_{ax}, was applied to the design values for both the unit side shear and unit end bearing. The multiplier for the lateral soil resistance, NQ_{lat}, was applied to the design values for the ultimate unit lateral resistance (note that this multiplier applies to the piles and the wells). For example, a combination of NQ_{ax} equal to 2.0 and NQ_{lat} equal to 1.0 means that the total axial capacity of each individual pile in the system is doubled while the lateral capacity of each individual pile is the same as the design case. These multipliers were selected by trial and error in order to increase design (estimated) foundation system capacities beyond Katrina loads. Results from the parametric analysis are shown in Figure 4.

The actual axial pile capacity for these two platforms is significantly greater than the design value (Figure 4). A multiplier of at least 1.5 on the axial capacity is needed to explain the survival of these platforms in Hurricane Katrina. This result is consistent with similar analyses of offshore platforms in Hurricanes Andrew (Aggarwal et al. 1996) and Roxanne (Bea et al. 1999). One unique aspect of Platforms A and B in comparison to earlier studies is that the axial capacities of the piles for these platforms are governed by side shear and end bearing in sand layers versus clay layers (Figure 1). Based on the design values, the sand layers contribute 70 percent of the total axial capacity. In addition, the contribution of end bearing is 30 percent. In contrast, the end bearing for a typical offshore pile in a marine clay deposit contributes less than 10 percent of the total capacity. Therefore, the collective hurricane experience indicates that there is an apparent conservatism in the design method for the axial capacity of driven piles in both sand and clay. Potential sources for this conservatism include limitations in the empirical design methods due to limited data used in their development, rate-of-loading effects due to the relatively short-term load applied by a wave over a duration of several seconds, aging effects due to set-up between the installation of these piles and the hurricane loading in 2005 and conservative biases in how design parameters were established. Bea et al. (1999) provide a detailed discussion of these issues for piles in clay.

The actual lateral pile capacity for these two platforms is also significantly greater than the design value (Figure 4). For Platform A, the survival of the structure in Hurricane Katrina cannot be explained by increasing the axial capacity alone. In this case, a multiplier of at least 2.0 on the design lateral capacity is needed. This resulting bias is greater than those estimated from Hurricanes Andrew (Aggarwal et al. 1996) and Roxanne (Bea et al. 1999). Had the contribution of well conductors not been included, this multiplier would have been greater than 2.0. These differences underscore that the hurricane loads only provide proof loading information and do not help determine the ultimate capacity when the foundations do not fail. However, this proof loading allows one to investigate the sources of conservatism and begins to justify the need to develop a specification for assessment of existing pile foundations.

There are several factors that could contribute to the discrepancy between the actual and design values for the lateral capacity. The lateral capacity is governed by the soil resistance in clay between the mudline and a depth of about 15 m (Stratum 1 in Figure 1). More than doubling the undrained shear strength would be required to

produce a multiplier of 2.0 on the design lateral capacity, even if the higher lateral resistance corresponding to static (versus cyclic) loading in the design method was used. The lateral capacity of a pile can also be increased by increasing the moment capacity of the steel pipe. The most likely mechanism for increased moment capacity is related to the lateral connection between the piles and the jacket legs. The jacket legs can penetrate below the mudline, increasing the effective moment capacity of the piles, which is not always accounted for when determining foundation capacity. In addition, the well conductors contain inner pipes with grouted annuluses (casing strings) that can effectively increase their moment capacity below the mudline. This is not typically accounted for when determining foundation capacity because the makeup of the inner pipes and grouting is not always known for older structures.

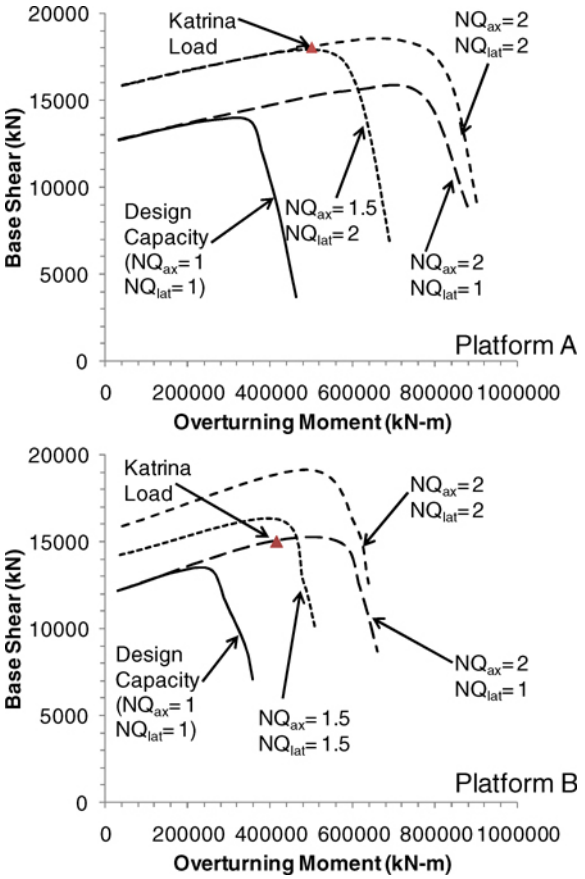

FIG. 4. Parametric results for foundation system capacity interaction curves.

CONCLUSIONS

A back-analysis of the pile foundation systems for two offshore structures that survived Hurricane Katrina shows that the actual foundation capacities were significantly greater than their design capacities. A parametric analysis indicates that both axial and lateral capacities need to be increased by factors up to 2.0 to explain the survival of these particular structures. The results in this paper expand upon findings from similar analyses of structures following previous hurricanes. A conservative bias in axial capacity has now been observed in hurricane loading for driven piles in both sand and clay. In addition, the conservative bias in lateral capacity is even higher than previously observed because Hurricane Katrina produced the largest waves of any hurricane in recent history. This work highlights the potential to update assessment practice, both for offshore and onshore pile foundations, based on proof loading of offshore structures during hurricanes.

ACKNOWLEDGMENTS

This work is supported by the American Petroleum Institute and the Minerals Management Service. Aditya Hariharan and Sean Verret of Energo Engineering, Inc. have been instrumental in providing information. Prof. Gilbert acknowledges the financial support of the Hudson Matlock Professorship Fund. The views and opinions expressed herein are those of the authors alone and do not reflect any of the organizations, parties or individuals who have supported the work.

REFERENCES

Aggarwal, R.K., Litton, R.W., Cornell, C.A., Tang, W.H., Chen, J.H., and Murff, J.D. (1996). "Development of pile foundation bias factors using observed behavior of platforms during Hurricane Andrew," Offshore Technology Conference, OTC 8078, pp. 445-455.

American Petroleum Institute (2000). *Recommended Practice for Planning, Designing and Constructing Fixed Offshore Platforms – Working Stress Design*, API RP 2A-WSD, 21st edition.

Bea, R.G., Jin, Z., Valle, C., and Ramos, R. (1999). "Evaluation of reliability of platform pile foundations," *Journal of Geotechnical and Geoenvironmental Engineering*, ASCE, Vol. 125, No. 8, pp. 695-704.

Energo Engineering, Inc. (2006). *Assessment of Fixed Offshore Platform Performance in Hurricanes Andrew, Lili and Ivan*, Final Report to MMS.

Energo Engineering, Inc. (2007). *Assessment of Fixed Offshore Platform Performance in Hurricanes Katrina and Rita*, Final Report to MMS.

Murff, J.D. and Wesselink, B.D. (1986). "Collapse analysis of pile foundations," 3rd International Conference on Numerical Methods in Offshore Piling, Nantes, France.

Tang, W.H. and Gilbert, R.B. (1992). *Offshore Pile System Reliability*, Final Report to API (Project PRAC 89-29).

Copyrighted Materials
Copyright © 2009 American Society of Civil Engineers (ASCE)
Retrieved from www.knovel.com

H-Piles Selected for New Power Plant Based on Pre-Award Testing Program and Cost Comparison

Kenneth Bell[1], PhD., P.E., F.ASCE Scott Newhouse[2], P.E., M.ASCE
Jeff O'Neal[3], P.E., M.ASCE

1. Chief Engineer Geotechnical Services
2. Senior Engineer Geotechnical Services
3. Engineering Group Supervisor Civil Engineering Group

Bechtel Power Corporation
5275 Westview Drive
Frederick, MD 21703

ABSTRACT

Detailed site investigation for a large power plant project in the mid-west US indicated that the heavily loaded and settlement sensitive plant structures would require deep foundations, and that the piles would need to be driven or drilled to the top of rock. Based on preliminary estimates and design calculations it was determined that the project would require upward of 5,000 to 6,000 piles. In order to determine the most economical pile solution it was decided to conduct a pre-award load testing program. The main goals of the program were to determine the variation in driving lengths across the site and the pile capacity that could be obtained by driving various size H-piles to rock. During the installation all piles were tested using dynamic testing (PDA), which was then followed by static load testing. The results of the testing were then reviewed to determine the pile that would provide the highest capacity at the least cost (tons/$). The tested H-piles were compared to Auger Cast Piles (ACP) that would be drilled to the top of rock. Based on evaluation of the tons/$ for the various H-sections and ACP, the project elected to go with driven H-piles. Design proceeded with two pile loading capacities: 1070 kN capacity pile using an HP 10 x 42 and 1780 kN capacity pile using an HP 12 x 74. The project is now under construction; the pile installation was recently successfully completed.

INTRODUCTION

The project entails construction of a large coal-fired power plant. The plant components include boilers, turbines, a stack, and extensive coal handling structures, all of which have heavy foundation loads. The site soil profile consists of a thick layer of clay above bedrock, as illustrated on Fig. 1. Engineers determined that the medium consistency of the upper clay would effect intolerable settlement for shallow

foundations for the heavy plant components. Thus, the design team decided on use of deep foundations of driven piling. The decision to use piling for the major foundations entailed the placement of over 5,000 piles. The piling works added a significant cost to the project with an increase to the overall project construction schedule. Ensuring the most cost and schedule effective foundation required choosing the type of pile or piles to be used and the related details:

- Diameter/size
- Capacity
- Length
- Spacing

SITE EXPLORATION, EVALUATION/ANALYSIS, DECISION TO USE PILING

Figure 1, as shown below, illustrates the typical soil conditions determined from the site exploration. The profile consists of clay soil extending to depth of 9 to 15 m. The clay consistency is typically medium from the surface to depth of near 5 m, and stiff below 5 m. Bedrock is shale or sandstone; exploration showed sandstone prevalent on one side of the site and shale prevalent on the other. Groundwater level in the exploration was typically initially encountered in bore-holes at depth of 5 to 6 m; the level would then rise in an open bore-hole to within 0.6 to 1.5 m of the ground surface.

Settlement analysis based on this profile for mat foundations with bearing pressure of about 190 kPa, which would be required, indicated unacceptable foundation settlement. Based on settlement and bearing capacity of saturated clay of medium consistency, engineers concluded that mat foundations were not cost effective, and deep foundations would be required..

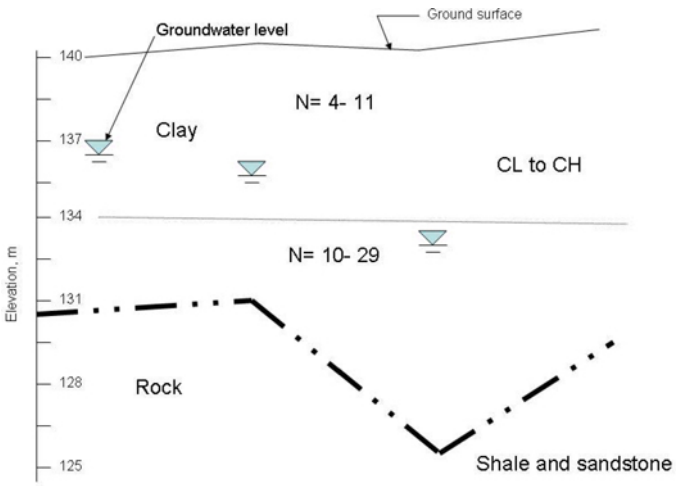

Fig. 1. Site Soil Profile

The choice of deep foundations - piles or piers was made based on company experience with similar soil profiles. With rock at depth 12 to 15 m, and clay soil above the rock that would allow driving or drilling piles, company experience suggested use of piles bearing on rock. The evaluation process is described below.

Piling Options

Pile types considered included:

- Driven closed-ended pipe piles, concrete filled after driving
- Auger Cast Piles (ACP)
- Drilled piers.
- Precast, pre-stressed driven concrete piles
- Driven H-piles

Driven closed-ended pipe piles

Initial evaluation indicated that steel H-Piles would have cost and schedule advantage over closed-ended pipe piles. Therefore, they were not considered as a viable option.

Precast Concrete Piling

This type of pile is a displacement type pile; it prompted concern about heaving of the soil between piles, especially at the projected spacing of 1 to 1.5 m. It should also be noted that the effort (time and money) required to cutoff a steel H-pile versus a concrete pile is typically considerably less. Typically for a precast concrete pile it is necessary to cut away the upper portion of the pile after driving to expose the rebar and tendons (if pre-stressed) in order to tie into the foundation. With a steel H-pile the top of the pile can easily be burned off and any required tension connection of the pile cap to the pile can easily be accomplished by burning holes through the flanges of the pile to allow the bottom mat of rebar to go through the piles, or adding a tension pile cap. In addition, when there is damage to the top of a concrete pile it becomes necessary to cutoff the pile below the planned final cutoff elevation and locally thicken the foundation.

The other concern with the precast concrete piles and driving the piles to refusal is the high risk in over stressing the piles when they reach the rock. When driving piles to rock, particularly when the driving goes from fairly easy driving to refusal in a very short distance, there is an extremely high risk of damaging concrete piles when hitting the rock. Pile driving logs often show that the driving resistance (blow count) increases significantly within a matter of inches. Pile driving logs from one recent project with a similar soil profile showed the blow count abruptly increase to almost 200 blows per 300 mm, which could have easily damaged the precast pile when it hit the rock and the driving resistance increased this quickly.

Company experience involved widespread use of precast concrete piles under the right soil conditions. These piles have worked very well when used, which was always under conditions where we were trying to develop friction in either a clayey soil or a dense sand and gravel. Company experience did not include precast piles driven to rock.

Auger Cast Piling (ACP)

Evaluation identified several disadvantages regarding use of ACP, as listed below:

- Grout used for construction of these piles would require a cure time
- Similar to the concern with drilled piers, cold weather will affect installation time, negatively affect quality control, and increase the cost of these types of pile
- No way to be sure (other than additional load testing of individual piles) that individual production piles will have the capacity of the original test piles
- Quality control after placement, e.g. potential for "squeezing" or "necking" along their length
- ACP cannot extend above grade without significant effort.

Driven H-Piles

When driving piles to end bearing in rock, a pile that provides the highest allowable structural capacity per pile is desirable; company experience held that it was provided by a steel H-pile. When the entire load on the pile is being transferred as end bearing

into the rock one would want a pile that provides the greatest ability to do so. The only reason this has come into some question lately is related to how the price of a steel pile has escalated more than the cost of concrete pile, although the cost of concrete piles has seen some increase in cost due to the requirements for reinforcement and prestressing strands.

There have been many recent studies when evaluating a pile foundation, one should not strictly look at the cost per pile, but should be really looking at cost per ton of capacity. Recent papers have presented data that show the cost per ton of capacity decreases with the increased allowable load per pile (Komurka, 2006). This function indicates that the most economical foundation would be one that maximizes the structural capacity of the pile while trying to match the soil-pile interaction capacity. Again this is most easily achieved by using a steel H-pile when driving piles to end bearing in rock. The effective use of a steel H-pile should result in the need for fewer piles to be used than precast concrete piles.

One of the other advantages of steel H-piles is that it is easy to vary the pile section based on the specific loading needs at various locations on the project to optimize the design and minimize the cost. For example, on another recent project, design engineers used four different steel H sections based on the required pile capacity, which varies anywhere from 890 up to 1960 kN. Varying the size of the pile is much easier and more economical for steel H-piles than with precast concrete piles.

Additional reasons for selecting driven H-piles include:

- Because of high capacity achieved with small width of pile, for 3 diameters (3D) spacing, can support very high foundation loads.
- No concrete involved during installation, a notable advantage for the planned winter pile installation.
- No cure or waiting time to start pile cap construction as would be required for ACP or concrete filled pipe piles.
- Easy to handle piles without overstressing.
- Easy to cut off and weld on, when required. Thus, can easily adapt to varying top of rock elevations.
- Verifiable capacity achieved by driving to refusal (or virtual refusal) in bedrock.
- PDA testing of H-piling during driving coupled with hammer performance information ensures production H-piling is meeting or exceeding the capacity of the original test pile.
- Driven piles can be driven in natural sequence rather than skipping alternate piles as might be required with ACP, thus minimizing the moving of the equipment and speeding installation, especially where piles are placed in a tight cluster under the heavy columns
- Driven pile installations usually produce no spoils for removal and therefore no exposure to, or costly disposal of, potentially hazardous or contaminated materials. The site is left clean and ready for the next construction activity.

Drilled Piers

Evaluation indicated that design of the pile/pier cap using drilled piers would entail added volume of concrete compared to a pile foundation. The main factors effecting decision not to select drilled piers were:

- Added volume of concrete in the cap.
- Requirement to place concrete during winter months for construction.
- Concerns regarding equipment access- much greater effort for access was identified to get pier drilling equipment onto the building footprints.

H-Piles versus ACP

Selection narrowed to H-Piles and ACP for reasons discussed above. The project engineers had to choose between these two options based on cost and schedule. The piling subcontractor stated that "We believe there are significant opportunities to lower and optimize the material costs for the H-pile material by utilizing techniques to match the allowable pile loads to the structural loads. We also believe that higher allowable pile loads may be achieved through the testing program, thus lowering the material costs per allowable ton of installed H-pile."

DEVELOPMENT OF LOAD TEST PROGRAM

Project engineers selected H-piles for a load testing program. The piling subcontractor proposed section/shapes based on availability, cost, and projected ability to sustain required design load; these included: HP 10 x 42, HP 12 x 63, HP 12 x 74. Project engineers accepted the proposed piling and the load testing commenced. All static and dynamic load testing was conducted in accordance with applicable ASTM standards. The load test had 2 test pile groups for each of these HP section/shapes. The groups were placed on opposite ends of the site. For one of the groups rock was predominantly sandstone; for the second test group at the other side of the site rock was predominantly shale. The piling subcontractor designed the test pile groups. Installation of the test pile groups included PDA tests on reaction piles to develop driving criteria. These criteria were then applied to driving the test piles. Test piles were driven to rock using a Delmag D46 hammer for HP 12 section piling, and a Delmag D30 hammer for HP 10. The HP 12 piles were fitted with hardened driving shoes (the HP 10 piles were driven without shoes). The test piles were driven to criteria established to maximize capacity while limiting stress in the pile to 90% of yield strength. Static load tests were run for compression, tension and lateral load for each of the section/shapes at each of the 2 test group locations. Test load for compression was developed from capacity estimates using WEAP prior to the test program. Capacity for tension and lateral load was established prior to the load testing program based on project requirements, 890 kN tension and 90 kN lateral load. Test load was applied at twice the design load.

LOAD TEST RESULTS

Project engineers determined compression capacity of the test piles from the load-deflection plots using Davisson's method; Table 1 lists this capacity as Q_{ult}.

Applying factor of safety and corrosion effects, project engineers then developed the recommended design loads indicated in Table 1 as Q_{rec}. Table 2 summarizes the measured deflections during load testing.

Dynamic PDA testing and resulting CAPWAP analysis indicated ultimate compression capacity that agreed well with results of static load testing. Dynamic testing indicated that pile stress during driving was typically about 92% of the yield strength. Dynamic testing did not accurately predict tension capacity; test piles showed capacity exceeding 890 kN, where dynamic testing indicated tension capacity of 396 to 672 kN for 3 of the 4 tension test piles. For the remaining fourth tension test pile, dynamic testing indicated capacity of 1308 kN; static load testing of this test pile showed capacity greater than the maximum test load of 890 kN.

TABLE 1. RECOMMENDED H-PILE COMPRESSION CAPACITY

Pile Shape/Section	Location	Q_{ult}, kN	Q_{all}, kN	Q_{rec}, kN
HP-12 x 74	Boiler	>4000	2000	1780*
HP-12 x 63		2935	1468	1335*
HP-12 x 74	Chimney	3630	1815	1600*
HP-10 x 42		2562	1281	1070*

*Values are reduced due to corrosion effect

TABLE 2. MEASURED PILE HEAD DEFLECTION DURING LOAD TESTING

Pile Shape/Section	Location	Max test load, kN	Deflection (cm)	
			Max (@ max test load)	Min. (after un-loading)
HP-12 x 74	Boiler	4090	2.8	0.2
HP-12 x 63		4090	3.6	1.0
HP-12 x 74	Chimney	3915	4.1	1.8
HP-10 x 42		2670	4.8	2.8

PRELIMINARY PILE DESIGN

Based on the results of the load testing program, the project engineers developed preliminary pile design structural capacity to maximize the pile allowable capacity (geotechnical capacity) and to minimize the required number of piles. Design was controlled by compressive capacity and by lateral load capacity to sustain both static loading and earthquake loading. Preliminary design allowed quantifying the total number of H-Piles according to section/shape and length. Bids were then solicited from piling contractors based on the quantity determined by preliminary design.

ACP Pile Design and Bids

Project engineers also developed bid documents for ACP. They bid this alternative in order to determine the pile type- H-pile or ACP that had the lower construction cost. The bid package also required the bidder to submit a preliminary

design. Ideally the ACP design would be based on load testing. However, load testing was not performed. There was not sufficient time or budget to support a second load test program on ACP. Consequently ACP pile capacity was established by analysis. Using predicted compression and lateral capacities, engineers determined the total number of required piles for use in bidding/cost evaluation. For bid purposes engineers used a common ACP diameter of 41 cm and a length based on depth to rock established by exploration, and assumed capacity of 1025 kN (based on analysis-predicted capacity).

SELECTION OF H-PILES

Bids for both piling types, H-piles and ACP indicated that H-Piles had advantage in both cost and schedule. Accordingly, final design proceeded based on H-Piles. For final design, design engineers chose 2 of the 3 section/shapes tested:

Pile	Design Load- Compression (kN)
HP 10 x 42	1070
HP 12 x 74	1780

Construction plans were prepared based on these design loads and production piling commenced. Piling work was recently completed. The piling work went smoothly with few problems and defects encountered. Engineers encountered challenges at times during construction in developing driving criteria for the lighter pile, HP 10 x 42, that maintained capacity without causing over-stress during driving. Engineers used PDA testing during construction to develop the driving criteria and change them to match change in ground conditions as work progressed.

SUMMARY

Project engineers used geotechnical analysis to identify the need for a deep foundation. They identified the optimal deep foundation based on company experience with similar soil profiles, and by evaluating the alternative foundation types. Detailed design was based on a load test program. Project engineers sought to maximize pile capacity and tons/$. The use of H-piles and load testing allowed customizing the pile design, matching capacity with demand. This approach creates an efficient foundation; pile capacity is customized to meet demand without expending cost on surplus capacity.

REFERENCES

Komurka, V. (2006). "Deep Foundation Support-Cost Components." *Proc., 7th Annual DICEP Conference and DFDTA Course, Pile Driving Contractors Association 2006, Design and Installation of Cost Efficient Piles and Deep foundation Dynamic Testing and Analysis* (CD-ROM), PDCA, Orange Park, FL.

Copyrighted Materials
Copyright © 2009 American Society of Civil Engineers (ASCE)
Retrieved from www.knovel.com

Driven Pile Foundation in the Offshore Fields of Qatar: Installation Problems, Challenges, and Potential Solutions

Waddah Akili Ph.D., P.E., M. ASCE

Professor of Civil Engineering (Retired), Principal, Geotechnical Engineering,
3222 Evergreen Rd. Ames, Iowa, email:w.akili@isunet.net

ABSTRACT

This paper addresses discrepancies between design of driven steel pipe piles for offshore platforms in Qatar, the Arabian Gulf, and their "as-installed" ultimate capacities and safety factors. The paper evaluates "as–installed" ultimate capacities and safety factors and recommends remedial installation procedures when piles refuse before design penetration is achieved. This case history offers guidance for installation of future offshore structures in the Region, thus gaining an added margin of confidence regarding the ultimate capacity of installed piles.

INTRODUCTION

The State of Qatar, situated on the southern shores of the Arabian Gulf, has - over the last two decades – experienced an unprecedented offshore construction boom, including design and construction of platforms, to facilitate the production and transport of its oil and gas. As noted by Akili (2004), much of Qatar's offshore "earthly" deposits (soil and rock) comprise calcareous soils, overlying diagenetic limestones interbedded with dolomites, marl and shale. Borehole data, derived from offshore sites, asserts that ground conditions for pile installation are highly variable. Ground variability plus inadequate soil investigation, results in misassessment of the insitu conditions, leading often to a huge discrepancy between ultimate pile capacity based on design, and actual capacity after installation. Obtaining valid samples and proper geotechnical data were affected, to a great extent, by the same difficulties that later affected installation. All of the piles reported on here, were installed under the extreme exigencies of the situation, and at serious over-runs of cost and time.

Driven piles in these deposits have, by and large, met refusal short of design penetration. In many cases, refusal was of an abrupt nature. The abruptness is a clear indication that the piles encountered resistance unaccounted for, such as: a rock layer, cemented soil layer, a boulder, or hard clay. Discrepancies may have also arisen from processes related to the construction of the piles, i.e., either inadequate construction control or from inevitable consequences of pile installation activities. Also, as noted by Poulos (2005), structural defects of the pile such as: size, strength, or stiffness

being less than assumed in design, do adversely affect outcome. The main difficulties are that the designer does not recognize the existence of the imperfections during the design process, or else they may only become manifest beyond the design process. Subsequent analysis has become a "must" remedial or, else, a forensic exercise.

PILE INSTALLATION: THE STATUS QUO

This paper focuses on installation and resulting discrepancies of driven pipe piles in the offshore of Qatar derived from fourteen platforms (three piles per platform), located 40 miles east of Doha, the capital of the State, in three adjacent fields: Idd El Shargi, Bul Hanine, and Maydan Mahzan, referred to here as: Fields No.1, 2, and 3.

Pile Driving and Related Information

Pile design penetrations - for the case reported on here - were, unfortunately, based on insufficient borehole data (i.e., number of borings were much smaller than required). Piles used on the jackets are 30 inch diameter open-end pipe piles with variable wall thickness. The minimum wall thickness was 1.0 inch and the piles were equipped with 10 ft long 1.5 in. wall thickness driving shoe. Design penetration has ranged from 270 to 190 ft. Hammers used for driving were the Vulcan 020 and the Vulcan 040.Typical blow count versus penetration is shown in Fig. 1. The blow count data presented is approximate and intended to reflect the character of pile driving. Fig.1 is typical, and reveals: i) the erratic behavior and extreme variability of blow counts as a function of penetration due to resistance encountered during driving, ii) welded sections and time delays (in hours) to finish welding the new section to the previous, and, iii) location and extent of pilot holes using 30 inch diam. underreamer.

The pile shown in Fig.1, as an example, met refusal twice, resulting in the drilling of two pilot holes. Refusal was first met at 238 ft penetration. As a consequence, the soil plug was drilled out and a pilot hole was advanced to 253 ft penetration. The pilot hole (Fig.1) was underreamed to 30 inch diameter from approximately 238 to 248 ft. Pile driving continued, but abrupt refusal was encountered again at 260 ft with a blow count of 705 blows per ft. Another pilot hole was drilled to 274 ft penetration, with the interval from 260 ft to 269 ft being underreamed. The pile was driven further on to 270 ft with a final count of 29 blows per ft. Table 1 shows typical pile installation data from piles driven in field No1, with number of times the pile refused, and remedial action taken to reach design penetration. Piles driven in the other two fields - No.2 and No.3- (data not shown) exhibited similar behavior, i.e., majority met refusal short of design penetration, and required remedial installation measures.

Pile Refusal

Almost all of the piles- a total of 42 piles- met refusal short of design penetration. Principal remedial measures taken to facilitate redriving after refusal were to drill out the soil plug and to advance a pilot hole below the pile tip. Evaluations of available boring logs have indicated that the deeper soils encountered layers of strong material, probably: rock, calcareous sands, or hardened clays.

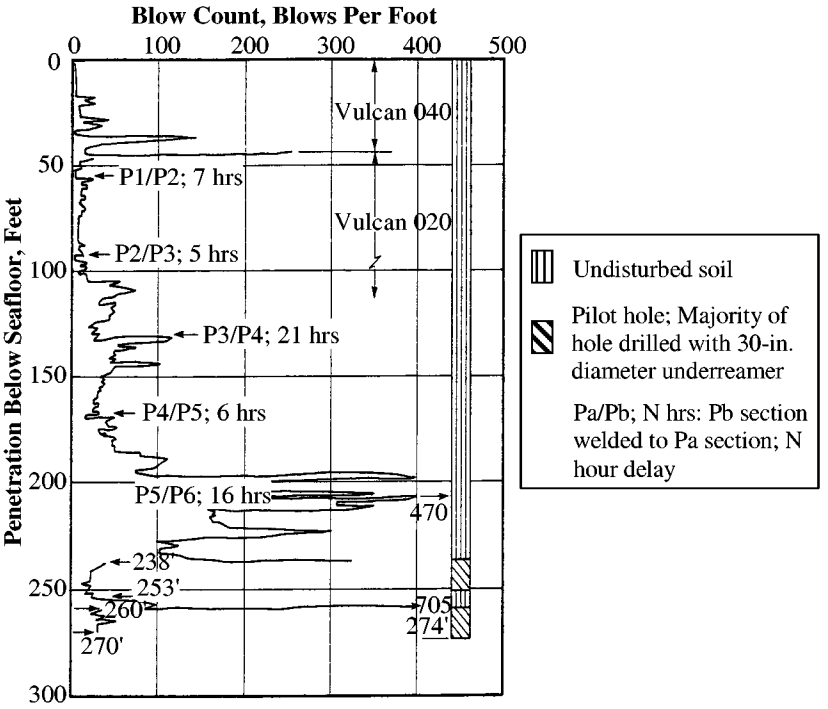

Fig.1. Blow Count versus Penetration of driven 30-inch diameter pipe pile (Jacket A, Pile A-1) Field No.1.

The inability to redrive piles after delays had been encountered was noted on several piles. This condition may be attributed, sometimes, to clay "set up" that occurs as clays and clayey silts regain strength over a period of time- primarily due to the dissipation of pore pressures that builds up during pile driving. Several instances were noted where a pile initially met refusal but was able to be redriven after a relatively short delay in driving. The excess pore pressures during driving causes swelling and weakening of the stiff clay, in addition to remolding. In dense silty sands, induced negative pore pressures inhibit the silty sand ability to deform during pile driving. Pore pressure dissipation during driving delays, may then reduce driving resistance.

Pilot Holes and Grout Plugs

At the time of the installations, the only remedial technique available on the barge was the drilling of pilot holes. The soil plug was drilled out using the 26 inch bit. When the bit was 5 ft below the pile tip, the underreamer was opened and a 30 inch diameter hole was reamed out for some distance below the pile tip.

Table. 1. Summary of typical pile installation data showing: design penetration, no. of refusal times, & remedial action to reach design penetration (Field No.1).

Jacket	Pile	Design Penet.	Refusal No.	Remedial Action
A	A-1	270 ft	2 Times	Two pilot holes with underreaming
	A-2		2 Times	One pilot hole with underreaming
	A-3		1 Time	One pilot hole with underreaming
B	B-1	262 ft	2 Times	Two pilot holes with underreaming
	B-2		2 Times	Two pilot holes with underreaming/grouting
	B-3		4 Times	Two pilot holes with underreaming/grouting
C	C-1	246 ft	2 Times	Two pilot holes with underreaming
	C-2		2 Times	One pilot hole with underreaming
	C-3		1 Time	One pilot hole with underreaming
D	D-1	245 ft	1 Time	No remedial installation measure was necessary
	D-2		1 Time	No remedial installation measure was necessary
	D-3		1 Time	No remedial installation measure was necessary
E	E-1	247 ft	3 Times	Two pilot holes with underreaming
	E-2		3 Times	Two pilot holes with underreaming
	E-3		2 Times	One pilot hole with underreaming

Underreaming a pilot hole to the same diameter as the pile, may have a detrimental effect on the skin friction in the underreamed zone, i.e., skin friction in the underreamed zone may be significantly lower than on piles driven through undisturbed soil. The drilling of pilot holes resulted in several piles with inadequate soil plug to mobilize end bearing. The recommendation, at the time, stated that grout plugs be installed to mobilize the necessary end bearing needed to achieve the desired pile capacity. Therefore, almost half of the piles were grouted from the bottom of the pilot hole to the sea floor. Needed grout plug length varied from 20 to 30 feet.

Hammer-Pile Combination

Pilot holes did not significantly increase pile drivability in many cases. In addition, pile refusal occurred within the zone of pilot holes at several locations. This finding supports the view that Vulcan 040 was too small to drive the 30 inch piles to design penetration. This discrepancy was further investigated by wave equation analyses to determine if a larger hammer would have increased the drivability of the noted piles in these soils. The results of the analyses are shown in Fig.2 as a plot of driving resistance in kips versus rate of penetration in blows per ft. As shown in Fig.2, the Vulcan 040 is able to overcome a driving resistance of about 2,000 kips at refusal (300 blows per ft). Under the same conditions, the Vulcan 060 is able to overcome a driving resistance of approximately 2,250 kips. This small increase indicates that little benefit would have resulted from the use of a Vulcan 060 vs. the Vulcan 040. The relatively low driving stresses shown in Fig.2 suggest that a larger hammer than the Vulcan 060 could probably have been used without incurring damage to the pile.

Refusal of a large number of piles, where pilot holes were drilled, has been of concern. Data shows that refusals are due to a combination of hammer size, pile size, and soil conditions, rather than any faults in the equipment used by the contractor.

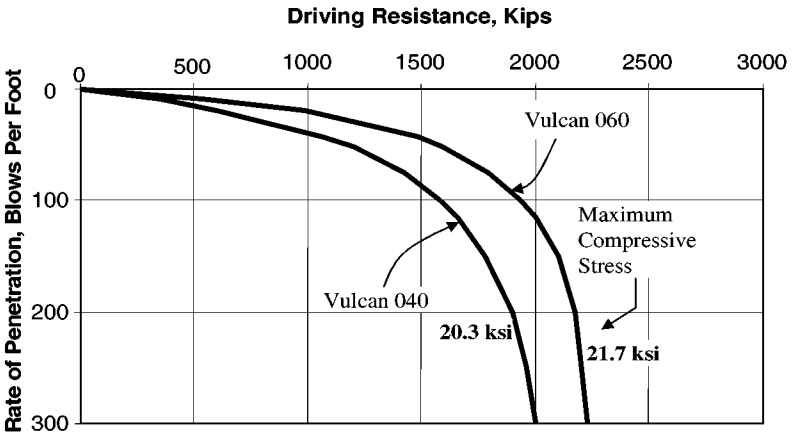

Fig.2. Wave equation analysis for the 30 in. diam. pipe pile (at 215 ft. penet.) showing: Driving Resistance in kips versus Rate of Penetration in blows per foot. (1 ksi= 6895 Kn/m^2)

Ultimate Pile Capacity and Safety Factors

The ultimate pile capacity at each pile location was evaluated from borings previously drilled in the area and from engineering evaluation of the installation records. Pile capacities were computed in accordance with the API RP 2A (1991) method. The unit skin friction on the piles was calculated using parameters appropriate for dense carbonate silty sand, believed to prevail in the vicinity of the majority of driven piles in field No.1. This assumption may have resulted in a conservatively low estimate of pile capacity, but the true soil type could not be determined based only on the driving records. The calculated ultimate compressive pile capacities, shown in Table 2, for some of the installed piles, are adjusted to reflect the "as-installed" pile penetrations in field No.1.

The weight of grout plugs, if any, and soil plugs inside the piles were added to the tensile capacities that are shown in Table 2. In the underreamed zones, very low limiting values of skin friction were used because of the potential reduction in lateral pressure on pile wall caused by the underream. Available ultimate pile loads were used to compute safety factors in both tension and compression, and the resulting safety factors are shown in Table 2.When site-specific geotechnical data are incomplete, evaluations of pile capacities may be based on assumed conditions. Then, an upper bound and a lower bound of ultimate capacity & safety factor are calculated.

This is by no means a substitute to values based on geotechnical data - it is only intended to provide guidance in the absence of credible geotechnical parameters.

Table 2. Ultimate pile capacities and safety factors of selected piles installed in Field No.1.

Jacket/ Pile	Ultimate Pile Load, kips*		Ultimate Pile Capacity, kips*		Safety Factor	
	Comp.*	Ten.*	Comp.*	Ten.*	Comp.*	Ten.*
C-1	1603	1404	1998	1761	1.25	1.25
C-2	1603	1404	1951	1768	1.22	1.26
C-3	1603	1404	1861	1675	1.16	1.19
D-1	1582	1386	1951	1815	1.23	1.31
D-2	1582	1386	1979	1844	1.25	1.33
D-3	1582	1386	1974	1838	1.25	1.33
E-1	1622	1421	1844	1703	1.14	1.20
E-2	1622	1421	1894	1752	1.17	1.23
E-3	1622	1421	1917	1775	1.18	1.25
F-1	1523	1333	1865	1722	1.22	1.29
F-2	1523	1333	1821	1679	1.20	1.26
F-3	1523	1333	1900	1759	1.25	1.32

1 kip* = 4.448Kn; Comp.*= Compression; Ten.*= Tension;

RECOMMENDATIONS FOR FUTURE INSTALLATIONS IN THE REGION

Author's experience (Akili 1998; Akili 2000; Akili 2004), supplemented by the experience of others (American Petroleum Inst. 1991; O'Neill & Raines 1991; Poulos 2005), supports the view that advanced planning coupled with specific measures will help in overcoming unpredictable difficulties when driving piles in the Region.

Recommended Measures

These measures should include some or all of the following:

- ***Appropriate geotechnical investigation should precede*** any installation work. At least one soil boring be drilled at each of the platform locations. Insufficient number or depth of boreholes to identify stratigraphic variations across the site, or result in inadequate testing, could lead to improper characterization of the site.
- ***Use of high strength steel with uniform constant wall thickness***, to eliminate the need for underdrive or overdrive allowances of a thick–wall section, is highly recommended! Also, fewer complications will occur during driving of soil plug.
- ***Selection of hammer sizes one or two sizes larger*** than that indicated by the drivability study is a must! Heavier ram weights are more important than energy!
- ***Any problem resulting from clay "set-up",*** due to normal increase in driving resistance or when encountering strong clays, can be reduced by keeping pauses very short and making final add-ons with the pile tip at the highest possible elevation, so driving at deeper penetration can be accomplished uninterrupted!

- ***When a pile reaches refusal*** in hard clays or dense sands, additional pile penetration may be facilitated by drilling or jetting the soil plug that forms inside the pile during driving. Since the purpose of removing the soil plug is to reduce end bearing during redriving, consideration should be given to the end bearing adequacy of the new plug formed by redriving, and to the possible need for reestablishing end bearing by the installation of a grout plug.
- ***Redriving to a greater penetration is achieved by drilling a pilot hole.*** A predrilled pilot hole should be terminated at least 5 ft above design penetration. The pilot hole length should be less than the length of pile remaining to be driven before the next add-on section must be made. For vertical piles, the maximum depth of pilot holes should not exceed 50 ft.The diameter of predrilled hole should be less than two–thirds of the outside pile diameter.
- ***The possibility of installing a grout plug*** in a pile that meets refusal short of design penetration - to mobilize the necessary end bearing needed to achieve the desired pile capacity - should always be under consideration. It is recommended that prior to placing the grout plug the soil plug be drilled out to a depth of 6 ft above the driven pile tip. The length of grout plug needed to produce the unit end bearing that the soil stratum can mobilize, i.e., the stratum in which the pile tip is embedded, can be computed using a limiting steel-to-grout adhesion value of 4 ksf. As a rule, it is recommended that the length of the grout plug be at least 10 ft.

Safety Factors and Pile Acceptance

The ratio of ultimate pile capacity to the design pile load is the safety factor. Determination of an adequate safety factor is based on experience in the locale. Structure serviceability, economy, and consequences of failure must be included in an assessment of an adequate safety factor. The probability of failure (reflected by the safety factor) depends on: the confidence in assigned soil properties, capacity computation method, and other details. These factors can significantly influence the ultimate pile capacity and, thus, the degree of certainty of the computed pile capacity.

If a pile reaches refusal after it has sufficient penetration to obtain a theoretical factor of safety of at least 1.35, as determined from the ultimate compressive pile capacity curves, it is recommend that no further attempt be made to install this pile to design grade. A safety factor as low as 1.25, based on static criteria, is considered acceptable provided dynamic monitoring plus a drivability study indicate that the pile has a minimum factor of safety of 1.5. The above- recommended criteria for acceptability of driven piles- intended for the Arabian Gulf shore- should be used only if the tensile capacity, based on static analysis, yields a safety factor of at least 1.5. A chart for pile installation procedures based on the recommended safety factors can be developed for each platform location. These charts provide the contractor with guidelines to follow if piles refuse above design penetration. The information needed to develop pile installations procedures, and henceforth the chart, are: i) reliable results of a geotechnical investigation at the proposed site, ii) pile size, and iii) general construction details, including available hammers, grouting equipment, drilling equipment, and proficiency and experience of the crew.

CONCLUDING REMARKS

This case history addresses the discrepancies between design penetration of steel pipe piles driven in the offshore of Qatar, the Arabian Gulf shore, and their "as-installed" ultimate capacities. It is revealed here, through subsurface data and pile driving records, that corrective steps to close the gap between design and field outcome, need to be taken rather than to just continue an inadequate approach to pile driving. Recommendations have been made to guide the installation process, focusing on: geotechnical parameters, hammer sizes, pile characteristics, remedial installation procedures, safety factors, and pile acceptance criteria. These recommendations should be an integral part of a "well thought out" strategy to solve pile installation problems and gain an added margin of confidence of installed capacities. Also, not having the right equipment on the barge such as: heavy ram weights, pumps, airlifts, drills, plus equipment for remedial installation, leads to over-runs in cost and time.

While modern geotechnical engineering makes it possible to carry out drivability studies on the basis of soil samples; the condition down below may vary. As pointed out by Gerwick (2004), "Pile driving is a mixture of engineering and art. Recent developments in the ability to measure and predict stresses are wonderful tools, -- but the high variability of geotechnical conditions also requires that we incorporate the lessons from prior experience to achieve both technical and economic success." Thus, it becomes inherent on the designer to provide for potential changes in geotechnical conditions, relying on competent staff, preferably with prior experience in the locale.

REFERENCES

Akili, W. (1998). "Shallow Foundations on a Digenetic Limestone Formation in Qatar".*Proc. 4th Int. Conf.on Case Histories in Geotechnical Engrg.,* St.Louis, MO.

Akili, W. (2000). "Pile Driving in the Offshore of Qatar: Problems, Challenges, and Potential Solutions". *In-house Report*, University of Qatar, Doha, Qatar.

Akili, W. (2004). "Foundations over Salt-encrusted Flats (Sabkha): Profiles, Properties, and Design Guideline".*Proc. 5th Int. Conf. on Case Histories in Geotechnical Engrg.,* New York, NY.

API. (1991). "Recommended Practice for Planning, Designing and Constructing Fixed Offshore Platforms".19th Ed., Am. Petroleum Institute API RP 2A, Dallas, TX.

Gerwick, B.C. (2004). "Pile Installation in Difficult Soils". *ASCE J. Geotech. and Geoenvironmental Engrg.*, 130, (5): 454-460.

O'Neill, M.W., and Raines, R.D. [1991]. "Load Transfer of Pipe Piles in Highly Pressured Dense Sand" .*ASCE J. Geotech. Engrg.* 117, (8):1208-1226.

Poulos, H.G. (2005). "Pile Behavior-Consequences of Geological & Construction Imperfections". *ASCE J. Geotech. & Geoenvironmental Engrg.*, 131, (5):538-563.

Copyrighted Materials
Copyright © 2009 American Society of Civil Engineers (ASCE)
Retrieved from www.knovel.com

Driven Pile Capacity in Intermediate Geomaterial Formations

Robert L. Mokwa[1], Ph.D., P.E., M. ASCE, and Heather Brooks[2]

[1]Associate Professor, Dept. of Civil Engineering, Montana State University, Bozeman, MT.
[2]Graduate Student, Dept. of Civil Engineering, Montana State University, Bozeman, MT.

ABSTRACT: The natural variability of intermediate geomaterials (IGMs) exacerbates uncertainties in deep foundation design and may ultimately increase construction costs. There are well-established analytical methods for evaluating pile capacity and for predicting pile driving characteristics for cohesive soil, cohesionless soil, and rock. However, past experience indicates these methods may not be reliable for piles driven into IGMs, which often exhibit a wide array of properties with characteristics ranging from stiff or hard soil to soft weathered rock. Analytical results are compared to field capacities determined using PDA measurements obtained during pile driving and wave equation analyses conducted using the CAPWAP program. Capacity comparisons clearly demonstrate the inherent variability of pile resistance in IGMs and indicate that traditional semiempirical methods developed for soil may yield unreliable predictions for piles driven into IGM formations. The synthesis described herein has the potential to improve the reliability and cost effectiveness of deep foundations supported in IGMs by comparing design methods and material characteristic techniques with measured pile responses.

INTRODUCTION

Engineering mechanical properties of intermediate geomaterials (IGMs) fall within the continuum bracketed by soil and rock. Various terms have been used to describe or classify IGM deposits, including: formation materials, indurated soils, soft rocks, weak rocks, and hard soils. Construction experience indicate that piles driven into IGMs do not always behave as predicted; i.e., piles may stop short of their design elevation (premature refusal) or require driving to greater depth (known as running) to achieve the required capacity. As a result, construction costs for foundations can be greatly increased due to unpredictable strength and drivability behavior of piles driven into IGM formations.

The purpose of this study was to determine if an improved method of analysis could be used to better predict the behavior of piles driven into IGMs with respect to axial capacity and depth of embedment. The accuracy of design methods were evaluated using measurements obtained during pile installation on nine Montana Department of Transportation (MDT) bridge construction projects.

OVERVIEW OF INTERMEDIATE GEOMATERIALS

Principles from both soil and rock mechanics are often applied to IGMs in terms of material behavior and design methodology. However, neither approach adequately addresses the unique and disparate nature of IGM formation processes, which generally fit into one of the following two basic descriptions: 1) soil has been strengthened to near rock-like characteristics, or 2) rock formations have been weakened to near soil-like levels. IGMs occur when the natural processes of soil or rock formation are incomplete or interrupted. For example, in some settings the soil strengthening process (deposition followed by lithification, diagenesis or cementation) may be interrupted before the creation of rock. In other settings, IGMs are the byproduct of weakening processes (e.g., weathering and disintegration) of intact rock (Gannon et al. 1999). Because of their variability, the behavior of IGMs is far from predictable. Wide ranges of material behavior have resulted in a multitude of disparate definitions in the literature, all based on material strength. Based on a synthesis of technical literature addressing IGM properties, it appears that a reasonable definition for most applications is that IGMs will have a uniaxial compressive strength in the range of 600 to 12,500 kPa, an SPT N-value greater than 50 blows per 0.3 m, and a stiffness modulus in the range of 100 to 1,000 MPa. Additional details regarding IGM properties are described by Mokwa and Brooks (2008).

For the analyses conducted in this study, IGMs were divided into two broad categories, cohesive and cohesionless. Cohesive IGMs have an intrinsic component bonding; for example, siltstone, claystone, mudstone, sandstone, argillaceous, and arenaceous materials. Cohesionless IGMs include very dense granular materials that derive strength predominately from frictional resistance rather than intrinsic particulate bonding.

DATA ANALYSIS

Data analyzed in this study were obtained from design and construction records from nine bridge projects in Montana. Information from each of the projects was collected and compiled, including initial drive and restrike data from CAPWAP reports, PDA records, foundation reports, and construction documentation. GRLWEAP and DRIVEN computer analyses were conducted by the authors using hammer and cushion information submitted by the contractor. Remaining information was determined using engineering judgment, based on the soil profiles and foundation reports. Detailed descriptions of the MDT project data and information is provided by Mokwa and Brooks (2008).

An iterative approach was used in this study. Evaluations were conducted by creating numerous parametric comparisons to search for trends or useful relationships within the data. The variability of IGMs provided an interesting challenge because of the unpredictable response of the material to pile driving, and because of the many variables involved with pile driving and pile resistance. The analytical comparison was divided into the following three phases:

1) evaluate the reliability of current design procedures;
2) investigate possible correlations between project data and predictive methods;
3) determine the accuracy of other capacity prediction methods.

CAPWAP results were used as the baseline standard in the analytical comparisons. The suitability of this assumption for piles in IGMs was evaluated using a database compiled by Likins and Rausche (2004) and further expanded using additional data obtained through an extensive literature review. A comparison of static load test (SLT) capacities to CAPWAP capacities is provided in Figure 1 for IGMs and traditional soils. Based on the reasonable correlation between SLT and CAPWAP measured capacities, the authors presupposed that CAPWAP results could be used as reliable estimates of axial capacity for the data evaluated in this study.

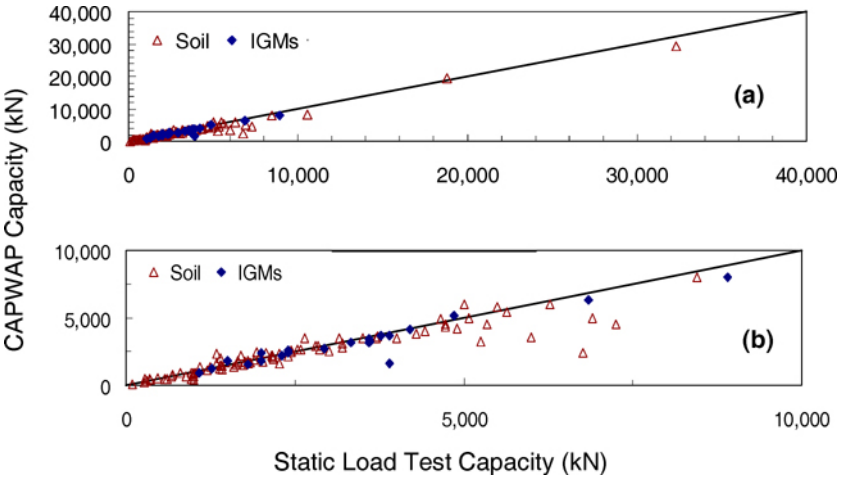

Figure 1. Comparison of static load test and CAPWAP capacities from the literature. (a) Full scale plot of all data. (b) Data points at lower capacities.

Reliability of Current Design Methods

The adequacy of current design methods commonly used by transportation agencies was evaluated by comparing calculated static capacities (using the program DRIVEN) to measured dynamic capacities from CAPWAP. The depths used to determine capacities were obtained directly from the MDT CAPWAP reports at the end-of-driving and restrike.

A comparison of the capacity values is shown in Figure 2. The ordinate of the plot represents the calculated capacities using original input parameters. The abscissa represents the measured dynamic capacities from CAPWAP tests, for end-of-drive and restrike. The diagonal 45° line in each plot can be used to qualitatively asses the accuracy of calculated predictions using original, unaltered parameters from the design reports.

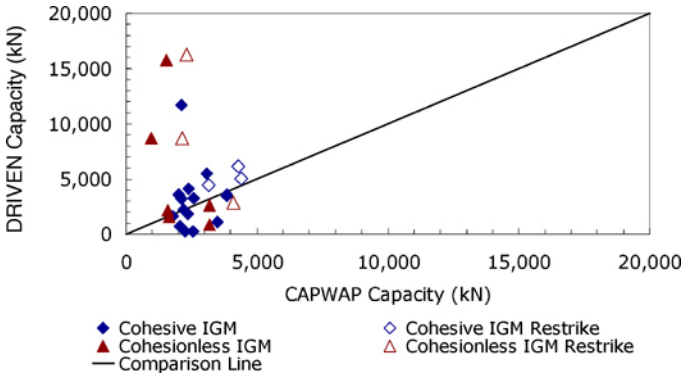

Figure 2. Measured CAPWAP capacities compared to calculated capacities.

The capacity comparisons shown in Figure 2 clearly demonstrate the inherent variability of pile resistance in IGMs. Most of the projects exhibited considerable variation between predicted capacities calculated using DRIVEN and measured CAPWAP capacities. For example, five of the six restrike analyses were over predicted using DRIVEN, one by as much as 580% (a factor of 6.8). Additional refinement of the analyses revealed that shaft resistance was under predicted in 12 out of 20 (60%) occurrences in cohesive IGMs; however, there were outliers in which capacity was over predicted by 150% to 380%. The majority of shaft capacity predictions for cohesionless IGMs were less than the measured CAPWAP capacities; the worse case was a 400% under prediction (a factor of 5). Toe capacity predictions were also quite variable and random, with no discernable trends.

These comparisons were made using the original DRIVEN computer files and soil parameters, with no after-the-fact modifications. This indicates that semiempirical methods developed for soil may yield unreliable predictions for piles driven into IGM deposits.

Investigation of Potential Correlations

By normalizing the capacity measurements, a potentially more accurate method of comparing data between projects is achieved by isolating material properties from measured values. The pile perimeter, the pile toe area, and the length of the pile within the IGM were used to normalize the CAPWAP shaft and toe capacities. For example, one form of normalized shaft resistance is shown in Eq. 1, as follows:

$$N_{shaft} = \frac{CAPWAP_{shaft}}{p} \tag{1}$$

where, N_{shaft} is the normalized shaft resistance, p is the perimeter of the pile and $CAPWAP_{shaft}$ is the measured CAPWAP shaft resistance.

One form of normalized toe resistance is shown in Eq. 2, as follows:

$$N_t = \frac{CAPWAP_{toe}}{A} \tag{2}$$

where, N_t is the normalized toe resistance, A is the plugged area of the pile, and $CAPWAP_{toe}$ is the measured toe resistance. The plugged area is the full toe area of the pile; a box area for H-piles and the entire circular area for pipe piles.

The length of pile within IGM layer is compared to N_{shaft} in Figure 3. There is potentially a slight trend within the data, which consists of a relatively weak linear relationship from coordinate point (0, 0) to (7, 1500). The data points trend downward and shows considerable scatter beyond about 7 m of pile embedment in the IGM layer. The CAPWAP shaft capacity included within this calculation is the total shaft capacity of the pile; unfortunately, this also includes the shaft resistance from the soil layers above the IGM deposit. For the projects evaluated in this study, the shaft capacity in the upper soil layers was not measured during pile driving. The authors believe the trends or correlations could be improved if the soil and IGM shaft resistances could be accurately separated from the total CAPWAP shaft resistance.

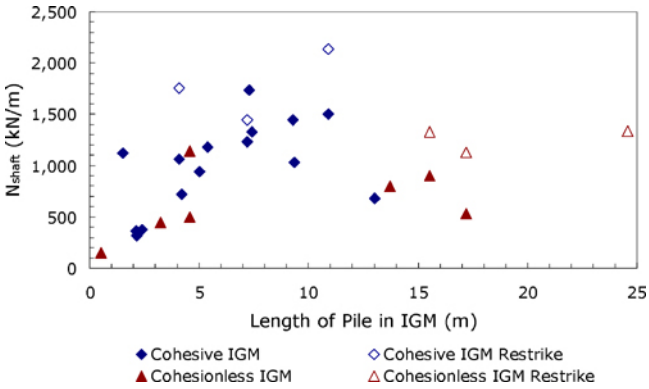

Figure 3. Normalized shaft resistance compared to pile length in IGM.

As shown in Figure 4, the comparison of normalized toe capacity (N_t) with unconfined compression strength indicates large data scatter with no apparent trend. Intuitively, an increase in toe capacity would be expected to occur as the unconfined compression strength of the IGM increased; however, this was not the case for the data evaluated. It is postulated that these uncharacteristic results could be attributed partially to changes in material properties during pile driving. Figure 5 shows a slight correlation of decreasing toe capacity with the length of pile driven into the IGM layer. However, because of changes in material properties during pile driving and geologic trends in which the IGM strength changes with depth, the correlation is limited in its usefulness.

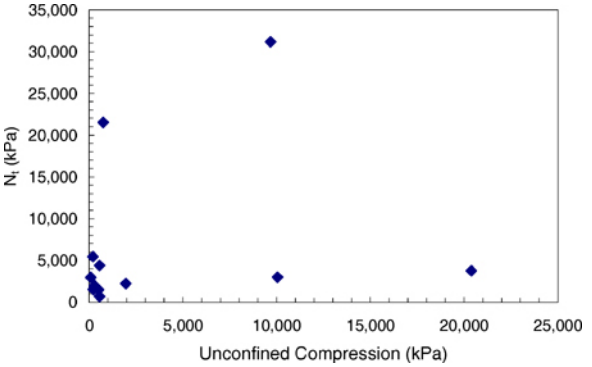

Figure 4. Comparison of normalized toe resistance with unconfined compression strength.

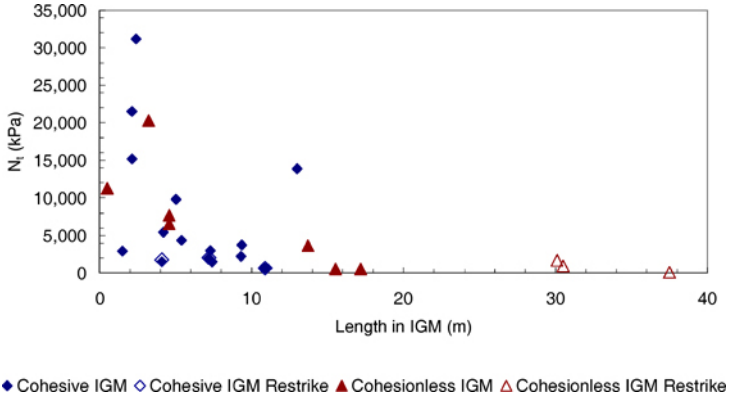

Figure 5. Comparison of normalized toe resistance with length of pile in IGM.

Accuracy of Other Analytical Methods

Additional approaches for predicting axial capacity were evaluated including the Gates dynamic formula, the WSDOT dynamic formula, and a method used by the Colorado Department of Transportation, herein called the CDOT method.

The Gates dynamic formula is shown in Eq. 3, as follows:

$$R_{Gates} = 1.75\sqrt{1{,}000 \times E^*}\log_{10}(10N_c) - 100 \quad (3)$$

where, R_{Gates} is the pile axial capacity, E* is the energy of the hammer in foot-pounds, and N_c is the pile penetration resistance in blows per inch.

The WSDOT formula represents a recent addition to the exhaustive collection of pile dynamic formulas. Allen (2007) used a large database of pile driving information to calibrate and modify the Gates formula to provide more accurate solutions for conditions encountered on transportation projects in the state of Washington. Pile capacities were calculated in this study with the WSDOT dynamic formula using two approaches based on the source of hammer energy values: 1) predicted hammer energy (R_{WA1}), and 2) measured hammer energy (R_{WA2}).

Approach 1 uses the predicted or assumed hammer energy as follows:

$$R_{WA1} = 6.6 \times F_{eff} \times E^* \times \ln(10N_c) \tag{4}$$

where, R_{WA1} is the pile axial capacity based on predicted hammer energies, F_{eff} is an efficiency factor for specific hammers and pile types, E* is the energy of the hammer in foot-pounds, and N_c is the pile penetration resistance in blows per inch. Hammers on all of the MDT projects were open-ended diesel hammers on steel piles; thus, based on recommendations by Allen (2007), $F_{eff} = 0.47$. E* in this case represents the potential energy of the hammer, or the stroke of the hammer multiplied by the ram weight. The penetration resistance, N_c, was obtained directly from the CAPWAP reports provided by MDT.

Approach 2 uses the measured hammer energy as follows:

$$R_{WA2} = 6.6 \times TE \times \ln(10N_c) \tag{5}$$

where, R_{WA2} is the pile axial capacity based on measured hammer energies, and TE is the energy transferred to the pile as measured by gauges attached to the pile during dynamic testing.

Axial capacity can be estimated using the CDOT method with Eq. 6 as follows:

$$R_{CDOT} = 0.25 \times f_y \times A_{open} \times FS \tag{6}$$

where, R_{CDOT} is the pile axial capacity, f_y is the yield stress of the steel, A_{open} is the cross sectional area of the pile, and FS is the factor of safety.

Comparisons of capacities calculated using the Gates dynamic formula, the WSDOT dynamic formula, the CDOT method, and the DRIVEN and GRLWEAP computer programs are shown in Figure 6 for cohesive IGM formations. Calculated capacities are compared to measured CAPWAP capacities using original unmodified input values obtained from the MDT project reports. Capacities calculated using the CDOT method and the Gates dynamic formula consistently under predicted the measured capacities by relatively large amounts. The predicted capacities determined from DRIVEN and GRLWEAP were in relatively good agreement; however, neither accurately matched the measured CAPWAP capacities. Overall, the WSDOT dynamic formula provided the best match to measured CAPWAP capacities. Analytical predictions for piles in cohesionless IGMs exhibited even greater scatter than the cohesive IGM capacity predictions.

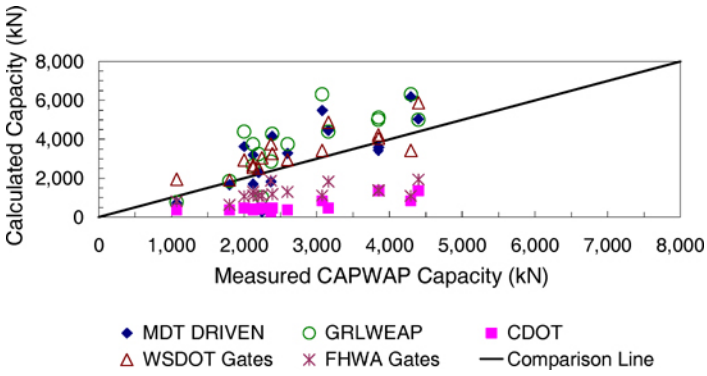

Figure 6. Comparison of capacity calculations in cohesive IGMs.

SUMMARY AND CONCLUSIONS

Construction experience with piles driven into IGM deposits indicates the predicted behavior frequently does not match the field-measured response. Piles either refuse early or drive further than anticipated. The capacity comparisons evaluated using measured data from nine Montana bridge projects clearly demonstrated the inherent variability of pile resistance in IGMs. Results from the majority of the projects exhibited considerable variation between predicted capacities calculated using DRIVEN and measured CAPWAP capacities. The error in predicted values ranged from a 580% over prediction of capacity to a 400% under prediction of capacity.

The authors recommend that during design, careful consideration be given to evaluating: 1) changes in IGM engineering properties that occur during driving, and 2) pile stresses and potential pile damage if IGMs are expected at the site. It would be prudent to use a range of IGM strength parameters (parametric study) in this evaluation because of the variable nature of these materials and the real potential for excessively strong and excessively weak anomalies within the IGM deposit.

ACKNOWLEDGEMENTS

Acknowledgement of financial support is extended to MDT and the RITA program through the Western Transportation Institute at Montana State University.

REFERENCES CITED

Allen, T. (2007). Development of New Pile-Driving Formula and Its Calibration for Load and Resistance Factor Design. *Journal of the Trans. Research Board. No. 2004; 20-27.*

Gannon, L.A., Masterton, G.G., Wallace, W.A. and Wood, D.M.. (1999). Piled Foundations in Weak Rock. Published by Ciria Press, Westminster, London.

Likins, G. and Rausche, F. (2004). "Correlation of CAPWAP with Static Load Tests." *Proceedings of the 7th International Conference on the Application of Stress-Wave Theory to Piles*: Petaling Jaya, Selangor, Malaysia; 153-165.

Mokwa, R.L. and Brooks, H. (2008). Axial Capacity of Piles Supported on Intermediate Geomaterials. Research Report FHWA/MT-08-8117-32, prepared for Montana Department of Transportation and the U.S. DOT, Helena, MT, July 2008.

Copyrighted Materials
Copyright © 2009 American Society of Civil Engineers (ASCE)
Retrieved from www.knovel.com

Use of Dynamic Measurements to Drive High Capacity Concrete Piles in Washington's Potomac Formation

John E. Regan, P.E.[1] and Karl A. Higgins, III, P.E.[2]

[1]Associate Principal, GZA GeoEnvironmental, Inc, One Edgewater Drive, Norwood, Massachusetts 02062: Tel: 781-278-5741: john.regan@gza.com

[2]Principal, ECS Mid-Atlantic, LLC, 14026 Thunderbolt Place, Suite 100, Chantilly, Virginia 20151: Tel: 703-834-2325: khiggins@ecslimited.com

ABSTRACT: Located along the eastern shoreline of the Potomac River, the Gaylord National Harbor Hotel and Convention Center is a massive development project supported on deep foundations. Deep foundations were designed to derived support within the underlying Potomac Formation, a highly variable mixture of sand, gravel, and clay. While other traditional deep foundation options typically used in the Washington DC region were considered, prestressed, square concrete piles driven to a 1335 kN (150 ton) design capacity were deemed most feasible.

Square (355 mm) prestressed concrete piles were dynamically load tested and monitored during impact driving using the Pile Driving Analyzer (PDA). Dynamic soil forces resisting pile penetration within the Potomac Formation exhibited significant elastic behavior at times, resulting in large pile rebound and substantial energy loss in the hammer-pile-soil system. Large soil quakes were observed during penetration within the bearing soils resulting in significant pile breakage. This paper discusses some of the challenges faced with installing prestressed concrete piles in the Potomac Formation and presents a case history of observations, dynamic test results and remedies employed to safely achieve the required design loads using a single-acting diesel hammer.

INTRODUCTION

The Gaylord National Harbor Hotel and Convention Center is just one of a growing number of projects in the Washington DC Metro region founded on high capacity prestressed concrete piles. Located along the Potomac River, just east of the Woodrow Wilson Bridge connecting Maryland and Virginia, this massive project was constructed in two phases. The first phase extends inland from the eastern shoreline of the Potomac and is founded on square (355 mm) prestressed concrete piles which achieve suitable bearing above the Potomac Formation. The Phase II portion of this project lies in an area described on geologic maps and geotechnical reports as an erratic transition zone between the overlying Terrace River Deposits and the deeper Potomac Formation. Phase II was initially designed to be supported on drilled shafts bearing within the underlying Potomac Formation, a highly variable mixture of sand, gravel, and clay. Driven, prestressed concrete piles were proposed as an alternate to more traditional deep foundation elements (i.e. drilled shafts) typically employed in the Washington DC region.

The site is located along the eastern shore of the Potomac River in the Coastal Plain Physiographic Province, known as Selby Bay, in Prince George's County, Maryland. The upper soil beneath a relatively thin layer of fill material consists of "Terrace River Deposits", alluvial/fluvial soils consisting predominately of sands with interbedded layers of low to high plasticity clay soils. Marine deposits of the Potomac Formation, consisting of very dense sands and highly overconsolidated clays, underlay the Alluvial Deposits. Groundwater was encountered at depths ranging from 12 to 20 meters below existing grades, ranging in elevation from el. + 6 m to el.+ 1.2 m, and may represent perched water within the Alluvial soils, above the Potomac Formation.

The Potomac Formation, generally consisting of fine sands, silt and clay, is the oldest sedimentary deposit in the Washington metro area and represents the bearing stratum for many shallow and deep foundations. The silts and clays of the Potomac Formation are often referred to as "marine clays", and typically have high plasticity characteristics and significant shrink-swell potential and are highly overconsolidated. With bedrock typically encountered at significant depth, usually greater than 60 meters below ground surface, the Potomac Formation represents the bearing stratum for many shallow and deep foundations in the Washington DC Metropolitan area.

FOUNDATION DESIGN CONSIDERATIONS

Preliminary geotechnical findings suggested that 1335 kN (150 ton) auger cast-in-place (CIP) piles and 1335 kN (150 ton) drilled shafts represented that most cost effective foundation options available in the region to support the required building loads. While driven 355mm square prestressed concrete piles were recognized as an alternative, design capacities for driven piles commonly used within

the Washington DC region are generally limited to 800-900 kN (80-90 tons) per pile, thereby rending their use more expensive than drilled foundation systems.

Prestressed concrete pile capacities have traditionally been limited in the Washington region to 800-900 kN (80-90 tons). While substantially higher design loads (i.e. 1335 kN) are common throughout many regions in the US, the variability of Washington's Potomac Formation presents challenges to ensure safe and economical installation of these large displacement piles. By executing a comprehensive dynamic test pile program to confirm that individual pile capacities in excess of 1335 kN (150 tons) were possible, the project schedule and cost constraints supported a driven pile foundation system over more traditional drilled cast-in-place piles or drilled shafts.

Square (355mm) prestressed concrete piles having a minimum 28-day compressive strength of 41.4 MPa (6,000 psi) and a prestress of 4.8 MPa (700 psi) were installed using a Delmag D46-32 single acting diesel hammer to an ultimate pile capacity of 2670 kN (300 tons). The D46 has a ram weight of 45.1 kN (10,143 lbs), a maximum stroke of 3.7 meters (12 feet), yielding a maximum rated energy of 165 kN-m (122,000 ft-lbs). The hammer cushioning material consisted of 5.1 cm (2 inches) of aluminum and conbest and the pile cushioning material consisted of 23.5 cm (9.25 inches) of plywood. Driven pile lengths ranged between 23 meters and 33.5 meters long. Maximum compressive and tensile stresses for this pile type are 29.6 MPa (4.3 ksi) and 7.1 MPa (1.1 ksi), respectively (per AASHTO Standard Specification for Highway Bridges).

Preliminary Driving Criteria – Phase I

Preliminary driving criteria were developed for the test pile program utilizing a combination of static pile capacity analyses (i.e. Meyerhof's formulae), along with pile-hammer-soil models developed using GRLWEAP, a one-dimensional wave equation program. Target pile lengths were developed based on the site geology and calculated end bearing and skin friction components.

The initial Test Pile Program performed for Phase I consisted of dynamic load testing using the Pile Driving Analyzer (PDA) to measure pile stresses, pile-soil displacement (i.e. quake), hammer performance and to estimate pile capacity. The PDA was used to make dynamic force and acceleration measurements of the test piles. These measurements were evaluated in the field to determine pile capacity, pile stress and hammer performance. Dynamic force and acceleration measurements obtained from the PDA during initial drive and restrike, and CAPWAP analyses were evaluated to develop a minimum embedment depth into the underlying bearing stratum. Target pile lengths varied by approximately 12 meters across the Phase I portion of the site.

Pile driving results during Phase I confirmed that the pile design load of 1335 kN (150 tons) could be achieved with reasonable driving effort using the Delmag D-

46 operating at a 2 meter (6.5 foot) stroke. Using the Delmag D-46 with plywood cushioning, the Phase I piles were installed without pre-augering. The production driving criteria was established such that pile installation would be terminated above the minimum embedment length provided that a minimum penetration resistance of 8 blows per 25.4 mm (8 blows per inch) for 305 mm (1 foot) was achieved using a 2 meter (6.5 foot) stroke. Restrike testing subsequently confirmed that significant pile set-up was achieved over time. Many of the production piles, therefore, were simply driven to the target tip elevation, developing the required capacity principally in the Terrace River deposits (i.e. Fluvium or Alluvium).

PHASE II DEVELOPMENT - *Geologic Transition*

The Phase II portion of the Site was planned in an area where erratic and abrupt changes in the underlying geology were identified by soil explorations. While portions of the site are underlain by relatively thick Alluvium and ultimately, at deeper depths, by the Potomac Formation, the eastern portions of the site, in the vicinity of the Phase II building addition, are underlain by thinner amounts of upper alluvium, and the Potomac Formation is encountered at shallower, more erratic depths. The soil stratigraphy resembles a wedge that grows thicker toward the west and the Potomac River; the Potomac Formation soils can be found at the ground surface at points just east of Phase II. This abrupt change in site geology presented challenges with respect to driven pile installation. Due to these known geologic conditions, the Phase II dynamic test program considered a higher density of dynamic test piles to determine pile lengths.

Dynamic Test Pile Program

Seventeen test piles were dynamically load tested and monitored using the PDA during initial drive and restrike. In addition, subsequent CAPWAP analyses were performed on selected blows. Each test pile location was pre-augered 15 to 17 meters (50-55 feet) below existing grade using a 355 mm (14 inch) diameter drill stem. Pre-augering was performed to improve the energy transfer from the pile top to the pile tip and improve pile embedments into the varying underlying soil conditions.

Three test areas were defined to coincide with changes in pile behavior. While pile penetration resistances required to achieve the pre-determined target tip elevation generally varied from 2 to 11 blows per 25.4 mm (28-130 blows per foot), difficult driving was concentrated in the northeast corner of Phase II. Ultimately, five of 17 test piles were broken during driving. The breakage was abrupt, and little warning was observed with regard to stresses measured at the pile heads. After further examination of the PDA data with CAPWAP analyses, it was determined that the piles developed tensile cracks and broke in the lower 1/3 to ½ of the pile length.

CAPWAP analyses performed on data recorded at the end of initial drive indicated pile capacities ranging from 1780 kN (400 kips) to 2800 kN (630 kips) with skin friction components ranging from 180 kN (10 %) in the southern most area to

1290 kN (70%) in the northeast area of the Site. CAPWAP analyses performed on data recorded at the beginning of restrike, typically following a 3 to 6 day set-up period, indicated a "Case Method" ultimate pile capacity of 2625 kN (590 kips) to 4400 kN (990 kips) with skin friction components ranging from 735 kips (25% percent) to 2310 kips (85%). With a few exceptions, the data obtained at the beginning of restrike testing indicated a significant increase in penetration resistance ranging from 20% to 260%.

High Quake – Pile Rebound

Dynamic soil forces resisting pile penetration within the Potomac Formation exhibited significant elastic behavior at times, resulting in large pile rebound and substantial energy loss in the hammer-pile-soil system. This elastic behavior, known as Quake, is defined as the displacement at which the initial elastic deformation of the pile and soil achieves its ultimate load and goes plastic. Studies have shown that soil quakes greater than 0.4-inches significantly alter the wave equation results (Likins, 1983).

Dynamic data from Phase II test piles indicated computed quake values during restrike between 16mm and 25mm (0.64 to 1.0 inches), with toe quake values as high as 20 mm (0.78 inches). Table 1 below provides a summary of select dynamic measurements for test piles driven within the Potomac Formation, including Dmax, the maximum pile displacement of the pile head (both elastic and plastic) under a single hammer blow. While measured compressive and tensile driving stresses were maintained within allowable limits (are 29.6 MPa (4.3 ksi) and 7.1 MPa (1.1 ksi), respectively) sudden pile breakage occurred at various tip elevations with moderate driving resistance.

Table 1 – Dynamic Measurements of Test Piles driven into the Potomac Formation prior to breakage

Test Pile	Total Embed. Length (m)	Embed. Length through Potomac (m)	Pile Tip Elev. (m)	Blow Count (blows per 25.4mm)	Measured Tensile Stress (MPa)	CAPWAP Toe Quake (cm)	Max Pile Displ. DMax (cm)
A7	19.8	19.8	+2.1	1	1.4 - 6.2	2.0	5.1
A7-R	18.3	18.3	+3.6	2	1.4 - 4.1	3.3	3.4
A7-R2	22.6	22.6	-0.6	3	2.1 - 6.9	2.7	3.4
A8	20.1	20.1	+1.2	3	1.4 – 5.5	2.0	4.7

Estimating static pile capacity requires a balance of energy between the total energy delivered by the hammer to the pile and the total work done by the resisting forces, both elastic and plastic, during penetration. The effect that large quakes have on the efficiency of the pile/hammer/soil system during impact can be significant. The occurrence of high soil quakes requires more energy to fully mobilize the pile tip

from elastic to plastic than would be needed under normal quake conditions. This behavior is represented below in Figure 2 by comparing the relationship of Pile/Soil resistance to elastic and plastic (i.e. permanent) Displacement, under each hammer blow (Smith, 1960)

With equivalent energy delivered to the pile/soil system, a pile will achieve substantially more permanent toe displacement (i.e. Set) under a normal quake condition (point c) than a pile driven under high quake conditions (point c'). However, the maximum displacement of the pile top under each hammer blow, which represents the total elastic and plastic displacement of the pile top, will be substantially lower for normal quake conditions (point b) than high quake conditions (point b'). Similarly, when driving a pile in high quake conditions, substantially larger energy transfer is required to produce the same permanent set (i.e. blow count where Set = 1/ Blow count), as compared to a pile driven in normal quake conditions.

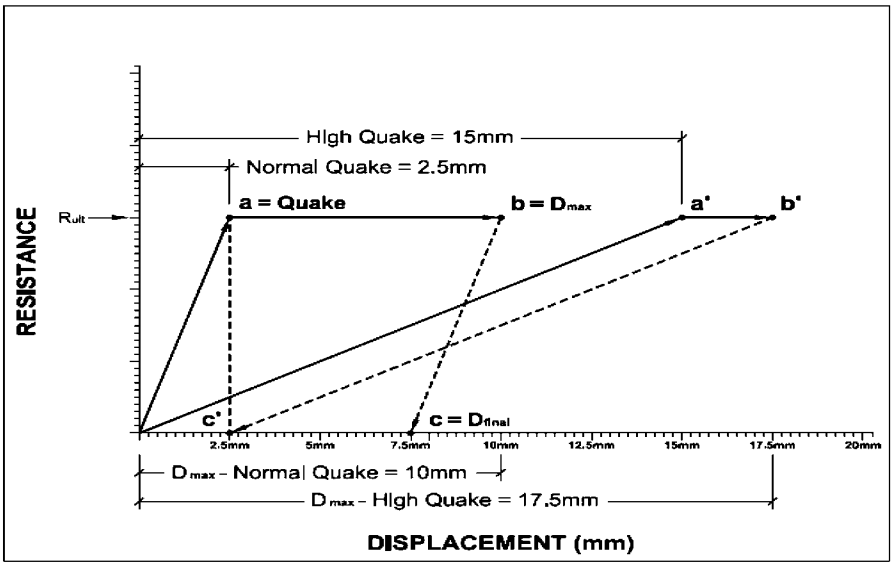

Figure 2 – Load vs. Displacement for Normal and High Quake conditions under each hammer blow (Smith, 1960).

This larger energy transfer is needed to overcome the elastic rebound of the high quake soil condition prior to fully mobilizing the full resistance at the pile tip (Likins, 1983). As such, high quake experienced in the overconsolidated Potomac Formation resulted in decreased energy transfer to the pile tip, thereby increasing the blow count required to mobilize the full pile resistance. High blow counts and corresponding high compressive stresses within the body of the piles contributed to

the cyclic loading condition which decreased pile embedment lengths into the Potomac Formation and increased the occurrence of pile breakage (Hannigan, 1985).

One dimensional wave propagation theory shows that impact loads (i.e. compression forces) imparted on piles with little to no tip resistance (i.e. early driving) cause tension reflections from the pile toe. As the pile tip resistance increases, the magnitude of these tension reflections are minimized. Pile driving systems are routinely selected so that the ram weight and stroke can be controlled to minimize early driving tensile stresses. Tension reflections are further increased, however, in high quake soil conditions due to the slow response time of the tension reflection along the pile. Under normal quake conditions, the full resistance of the pile tip are mobilized at the time of the first reflection at the pile tip thereby reducing the tension reflection. In high quake soils, the full toe displacement may not be mobilized at the time of first arrival of the peak input velocity, thus higher tension reflections are generated even under refusal conditions (Likins 1983).

As shown in Table 1, recorded blow counts for four test piles driven in the geologic transition zone ranged from 1 to 3 blows per 25.4 mm (12-40 blows per foot), demonstrating sufficient pile tip resistance to maintain acceptable tension reflections from the pile tip. This was substantiated by the measured tensile stresses which ranged from 1.4 to 6.9 MPa (0.2-1.0 ksi) The driving conditions, however, changed abruptly within the Potomac Formation as the frequency of pile breakage increased substantially with very little warning. Cyclical loading imparted by the driving system and large toe quakes enpcountered in the Potomac Formation induced tension reflections causing pile breakage little typically within the lower ½ to 1/3 of the pile.

Previous studies concerning high quake soils relate pile installation difficulties to excess pore pressure build-up during cyclical loading (i.e. impact driving) in saturated soil conditions (Likins, 1983 Hussein, 2006). Interestingly, on-site observations of open cut excavations in the Phase II area, in addition to examination of soil boring data, suggest that perched groundwater is present and that the upper Potomac Formation at the Site is dessicated and very hard. The large soil quakes observed are likely related to the degree of overconsolidation of this bearing stratum, as well as the development of excess pore water pressure that may increase during driving.

REMEDIES / RESULTS

The results of the dynamic test program were instrumental in developing measures to address the issue of excessive pile breakage. To improve energy transfer to the pile tip, production pile driving procedures were modified to include pre-augering through the upper 15 meters of overburden for all production pile locations prior to installation. In addition, plywood pile cushioning material was maintained at 235 mm (9.25 inches) to minimize pile top damage. While these measures helped minimize pile breakage, ultimately the required pile capacity of 1335 kN (150 tons) was lowered down to 890 kN (100 tons) along the easternmost one-third of the

building footprint, where most of the test pile damage occurred. By lowering the capacity, the piles required less tip embedment into the Potomac Formation, and thereby the chances of pile breakage were limited. The remainder of Phase II was supported by 1335 kN (150 ton) piles consistent with Phase I.

Production testing included a careful review of driving records for damage, followed by frequent PDA tests on production piles and occasional Pile Integrity Testing (PIT). As a result of these changes, the frequency of production pile damage was low for Phase II, decreasing from approximately 10% to less than 5% for the balance of Phase II (500 piles).

CONCLUSIONS

For square (355mm x355 mm) prestressed concrete piles and other large displacement piles penetrating high rebound soils such as Washington's Potomac Formation, driving system energy dissipates through the elastic rebound of the pile tip thereby increasing the driving resistance (i.e. blow count). The driving inefficiencies experienced due to highly elastic conditions in the hard Potomac Formation induced cyclical loading conditions resulting in compounding stresses that increased the occurrence of pile breakage under hard driving conditions. The variability of the driving conditions encountered at this site relate to large energy losses experienced due to elastic compression of the pile tip (i.e. high tip quakes) in very hard (N values > 50), overconsolidated clays.

The use of the PDA to obtain real-time dynamic measurements during pile installation aided in the field evaluation of hammer performance, structural integrity, pile capacity estimates and driving stresses under each hammer blow. This valuable information guided the Project team in making on-site changes to the driving criteria and helped maintain critical project milestones. By implementing routine changes to the driving criteria, square prestressed concrete piles were successfully installed within Washington's Potomac Formation using a single-acting diesel hammer.

REFERENCES

Hussein, M.H., Woerner, W.A., Sharp, M. and Hwang, C. (2006) "Pile Driveability and Bearing Capacity in High-Rebound Soils" *ASCE Proceedings of GeoCongress 2006.* Atlanta, Georgia, USA.

Likins, Garland E. (1983). "Pile Installation Difficulties in Soils with Large Quakes", *Proceedings of Symposium 6 at the ASCE Convention*, Philadelphia, PA, USA.

Hannigan, P.J. (1985). "Large Quake Development During Driving of Low Displacement Piles", *Proceedings of the 2nd International Conference on the Application of Stress-Wave Theory to Piles*, Stockholm, Sweden.

Smith, E.A.L. (1960). "Pile Driving Analysis by the Wave Equation", Journal of Soil Mechanics and Foundations, *American Society of Civil Engineers*, August 1960,

Copyrighted Materials
Copyright © 2009 American Society of Civil Engineers (ASCE)
Retrieved from www.knovel.com

Measured Versus Predicted Shaft Resistance of H- and Closed Ended Pipe Piles in Sands

Scott M. Mackiewicz, PhD, PE[1]

[1]Principal Geotechnical Engineer, Kleinfelder, 7802 Barton, Lenexa, Kansas, 66214, USA, (913)962-0909, smackiewicz@kleinfelder.com

ABSTRACT

There are many factors that influence the skin friction capacity of steel H- and closed ended pipe (CEP) piles driven into sands. As part of a bridge replacement project near the Texas gulf coast, we evaluated the performance of various design methodologies for predicting driven pile shaft resistance in sands. We predicted the shaft resistance of steel H- and CEP piles at one bridge location using the SPT Method (Meyerhof, 1979), FHWA DRIVEN computer program, and WEAP-SPT Method. The actual pile shaft resistances were then determined during end-of-drive (EOD) and at beginning of restrike (BOR) using dynamic testing and CAPWAP.

This paper describes the installation of the driven steel H- and CEP piles, presents the dynamic load test results as compared with predicted design values and evaluates the performance of the predictive methods. Based on the data obtained, it appears that the DRIVEN and WEAP-SPT (for H-piles only) tend to largely over predict skin resistance in sands and the SPT and WEAP-SPT (for CEP piles) methods provide a reasonable but slight overestimation of the skin resistance in sands.

INTRODUCTION

As part of a bridge replacement project, a dynamic pile (i.e., PDA and CAPWAP) load test program was conducted to evaluate the driven H-pile and closed-ended pipe (CEP) pile capacity predictions. The static capacity prediction methods used for this project include the SPT method (Meyerhof, 1976), Federal Highway Administration (FHWA) DRIVEN program and GRL-WEAP simplified SPT Analysis. The pile load test program for this bridge replacement consisted of dynamically monitoring three test piles, two 14x89 H-piles and one 20-inch diameter CEP pile, during initial driving and at the beginning of restrike. This paper describes the prediction of shaft resistance and installation of the driven piles as well as presents the dynamic load test results as compared with predicted shaft resistances.

PROJECT SITE

The project site is located within the Texas Gulf coast about 3.4 miles southwest of Beasley, Texas, see Figure 1. The bridge location is along an existing, but abandoned railroad corridor that parallels Highway 56. At the time of our study, the existing railroad bridge was being removed and a new bridge was being constructed.

Figure 1. Project Location

GEOLOGY/SOIL PROFILE

The project site is located where the subsurface materials are comprised of the Beaumont Formation, which is the youngest coast-wise or coast-paralleling Pleistocene unit in the Texas Gulf Coast. The Beaumont is comprised of fluvial and delta sands with intervening layers of clays, silty clays, sandy clays, and clayey silts. These fine grained, overbank deposits are generally 10 to 30 feet thick and were most likely placed by receding floodwaters. The Beaumont formation extends to depths greater than 200 feet in this area.

In general, the Beaumont Formation in this area was comprised silty sands, clayey sands and sands with intervening clay seams deposited by slack water. In general, the clay seams were comprised of high plastic clay and were between 5 to 10 feet thick. The poorly to well graded, silty and clayey sands had fines contents (-#200 sieve) of 14 to 41 percent. The poorly graded sands had fines contents (-#200 sieve) of about 7 percent. The N_{60} value and fines content test results for the boring performed at the site are presented in Figure 2. Groundwater was encountered during our subsurface exploration at depths of about 37 feet below existing grades.

PILE CAPACITY PREDICTION/MEASUREMENT METHODS

The ultimate static axial shaft resistance of each test pile was initially estimated using the SPT method (Meyerhof, 1976), DRIVEN program (FHWA), and the Simplified SPT N-value methods included in the GRL-WEAP program and the subsurface profile outlined previously. The following presents the background of the methods that were used to predict the pile shaft resistances.

SPT Method (Meyerhof, 1976): The SPT method developed by Meyerhof was based on existing correlations between the SPT results and static pile load test in a variety of cohesionless materials. This method takes into account the difference in stress conditions caused by displacement (CEP or concrete) piles and non-displacement (H-) piles by varying the constant. The "N" value used in this paper was corrected to 60 percent hammer efficiency and also corrected for overburden. Since this method can be influence by numerous factors, Hannigan, (1997) recommends that this method only be used for preliminary design. It should be noted

that this method limits the shaft resistance to a maximum of 2 ksf. The SPT Method is outlined below:

Shaft Resistance, f_s (ksf)

Non-Displacement (H-piles)	f_s (ksf) = $(0.02)N_{60}' \leq 2$ ksf
Displacement (pipe or concrete)	f_s (ksf) = $(0.04)N_{60}' \leq 2$ ksf

Where: N_{60}' = SPT N_{60} value corrected for overburden pressure

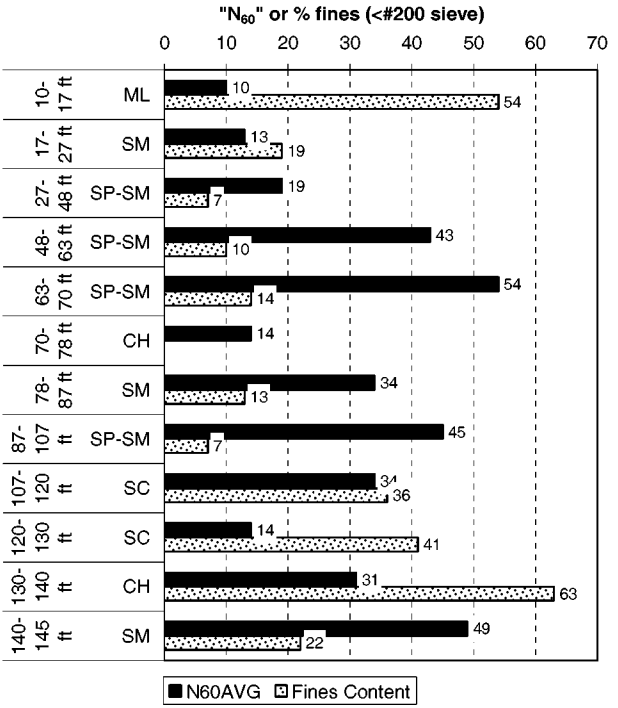

Figure 2. Subsurface Profile Information

DRIVEN Program (v 1.2): The DRIVEN program was developed for the Federal Highway Administration (FHWA) and follows the methods and equations presented by Norlund (1963, 1979), Thurman (1964), Meyerhof (1976), and Tomlinson (1979,1980). The user inputs the soil profile, groundwater levels, strength properties, and pile type. The shaft resistance, f_s, for cohesionless materials is estimated using Norlund's methods. It should be noted that Norlund's method does not put a limiting value on the effective stress, which is used in the computation of the shaft resistance. The Norlund method is outlined in detail in the FHWA "Design and Construction of Driven Pile Foundations" manual (Hannigan, et.al., 1997).

WEAP SPT N–value Based Method: For this paper, we used the simplified SPT N value method included in GRL-WEAP 2005 as one of our predictive methods. The details on the basis for the calculations in this method are outlined in the GRL-WEAP 2005 user manual. It should be noted that the SPT N value method used in the WEAP program does not correct the N values for overburden as in Meyerhof's SPT method but does adjust them to a N_{60} value. The manual does indicate that the SPT method used for determination of pile capacity is generally inaccurate due to variability in SPT values and soil behavior.

PILE INSTALLATION

A Pileco 30-32 single-acting diesel hammer was used to drive all piles. This hammer has a ram weight of 6.61 kips and a manufacturer's rated energy of 70.066 foot-kips at a 10.6-foot stroke at the maximum fuel setting (No 4). Fuel setting No.4 was used for all installation and restrikes.

The 14x89 steel H-piles were installed to a maximum depth of 163 feet and had minimum yield strength of 50 ksi (ASTM A-572 Grade 50). The steel CEP pile was installed to a maximum depth of 76 feet and had minimum yield strength of 45 ksi (ASTM A-252, Grade 3). The piles were driven in 60-foot sections and spliced with full penetration groove welds. The CEP piles were closed on the end by welding a 1-inch thick plate to the bottom section.

DYNAMIC PILE LOAD TEST PROGRAM

The purpose of the dynamic load test program was to monitor the performance of the driving system and evaluate the pile capacity. The dynamic testing was performed using a PAK Model, Pile Driving Analyzer® (PDA) to acquire data from the strain transducers and accelerometers. The evaluation of the soil resistance distribution was performed using CAPWAP®, which computes soil resistance forces and approximate distribution using the force velocity data recorded in the field.

CAPWAP analyses were performed on selected data obtained at the end of drive for the initial pile segment (ID), the end of drive (EOD) and the beginning of restrike (BOR). Table 1 summarizes the test piles that were driven and the depths at which the CAPWAP analyses were performed. Based on the CAPWAP data, it appears that the shaft resistance for the H-piles accounts for about 61 to 77 percent of the total capacity and for the CEP's about 27 to 66 percent of the total capacity.

Table 1. Summary of Test Piles and CAPWAP Information

14x89 H-pile	20 in. CEP
103 ft ID	61 ft ID
163 ft EOD	81 ft EOD
163 ft BOR	81 ft BOR

ID-Initial Drive, EOD-End of Drive, BOR-Beginning of Restrike

The shaft resistance for each soil layer was estimated from the CAPWAP unit resistance (area) results. The reported soil segment unit resistances were averaged over the soil layer. The distribution of the shaft resistance with respect to the individual sand layers is shown in Table 2 for the H-piles and Table 3 for the CEP's. The tables also show the shaft resistance predicted by the SPT method (Meyerhof, 1976), DRIVEN program (FHWA), and the Simplified SPT N-value methods included in the GRL-WEAP program.

Table 2. Ultimate Shaft Resistance Predictions in Sand: 14x89 H-Pile

Soil Layer	USCS	N_{60}	SPT	DRIVEN (FHWA)	WEAP-SPT	CAPWAP (ID/EOD) 103 ft/163 ft	CAPWAP (BOR-7 day) 163 ft
			ksf	ksf	ksf	ksf	ksf
10-17 ft	ML	10	0.19	0.58	0.19	0.03/ -	--
17-27 ft	SM	13	0.21	0.99	0.49	0.05/ -	--
27-48 ft	SP-SM	19	0.27	1.72	0.79	0.29/0.16	0.03
48-63 ft	SP-SM	43	0.55	3.34	1.06	0.72/0.12	0.06
63-70 ft	SP-SM	54	0.67	4.42	1.21	0.32/0.10	0.23
70-78 ft	CH	14					
78-87 ft	SM	34	0.36	3.29	1.46	0.71/0.13	0.18
87-107 ft	SP-SM	45	0.48	4.16	1.75	0.53/0.21	0.47
107-120 ft	SC	34	0.34	3.87	1.88	- /0.41	0.76
120-130 ft	SC	14	0.13	3.05	2.06	- /0.52	0.81
130-140 ft	CH	31					
140-145 ft	SM	49	0.43	4.81	2.59	- /1.53	1.36

Table 3. Ultimate Shaft Resistance Predictions in Sand: 20 inch –CEP

Soil Layer	USCS	N_{60}	SPT	DRIVEN (FHWA)	WEAP -SPT	CAPWAP (ID/EOD) 61 ft/ 81 ft	CAPWAP (BOR-1 day) 81 ft
			ksf	ksf	ksf	ksf	ksf
10-17 ft	ML	10	0.38	0.77	0.19	0.17/0.20	0.11
17-27 ft	SM	13	0.42	1.32	0.49	0.32/0.11	0.17
27-48 ft	SP-SM	19	0.54	2.34	0.79	0.58/0.26	0.24
48-63 ft	SP-SM	43	1.11	5.00	1.06	1.63/1.06	0.98
63-70 ft	SP-SM	54	1.33	6.92	1.21	- /2.15	2.44
70-78 ft	CH	14					
78-87 ft	SM	34	0.76	4.64	1.46	- / 1.58	2.34
87-107 ft	SP-SM	45	0.95	6.02	1.75		
107-120 ft	SC	34	0.67		1.88		
120-130 ft	SC	14	0.26		2.06		
130-140 ft	CH	31					
140-145 ft	SM	49	0.86	7.63	2.59		

FINDINGS

The ultimate shaft resistance measured during the dynamic load testing when compared to the predictive methods varied significantly with the method, depth and soil type as shown in Figures 3 and 4. Table 4 summarizes the range of predicted/measured ratios for the skin friction resistance on the test piles. The measured resistance was taken at the beginning of restrike (BOR), which included a 7-day delay on the H-pile and a 1-day delay on the CEP.

Table 4. Ultimate Skin Friction Prediction/Measured Ratios

	14x89 H-Pile	20 inch CEP
SPT (Meyerhof)	0.2 – 2.9	0.5 – 3.5
DRIVEN	3.5 - 20	2.6 – 9.8
WEAP-SPT	1.9 – 8.0	0.5 – 3.3

A simple statistical analysis, calculation of mean and standard deviation, was performed to determine the accuracy of the predictive methods to the CAPWAP resistance distributions at ID, EOD, and BOR. Since the distribution of predicted to measured capacity has been noted to be lognormal (Long, et. al, 2002), the computation of the mean and standard deviations were based on a lognormal distribution. The mean values from this statistical analysis are shown in Table 5. A mean value (μ) of unity represents, on average, that the predicted capacity equals the measured capacity. A $\mu < 1$ indicates under prediction, a $\mu > 1$ indicates over prediction of the method. The standard deviation of the analyses ranged from 0.17 to 0.97 (poor quality) for the CEP data and 0.99 to 1.89 (very poor quality) for the H-Pile data.

Table 5. Mean Values (μ) of Prediction/Measured Ratios

	14x89 H-Pile			20 inch CEP		
	ID	EOD	BOR	ID	EOD	BOR
SPT (Meyerhof)	1.51	1.45	1.35	1.17	1.29	1.14
DRIVEN	9.13	13.58	12.69	3.90	5.14	4.54
WEAP-SPT	3.50	5.92	5.54	1.11	1.37	1.21

In addition, based on the CAPWAP results, the shaft resistance of the piles generally increases with time. The ultimate skin resistance measured on the 1 and 7-day restrikes on the H-pile and CEP pile, respectively was 1.4 to 2.3 greater and 1.1 to 1.7 greater than the measured end of drive shaft resistance.

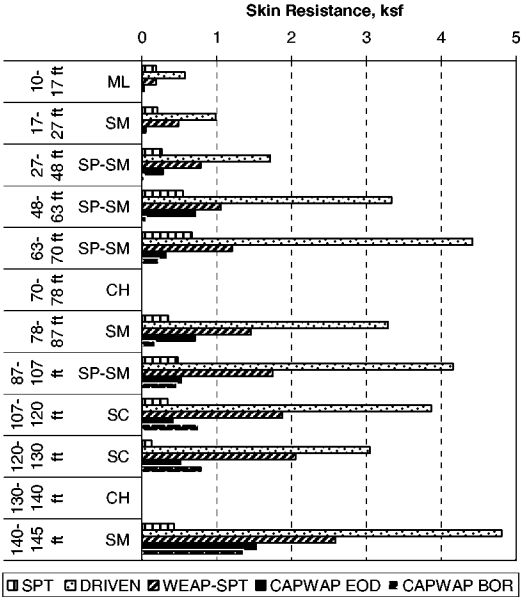

Figure 3. H-Pile Predicted and Measured Shaft Resistance

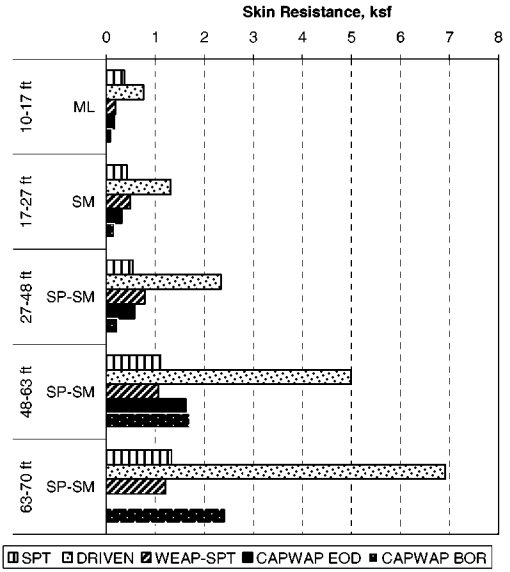

Figure 4. CEP-Pile Predicted and Measured Shaft Resistance

CONCLUSIONS

Based on the subsurface information as well as field and laboratory test results, the ultimate shaft resistance predicted using the FHWA DRIVEN program appear to be considerably larger than (2.6 - 20 times) the ultimate shaft resistance measured by dynamic load testing and the CAPWAP analysis for the H- and CEP piles. In addition, the WEAP-SPT method also appears to over predict the skin friction resistance (1.9 - 8 times) of the H-Piles. The SPT method on the other hand appears to provide a more reasonable estimate (μ = 1.14 to 1.51) of the ultimate shaft resistance for these materials. The WEAP-SPT also appears to provide a reasonable estimate (μ = 1.11 to 1.37) of the skin resistance for the CEP piles. Based on the simple statistical analysis, it appears that the prediction methods are generally of higher quality at ID and become more scattered at the EOD and BOR.

This study indicates that the shaft resistance in sands can be very difficult to estimate using the available methods and guidelines. Thus, the use of dynamic pile testing can provide the designer better information that can be used to refine shaft resistance estimates and, in turn reduce project costs.

REFERENCES

GRL WEAP (2005), Wave Equation Analysis of Pile Driving, Procedures and Models, Pile Dynamics, Inc., 4535 Renaissance Parkway, Cleveland, OH, 44128

Hannigan, P.J., et. al. (1998) *Design and Construction of Driven Pile Foundations*, Volumes 1 and 2, FHWA HI 97-013, November 1998.

Long, J.H., M. Maniaci, E.A. Samara (2002) Measured and Predicted Capacity of H-Piles, ASCE, *Deep Foundations 2002,* Vol. 1, pp. 542-558.

Meyerhof, G.G. (1976). Bearing Capacity and Settlement of Pile Foundations. , ASCE, *Journal of the Soil Mechanics and Foundations Division*, Vol. 85, SM6, December, pp. 1-29.

Norlund, R.L. (1963) Bearing Capacity of Piles in Cohesionless Soils. ASCE, *Journal of the Soil Mechanics and Foundations Division*, SM3, pp. 1-35.

Norlund, R.L. (1979) Point Bearing and Shaft Friction of Piles in Sand. Missouri-Rolla 5th Annual Short Course on Fundamentals of Deep Foundation Design.

Thurman, A. G. (1964) Discussion of Bearing Capacity of Piles in Cohesionless Soils. American Society of Civil Engineers, ASCE, *Journal of the Soil Mechanics and Foundations Division*, SM1, pp. 127-129.

Tomlinson, M. J. (1980) *Foundation Design and Construction*, Fourth Edition, Pitman Advanced Publishing Program.

Copyrighted Materials
Copyright © 2009 American Society of Civil Engineers (ASCE)
Retrieved from www.knovel.com

Intelligent Pile-Driving with a Diesel Impact Hammer

Michael D. Justason[1], M.Eng., P.Eng., M.ASCE

[1]Product Manager, Bermingham Foundation Solutions, Hamilton, Ontario, Canada L8L 4Z9; mjustason@berminghammer.com

ABSTRACT: This paper describes an automated energy control system for a diesel pile hammer. Some background is given on experience using an energy monitoring system on the Route 1/I-95 interchange in Alexandria, Virginia. An adjustable hammer throttle and feedback from an energy monitoring system was then used to create a fully automated hammer energy control system. The performance of this system is described in reference to a piling project in Canada where the automated energy control system was used to obtain a high level of quality control and assurance – data and graphs from the project are presented. The hammer energy control system (ECS) was used to successfully control and maintain a prescribed impact (kinetic) energy for the diesel hammer. This paper presents the results from the first ever use of a partially automated diesel pile hammer and points to a new direction in quality control and assurance in pile driving.

INTRODUCTION

The performance (defined as the kinetic or impact energy of the ram) of a *diesel* hammer depends on the soil resistance, and the mass and stiffness of the pile foundation being driven. Likewise, the resulting capacity of the pile foundation depends on the performance of the pile-driving hammer. In contrast, the impact energy of a *hydraulic* hammer is relatively independent of the pile resistance. The interdependency of the pile capacity and the hammer performance for a diesel hammer adds an extra level of complexity to the QA and QC of the pile driving operation.

Proponents of diesel hammers tend to view the interdependency of pile resistance and hammer performance as an advantage rather than a disadvantage. When driving concrete piles the impact energy of a diesel hammer will be low when the soil resistance is low, thus helping to minimize potentially damaging tension stresses. Another concern with diesel hammers is that the impact energy may suddenly increase and over-stress the pile. This can be a concern when driving piles through very soft soil to a hard rock bearing layer.

Traditional diesel hammers are equipped with discrete 'energy settings' (4-settings are common). These settings control the amount of fuel delivered to the hammer, and

thus indirectly control the resulting impact energy of the hammer. Some diesel hammers are equipped with an infinitely adjustable fuel delivery or throttle mechanism, which gives the operator some control over the hammer performance, up to the maximum performance 'permitted' by the pile resistance. One such throttle mechanism uses a small hydraulic line connected to a hydraulic hand-pump to control the position of a needle valve. The needle valve regulates the flow of fuel to the combustion chamber of the hammer and hence the impact energy, allowing a direct relation between the impact energy of the hammer and the hydraulic hand-pump pressure.

VERIFYING HAMMER PERFORMANCE (IMPACT ENERGY)

In pile driving, 'QA' and 'QC' typically consist of pile installation records that log the number of blows per unit of penetration, and the final tip elevation for each pile. Very often, however, the performance of the pile hammer is not logged on the pile installation record, or more disturbing, the pile hammer may appear to be operating at the desired impact energy, while in fact it is not. This can lead to a potentially dangerous situation, whereby piles are believed to have more capacity than they actually do.

Historically, the most common problem with diesel hammers has been the phenomenon of 'pre-ignition'. Pre-ignition occurs when the hammer becomes very hot and combustion begins prior to the impact of the ram. Unfortunately, a diesel hammer that is experiencing pre-ignition may not show any visible signs of a problem. The combustion pressure may still be sufficient to 'run' the hammer with the desired stroke, yet the impact energy may be reduced because of the increased gas pressure beneath the falling ram prior to impact.

Diesel hammers that operate using a fuel injection system do not experience pre-ignition. This can be verified using an instrumentation port that allows for monitoring the impact velocity of the ram using magnetic proximity switches. Typically, two proximity switches located on the body of the hammer sense the position of a particular machined 'feature' of the ram. Knowing the distance between these two proximity switches and the difference in time between switching signals the velocity of the ram just prior to impact can be calculated. Testing has shown that fuel injected hammers do not experience a loss in impact velocity as the hammer temperature increases.

Further development of the velocity monitoring system included the addition of other features for greater QA and QC in pile driving. In 1990, a device was introduced called a Pile Driving Monitor (PDM) that included a depth logger and blow counter, calculated impact energy, pile number, cut-off elevation, date, time, project name, splice location, and various other pertinent information. Early versions of these energy monitoring devices included on-board printers for record-keeping, but these have been replaced with newer PDMs that include USB ports for connection to a computer or direct connection to a USB memory key for downloading of data.

FIG. 1 – Pile Driving Monitor

During the 1980's and 90's, companies in America and The Netherlands were also developing and popularizing the use of high strain dynamic testing of piles, commonly known as PDA (Pile Driving Analysis or Pile Dynamic Analysis). Using PDA, engineers can affix strain and acceleration transducers to the pile and monitor the pile stress, delivered (transferred) energy to the pile, and using computer models they can predict pile capacity. This innovation has proved extremely useful in assessing the suitability of a pile hammer for a particular job.

Another innovation used to improve the QA and QC for pile driving was an acoustic blow-counter called the Saximeter™. This device 'listens' to the blow-rate of a hammer, and using a basic formula, estimates the stroke, or the potential energy of a hammer (not to be confused with the impact or kinetic energy). It also offers the ability to record blow counts, and to store other pertinent QA and QC information. While the original versions of this device offered no ability to detect impact velocity, there is a newer version of the device that uses proximity switches, very similar to the PDM that allows it to monitor impact velocity. This device is called the E-Saximeter™.

ROUTE 1/I-95

In specifying the pile driving hammer for the Virginia side of the Woodrow Wilson Bridge near Washington, D.C., the Virginia DOT specified that the pile-driving hammer shall have energy monitoring and reporting capabilities. For this reason the project specifications explicitly called for the use of a hydraulic pile driving hammer. This project was one of the several contracts for the construction of the highway approaches on the Virginia side of the Woodrow Wilson Bridge. After meetings with the Virginia DOT as well as the project consultants, it was decided that a diesel hammer would be allowed, provided that the hammer was equipped with an impact energy monitoring system, such as the one shown in Fig. 1.

The piles for this project were 610-mm (24-inch) square pre-stressed concrete piles. The piles ranged in length from 15-24-m (50-80-ft). The soil conditions consisted mainly of sand and silt layers on top of a stiff clay. The contractor for this section of the approach bridges was Dawson Bridge Company from Lexington, Kentucky. The hammer was a Berminghammer B-6505 with 275-kJ (202,000-ft-lb) of rated energy

and an 8,000-kg (17,600-lb) ram. PDA testing was performed by Aver Technologies, Inc. of Virginia.

Results

To truly verify the accuracy of the hammer energy monitor, the data from the monitor was downloaded to a computer and then combined on a common scale with the PDA data from the pile. Fig. 2 shows the theoretical 'potential energy' of the ram (stroke x acceleration of gravity x ram mass). The stroke data is calculated by the PDA system using an empirical formula used to relate blows-per-minute to stroke for a typical diesel hammer. Notice that the stroke vs. the impact (kinetic) energy is a near-linear relation.

Fig. 2 also shows the impact (kinetic) energy as measured by the on-board energy monitor (PDM). Notice that about 54-kJ (40-kip-ft) of the 'potential' energy is used to compress the gas for combustion. This energy value is calculated used the formula $E = \frac{1}{2}\, mv^2$, where m is the ram mass and v is the impact velocity measured by the proximity switches.

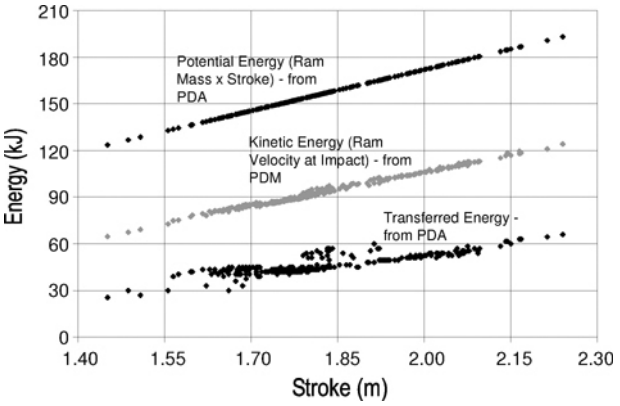

FIG. 2 – PDM and PDA Energy Data

Finally, Fig. 2 shows the transferred energy to the pile as calculated by the PDA system. Notice that this data series shows more 'scatter' than the PDM measured impact energy since it is affected by more variables such as pile/hammer alignment, cushion wear, small changes in driving resistance, etc.

In general, the energy monitoring system (PDM) used at the Woodrow Wilson Bridge was used as a quality assurance tool for the performance of the hammer. This energy monitoring system was used to verify that consistent energy was used to achieve the required blow counts. Combining the PDM data with the PDA data is instructive since the potential, kinetic (impact), and transferred (delivered) energies can be studied.

THE ENERGY CONTROL SYSTEM (ECS)

The next logical step in the advancement of technology for diesel hammers was the invention of a hammer energy control system. By combining the functions of the PDM (Figure 1) and the remote hydraulic throttle and adding basic control-system programming, the first ever diesel hammer energy control system was created (ECS) – see Fig. 3.

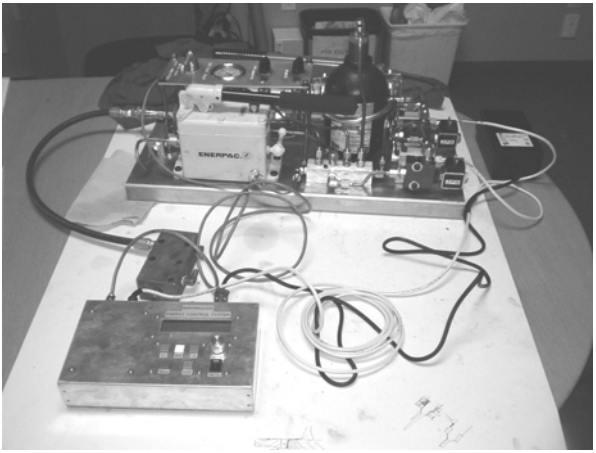

FIG. 3 – Prototype Energy Control System

The ECS contains a small hydraulic accumulator that provides a source of hydraulic flow to operate the throttle. The accumulator is 'pumped-up' at the beginning of the day, and stores enough oil to operate the system for several hours, depending on the amount of 'throttling' the system performs. The control box houses the programming and provides the control for two electronically activated valves that either let more oil into the throttle line (for more hammer impact energy), or release oil to a tank (to decrease the hammer impact energy).

Using the ECS requires no modifications to the diesel hammer and requires no additional control lines going to the hammer. The ECS simply makes use of the existing hydraulic throttle line in combination with the cable carrying the data from the proximity switches. The ECS allows the user to set an allowable maximum impact energy – this could be determined by a test pile with PDA testing, or determined theoretically using a wave-equation simulation program. The ECS also allows the user to select a specific target impact energy for the hammer and automatically tries to achieve that energy regardless of the driving resistance (the preset energy is not always attainable, especially near the beginning of driving or at other times when the driving is 'soft'). The small hydraulic pressure adjustments occur in after every hammer-blow for real-time control of the hammer impact energy. When the target impact energy in not attainable, the ECS stops increasing the throttle pressure when it reaches a pre-set maximum allowable pressure.

BUNGE EDIBLE OIL PRODUCTS FACILITY

The Bunge Facility is located in Hamilton, Ontario, Canada on the south shore of Lake Ontario. The pile driving undertaken at this project was performed by Bermingham Construction Limited, also of Hamilton. The project consisted of three pile types; 890-kN (100-ton) design load 273-mm (10.75-inch) pipe with 9-mm (0.365-inch) wall thickness, 1,335-kN (150-ton) design load 302-mm (11.875-inch) pipe with 15-mm (0.582-inch) wall, and 1,690-kN (190-ton) design load 346-mm (13.625-inch) pipe with 16-mm (0.625-inch) wall. All piles were driven closed-end. A total of 268 piles were driven on this site.

Soil conditions on the site varied due to the presence of a variety of fill materials. SPT blow counts in the upper layers ranged from 2-30. The underlying native material consisted primarily of silt over stiff clay-till. A weathered shale bedrock was present at a depth of approximately 30-m (100-ft). All of the piles were anticipated to be driven to either the stiff clay-till or the shale. Driving was performed using a Berminghammer B-32 Diesel Impact Hammer, with a rated (maximum potential energy) of 110-kJ (81,000-ft-lbs). PDA testing was planned for 10% of the piles. Driving was facilitated by a 70-tonne crane equipped with fixed-leads. The PDA testing was performed by AA Tech, Inc. of Ottawa, Ontario.

Results from the ECS

Approximately one-quarter of the piles on the project were driven using the ECS. Of this number, the first 17 piles were used to refine the programming of the ECS control logic based on the site and hammer. This process was necessary since this was the first time using the ECS in a project setting. Once the performance of the ECS was deemed satisfactory, 19 piles were driven with the ECS in complete control of the hammer. Of these 19 records, 2 records have been chosen for discussion. Both piles selected were 302-mm (11.875-inch) pipe with 1,335-kN (150-ton) design load. The termination criteria for these piles was 12-blows/25-mm with a hammer potential energy of 85-kJ (63-kip-ft) corresponding to a 2.75-m (9-ft) hammer stroke. The ECS target impact velocity was set to 5.5-m/s (18-ft/s) which corresponded to an impact (kinetic) energy of 49-kJ (36-kip-ft).

In both graphs the hammer impact velocity is on the left-vertical axis and the hammer throttle pressure is on the right vertical axis. The target impact velocity (usually 5.5-m/s (18-ft/s)) is shown as a dashed-line, the actual impact velocity is the solid black line, and the throttle pressure is the grey line. Each of these variables is graphed as a function of the cumulative number of blows on the horizontal axis.

In Figures 4 and 5, observe how close the actual impact velocity is to the target impact velocity and notice how the throttle pressure adjusts automatically to achieve the desired impact velocity. Also note in Figure 4 that the 'maximum' throttle pressure (grey line) is 3,100-kPa (450-psi) during the soft driving between blows 25-200. Increasing the pressure higher than 3,100-kPa (450-psi) does *not* deliver more fuel to the injectors, thus the threshold of 3,100-kPa (450-psi) was programmed into the ECS as the maximum allowable throttle pressure.

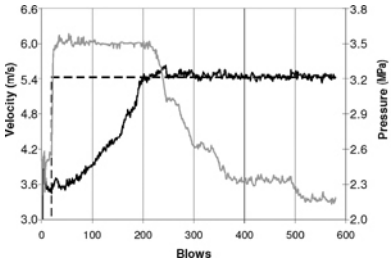

FIG. 4 – Record 080606B

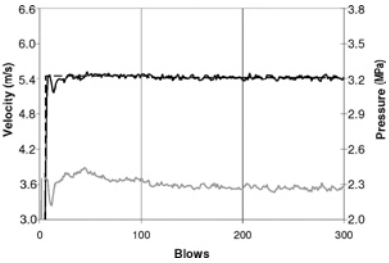

FIG. 5 – Record 140606D

In each graph note that the ECS was programmed for a hammer start-up pressure of 2,300-kPa (330-psi). This was the throttle pressure at which the hammer was known to start. Observe that after 10 blows, the ECS 'engaged' its control logic and attempted to achieve the target impact velocity. This can be seen by the pressure moving up (when necessary) to attempt to increase the impact velocity.

In Fig. 4 the ECS continuously lowers the hammer throttle pressure to maintain a constant 5.5-m/s (18-ft/s) impact velocity. This occurs as the blow-count (driving resistance) increases. On these piles the hammer and ECS could maintain the target impact velocity over the range of blow counts from about 2-blow/25-mm to 12-blows/25-mm. The hammer ran at lower than the target impact velocity for lower blow-counts (soft driving).

In Fig. 5, the hammer starts driving and is immediately able to achieve the target impact velocity. The ECS makes minor pressure adjustments to maintain the target velocity of 5.5-m/s (18 ft/second). Variations in the impact velocity are minimal; corresponding to stroke variations of about +/- 75-mm (3-inch).

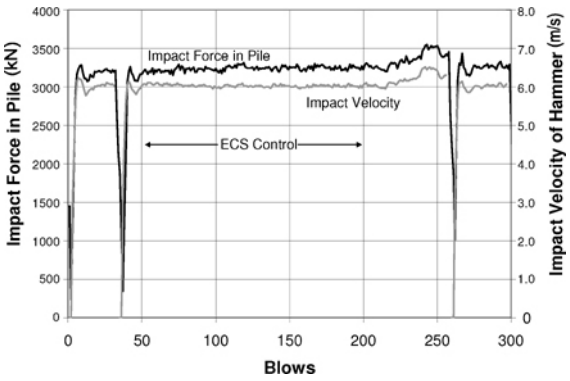

FIG. 6 – Impact Velocity of the hammer (ECS) and Impact Force in the Pile (from PDA)

Fig. 6 shows a comparison between the impact velocity of the hammer (controlled by the ECS) and the impact force in the pile. This figure shows how well the pile stress could be controlled using the ECS. From blow 50 to blow 200, the target impact velocity was left constant (not adjusted by the operator) and the impact force varies between 2,810-kN and 2,940-kN (630 and 660-kips), in direct proportion to the impact force. For this pipe pile (302-mm, 15-mm wall), these forces translate into stresses ranging from 200-MPa (29.0-ksi) to 209-MPa (30.4-ksi); a range of only 9-MPa (1.4-ksi).

FUTURE DIRECTION

Other experiments planned for the ECS include 'optimizing' the speed of the driving, minimizing fuel consumption, and pre-programming the ECS to drive through a given soil profile. It will also be possible to connect the ECS to a PDA device whereby the PDA can inform the ECS if the driving stress is too high and the ECS can reduce the impact force of the hammer accordingly. Additional programming will also be added to inform the operator when the hammer requires service – i.e. greasing and oiling, or when there is an obvious hammer malfunction.

The ECS also has the potential to be connected to other monitoring systems such as sound and vibration monitors. This would allow any measured parameter to be used as the control variable for the hammer impact energy. In other words, the ECS could ensure that measured sound or vibration levels from pile driving do not exceed a maximum allowable value.

CONCLUSIONS

This paper has demonstrated the use of an energy monitoring system at the Route1/I-95 project driving 610-mm (24-inch) square concrete piles. This paper has also demonstrated the use of the ECS on a project in Canada. This project represents the first attempt (known to this author) to automatically control the impact velocity of a diesel pile driving hammer.

After the initial period of program refinement, the ECS proved that a diesel pile driving hammer can be controlled automatically. In addition to the QA and QC functions already mentioned the ECS is capable of other functions described in the following paragraph. The ECS's full potential has not been realized, but the 19 piles driven at the Bunge Facility have proven that the concept is not only feasible, but that the energy control is very accurate.

Plans for the future direction of this technology have also been discussed.

REFERENCES

Virginia DOT – *Project Specifications,* Route 1/I-95 Interchange, (2003)

Pile Dynamics Inc. – *Product Specification Sheets:* Saximeter™ and E-Saximeter™ (2007)

Bermingham Foundation Solutions – *Product Specification Sheet:* Pile Driving Monitor (2007)

Copyrighted Materials
Copyright © 2009 American Society of Civil Engineers (ASCE)
Retrieved from www.knovel.com

DRIVEN DUCTILE IRON PIPE PILES DESIGN, INSTALLATION AND PERFORMANCE

Frank Schmidt[1]
Thomas N. Dobras, P.E. Member ASCE[2]

[1]DSI (DYWIDAG-Systems International GmbH), Siemensstrasse 8, 85716 Unterschleissheim, Germany, PH +49 / 89 / 30 90 50 – 182, FAX +49 / 89 / 30 90 50 – 170, email: frank.schmidt@dywidag-systems.com

[2] DSI (DYWIDAG-Systems International USA, Inc.), 4732 Stone Drive, Tucker, GA 30084, PH (770) 491-3790 Ext. 223, FAX (770) 938-1219, email: thomas.dobras@dsiamerica.com

ABSTRACT

The driven ductile iron pile system is a simple and economical driven foundation system, requiring only a medium sized excavator equipped with a hydraulic, breaker-type driving hammer and a specially fabricated driving shank. The pipe material is centrifugally-cast ductile iron, with decades of proven success in underground applications, and which has excellent tenacity, ductility, strength, and corrosion resistance properties. The individual pipe sections, 5 m (16.4 ft) in length and outside diameter of either 118 mm (4.6 in) or 170 mm (6.7 in), are joined together via a conical bell end on one side, and tapered spigot on the other side. The length of each pile can be adapted to the actual ground conditions. The upper most pipe section is cut with a standard pipe cutting saw and then fitted with its own driving shoe for use as the first pipe section for the next pile, thereby minimizing waste. End-bearing piles are filled with concrete/grout after driving creating a continuous load bearing structural member. Friction-bearing piles are grouted simultaneously to driving, both through the interior of the pile and along the exterior annulus to provide both the required frictional resistance and excellent protection against corrosion. The driven ductile iron piles represent a proven and economical alternative for driven micropiles with the following primary advantages: low mobilization cost; rapid installation up to 400 meters (1300 feet) per day utilizing lightweight and easily manoeuvrable equipment; robust (i.e. impact resistant) piles; and high corrosion resistance.

ABOUT THE DRIVEN DUCTILE IRON PILE SYSTEM

General

The driven ductile iron pile system is an easy foundation system to mobilize and install. The installation requires a medium sized hydraulic excavator weighing 25-30 tonnes, (28-34 tons) with a hydraulic breaker-type hammer with the following approximate specifications: hammer energy: 4000-5000 Joules (3000-3700 ft-lbs); hammer blow rate: 300-600 BPM; hammer length: 2m (6.5 ft); and hammer weight: 1.7-2.2 tonnes (1.9-2.5 tons)

The ductile iron pipe piles are typically driven down to the bearing soil layer. Alternatively, they can serve as friction-bearing piles which are grouted inside and out to provide similar frictional resistance as auger cast-in-place piles. For the friction-bearing piles, grouting is done simultaneously to driving using a specially fabricated grout injection shank and an oversized grout shoe creating an annulus along the exterior of the pile which allows the grout to flow uniformly to the surface. The first pile section has small triangular pieces cut out on one or both sides of the pile section to allow the concrete/grout to flow through the pile section and around the exterior annulus.

The individual pipe segments have a length of 5 m (16.4 ft) and outside diameter of either 118 mm (4.6 in) or 170 mm (6.7 in). The bell end is fabricated with a double wall thickness socket wall and internal shoulder to provide a spigot end stop. The pipe segment extending beyond the surface after driving to the desired length can be cut with standard pipe cutter after driving and the remaining segment can be fitted with a driving shoe and used as the first pipe segment of the next pile. The individual pipe sections are cold-welded together at the bell-and spigot joint locations during driving creating a significantly more stable system and allowing the designers to consider each pile as a continuous monolith rather than individual discreet sectional components.

Free standing non-grouted pile

View on the hydraulic hammer

Installation of non-grouted end bearing pile

Installation of grouted friction bearing pile

Grouted pile driving shoe

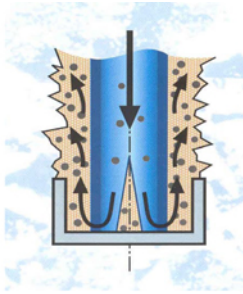
Schematic of first pipe section with grouted pile driving shoe and cut-away area

Installation Procedure

The illustration below demonstrates the ease of setup and installation which can be performed at a rate of approximately 200 to 400 meters per day (650-1300 feet/day), depending on the ground and site conditions.

Unloading the pipe sections

Positioning of the first section onto the shoe

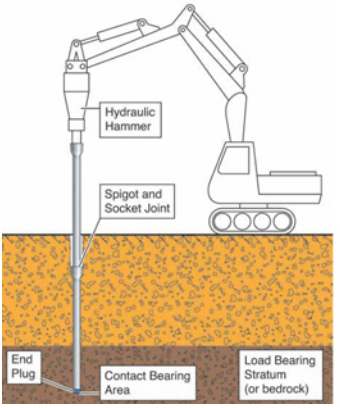

Dry driving to end bearing

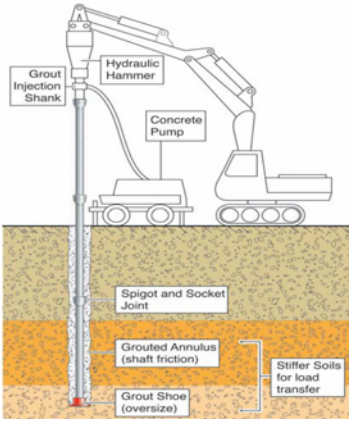

Driving to design bond length while grouting interior and exterior annulus

The pile components

Raw Material

The raw material of the spun-cast iron pipes is ductile cast iron, a development of gray cast iron which has been used worldwide in the sewer and water industry for more than a hundred years. Ductile iron is produced by treating molten low sulphur iron with magnesium creating free graphite deposits in a spheroidal or nodular form, replacing the flake form of graphite in the old gray cast iron. The free graphite in nodular form improves its strength, ductility, and impact resistance while maintaining the excellent corrosion resistant properties of gray cast iron and the ductility properties of Grade 50 steel.

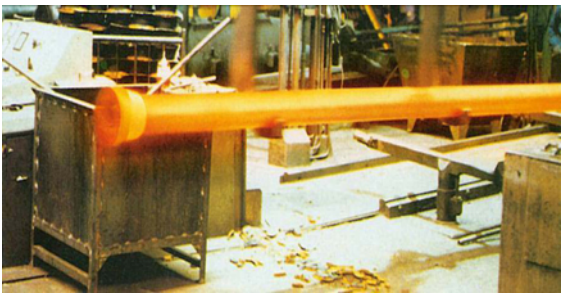

Spin-casting of ductile iron pipe piles

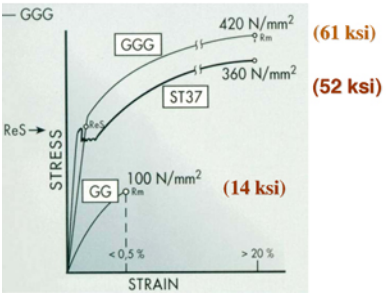

Stress-strain curves of ductile cast iron, (GGG), gray cast iron (GG), and Grade 50 steel (ST37)

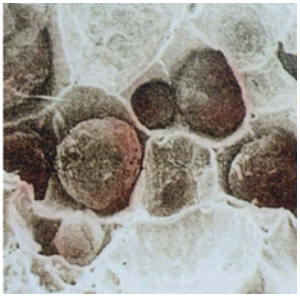

Microscopic view of nodular graphite in ductile iron

Pipe Pile Components and Specifications

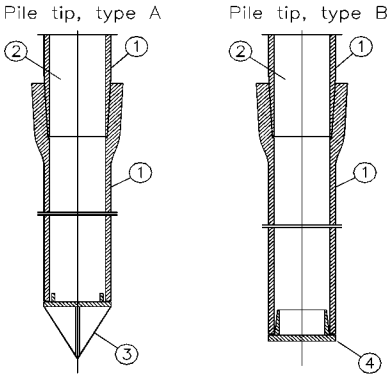

① Cast iron pipe
② Cement grout or concrete filling strength class corresponding to B25
③ Ram bit
④ Ram shoe

O.D. mm (in)	Wall Thick mm (in)	Weight per 5m kg (lbs)	Tensile Stress MPa (ksi)	Yield Stress MPa (ksi)	Ultimate Load kN (kips)	Yield Load kN (kips)	Sect Mod cm^4 (in^4)	Mom. Inertia cm^3 (in^3)
118 (4.6)	7.5 (0.3)	105 (231)	420 (61)	300 (44)	1093 (246)	781 (176)	68 (4.2)	399 (9.6)
118 (4.6)	9.0 (0.35)	123 (271)	420 (61)	300 (44)	1294 (291)	925 (208)	78 (4.8)	461 (11.1)
170 (6.7)	9.0 (0.35)	186 (410)	420 (61)	300 (44)	1912 (430)	1366 (307)	174 (10.6)	1480 (35.6)
170 (6.7)	10.6 (0.42)	213 (470)	420 (61)	300 (44)	2229 (501)	1592 (358)	199 (12.1)	1683 (40.4)

Distinction between grouted piles and non-grouted piles

Corrosion protection

It has been proven through decades of research[2] that unprotected ductile iron pipes in corrosive environments will not corrode uniformly as might be expected in standard steel pipes, but rather in isolated areas as evident by pitting. For bare uncoated pipe this pitting occurs at an average rate of 0.4 mm (0.015 in) per year. It can therefore be calculated that the time to penetration will be approximately 19 years for 7.5 mm pipe and 22 years for 9 mm pipe. Additional research[3] has shown that even with heavy concentration of pitting due to highly aggressive soils the 0.2% yield strength is not reduced by more than 50% over the life of the pile from its original value. Therefore a maximum allowable compressive load of 33% of its 0.2% yield load capacity should provide adequate safety factor against the pitting effects of corrosion in even the most aggressive environments and will also comply with the requirements of the *International Building Code 2000*.

Grouted piles with a uniform grout layer both inside the pile and outside in the surrounding annulus area will provide excellent protection against corrosion by maintaining a uniform, high alkaline environment surrounding the pipe. The Ductile Iron Pipe Research Association, (DIPRA) a non-profit trade association representing the US ductile iron pipe manufacturers, has developed a 10-Point System[2], as described in Appendix A of ANSI/AWWA C105/A21.5 as a basis to predict a soil's long term corrosivity effects on ductile iron pipes.

DIPRA recommends testing of the soil at the actual location and depth that the piles are to be installed using the following soil tests to determine its overall corrosivity score on the 10-point scale: resistivity, moisture content, pH, chlorides, sulphides, and Oxidation-Reduction Potential (REDOX).

Excavated grouted pile showing uniform grout coverage

Grouted pile showing grout apparent at surface

Installation of grouted (friction-bearing) piles

If the soils are non-cohesive with medium density, or mixed soils with a high percentage of gravel and sands, then the grout driving shoe can be used to create the grout annulus and transfer the pile load via skin friction into the surrounding ground. The concrete/grout flows through the pile down to the bottom, and through the opening of the pile foot into the annulus and up to the surface. Grouting inside and outside along the annulus is performed simultaneously to driving of the pile.

Installation of non-grouted (end- bearing) piles

For end-bearing piles, the ductile iron piles are driven into the ground until the load bearing layer is reached. A grout shoe which fits snugly inside the first pile section being driven aids in the driving. A rock point shoe will assist in driving through harder soils which contain gravels and aggregates. If the driving progress of the pile achieves refusal, typically defined in the pile driving industry as approximately 2-3 cm (1 in) of penetration per minute, depending on the specific soil type, then the load capacity of the pile is automatically at least as large as the maximum force of the hydraulic hammer. After the pile driving has been terminated, the pile is cut with a pipe cutting saw at the required level and the cut section reused for the next pile.

End-bearing driving shoe fits inside pipe

Friction-bearing driving shoe fits outside pipe

Grout injection shank for driving grouted piles

Cutting piles to the required length. Cut section can be fitted with a grout driving shoe and reused

Noise and Vibration Concerns

Because of the low vibrations and noise levels associated with driven ductile iron piles it is possible to drive piles for the foundations of an add-on/rehabilitation of an existing building, in reasonable close proximity to the existing structure. On a jobsite in Berlin, driven ductile piles were installed near the renowned hospital Charité[1]. A continuous surveillance of the construction site noise was performed at the entrance to the hospital, approximately 50 m (165 ft) from the site. The data indicated that the noise-level of the pile driving alone was only slightly higher than the basic noise-level of the construction site, or equivalently the same noise levels as a car driving directly by the measuring point. The following noise-levels were recorded:

Noise levels measured at a point 50 m from project site, at hospital entrance:

	values in dB(A)		
	L_1	L_{50}	L_{95}
Basic noise-level of the construction site, no driving	76.0	71.1	68,8
Noise level during pile-driving	79.0	74,1	69,7

$L_{1,50,95}$ = level, which is reached or exceeded in 1, 50 or 95% of the measuring period

On a job site in Salzburg[1], vibration-detectors were installed on a concrete wall located approximately 10 to 30m (33 to 98 ft) away from the driving location. Vibrations were measured during parallel installation of two ductile iron piles and the following vibration-velocities were measured by the vibration detectors:

Max. values: 0.22 – 0.77 mm/s (0.009 – 0.03 in/s)
Mean values: 0.04 – 0.13 mm/s (0.002 – 0.005 in/s)

As indicated from the data listed above, the vibrations that occur while ductile iron piles are driven are significantly below the permissible values even for a sensitive historic buildings which is 2.0 mm/sec (0.08 in/s) per the German building code standard DIN 4150-3 (1999.

References

[1]Schmidt, F. (2004). "Geotechnics - Ductile Driven Piles, Report No. 58." *DSI Internal Technical Document,* DYWIDAG-Systems International GmbH Technical Services, Munich, Germany: 1-33

[2]Horn, L.G. (2006). "The Design Decision Model™ For Corrosion Control of Ductile Iron Pipelines." Ductile Iron Pipe Research Association, Birmingham, AL:1-8

[3]Schütz, P., Hirhager, R., Pommer, G. (1999). "Prefabricated Driven Piles Made of Ductile Cast Iron." Vienna Municipal Corporation, Department MA 3-VFA Vienna Municipal Test and Research Institute, Vienna, Austria: 1-30

Copyrighted Materials
Copyright © 2009 American Society of Civil Engineers (ASCE)
Retrieved from www.knovel.com

Characterization of Precast UHPC Pile Driveability

Thomas Vande Voort1, Muhannad Suleiman2, Sri Sritharan3

In 2005, AASHTO identified extending the service life and optimizing structural systems of bridges as two grand challenges for bridge engineering. Ultra High Performance Concrete (UHPC) possesses superior strength and durability, which can assist in meeting these challenges. The research team has explored the use of UHPC in deep foundation applications. H-shaped precast, prestressed UHPC piles have been designed and prefabricated. The UHPC piles were designed with comparable overall dimensions and self weight to a steel HP 250×85 pile. The driveability of the UHPC piles compared to normal concrete, high performance concrete, and steel piles has been examined through a driveability study using a wide range of driving parameters and GRLWEAP. UHPC piles demonstrate increased driveability over NC and HPC and can be driven with comparable ease to steel piles.

INTRODUCTION

In 2005, the American Association of State Highway Transportation Officials (AASHTO) issued a strategic plan for bridge engineering, which included seven "grand challenges", two of which were extending service life and optimizing structural systems. One of the greatest obstacles to achieving the target 75-year service life for a typical bridge is material deterioration, including deterioration of foundations. Steel piles and steel reinforcement in concrete piles are subject to corrosion. Even in non-marine environments, corrosion can lead to significant section loss. For example, steel piles supporting integral bridge abutments have experienced high levels of corrosion due to the alternate wetting and drying of the pile in a soil gap that forms under the abutments (White et al. 2007).

One of the areas highlighted by AASHTO in optimizing structural systems is using high performance materials such as Ultra High Performance Concrete (UHPC). UHPC is a new concrete mix with a very high compressive strength, which is achieved through mix optimization and heat treatment. Typical material properties of UHPC are compared to normal concrete (NC) and high performance concrete (HPC) in Table 1. The low porosity of UHPC also makes it extremely durable, up to several orders of magnitude more durable than HPC or NC (Roux et al. 1996).

---

[1]Graduate Student, Dept. of Civil, Construction, and Environmental Engineering, Town Engineering Building, Iowa State University, Ames, IA, 50011. E-mail: tomvv@iastate.edu
[2]Assistant Professor, Dept. of Civil and Environmental Engineering, 321 Acopian Engineering Center, Lafayette College, Easton, PA, 18042. E-mail:suleimam@lafayette.edu
[3]Associate Professor, Dept. of Civil, Construction, and Environmental Engineering, 406 Town Engineering Building, Iowa State University, Ames, IA, 50011. E-mail: sri@iastate.edu

TABLE 1. NC and HPC Properties Compared to UHPC

Property	NC	HPC	UHPC
Compressive Strength	25 – 55 MPa	80 – 125 MPa	180 – 210 MPa
Tensile Strength	2 – 5 MPa	5 – 6 MPa	12 MPa
Elastic Modulus	25 – 35 GPa	33 – 44 GPa	55 GPa

DESIGN OF A UHPC PILE SECTION

With the high strength and durability of UHPC comes a relatively high cost, which emphasizes the need to develop optimized sections. A tapered H-shaped section was chosen over hollow sections, since this section is easy to form and does not require collapsible forms. The taper also reduces the risk of air pockets forming on the top surfaces of the bottom flanges during casting.

The UHPC pile section was reinforced with ten, 13-mm diameter prestressing strands and no mild steel. The high strength and durability of UHPC allowed a reduction in the concrete cover required on the prestressing strands from 32 mm to 19 mm. The final UHPC section is a 254 by 254-mm tapered H-shaped section, which is shown next to a steel HP 250×85 pile with roughly the same outer dimensions in Fig. 1. The HP 250×85 steel pile section is commonly used by many states, including Iowa, in bridge foundations (Iowa Department of Transportation 2007).

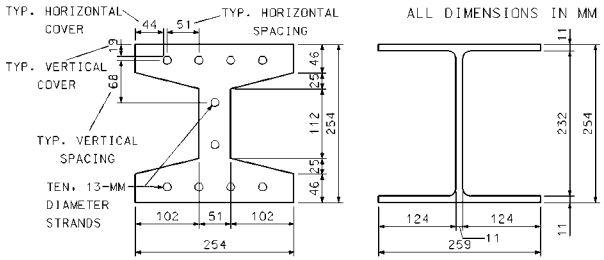

FIG. 1. Comparison of Dimensions of UHPC Pile and Steel HP 250×85 Pile

The area of the UHPC pile is 3.4 times that of the steel pile, but the weight of each pile per unit length is similar, as shown in Table 2. The stiffness term, E·A, of the UHPC pile is only reduced by about 7 percent compared to the steel pile.

TABLE 2. Comparison of Section Properties of UHPC and Steel HP 250×85 Pile

Property	Steel HP 250×85 Pile	UHPC Pile
Area	10,800 mm^2	36,600 mm^2
Weight	85.1 kg/m	90.9 kg/m
Stiffness Term, E·A	2.17×10^6 kN	2.02×10^6 kN

DRIVABILTY STUDY

In addition to having sufficient strength and durability, UHPC piles must be driveable. A driveability study was conducted using the wave equation program GRLWEAP (2005) to compare the driveability of a UHPC pile to NC, HPC, and steel piles in a variety of soils with different driving systems.

Material Types

The square NC and HPC piles used in the driveability study were proportioned to give each pile approximately the same factored axial compressive strength as the UHPC pile (See Fig. 3). The HP 250×85 steel pile was also analyzed because it has similar outer dimensions to the UHPC pile. Eight, 13-mm diameter prestressing strands were used in the NC pile and four in the HPC pile. Each strand was stressed to 70 percent of its 1860 MPa ultimate strength (f_{pu}) and had estimated prestress losses of 310 MPa after AASHTO (2004). The ten prestressing strands in the UHPC pile were stressed to $0.75 \cdot f_{pu}$ and prestressing losses were calculated to be 326 MPa. The tension and compression stress limits calculated using AASHTO formulas are shown in Table 3. The high compressive strength and high prestressing in UHPC allow the UHPC pile to have much higher stress limits than NC and HPC.

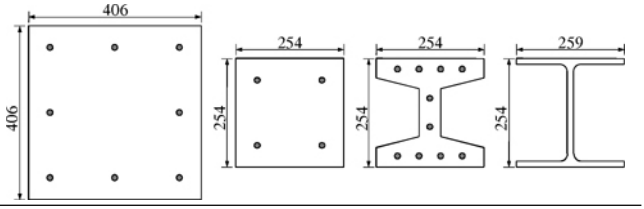

Pile	NC – 406 mm Sq.	HPC – 254 mm Sq.	UHPC – 254 mm H	Steel HP 250×85
Area	165,100 mm²	64,500 mm²	36,600 mm²	10,800 mm²
Comp. Str.	35 MPa	85 MPa	180 MPa	345 MPa (Yield)
Pile Axial Str.	4060 kN	4140 kN	4470 kN	2240 kN

FIG. 2. NC, HPC, UHPC, and Steel Cross-Sections Used in Driveability Study

TABLE 3. Driving Stress Limits for Piles Used in Driveability Study

Pile	NC	HPC	UHPC	Steel
Tension Driving Stress Limit	6.2 MPa	8.3 MPa	37.3 MPa	310.0 MPa
Compression Driving Stress Limit	24.5 MPa	64.3 MPa	122.0 MPa	310.0 MPa

Soil Profiles

Three different soil profiles were used to examine the driving behavior of each of the pile types. The DRIVEN computer program was used to create input files for the GRLWEAP analysis from the soil profiles. The first soil profile, called "Bearing Soil", is characterized by a large end bearing resistance and is similar to one from Colorado reported in a paper by Goble and Hussein (2000) analyzing the driving of

HPC piles. The soil layer details are shown in Table 4. Each pile was modeled as being driven 13.1 m into this soil.

TABLE 4. Details of "Bearing Soil" Profile

Depth to Bottom of Layer (m)	Type	Unit Weight (kN/m^3)	Undrained Shear Strength, s_u (kPa) or Friction Angle, ϕ
2.5	Cohesionless	18.0	$\phi = 30.8°$
13.0	Cohesionless	18.0	$\phi = 31.5°$
16.0	Cohesive	22.0	$s_u = 3000.0$

The second soil profile, "Combination Soil", provides resistance through both end bearing and friction. This soil profile is also similar to one presented by Goble and Hussein (2000), and its details are shown in Table 5. Each pile was modeled as being driven 22.3 m into this soil.

TABLE 5. Details of "Combination Soil" Profile

Depth to Bottom of Layer (m)	Type	Unit Weight (kN/m^3)	Undrained Shear Strength, s_u (kPa) or Friction Angle, ϕ
1.5	Cohesionless	18.0	$\phi = 28.5°$
6.0	Cohesive	14.0	$s_u = 25.0$
18.0	Cohesionless	18.0	$\phi = 32.9°$
22.0	Cohesionless	18.0	$\phi = 34.8°$
30.0	Cohesionless	18.0	$\phi = 38.9°$

The final soil profile was designed as a cohesive soil with very little end bearing, called "Friction Soil". The details of the soil are shown in Table 6. Each pile was modeled as being driven to a depth of 18.3 m in this soil.

TABLE 6. Details of "Friction Soil" Profile

Depth to Bottom of Layer (m)	Type	Unit Weight (kN/m^3)	Undrained Shear Strength, s_u (kPa) or Friction Angle, ϕ
1.2	Cohesive	15.7	$s_u = 23.9$
6.1	Cohesive	16.5	$s_u = 47.9$
16.8	Cohesive	16.5	$s_u = 95.8$
18.6	Cohesive	16.5	$s_u = 71.8$

Driving System

A DELMAG D19-42 open-ended diesel hammer was used for most of the driveability analyses, but some additional analyses were conducted using D8-22, D36-32, and D100-13 as well. The details of each hammer are shown in Table 7. The D8-22 was included since it has a low ram weight. The D19-42 is a common hammer that has been used to drive two UHPC piles (Vande Voort 2008). The D36-32 was used in the HPC study by Goble and Hussein (2000). The D100-13 is the largest

DELMAG hammer with a recommended pile weight range that includes the weight of the heaviest pile in this study, the 22.3-m long NC pile (8830 kg).

TABLE 7. Details of Hammers Used in Driveability Study

Hammer	Ram Weight[a] (kN)	Maximum Stroke[a] (m)	Maximum Energy[a] (kJ)	Combustion Pressure[a] (kPa)	Recommended Pile Weight Range[b] (kg)
D8-22	4.90	3.48	27.3	12,270	500 – 3000
D19-42	17.80	3.30	58.6	10,480	1100 – 6000
D36-32	35.29	3.48	122.8	10,000	2500 – 12,000
D100-13	98.19	3.67	360.2	10,410	7000 – 100,000

Notes: [a]Source: GRLWEAP 2005; [b]Source: DELMAG 2007

For each analysis, a 102-mm thick hammer cushion (between the hammer and helmet) was used. The cushion had an elastic modulus of 3650 MPa and a coefficient of restitution of 0.8. The helmet weight and hammer cushion area were varied according to the standard equipment for each hammer. The pile cushion (between the helmet and the top of the pile) was plywood with an elastic modulus of 210 MPa and had thicknesses ranging from 0 mm to 305 mm. The deterioration of the pile cushion during driving was modeled by multiplying the stiffness by an initial factor of 0.8, increased to 1.0 over the duration of driving. The coefficient of restitution was also reduced from an initial value of 0.5 to 0.45 at the end of driving.

Analysis Parameters

The "driveability" analysis option in GRLWEAP was used for the study rather than the bearing graph options. Smith soil damping was used. GRLWEAP allows the user to fix the stroke or combustion pressure of the diesel hammer or both. A fixed stroke was used in each analysis, but if the computed combustion pressure exceeded the maximum pressure for the hammer, both parameters were fixed. Stresses calculated by the program were ignored if the number of blows per meter of driving was lower than 15, since the program may be sensitive to small changes at very low resistance.

Results from Pile Types in Different Soils

The maximum stresses during the driving of each of the piles were calculated for each of the soil profiles for cushion thicknesses ranging from 0 mm to 152 mm. The stresses are shown in Fig. 5, Fig. 6, and Fig. 7 for the "Bearing Soil", "Combination Soil", and "Friction Soil", respectively. In each type of soil, the NC pile exceeded the tension stress limit, except with a 152-mm thick pile cushion in the "Bearing Soil". The NC pile also exceeded the compression limit in each soil with 0 mm and 51 mm pile cushion thicknesses. HPC also had tension problems with no pile cushion in the "Combination Soil" and "Friction Soil" and exceeded the compression limit with no pile cushion in the "Bearing Soil". The stresses in the UHPC and steel piles were well below limits in every soil with any pile cushion thickness. (The steel pile was modeled without a pile cushion, as is common construction practice.)

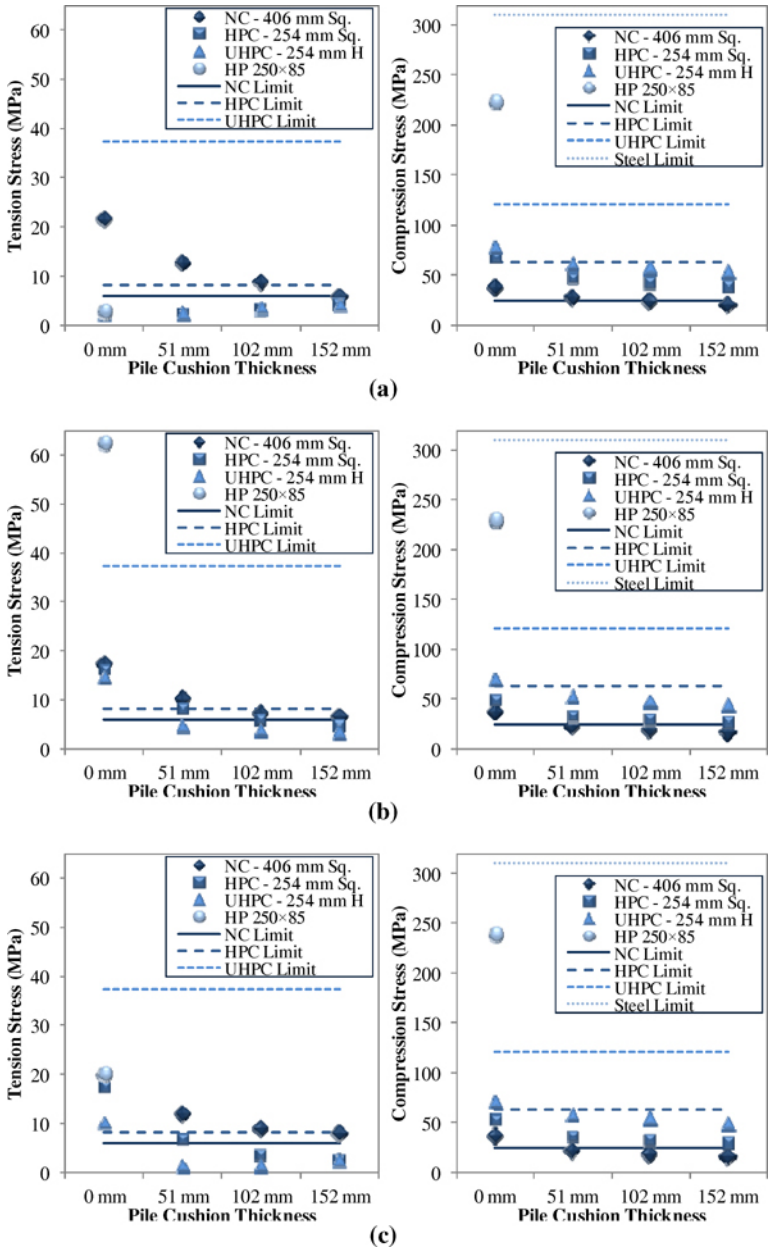

FIG. 3. Tension and Compression Stresses with a D19-42 hammer and 3.0 m stroke in (a) Bearing Soil, (b) Combination Soil, and (c) Friction Soil

Table 8 shows the ratios of the calculated tension and compression stresses with a 102-mm thick pile cushion (except for the steel pile) from Fig. 3c to the stress limits shown in Table 7. The table shows that the UHPC pile has the lowest ratios in both tension and compression in this case, indicating it has significant reserve capacity to handle driving stresses.

TABLE 8. Ratios of Calculated Stresses to Stress Limits for 102-mm Thick Pile Cushion with a D19-42 Hammer, 3.0 m stroke, and Friction Soil

Pile	(1) Calc. Tens. Str. (MPa)	(2) Tens. Str. Limit (MPa)	(1)/(2)	(3) Calc. Comp. Str. (MPa)	(4) Comp. Str. Limit (MPa)	(3)/(4)
NC	9.1	6.2	1.47	18.3	24.5	0.74
HPC	3.6	8.3	0.44	32.1	64.3	0.50
UHPC	1.8	37.3	0.05	53.0	122.0	0.43
Steel	20.2	310.0	0.07	238.6	310.0	0.77

Results Using Different Hammers

The NC and UHPC piles were also analyzed with all four hammers, each with a 2.1 m and 3.0 m stroke, in the "Friction Soil". The maximum tension and compression stresses calculated during driving with a 0-mm thick and 102-mm thick pile cushion are shown in Fig. 4a and 4b, respectively. For both cushion thicknesses, the NC and UHPC piles experienced refusal before reaching their full penetration with the D8-22 hammer with the 2.1 m stroke. Refusal, defined as a driving resistance of 790 blows/m or greater (DFI 2008), was also experienced for each pile with the 3.0 m stroke and the D8-22 when the 102-mm thick pile cushion is used. For the other hammers, the figures show that NC exceeds its tension limit for every hammer except the D100-13, and it exceeds its compression limit with every hammer. In other words, the NC pile cannot be driven in this soil profile with no pile cushion. Even with a 102-mm thick pile cushion, the NC pile can only be driven with the D36-32 hammer with a 2.1 m stroke. UHPC, however, can be driven without a pile cushion with any hammer and stroke except the D8-22 with a 2.1 m stroke or the D100-13 with 3.0 m stroke.

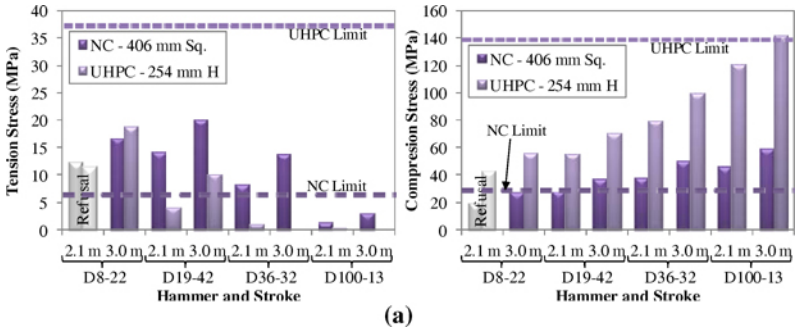

(a)

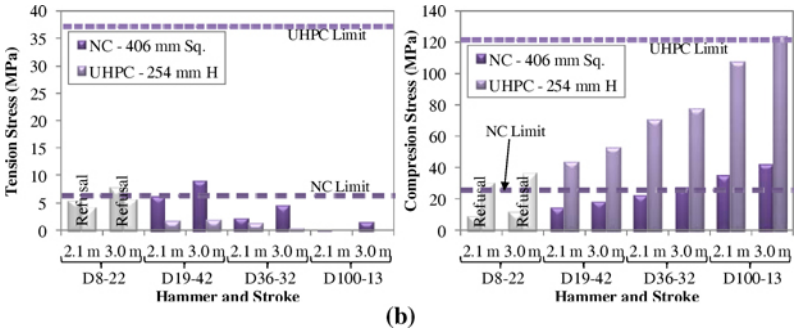

FIG. 4. Tension and Compression Stresses with Various Hammers and Strokes in Friction Soil with (a) 0-mm thick and (b) 102-mm thick pile cushion

CONCLUSIONS

The high compressive strength and high prestressing that can be used in UHPC piles allows them to have high driving stress limits. The driveability analysis using different soil types shows that stresses induced in a UHPC pile during driving are not much higher than those in NC or HPC, and the ratio of the calculated stresses to the limits are much lower for UHPC than NC or HPC and are comparable to steel. The analyses showed that UHPC may be able to be driven with no pile cushion in most situations, and it also may be driven with a wide range of hammers and strokes.

REFERENCES

AASHTO. (2005). "Grand challenges: a strategic plan for bridge engineering." AASHTO Subcommittee on Bridges and Structures.

White, D.J., Mekkawy, M.M., Sritharan, S., and Suleiman, M. (2007). "Underlying causes for settlement of bridge approach pavement systems." *J. of Performance of Constructed Facilities*, ASCE, Reston/VA: 273-282.

Roux, N., Andrade, C., and Sanjuan, M.A. 1996. "Experimental study of durability of reactive powder concretes." *J. of Materials in Civil Engrg.* 8 (1): 1-6.

Iowa Department of Transportation. (2007). *ASD/LFD Bridge Design Manual.* http://www.dot.state.ia.us/bridge/manualasd.htm.

GRLWEAP. (2005). GRL Engineers, Cleveland/OH.

AASHTO. (2004). *AASHTO LRFD Bridge Design Specifications*, Third Ed.

DRIVEN. (2001). Version 1.2, FHWA, Washington/DC.

Goble, G., and Hussein, M. (2000). "Potential for HPC in driven pile foundations." *Symposium Proc. – PCI/FHWA/FIB Intl. Symposium on High Performance Concrete, Orlando, FL, Sept. 25-27*, Johal, PCI, Chicago/IL: 608-625.

Vande Voort, T. (2008). Design and field testing of tapered H-shaped Ultra High Performance Concrete piles. *MS Thesis*, Dept. of Civil, Construction, and Environmental Engineering, Iowa State University, Ames, IA, 229 p.

DELMAG. (2007). *Diesel Pile Hammer Technical Data*, Esslingen, Germany.

DFI. 2008. *Online term search*, http://www.dfi.org/, Hawthorne/NJ.

Copyrighted Materials
Copyright © 2009 American Society of Civil Engineers (ASCE)
Retrieved from www.knovel.com

The Vibro-Jetting Driving Method

Hermann Zeilinger, M, PDCA, Dipl.- Ing. TU

Partner, Harland Associates, 1, rue du Moulin, 7423 Dondelange, Luxemburg, zeilbuch@pt.lu

ABSTRACT: The driving procedure using vibratory hammer in combination with specific water jetting, preparing the soil at the piles tip for easy penetration became the standard installation in cases where environmental regulations and difficult soil conditions did eliminate the usual methods. The vibro-jetting procedure requires well equipped and trained driving crews to meet the restrictions in sensitive areas, concerning limited ground vibration, low noise levels and short construction time. The paper presents the equipment needed, operation areas and calculation of the cost. It answers questions regarding the change and influence of the soil conditions.

INTRODUCTIONS

The combination of vibratory hammers and water jetting as aid easing the driving process is pretty well known since decades. In the very beginning of this unusual driving assistance, contractors used big lances, tubes up to 4 inches in diameter transporting a high amount of water into the ground. The soil became almost liquid around the piling and the vibratory hammer pushed the piling down in this kind of mud easily. But as consequence the soil parameter were never the same as before. The system did work only in cases where these changes were of no importance.

DESCRIPTION OF THE PROCUDURE; EQUIPMENT REQUIRED

The modern controlled jetting was developed in the late seventies in Munich. The construction of the subway through the inner city with small streets and historical buildings on both sides required an adjusted construction process. This process had to meet a list of requirements in particular: low ground vibration, low noise emission: factors which concerned people living near by. The groundwater is used as drinking water reservoir, and the soil condition of this area are extremely difficult with glacial compacted layers of marl, hard like natural concrete.

Tunneling was excluded, because of the two different water floors, with the lower one under artesian pressure. Required was an open excavation protected by a removable cofferdam system to restore the groundwater flow after the construction. Steel sheet piling was the only reliable solution left, but faced difficulties. No pile

driver knew how he could meet the limits of the codes. Finally two solutions, which did meet the requirements, were discussed: Drilling of overlapping boreholes, replacing the soil by a loose sand gravel mixture, setting up the sheet piling into this trench using first a vibratory hammer and finally an impact hammer for the last 1 m.

Finally the modern controlled vibro-jetting did prove its efficiency. The daily, the number of doubles was several times higher as per drilled soil exchange. Ground vibration, noise or water tightness was never a question.

This was the beginning of a successful period of this modern driving procedure. Today pile drivers in many countries, even in Australia or South Africa, use the vibro-jetting method to meet environmental regulations.

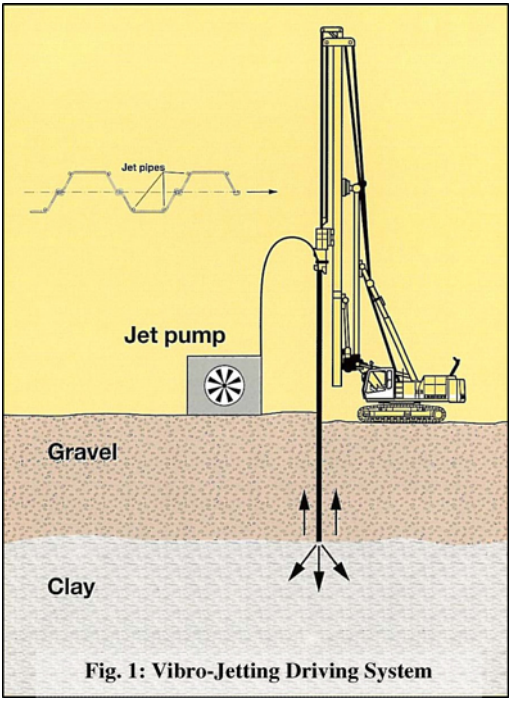

Fig. 1: Vibro-Jetting Driving System

What are the basics of success of the modern controlled vibro-jetting method? Driving of piles has to overcome the soil resistances: such as the friction along the piles, the interlock friction, the resistance at the pile tip. Small lances welded to the piles transporting a controlled amount of water under low constant pressure down to the tip of the sheets. The pressure is high enough causing the backflow of the water to the surface, acting like a lubricate film reducing the skin friction and adhesion to almost zero. The flowing water is also washing out the loose soil particles in the small gap caused by the up and down of the vibration at the pile's end, preparing further penetration. Before this driving procedure could become state-of-the-art as it is accepted in our days, the influence and changes of the jetting concerning the subsoil conditions had to be answered. Usually subsoil investigations are based on boring logs and the laboratory tests of disturbed and undisturbed soil samples.

The first step was simple: borings done before and after the vibro-jetting driving were compared. The results of all investigations did not show any significant differences which could be related to the jetting. All compared data did lie within the tolerance of the testing process. The conclusion of all comparisons for non cohesive as well as for cohesive soils did indicate that parameters are not inflicted by this controlled low pressure jetting, the density, submerged or dry, the angle of internal friction and of the wall friction, the coefficient of compressibility remain unchanged.

Fig. 2: Jetting Container for Water + Air

Shear tests of cohesive soil strata show the same cohesion values for all samples. Further investigations of the water flow did confirm the conclusion above. Piezometer and pore water gages were placed under 90 degrees to the driving direction controlling the water pressure during the jetting in non cohesive and the pore water pressure in cohesive soil layers. In sand and gravel the jetting water flew back up along the skin. In 0.5 m distance from the sheets no influence was registered. In clay the gages, controlling the pore water pressure, did show no change during the jetting. A lubricant emulsion of water with clay particles did flow from the tip of the sheeting to the surface reducing the skin friction and adhesion to zero.

The angle of wall friction delta is direct proportional to the skin friction of the piling and the soil and is therefore most important for any static analysis for retaining walls and the stability checks of any structure. The indirectly done investigations and the conclusions above should be confirmed by appropriate field investigations. These tests were executed under the leadership of the "Physical Laboratory of Soil Mechanics and Foundation of the Technical University of Munich" under Prof. Dr. Jelinek and his successor Prof. Dr. Floss.

The test arrangement show to rows of reaction piles in a distance of 5.22 m, a bridge of beams carrying the hydraulic tension and measurement equipment connected to the test pile in the middle. A series of piles of different length were set up using vibro-jetting and after some weeks in rest the extraction tests were carried out. Hydraulic presses did activate the vertical uplift forces. The process was recorded and later analyzed in the laboratories. It is not very much opportune going into the details regarding the description of the testing, the electronic controls, the monitoring etc. Important is the final conclusion and the recommendations for the soil engineers in charge for any static analysis of retaining walls.

Evaluating the final results at this particular site, the Institute of the Technical University of Munich stated as follows concerning the design and calculation of steel sheet piling structures and their stability checks required:

"The calculation of cofferdams, retaining walls and the states of failure should be based on an angle of internal friction phi = 37.5 degrees. For the calculation of the active as well as the passive pressure diagram, the value of the angle of wall friction should be determined as 2/3 of the internal friction ph."

During the last 30 years the equipment required for this particular driving procedure was permanent improved. The process of its quality process was optimized meeting the environmental codes. Vibro-jetting became state-of-the-art.

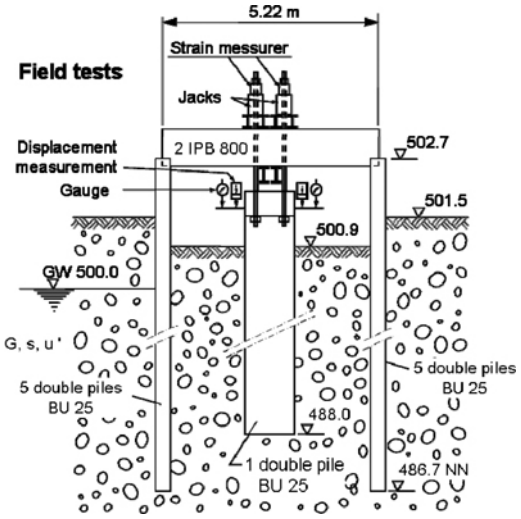

Fig.3: Influence on the Wall Friction

One important almost cultural difference between the American pile driver and his European counterpart is the way they do install steel sheet pilling elements: the Americans are setting up panels and drive the sheets step by step back and forth, the Europeans are picking up one double and drive the element in once to its final depth.

The basic machinery for vibro-jetting consists of a solid carrier with a robust leader. Its size should match the size of the piling. Modern carriers are entirely controllable from the cab. They have speed control, high push and pull forces, are completely self-rigging, they have inclination adjustment, alignment systems and meet all standards concerned.

The modern hydraulic vibratory hammers are able to adjust moment and frequency to the soil. With the opportunity to start the vibration with static moment of zero and regulating the amplitude after, the system avoids the dangerous resonance.

The typical jetting unit contains all its equipment in a 20 ft. standard container. The water reservoir has a capacity of 8 m3. The platform has two centrifugal pumps, each with a capacity of 18 m3/ hour, a maximum pressure of 20 bars. Converters are adjusting the pumps. If a mixed jetting of water and air might be opportune, a piston compressor is added. For the lances four connections for the water flushing hoses are installed together flow controls and pressure gauges and a connection to add compressed air. Radio remote control receiver, electrical switch cabinet and other elements are completing the platform. Such unit is ready for use at any site. For the lances, standard industrial pipes of ¾ inch in standard length are sufficient. Usually 2-4 lances are talk welded along the sections. Hoses are connecting the pipes to the pumps. To understand the system and to learn the interaction of soil, sheet piling vibration and jetting, it is necessary recording all available and relevant data of the process and to investigate their coherencies. Relevant are all soil and driving data.

The soil data are usually well known in advance. Because the soil reports with boring logs and tests are done during the design phase. But they contain almost no information regarding the drivability except the SPT or CPT values, which are not sufficient, to select the best driving equipment and calculate performance and cost.

For the vibro-jetting method important are the engine data of the vibratory hammer. The performance of the vibrator is determined, first: by the pressure of the oil flow which powers the hydraulic motor, second: by the frequency and the

amplitude, third: a variable static moment should be a must to adjust the driving forces to changing soil layers and environmental regulations. Further measurements: such as the driving performance recorded by a diagram of driving depth and time, the acceleration measured by specific sensor placed inside the hammer, quantity and pressure of the water flow through the lances, are completing the required data. All data, including ground vibration, are shown on displays in the cab of the carrier giving the operator the tools on hand optimizing and adjusting the driving process to the situation he is facing. The variations can be done manual by the operator or by a computer controlled software system as additional assistance to the operator. Each pile, each single change should be recorded for any further investigation, this is important for any recalculation, any performance control and any improvement, the monitoring and recording should be part of the quality control system of any project. Beside the machinery and all the electronic equipment, the human resources are extremely important for any success of such modern sophisticated systems. The experiences of the operator are the key for his correct interpretation of the changing data and the adjustments he has to make. The whole crew should understand all actions and interactions of each single operation. The training and education of the crew, according to the permanent modernization, should be considered as positive investment into the human capital of your company

APPLICATIONS OF THE VIBRO-JETTING DRIVING PROCEDURE

The vibro-jetting driving procedure is standard in many countries of Europe. The method was also accepted and successfully used in different areas of Asia, Australia and Africa. For almost all piling projects located in sensitive areas where ground vibration and noise emissions are limited by codes and environmental regulations vibro-jetting did offer a way to meet the limits. At sites where soil layers are considered as non penetrable, when extremely high SPT values are signaling glacial compacted marl or weathered rock, vibro-jetting is the solution.

Two classical projects will demonstrate these two major applications:

First example is a test site where impact driving and vibro-jetting did compete side by side. An inland harbor located in Straubing on the Danube was under construction with 6000 tons of steel sheet pilling for the basin. The boring logs did show an overlaying formation of sand and gravel, followed by 2-3 m of firm clay. The under laying strata consisted of dense to very dense fine sand, followed by stiff to hard tertiary clay down to the end. The numbers of blows per 10 cm of the SRS tests grow continuously with the depths up to 60 0r even 100 blows, comparable to the SPT values of 180 to 300 per ft.

Because of these extreme conditions the port authorities did organize a driving test. From previous projects nearby it was known that vibrating was impossible. First a diesel hammer D 30 was ordered to drive the 20 m long piling sections: L 24, L 25, doubles of 1.00 m width and PU 25, PU 32 of 1.20 m.

The results were negative: the D 30 did need between 2.000 and 2.700 blows or 60 to 75 minutes for one pair. The diagram of the driving progress did follow exactly the SRS tests .Considering the noise level and the time needed impact driving was not appropriate The Technical Department of Profil Arbed Luxemburg and

Techno-Grundbau, a pile driver, did offer the vibro-jetting method. They used a standard carrier, a high frequency vibratory hammer PTC 60 HFV with a static

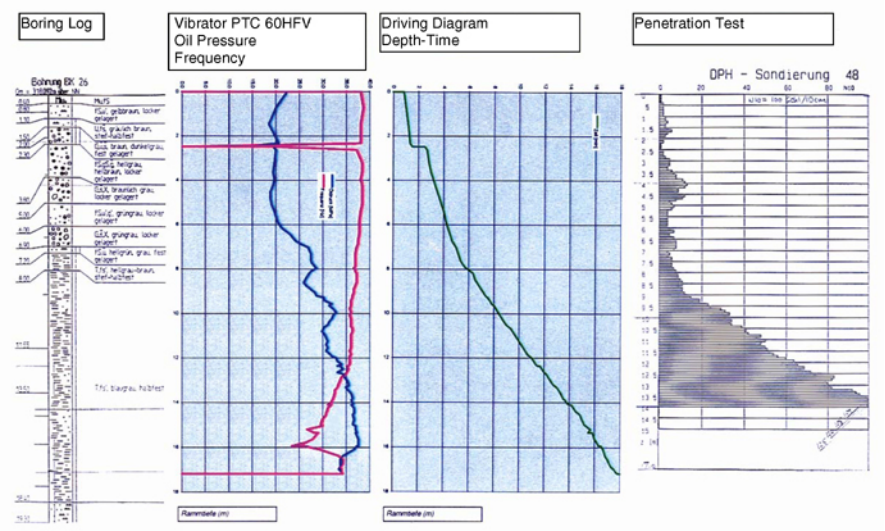

Fig. 4 : Driving Records

moment of 54.0 mkg. The eccentric moment was variable from zero up to maximum when the hammer was in operation. The 4 jetting lances of 20 mm were powered by 2 rotary pumps. For the tests two areas were selected with the dominating soil formations: one with mostly sandy, very dense, high compacted soil layers and SRS values up to 60 blows with a firm clay layer of 2.4 m thickness about 5.1 m below surface. The second area had 4 to 5 meter of sandy soil followed by 13-16 m of firm to stiff clay and marl with SPS up to 100 blows.

The driving diagrams of area one show a constant progress. The piling reached the final depth of 20 m after 14 minutes. The curves of the oil flow pressure and the frequency indicating that the pressure is well below the maximum of 380 bars and the frequency is almost constant. Of interest were the results of 3 geophones placed in certain distances from the piling. The average values measured were between 2 3 mm/sec. But as the piling did pass through the clay, the peak reached 7 mm/sec. In area two with its hard clay the driving time for the 20 m was just over 16 min. The oil pressure grew steadily up to 380 bars, consequently the frequency dropped. After passing the 16 m level the frequency recovered and the pressure dropped, indicating a lower overall resistance. The geophones showed only 1.5 mm/sec as long as the frequency was high. Reaching the 13 m level, the ground vibration went up to 4.5 mm/sec, after passing this layer the speed did decline again. As conclusion: the PTS 60 HFV has reached the limits. The next bigger size would be appropriate.

The most interesting applications for vibro-jetting are projects where noise and ground vibration are limited. This is the case when new buildings in cities with historical landmarks are on the agenda. If the project is important, owners are often willing financing a field test under real conditions. This was the case for a combined apartment and office building in the city of Karlsruhe. A cofferdam was needed for a 2 floor underground. Because of the sensitive groundwater situation the contractor selected a sheet piling retaining wall. The borings show an overlaying combination of fill and rubble of 4.5 m followed by 3 m of peat and silt, followed by alternating medium to dense sand and gravel. The clay below did build a watertight layer. Out of different alternates, the steel sheet piling solution was selected. Before construction a field test was set up to prove that vibro-jetting meets the limits of ground vibration, noise and groundwater. The equipment consisted of a carrier, with leader, high frequency vibrator with variable moment and a jetting unit. Because of the possible settlement, the code limit of 8 mm/sec was lowered to 2 mm/sec. 3-axial sensors were placed in the buildings. Further sensors controlled the spreading of the vibration over the whole area. The testing confirmed that vibro-jetting keeps the ground vibration below the value of 2 mm/sec. During construction 3-axial sensors controlled all buildings. Because daily checks were too expensive, calibrated and sealed systems were installed guarantying quality control, excluding manipulations. Protocols were printed during driving to control the vibration. The pile driver worked carefully, recorded each sheet and adjusted the vibratory hammer accordingly. The ground vibration was always within the limits. No damages were reported.

INVESTMENT REQUIRED; CALCULATION OF DRIVING COST

Important for any performance is the overall time of one driving cycle. Beside setting up and trimming, the time depends on the interaction between the vibrator and the jetting. The reduction of the resistances determines the speed of the progress. Side jobs should never slow down the cycle. Vibro-jetting requires a high amount of investment of modern machinery as described above. A second crane is needed for handling, welding and placing. Using renting prices for the fix-cost of a vibro-jetting and a diesel hammer unit we may compare the following numbers:

Vibro-jetting unit:	with 5 men per shift and 1.000 hours per month	
	Carrier: Liebherr LRB 255 rent:	$ 69.000 per month
	Dieseko Vibratory hammer	$ 11.600
	Second crane	$ 6.700
	Jetting, welding platform	$ 8.000
Diesel hammer unit:	with 3 men per shift and	600 hours per month
	Carrier: Hitachi KH 180 rent	$ 22.400 per month
	Diesel hammer D30	$ 11.800
	Second crane	$ 6.700

Each contractor has a specific way calculating prices for tender. The values for his machinery depend on factors, such as age, booking value, and stage. But the most significant influence has the quality of the crew. The knowledge and motivation of these men are the most important factor for any success.

The operator should be well trained. He has to understand the interaction of changing soil, the reaction of the vibratory hammer and water jetting and how he has to react. The numbers above should be considered only as relation between the two different driving methods. The investment for vibro-jetting is more than twice as high as the total required for the standard diesel hammer unit. Therefore the performance per linear meter of wall must be much higher to compensate its bigger investment cost. Above we did describe two niches: extremely difficult soil conditions and situations where impact driving is excluded because of ground vibration and noise regulations. The example of the inland harbor delivers interesting comparison of the performance of the two systems. During the tests the driving cycle of the D 30 the 20 m piling was never below 60 minutes. With an estimated cycle of 70 min., the performance would reach 8 doubles or 160 m2 a day. The maximum of the vibro-jetting method during the construction reached 32 doubles or 640 m2 / day. The average for the whole tonnage of 6.000 tons was recalculated and did result 25 doubles or 500 m2 / day. For the tender the estimate was based on an average p of 18 doubles per day. This jobsite was ideal for the vibro-jetting method, because of its high performance, its low noise emission and that the port was open for business earlier as expected.

Six major points determine the calculation:

The selection of the most appropriate driving technique
The optimization of low cost and high performance
The consumption of energy and other sources
The reliability of the machinery units involved
The high level education of a well trained crew

Conclusion

Vibro-jetting is an appropriate way when environmental regulations are excluding the regular standard driving and other installation procedures, such as drilling, or slurry walls. Over the last three decades the tonnage installed with the vibro-jetting method increased slowly but steadily. As more difficult the soil conditions, as stricter and more rigid the regulations and codes were handled by the public authorities, as more the vibro-jetting method was accepted and became "state of the art".

REFERENCES

Forst, M., Hudelmaier, K.,"Sondervorschläge in Spundwandbauweise: Weiherhof-Center, Teil 1 & 2,". (2000), *Stahl-Informations-Zentrum*, Dok. 549, 81-87.

Unknown, P., "Scherspannungen verschiedener Rammverfahren".(1992), Internal research report, *T. U. Munich, BVV Spezialtiefbautechnik.*

Zeilinger, H. "Proberammung Donauhafen Sand, Vergleichsrammung", (1994), Internal research report, *ISPC Profil-ARBED Luxemburg.*

Copyrighted Materials
Copyright © 2009 American Society of Civil Engineers (ASCE)
Retrieved from www.knovel.com

CENTRIFUGE MODEL TESTS ON INSTABILITY OF AUTOMOTIVE PILE DRIVERS

Tomohito Hori[1] and Satoshi Tamate[2]

[1]Researcher, National Institute of Occupational Safety and Health, Japan, 1-4-6 Umezono, Kiyose, Tokyo, JAPAN, 204-0024; horito@s.jniosh.go.jp
[2]Senior Researcher, National Institute of Occupational Safety and Health, Japan, 1-4-6 Umezono, Kiyose, Tokyo, JAPAN, 204-0024; tamate@s.jniosh.go.jp

ABSTRACT: The automotive pile driver is a piece of large-scale construction machinery. This machinery is used for ground improvement and foundation work. In recent years, there have been some reports of accidents in which the machinery overturned. In this study, a 1/25 scale model of an automotive pile driver was made to clarify the mechanism making the pile driver unstable, and centrifuge tests were performed. The load of each axle and the behavior of the model were measured in a centrifuge test. The grounds used with the model are two types of urethane foam with different strengths, with conditions imitating the uniform ground and non-uniform ground. As a result, the response acceleration did not have a significant difference due to differences in ground conditions. On the other hand, the effect of the ground condition was different in the axle load, and it was possible to evaluable the instability of the automotive pile driver when self propelling.

INTRODUCTION

The automotive pile driver (hereinafter referred to as the machinery) is mainly used for the foundation work of high-rise buildings and ground improvement. A photograph of the automotive pile driver is shown in Photo 1. This machinery is frequently used in urban areas. Recently, there have been accidents in which this machinery has overturned. In cases where the machinery topples, the risk to the lives of workers is not only a problem but this can also block trunk roads etc., having a great impact on society. Investigation revealed that overturning accidents of this machinery often occur during relocation to another pile. There are two factors in the background of the overturning of the machinery. One is structural instability stemming from a high center of gravity, and another is the ground where the machinery is set up being too soft. It is necessary to conduct a quantitative assessment of the fluctuation in the ground contact pressure while the machinery is running.

In this study, a 1/25 scale model of the automotive pile driver was made to clarify the mechanism of the instability of the pile driver during self propelling, and centrifuge

Photo 1. Automotive pile driver

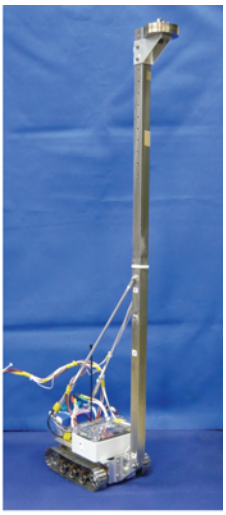

Photo 2. Automotive pile driver model

tests have been performed. In the experiment, the behavior of the model when self propelling was measured by installing an accelerometer, and the load placed on the each axle of the model was measured to investigate the instability of the automotive pile driver.

This paper presents the safety factor of bearing capacity that is necessary to prevent the overturning of the machinery.

OUTLINE OF THE AUTOMOTIVE PILE DRIVER MODEL

The automotive pile driver model (hereinafter referred to as the model) was made by referring to the machinery subject to overturning accidents in the past. Table 1 shows a comparison between the specifications of the actual machinery and the model. The gross weight of this machinery is 539kN (55ton), and it is medium-sized in terms of this kind of machinery. The centrifuge tests were conducted at 25 g. This is the reason for the 1/25 scale mode. The positions of the motor, reduction gears, and battery of the

Table 1. Comparison of the specifications of the actual machinery and the model

		Automotive pile driver			
		original		model (1/25 scale)	
Center of gravity		Horizontal x(m)	Vertical y(m)	Horizontal x(mm)	Vertical y(mm)
Lower part (crawler)		-0.83	1.43	6.5	2.7
Upper part	body・leader	3.35	12.42	213.0	198.8
	auger・etc.	4.20	15.98	-5.8	32.2
Gross weight		539kN		29.9N (25g in 747N)	
Ground contact pressure (kPa)		101		133	
Velocity (km/h)		1.2 (=33cm/sec)			

model were designed relative to the machinery in terms of the center of gravity. The weight of the model is 29.9N. In a centrifugal field, the weight of the model is increased by up to 25 times. As a result, the ground contact pressure that acts on the crawler can be reproduced with the machinery.

Feedback control of the rotation rate of the motor was carried out to make it possible to hold a straight line. The velocity of the model can be changed by exchanging gears. The model is operated wirelessly. The stability angle of the model can be freely changed by changing the position of the additional weight. This is because the additional weight is loaded into the construction machinery (auger, sand compaction pile, etc.). Ground contact pressure was measured on the crawler by putting the strain gauge on the arm part of each axle, which has a cantilever structure. A calibration test was carried out to investigate the relation between the load and response of strain. As a result, it was confirmed that there were linear relationships in the load and the response of strain even if 300N (30kg) was applied. In addition, the behavior of the model was measured by putting accelerometers in three places (upper part and lower part of the leader, and the body). Photo 2 shows the automotive pile driver model.

MODELING OF THE GROUND

Material

To obtain basic data on the behavior of the model, urethane foam was used for ground in the model. Two types of urethane foam with different strengths are used. One is hard FP15, and another is soft FP30. Table 2 shows the density and hardness of the urethane foams.

Table 2. Density and hardness of urethane foams

	Density (kg/m^3)	Degree of hardness (kPa)
FP15	61	139
FP30	28	50

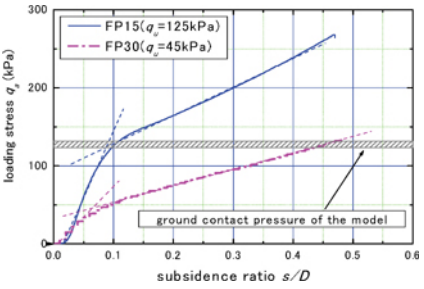

FIG. 1. Bearing capacity test results

Bearing Capacity Tests on Urethane Foam

The bearing capacity tests were performed to investigate the strength characteristics of the two types of urethane foam. This was examined using strain control and the rate of loading is 1 mm/min. The size of the loading plate used for the experiment is

25mm×50mm. Fig.1 shows the relation between loading stress and subsidence ratio (s/D) in which the amount of subsidence (s) is divided by the short side of the rectangle (D) of the loading plate. The q_a value of the intersection of two tangents in front and behind the winding point is defined as the ultimate bearing capacity.

The ultimate bearing capacity of FP15 and the ground contact pressure of the model are almost equal. On the other hand, the ultimate bearing capacity of FP30 is lower than the ground contact pressure of the model.

TEST PROGRAM

Test Apparatus

The test of the performance (operation) of the model was carried out in a centrifuge. Centrifuge testing was performed at the National Institute of Occupational Safety and Health, Japan (JNIOSH). A photograph of the NIIS Mark-II Centrifuge is shown in Photo 3. This apparatus has an effective radius of 2.3m, and the maximum acceleration of gravity is 100g. This is a medium-sized centrifuge compared to others in the world. As in other centrifuges, it has a main shaft, a drive unit, two arms, two swinging platforms, a signal and power supply interface and a control box. However, its arms are asymmetrical, which is its special feature.

Fig. 2 shows the outline of the centrifuge model test. The size of the soil container is 920mm in length, 465mm in height, and 450mm in width. To prevent the wind from influencing it when experimenting, the whole unit was covered with a windshield cowl. The velocity of the model was measured with a wire-type displacement sensor. In this study, each axle was defined from the front wheel as FS (Front Sprocket), FR (Front Roller), CR (Center Roller), RR (Rear Roller), and RS Rear Sprocket).

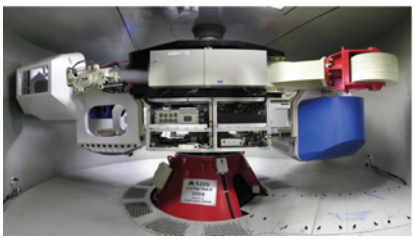

Photo 3. NIIS Mark-II centrifuge

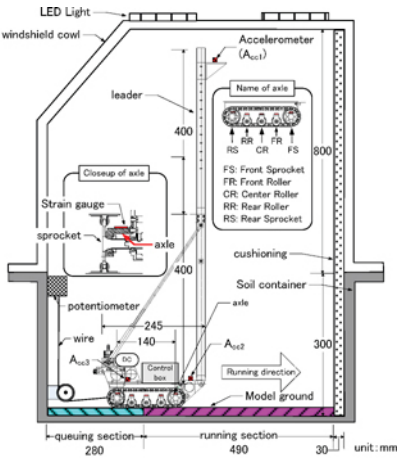

FIG. 2. Outline of the centrifuge test

Test Condition

The stability angle of the machinery should be five degrees or more according to the standard of Japan. In addition, the stability angle when running is ten degrees or more according to the British Standard. Therefore, the experiment was performed on the condition of a stability angle of fifteen degrees.

The model grounds are the two types shown in Fig 3. One is "the uniform ground" that using F15 and imitates the ground where strength is uniform. Another is "the alternating ground" using an alternating combination of FP15 and FP30 in bands 1/2 of the crawler length, and imitates the non-uniform ground. The model was made to run after centrifugal acceleration had been increased up to 25g.

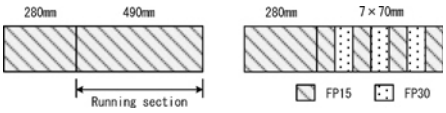

(a) Uniform ground (b) Alternating ground

FIG. 3. Model grounds

TEST RESULTS

Typical Test Results

Fig.4 and Fig.5 show typical test results of the uniform ground and the alternating ground. The data shown in figure is a result for after 150mm when the entire band is in the running section. The velocity of the model was constant and it was about 30cm/sec. The acceleration shown in figure is the direction of travel. The acceleration data in the

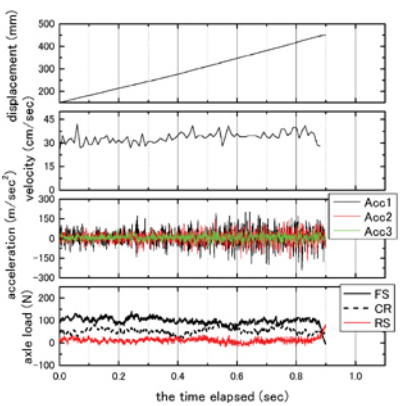

FIG. 4. Typical test results of the uniform ground

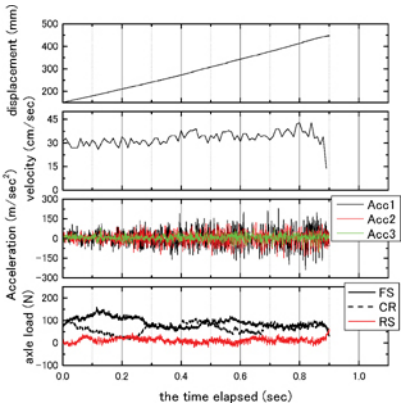

FIG. 5. Typical test results of the alternating ground

upper part of the leader was defined as Acc1, the lower part was defined as Acc2, and the body part was defined as Acc3. When accelerations are compared, Acc2 and Acc3 are almost equal regardless of the ground condition. In contrast, Acc1 is slightly larger than others. It was clarified that Acc1 was amplified by the leader. Meanwhile in the result of the axle load, the load of the front wheel is larger and the overturning moment more impactful than the rear wheel. In the case of the uniform ground, each axle load is almost constant. On the other hand, in the case of the alternating ground, the increase and decrease of the axle load on the front wheel side is especially large.

Frequency Analysis of Acceleration

Fig. 6 shows the result of the Fourier transform after conversion from the model scale into a full scale. The dominant frequency is seen in about 2Hz for both the uniform ground and the alternating ground. This is an influenced by structural unevenness of the crawler. In the case of the alternating ground, the dominant frequency is seen in about 0-2Hz. Therefore, the model shakes for a longer period.

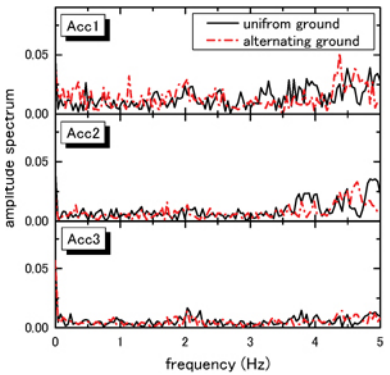

FIG. 6. Frequency analysis of acceleration

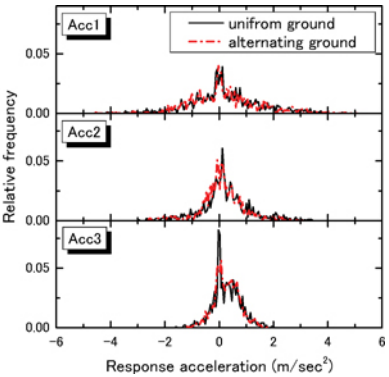

FIG. 7. Frequency distribution analysis of acceleration

Frequency Distribution Analysis

Fig. 7 shows the result of frequency distribution analysis of response acceleration. The frequency distribution analysis was carried out in 0.005g steps. There was no significant difference when the uniform ground was compared with the alternating ground. As mentioned above, there were no differences in the results of the Fourier transform and the frequency distribution analysis at the response accelerations.

Fig. 8 shows frequency distribution analysis results for the axle loads. In this study, the load acting on each crawler is divided by the weight of the model to define the load distribution ratio. There is little subsidence caused in the crawler because the ultimate bearing capacity of the urethane foam and the ground contact pressure of the model are

almost equal in the uniform ground. Therefore, the maximum relative frequency of each axle showed comparable results. On the other hand, there is a difference in the distribution shape of I_{fr} when each axle is over alternating ground, and the front axle load is distributed widely. For that reason, the influence by the effect of the ground condition at the axle load where strength changes periodically appear.

Fig.9 shows the comparison between the theoretical value and the experimental value. The theoretical value of the ground contact pressure was calculated as established in the Japan Industrial Standards (JIS). The numerical expression is the same as in the British Standard. The mean and standard deviation are shown in figure. When the means are compared, the theoretical value and the average of experimental value are almost equal for both the uniform ground and the alternating ground. The error bar indicates two standard deviations (2σ). In a comparison of the uniform ground and the alternating ground, the standard deviation of the alternating ground is larger. The short-term safety factor of the foundation work is 1.5 in Japan. In addition, the same safety factor is adopted in CIRIA. For the biggest FS of the axle load, both the uniform ground and the alternating ground fall below the safety factor threshold of 1.5. Accordingly, it is

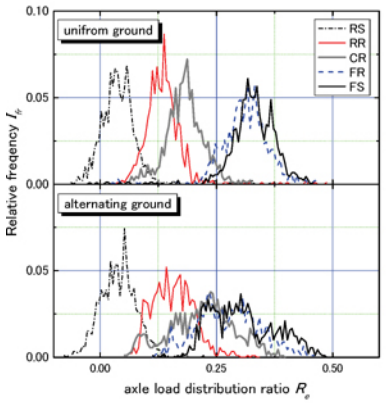

FIG. 8. Frequency distribution analysis of axle load distribution ratio

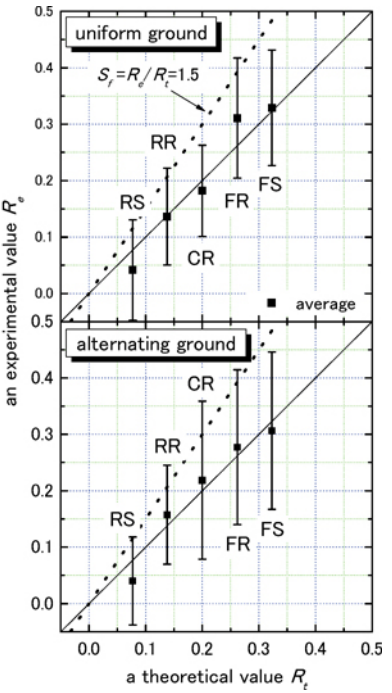

FIG. 9. Comparison between the theoretical value and the experimental value

thought that a safety factor of 1.5 is appropriate. However, FS and RS, tensile force acts on the crawler part when running, and bending-torsion force acts on the axle part. This is due to the effect of a structural problem in the axle part. Therefore, there is a problem where this is underestimated compared with the actual load. There are plans to improve the structure of the axle part examine it in the future.

CONCLUSIONS

The following conclusions were obtained on the centrifuge model test results performed on two types of the model ground:
(1) The acceleration did not result in any marked difference due to differences in the ground condition. On the other hand, there was a clear effect of the ground condition in the axle load, and it was possible to evaluate the instability of the model.
(2) The average of the experimental value of axle load was almost equal to the theoretical value.
(3) Two standard deviations in the frequency distribution analysis of the axle load were for a safety factor of roughly 1.5 or less. Therefore, it is thought that the safety factor for the bearing capacity of the ground must be at least 1.5 or more.

REFERENCES

British Standard , BS EN 791:1996 *Drill rigs - Safety.*
CIRIA, 2003, *Crane stability on site*, SP131, pp.48.
N. Horii, K. Itoh, Y. Toyosawa and S. Tamate (2006), "Development of the NIIS Mark-II geotechnical centrifuge" *Proceedings of the 6th international conference on physical modeling in geotechnics*, vol.1, pp.141-146.

Copyrighted Materials
Copyright © 2009 American Society of Civil Engineers (ASCE)
Retrieved from www.knovel.com

SEISMIC HAZARDS AND CONSTRUCTION VIBRATIONS

Justin Moderie[1], P.E., A.M.ASCE and Arlan H. Rippe[2], P.E., F.ASCE

[1]Geotechnical Engineer, Kleinfelder, 15050 SW Koll Parkway, Suite L, Beaverton, OR 97006; arippe@kleinfelder.com
[2]Senior Principal Geotechnical Engineer, Kleinfelder, 15050 SW Koll Parkway, Suite L, Beaverton, OR 97006; arippe@kleinfelder.com

ABSTRACT

Redevelopment of an area along the waterfront in Portland, Oregon presented many geotechnical design and construction challenges for a 16-story building. Saturated river sediments and old industrial fills were susceptible to liquefaction and required seismic hazard mitigation, deep foundations, ground improvement, construction near sensitive structures, and a basement below groundwater. Many of these challenges on this 0.4-hectare (1-acre) site currently are being researched, and consequently are often subject to differing engineering judgment and analysis rationale. Design and constructability of the foundation elements of this 16-story building present a case worthy of study. Three important questions resolved during the project include:

- Will installation of stone columns densify lithified deposits of non-plastic silt and sand?
- What is the magnitude of vibration at varying distances from pile driving and from installation of stone columns, near a historic, active, fragile composite concrete and brick storm sewer pipe?
- Will pile driving and installation of stone columns cause liquefaction of nearby soils supporting the storm sewer pipe?

These questions were answered during construction. Pre and post-construction CPT testing, vibration monitoring, survey markers, and video monitoring of the storm sewer were used. Data collected provide supportive proof of the approaches, research, and rationale.

SITE HISTORY

Redevelopment of an area along the waterfront in Portland, Oregon presented many geotechnical design and construction challenges for a 16-story condominium and retail building. The building is located on a 70 by 70 m (200 by 200 ft) block surrounded by proposed city parks and existing city streets. A two-level basement for below-grade parking extends from about 4.6 to 6.1 m (15 to 20 ft) below the existing ground surface over the entire block. The design load averages on the order of 153 kPa (3200 psf) across site. On two sides of the building, a 6.1 to 9.1 m (20 to 30 ft) deep functioning old storm sewer line is located as close as 6.1 m (20 ft) from the perimeter of the basement. The sewer is approximately 90 years old and consists of an 2.4 m (8 ft) high composite concrete arch structure with a brick-lined bottom. A site sketch is provided as Figure No. 1.

SUBSURFACE CONDITIONS

Prior to development in the late 1800s, the vicinity of the site was marshland with a lake and creek feeding into the adjacent Willamette River. The area was filled at the turn of the previous century and used for a variety of industrial purposes, including a railroad fueling and maintenance facility. Measured from the original ground surface downwards, soil conditions consisted of about 7.0 to 10.7 m (23 to 35 ft) of fill overlying about 6.1 to 13.4 m (20 to 44 ft) of soft to stiff native clayey silt grading to very loose to medium dense fine sand with silt. Much of the sand and silt materials are stratified alluvial deposits. Below the silt and loose sands, at about 18.3 to 20.1 m (60 to 66 ft) deep, 3.0 to 4.6 m (10 to 15 ft) thick dense to very dense sandy gravel exists. Beneath the sandy gravel, at about 21.3 to 27.4 m (70 to 90 ft) deep, a layer of dense to very dense sandy gravel to gravelly sand was encountered. Groundwater is typically below the basement elevation, but rises above the bottom of the basement during river flood conditions. A representative subsurface profile is provided as Figure No 2.

The saturated river sediments and old industrial fills were determined to be susceptible to liquefaction and required seismic hazard mitigation. A steep river bank approximately 152 m (500 ft) away posed a significant risk of lateral spreading during a design earthquake based on Youd et al. (2002). The maximum considered earthquake is primarily based on either a M8.3 to M9.0 subduction event about 100 km (62 miles) from the site or shallow crustal earthquakes with magnitudes as high as M6.0 to M6.9, with one potentially active fault as near as about 1 km (0.6 miles) from the site. Deep foundations were used for building support, and stone columns were used for ground improvement across the entire site. Due to access constraints, a stone column buttress was located under the perimeter of the building to mitigate the potential lateral spreading. Additional lateral reinforcement was added for the piles and building structure within this perimeter zone. Additionally, 1.1 m (3.5 ft) diameter stone columns were used across the site to improve the IBC Site Class from an "F" or "E" to a "D" by replacement and not necessarily densification.

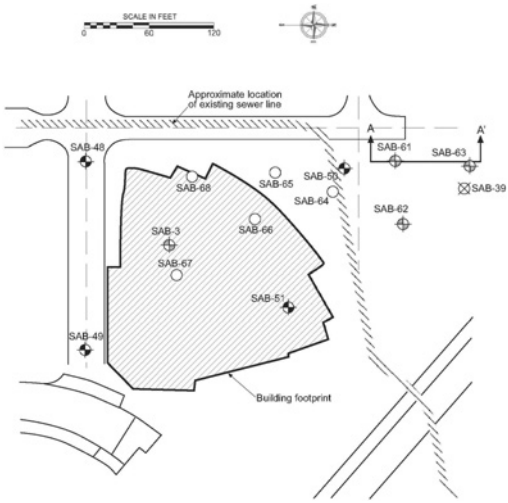

FIGURE No. 1. Site Sketch

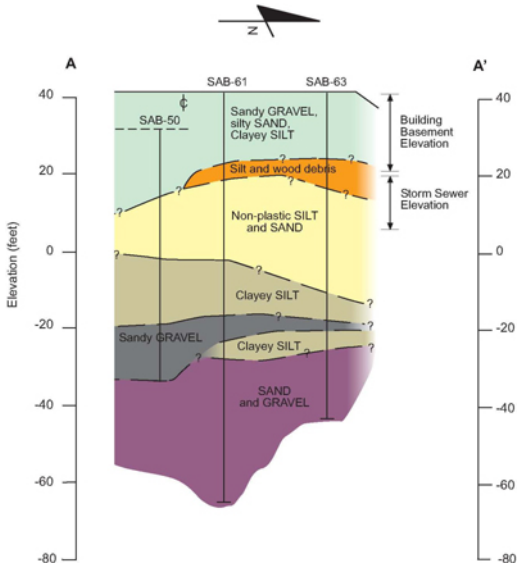

FIGURE No. 2. Soil Profile

DESIGN CHALLENGES

Many of these geotechnical and foundation challenges on this 1-acre site currently are being researched, and consequently are often subject to differing engineering opinions and analysis rationale. Three specific questions addressed herein are: 1) will installation of stone columns densify stratified deposits of non-plastic silt and sand; 2) what is the magnitude of vibration at varying distances from pile driving and from installation of stone columns near a historic, active composite concrete and brick storm sewer pipe; and 3) will pile driving and installation of stone columns cause liquefaction of nearby soils supporting the brick storm sewer pipe?

DENSIFICATION OF STRATIFIED DEPOSITS OF NON-PLASTIC SILT AND SAND

Stone columns are often used to densify relatively clean sand to a relative density not significantly susceptible to liquefaction. Also, reinforcement and drainage of the soil by the stone columns provides some resistance to liquefaction. Approximately 1.1 m (3.5 ft) diameter stone columns on a 2.7 m (9 ft) triangular matrix were installed across the entire site to depths of 12.2 to 15.2 m (40 to 50 ft). Approximately 0.61 m (2 ft) thick lenses of relatively clean sand and on the order of 3.0 m (10 ft) thick deposits of non-plastic silty sand and sandy silt were present on the site. As a design issue, it was useful to estimate and validate whether or not these potentially liquefiable soil units would densify. This was useful for estimating the buttressing effect of the perimeter stone columns, and the contribution of potentially densified soils to the overall buttressing effect. Additionally, since the building was founded on piles installed within the stone column matrix, the liquefaction susceptibility, static soil strength, and liquefied residual shear strength after installation of the stone columns affected the pile design.

Four Cone Penetrometer Tests (CPTs) were conducted within the basement excavation prior to installation of stone columns. About one month after completion of stone column installation, four CPTs were again conducted within several feet of the first CPTs and at the midpoint of the triangular stone column matrixes. Table No. 1 below presents the major soil units based on CPT data and validated by nearby borings. Additionally, Table No. 1 also provides pre and post-installation cone tip resistance (Q_c) and cone friction ratio, which consists of the cone side friction (f_s) divided by Q_c. Pore water pressure was observed by the CPT piezo-cone transducer during probing, both before and after stone column placement. However, post-installation CPT testing was conducted one month after completion of stone columns. No discernable trend was noted between pore water pressure measurements before and after construction; and in our opinion, any trends would have been inconclusive due to the duration of time during which excess pore water pressure may have dissipated.

TABLE No. 1. Stone Column Soil Densification.

Depth Range (m)		Generalized Soil Description (based on borings and CPTs)	Before Q_c (kPa)	Before Friction Ratio (f_s/Q_c)	After Q_c (kPa)	After Friction Ratio (f_s/Q_c)
CPT 1						
1.5	3.0	silty CLAY	958	2.3	1149	4
3.0	7.6	SILT / clayey SILT	958	1.5	958	3.4
7.6	10.7	lithified sandy SILT to clayey SILT	2873	2.8	2394	3.8
10.7	11.6	lithified SAND to sandy SILT	8140	1.6	2873	2.5
CPT 2						
0.9	3.0	FILL: SILT / SAND / DEBRIS	9576	1	9576	2.2
3.0	5.5	clayey SILT / silty CLAY	958	0.6	958	3
5.5	6.4	lithified silty SAND / SILT	1915	0.9	1915	2.3
6.4	10.4	SILT	2394	2	2394	2.7
10.4	11.9	lithified SAND to sandy SILT	4788	0.9	4309	2.5
CPT 3						
1.5	3.0	clayey SILT / silty CLAY	1915	2	2394	3
3.0	5.5	clayey SILT	766	1	766	3.5
5.5	6.1	silty SAND / sandy SILT	2394	0.3	3830	1.2
6.1	8.5	lithified sandy SILT / silty CLAY	1436	1	1915	2.7
8.5	11.6	lithified silty SAND / clayey SILT	3830	2.5	2490	3
11.6	12.2	SAND / sandy SILT	7661	1	6224	2
CPT 4						
1.5	4.3	clayey SILT / CLAY	766	2	958	2.7
4.3	6.1	lithified SAND / sandy SILT	4309	0.7	4788	1.5
6.1	11.0	sandy SILT / clayey SILT	958	1.5	1149	2.5
11.0	11.9	silty SAND / sandy SILT	4309	2.5	3352	2.5

As evidenced by the CPTs, some densification was attained from stone column installation, as correlated to Q_c, in the thin, sandier layer near bottom of the stone column installation depth. Throughout the rest of the soil stratigraphy, Q_c did not significantly increase, thus indicating significant densification did not occur in these soil units. However, f_s did significantly increase, which strongly suggests that some limited densification did occur. To validate this conclusion, the theoretical volume of stone columns was related to the volume of soil spoils removed from the site to return the site to pre-installation grades. It should be noted that limited ground heave occurred during stone column installation, and much soil was ejected to the surface as a liquefied mud. On the order of 3,823 m^3 (5,000 cubic yards (CY)) of crushed rock was inserted into the soil during installation of the stone columns. Based on records of the earthwork contractor, about 1912 to 2294 m^3 (2,500 to 3,000 CY) of soil was removed from the site to re-grade the site after stone column installation.

In conclusion, neither the thin layers of sand nor the non-plastic silty sand to sandy silt densified at the midpoints of the triangular matrixes (about 1.5 m (5 ft) from the center of the columns). However, the volume of soil removed from the site indicates that some densification occurred, but it may have occurred in a limited radius from each stone column. Additionally, some of the soil may have filled in the voids within the open-graded crushed rock used to construct the stone columns. CPTs indicated that the friction ratio increased, implying that lateral pressure coefficient (K_o) within the soil increased as a result of stone column installation. It is not currently known if

this increased lateral pressure coefficient is permanent, or if it will return to the pre-construction lateral earth pressure.

Magnitude of Vibrations at Varying Distances

Wiss (1981) provides a method for estimating vibrations from pile driving at varying distances from the source, when vibrations are already known at a specific distance from the source. Woods and Jedele (1985) collected data from vibrations at construction projects and plotted the peak particle velocities vs. distance from the source for varying different construction equipment, including pile driving hammers and vibratory equipment. Woods (1997) developed a chart relating equipment energy, soil type, and peak particle velocity. Both of these latter charts were based on the Wiss method.

Using the Woods (1997) chart, peak particle velocities were estimated based on medium stiff to stiff soils (N=5 to 15) for pile driving. Figure No. 3 below shows the predicted relationship specific to the pile driving equipment used and soil conditions at the site. However, higher peak velocities were measured. Since the piles were driven following stone column installation, the higher than predicted velocities most likely are due to an increase in overall site stiffness from stone column installation. Relationships regarding vibrations from stone column installation equipment are not well documented. Therefore a "best fit" line is provided in Figure No. 3 below for maximum measured vibrations during stone column installation.

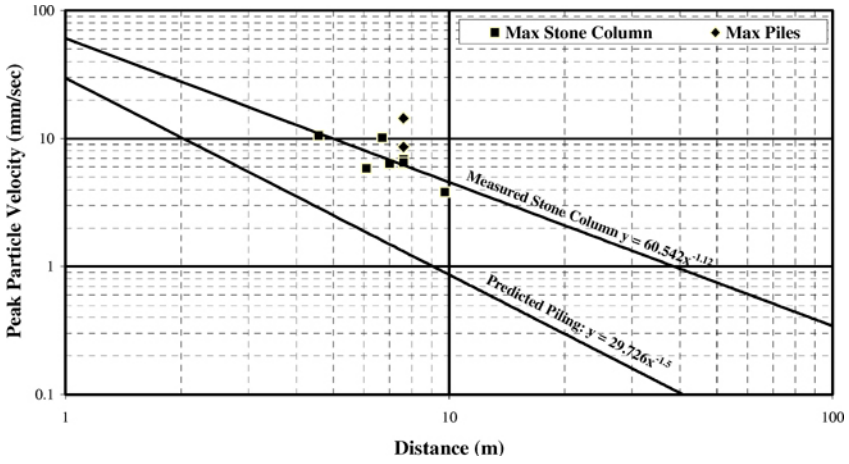

FIGURE No. 3. Peak Particle Velocity vs. Distance.

The entire record of vibration monitoring was recorded for several stone columns and piles. Peak particle velocities at about 7.6 m (25 ft) from the source varied relatively evenly between approximately 1.3 and 10.2 mm/s (0.05 and 0.4 in/s) for the

pile driving, and between approximately 2.6-10.2 mm/s (0.01 and 0.4 in/s) (with a concentration of readings around 5.1 mm/s (0.2 in/s)) for the stone column installation. As a side note, the stone column vibration equipment typically peaked at about 300 Amps during installations which corresponded to the recorded peak velocities. The vibratory probe had a rated energy input of 112 kW (150 horsepower).

POTENTIAL DAMAGE TO NEARBY SEWER

The historic composite concrete arch storm sewer pipe with a brick-lined bottom was located about 6.1 m (20 ft) away from pile and stone column locations. Potential damage to the storm sewer from various modes included:

- Vibration – damage may occur due to excessive magnitude of vibration.
- Settlement - due to densification and/or liquefaction of soils under the pipe during stone column installation.
- Excess Pore Water Pressure – could cause collapse of the pipe if compressed air used to inject the stone forming the columns created excess pore water pressure within the soil.

A monitoring program was conducted to evaluate each of these potential modes of damage.

Since vibration readings inside of the pipe were not practical and the storm sewer pipe was near the same elevation as the bottom of the excavation, a seismograph was used to measure and record vibrations at the ground surface within the excavation. No suggested maximum vibrations for pipes of similar construction were found in a literature search, and so a peak particle velocity of 6.4 mm/s (0.25 in/s) was selected as a conservative measure, relatively consistent with correlations for residential buildings with plastered walls. Some of the measured peak particle velocities exceeded 6.4 mm/s (0.25 in/s). These peak velocities approached 15.2 mm/s (0.6 in/s) for the piles and 10.2 mm/s (0.4 in/s) for the stone columns with frequencies of vibrations between about 20 and 50 Hz for both the piles and stone columns.

Settlement monitoring points were installed adjacent to the sewer, located at the same elevation as the bottom of the sewer. Points consisted of a sleeved rod embedded into the soils at the bottom of the sleeve. The purpose of these monitoring points was to check for settlement near the most sensitive portions of pipe. Although the pipe was near the groundwater elevation and underlain by potentially liquefiable soils, no discernable settlement was observed during weekly survey monitoring throughout stone column and pile installation. Hence, no discernable liquefaction or soil densification occurred approximately 6.1 m (20 ft) away from the stone column or pile locations.

Establishing a defensible method for checking existence of excess pore water pressures was challenging. Due to various constraints, including monitoring costs, electronic piezometers or pressure cells were not installed adjacent to the sewer. Instead, the radius of water and air extrusion at the ground surface was observed and

documented. In general, water and air extrusion was limited to a radius of about 3.0 m (10 ft) from the point of insertion. It was therefore concluded that water and air migration, and hence excess pore water pressure, were not present adjacent to the storm pipe 6.1 m (20 ft) away.

A remote video camera was used to document the visual condition of the interior of the storm sewer pipe before and after basement construction. It was determined that no discernable visual damage or distress occurred as a result of the construction activities.

CONCLUSIONS

Several relevant conclusions can be formed from the discussion and results above. The conclusions related to the technical aspects are as follows:

- Deposits of relatively clean sand of much greater thickness than 0.9 m (3 ft) are needed in order to effectively achieve significant densification during stone column installation.
- Based on amount of spoils generated during construction, increase in measured f_s, and by vibration response during pile driving, overall site subsurface conditions (Site Class) appears to have been stiffened by replacement stone columns in liquefiable, non-densifiable soil, such as non-plastic silt.
- Further research is needed to complete relationships between stone column installation and vibration at varying distances from the installation equipment.
- A vibration threshold of 6.1 mm/s (0.25 in/s) may be conservative for old composite concrete and brick storm sewer pipes.

REFERENCES

Wiss, J.F. (1981), "Construction VIbrations: State-of-the-Art," *Journal of the Geotechnical Engineering Division*, ASCE, (Vol. 107, No. GT 2, February, 1981) pp. 167-181.

Woods, R.D. and L.P. Jedele (1985), "Energy Attenuation Relationships from Construction Vibrations," *Vibration Problems in Geotechnical Engineering,* Proceedings of a symposium sponsored by the Geotechnical Engineering Division, ASCE, Detroit, Michigan, (October 1985) pp 229-246.

Woods, RD (1997), "Synthesis of Highway Practice 253, Dynamic Effects of Pile Installations on Adjacent Structures," Transportation Research Board, Washington D.C.

Youd, T.L., Corbett, C.M., Bartlett, S.F. (2002), "Revised Multilinear Regression Equations for Prediction of Lateral Spread Displacement," *Journal of Geotechnical and Geoenvironmental Engineering,* ASCE, (Vol 128, No. 12, December 1, 2002) pp. 1007-1017.

Copyrighted Materials
Copyright © 2009 American Society of Civil Engineers (ASCE)
Retrieved from www.knovel.com

Monitoring Pile Driving Vibrations – Problem Avoidance and Case Studies

David Harrison[1]

[1]Vice President and Principal, Seismic Surveys, Inc, 4375 Gibsonia Road, Suite 4, Gibsonia, Pennsylvania; dharrison@seismicsurveys.net

ABSTRACT: Vibration monitoring is important to protect against fraudulent claims and for regulatory compliance and public relations. There are various levels of allowable vibrations from pile driving activities in relation to vibration limits that are typically applied. The difference between impact and transient vibration levels as compared to steady state vibration levels is also an important distinction. Precautions are possible, such as pre-piling condition surveys and vibration monitoring with seismographs. This paper presents an overview of the various areas of concern surrounding pile driving vibrations as well as a summary and discussion of mitigating actions that can be taken to prevent real or perceived problems caused by pile driving vibrations. This paper illustrates the various points of discussion using two case studies involving pile driving projects with actual vibration measurements.

INTRODUCTION

In today's legal environment, protecting pile driving projects from fraudulent or errant claims resulting from vibrations produced from those pile driving or other construction activities is important. This can be achieved with good science and data collection prior to and during pile driving activities. This paper explains the difference between impact and transient vibration levels and steady state vibration levels associated with vibratory pile driving. This paper also discusses various vibration limits that have been applied over the years, including the use of frequency-based limits that are currently used in other vibration generating activities, such as blasting, and their possible application to pile driving.

Also discussed in this paper are the precautions that can be taken to protect contractors. Precautions, such as pre-piling condition surveys and inspections of the properties around a project in order to mitigate unwanted claims of damage of pre-existing defects. Other precautions, such as vibration monitoring with seismographs will be explored, as well as a discussion of public relations strategies to lessen claims from vibrations from pile driving activities. Lastly, some case studies of actual vibration levels recorded will be presented.

Ground vibration is essentially wasted energy. Not all of the energy from the pile driving hammer goes into driving the pile in the ground. Some "wasted" energy is released as ground vibrations, air concussion, and noise. The primary concern with ground vibration is its potential to damage surrounding properties. It is important to distinguish between structural damage and damage that is of a cosmetic nature.

Seismographs are used to monitor ground vibrations and impulse noise levels. These instruments continuously monitor the two horizontal and one vertical component of motion and record the maximum resultant vector. The maximum

resultant vector of velocity in these three directions is called the Peak Particle Velocity (PPV) and is the main output parameter reported by the seismograph. PPV is typically measured in inches per second. The seismograph also monitors impact noise levels. Overpressure is the acoustic parameter measured by the seismograph and is measured in decibels indicated by the symbol dB(L).

Another measurement tool is human perception People can feel vibrations well below those levels necessary to cause damage and as such, human perception should not be used as an indicator of the damage potential of vibrations.

Understanding vibrations and measuring them using reliable, scientific instruments allows further examination into the following topic areas: 1. Areas of concern and associated vibration standards, and 2. Liability protection measures

PILE DRIVING VIBRATIONS – AREAS OF CONCERNS

The following are areas of concern for vibrations from pile driving operations: building damage, green concrete, soil settlement/buried utilities, human perception, toppling of loose objects, and sensitive equipment and computers. Each of these topics is discussed in greater detail in the following sections including typical industry standards where applicable.

Damage Potential to Buildings

Vibration standards are in units of particle velocity with frequency dependency. These standards are designed to protect drywall and plaster from cosmetic cracking; structural damage would require two to five times higher vibrations than the generally applied standards.

Vibration Standards-Transient (Impact Hammer)

Below is a list of acceptable vibration limits for transient vibration levels for pile driving and other construction activities developed by the US Bureau of Mines (RI 8507):

- Limits PPV to 19.05 mm/sec (0.75 in/sec) for low frequency vibrations (<12 Hertz)
- PPV of 25.5 mm/sec (1.0 in/sec) for frequencies of 20 Hz and PPV of 50.8 mm/sec (2.0 in/sec) for higher frequency vibrations.

Vibration Standards-Steady State (Vibratory Hammer)

Below is a summary of information on vibration limits for steady state vibration levels for pile driving and other construction activities (Dowding, 1996):

- Vibrations from steady state sources are typically limited to a PPV of 12.7 mm/sec (0.5 in/sec) or less.
- Greater potential for resonance due to number of cycles/duration
- Fatigue cracking a concern due to the number of cycles
- Low frequency vibrations typically occur during ramping up and down at start up and stop (vibratory hammer for instance)

- Objects "walking" across shelves are more of a concern with steady state vibrations, even well below safe structure standards

Green Concrete

When pile driving or blasting is conducted in close proximity to freshly poured concrete, special care must be taken not to damage the cement bonds. The limits in Table 1 for controlling transient vibration impacts (from pile driving with an impact hammer or from blasting) on green concrete foundations have been successfully applied on similar projects (Oriard and Coulson, 1980).

Table 1 – Recommended Vibration Limits for Mass Concrete

Concrete Age from Batching	Allowable Particle Velocity (mm/sec) x Distance Factor (DF)
0 to 4 hrs.	50.8 x DF
4 hrs. to 1 day	76.2 x DF
1 to 3 days	114.3 x DF
3 to 7 days	152.4 x DF
7 to 10 days	190.5 x DF
10 days or more	254 x DF

DF is defined as follows:

Distance = 0 to 15.24 meter	DF = 1.0
Distance = 15.24 to 45.72 meter	DF = 0.8
Distance = 45.72 to 76.2 meter	DF = 0.7
Distance = over 76.2 meter	DF = 0.6

- A minimum distance of 30.48 meter is recommended between pile driving and freshly poured concrete elements less than three days old. Vibrations shall be controlled to the levels detailed in Table 1 for curing mass concrete.
- Concrete forms must be braced sufficiently to withstand vibration during the first 24 hours after concrete is poured, before it has attained sufficient strength.
- For above grade walls, the vibrations should be limited to one half of the limits listed in Table 1.

As discussed above, driving of sheet piles using a vibratory hammer produces continuous steady state vibrations as opposed to the transient vibrations generated by impact pile driving hammers. Limits for continuous vibrations should be established at 25% of those established for transient vibrations (Oriard and Coulson, 1980).

Soil Settlement from Pile Driving and Construction Vibration

There are two possible foundation related effects from vibrations; direct vibration effects on a house and effects on the foundation soils, which can then affect the house (Siskind, 2000). The direct effects were discussed previously.

Saturated cohesionless soils, like the poorly graded beach sand underlying the site, are known to be susceptible to a vibration effect called liquefaction (beach sand is the

best known example of this). Vulnerability requires susceptible soils (saturated and cohesionless), long duration vibration (tens to hundreds of cycles), and high vibration amplitudes (Siskind, 2000). The concern is not vibration velocity, but acceleration and the conditions that sometimes occur in earthquakes, but seldom manifests in blasting or dynamic compaction.

The lowest known examples of vibration induced liquefaction were 80 cycles of vibration at 0.165 g (equivalent to 63.5 mm/sec (2.5 ips) at 4 Hz) and observed liquefaction at a PPV of 50.8 mm/sec (2.0 ips) (Siskind, 2000). Because liquefaction concerns are earthquake driven, frequencies required to induce liquefaction are very low and therefore strain levels are very high (displacements and strains are inversely proportional to frequency). Therefore, it is reasonable to assume that the accelerations associated with the observed liquefaction examples apply only to low frequencies, likely below 4 Hz (Siskind, 2000).

Dowding (1985) describes blast densification of loose sand. Dowding reiterates that very high velocities are required to induce liquefaction or settlement. Dowding presents an example where 5 kg of high explosives was detonated in loose to medium-dense sands, measurable settlement occurred out to a distance of 17.98 meter. The estimated PPV at 17.98 meter from the blast was between 25.4 and 76.2 meter per second (mm/sec). These sands were extremely loose and had standard penetration resistance blow count numbers (N) of less than 10.

Oriard (2002) reports that the minimum threshold for ground shear strain to induce liquefaction is about 0.02 percent for a very wide variety of soil conditions independent of the duration of the shaking. In the case of construction activity, this would mean that the dynamic compaction source would have to be located in the immediate area, within the deposit itself. Strain is equal to particle velocity divided by the shear wave velocity.

Standards for Buried Utilities

- Restrained in-ground resonance unlikely
- Less susceptible to vibration effects than above ground structures
- PPV limits published for pressurized gas transmission pipelines and for fiber optics-101.6 to 127 mm/sec.

Engineered Commercial Structures

- PPV standards 2 or 3 times safe levels for residences
- Can be up to 76.2 to 127 mm/sec.
- Displacement of 0.020 mm can be applied

Toppling of Loose Objects

Movement of pictures, items on shelves, dishes rattling, and toppling of tall knick-knacks occurs at PPV levels below cracking thresholds. Oriard (1999) indicates that based on personal experience, for lower frequencies and greater durations, many objects are more responsive and for higher frequencies and short durations, many

objects are less responsive. Table 2 illustrates a generalized sensitivity range, where 0.1 ips is 2.54 mm/sec, 1 ips is 25.4 mm/sec and 4 ips is 101.6 mm/sec.

Table 2 – Vibration Effects on Loose Objects (Oriard, 1999):

Risk of Toppling Objects	Particle Velocity (mm/sec)
Rare	Under 2.54
Occassional	2.54 to 25.4
Common	25.4 to 101.6
Extensive	Above 101.6

Sensitive Equipment and Computers

- Standards are typically in accelerations expressed in (g)
- Common acceleration standard is 0.25 g. At a frequency of 20 Hz, the equivalent PPV is about 19.04 mm/sec (0.75 in/sec).
- These standards are typically designed for earthquake standards or steady state vibrations during operation
- Equipment and computers are far less susceptible to short term transient vibration effects from construction than from the steady state operating standards usually published

LIABILITY PROTECTION

In order to protect a project from liability, the following needs to be addressed: seismograph monitoring, pre-construction photographic surveys/inspections, notification and education of the public, communication, recordkeeping, and mitigation.

Monitoring

There are various types of instruments or seismographs available to measure ground vibrations and impact noise levels. Manufacturers of seismographs can recommend suitable equipment based on the needs of a particular project. To obtain reliable vibrations measurements the seismograph's geophone must be well connected to the ground or the recording location – this is called 'coupling'. For earth locations, the geophone should be buried at least 152 mm, spiked and covered with a sandbag.
In an urban environment, the geophones should be bolted or otherwise adhered to the ground. Areas to avoid include unstable ground or hollow areas. Various options exist for the recording and reporting of vibration data ranging from on-site monitoring by personnel, to new technologies such as automatic web-based posting of data and automated transmission of vibration data to email, pagers and cell phones.

Pre-Piling/Construction Surveys/Inspections:

Pre-piling building condition surveys/inspections provide a baseline of how the properties appear prior to the start of piling. Performing these surveys does not mean that damage will occur or that it is anticipated. The surveys should be conducted by competent and experienced individuals and companies. Typically, this is a cosmetic survey of the surface condition of the properties around the project. Structural defects are unlikely to occur with the typical vibration levels experienced from impact pile driving.

The survey perimeters vary from project to project. Typically, a range of 30.48 to 182.9 meter from the piling is standard. At minimum, a 91.4-meter survey perimeter would suffice. The formats of these surveys also vary. Typical format consists of diagram sheets of each room and wall, 3x5 color photos and supplemental videos of existing conditions. The use of high quality digital photographs and scanned (pdf) files incorporated into electronic copies of the surveys puts the data into a usable format for today's construction project software. These surveys are a documentation of *cosmetic* defects and need to be very detailed. If damage were to occur, it would be to those minor cosmetic areas first and not major structural damage, in most cases.

Notification/Education of Public and Communications

A great deal of prospective problems, complaints and claims of damage from pile driving vibrations can be reduced with good communication at the onset of the project. Simply explaining to the surrounding property owners what they may expect to feel from pile driving activities and that feeling vibrations does not mean that damage will occur can go a long way in the overall reduction in complaints. Furthermore, performing a pre-pile property condition survey does not mean that damage is expected. Public education is critical, as it has been important in the blasting industry for years; it is also equally significant for the pile driving industry.

Recordkeeping

Good record keeping is essential for liability protection. The following information has to be documented at a minimum: what piles (type and length) are driven, when and where, seismograph serial number and location, distance and direction from seismograph to each pile, and make, model and energy of the hammer.

Mitigation Techniques

The following actions can be taken to mitigate vibrations and/or help prevent complaints related to piling driving: Public relations and monitoring, Pre-drilling of piles, Reduction of hammer stroke to reduce energy and/or reduction of hammer size, Mitigation trenches/sheeting, and Time of work.

CASE STUDY 1

This case involved a new bridge ramp and elevated roadway extending from an existing tunnel, running adjacent to historical buildings, which were located on a riverbed. The project specifications included the following requirements for vibration control:

- Submission of a vibration monitoring and control plan and qualifications of seismic engineer (5 years minimum experience). Include predicted anticipated vibration readings at recording locations.
- Extensive pre-construction property condition surveys/inspections required – 152.4 meter from pile driving (very conservative).
- Ambient vibration and sound levels has to be collected.
- Installation of survey monitoring points at specific locations and reference points (.0.0003048 meter).

Additionally, the vibration limit for the project was 50.8 meters per second and an imposed action level required action if 10.16 meters per second was exceeded. A reading at that level required contractor notification. Vibration monitoring was required for every new construction activity. Assuming 12.7 meters/sec was not exceeded continual monitoring was not required.

Sound levels from 8 am to 8 pm were limited to 91dBA at commercial structures and 80 dBA at residential structures. There was an optional limit to use 5 db over ambient levels. Ambient levels in this case were as high as 96 dBA.

Typical Recorded Levels:

- Pile driving activities – diesel hammer – Delmag 4500 lbs
- 2.28 mm/sec @ 4.57 meter
- 85 dBA @ 30.48 meter
- Pre-drilling for caissons – 2.54 mm/sec @ 21.34 meter

For this project there was no real difference between a hydraulic hammer and diesel hammer for vibration or sound levels. Sound proofing was used around the hydraulic hammer in close proximity of buildings, as per specifications.

CASE STUDY 2

This case involved the demolishing and rebuilding of a steel bridge along with the construction of a large retaining wall near historic and older properties. The project specifications included the following requirements for vibration control:

- Submission a vibration monitoring and control plan along with qualifications of seismic engineer (5 years minimum experience).
- Extensive pre-construction property condition surveys/inspections were required 91.44 meter from pile driving operations.
- On site, third-party vibration monitoring was required for all piling activities.

In this case, the requirement for third-party, independent vibration monitoring was met with remote monitoring stations that allowed the real time posting of vibration data to a secure website that could be accessible by the contractor and state regulatory authority as needed. Action was set on the equipment to transmit data over 2.54

mm/sec and text message and emails could be sent when those levels were recorded. The typical recorded vibrations were as follows:

- Pile driving activities – impact hammer – 3.68 mm/sec @ 15.24 meter
- Bridge span fall during demo – 6.49 mm/sec @ 10.66 meter

CONCLUSION

For the presented case studies, the data collection and precautions taken proved to be very helpful. Unfortunately, there is no perfect solution to dealing with the problems of pile driving near properties. However, there are some things that can be done to reduce the problems, such as:

- Maintenance of good public and community relations.
- Performance of appropriate and detailed pre-construction surveys/inspections – establish base line condition of neighbors.
- Undertaking of seismic monitoring.

Following the above recommendations and having a good understanding of vibrations and techniques for measuring them are necessary to mitigating problems related to pile driving vibrations.

REFERENCES

Chae, Y.S., 1978, "Design of Excavation Blasts to Prevent Damage", Civil Engineering, ASCE, Vol. 48, No. 4, pp. 77-79.

Dowding, C.H., 1996, "Construction Vibrations", Prentice-Hall, Inc. Upper Saddle River, NJ.

Konon, W., and Schuring, J.R., 1983, "Vibration Criteria for Historic and Sensitive Older Buildings," American Society of Civil Engineers, Pre-print 83-501.

Institution of Swiss Highway Engineers, (VSS), Swiss Standard SN640312: "Vibration Effects on Structures", VSS Secretariat Zurich, Nov., 1978.

Oriard, L.L., and Coulson, J.H., 1980, "TVA Blast Vibration Criteria for Mass Concrete", Minimizing Detrimental Construction Vibrations, ASCE Preprint 80-175, ASCE, New York, pp. 101-123.

Oriard, L.L., 2002, Explosives Engineering, Construction Vibrations and Geotechnology, International Society of Explosives Engineers, Cleveland Ohio.

Oriard, L.L., 1999, "The Effects of Vibrations and Environmental Forces: A Guide for the Investigation of Structures," International Society of Explosives Engineers, Cleveland, Ohio.

Siskind, D.E., Stagg, M.S., Kopp, J.W., and Dowding, C.H., 1980, "Structure Response and Damage Produced by Ground Vibrations from Surface Mine Blasting", Report of Investigations 8507, U.S. Bureau of Mines (USBM), Wash., DC.

Siskind, D.E., Stagg, M.S., 1994, "Surface Mine Blasting Near Pressurized Transmission Pipelines", Report of Investigations RI 9523, USBM, Wash., DC.

Siskind, D.E., 2000, Vibrations from Blasting, International Society of Explosives Engineers, Cleveland, Ohio.

Wiss, J. F., "Construction Vibrations: State-of-the-Art" Journal of the Geotechnical Division, ASCE, Vol. 107, No. GT2, Feb 1981.

Copyrighted Materials
Copyright © 2009 American Society of Civil Engineers (ASCE)
Retrieved from www.knovel.com

An Overview of Relevant Guidelines for Deep Foundation Generated Ground Vibrations

Edward L. Hajduk[1], M. ASCE, D.Eng, PE, Les R. Chernauskas[2], M. ASCE, PE, Stephanie van der Horst[3], S.M. ASCE, and Elizabeth Penn-Sanders[4], S.M. ASCE

[1]Assistant Professor, The Citadel, Department of Civil and Environmental Engineering, 171 Moultrie Street, Charleston, SC 29409, ed.hajduk@citadel.edu
[2]Principal, Geosciences Testing and Research Inc., 55 Middlesex Street, North Chelmsford, MA 01854, les@gtrinc.net
[3]Undergraduate Student, The Citadel, Department of Civil and Environmental Engineering, 171 Moultrie Street, Charleston, SC 29409, vanderhou1@citadel.edu
[4]Undergraduate Student, The Citadel, Department of Civil and Environmental Engineering, 171 Moultrie Street, Charleston, SC 29409, penne1@citadel.edu

ABSTRACT: Ground vibrations can be a major concern during the installation of various types of deep foundations, such as casing installation for drilled shafts and vibratory and impact driven piles. Vibration concerns can be either nuisance issues (e.g. disturbance of neighboring residents) or relate to cosmetic or structural damage of nearby buildings. Available vibration criteria commonly used to address both of these concerns vary significantly, which can lead to confusion when selecting an appropriate vibration criterion. The following paper presents a review of commonly used vibration criteria and examines their applicability for use with regards to deep foundation installations.

INTRODUCTION

Ground vibrations generated from deep foundation installations (e.g. driven piles, casing installations for drilled shafts) have long been a concern for construction projects. The major concerns are that generated ground vibrations will either cause damage (cosmetic or structural) to adjacent structures (e.g. existing buildings, freshly placed concrete) or annoyance to the neighboring people (e.g. disturbing work productivity or sleep). Annoyance to neighboring people is of particular concern in urban areas, where new projects on deep foundations typically abut existing residential and/or professional buildings. Inhabitants within these structures may have the ability to cause project delays or changes in construction schedules with complaints about vibration annoyance. Damage to freshly placed concrete is a concern to any construction site where concurrent operations of deep foundation installations and concrete placement occurs (e.g. concrete for pile caps or drilled

shafts being placed while deep foundation installations are ongoing). Damage to structures from ground vibrations can be from either direct damage caused by the vibration excitation or damage relating to vibration induced soil settlement.

COMMONLY USED EXISTING VIBRATION CRITERIA

Ground vibrations can be examined in a variety of ways (e.g. via acceleration, velocity, or displacement). Most research into ground vibration and their affects on people and structures use peak particle velocity (PPV) as the basis for their analysis and comparisons. Other vibration criteria relating to the effects on structures and/or human perception have been published using vibration measurements in terms of decibels (e.g. Hanson et al., 2006) and weighted root mean square accelerations (e.g. ISO, 1989). However, the majority of commonly used criteria provide limits in terms of PPV, typically in relationship to vibration frequency. The vibration criteria and thresholds examined in this paper are based on measurements of peak particle velocity (PPV).

Vibration Criteria based on Direct Damage to Structure

Vibration effects on a wide variety of structure types have been examined to develop vibration criteria, such as residential structures (e.g. Siskind et al., 1980), massive concrete structures (e.g. Oriard and Coulson, 1980), and buried pipes (e.g. Atalah, 2006). The most commonly used ground vibration criteria for structures was developed by Siskind et al. (1980), who examined the effects of surface mine blasting on residential structures for the United States Bureau of Mines and developed a criteria for the onset of threshold (i.e. cosmetic) damage. This criterion is commonly referenced as USBM (1980) and provides limits of peak particle velocity (PPV) relative to vibration frequency. Figure 1 presents the USBM (1980) criteria.

In addition to the USBM (1980) criteria, several other commonly used criteria relating PPV to threshold (i.e. cosmetic) damage for residential and commercial buildings are Rosenthal and Morlock (1987) (commonly referred to as OSMRE 1987), British Standard BS 7385 (1993) and German National Standard DIN 4150 (1999). These standards are also presented in Figure 1. Also provided in Figure 1 is the typical range of ground vibration frequencies associated with pile driving (i.e. 10 Hz to 40 Hz). The vibration criteria provided in these standards also apply to the onset of "threshold" or "cosmetic" damage. Potential ground vibration damage criteria not related to vibration frequency for continuous/frequent intermittent vibration sources, such as pile driving, was compiled by Jones & Stokes (2004) using a variety of sources. Their summary is provided in Table 1.

Direct Damage to Historic Structures

Of additional concern relating to direct damage to structures are those buildings deemed as historic, since they cannot be replaced and repairs can be difficult and expensive. Several commonly used vibration criteria relating to historic (a.k.a. older or fragile) structures include Konon and Schuring (1983), Swiss Standard SN640312

(1992), DIN 4150 (1999), and Hajduk et al. (2004). These standards are also based on PPV and vibration frequency and are presented in Figure 2.

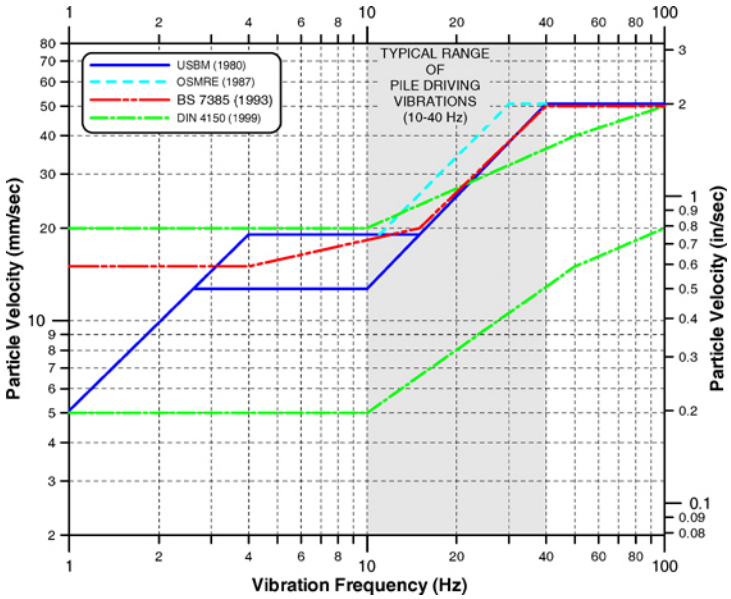

FIG. 1. Commonly Used Vibration Criteria for Typical Residential and Commercial Buildings (after Dowding, 1996).

Table 1. Vibration Damage Potential Threshold Criteria (Jones & Stokes, 2004).

Structure and Condition	Maximum PPV mm/sec (in/sec)
Fragile Buildings	2.5 (0.1)
Historic and Some Old Buildings	6.4 (0.25)
Older Residential Structures	7.6 (0.3)
New Residential Structures	12.7 (0.5)
Modern Industrial/Commercial Buildings	12.7 (0.5)

Human Perception Vibration Criteria

Bay (2003), after examining several studies evaluating human perceptions to vibrations, stated that in general, humans will perceive vibrations greater than 0.25 mm/sec (0.01 in/sec), are strongly perceptible/possibly disturbed by vibration levels greater than 2.5 mm/sec (0.1 in/sec), and are likely to be very disturbed at vibration

levels greater than 25 mm/sec (1 in/sec). The human perception vibration levels from Bay (2003) are shown relative to typical structure vibration levels in Figure 3.

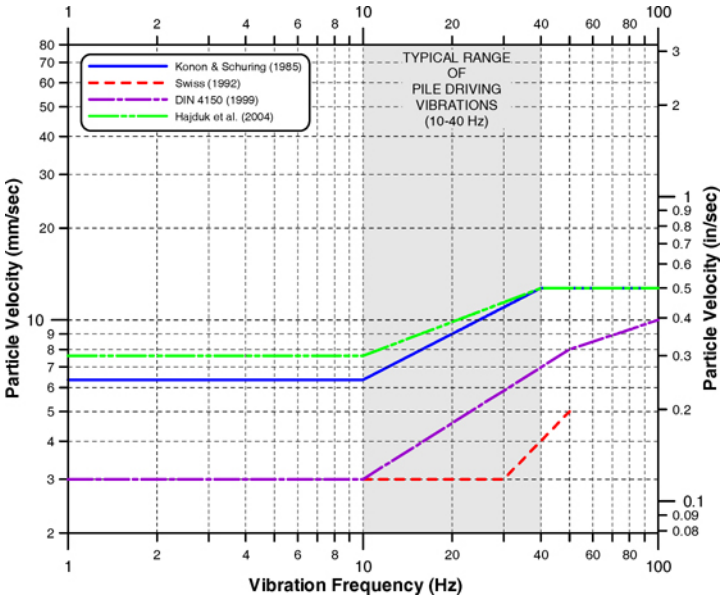

FIG. 2. Commonly Used Vibration Criteria for Historic/Older/Fragile Structures.

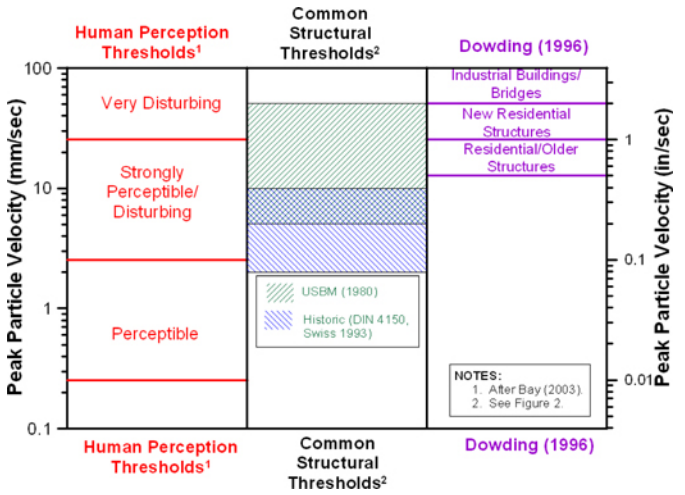

FIG. 3. Typical Levels of Human Perception Relative to Common Structural Vibration Criteria (after Bay, 2003).

Concrete Vibration Criteria

Concerns relating to ground vibrations effects on concrete are typically divided into two (2) categories; effects on "green" (i.e. freshly placed) concrete and fully hardened (i.e. cured or set) concrete. A summary of commonly used ground vibration criteria for concrete is presented in Table 2.

Table 2. Ground Vibration Criteria for Concrete (after Tawfiq and Abichou, 2003).

Reference	Permitted Peak Particle Velocity mm/sec (in/sec)	
	Green Concrete[1]	Set Concrete[2]
Oriard and Coulson (1980)	102-381 (4-15)	508 (20)
Bryson and Cooley (1985)	5.1-102 (0.2-4)	102 (4)
Gamble et al. (1985)	5.1-51 (0.2-2)	102 (4)
Olofesson (1988) Curing at 5°C	<36 (< 1.4)	76 (3)
Tawfiq and Abichou (2003)	51 (2)[3]	NA

NOTES:
1. Green Concrete is defined as concrete up to 10 hours from placement.
2. Set concrete has had a minimum time of 28 days from placement.
3. At a minimum distance of 1m (3ft) from placed concrete.

APPLICABILITY OF EXISTING CRITERIA TO DEEP FOUNDATIONS

At present, there is no universally accepted standard for limiting earth-borne vibrations (AASHTO, 2004). The lack of a universally accepted criteria is due to the complexity of variables involved, such as type of structure (e.g. historic to newly built), type of structure foundation (deep vs. shallow), type of damage (e.g. cosmetic to structural failure), and level of annoyance (i.e. disturbed to annoyed). Given that "threshold" or "cosmetic" damage will most likely occur prior to damage that could significantly alter the load bearing capabilities of a structure, a limit relating to this level of damage is appropriate. However, damage to different materials usually occurs at different levels. An example of different criteria for different materials is shown in Figure 1 for the USBM (1980) criteria, which has different limiting PPV magnitudes depending on the residential wall materials (i.e. drywall vs. plaster).

Since the commonly used vibration criteria for "cosmetic" damage and historic structures are mainly based on blast vibrations (e.g. Siskind et al, 1980 and Rosenthal and Morlock, 1987) or from unknown data sources (Swiss, 1992 and DIN, 1999), the applicability of these criteria to deep foundation generated vibrations may be questionable. Blast generated vibrations are predominantly comprised of surface waves. Depending on the soil profile and installation methods, the primary component of ground vibrations generated during deep foundation installation may not be surface waves. Using dynamic pile measurements, Hajduk and Adams (2007)

showed that maximum ground vibrations generated during driven pile installation correlated to maximum pile capacities. If maximum pile capacities are generated with depth during installation through dense/stiff layers, the primary component of the ground vibrations could be compression waves. As the previous studies based on blasting focused on peak vibrations, this may not be a concern. Additional research in this field is needed.

The use of low vibration levels for historic structures is also questionable. Bay (2003) suggested that the vibration criteria of 12.7 mm/sec (0.5 in/sec) for residential structures in poor condition proposed by Chae (1978) would be more appropriate for historic buildings, since the existing European vibration standards for historical structures (e.g. Swiss, 1992 and DIN 4150, 1999) are unreasonably low and that buildings which cannot withstand these vibration levels are too fragile to have substantial function. This is the same PPV level for some historic/older structures suggested by Dowding (1996). Using ground vibration data from driven pile projects, Hajduk et al. (2004) suggested higher PPV levels could be used for historic/older structures in the Charleston, SC area, but not at the levels suggested by Bay (2003), though they do acknowledge that low vibration standards which are near the levels generated by vehicle and pedestrian traffic or other everyday activities are impractical.

While establishing vibration criteria for structures is important to deep foundation projects, of greater significance may be the establishment of vibration criteria for human perception. As shown in Figure 3, the general human PPV perception level summarized by Bay (2003) is approximately an order of magnitude lower than even the most conservative PPV level for historic structures and approximately twenty (20) times lower than lowest PPV level for residential structures from the USBM (1980). Human perception of ground vibrations is often the primary concern relating to deep foundation projects, since complaints from neighboring professional workers and/or residents can lead to work stoppage and/or lawsuits. The authors' general experience relating to deep foundation generated ground vibrations is that once neighboring people (especially residents) sense ground vibrations, they tend to notice existing defects (e.g. cracks) and subsequently file complaints and/or lawsuits. To reduce delays and/or additional project costs related to human perceived vibrations, the use of vibration criteria related to human perception PPV levels may be desirable.

In addition to reducing project delays and/or costs, the use of vibration criteria based on human perception levels may also be desirable for another reason; reducing the risk of damage to structures due to soil settlement. Lacy and Gould (1985) concluded that settlement from pile driving vibrations can result from vibrations at peak particle velocity levels much lower than those that can cause damage to structures in loose to medium dense uniform sands. Since current vibration criteria relating to structures do not address damage from soil settlement, a reduction to human perception PPV levels could be used. The use of human perception PPV levels is not meant as a replacement to a detailed examination of soil settlements from expected deep foundation generated ground vibrations. As the vibration criteria for concrete, either "green" or set, is significantly greater than those for cosmetic structural damage and human perception, the use of human perception levels would also address any concerns in this area.

The use of any existing vibration criteria for deep foundation projects should be thoroughly examined on an individual case basis. The complexity of the variables involved, such as adjacent building types, existing soil conditions, neighboring population, prevent the use of a single blanketing criteria that covers all situations. Monitoring ground vibrations during deep foundation installation or testing and comparing them to selected criteria should just one component in addressing ground vibration concerns. Other components should include education of neighboring people with regards to the project, pre and post condition surveys of adjacent structures, prediction of ground vibration magnitudes, evaluation of the affects of ground vibrations on people and structures (to include examination of the possibility of soil settlement and fundamental adjacent building frequencies if warranted), and development of a monitoring plan for adjacent structures (if deemed necessary). Dowding (2001) suggests measuring cracks instead of ground vibrations, since cracks are directly visible to the structure owners and ground motion complexities and their indirect relationship to potential damage are avoided.

CONCLUSIONS

A review of some commonly used vibration criteria applied to deep foundation generated ground vibrations have been presented. These criteria address concerns relating to cosmetic damage to adjacent buildings, neighboring human perceptions, and the affects on concrete. It is noted that other vibration criteria that can be applied to deep foundations exist that have not been presented in this paper. Focusing on human perception levels in selecting vibration criteria for a specific project has the possibility of addressing other common concerns, such as neighbor annoyance and soil settlement.

REFERENCES

American Association of State Highway and Transportation Officials (AASHTO) (2004). R8-96 *Standard recommended practice for evaluation of transportation-related earthborne vibrations.* Washington, DC.

American National Standards Institute (ANSI) (1983). "Guide to the evaluation of human exposure to vibrations in buildings." *ANSI S3.29-1983*, New York.

Atalah, A. (2006). "Safe Distance between Large-Diameter Rock Pipe Bursting and Nearby Buildings and Buried Structures." *J. Transp. Engrg.*, 132 (4): 350-356.

Bay, J.A. (2003). "A Summary of the Research on Pile Driving Vibrations." *Proc. 7th Pile Driving Contractors Association Annual Winter Round Table*, Atlanta, GA.,

British Standards Institution. (1993). "Evaluation and Measurement of Vibration in Buildings, Part 2: Guide to Damage Levels from Ground-borne vibration." BSI, London, BS 7385: Part2.

Bryson, B. and Cooley, T. "Blasting procedures, Veterans Administration Medical Centre, Birmingham, Alabama", *Proc. 11th Conference on Explosives and Blasting Technique*, Society of Explosive Engineers: 272-283.

Chae Y.S. (1978). Design of Excavation Blasts to Prevent Damage." *Civil Engineering*, 48 (4): 77-79

Dowding, C.H. (2001). "Measure the Crack Instead of Construction Vibrations." *Geo-Strata - Geo Institute of ASCE*, 2 (3): 20-23

Dowding, C. H. (1996). *Construction Vibrations*, Prentice-Hall, Upper Saddle River, N.J. 610p.

Gamble, D. L.; Jow, Y. K.; and Simpson, T. A. (1985). "Effects of blasting vibrations on uncured concrete foundations", *Proc. 11th Conference on Explosives and Blasting Technique*, Society of Explosive Engineers: 124-136.

German Standards Organization. (1999). "Vibrations in Building Construction." DIN 4150.

Hajduk, E.L., D.L. Ledford and W.B. Wright. (2004). "Construction Vibration Monitoring in the Charleston, SC Area." *Proc. 5th Intl. Conference on Case Histories in Geotechnical Engineering*, New York, NY.

Hajduk, E.L. and Adams, J.C. (2008). "Examination of Ground Vibrations and Dynamic Pile Measurements during Driven Pile Installation", *Proc. 8th Intl. Conference on the Application of Stress-Wave Theory to Piles*, Lisbon, Portugal.

Hanson, C.E., Towers, D.A., and Meister, L.D. (2006). "Transit Noise and Vibration Impact Assessment." Report FTA-VA-90-1003-06, Federal Transit Administration, Washington, DC.

International Organization for Standardization. (1989). *ISO 2631-2 - Evaluation of human exposure to whole-body vibration - Continuous and shock-induced vibration in buildings*. 18 pp.

Jones & Stokes (2004). *Transportation- and construction-induced vibration guidance* June. (J&S 02-039.) Sacramento, CA. Prepared for California Department of Transportation, Noise, Vibration, and Hazardous Waste Management Office, Sacramento, CA.

Konon, W. and Schuring J.R. (1985). "Vibration Criteria for Historic and Sensitive Buildings." American Society of Civil Engineers (ASCE) Preprint 83-501.

Lacy, H. S., and Gould, J. P. (1985). "Settlement From Pile Driving in Sands." *Proc. Symp. Vibration Problems in Geotechnical Engineering*, ASCE, Detroit, MI: 152-173.

Olofesson, S.O. "Applied Explosives Technology for Construction and Mining, Applex, Ärla, Sweden: 236-237.

Oriard, L.L. and Coulson, J.H. (1980). "TVA's Criteria for Blasting Effects on Concrete", *Specialty Conference on Minimizing Detrimental Construction Vibrations*, ASCE, Portland, OR.

Rosenthal, M.F. and Morlock, G.L. (1987). Blasting Guidance Manual, Office of Surface Mining and Reclamation and Enforcement, US Dept of the Interior.

Siskind, D.E., M.S. Stagg, J.W. Kopp, and C.H. Dowding (1980). "Structure Response and Damage Produced by Ground Vibration from Surface Mine Blasting", Report of Investigations 8507, United States Bureau of Mines, Washington, D.C.

Swiss Standard SN640312 (1992), "Effects of Vibration on Constructed Facilities," Swiss Consultants for Road Construction Association.

Tawfiq, K. and T. Abichou. (2003). "Effects of Vibration on Concrete Strength During Foundation Construction." Report BC-352-14, Florida Department of Transportation, Tallahassee, FL.

Copyrighted Materials
Copyright © 2009 American Society of Civil Engineers (ASCE)
Retrieved from www.knovel.com

Development of a Driven Pile Ground Vibration Case History Database

Edward L. Hajduk[1], M. ASCE, D.Eng, PE, Kevin C. Bower[2], M.ASCE. Ph.D, PE, Timothy W. Mays[3], M.ASCE. Ph.D, PE, David A. Falatok[4], and Timothy S. Perkins[4]

[1]Assistant Professor, The Citadel, Department of Civil and Environmental Engineering, 171 Moultrie Street, Charleston, SC 29409, ed.hajduk@citadel.edu
[2]Assistant Professor, The Citadel, Department of Civil and Environmental Engineering, 171 Moultrie Street, Charleston, SC 29409, kevin.bower@citadel.edu
[3]Associate Professor, The Citadel, Department of Civil and Environmental Engineering, 171 Moultrie Street, Charleston, SC 29409, timothy.mays@citadel@citadel.edu
[4]Formerly Undergraduate Student, The Citadel, Department of Civil and Environmental Engineering, 171 Moultrie Street, Charleston, SC 29409

ABSTRACT: Ground vibrations are a major concern for driven pile projects. Although experience has shown that vibration concerns from pile driving operations can be managed, it is difficult to illustrate this concept based on the available information. This difficulty is evident in the wide range of vibration criteria applied to pile driving in use today. While there is extensive technical literature on ground vibrations generated from pile driving, no central database exists that incorporates the various case history data. The creation of a central database of driven pile vibration case histories is an important first step towards future research examining these environmental effects of pile driving on adjacent structures and residents.

A pile driving vibration case history database was developed that incorporates available data from the technical literature and data provided by professionals within the pile driving industry. The following paper details the background related to the database creation, the data collection and review process, and development of the data into a database format.

INTRODUCTION

As projects within urban areas with limited space increase in frequency, driven pile foundations are routinely being discounted as a foundation option due to concerns with ground vibrations. In some cases, driven piles are being ruled out as a foundation option in the planning stages due to this concern alone without an engineering evaluation.

The perception that driven piles generate unacceptable levels of ground vibrations stems primarily from a general lack of knowledge. The ignorance relating to this pile driving environmental issue is connected in part to the unconsolidated nature of the available technical data related to driven pile generated ground vibration.

Over the years, a significant number of pile driving vibration case histories have been published for a wide variety of purposes, such as examination of ground vibration attenuation characteristics (e.g. Attewell and Farmer (1973), Wiss (1981), Woods and Jedele (1985), and Hajduk et al., 2004); investigation of the affects of driven pile generated ground vibrations on structures (e.g. Selby, 1989); detailing case histories relating to settlement of in-situ soils (e.g. Lacy and Gould, 1985); and examination of the generated ground vibration characteristics (e.g. Thandavamoorthy, 2004). Recently, there have been efforts to examine the relationships between dynamic pile measurements during installation and generated ground vibrations (e.g. Robinson 2006, Hajduk et al., 2006, Heung et al., 2007, and Hajduk and Adams, 2008).

Although the technical literature has a large sample of pile driving vibration case histories, the relative number of published case histories is small when compared to the number of driven pile projects. Smaller still is the number of attempts that have been made to collect and centralize the available data in one location. Of these attempts, the most comprehensive was conducted by Woods (1997), who collected ground vibration data from nineteen (19) driven pile projects. While Woods (1997) conducted a thorough examination of the effects of ground vibrations on adjacent structures, the case history data presented is limited to general information summaries of the major factors (i.e. pile type, soil conditions, and measured vibration levels). Individual data points relating pile type, distance(s) to ground vibration measurements, and ground vibration magnitudes and frequencies are not provided. In general, the case histories on the technical literature provide general data summaries and not detailed individual measurements that could be used in future research efforts. Only a few case histories provide detailed measurements of ground vibrations with individual pile installations (e.g. Robinson, 2006).

While much is known regarding ground vibrations generated during driven pile installation, much remains to be investigated. For example, attenuation characteristics for driven pile ground vibrations have been developed relating to hammer energy (either rated or measured) and distance from the pile. However, only a few of these correlations also account for the type and strength of the soils the piles are penetrating (e.g. Woods and Jedele, 1985). Given that past research has shown that maximum ground vibrations measured at the ground surface can correlate to the stiffest soil layers encountered during pile penetration (Hajduk et al., 2006), the penetrated soils could be an influential factor in attenuation relationships.

Future research of driven pile generated ground vibrations would benefit from a centralized case history database that is readily available. This database would contain specific data relating to the major factors influencing generated ground

vibrations (i.e. pile type, soil conditions, and measured vibration levels and frequencies) as well as case history data not commonly found in the technical literature case histories (e.g. if pre-condition surveys were conducted, complaints and/or lawsuits relating to generated ground vibrations were filed), which could also be useful in future research efforts.

DATABASE DEVELOPMENT

The development of a centralized driven pile ground vibration case history database was divided into the following four-step process:

1. Identify relevant data to be collected.
2. Accumulate case history data from the driven pile industry and associated technical organizations.
3. Develop a database format within a commercially available database program.
4. Review and enter case history data.

In addition to the four-steps listed above, a literature survey was conducted and a questionnaire was sent out to State Transportation Departments (DOT), pile driving contractors, and engineering consultants to sample the industry's experience with pile driving vibration. The questionnaire was modeled directly after Woods (1997). The literature survey and results of the questionnaire are beyond the scope of this paper.

A list of relevant data for the individual case histories was developed based on the primary author's experience with driven pile vibration projects and common data presented within the available case histories found during the literature survey. These data included soil information (e.g. soil type), pile information (e.g. pile type and size), hammer information (e.g. hammer type), vibration measurements (i.e. peak particle velocity), and project information (e.g. pre-condition surveys). The desired relevant data are summarized in Table 1.

Case history collection began with twenty-three (23) case histories containing 1793 individual pile-ground vibration measurements provided by the primary author from projects within the Charleston, SC area. These case histories are summarized in Table 2. Additional case histories were solicited from the members of the Pile Driving Contractors Association (PDCA), which sponsored the database development, and other technical organizations dealing with driven piles such as the Deep Foundations Institute. Given that monitoring of ground vibrations is being increasingly required for deep foundation projects, it stood to reason that additional driven pile ground vibration case history data would be readily available from within the driven pile industry. For the initial database development, only the case histories submitted by the primary author were used since they had undergone a rigorous data review prior to their submittal. Future case history data would be reviewed prior to their inclusion into the database.

Table 1. Desired Relevant Driven Pile Ground Vibration Case History Data.

Factor	Desired Relevant Data
Pile	Pile Type
	Pile Size
	Pile Length
	Pile Cushion Type & Thickness
	Pre-Auger Diameter
	Pre-Auger Length
	Pile Penetration Start Depth
	Highest Blow Count (BC)
	Penetration @ Highest BC
	Observed Stroke
	Final Penetration Embedment
	BC @ Final Embedment
	Measured Energy (if dynamically monitored)
Hammer	Hammer Type
	Hammer Manufacturer
	Hammer Model
	Ram Weight (Impact)
	Maximum Stroke (Impact)
	Hammer Speed (Impact)
	Maximum Rated Energy (Impact)
	Maximum Amplitude (Vibratory)
	Centrifugal Force (Vibratory)
	Suspended Weight (Vibratory)
	Vibration Frequency (Vibratory)
Vibration	Distance from Pile
	Peak Particle Velocity – Transverse Direction (PPV-T)
	PPV-T Frequency
	Peak Particle Velocity – Longitudinal Direction (PPV-L)
	PPV-L Frequency
	Peak Particle Velocity – Vertical Direction (PPV-V)
	PPV-V Frequency
	Peak Vector Sum (PVS) Vibration Magnitude
Soil	Soil Type – Toe
	Predominant Soil Type - Skin
	In-situ Testing Data (e.g. SPT, CPT, DMT, etc.)
Project	Pre-Condition Survey (Y/N)
	Post-Condition Survey (Y/N)
	Adjacent Building Existing Crack Monitoring (Y/N)
	Adjacent Building Existing Crack Monitoring (Y/N)
	Distance to
	Settlement Monitoring (Y/N)
	Settlements (Y/N)
	Maximum Settlement
	Adjacent Structure Damage (Y/N)
	Damage Type (Cosmetic/Structural)
	Known Complaints or Lawsuits (Y/N)

Table 2. Summary of Initial Database Case Histories.

Case No.[1]	Location	Pile Size	Hammer Type	Hammer	Data Points
1	Charleston, SC	HP305x79 (HP12x53)	Hydraulic	ICE 75	203
		30.5cm (12in) OEP	Hydraulic	ICE 75	7
2	Charleston, SC	30.5cm (12in) PSC	Hydraulic	ICE 75	396
3	Sullivan's Is., SC	20.3cm (8in) Timber	Air	Vulcan 6 ECH	108
4	Isle of Palms, SC	25.4cm (10in) Timber	Air	Vulcan 06	56
5	Charleston, SC	25.4cm (10in) PSC	Hydraulic	ICE 115	35
		30.5cm (12in) PSC	Hydraulic	ICE 115	72
6	Charleston, SC	HP305x79 (HP12x53)	Air	Vulcan 01	9
7	Charleston, SC	HP305x79 (HP12x53)	Vibratory	APE 200	22
		AZ 13	Vibratory	APE 200	71
		AZ 18	Vibratory	APE 200	28
8	Charleston, SC	30.5cm (12in) PSC	OED	Delmag D30-23	40
9	Charleston, SC	HP305x79 (HP12x53)	Hydraulic	Conmaco C65	7
10	Charleston, SC	HP305x79 (HP12x53)	Air	Vulcan 06	6
		30.5cm (12in) PSC	Air	Vulcan 06	18
11	Isle of Palms, SC	20.3cm (8in) Timber	Air	Vulcan 01	16
12	Sullivan's Is., SC	25.4cm (10in) PSC	Air	Vulcan 01	109
13	Kiawah Island, SC	20.3cm (8in) Timber	Air	Vulcan 06	3
14	Kiawah Island, SC	30.5cm (12in) PSC	Air	Vulcan 06	74
15	Charleston, SC	HP305x79 (HP12x53)	Air	Vulcan 06	95
16	Seabrook Is., SC	20.3cm (8in) Timber	Air	Vulcan 01	94
17	Folly Beach, SC	30.5cm (12in) PSC	Air	Vulcan 06	4
		20.3cm (8in) Timber	Air	Vulcan 06	16
18	Mt. Pleasant, SC	Fordingham 3NA	Vibratory	PVE 1420	46
19	Charleston, SC	30.5cm (12in) PSC	Hydraulic	ICE 115	5
20	Sullivan's Is., SC	25.4cm (10in) Timber	Drop	Drop Hammer	18
21	Charleston, SC	30.5cm (12in) PSC	Hydraulic	ICE 115	6
		30.5cm (12in) PSC	Hydraulic	ICE 75	143
22	Folly Beach, SC	30.5cm (12in) Timber	Drop	Drop Hammer	48
23	Sullivan's Is., SC	20.3cm (8in) Timber	Drop	Drop Hammer	38
				TOTAL	**1793**

NOTES:

1. Site Case History. Note five case histories have two pile types, and one case history has 3 pile types.

Microsoft Excel™ and Access™ were chosen as the software programs for use in the database development due to their ubiquitous presence in civil engineering and pile driving contractors offices and their compatibility with each other. For each case history, an Excel workbook was developed. The first worksheet within an individual case history workbook contained the project information (i.e. case history data, hammer model and specifications for impact or vibration hammers, soil data availability, and pre/post-condition survey availability). The second worksheet contained the individual pile specifications with type, size, length, cushion, pre-auger diameter and depth, blow count data, hammer stroke, energy, distance to pile, scaled distance, peak particle velocity (PPV) amplitude with frequency on three axes, maximum PPV with amplitude, and Peak Vector Sum. The third worksheet contained any available in-situ soil data (e.g. CPT data, N-values with depth and soil stratigraphy). The individual case history Excel workbooks were then imported into an Access database file, where the data was arranged to allow for quick searches of data based on pile, soil, and hammer attributes. Data within the Access database file could still be accessed via Excel, although the search features would not be present.

Upon entry of the first twenty-three (23) case histories, the ground vibration database was placed on the Pile Driving Contractors Association (PDCA) website to assist pile driving contractors, project engineers, developers, and owners with regards to this driven pile environmental issue and aid in future research. The database can be accessed at http://www.piledrivers.org/vibrational.php.

FUTURE ACTIVITY

An additional twenty-eight (28) case histories have been submitted for inclusion into the case history database and are currently being reviewed. Planned analyses of the case history data includes:

- Examination of ground vibration dissipation with respect to scaled distance from the pile installation and the relationships between the data determined from these lines (i.e. slope, intercept, coefficient of determination) and the major factors that influence ground vibrations from pile driving (i.e. pile type, soil type, hammer type).

- Comparison of peak vibrations with respect to vibration frequency.

- Statistical examination of peak vibrations and peak vibration frequencies.

CONCLUSIONS

The development of a driven pile ground vibration case history database intended to assist people associated with the driven pile industry and future research in the field was presented. The database contains relevant project information and vibration, pile, and hammer measurements from individual pile installations. The database was initially complied using twenty-three (23) case histories from the Charleston, SC

area. The initial database can be accessed at the Pile Driving Contractors Association (PDCA) website (http://www.piledrivers.org/vibrational.php). Additional case histories have been submitted and future examination of the data is planned.

ACKNOWLEDGEMENTS

The authors deeply appreciate the support of the Pile Driving Contractors Association (PDCA), The Citadel Foundation, and WPC Inc. for funding the development of the driven pile ground vibration case history database. Individual people within the PDCA who provided support and assistance include Mr. John Linscott (Environmental Committee Chair), Mr. Harry Robbins (Past National President), Stevan Hall (Executive Director), Tanya Goble (past Executive Director), and Van Hogan (Webmaster). Individual people within WPC Inc. who provided support and assistance include Mr. Reg Christopher, PE (President and CEO), Mr. Bill Wright, PE, Mr. Josh Adams, and Mr. Craig Skiles. Finally, the support of The Citadel's Department of Civil and Environmental Engineering is also appreciated.

REFERENCES

Attewell, P. B., and Farmer I.W. (1973). "Attenuation of Ground Vibrations from Pile Driving," *Gnd Engrg,* 3(7), 26-29.

Hajduk, E.L., D.L. Ledford and W.B. Wright. (2004). "Pile Driving Vibration Energy-Attenuation Relationships in the Charleston, SC Area." *Proc. 5th Intl. Conference on Case Histories in Geotechnical Engineering*, New York, NY.

Hajduk, E.L., Adams, J.C., Hill, T.E., and Chernauskas, L.R. (2006). "Vibration, Energy, and Pile Embedment Relationships during Driven Pile Installation", *GeoShanghai 2006*, GSP No. 153, ASCE, Reston, VA: 182-188.

Hajduk, E.L. and Adams, J.C. (2008). "Examination of Ground Vibrations and Dynamic Pile Measurements during Driven Pile Installation", *Proc. 8th Intl. Conference on the Application of Stress-Wave Theory to Piles*, Lisbon, Portugal.

Heung, W., Morgan, K., Yoon, Y.H., Gobin, R., and Gollamudi, S. (2007). "Vibration due to Driving Concrete Piles Using Open-Ended Diesel Hammer in Central and South Florida" *Proc. 7th Intl. Symposium on Field Measurements in Geomechanics*, Boston, MA.: 1-12.

Lacy, H., and Gould, J. P. (1985). "Settlement from Pile Driving in Sands." *Proc. Symposium on Vibration Problems in Geotechnical Engineering,* ASCE, Detroit MI: 154-173.

Robinson, B.R. (2006). Models for Prediction of Surface Vibrations from Pile Driving Records. MS Thesis, Dept. of Civil Engineering, North Carolina State University, Raleigh, NC, 231 p.

Selby, A.R. (1989). "Strains in Brickwork due to Ground Vibration Caused by Pile Driving – A Controlled Test Series", *Research Report for the Applied Mechanics Group, School of Engineering and Applied Science*, University of Durham, Durham, England.

Thandavamoorthy, T. S. (2004). "Piling in Fine and Medium Sand- A Case Study of Ground and Pile Vibration." *Soil Dynamics and Earthquake Engineering*, 24, 295-304.

Wiss, J. F. (1981). "Construction Vibrations: State of the Art," *J. Geotechnical Division,* 107 (GT2): 167-181.

Woods, R. S., and L.P. Jedele (1985). "Energy-Attenuation Relationships from Construction Vibrations," *Vibration Problems in Geo. Engrg*, Special Technical Publication, ASCE, New York, NY: 187-202.

Woods, R.D. (1997). "Dynamic Effects of Pile Installation on Adjacent Structures", *Synthesis of Highway Practice 253*, National Academy Press, Washington, D.C.

Copyrighted Materials
Copyright © 2009 American Society of Civil Engineers (ASCE)
Retrieved from www.knovel.com

High Capacity Micropiles in Wissahickon Schist Bedrock

Terence P. Holman, Ph.D., P.E., M.ASCE

Senior Engineer, Moretrench, 100 Stickle Avenue, Rockaway, NJ 07866, tholman@mtac.com

ABSTRACT: Urban construction frequently dictates that new foundations are capable of supporting very high structural loads within project sites of a limited footprint. In the interest of limiting pile diameters for constructability, the structural loads per unit cross-section have increased significantly in recent years. This paper details a case history of high capacity micropiles founded in Wissahickon Mica Schist bedrock in Philadelphia, Pennsylvania. Sixty production piles were installed at the project site to carry the load of a new 10-story building addition with heavy new foundation loads on a cramped site. The structural loading demands on these rock-socketed micropiles necessitated an aggressive approach to design. A heavily instrumented compression load test was conducted to confirm the pile performance. Observed strain compatibility between the structural elements of the pile and the high degree of confinement validated the use of high-strength steel reinforcement and high allowable stresses. The load distribution in the bond zone was found to be nonlinear and concentrated in the upper ¼ to ½ of the socket length, and mobilized bond stresses were shown to be higher than reliable, published values for similar geologic materials and environments.

PROJECT DESCRIPTION

The National Board of Medical Examiners (NBME) facility is located in the University City section of Philadelphia, Pennsylvania at the southeast corner of 38th and Market Streets. NBME constructed a multi-story structure in the early 1990s and founded it on caissons (drilled shafts) bearing in the upper portion of the Wissahickon Schist bedrock. In 2006, NBME began to develop plans for an expansion of their headquarters into a landscaped portion of their existing property. The new structure, to be constructed in a very limited footprint of about 21 m by 32 m, is 10 stories high. Furthermore, four of the new columns had to extend through the adjacent below-grade parking garage and be constructed in low-headroom conditions. The maximum column loads for the addition were to range from 6.0 to 10.0 MN in compression.

Specialty foundation construction techniques became a necessity because of the high column loads, small site footprint, and low-headroom conditions. The specialty contractor investigated the feasibility of developing very high structural and geotechnical capacities for micropiles in consideration of the inherent variability of

the underlying subsurface conditions. The use of high capacity, rock-socketed micropiles was feasible given the site geometry, loading requirements, and ultimately the construction schedule. A design (working) compression capacity of 2.0 MN was selected in order to develop the final foundation design. A 0.67 MN tension capacity was required for many of the piles to resist wind and seismically driven uplift loads. The structural design plans called for a total of 60 production piles, 14 of which were to be constructed in low-headroom conditions in the parking garage.

PILE DESIGN

The specialty contractor designed the micropiles and the pile-top connections into the pile caps in conjunction with their consultant. Following the preliminary design stage, the contractor determined that a 244 mm OD pile casing would result in the most constructible design to achieve the 2.0 MN design capacity. The governing building code for the pile design was the 2003 International Building Code (IBC 2003) which designated the allowable stresses for the pile materials as $0.35\ F_{yc}$, $0.50F_{yb}$, and $0.33f'_c$, respectively for the permanent steel casing, centralized reinforcement, and the neat cement grout. A further provision in the code indicated that strain compatibility had to be considered for the structural design, effectively limiting the usable yield strength of the centralized reinforcing bar to 600 MPa (based on a 0.3% failure strain in the grout). However, this concept was not considered applicable to a rock-socketed micropile in competent rock due to the high degree of confinement (both in the cased portion of the pile and socket), and socket roughness resulting in dilation and increased normal stresses. The micropile structural design was completed using high strength 63 mm diameter, Grade 1035 reinforcement in the rock socket and No. 57 Grade 520 reinforcement in the cased portion and extending up into the pile caps. The design compressive strength of the grout was 41.4 MPa and the minimum yield strength of the API N80 casing was 552 MPa. The assumed neat diameter of the rock socket was taken as 210 mm for design. Refer to Figure 1 for a cutaway view of the micropile.

The geotechnical design of the rock socket consisted of analyzing the subsurface conditions, particularly the rock quality, and selecting a unit bond shear stress to represent the load transfer at the interface between the socket sidewalls and the micropile grout. The typical subsurface profile of the site from drilling grade (at site subgrade, roughly 3 m below street level) is shown in Figure 2. It was assumed that the pile casing would be advanced to a minimum depth of 7.6 m below subgrade, followed by construction of the socket using down the hole hammers in the competent, coreable rock. The bond length design was predicated on having the socket extend well into the high-RQD, moderately weathered, moderately hard schist. Based primarily on historical, high quality load test data from Koutsoftas (1981), an ultimate bond shear stress τ of 1,380 kPa was selected for design and reduced to arrive at a working τ of 550 kPa. It is worth noting that while these bond stresses may seem conservative for intact metamorphic rock, the Wissahickon Schist in the Philadelphia area is notorious for having variable quality, weathering, and strength. The contractor's design consultant selected a socket length of 6.1 m for construction.

RESULTS OF COMPRESSION LOAD TEST

The specialty contractor performed a Quick Method compression load test as part of the micropile construction contract prior to the installation of production piles. The test load to be applied to the sacrificial pile was 4.0 MN, twice the design capacity of 2.0 MN. As a result of the high design load, the specialty contractor elected to install a significant amount of vibrating wire strain gauge instrumentation within the test pile. Eighteen strain gauges were employed with three pairs of spot-weldable strain gauges mounted directly onto the high-strength centralized steel reinforcing bar and twelve embedment gauges situated within the neat cement grout, allowing for an examination of strain-compatibility within the pile. A computer-controlled data acquisition system was used to continuously record all strain gauge data.

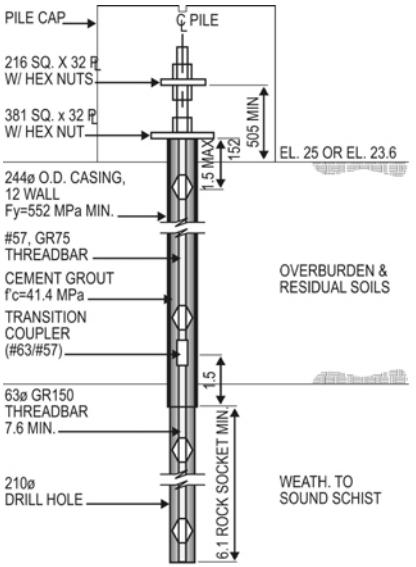

FIG. 1. Cutaway view of pile design section (all dim. in mm unless noted)

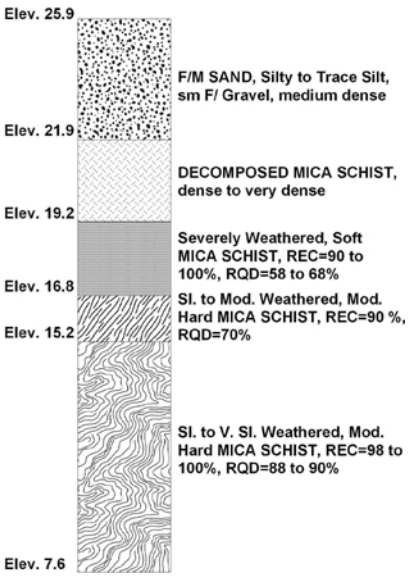

FIG. 2. Subsurface profile below excavation subgrade

The micropile load test was conducted in August 2007 after mobilization to the site and the results indicated that the single-pile design and performance was acceptable. The sacrificial test pile was comprised of a 8.7 m cased length and 6.1 m bond length, resulting in a total length of 14.8 m. The pile-top settlement at the design load of 2.0 MN and the test load of 4.0 MN was 9 mm and 20 mm, respectively. The pile-top settlement data is based on the average of 4 micrometer dial gauges. Refer to Figure 3 for the load-settlement plot. The test pile behavior was essentially elastic (fully recoverable) with very little load transfer evident below the ¼ point of the socket until after the design load was exceeded. The strain generated at each gauge level

within the test pile reflects the load distribution as well as the pile section and geometry changes. Figure 4 presents the average strain distribution along the length of the pile during the load test.

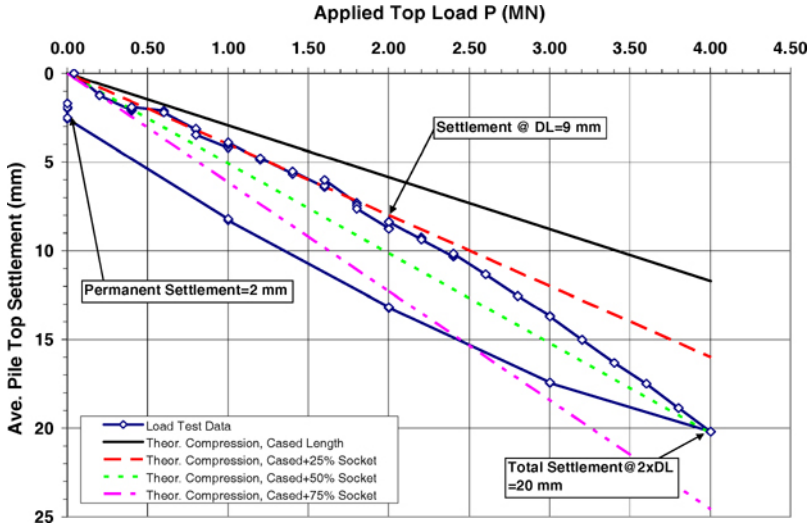

FIG. 3. Load-settlement plot for compression load test

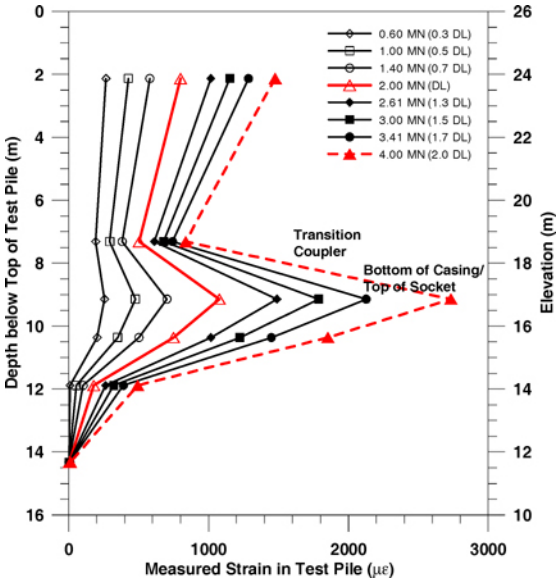

FIG. 4. Strain distribution in test pile

ANALYSIS AND IMPLICATIONS FOR DESIGN OF HIGH CAPACITY MICROPILES

Strain Compatibility

Strain compatibility between the various structural components of the micropile was a concern for design and performance. Many design codes and references incorrectly specify the use of maximum reinforcement steel yield strengths matched up with failure strains for unconfined concrete. These concepts are rooted in design theory for unconfined beams and columns. Even limited confinement significantly increases the ductility, or compressive strains, of cementitious materials at failure. The confinement offered by heavy-walled, high strength steel micropile casing, rock sockets, and even competent soils under modest effective stresses eliminates this concern and allows for safe, economical use of higher yield strength reinforcement steel.

The strain gauge instrumentation employed for the test micropile in this project was specifically designed to allow for a comparison of strain mobilization between the grout and centralized reinforcement in both the cased zone and rock socket. Companion sets of gauges were placed at the top of the casing (Elev. 23.5 to 23.8), top of the socket (Elev. 16.7 to 16.9), and tip of the socket (Elev. 11.4 to 11.6). Table 1 summarizes the mobilized strains in these companion gauge sets for various stages of the compression load test. Spot weldable gauges and embedment strain gauges are designated as SW and EB, respectively. Within the cased zone, near the top of the pile, the average difference between the measured strain in the reinforcing steel and grout is about 14%, with the strain in the steel typically being higher. At the top of the rock socket, the measured strain in the grout is about 42% higher than in the steel, with the difference shown to decrease with increasing pile-top load. Similar responses were reported in Holman and Barkauskas (2007) for micropiles in granular soils that were loaded to failure. These deviations from complete theoretical compatibility are considered minor when considering that the embedment strain gauges, while situated within the grout, are only about 50 mm from the reinforcing steel and may be subjected to some strains resulting from shear stress transfer at the grout-steel interface. It is important that near the top of the socket, where the loading is most intense, the equality in measured strain (compatibility) increases with increasing pile-top load.

The strain-response of this rock-socketed micropile, coupled with the recoverable load-settlement response, reinforces the point that compatibility need not be strictly considered for adequate design and performance. At the test load of 4.0 MN, just less than the computed ultimate bond zone structural capacity of 4.8 MN kips (using ultimate reinforcement strength of 1035 MPa and grout compressive strength of 41.4 MPa), the grout strain was only estimated to be about 2700 με. This value is approaching the accepted unconfined failure strain level for grout and cementitious materials of 0.2 to 0.3%. However, the load-settlement data for this test pile indicated that the maximum settlement was less than 20 mm and the permanent settlement was only 2 mm, less than 10% of the maximum. This means that the pile response is largely elastic, fully-recoverable, and under no structural distress. The convergence of the measured strains with increasing load, as noted above, supports

the elastic nature of the pile's structural section. Based on these accumulated data, high-strength reinforcing steels can be used in computations of pile structural capacity as long as reasonable allowable-stress coefficients are employed for assignment of safe working load levels.

Table 1. Comparison of spot weldable and embedment strain gauge readings

Applied Load (MN)	Elev. 23.6		Elev. 16.8		Elev. 11.4	
	SW	EB	SW	EB	SW	EB
0.6	295.0	227.0	221.2	396.4	1.8	1.0
1.0	456.2	379.9	355.4	579.2	1.7	1.5
2.0	831.0	801.1	990.1	1213.4	3.3	3.8
3.0	1271.9	1186.1	1821.8	1906.2	4.9	7.7
4.0	1609.1	1283.1	2730*		8.5	16.2
Ave. Difference	14%		42%		43%	
NOTE:	All SW and EB readings in microstrains (με)					
	* Strain gauge readings at max. test load interpreted from data trend					

Load Transfer in Wissahickon Mica Schist

Load transfer capabilities of the Wissahickon Mica Schist have not been adequately documented throughout the history of deep foundation design in the Philadelphia area. Available data on conventional drilled shaft (caisson) foundations are very limited and none are available for long, slender elements such as micropiles. The high-quality strain-gauged load test data presented in Koutsoftas (1981) are used as the basis for comparison with the load-transfer data generated from this project.

The strain versus depth profile in the test pile at various load levels was used to estimate the load in the pile cross section at each gauge level. The load P_i at a given depth can be calculated using the measured strain ε_i, cross sectional area A_i, and the secant modulus E_{pi}. However, the modulus at a given point is not constant but changes with increasing strain, as discussed in previous sections. Using the methods of Fellenius (1989), the secant moduli E_{pi} were estimated as a function of strain and calculated as

$$\text{Cased Zone: } E_{sec}\,(\text{GPa}) = 5.67\text{x}10^{-3}\varepsilon + 49.68 \qquad (1)$$

$$\text{Rock Socket: } E_{sec}\,(\text{GPa}) = -11.75\text{x}10^{-3}\varepsilon + 48.47 \qquad (2)$$

where ε is in microstrains (με). The calculated load distribution (using Eq. 1 and 2) along the length of the test micropile is shown in Figure 5 for four applied pile-top loads. The back-calculated grout-rock bond shear stress τ is also shown in between each strain gauge level. Significant load was shed to the ground along the cased length of the pile, resulting in a mobilized τ of 170 kPa at the conclusion of the test. Beginning at the top of the rock socket, Elev. 17.2, load was rapidly, but nonuniformly transferred to the surrounding rock. The mobilization of bond shear in

the grout-rock interface is significant below Elev. 16.8. The more weathered rock between Elev. 16.8 and Elev. 15.2 provided a mobilized τ of 790 kPa, while 1570 kPa bond shear stress was estimated for the sound, high RQD rock below Elev. 15.2. The socket did not transfer a significant amount of load below Elev. 14, the bottom 40% of the socket, and virtually no tip resistance was generated.

The data obtained from this instrumented load test demonstrate that the mobilized bond shear stresses in the Wissahickon Schist are very high, particularly in the fresh, hard rock. Considering the elastic nature of the pile response and the distribution of load in the rock socket, this test pile was not near a geotechnical failure condition and could likely have sustained substantially more total load, possibly greater than 50% more. The only portion of the rock socket that appeared to have reached a constant mobilized bond stress was the portion from Elev. 17.1 to Elev. 15.2, where the mobilized τ was 720 kPa at a load of 3.0 MN and 790 kPa at 4.0 MN. This zone would likely have begun progressive bond failure at loads exceeding 4.0 MN.

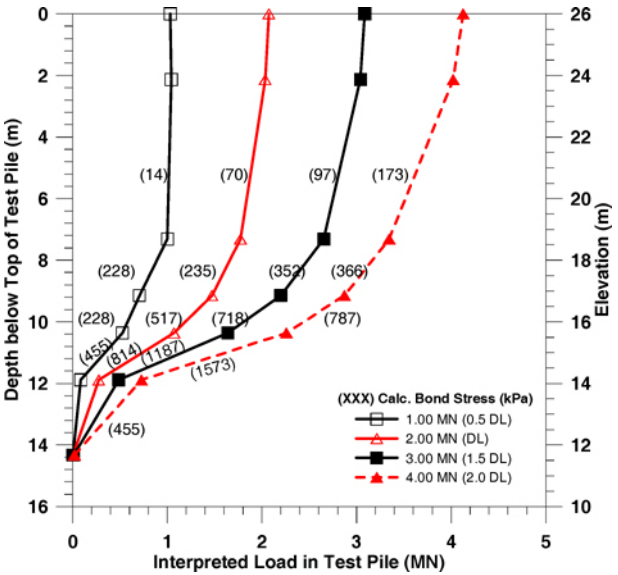

FIG. 5. Calculated load distribution in test pile

The lower portion of the rock socket, from Elev. 15.5 to 11.6 was in fresh, hard Schist and can be compared to the only other well-documented case study in the Philadelphia area. The case history of the Philadelphia Federal Courthouse (PFC) caisson failure and remediation program, documented in Koutsoftas (1981), involved instrumented underpinning caissons in the same quality Schist. The back-calculation of the maximum mobilized bond shear stress was 1365 kPa for a load of 8.2 MN at the top of this 610 mm diameter, 9.1 m long socket. The rock sockets for the NBME and PFC have normalized lengths L_s/d of 30 and 15, respectively where L_s is the

socket length and d is the socket diameter. The rock socket for the NBME test pile is by virtue of its slender normalized geometry more elastically compressible than that for PFC for similar relative pile stiffnesses, E_p/E_{rm}. The performance of both instrumented rock sockets was very similar in consideration of these factors.

CONCLUSIONS

Very high capacity micropiles can be constructed in the Wissahickon Mica Schist, well known for having variable quality, weathering, shear strength, and compressibility. For the NBME project, 2.0 MN design capacity piles were designed, load tested, and constructed. A heavily instrumented compression load test to 4.0 MN revealed much about strain compatibility between the structural elements and load transfer to the Wissahickon Mica Schist. The pile response was elastic, with nearly full recovery of the axial deformations upon unloading. Instrumentation data demonstrated that strain compatibility exists within the pile cross section, and no grout failure was occurring even though measured grout strains were very near to the previously accepted 0.3% limit. Based on these data, the use of high capacity reinforcing steel on the interior of the micropile is considered safe practice as long as suitable allowable stress coefficients are employed for assigning working capacities. The load transfer to the rock mass is nonlinear and varies as a function of the rock quality, weathering, and hardness. In the sound, fresh Schist, the maximum mobilized bond shear stress was 1570 kPa. Significantly greater bond stress in the sound rock can likely be activated, perhaps up to 50% more, especially since the test pile's overall response was largely elastic.

ACKNOWLEDGEMENTS

The construction manager, Tamora Building Company, provided the cooperation necessary to conduct this work. Peirce Engineering Inc. of Phoenixville, Pennsylvania provided micropile design engineering. The author would like to thank the staff of Moretrench for their diligence in ensuring that the instrumented load test was conducted in the most careful manner; specifically Peter Erik, Jeff Marron, Michael McNicholas, and Jeff Long. Tara Holman produced many of the graphics used in this paper. TRC Solutions, the owner's geotechnical engineer, deserves recognition for involving the author in the preliminary phases of this project.

REFERENCES

Fellenius, B. (1989). "Tangent modulus of piles determined from strain data." *Proc. of the Congress on Foundation Engineering: Current Principles and Practices*, ASCE, Vol. 1, 500-510.

Holman, T.P. and Barkauskas, B. D. (2007). "Mechanics of micropile performance from instrumented load tests," American Society of Civil Engineers, Geo-Institute, *7th Intl. Symposium on Field Measurements in Geomechanics*, Boston, 14 pp.

Koutsoftas, D.C. (1981). "Caissons socketed in sound mica schist." *Journal of the Geotechnical Engineering Division*, ASCE, Vol. 107, GT6, 743-757.

Copyrighted Materials
Copyright © 2009 American Society of Civil Engineers (ASCE)
Retrieved from www.knovel.com

Influence of Confining Micro Piles on the Bearing Capacity of Sand

Unnikrishnan, N[1] and Sachin, P[2]

[1]Lecturer in Civil Engineering, College of Engineering Trivandrum, Kerala, India 695 016; unnikrishnan_n@yahoo.com
[2]Graduate Student, Civil Engineering, College of Engineering Trivandrum, Kerala, India 695 016.

ABSTRACT: The benefit of providing confinement to footings on loose sand deposits using small diameter timber micro piles driven around footings is explored. The technique can be utilised for improving the bearing capacity of footings on loose sand deposits. Experimental investigations on laboratory model footings on loose sand deposits were undertaken. Timber confining piles were employed. Influences of various pile configurations were investigated. The response of footings with micro pile confinement was compared with that of a footing without confinement. The results indicate that the confining piles can appreciably increase the load carrying capacity of footings on loose sand deposits. The piles impart additional confinement by providing lateral restraint. Closer spacing tends to improve the confinement and thus the load carrying capacity. Extending the length of the confining pile beyond an optimum value was found not advantageous. Attempt has also been made to explain the underlying phenomenon on the basis of possible mechanisms developed within the confined soil.

INTRODUCTION

Many localities in the World have infrastructure developments near coastline. The coastal areas are characterized by ample loose sand deposits. These depositions result out of the action of wind and water. Typically, these deposits consist of uniformly graded medium to fine sand. Such deposits offer very poor shear strength. Often these sand deposits extend to great depths. This poses difficulties in providing shallow foundations for even light buildings. To avoid the high cost of deep foundations, ground improvement techniques are adopted. Loose sands are densified by employing several techniques. Densification may be achieved though sand piling or using vibroflots. Jet grouting is another technique that can be adopted for important structures. However, these techniques are often not cost effective for light residential buildings.

Sand is considered to be an ideal material to support foundations, if it is confined. Loose sand deposits can be improved to support more load, if sufficient confinement

is provided. Though loose sand can be cheaply compacted, such compaction is usually be done only for a small area within and around the building. The improved density thus created may get reduced over a period of time due to seepage and changes in water table level. However, providing confinement may reduce the chance of such reduction. There is a need for a technique that is (i) cheap (ii) requiring less skilled labours and (iii) practical to implement for light residential building foundations in loose uniform sand deposits.

The present investigation was carried out to study the effect of driving small diameter piles around a footing on loose sand deposit for improving the bearing capacity. Relative improvement in performance of footings located on loose sand due to the introduction of confining piles was investigated through laboratory model studies. The influences of various confining pile configurations were investigated. Some of the results are discussed here in.

CONFINED FOUNDATIONS

There are several ground improvement methods employing the principle of "inclusion" of which the most prominent example is reinforced earth Vidal (1968). The essential phenomenon in reinforced earth is the confinement induced by the friction between the earth and the reinforcements. Several experimental investigations and theoretical formulations were carried out on the application of soil reinforcement for the improvement of the bearing capacity of loose sands (Binquet and Lee, 1975, Akinmusuru and Akinbolade, 1981, Omar et al., 1993a,b, Adams and Collin, 1997). The principle behind the use of geocells is also confinement (Rajagopal et al., 1999, Dash et al., 2003).

Skirting is another technique that falls in the category of "inclusion technique". In this method a rigid reinforced concrete or ferro-cement wall called "skirt" is constructed around a footing in order to confine the soil below the footing. The skirts are vertical walls around the footing at distance from the edge of footing. The provision of such skirt is found to increase the bearing capacity and reduce the settlement significantly (Nirmala Devi et al., 1997, Purohit and Ameta, 1999). Sawwaf and Nazeer (2005) studied the significant effects of confinement on soil by using confining cylinders made of unplastcised polyvinyl chloride (UPVC). However the skirted foundation technique has the inherent disadvantage of being uneconomical. This is because (i) steel and concrete are expensive (ii) provision of skirt box requires excavation of an area larger than that of the footing (iii) excavation in loose sand may require side support to prevent collapse of sides.

The application of a number of small diameter confining piles in the form of a skirt is thought to be an alternative solution for providing confinement. Small diameter piles of concrete or timber can be used as confining piles. However, application of locally available timber makes more sense from the economical point of view. These piles can be easily driven beside and around the footing to impart confinement to the soil, which helps in the improvement of bearing capacity of the soil. This technique of providing confining piles overcomes the disadvantages of skirted footing mentioned above. Since most of the loose sand deposits near coast line have water table close to the ground level itself, timber piles may not be subjected to

degradation. In the investigation reported herein, locally available coconut timber piles were used for providing confinement.

EXPERIMENTAL INVESTIGTIONS

Load tests were conducted on laboratory model footings on loose sand with confining piles and also without confining piles. Confining piles were driven into the soil for the purpose. Various pile lengths and pile spacing were tried. Different pile skirt sizes were also used. Loads were applied to soil in cumulative increments of one-fifth of the estimated ultimate bearing capacity of the unconfined footing. A model tank size of 1.5m x 1.5m x 1.5m depth was used. A square mild steel plate of size 15cm x 15cm and thickness 20 mm was used as the model footing. The sand used was sea sand of uniform grade (effective size D_{10}=0.23, uniformity coefficient = 1.7, specific gravity = 2.65). A relative density of 30% was used throughout the test. This was achieved by employing sand raining technique , keeping the height of fall of sand pouring a constant, using a cone with scale arrangement. An average density of 1.45g/cc was achieved through this method.

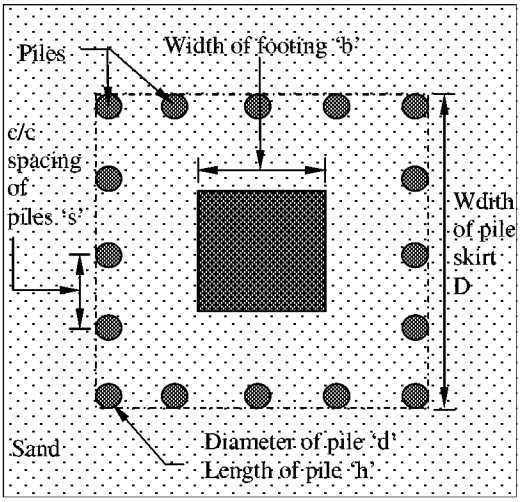

FIG. 1. Schematic diagram of footing with confining piles around.

The confining piles used in the study were made of coconut timber of 1.5 cm diameter. Results of three pile lengths (h), 15 cm, 22.5 cm, and 30 cm are presented here in. The general arrangement of confining piles around the footing is shown in Figure 1. Three different pile spacing (s) values viz. 4cm, 5cm, 6.6cm, 10cm and 20cm centre to centre were used. The lengths of piles as well as spacing are normalized with the plate dimension b (15 cm). Different skirt sizes were also used

in the investigation (Sachin, 2006). Results corresponding to a skirt size of 20cm (D/b = 1.33) is reported herein.

RESULTS AND DISCUSSIONS

The displacements of the footing (S_p)were normalised with respect to the size of the plate 'b' and are reported in percentage. Applied stress corresponding to a normalised displacement of 20% was taken as the ultimate stress for comparison as there was no defined failure location available from the load settlement curve of the footing without confinement.

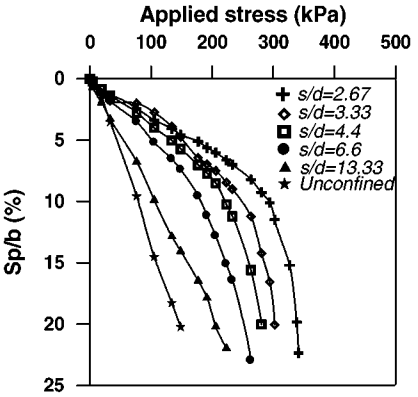

FIG. 2. Aplied stress vs normalised settlement for h/b =2

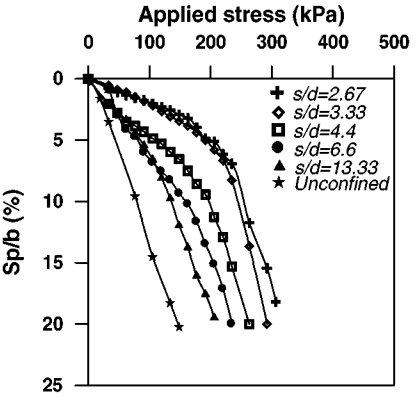

FIG. 3. Aplied stress vs normalised settlement for h/b =1.5

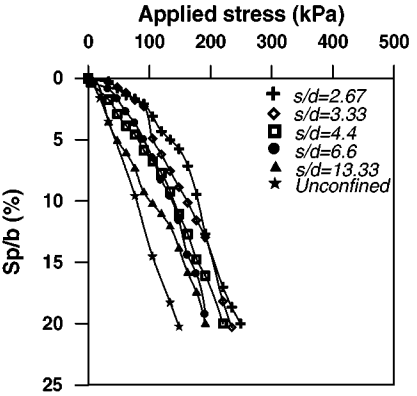

FIG. 4. Aplied stress vs normalised settlement for h/b =1

The applied stress vs normalised settlement of the test for different spacing of confining piles is shown in Figure 2 for a pile length h =30cm (h/b=2). From the Figure, it can be observed that the applied stress corresponding to a normalised settlement ratio of 20% is 148 kPa for the unconfined soil. This was taken as the ultimate applied stress for comparison purpose. The load settlement behaviour was suggestive of punching failure (Das, 1999). Responses of the confined footing with different s/d ratios of 13.33 cm, 6.67 cm, 4.4 cm, 3.33 cm and 2.67 cm are also shown in the same figure. Tests were repeated with an h/b ratio of 1.5 and 1 (length of pile 22.5cm and 15cm respectively). The same s/d ratios of 13.33, 6.67, 4.4, 3.33 and 2.67 were used. Corresponding applied stress vs normalized settlement plot are given in Fig.3 and 4.

With the reduction of spacing between the piles, a definite change in the load – settlement behaviour indicated by the lateral shift in the ultimate stress-settlement curve. As the spacing of piles reduced, the mode of failure showed tendency to change to general shear failure. Well defined failure is indicated with closer spacing of piles. This points to the mobilisation of more shear strength of the same soil with the introduction of the confining piles.

A non-dimensional factor, called the bearing capacity ratio (BCR) is used for the purpose of comparison. BCR is defined as ratio of the ultimate applied stress of the footing with confining piles to that of the footing without confinement. Figure 5 shows the variation of BCR with normalised spacing for three pile lengths. It can be noticed that the reduction in spacing leads to an improvement in the ultimate applied stress. As the spacing between the piles increased, the improvement in BCR reduced. The curve relating the BCR with normalised spacing showed tendency to become parallel to the X axis, rather than becoming asymptotic. This could be due to improvement resulting from the densification of the loose sand bed because of the pile driving.

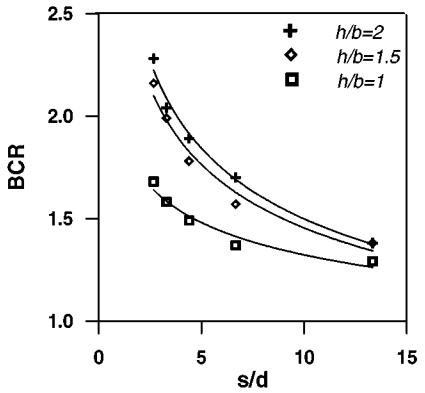

FIG. 5. Change in the BCR with the pile spacing

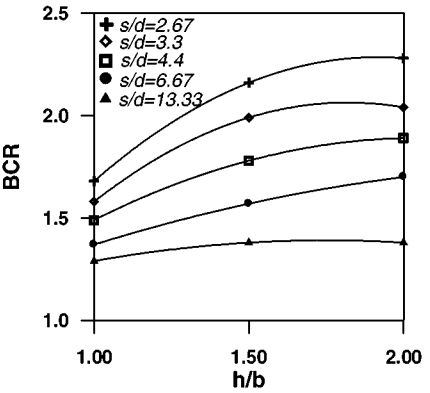

FIG. 6. Variation of BCR for different pile lengths

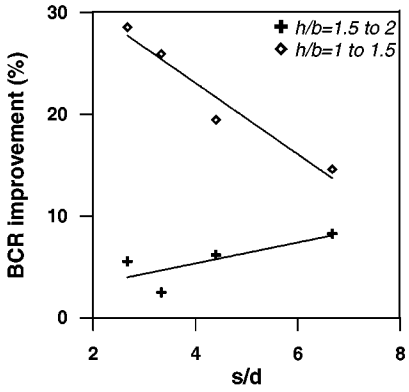

FIG. 7. Relative BCR improvement for increase of pile length from h/b = 1.5 to 2 and h/b=1 to 1.5

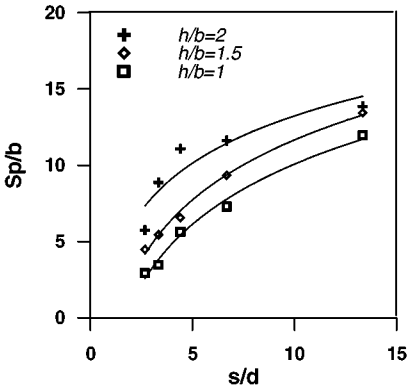

FIG. 8. Variation of settlement of footing for various pile spacing and pile lengths.

Maximum BCR improvement noticed was 2.28 for a normalised spacing of 2.67 and a normalised pile length (h/b) of 2. For the same configuration, with a normalised pile length of 1, the improvement was 1.68. By increasing the normalised pile length to 1.5 from 1, the improvement in BCR was 28.5%. However, the corresponding improvement in BCR between the normalised pile lengths of 2 and 1.5 was only 5.5%. This point to an optimum length of pile beyond which the improvement in bearing capacity will not be significant. Figure 6 shows the relationship between BCR and the normalised pile length (h/b) for various pile spacing. It can be noticed that the influence of pile length is dependent on the pile spacing. As already mentioned, with closer spacing of piles (s/d =2.67), significant improvement in BCR took place as the normalised pile length became 1.5. The improvement that resulted in further increase of pile length was not significant. However, for wider spacing, the increase in BCR for pile length beyond the normalised pile length of 1.5 was significant. This is evident from the Figure 7. The figure separates the BCR improvement to two stages. First stage is the improvement resulting from the increase of pile length from h/d=1 to 1.5. The second stage is the BCR improvement resulting from the increase of h/d from 1.5 to 2. Hence for closer spacing, a shorter optimum pile length is sufficient. The difference in the quantum of improvement clearly suggests the early mobilisation of shear strength and shifting of the failure pattern from local to general shear failure with well defined failure planes.

A possible mechanism that is responsible for the improvement is the formation of an arch of soil grains that provides confinement to the footing (Figure 9). The arch prevents lateral movement of soil grains resulting in a reduction in the settlement. This causes an improvement in the ultimate load. In this process, the arch transfers its end reaction to the piles and the piles resist the same by way of their stiffness. With the increase in the spacing of the piles, the arch span also increases, and the collapse of the arch takes place at a smaller lateral load. The development of a well

defined failure in the case of footings with close pile spacing is indicative of this mechanism.

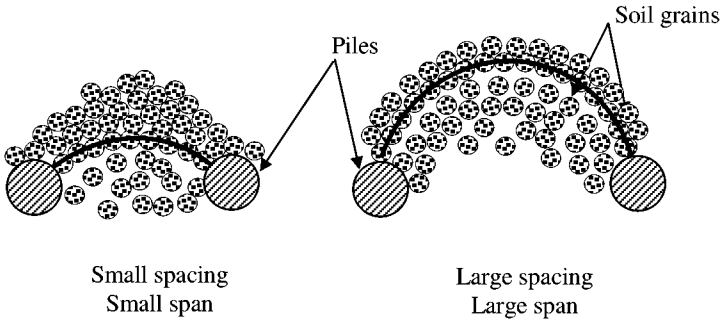

FIG. 9. Mechanism of confinement with confining piles

CONCLUSIONS

Confining piles can be successfully employed to improve the bearing capacity of loose sand deposits. Coastal areas are typically characterized by loose sand deposits with ground water table near to the ground level. Though there are several techniques of improving the relative density of loose sand deposits, confining timber piles attract more interest owing to the fact that the technique can utilize locally available timber. In comparison to the reinforced soil technique, installation of confining piles does not require any excavation. The technique is thus economical to implement. Higher load carrying capacity for footings on loose sand deposits can be obtained with closer spacing of confining piles. Improvement of bearing capacity up to 2.28 times that of unconfined footing was observed with close spacing of piles (s/d=2.67). As the spacing of piles reduced, the mode of failure showed tendency to change to general shear failure. Load settlement relation showed well defined failure with closer spacing of piles. This points to the mobilisation of more shear strength of the same soil with the introduction of the confining piles. Length of confining piles defines the depth up to which confining has to be provided. Increasing the pile length (h) beyond certain optimum value did not significantly improve the ultimate load bearing capacity. Though the optimum pile length was found to be dependent on the pile spacing, an optimum h/b ratio of 1.75 can be generally recommended. The technique also finds application in stabilizing foundations on loose sand deposits under distress.

REFERENCES

Adams, M. T., and Collin, J. G. (1997). "Large model spread footing load tests on geosynthetic reinforced soil foundations", *J. Geotechnical & Geoenv. Engrg.*, Vol. 123(6): 66 – 72.

Akinmusuru, J. O and Akinbolade, J. A. (1981). "Stability of Loaded footings on reinforced soil", *J. Geotechnical & Geoenv. Engrg.*, Vol. 107(6): 819 – 827.

Binquet, J. and Lee, K. L. (1975). "Bearing capacity test on on reinforced earth slabs", *J. Geotechnical & Geoenv. Engrg.*, Vol. 101 (12):1241 – 1254.

Consoli, N. C., Schnaid, F., and Milititsky, J. (1998). "Interpretation of plate load tests on residual soil site", *J. Geotechnical & Geoenv. Engrg.*, Vol. 124(9): 857-867.

Consoli, N. C., Vendruscolo, M. A., and Prietto, P. D. M. (2003). "Behaviour of plate load tests on soil layers improved with cement and fiber", *J. Geotechnical & Geoenv. Engrg.*, Vol. 129(96): 96-101.

Das, B. M. (1999) Shallow foundations: Bearing capacity and settlement, *CRC Press*, Florida

Dash, S.K., Sireesh, S., and Sitharam, T. G. (2003). "Behaviour of geocell-reinforced sand beds under circular footing", *Ground Improvement* , Vol. 7 (3): 111–115.

Nirmala Devi, N.C. and Nainan P. Kurian (1997). "Performance of skirted footings in sand", *Proc. 14th Intl. Conference on Soil Mechanics and Foundation Engrg., Hamburg,*827 – 830.

Omar, M. T., Das, B. M., Puri, V. K. and Yen, S. C. (1993a). "Ultimate bearing capacity of shallow foundations on sand with geogrid reinforcement", *Canadian Geotechnical Journal*, Vol. 30(3): 545 – 549.

Omar, M. T., Das, B. M., Yen, S. C., Puri, V. K. and Cook, E. E. (1993b). "Ultimate bearing capacity of rectangular foundations on geogrid reinforced sand", *Geotechnical Testing Journal,* Vol. 16(2): 246 – 252.

Purohit, D. G. and Ameta, N. K. (1999). "Behaviour of annular skirted footing on dune sand", *Proceedings of the Indian Geotechnical Conference*, Calcutta, Vol. 1:116-119.

Rajagopal, K., Krishnaswamy, N.R. and Madhavi Latha. G (1999). "Behaviour of sand confined with single and multiple geocells", *Geotextiles and Geomembranes,* Vol 17(3): 171 – 181.

Sachin, P. (2006) Investigation on the influence of confining piles on the bearing capacity of loose sand, *M.Tech. Thesis*, Kerala University, Trivandrum, India.

Sawwaf, M. and Nazer, A. (2005). "Behaviour of circular footings resting on confined granular soil",. *Geotechnical & Geoenv. Engrg.*, Vol. 131(3): 359-366.

Vidal, H. (1969). "The principle of reinforced earth", *Highway Research Record*, No. 282: 1 – 16.

Copyrighted Materials
Copyright © 2009 American Society of Civil Engineers (ASCE)
Retrieved from www.knovel.com

Micropile Foundations for ESSROC Cement Plant Expansion

Paul D. Martin

Group Manager: Drilling and Grouting, Foundation Division
Brayman Construction Corporation
1000 John Roebling Way
Saxonburg, Pennsylvania 16056

ABSTRACT

This paper will present a case study of the ESSROC Cement Plant Expansion Project located in Martinsburg, West Virginia. Over 1,600 total micropiles have been installed through highly karstic limestone for the expansion of the existing plant.

Figure 1 - Aerial view at Low Alkali Silo, including 143-each micropiles with an average depth of 57-feet

The micropiles are designed for 350-tons axial compression, 125-tons axial tension, and 15 tons lateral load capacity. Throughout the course of the work significant voids were encountered that required a grouting program to fill the voids and stabilize the free length of the micropiles. Casing installed was both $11^{7/8}$ inch x 0.582 inch wall pipe and $11^{3/4}$ inch x 0.534 wall pipe, with drilling depths up to 180 feet from existing grade. Numerous load tests were performed to verify the capacity of the micropiles in rock and grouted zones of the project.

During the construction process adaptations to normal installation of the micropiles were necessary in order to grout highly voided areas. Multiple drill rigs were used throughout the course of the work in order to facilitate the installation of the micropiles and low mobility grouting.

This paper will cover the design challenges incurred during the construction process to address the voids, the construction process with respect to drilling complexities within the geologic formations, and the specialized equipment used to install the piles.

PROJECT OVERVIEW

ESSROC, a member of the Italcemente Group of companies is a leading North American cement producer with over 6.5 million metric tons of annual capacity. With headquarters in Nazareth, Pennsylvania, ESSROC operates multiple production facilities strategically located throughout the United States, Canada, and Puerto Rico. As such, the Martinsburg, West Virginia facility, as shown in *Figure 2*, had budgeted $320 Million for plant renovations and expansion.

Figure 2 - Aerial view ESSROC Cement Plant, Martinsburg, WV

Included in the expansion was the addition of a completely new production line. Structures required to support the new addition included: a coal storage building, finish mill building, conditioning tower, heat exchanger, and related administrative and processing equipment. In total, there would be over twenty structures that would require appropriate foundations to satisfy the operational requirements and strict tolerances of the machinery to be used coupled with the unique composition of the soil and rock upon which these structures would be constructed.

Upon completion, it is anticipated that the renovation and expansion of the facility will more than double the existing capacity of 2,350 metric tons per day to over 6,000 metric tons per day. In addition to increasing the plants production capacity, another goal for the renovation of the facility is to lower the overall process emissions from the plant.

SITE ASSESSMENT

Prior to starting the expansion efforts, comprehensive geological assessments were accomplished throughout the proposed expansion areas and foundation evaluations of existing structures were developed. In general, the initial subsurface explorations of the existing cement plant boundaries indicated the presence of karstic dolomite/limestone bedrock. The term *"karstic"* describes a terrain of characteristic landforms and subsurface features produced primarily as a result of dissolution of soluble bedrock - such as limestone or dolomite by groundwater. As such, the general description of the soil and rock onsite identified the top of the competent rock as relatively non-voided and un-solutioned rock (hard dolomite) that is generally un-weathered with minimal evidence of air or clay-filled voids. However, it was determined that there were exceptions to this within the proposed Finish Mills area – with the existence of large clay filled voids, as well as the existence of a small clay filled void in the area of the proposed Coal Storage area. A typical boring as shown in *Figure* 3 displays the seams of rock and clay encountered during the micropile installation. In addition, rock in these areas was determined to be highly irregular with depressions in the top of competent rock surfaces and pinnacles prevalent throughout the area.

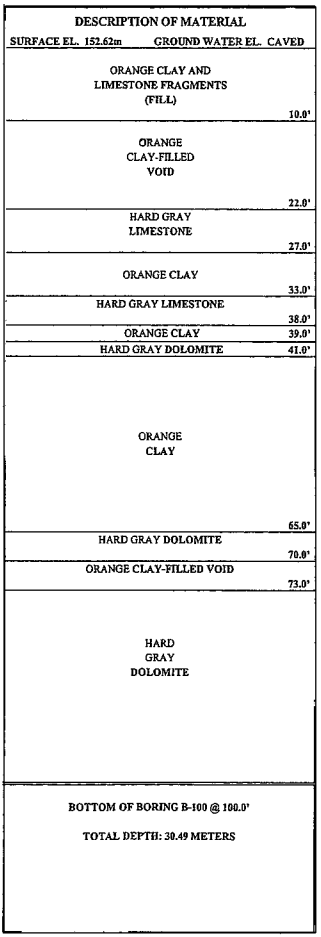

Figure 3 – Soil boring example

These karstic conditions exhibited features that included pinnacled limestone, sinkholes, and voids in the bedrock. While in most areas of the site the voids were clay-filled, some locations had been characterized with air or mud filled seams. During micropile installation top of rock varied drastically at every location. The deepest micropile installed with the designed rock socket was 177-feet.

MICROPILE DESIGN

Proposed Site Uses/Plant Equipment Operational Requirements

Various foundation designs were evaluated for compatibility with the existing geologic strata, in combination with the type of structures to be built, and the specifications of the equipment to be used within each structure. Requirements of the various new facilities to be constructed mandated minimal foundation settlement due to the precise requirements

and tight tolerances of the machinery to be installed. Likewise, the new plant facility will have steady, large loads, which will be distributed over the extremely karstic soil.

Given the site conditions, multiple foundation designs were evaluated – including spread footers and caissons. Due to the significant foundation loadings and significant settlement potential in the karstic limestone, spread footers were ruled out. A caisson design with the abundance of voids below the top of rock and the potential for the need of casing rendered this option unfeasible. As such, the evaluation of design options for micropile use as a viable foundation support solution was the best option given the project site geology. Constructability concerns with drilling pinnacled bedrock and installing temporary casing through multiple soil seams/voids rendered the caisson option as unfeasible.

Micropile Design

The micropile design for this project site was performed by the engineering firm of D'Appolonia – located in Monroeville, Pennsylvania. The micropiles were designed using FHWA methodology, but to the 2006 International Building Code's allowable limits for stress and strain. The specific design load requirements for the micropiles, stipulated an allowable axial compression capacity of 350 tons, an allowable lateral load capacity of 15 tons, and an allowable axial tension capacity of 125 tons. This standard design loading was used primarily throughout the site by the structural design engineers.

Exhibit Design Detail – Typical Micropile Detail

In order to incorporate the behavior of the micropiles in a finite element model for structural design of supported structures, a strength reduction factor of 0.65 was applied to each pile. The rationale for this reduction factor for the compression-controlled sections was that these sections have less ductility, are more sensitive to variations in concrete strength, and generally occur in members that support larger loaded areas. Due to the total quantity of casing needed to support this project - two main types of 80 ksi casing were used. These included a casing with a $11^{3/4}$ inch outside diameter and a wall thickness of 0.534 inch and a casing of $11^{7/8}$ inch outside diameter and a wall thickness of 0.582 inch. Typical reinforcement included a bundle consisting of one (1) #20 Grade 85 (18 feet) with two (2) #18 Grade 75 (17 feet) all-thread bars located at the bottom of the pile, with one (1) #20 Grade 85 (16 feet) and one (1) #14 Grade 75 (16 feet) all-thread bars hung from the top of the pile. Micropiles acting in tension received the same bottom reinforcement coupled together with a full-length #20 Grade 85 all-thread bar. The bearing plate would be 15 inches x 15 inches x 2.5 inches utilizing ASTM A-572 steel. The design also called for the pile to extend 3.5 feet into the pile cap and a 14 foot long rock socket drilled with a 3.5 foot casing plunge into the bedrock. Initially, the design had called for a bond length of 14 feet; however, due to the successful completion of the initial pre-production load test in which a micropile with a 10.5 foot bond zone was able to support two times its design load, the production pile bond length was set at 10.5 feet. The original bond strength for the rock was adopted based on tests of rock cores from the drilling explorations. The bond strength back calculated from the load test actually exceeded the initial value and allowed the bond length to be shortened, the value was

quite high q-ult = 216psi; q-allowable = 87psi. The bond zone was set below any voids encountered in solid competent rock or later in LMG modified rock. In the LMG cases a load test was run for capacity. The load test confirmed there was no noticeable loss in bond strength with the LMG micropiles.

In summary, the typical pile had a capacity of 350 ton in comparison. However, pile selections to accommodate 225 ton, 200 ton, and 130.5 ton capacity micropiles were also designed and incorporated on a limited basis throughout the work.

CONSTRUCTION PROCESS AND SEQUENCE

Phased Installation of Micropiles

The micropile installation was sequenced into three major phases of work due to the release of design for specific structures. This allowed for easier job tracking, along with allowing all increased material costs to be examined by both owner and contractor

Phase I – consisted of the installation of 905 micropiles with a total drilled footage of 48,120 linear feet, along with 52,313 cubic feet of grout pumped. Three drills, as shown in *Figure 4*, were mobilized to start the project and included a Casagrande C-14, a Casagrande C-8, and an ABI rig converted to a micropile rig.

Figure 4 – Three micropile drill rigs including a Casagrande C-14, Casagrande C-8 and an ABI drill installing micropiles

These larger style micropile drills were needed due to the weight of the pipe and the overburden drilling system used with respect to the depths needed to drill to. An automated grout plant and silo were used. All cement requirements for the project were provided by the owner. Piles were installed using the Numa Super Jaws drilling system with the combination of high-air and the introduction of water to advance piles to tip elevation. Due to the geology and the presence of multiple layers of rock with interbedded seams of clay, mud and voids, the extended wings on the bit provided a bit

face striking area larger than the outside diameter of the casing. This enabled the casing to be installed into a rock seam that met the design criteria. The bits utilized for this project, T-265ND Numa Super Jaw – *Figure 5*, were custom made for the non-standard casing with a retracted diameter of 10.5-inches and an expanded diameter of 12.4-inches. The extended wings were also customized by reconfiguring the button layout to provide stability, as there was a large shearing action due to the pinnacled rock encountered. Upon completion of the drilling, the pipe was set and secured for the grouting operations. All piles were tremie grouted and reinforcement installed per design.

Figure 5 – Numa T-265ND Super Jaws Bit with wings

Phase II – consisted of the installation 662 micropiles with a total drilled footage of 35,743 linear feet along with 54,075 cubic feet of grout pumped. Also included within Phase II was the drilling of approximately 18 test holes – totaling 3,011 linear feet-drilled in the Coal Storage area. The purpose for the test program was to find the top of rock locations along the existing clay seam. This gave both contractor and owner the ability to locate exactly where piles would encounter the required rock socket thus providing a more efficient construction sequence.

Phase III – consisted of the installation of 121 micropiles with a total drilled footage of 6,936 linear feet along with 3,428 cubic feet of grout pumped. Due to the significant variations of rock elevation in the Coal Storage area, the majority of the piles for Phase III were required to provide a uniform stiffness for this structure. The piles were drilled to specified lengths to provide the required design needs to satisfy differential settlements.

Low Mobility Grout

During construction and excavation operations, continual physical investigations of the strata were accomplished. Investigations included the use of probe drilling, sonar, radar, as well as physically inserting cameras down into the drill holes and voids for inspection.

As the micropiles are being used for structural support - given the situations when an open void, a continuous clay seam, or no rock was found - low mobility grouting or void filling techniques were used to achieve appropriate ground modification. Low mobility grouting is the process of injecting grout into voids/seams. Void filling in areas of large voids was used by pumping lean mix concrete to fill cavities found during micropile installation.

With the abundance of fractured rock in the area, low mobility grout was used as a bonding agent with the fractured rock layers to enhance the bond strength of the micropiles. Low mobility grout was delivered to the job site in ready-mix trucks and placed using a concrete pump.

Pile Load Tests Performed

Throughout construction multiple pile load tests including compression, tension and lateral tests were performed. A total of five (5) sets of load tests were completed throughout the various phases of installation and typically when a significant change of subsurface condition was encountered. Of the five total tests, two load tests were performed on the standard micropile design to verify the grout to rock bond stress. One test was performed on a micropile in which fractured rock and clay was prevalent in the rock zone. A fourth load test was performed on a micropile where low mobility grout was used to achieve the bond zone. In each of these cases the micropiles tested were acceptable.

A wide and deep clay filled fracture was encountered through the middle of the Coal Storage area. As a result, micropiles along this seam could not be installed with the designed rock socket. Subsequently, an additional pile test was performed in this area to determine the limiting-load that the clay in the fracture could sustain. Given the sensitivity of the structure to differential settlement, the initial plan was to use a system that could support the span over the clay seam by using the existing micropiles and a grade beam. Design parameters of this area called for a load capacity of 400 kips. Unfortunately, the micropiles only achieved a loading of 200 kips. As a result, additional micropiles were required along the outskirts of the clay seam to provide the necessary load support. Overall the piles were more than adequate and were tested to twice their design capacity (tested to 1400 kips). All movements followed the calculated stress-strain curves used for the tests.

Figure 6 – Initial load test setup utilizing four reaction anchors to obtain the test load of 1400 kips.

Conclusion

Throughout the project the micropile installation was faced with multiple challenges including open voids, fractured rock or areas of no rock at all to depths over 200-ft. The use of low mobility grouting increased the bond strength at areas of fractured or no rock to enable micropile installation. In certain instances where open voids were present, lean mix was pumped directly into the void in order to support the micropile cased length. Due to the extreme differences in micropile lengths caused by the varying rock depths additional micropiles were required to balance the settlements for certain structures. The ESSROC Project is an example of the effective use of non-traditional applications and techniques designed and implemented for the effective installation of micropiles supplemented with low mobility grouting and void filling to achieve design loads. In excess of 1,600 total micropiles with a total of over 93,000-lf were installed in highly karstic dolomite and limestone – providing the necessary foundation supports required for the expansion efforts.

Copyrighted Materials
Copyright © 2009 American Society of Civil Engineers (ASCE)
Retrieved from www.knovel.com

Micropiles for Re-support and Lifting of Two Buildings under Construction

Brent Byford[1] and Mark Hampton[2]

[1]Project Manager, Hayward Baker, Inc., 1350 W. Lake Street, Roselle, IL 60172; bmbyford@haywardbaker.com
[2]Project Engineer, Hayward Baker, Inc., 1350 W. Lake Street, Roselle, IL 60172; mrhampton@haywardbaker.com

ABSTRACT: A pair of new barracks buildings at the Great Lakes Naval Base in Great Lakes, Illinois was settling during their construction due to consolidation of a zone of poorly compacted material that was used to backfill a former basement. Both buildings needed to be re-supported, and one needed to be re-leveled. The geotechnical contractor designed and installed a lifting/permanent support system utilizing micropiles and hydraulic jacks. The design scheme consisted of a micropile setup that accomplished the re-support and re-leveling requirements from within the tight dimensions required by the project. Valuable information was taken from the project concerning the use of micropiles in the application noted as well as an efficient method of transferring load from existing footings into micropiles.

INTRODUCTION

The newly constructed barracks at the Great Lakes Naval Base presented a difficult design and constructability challenge to rectify the settlement problem (Fig 1). Since the new buildings were under construction when the settlement problem was found, there were additional considerations that would influence the design solution, such as an existing slab-on–grade, first floor supports, and newly placed electrical and plumbing pipes.

The building needed a pile that would effectively correct the problem but with minimal disturbance to portions of the buildings that had already been constructed. The existing soil conditions had to be evaluated to determine if it would be sufficient to extend the micropiles to rock, or if a friction element would be necessary. This design also had to work into the overhead constraints of the drilling operation inside the building.

Micropiles were utilized to preload/lift the buildings. Since one building had settled less than the other and thus did not induce as much unexpected stress on the structure, the micropiles only had to be preloaded. The other structure had to be lifted to return it to its intended location and reduce the unexpected stresses.

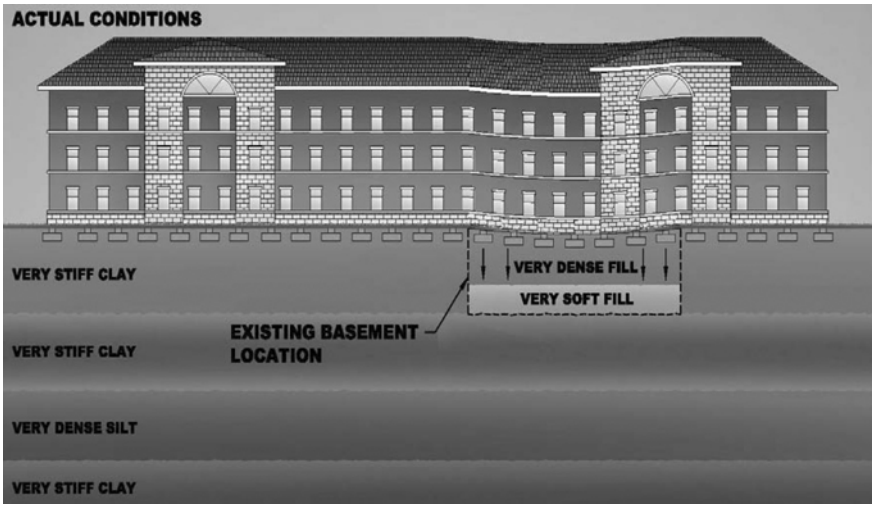

Fig. 1 – Illustration of the pre-repair condition.

After preloading/lifting the structures, the load transfer mechanism had to be incorporated into the footing and thus be covered by the newly constructed slab. The load transfer mechanism needed to be protected from potential corrosion prior to the slab being replaced. This was done by pouring concrete over the entire mechanism while still remaining below the bottom of slab elevation.

PROBLEM

The newly constructed barracks were resting on shallow spread footings. About halfway through construction, it was noticed that the structure was settling. In some areas the building had settled up to 101.6 mm (4"). Investigations revealed that the settlement was caused by an underlying basement that was demolished and backfilled with a very weak, compressible, and uncompacted fill material. The fill was a combination of sand, gravel and silty clay that was very moist and in some areas saturated. Fig. 2 shows the typical soil data for the upper fill area. As the buildings were constructed, the additional weight compressed the weak fill.

Construction on the buildings was halted until the problem could be solved. Since the building was still under construction, it presented some additional considerations in determining a solution. The floor slab in one building had already been constructed, so in order to install any remedial foundation system, a portion of the slab had to be removed. There were also newly installed electrical and plumbing lines that presented an additional obstacle for the design below the newly constructed slab. The overhead utilities and ceiling height also posed a limitation on the system that could be installed.

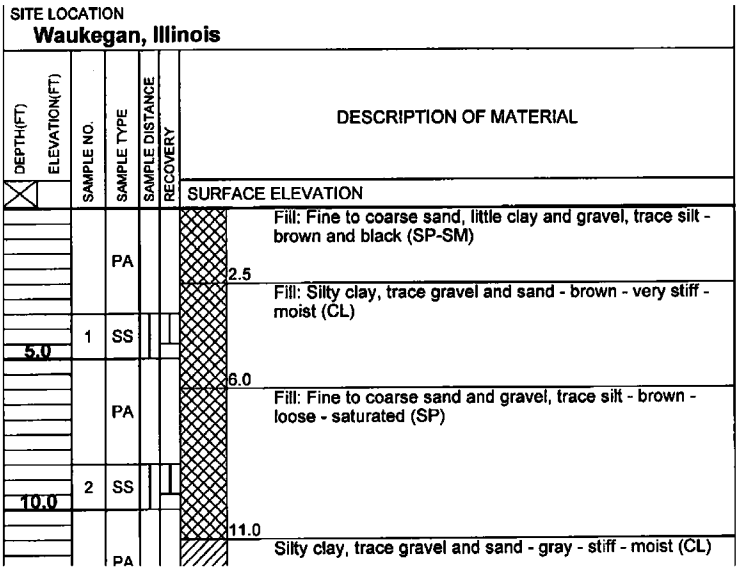

Fig. 2 – Typical upper fill soil data.

MICROPILES

The structural engineer of record specified that a form of micropile was needed to prevent further settlement and also could perform as an element to lift the building. A few different micropile options were analyzed in order to determine the best solution for the problem. Hydraulically pushed (jacked) piers of smaller capacity, larger quantity and installed in a configuration around the exterior of the footing was evaluated. This system provided difficulties in making a connection to the existing footing that would allow for the load transfer to take place and also raised concerns that due to the large footprint of the footings (up to 3,200 mm x 3,200 mm) and shallow depth (+/- 762 mm), the footing could fail while loading.

A system of hydraulically pushed piers pushed through the existing footings was also evaluated. This system had the advantage of requiring a smaller hole through the existing footing, but due to the smaller capacity, it also required a greater number of piles be installed. The greater number of piles caused difficulty in providing an efficient connection to the existing footing for the purpose of lifting and preloading.

The geotechnical contractor determined that a 203.2 mm (8") friction micropile with 43 mm (#14) threadbar reinforcement was the appropriate element for this application. These piles provided the 658 kN (148-kip) maximum capacity requirements of the project. Due to the very soft fill material, a 177.8 mm (7") diameter by 3,048 mm (10') long piece of casing was used at the top of the hole to prevent the fill material layer of soil from raveling into the hole. The piles extended to a hard pan layer approximately 19.812 m (65') below grade.

These piles required removal of the floor slab by sawcutting, and removal of the 609.6 mm (2') of fill above the footings. The locations of the piles were then laid out on the footings in order to determine if there was any conflict with any electrical or plumbing pipes. After this was determined, the geotechnical contractor utilized a coring machine to drill a 254 mm (10"0) diameter core hole. Upon completion of the core hole, the micropiles were installed. See Fig. 3 for typical pile configuration.

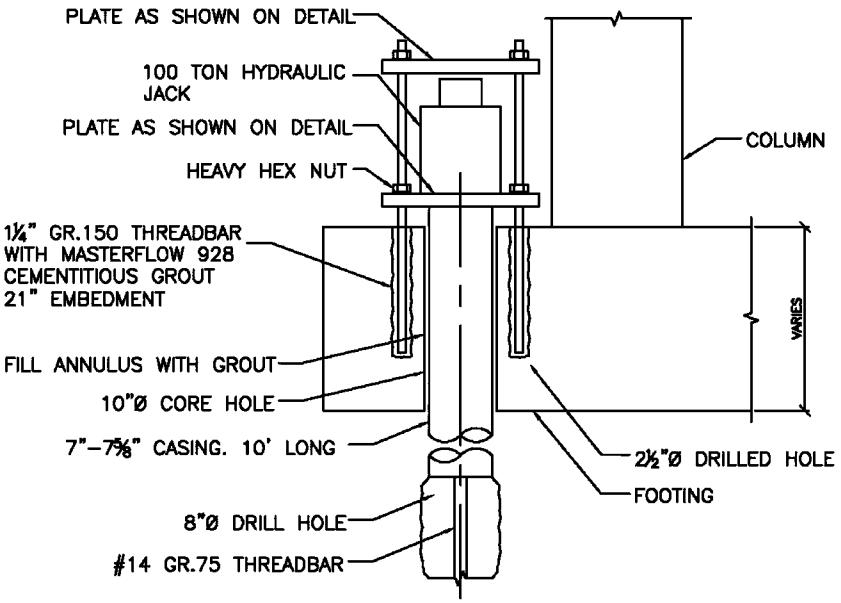

Fig. 3 – Typical pile and connection detail

The micropiles were installed utilizing hollow stem augers to the required 19.812 m (65') depth. As the hole was grouted, utilizing neat cement grout with a 28-day compressive strength of 34.47MPa (5,000 psi), the augers were removed from the hole. After the hole was grouted full, the casing was dropped into the hole to the required depth. Each pile was post grouted following the initial installation due to the soft clay.

CONNECTION DETAIL

The connection detail provided a significant challenge in order to provide a system that could transfer the load from the existing column and footings into the newly construction micropiles and still remain under the floor slab. There was only 609.6 mm (2') of space between the top of the existing footing and the bottom of the floor slab that was to be poured back. This space did not allow for a more conventional method of attachment such as walers connecting to the columns.

A system of steel plates and high strength threaded rods was developed to overcome the space limitations. Large steel plates (609.6 mm x 609.6 mm x 50.8mm thick) were installed over the protruding micropile casing. After the plate was in place, four high-strength 32 mm (1 ¼") threaded bars were drilled and grouted into the existing footing through predrilled holes in the steel plate. Nuts were then attached to each rod and hand tightened to the top of the plate. At this point, the micropile was connected to the footing and ready to be preloaded/lifted. See Fig. 3 for typical connection detail.

PRELOAD

It was determined that for one of the barracks buildings the micropiles would only be preloaded to the theoretical load that was already in the footings. For the other building, the structure would be jacked/lifted to bring it back closer to the design elevations and help reduce the stress that was imparted on the structure as it settled. The geotechnical contractor used a system of 890 kN (100–ton) jacks to perform both the preloading and the lifting.

For the building that was being preloaded, four to six jacks were chained together for each footing (see Fig. 4) and then connected to a hydraulic pump. Loading of the jacks occurred equally and simultaneously. The loading process proceeded in small increments so as to not produce an unwanted sudden lift of the footings. During loading, pressure gauges measured how much load was being inserted into the footings. The columns were also monitored to make sure that no lift was occurring as the footings were loaded.

Fig. 4 – System of 100-ton hydraulic jacks connected to perform the preloading

Upon loading the footings to a predetermined load, each micropile setup had to be locked off to insure that the load continued to be transferred from the footing. This was accomplished by tightening each nut on the micropile plate. After the nuts were locked into place, the jacks could be depressurized and removed.

JACKING/LIFTING

The system for lifting the building was similar to the used for the preloading except that more than one footing needed to be lifted at one time. Multiple sets of jacks needed to be operated simultaneously to perform the lifting. This was done by taking each set of footing jacks that were chained together in the same fashion that was used for the preloading, and chaining up to eight footings together to one pump.

	# of Columns	Lift Ht - mm (in)	Duration
Day 1			
	3	12.7 (0.5)	2 hrs
	1	6.35 (0.25)	
Day 2			
	5	19.05 (0.75)	4 hrs
Day 3			
	6	12.7 (0.5)	4 hrs
	1	6.35 (0.25)	
Day 4			
	10	19.05 (0.75)	
	3	12.7 (0.5)	4 hrs
	2	6.35 (0.25)	
Day 5			
	21	12.7 (0.5)	6 hrs

Table 1 – Breakdown of jacking sequence

The lifting sequence was calculated by the owner's engineer prior to the geotechnical contractor beginning the process. The sequence was set up over five continuous days and each day had specific footings and lift heights that were to be performed (see Table 1). Each day's sequence also had a specified time that it was to be completed in order to allow for the structure to be monitored thoroughly as the lift was taking place. After completion of each daily lift, the nuts on the micropile plates were locked off and the jack pressures were released. Surveys conducted at the end of each day and at the beginning of the following day determined if any rebound had occurred from the prior day's lift.

The final lift incorporated 21 footings to be lifted simultaneously. This was performed by incorporating 3 separate pumps and 92 jacks into one operation. The load at each pump was increased simultaneously in specified increments. After reaching each increment, each footing was measured to determine if it had reached its predetermined lift height. If an individual footing reached its specified lift height, the jacks for that footing were turned off and the nuts were locked off to prevent the load from being released. After the load induced in the piles reached the maximum design load each nut was locked off and the jack pressures released, completing the lift process. See Fig. 5 for illustration of repaired condition.

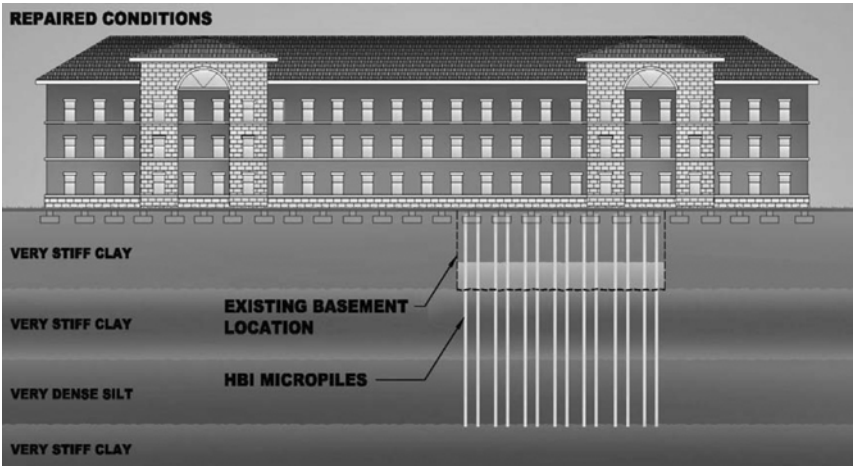

Fig. 5 – Illustration of the post-repair condition

The final results of the lifting were that the footings were raised up to 63.5 mm (2.5"). This was less than originally specified maximum lift of 76.2 mm (3"), but the maximum load that could be jacked into the piles could not exceed the micropiles design capacity. The final height that each footing was lifted varied depending on the original specified lift height and the number of times each footing was lifted.

CONCLUSIONS

The settlement issues encountered at the Great Lakes Naval Base presented a variety of design and constructability issues. By utilizing micropiles and a lifting/lock off mechanism in an efficient manner, the structures were able to be restored so they could continue construction. The use of micropiles offered the solution to solve a difficult problem.

ACKNOWLEDGMENTS

General Contractor – Clark/Blinderman Camp Porter, LLC
Geotechnical Contractor – Hayward Baker, Inc.
Structural Engineer – Graef, Anhalt, Schloemer, & Associates

Copyrighted Materials
Copyright © 2009 American Society of Civil Engineers (ASCE)
Retrieved from www.knovel.com

Use of Multiple Techniques to Support Construction of a New Hospital Addition

James B. Pease, P.E., M. ASCE[1]

[1] Project Manager, Hayward Baker Inc., P. O. Box 154, Palmyra, PA 17078-0154; jbpease@haywardbaker.com

ABSTRACT

Geisinger Health System planned a nine-story addition that will hold a variety of patient services. Deep foundation support, excavation support, and underpinning of the existing structure were required to facilitate construction. Micropiles, soil-nailing, and jet grouting were utilized.

Two-thousand-kilo-Newton (200 ton) capacity micropiles were specified for foundation support. Two pre-construction load tests were performed – one in limestone and one in grey shale – to further characterize the site geology, especially as it related to the design of the micropiles. The load test results indicated the limestone provided approximately three-times higher bond strength than the shale. Two-hundred and eighteen, 2,000 kN (200-ton) micropiles were installed. The design of the micropiles also included a 500 kN (50-ton) uplift capacity. Some piles were battered for lateral capacity.

Jet grouting was selected as the preferred underpinning technique for several pile caps of the existing building since it would provide the least disturbance to hospital operations and other construction trades. Thirty-three 1,067 mm (3.5 foot) diameter jet-grouted soilcrete columns (some battered) and seven tie-back anchors were installed.

A soil nail wall was proposed for temporary excavation support. The geotechnical contractor constructed a 280 m^2 (3,000 square foot) soil nail wall including 88 soil nails with a 100 mm (4-inch) thick reinforced shotcrete facing.

Site, geologic, and operational constraints caused engineers to select three distinct geotechnical construction techniques to solve specific problems and support construction of a new patient addition. Minimization of noise, vibration, and other disturbances were critical to the success of the project.

PROPOSED CONSTRUCTION

Geisinger Health System, a regional healthcare, education, and research service spanning 40 counties of 20,000 square miles and serving 2.5 million people, operates its main medical center and corporate headquarters in Danville, PA. The Geisinger Medical Center has operated for over 90 years, and has undergone several stages of growth over those years.

Most recently, Geisinger planned a significant expansion named the "Patient Pavilion" that will hold a variety of patient services. The addition was proposed to be 9-stories and would add 27,870 m^2 (300,000 square feet) of hospital space. The new space was proposed to house orthopedic and heart "hospitals" and new patient beds.

The construction site was adjacent to the hospital's exiting maternity ward and surgical recovery areas. Minimization of noise, vibration, and other disturbances were critical to the success of the project. Disruption of hospital operations was not possible.

To support the high foundation loads from the 9-story structure, the geotechnical engineer specified micropiles. Two-thousand-kilo-Newton (200 ton) capacity micropiles, constructed with minimum 244 mm ($9^5/_8$") outside diameter casing, were specified.

SUBSURFACE CONDITIONS

The regional geology of the Danville area is a sedimentary environment, consisting of alternating layers of sandstone, shale, and limestone. Nine (9) test borings were completed by the geotechnical engineer to characterize the approximately 2,800 m^2 (30,000 square foot) building footprint. This site was characterized by approximately 7.6 m (25 feet) of silty sand overburden underlain by approximately 3.0 to 6.1 m (10 to 20 feet) of weathered red shale; 3.0 to 6.1 m (10 to 20 feet) of slightly weathered, fractured, soft grey shale; and finally moderately weathered hard limestone.

Typical rock core recovery in the shales ranged from 30% to 100%, with an average of less than 65%. Average rock quality designation (RQD) of the shales was less than 30%. Average rock core recovery and RQD in the limestone was approximately 94% and 38%, respectively.

PROJECT SOLUTION

Micropiles are drilled-in, grouted steel pipe piles with central threadbar for reinforcement. Micropiles are installed with down-the-hole drill tools to advance steel pipe (casing) to the design depth above the bond zone. The bond zone is then drilled out, followed by grout placement, and finally the insertion of central reinforcing bar.

The geotechnical contractor performed two pre-construction compression load tests. The objective of these tests was to further characterize the site geology, especially as it related to the grout-to-ground bond strength of the bedrock. This is the primary component of the geotechnical design of micropiles. The first test was completed with the bond zone constructed in limestone, with a rock socket length of 4.6 m (15 feet). The test results yielded a bond nominal strength of approximately 1,035 kPa (150 psi).

The second test was a value-engineering effort to reduce the pile lengths. It was conducted with the bond zone constructed in the softer grey shales, with a socket length of 6.7 m (22 feet). This test resulted in a bond nominal strength of only approximately 317 kPa (46 psi). Additionally, complications were encountered in drilling and grouting the test anchors for this load test. Two of the anchor holes communicated during drilling. When these anchors were grouted, excessive grout was required to fill the holes. It was suspected that there were voids in the subsurface that were being filled with the excessive grout.

As can be seen from the discussion of test results above, the limestone provided approximately three-times higher bond strength than the shale. It was decided that a composite bond zone utilizing partly shale and partly limestone would be acceptable as long as all the rock was competent (i.e. no voids or soil seams). The project team settled on 45 kN per m of shale and 149 kN per m of limestone (9 kips and 30 kips per lineal foot respectively) based on a bond diameter of 262 mm (10.3 inches). Figures 1a and 1b show these load test results.

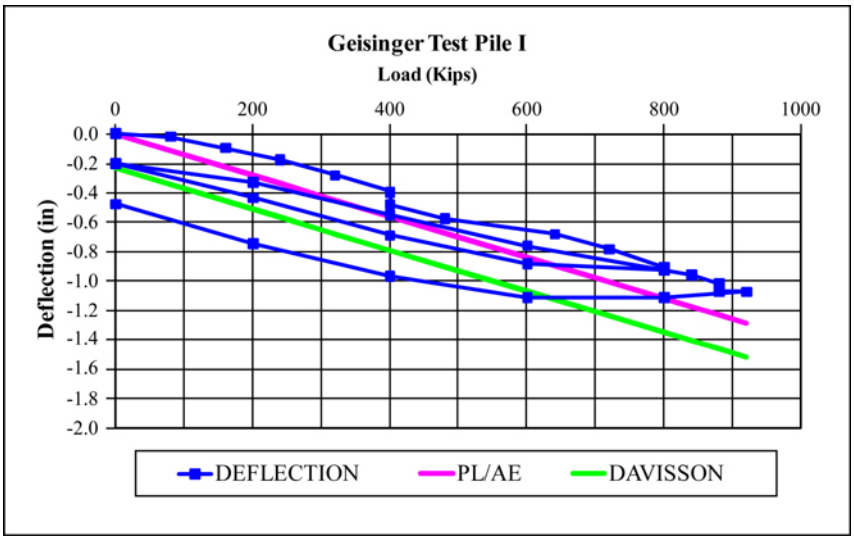

Figure 1a – Initial Load Test in Limestone

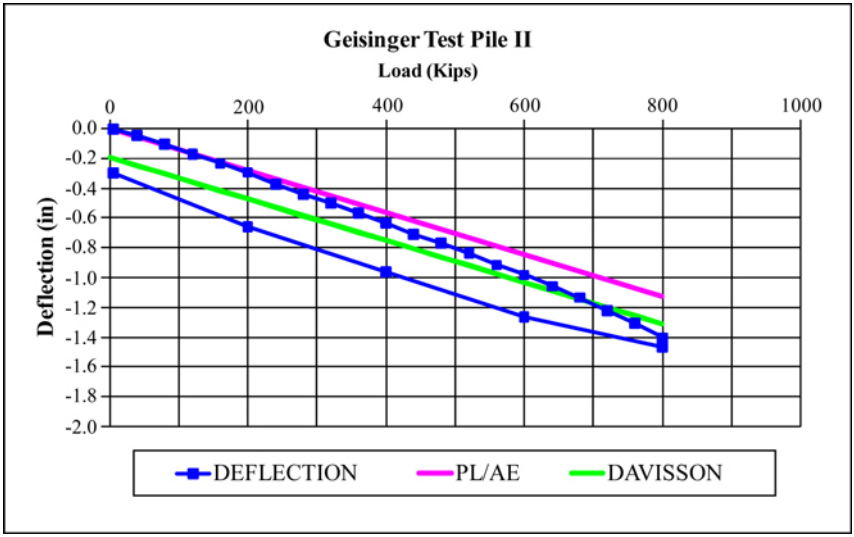

Figure 1b – Second Load Test in Shale

The geotechnical contractor installed two-hundred and eighteen two-thousand-kilo-Newton (200 ton) micropiles for foundation support. During production, it was determined that the quality of the shale was insufficient to rely on its bond capacity. For the majority of the piles, the casing (244 mm [$9^5/_8$"] O.D. with 13.8 mm [0.545"] wall thickness) was extended through the poor-quality shale, bonding in the hard limestone. Then the 4.6 m (15 foot) long, 262 mm (10.3 inch) rock socket was drilled out. A #28 Grade 75 central reinforcing bar was utilized to transfer the load from the cased section of the pile to the rock socket. This was installed in the rock socket and up into the casing the minimum development length. Minimum 34,500 kPa (5,000 psi) neat cement grout was placed in the piles using a tremie method.

The micropiles were also required to provide a minimum 500 kN (50-ton) uplift capacity. To transfer the tensile load from the pile cap to the bond zone, a central reinforcing bar was utilized the full length of the piles. In a value-engineering effort, the geotechnical contractor recommended a composite central reinforcing bar. This included a transition coupler from the #28 Grade 75 bar required in the bond zone to a #14 Grade 75 bar. The #14 Grade 75 bar was then extended up to the top of the pile. Threaded nuts secured a 44.4 mm x 203 mm x 203 mm (1 ¾" x 8" x 8") steel plate to the top of the #14 bar. All reinforcing steel and connecting hardware was plain (uncoated).

Four verification tension load tests were performed on throughout installation of the piles. These tension tests, performed on production piles, were loaded to 115% of the

design capacity, with one re-load cycle. The results of these tests consistently confirmed the design capacity of the piles.

UNDERPINNING

The new patient pavilion was planned to be attached to the existing hospital. The close proximity of the proposed structure and the depth of the proposed footings in the area of new elevators required underpinning of several existing pile caps. The proposed depth of excavation below the existing footings was approximately 1,500 mm (5 feet). As with every other aspect of construction on this project, disturbances to hospital operations must be minimized. Additionally, with multiple trades working on the job site concurrently, construction techniques were selected to result in the least disturbance to other construction activities.

Jet grouting was selected as the preferred underpinning technique since it would provide the best technical approach (based on the subsurface conditions) and the least disturbance. Thirty-three, 1,067 mm (3.5 foot) diameter jet-grouted soilcrete columns and 7 tie-back anchors were installed for underpinning. The soilcrete columns extended to a depth of 3.0 m (10 feet) below the bottom of existing footings.

Jet grouting is a replacement grouting technique that was developed in Japan approximately 30 years ago. It was introduced in the United States about 20 years ago, and has been a vital tool in providing underpinning of buildings, excavation support, and tunnel pre-support. Triple-fluid jet grouting was utilized for this project. Triple-fluid jet grouting has been relied upon for underpinning because it provides high quality soilcrete. This method was also used at this hospital on a previous underpinning project with excellent results. The technique consists of drilling a hole into the specified depth of treatment. At this depth, a high pressure water jet, sheathed in air, is induced just above the drill bit. The jet is created by pumping high pressure water (41,400 kPa [6,000 psi]) and air (800 kPa [120 psi]) through a 2.6 mm diameter nozzle at high velocity. The jet is rotated slowly during extraction from the borehole, during which time grout is placed through the drill bit. The process erodes the in situ soils and replaces them with a column of grouted soil. After several hours of curing, the cut soil, cement and water (soilcrete) hardens in a similar manner as concrete, with strengths between 350 and 6,900 kPa (50 and 1000 psi) possible. Three-day test results on this project yielded average strengths of approximately 5,000 kPa (750 psi).

Due to the high pressures that are used during the jet grout process, it is essential that "return" of drill spoil be maintained to the surface at all times. Drill flush return is the excess liquid soilcrete that travels up the drill string as waste. By constantly exhausting this material via return, heave at the surface is mitigated and no unnecessary loads are imparted on the existing structure. For this reason, the existing footings were cored prior to the jet grouting operation.

Since interior access could not be provided, some jet grouted soilcrete columns were battered under existing foundations. After the soilcrete cured for a few days, the excavation proceeded to a depth of approximately 305 mm (12 inches) below the bottom of footing to allow access for installation of tie-back anchors. Seven tie-back anchors were installed through the soilcrete columns. A 51 mm x 381 mm x 381 mm (2 inch x 15 inch x 15 inch) steel plate was secured on the end of the tie-back at the face of the soilcrete column with a hex nut (Figure 2).

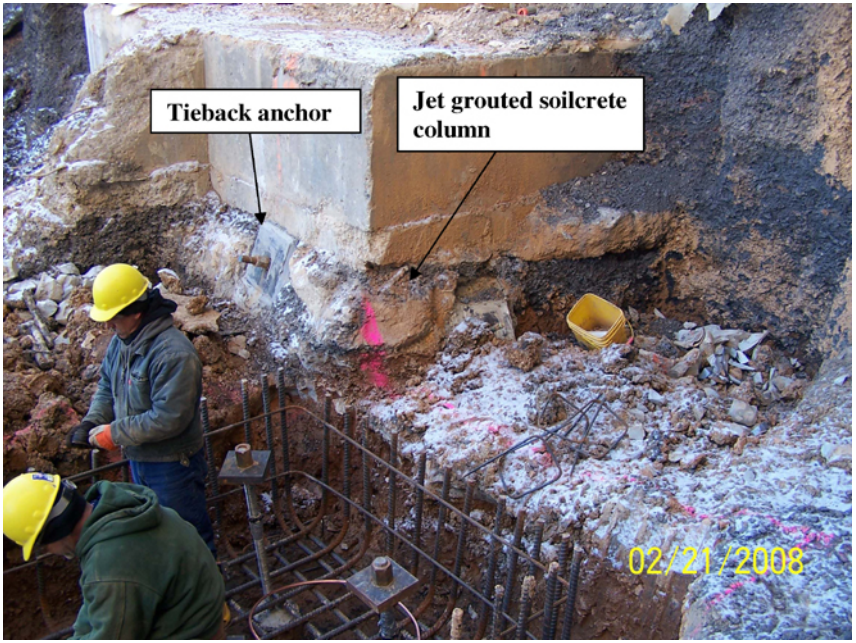

Figure 2 – Jet grouted soilcrete column shown at the corner of an existing footing; tie back on left side of footing, installed through the soilcrete.

EXCAVATION SUPPORT

Construction of the new Patient Pavilion required excavation support along an approximately 49 m (160 foot) length of the proposed building where it abutted existing underground utilities. The specialty geotechnical contractor proposed a soil nail wall based on previous similar excavations on the campus and the flexibility of the soil nail system around existing structures. Several underground utilities existed behind the soil nail wall and could not be interrupted without disrupting hospital operations. Although the soil nail system provided flexibility around these utilities, their presence in this case greatly complicated the installation of the soil nails.

The contractor constructed an approximately 280 m^2 (3,000 square foot) soil nail wall composed of 88 soil nails and a 100 mm (4-inch) thick reinforced shotcrete facing. The maximum exposed wall height was approximately 6.4 m (21 feet). Soil nails ranged in length from 6.1 to 7.9 m (20 to 26 feet). A 19 mm x 203 mm x 203 mm (¾ inch x 8 inch x 8 inch) steel plate was secured to a #8 Grade 75 soil nail on the face of the shotcrete with a nut.

SUMMARY

Site, geologic, and operational constraints caused engineers to select three distinct geotechnical construction techniques to solve specific problems and support construction of a new patient addition. The high loads and poor quality shale called for utilizing micropiles bonded in hard limestone encountered below the shale. To minimize the impact on patients at the existing facility, jet grouting was used to underpin existing footings adjacent to the proposed construction. Existing underground utilities adjacent to the proposed structure required the careful installation of a soil nail excavation support wall.

Figure 3 – Installing micropiles in foreground, jet grouting in background, and soil nail wall on right side of photograph.

The construction site was adjacent to the maternity ward and surgical recovery areas of the existing hospital. Minimization of noise, vibration, and other disturbances were critical to the success of the project. All these factors played into the selection of micropiles for foundation support, jet grouting for underpinning, and soil nails for temporary excavation support.

REFERENCES

FHWA, (2000), "Micropile Design and Construction Guidelines," Federal Highway Administration, FHWA-SA-97-070.

PROJECT CREDITS

Owner: Geisinger Health System, 100 N. Academy Ave., Danville, PA 17822

Construction Manager: Torcon, Inc., 328 Newman Springs Rd., Red Bank, NJ 07701

Geotechnical Engineer: Geo-Science Engineering Co., Inc., 1252 Mid Valley Dr., Jessup, PA 18434

Architect: Ewing Cole, 100 N. 6th St., Philadelphia, PA 19106

Copyrighted Materials
Copyright © 2009 American Society of Civil Engineers (ASCE)
Retrieved from www.knovel.com

BANJO BILL ROCK CATCHMENT BASINS

Paul B. Groneck, P.E. Vice President & Tom Armour, P.E. President
DBM Contractors, Inc. P.O. Box 6139, Federal Way, WA 98063, U.S.A.
Email paulg@dbmcm.com tarmour@dbmcm.com

ABSTRACT

Public safety and maintaining environmental integrity are the two most important features highway departments consider when designing and procuring construction projects along scenic highway corridors. Design, contract procurement and construction of two rock catchment basins on SR 89A in scenic Oak Creek Canyon near Sedona, Arizona required innovative thinking to meet the many environmental and technical challenges presented on this project. Anchored micropile earth retention structures were chosen as the most feasible alternative to create the two basins to catch and contain falling boulders and rocks from entering the roadway and adjacent campground.

This paper will present and discuss descriptions of the environmental and geotechnical assessments, retention method selection, anchored micropile wall design features, alternative procurement technique used to contract the project, construction and site challenges, monitoring; and performance of the basin retention system.

PROJECT DESCRIPTION

The project site is located in Oak Creek Canyon approximately 11-kilometers north of Sedona, Arizona on State Route 89A. One side of the canyon consists of scenic sandstone cliffs, with Oak Creek following the roadway alignment below. The project side of the canyon consists of a boulder strewn talus slope with an inclination of 30 to 40-degrees rising towards the canyon rim which is located 430-meters above the roadway. In the slope across the roadway from the Banjo Bill day use site are two natural drainage swales which terminate at the roadway. These drainage swales are within approx 90-meters of each other, and are the sites for this project. For the purpose of the project they are referred to as the north and south basins.

PROJECT DESIGN CONCEPT

SR89A had been blocked on six occasions over a fifteen year period by rockfall and debris flows thru the two basins. In the fall of 1999, two 2-meter diameter boulders rolled down the slope between the two basins, breaking trees and coming to rest against the guardrail across the roadway. A debris flow north of the north basin in December 2003 included a 2-meter diameter boulder which bounced across the road and came to rest against a large tree in the campground area. There had luckily been no injuries from the rockfall and debris flow incidents.

Photo 1 - Looking Down Canyon at Site

Photo 2 – Base of South Basin

Starting in 1991 ADOT commissioned several studies to develop concepts to deal with the rockfall and debris flow problem. The conclusion of the study by URS Corporation in 2002 was that the rockfall was attributed to undercutting of the talus slopes by water runoff resulting in loosening of the boulders in the slope. Options for reducing the risk to the roadway and public from the rockfall were considered. Scaling to make the slopes safer was not considered practical due to the extensive range of the upslope boulderfields. The Forest Service did not want to use fences for the containment due to aesthetic considerations. Realignment of the roadway was not feasible due to the close proximity of Oak Creek.

It was decided that the best plan was to provide basins at the base of the slope next to the roadway for containment of the rockfall. Based on volumes of previous slides, the basins needed to be designed to contain 190 and 380 cubic meters of material for the north and south basin respectively. Retaining walls up to approximately 9-meters in height would need to be installed to form the uphill side of the catchment basins. Due to the difficult terrain and ground conditions it was obvious that a unique retaining wall design would be necessary to meet the challenges of the site.

SUBSURFACE CONDITIONS

Geotechnical investigations were performed at the site in late 2000 and late 2003/early 2004 to determine the ground conditions and design parameters of the walls. The ground conditions were shown to consist of a steep boulder filled "talluvium" slope over Coconino sandstone. The top surface of the sandstone was somewhat irregular but was generally in close proximity to the roadway grade elevation, and sloped uphill from the roadway at approximately five-degrees.

Inclinometers and piezometers were installed in several of the borings to measure for slope movement and ground water elevation. The inclinometers indicated a slow downhill creep of the talluvium layer. The static water table elevation was approximately at the top of the sandstone layer.

CATCHMENT WALL DESIGN PARAMETERS

Due to the difficult boulder filled ground conditions and steep slope access conditions, it was decided that an anchored micropile wall would be best suited for the back walls of the catchment basins. An "A-frame" battered arrangement of the micropiles with a single row of anchors on a top cap beam was considered, but the large bending moments induced by the span between the top cap and sandstone embedment was considered to be more than the micropiles could support. Vertical micropiles laterally supported by multiple rows of anchors was determined to be the best solution.

Testing was performed on the collected samples to determine the design properties of the taluvium and weak sandstone. A variety of methods of analysis were used to examine the wall lateral design pressures, including finite element analysis. Analyses were run with the following parameters to examine the range of resulting lateral design pressures:

- Talluvium – φ = 42-degrees, c from 0 to 200-psf, γ = 130-pcf
- Sandstone – φ = 41 to 42-degrees, c from 0 to 1,000-psf, γ = 130-pcf
- Top of Sandstone Elev assumed to be either at the base of the wall or 40% of the wall height above the base.
- Target factor of safety = 1.5

The finite element analysis produced a range for the rectangular lateral earth pressures of 62H to 100H psf (H = wall height). The 100H value was considered to be too conservative as it ignored all cohesion. The next most conservative value of 78H was selected for the wall design which considered φ = 42-degrees and c = 100-psf for both materials. In addition to being used for determining the lateral earth pressures, finite element design methods were also employed in analyzing the stresses in the micropiles and shotcrete facings.

WALL DESIGN DETAILS

Each wall is approximately 27-meters long, and aligned to follow the contours of each basin location. The walls were installed to support the design height for the full length of the wall. The basic features of the walls are as follows:

- Vertical micropiles which are spaced at 41-cm on-center along the length of the wall. The piles consist of a 14.3-cm OD steel pile in a 25.4-cm diameter drilled hole grouted with neat cement grout. The micropiles provide vertical support for a shotcrete facing and the vertical load component of the anchors. The micropile embedment also provides lateral support for the base of the wall. The piles were designed to have adequate bending strength to support the full lateral soil design pressure while spanning between each row of anchors.

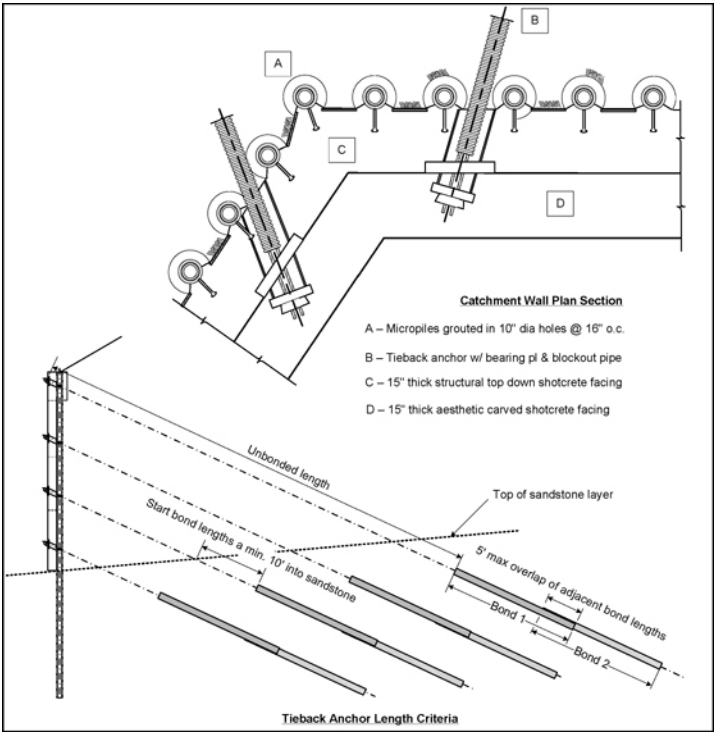

Figure 1 – Wall Design Details

- A 0.9-meter square reinforced concrete cap beam located at the top of piles to connect the piles together and provide a connection point for the top row of anchors.
- A 0.4-meter thick structural shotcrete facing which served to distribute the soil loads to the micropiles and provide connection points for the remaining rows of anchors. This facing was heavily reinforced to act as a waler along the anchor rows. The facing was installed in a top-down manner in lift heights which matched the anchor row spacing.
- The final walls were anchored with four rows of double corrosion protected tieback anchors. The anchors were connected to the structural shotcrete facing with bearing plates and embedded blockout pipes. The anchor bond lengths were founded in the underlying sandstone bedrock.
- A 0.4-meter thick aesthetic outer shotcrete facing which was carved and stained to emulate the features of the natural rock in the area.

Additional features of the basin construction included the following:

- Temporary soil nail walls which support the sides of the excavations from the ends of the micropile walls down to the edge of roadway.
- Gabion berms which form the permanent side slopes of the basins and bury the temporary soil nail walls.
- Drilled horizontal drains were constructed to relieve hydrostatic water pressure at the base of wall.

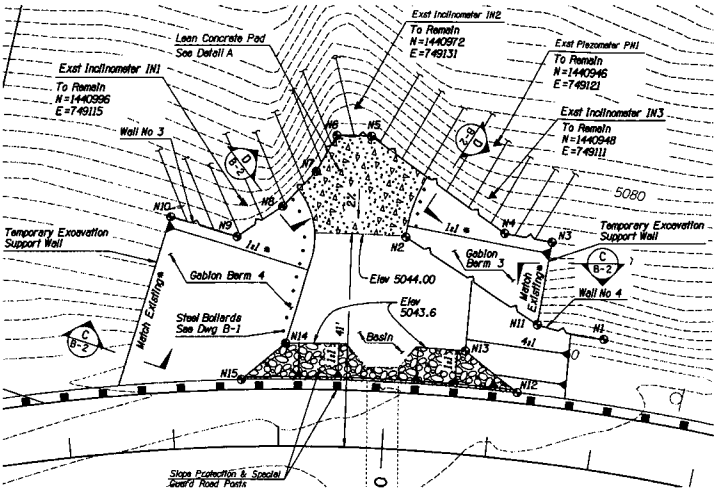

Figure 2 – North Wall Layout Plan

PROJECT CHALLENGES

The construction of the project presented many unique challenges, including:

- *Equipment Access* – Prior to the start of work the access along the wall alignment was a steep boulder strewn slope (approx. 40-deg inclination). Reinforced soil benches were built to provide a 9-meter plus bench width for access by the drill rigs and excavators along each top of wall location. The bench soils were reinforced with geotextile fabric at the South wall, and ecology blocks plus fabric for the North wall where room to build stable walls was more limited.
- *Difficult Ground Conditions* – The boulder filled upper soils were a challenge to the drilling of the micropiles and anchors. Care had to be taken to maintain verticality of the micropiles due to their close spacing and the need to thread the splayed anchors between them. Cased hole drilling techniques using down-the-hole hammers and "Super-Jaw" wing bits successfully met these challenges.
- *Limited Construction Schedule* – The project had to be completed during a construction window between September 1st, 2007 and March 30th, 2008. This limit was set to complete construction outside of the busy local tourist season, and

Photo 3 – North Wall Access Bench

to avoid interfering with the breeding season of the Mexican Spotted Owl, which is protected under the Endangered Species Act. Expanding the schedule outside of this allowed time was not an option. Double shifts, Saturday work, and contractor initiated alternative design changes aided in completing the project on schedule.

- *Environmental Aspects* - The Oak Creek Canyon is a very scenic and protected area of Arizona. The project is located on Coconino National Forest lands. The Forest Service played a major role in establishing the aesthetic requirements for the project design and monitored the impact to the site during construction. The foliage could not be disturbed outside of the direct wall locations. Weekly testing and inspection of the adjacent creek waters and spring water source for the local residences was done to monitor for contamination from the surface runoff and placement of grout in the anchors and micropiles.
- *Slope Stability During Construction* – There was concern for movement of the slopes during the interim phases of the top down wall construction. The support provided by the temporary access benches helped address these concerns. Movement of the slopes was monitored on a daily basis throughout the drilling work with reading of the inclinometers and the surveying of a series of points on the slopes above the walls.
- *The Need for a Successful Completion* – There was an initial failed attempt at completing this project in 2004. The General Contractor and Drilling Subcontractor were apparently not up to the site difficulties and contractor design aspect of the work. This first attempt resulted in a cancelled contract and completion of only 16 of the micropiles, which were subsequently removed as part of the successful wall installation.

Photo 4 – Shotcrete Fascia @ Anchor Row 2

The method of contracting the job was changed for the 2007 project. ADOT selected a procurement process where a select group of contractors were prequalified prior to bid time with their capabilities for completing the work established ahead of time. The project specifications required that the general contractor self perform the installation of the micropiles and tieback anchors.

ALTERNATIVE DESIGN

The project specifications allowed the contractor to propose an alternative design for the reinforcement of the micropiles and anchors as well as an alternative number of anchors. The original project design included five rows of anchors with a working load which ranged from 250 to 550-kN's. There was also a requirement for the anchor tendons to have a minimum steel area of 6.5 to 16-square cm which provided the stiffness values use in the wall design finite element analysis.

An alternative design was proposed by DBM which included reducing the number of anchor rows from 5 to 4, increasing the bending strength of the piles and shotcrete facing to support the larger span between anchor rows, and using an anchor tendon design which was based on strength instead of stiffness. The contract allowance for constructing the alternate design greatly aided in being able to meet the specified project completion date, which was in the interest of all involved parties.

CONCLUSION

The project was successfully completed in more ways than one. The walls have performed well to date as indicate by the installed instrumentation, which includes six

Photo 5 – Completed North Basin

inclinometer casings located above the wall for monitoring wall movements and two load cells on each anchor row on each wall (8-total) for monitoring changes in the anchor loads. No notable changes in the readings have been reported to date.

ADOT has a program for implementing a formal partnering procedure on all of their projects. This process was particularly successful and beneficial on this project and aided in dealing with the constant flow of structural and aesthetic design issues. The open lines of communication greatly aided to the successful completion of the project and the satisfaction of the Ownership group and Contractor. The project was recently announced as a winner of one of the 2008 ADOT Partnering Excellence Awards.

Key members of the team that completed the project include:

- Arizona DOT – Owner - Astrid Potter & Jim Monnett
- DBM Contractors – GC – John Bickford, Craig Henke, Paul Groneck
- URS Corporation – Structural Design – Randy Simpson
- NCS Consultants – Geotechnical Design – Naresh Samtani
- Schraner Associates – Architectural Design – Dave Schraner
- Forest Service – Owner – Judy Adams
- Boulderscape – Carved Shotcrete – Steve Jimenez
- Ground Support – Alternative Designer – Chris Wolschlag

Copyrighted Materials
Copyright © 2009 American Society of Civil Engineers (ASCE)
Retrieved from www.knovel.com

Seismic Analysis of Inclined Micropiles Using Numerical Method

Reza Noorzad[1] and G.Reza Saghaee[2]

[1]*Nooshirvani Institute of Technology, Civil Engineering Faculty, Babol, Iran; rnoorzad@nit.ac.ir*
[2]*Khazar University, Civil Engineering Department, Mahmoodabad, Iran; Grezasaghaee@stu.nit.ir*

ABSTRACT: Some design codes have restricted the use of inclined micropiles in seismic zones. Recent observations following seismic events have shown however, that inclined micropiles behave efficiently when subjected to earthquake loading. In this study, seismic analyses have been performed on two dimensional plain-strain models of inclined micropiles, using finite element code PLAXIS. Parametric analyses were performed to assess effects of batter angle. Results of the analyses showed an increase in axial force and a decrease in shear force and bending moments with increasing batter angle due to seismic loading. The results show that inclined micropiles have good performance under seismic loading.

INTRODUCTION

Micropiles are generally defined as piles with a diameter less than 300 millimetres and are constructed by boring holes in the ground, placing reinforcements and filling the void spaces by means of grouting. Substantial advantages in using micropiles have resulted in an increasing applicability of this technology in foundation retrofitting. Some of the advantages associated with micropiles are: Minimal disturbance in the soil, low excavation volumes involved, simplicity in construction of inclined micropiles, possibility of construction under low overhead space conditions in retrofitting of existing foundations.

Field observations following earthquake events provide a valuable source for evaluating the behaviour of piles. The level of damage caused by various piles having different batter angles is relatively diverse. Observations following the Kobe earthquake of 1995 with an intensity of 6.9 M_W showed that one of the few wharf walls which survived the earthquake loading in the Kobe port was a composite wall supported by inclined piles, although a nearby wall supported by vertical piles suffered extensive damage. These observations revealed the importance of seismic behaviour of inclined piles.

Micropiles, which may be regarded as frictional piles, have shown satisfactory seismic performance during recent earthquakes. Yet, behaviour of inclined micropiles has not been given the needed attention in the literature, and there is an obvious need for further evaluation of seismic performance of these structures. In the lack comprehensive full-scale performance data, numerical assessment deems one of the most suitable alternatives to study the seismic behaviour of inclined micropiles.

This study seeks to evaluate the effect of batter angle on seismic behaviour of micropiles. Commercial finite element code PLAXIS has been used in performing the dynamic analyses.

NUMERICAL MODELING

The finite element code used in the analyses is capable of modeling two dimensional plain strain and axisymmetric conditions. However, due to the presence of inclined elements in the model, axisymmetric conditions cannot be achieved. Therefore, following the modeling procedure used by Sivakumar et al (2004) which used plain strain conditions, and referring to the studies conducted by Anandarajah (1990) which showed that two dimensional modeling of soil-structure interaction (SSI) problems agree well with centrifuge model results, in this study, two dimensional plain strain conditions have been selected for modeling. This procedure is supported by other researches such as numerical modeling of grouted soil-cement columns by Omine, Ochiai and Bolton (1999). The Schematic model configuration and finite element mesh used in the analyses is shown in Figure 1.

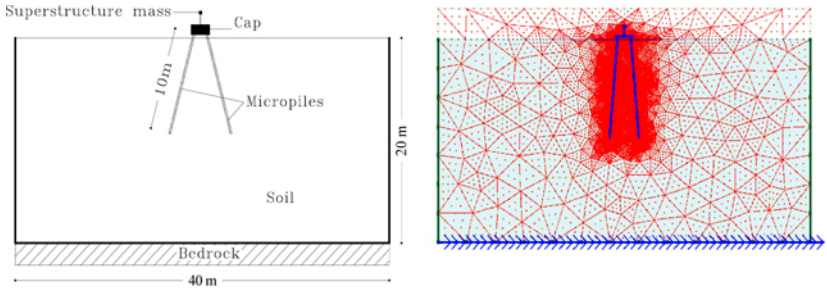

(a) **(b)**

FIG. 1. a) Schematic model configuration, b) Finite element mesh.

Referring to the literature, the distance from the pile to the vertical boundaries was suggested as 50 times the pile diameter, and a length equal to the pile length was suggested for the distance from the pile tip to the bottom of the model (Neves et al, 2001). For the models used in this study, the model depth was selected as 20 meters, and due to the use of dynamic boundary conditions at the vertical boundaries, the model length was selected as 40 meters. The distance between micropiles at the cap connection level was taken as 1.4 meters and the distance between cap and ground surface was taken as 0.3 meters.

The soil used in the analyses was Fontainebleau sand (FS) which is standard uniform silica sand. Mohr-Coulomb elastoplastic model was for the sand. The physical and mechanical properties of the FS are given in table 1. Two inclined micropiles of the B type (reference to FHWA micropile manual) with a diameter of 20 centimeters (equivalent structural cross section used for sum of grout and steel bar), 10 meter length and CTS-TITAN103/78 steel reinforcements were considered in each model. Table 2 lists the parameters used for the micropiles.

Table 1. Soil properties used in numerical analysis.

Soil	γ (KN/m^3)	E (MPa)	ν	ϕ°	C (Mpa)	ψ°
Fontainebleau Sand (FS)	16.77	117	0.3	39	0	14

Table 2. Properties of micropile cross-section used in numerical analysis.

Reinforcement Type	D_m (m)	ν	ω (Kg/m)	EA (KN)	EI $(KN.m^2)$
TITAN-IBO (103/78)	0.2	0.2	100.41	1401528	2597.59

The inclination angles of micropiles were selected as 0, 5, 15, 30, 45 and 60 degrees. Micropiles were modeled by beam elements with elastic behavior available in PLAXIS. Beam elements of the finite element model have three degrees of freedom in each node. Since 15 node elements were used to model the soil, beam elements were modeled using 5 node elements. Beam elements are based on Mindlin's beam theory (Bath, 1982).

One of the important considerations in SSI problems is the soil-structure interface which in this case is the micropile-soil interface (Wehnert and Vermeer, 2004). In order to correctly model this, interface elements were utilized to model the soil-micropile contact surface. In the construction of B-type micropiles, pressure grouting is performed after placing the grout under self weight by tremie. Grouting yields a cross section similar to the one shown in figure 2 (Astenbroich, 2001). This figure shows the cross section of a micropile with TITAN-IBO reinforcement which was used in this study. It can be seen from the figure that structural bearing section is actually the combination of the grout and the reinforcement. Adjacent to the grout, cemented soil and densified ground.

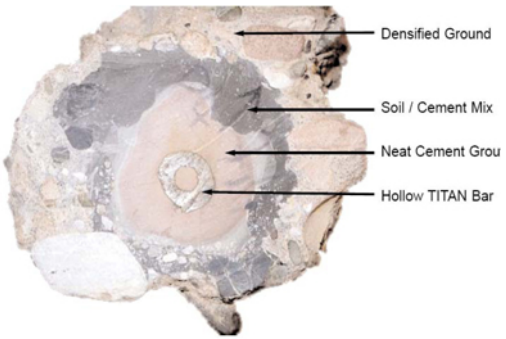

FIG. 2. Section of exhumed TITAN/IBO micropile.

The ribbed reinforcement provides adequate bond between grout and the reinforcement. This is why no reports have been given of failure of grout-reinforcement bond (FHWA, 2000). The grout-reinforcement bond strength is not dominant in the bearing capacity of micropiles compared to bond strength of soil-micropile interface. Therefore, it can be neglected in the modeling (Bruce, Ingle and Jones, 1985). Thus, the soil-micropile interface may be modeled as cemented soil formed as a result of grouting and the interface element diameter is 0.2 meters.

In the present study, the interface parameters are actually those of the sand in the vicinity of the micropile which has improved properties as a result of grouting. Properties of the cemented sand were derived from published data by Dano, Hicher and Tailliez (2004) who derived parameters for the Mohr-Coulomb model. They also showed that the Mohr-Coulomb model can be used effectively for modeling cemented sand. Since grouting adds tensile strength to soil, tensile strength of cemented sand was considered for interface element in order to enable gapping in the interface. This tensile strength was calculated from eq. 1 and was implemented as tensile failure in PLAXIS. Table 3 lists properties of the interface element.

Table 3. Soil-micropile interface element properties used in numerical analysis.

Interface Element	γ (KN/m^3)	E (MPa)	ν	ϕ°	C (Mpa)	ψ°	$R_{(cut)}$ (Mpa)
Grouted Fontainebleau Sand (FS)with cement grout	19	406	0.3	42	0.2	24	0.178

$$R_{cut} = \frac{2C' \times Cos\,\phi'}{1 + Sin\,\phi'} \tag{1}$$

In order to take into account the effect of inertial forces due to superstructure on seismic behavior of inclined micropiles in the numerical modeling, a single-degree-of freedom (SDOF) superstructure was modeled using a concentrated mass resting on a zero mass column connected rigidly to the micropile cap. The natural frequency of the SDOF was assumed to be same as that of a ten-story building with average story height of 3 meters. The natural period of a ten story building can be obtained from the empirical relation $T=0.05H^{3/4}$ (Kramer, 2007). Based on this relation, the natural frequency of the ten-story superstructure is equal to $f_0=f_{SDOF}=1.56$ Hz. Length of the column supporting the superstructure was taken as one meter. The SDOF superstructure mass was 20 tons for two micropiles based on plastic analysis. Micropile cap was modeled as a concrete slab with a one meter thickness.

The side and bottom of the model were assigned vertical and horizontal boundaries, respectively. Under static conditions, nodes on vertical boundaries were fixed in the horizontal direction and nodes on the horizontal boundary were fixed in both vertical and horizontal directions. Under Dynamic conditions, these boundaries were removed and absorbent boundaries based on formulation given by Lysmer and

Kuhlemeyer (1969) were employed for vertical boundaries, while bedrock was assumed to exist at the horizontal boundary.

Acceleration time history of 01/16/1995 Kobe earthquake at Takarazu station, 090 components was used as seismic loading at the base of the model. Figure 3 shows time histories of acceleration, velocity and displacement of Kobe earthquake.

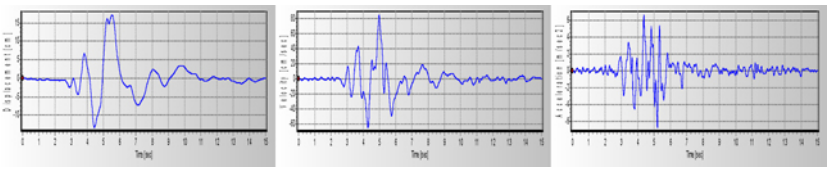

FIG. 3. Time histories of Kobe earthquake.

Rayleigh damping was used to model energy dissipation in the material. Damping ratios of 8% and 2% were used for the FS and the micropile, respectively, the latter of which was decided based on study conducted by Sadek and Shahrour (2004).

DYNAMIC ANALYSIS

Five different batter angles were selected to study the effect of inclination on seismic behaviour of inclined micropiles. Theses angles are 0, 5, 15, 30, 45 and 60 degrees where for $\alpha = 0$ implies a vertical micropile (α is the angle between micropile and the vertical direction). Fig 1 shows an example of finite element model employed to perform dynamic analyses. In each analysis, micropiles were connected fixedly to the cap.

Figure 4a and 4b show the profile of axial force envelopes in micropiles due to seismic loading versus X/L, where X is the distance from micropile head and L is the micropile length. These profiles indicate that maximum axial force at cap-micropile

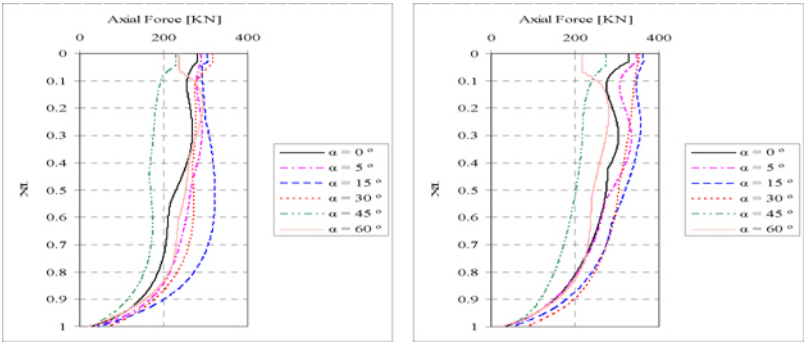

(a) **(b)**

FIG. 4. Envelope of axial force for: a) left micropile, b) right micropile

connection level is larger in inclined micropiles than vertical micropiles. This is also depicted in the figures which show that increasing the batter angle up to 30 degrees results in a decrease in axial force. This observation may be attributed to diminishing of the column-like behaviour of micropiles.

Profiles of shear force envelopes in micropiles under earthquake loading are shown in figures 5a and 5b. These profiles show that increasing the batter angle up to 30 degrees decreases maximum shear forces in micropiles. For batter angles of 45 and 60 degrees, shear force increased severely. A significant point in these two graphs is that shear force in depth X/L>0.5 reaches a constant value equal to 5% of maximum shear force at cap level. Shear forces increase intensively along the micropile for X/L values below 0.2.

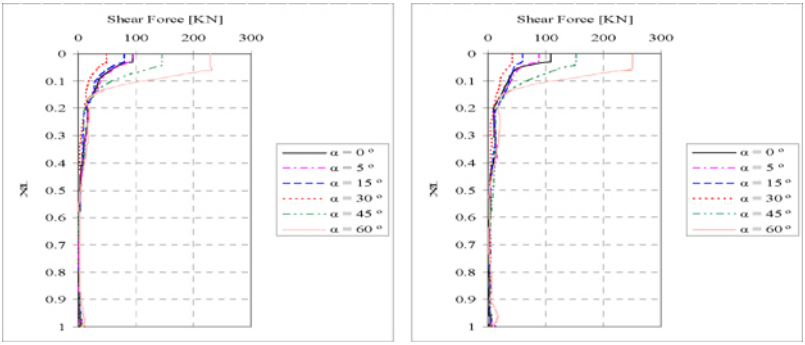

(a) **(b)**

FIG. 5. Envelope of Shear force for: a) left micropile b) right micropile.

Envelopes of bending moment along micropile under seismic loading are given in figures 6a and 6b. The occurrence of maximum bending moment and maximum shear force at micropile-cap connection level indicates that inertial forces have noticeable effect on seismic response of micropiles. Varying the batter angle from 30 degrees to 45 degrees increases the maximum bending moment by a factor of 2.5, and at a batter angle of 60 degrees, the increase factor reaches value of 5. This raise may be caused by change in micropile behaviour in higher inclination angles where micropiles operate as a bending beam and not as mere axial force elements. It can be seen that bending moment at micropile tip is almost zero in all cases. It means that there is no fixity at micropile tip in FS.

Results of the parametric analysis may be better interpreted if the significant parameters are plotted against different batter angles, as in figures 7.a, 7.b and 7.c. The aforementioned trends are better shown in these figures. It may be suggested from these figures that the optimum batter angle for design in seismic zones should be in the range of 30 degrees.

The maximum horizontal cap acceleration response for inclined micropiles is smaller than vertical one. By increasing the batter angle, maximum acceleration response decreases (Figures 8a and 8b).

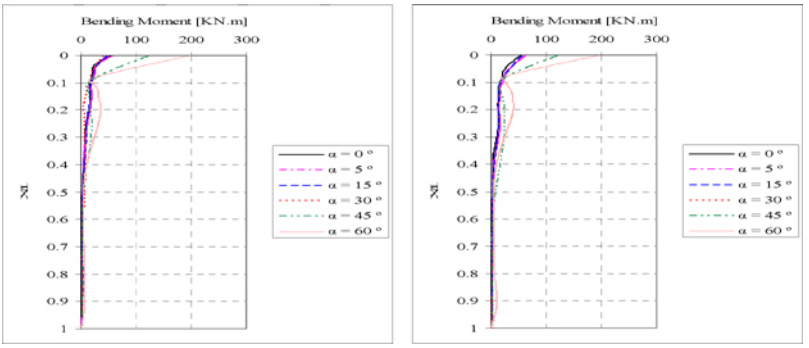

(a) (b)

FIG. 6. Envelope of bending moment for: a) left micropile, b) right micropile.

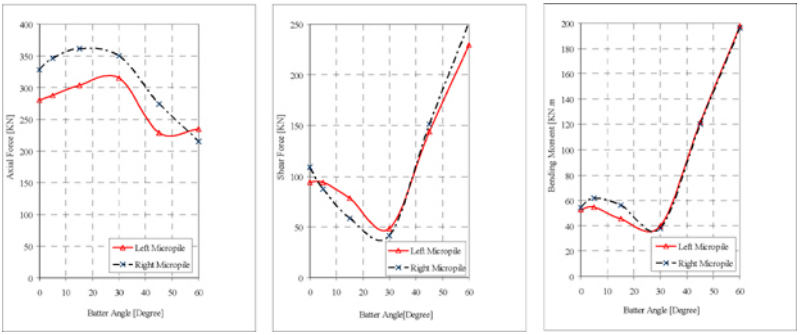

(a) (b) (c)

FIG. 7. Maximum of internal forces in different batter angles.

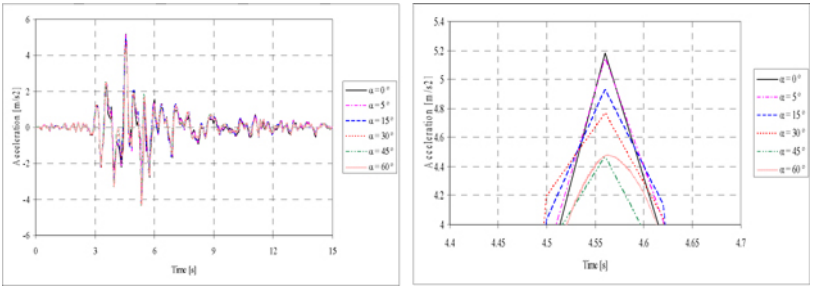

(a) (b)

FIG. 8. a) Time history of horizontal cap acceleration reponse, b) The maximum horizontal cap acceleration response.

CONCLUSIONS

This paper provides useful information about seismic behaviour of inclined micropiles. The results show that inclined micropiles have good performance under seismic loading. However both shearing forces and bending moment increased severely in large batter angles. As a result of this study, the optimum batter angle for micropile construction in seismic zones is in the range of 30 degrees. Superstructure presence has an important effect on the seismic response of micropiles, and leads to maximum internal forces occurring near the ground surface.

REFERENCES

Anandarajah, A. (2000). "Fully-coupled analysis of a single pile founded in liquefiable sands." *Proceedings of Sessions of Geo-Denver 2000 – Computer Simulation of Earthquake Effects, Geotechnical Special Publication.* No.110, ASCE:117- 131.

Astenbroich, H. (2001). "Micropile reinforcement systems and corrosion protection." *Presented at the ADSC Micropile Seminar,Charlotte NC,November 2001.*

Bruce,D.A., Ingle,J.L. and Jones,M.R. (1985). "Recent examples of underpinning using minipiles." *Proceeding of 2nd International Conference on Structural Faults and Repairs, London,* April 30 - May 2: 13-28.

Dano, C., Hicher, P.Y. and Tailliez, S. (2004). "Engineering properties of grouted sands."*Geotechnical and Geoenviromental Engineering.* March,ASCE: 328-338.

FHWA, (2000)."Micropile design and construction guidelines." *US department of transportation, Federal Highway Administration, priority technologies program, implementational manual*: SA-97-070.FHWA.

Kramer, S.L. (2007). "Geotechnical earthquake engineering." ISBN. B1317 07180 . A.C.E. International publication.

Lysmer, J. and Kuhlmeyer, R.L. (1969). "Finite dynamic model for infinite media." *Journal of the Engneering Mechanics.*Div, ASCE:859-877.

Neves, M., Mestat, Ph., Frank, R. and Degny, E. (2001). "Research on the behavior of bored piles II. Finite element modeling."BL-231-055-GB.

Omine, K., Ochiai, H. and Bolton, M.D. (1999). "Homogenization method for numerical analysis of improved ground with cement-treated columns." *Proceedings of the International Conference on Dry Mix Methods for Deep Soil Stabilization,* ISBN 9058091082:161-168.

Sadek, M. and Shahrour, I. (2004). "Three–dimensional finite element analysis of the seismic behavior of inclined micropiles." *Soil Dynamics And Earthquake Engineering* 24:473-485.

Sivakumar Babu, G.L., Srinivasa Murthy, B.R., Murthy, D.S.N. and Nataraj, M.S. (2004). "Bearing capacity improvement using micropiles a case study." ,*Geotechnical Special Publication* 124,ASCE,692-699.

Wehnert, M. and Vermeer, P.A. (2004). "Numerical analysis of load tests on bored piles." *Proceeding of NUMOG9th*.Ottawa, Canada:1-6

Copyrighted Materials
Copyright © 2009 American Society of Civil Engineers (ASCE)
Retrieved from www.knovel.com

Design, Testing and Automated Monitoring of ACIP Piles in Residual Soils

Stephen W. Lacz[1], M. ASCE, P.E. and Richard C. Wells[2], F. ASCE, P.E.

[1]Senior Professional, Trigon|Kleinfelder, Inc., 313 Gallimore Dairy Road, Greensboro, NC 27409; slacz@kleinfelder.com
[2]Vice President Corporate Development, Trigon|Kleinfelder, Inc., 313 Gallimore Dairy Road, Greensboro, NC 27409; rwells@kleinfelder.com

ABSTRACT: The new FedEx Mid-Atlantic Hub Sort/Truck Building contains an automated network of scanners and conveyors, moving the packages for mainly air to air transfer. Original site topography included a significant drainage feature and pond transecting the site directly below the proposed structure. Deep structural soil fill depths up to 18.3 m (60 feet) were placed by the grading contractor to level the site prior to property transfer.

Due to the variable subsurface profile, including deep alluvial soils and depth to partially weathered rock, groundwater elevation, economics and an accelerated construction schedule, augered cast-in-place (ACIP) piles were selected. The 406.4 mm (16 inch) diameter ACIP piles were designed using an allowable load of 889.6 kN (100 tons) each, bearing in partially weathered rock. A load test program consisting of two compression tests and three tensile tests was performed to confirm the design parameters.

As part of the Quality Control Program and due to the subsurface variability, all of the piles installed on site were monitored using an automated monitoring equipment (AME) system to measure the drilling and grouting parameters. The benefit of this system included efficient drilling, operator confidence and not drilling "blind" between borings.

Careful consideration of the subsurface profile, structure performance criteria and deep foundation system design, load testing and installation, combined with good design team communication, resulted in the successful execution of this phase of the project.

INTRODUCTION

The Federal Express Mid-Atlantic Hub is located on the northeast side of Piedmont Triad International Airport (PTIA) in Greensboro, North Carolina. The hub will be

capable of sorting 24,000 packages per hour and be served by 20-25 aircraft each weekday. The site for the FedEx facility encompasses approximately 68.8 hectares (170 acres) and includes various buildings for sorting, trucking and support. Adjacent to and surrounding these buildings are aircraft apron areas, parking, and access drives for on-site traffic.

The heart of the facility is the Sort/Truck Building encompassing approximately 28,465 square meters (306,400 square feet) in the planned area, with maximum building dimensions of approximately 155.4 m (510 feet) by 192.0 m (630 feet) and a height of 18.3 m (60 feet). Maximum column loads were estimated at 4114.6 kN (925 kips) in compression, 667.2 kN (150 kips) in uplift and 200.2 kN (45 kips) in shear during the design phase.

Floor loading was anticipated to be moderate to heavy, with floor loads of approximately 23.9 kPa (500 pounds per square foot). To reduce the settlement potential of the newly placed structural fill, future floor slabs and sorting equipment, the Sort/Truck Building area was surcharged using a minimum 38.3 kPa (800 psf) load as shown in Figure 1. Monitoring of the settlement was performed by others using settlement hubs. Between 20.3 mm (0.8 inches) to 152.4 mm (6.0 inches) of settlement was recorded in the monitoring program. This range indicates the amount of significant differential settlement across the building site that would have occurred under an equivalent loading condition similar to the surcharge loading.

FIG. 1. Surcharge loading of the Sort/Truck Building area

GEOLOGY AND SUBSURFACE CONDITIONS

The site is located in the Carolina Slate Belt of the Piedmont Physiographic Province of North Carolina. The parent bedrock underlying the property generally consists of well-foliated metamorphosed granitic parent bedrock. The on-site residual soils are the product of the in-place weathering of the parent bedrock. The subsurface conditions at the site generally consisted of soil fill, alluvial, residual soils and partially weathered rock.

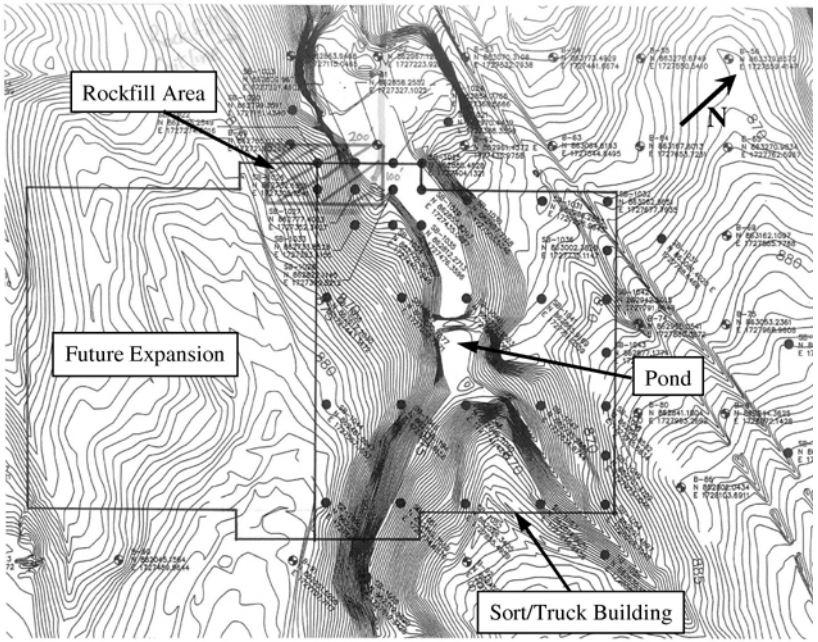

FIG. 2. Original Site Topography

Prior to current grading activities, the site contained open areas with grass and weed ground cover, as well as wooded areas. The northern portion of the site generally sloped downward from the south towards the north. Several drainage features were located in this portion of the site, some of which contained wetland areas. Spring activity was likely present in the drainage features, as evidenced by standing water and numerous wetland areas. A small pond and dam was present in an area located below the proposed Sort/Truck building. French drains were installed in the drainage features outside of the building areas. The extreme northern portion of the site was bordered by a large wetland area. Elevations across the site ranged from a high of approximately 275.8 m (905 feet) to a low of approximately 243.8 m (800 feet) at the wetland areas located in the northern portion of the site. Cut and fill depths on the order of 7.6 m (25 feet) and 18.3 m (60 feet), respectively, were required to bring the

site to the proposed subgrade elevation of 265.7 m (871.8 feet) prior to property transfer from PTIA to FedEx. Several deep fill areas on site contained 50.8 mm (2 foot) thick zones of rockfill, as permitted by the site grading contract. At the time of the subsurface investigation, groundwater was observed at depths ranging between 4.6 m to 13.6 m (15.0 to 44.6 feet) below the existing ground surface. The original site topography and location of the Sort/Truck Building, future expansion and rock fill area are shown in Figure 2.

FOUNDATION RECOMMENDATIONS

Based on the proposed column loads and sorting equipment settlement criteria, several deep foundation systems were considered for support of the Sort/Truck structure including auger cast piles, H-piles, pipe piles, drilled shafts and precast concrete piles. The majority of these methods were removed from consideration due to the variable bearing material elevation, groundwater elevation or inapplicability for the project conditions. Auger pressure grouted displacement (APGD) piles were initially considered due to the limited amount of spoils generated but were not deemed practical for the entire foundation area due to dense layers (greater than 25 bpf) in the subsurface soils. Ultimately, 406.4 mm (16 inch) diameter auger cast piles bearing on partially weathered rock, with a 889.6 kN (100 ton) allowable design capacity, were recommended due their ease in handling variations in the subsurface conditions and project schedule.

INSTALLATION MONITORING

The use of automated monitoring equipment (AME) during the installation process was utilized for the load test program and the productions piles. Berkel and Company Contractors, the auger cast pile contractor for the project, selected the PIR-A pile installation recorder, manufactured and installed by Pile Dynamics, Inc., The parameters measured by the PIR-A included time, depth and hydraulic pressure during drilling and time, depth, grout volume and grout pressure during grouting. Components of the AME included a display unit (Figure 3), depth sensor, magnetic flow meter (Figure 4), grout pressure sensor, field printer, torque pressure sensor and angle analyzer.

FIG. 3. Control unit mounted inside the crane cab

FIG. 4. Magnetic flow meter mounted inline on the crane

As this was the first time an AME was used by the project team, conventional auger cast pile observations were performed including shaft diameter, drilling procedures, eccentricity, plumbness, bearing materials, grout usage, and grout procedures.

TEST PILE PROGRAM

In order to confirm the design parameter and capacity, two static load tests (TP-1 and TP-2) and three tension load tests (TP-3, TP-4 and TP-5) were performed for the project at select boring locations. TP-1 was 19.8 m (65 feet) long and was located in the former pond, an area with deep fills underlain by alluvial, residual soils and weathered rock. TP-2 was 16.8 m (55 feet) long and installed in a shallow fill zone. TP-3 and TP-4 were both 12.2 m (40 feet) long and installed in areas of residual soils and moderate fill depths underlain by partially weathered rock, respectively. TP-5 was also installed in the former pond area to a depth of 18.3 m (60 feet).

The compression test piles were load tested in general accordance with ASTM D-1143, with a final test load of 200 percent of the 889.6 kN (100 ton) design load or 1,779.2 kN (200 tons). After unloading, the test pile was loaded to 2,668.8 kN (300 tons) or 300 percent of the design load. The tension test piles were load tested in general accordance with ASTM D-3689, with a final test load of 200 percent of the 400.3 kN (45 ton) design load or 800.6 kN (90 tons). The compression and tension load test setups are shown in Figure 5 and Figure 6.

All test piles were installed using the equipment proposed for the production piles (Figure 7). This included a crawler mounted crane with 27.4 m (90 feet) of auger, a 2,268 kg (5,000 pound) gear box capable of 50.14 kNm (36,985 ft-lbs) of torque and a Reinert P-3 grout pump with a pumping capacity of up to 30.4 cubic meters per hour (40 cubic yards per hour).

FIG. 5. Compression Load Test at TP-1

FIG. 6. Tension Load Test at TP-4

A secondary function of the load test program was to calibrate the automated monitoring system with the subsurface conditions. This was planned by having each of the test piles installed in close proximity to a soil test boring performed during the subsurface investigation phase of the project. This allowed for the correlation of the recorded PIR-A parameters to the subsurface conditions with respect to the top of partially weathered rock. As a result, the penetration rate and gear box pressure (torque) were used, in part, as production pile installation criteria for determination of auger penetration into the required bearing material.

FIG. 7. Test Pile and Production Pile Installation

PRODUCTION PILE INSTALLATION

Using the information gathered during the load test program, and the installation criteria correlated by the PIR-A parameters, a total of 821 auger cast piles were successfully installed from October 25, 2006 to December 4, 2006. Pile lengths ranged between 14.6 m (48 feet) to 23.6 m (77.5 feet) below grade.

The installation of the piles progressed steadily and ahead of schedule with the exception of one anomaly. Although the majority of the existing rockfill was understood to be undercut and backfilled prior to pile installation, several pile locations still encountered large shot rock fragments that required excavation. Good communication and coordination between the parties was essential to working around this issue.

CONCLUSIONS

Careful consideration of the subsurface profile, structure performance criteria and deep foundation system design, load testing and installation, combined with good design team communication, resulted in an economical solution and the successful execution of this phase of the project (Figure 8). It is the opinion of the author that using the automated monitoring equipment allowed for an efficient, confident installation by giving the operator real time feedback while drilling in these variable Piedmont subsurface conditions. Use of the AME, and essentially not drilling "blind" between boring locations, also gave the contractor and design team added assurance that the completed auger cast piles were installed to the required specifications.

FIG. 8. View of the Sort/Truck Building nearing completion

ACKNOWLEDGEMENTS

The authors would like to thank the following members of the design and construction team involved with the auger cast pile installation: FedEx, Frankfurt Short Bruza/Texas, Rentenbach, Kajima and Berkel and Company Contractors. A special thanks to Mr. Xavier Barrett, P.E., Mr. Thomas Wells, E.I., and Mr. Nazeer Brifkani, E.I. for their assistance during the load test program and production pile installation.

REFERENCES

ASTM D-1143 (1994), "Standard Test Method for Piles Under Static Axial Compressive Load", ASTM International, West Conshohocken, PA.

ASTM D-3689 (1995), "Standard Test Method for Piles Under Static Axial Tensile Load", ASTM International, West Conshohocken, PA.

Deep Foundations Institute (2003), *Augered Cast-in-Place Manual*, Third edition.

NeSmith, W.M (2006), Personal communication.

Copyrighted Materials
Copyright © 2009 American Society of Civil Engineers (ASCE)
Retrieved from www.knovel.com

Load Displacement Behavior of ACIP Piles in Cohesive Soils

C. Vipulanandan[1], Kalaiarasi Vembu[2] and Tracy Brettmann[3]

[1]Chairman, Professor, Director of Center for Innovative Grouting Materials and Technology (CIGMAT), and Director of Texas hurricane Center for Innovative Technology, Department of Civil and Environmental Engineering, University of Houston, Houston, Texas 77204-4003; cvipulanandan@uh.edu
[2]Graduate Student, Center for Innovative Grouting Materials and Technology (CIGMAT), University of Houston, Houston, Texas 77204-4003; kvembu@mail.uh.edu
[3]Regional Manager, Berkel & Company Contractors, Richmond, Texas; tbrettmann@berkelapg.com

ABSTRACT: In order to better quantify the performance of ACIP piles in cohesive soil the load-displacement behavior of ACIP pile at the NGES-UH was investigated. A database of ten other full-scale ACIP piles in cohesive soil with diameters ranging from 406 to 457 mm and lengths varying from 9.7 to 28 m was also investigated. The measured pile capacities varied from 898 to 3648 kN (100 to 410 tons). A non-dimensional hyperbolic relationship was used to verify the non linear load-displacement behavior of full scale load test data of eleven ACIP piles in cohesive soils in Texas. For the ACIP piles in cohesive soils, 50% of the ultimate load was achieved in the displacement range of 0.3% to 2% of the diameter. The ultimate capacity of the piles was determined using the hyperbolic relationship. The load transfer behavior of ACIP pile in cohesive soil was also studied.

INTRODUCTION

Augered cast-in-place (ACIP) piles are drilled foundation in which the pile is drilled to depth in one continuous process using a continuous flight auger. The equipments and techniques of ACIP piles have evolved in the 1940s (Neate, 1988). These piles have been used in the private sector in the United States for over 50 years (O'Neill, 1994) and became very popular in the early 1990's because of the developments in the construction quality control systems. In buildings and bridges displacement of piles under loading is important criteria, and hence it is important to determine the load-displacement relationship for the piles (Vipulanandan et al., 2005). But most of the load tests are performed to a load twice or thrice of the design load and not to the complete failure of the pile. Ultimate capacity criteria such as load at 5% or 10% of diameter of pile or Davisson's criterion (Davisson, 1972) are used to predict the ultimate capacity of the pile. Hence it is necessary to develop the representative models for load-displacement relationships for ACIP piles. In general

non-displacement piles carry most of the applied load by shaft friction under the working load and design load and the magnitude of the skin friction depends on the soil type, construction method and the loading type. In this paper the load-displacement and load transfer behavior of an instrumented pile in National Geotechnical Experimentation Site at the University of Houston was studied. The load-displacement behavior of full scale load tests was verified with a non-dimensional hyperbolic relationship.

OBJECTIVE

The overall objective of this study was to investigate and model the load-displacement relationship for ACIP piles in cohesive soil.

NGES-UH

The site was located in National Geotechnical Experimentation Site at the University of Houston (NGES-UH), which consists of a clay soil profile. The clay has been preconsolidated. It is a microdelta depositional site of Pleistocene age within the Beaumont formation. The test pile layout is shown in Fig. 1. A soil boring log is shown in Fig 2. N_{TXDOT}, N_{SPT}, undrained shear strength s_u, and soil classification are listed on the log. The ground water was encountered at a depth of 2.1 m (7 ft) below the existing ground surface after completion of the boring. The length and diameter of the pile was 15.2 m (50ft) and 0.457 m (18 in.) respectively. The length and diameter of the reaction piles were 12.2 m (40 ft) and 0.457 m (18 in.). A PIR (Pile Installation Recorder) was used to monitor the installation of the CFA piles. The grout volume ratio exceeded 1.0 except from depths 0.6 m to 4.2 m, where the grout volume ratio is slightly less than 1.0. The low grout take ratios near the top of the test pile were probably caused by the fact that grout was observed returning to the surface through the auger flights when the auger

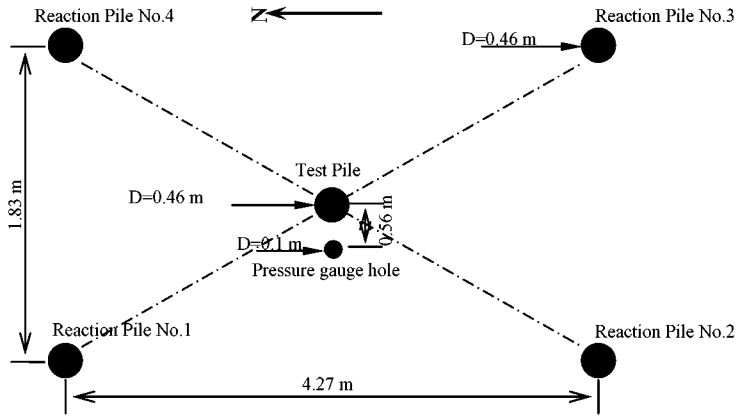

Figure 1 Layout of the Test Pile and Reaction Pile.

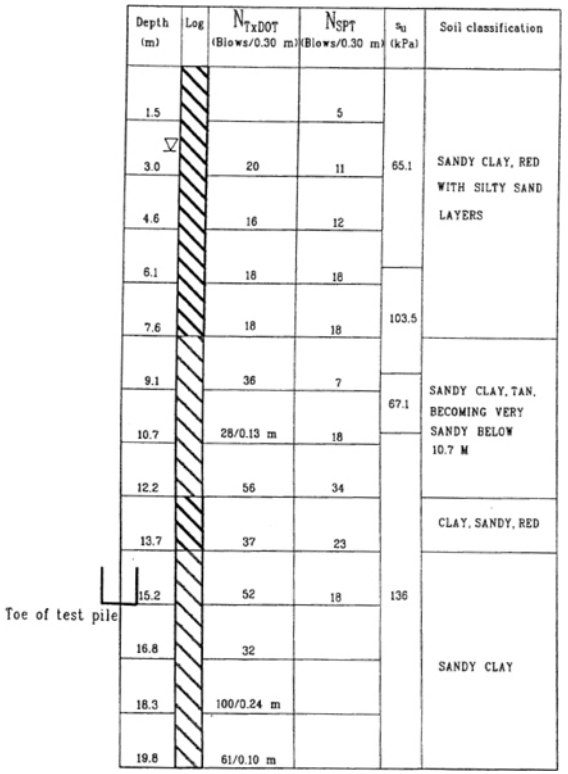

Figure 2 Boring Log for the UH Test Site

tip was at a depth of about 4.6 m (15 ft). The test pile was instrumented by using eight vibrating wire sister bars at four levels. The vibrating wire sister bars measure strains in a member by measuring the change in the frequency of a tensioned piano wire clamped in a fixture securely attached to the member.

Load-Deformation Behavior

The full-scale axial load test was performed by jacking the test pile against reaction beams anchored by four piles using a pneumatically powered jacking system. The jacking system consists of a hydraulic jack and an electronic load cell. Two dial gauges attached on the top of the pile were used to measure the axial settlement of the pile. The tests were conducted according to the Texas Quick Load Test Method, in which small increments of load are added every three minutes monotonically until failure occurs. The pile was loaded in 178 kN (20 tons) increments till the failure. The maximum deflection measured was 50 mm (2 in.) at the final load of 1660 kN (187 tons). The pile was unloaded in 534 kN (60 tons) increments until the load is zero.

The load settlement curve of the test pile is as shown in Fig. 3. The ultimate capacity of pile was estimated as 1666 kN based on the hyperbolic approach (Vipulanandan et al. 2005).

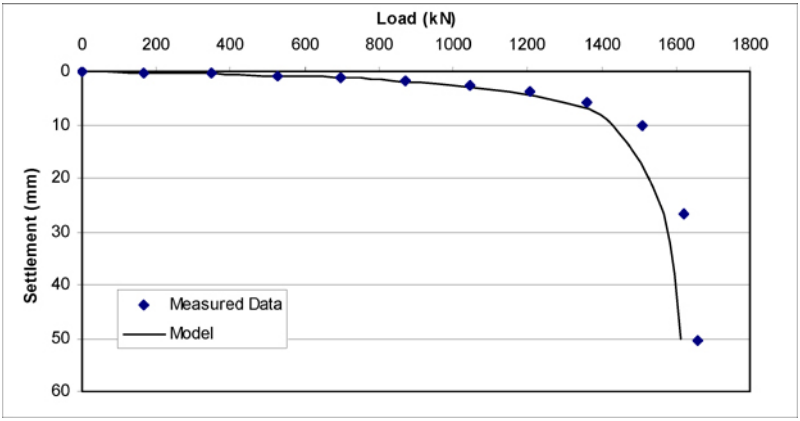

Figure 3 Load-Settlement Relationship for the Test Pile

Figure 4 shows the load distribution along the length of the pile which was calculated from the strain measured with the sister bars. Measured strains from the sister bars were converted into loads by multiplying with the axial rigidity which was back calculated using the measured data at the top of the test pile. Axial rigidity was assumed to be constant all along the length of the test pile. The averge unit side resistance and toe resistance was calculated from the load distribution of the pile and were 69 kPa and 232 kPa respectively. The percentage ratio of toe resistance to side resistance at the final load was 10% whereas the ratio was 2.3% at 50% of the failure load. Hence the pile carried most of the applied load by shaft resistance and the percentage contribution of the toe resistance increased close to the failure load.

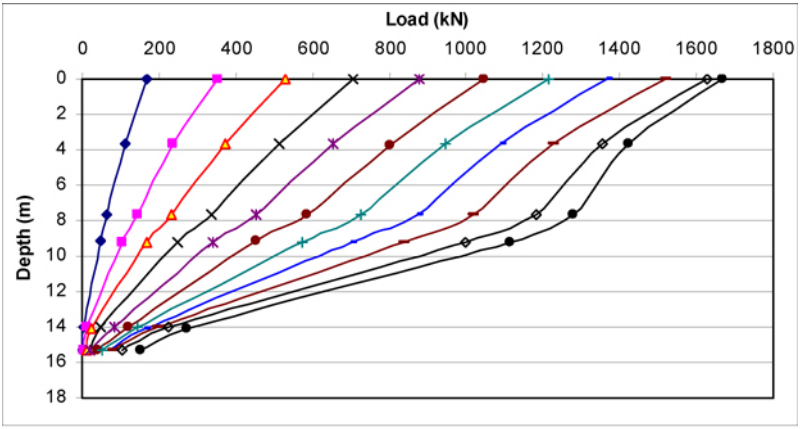

Figure 4 Load Distribution Along the Test Pile

LOAD TEST DATABASE

A total of ten load tests, on ACIP piles in cohesive soil in Texas were studied. Load tests were performed using conventional static loading system in accordance with ASTM D1143, "Quick Load Test Method for individual piles". The displacement of pile head was measured with at least three dial gages supported on reference beam. Characterization of overburden soil in original boring log has been reported in terms of Pocket Penetrometer (PP) values or SPT (N blows / 300 mm). General information on all ten load test sites are as follows:

Case 1: This site was located McAllen, Texas and the ACIP pile was used to support an office building. The length and diameter of the pile was 13.7 m (45 ft) and 0.406 m (16 in.) respectively (Table 1). The pile was supported on hard clay with SPT N value above 50. The pile was loaded to twice the design load.

Case 2 & 3: This site was located in Kemah, Texas and the ACIP piles were used to support the parking garage. Two piles were tested and the lengths of the piles tested was 18.3 m (60 ft) and 21.3 (70 ft) and the diameter of the pile was 0.406 m (16 in.) (Table 1). The piles were tested till failure based on the Davisson's criteria.

Case 4 & 5: The site was located in Freeport, Texas and the ACIP piles were used to support an office building. Two piles were tested and the lengths of the piles tested were 9.2 m (30.3 ft) and 16.4 m (54 ft) (Table 1) and the diameter of the pile was 0.406 m (16 in.). The piles were supported on stiff clay. One of the piles was tested till failure based on the Davisson's criteria.

Case 6: The site was located in Bryan, Texas and the ACIP pile was used to support a water tank. The length and diameter of the pile was 15.2 m (50 ft) and 0.457 m (18 in.) (Table 1). The pile was supported on very stiff clay.

Case 7: The site was located in Houston, Texas and the ACIP pile was used to support a parking garage. The length and diameter (Table 1) of the pile was 28.3 m (93 ft) and 0.457 m (18 in.) respectively. The pile was supported on fat clay. The pile was loaded till failure and at the maximum load of 3380 kN.

Case 8 & 9: The site was located in Houston, Texas and the ACIP pile was used to support a multistory tower. Two piles were tested and the length and diameter (Table 1) of the pile was 22.9 m (75 ft) and 0.457 m (18 in.) respectively. The piles were supported on very stiff fat clay.

Case 10: The site was located in Houston, Texas and the ACIP pile was used to support a conference center. The length and diameter (Table 1) of the pile was 24.4 m (80 ft) and 0.457 m (18 in.) respectively. The pile was supported on very stiff to hard clay.

Table 1. Load Test Results for ACIP Piles in Cohesive Soil

Case No.	Location	Length (m) (ft)	Diameter (mm) (in.)	Max. Load* (kN) (tons)	Max. Displacement % D
1	McAllen, TX	13.7(45)	406 (16)	2135 (240)	4.12
2	Kemah, TX	18.3 (60)	406 (16)	1423 (160)	4.69
3	Kemah, TX	21.3 (70)	406 (16)	1779 (200)	6.37
4	Freeport, TX	9.2 (30.3)	406 (16)	898 (101)	7
5	Freeport, TX	16.4 (54)	406 (16)	1000 (112.5)	1.81
6	Bryan, TX	15.2 (50)	457 (18)	2648 (298)	6.98
7	Houston, TX	28.3 (93)	457 (18)	3380 (380)	5.55
8	Houston, TX	22.9 (75)	457 (18)	2891 (325)	5.65
9	Houston, TX	22.9 (75)	457 (18)	3202 (360)	7.11
10	Houston, TX	24.4 (80)	457 (18)	3648 (410)	4.52
Range		9.2-28.3 m	406-457 mm	898-3648 kN	1.81% - 7.11% of D

*** Maximum load reached in that load test, not actual maximum.**

ANALYSIS AND DISCUSSIONS

Ultimate Capacity

One mathematical relationship that will satisfy the ACIP pile behavior is the two parameter hyperbolic equation (Vipulanandan et al 2005) which can be represented as follows:

$$Q = \frac{\rho}{A + B\rho} \tag{1}$$

By rearranging the Eqn. (1) to represent a linear relationship as follows:

$$\rho / Q = A + B\,\rho \tag{2}$$

All the pile test data were verified by the linear relationship (Eqn. (2)) within an acceptable limit (high coefficient of correlation). The agreement was very good. Parameter B was obtained from the linear relationship for further analyses. When the displacement becomes large the pile capacity reaches its theoretical maximum (Q_{ult}) and it will be related to parameter B as follows:

$$Q_{ult} = 1/B \tag{3}$$

The ultimate capacity for each case was determined and the $Q_{measured}$ to Q_{ult} ratio varied from 0.76 to 0.98.

Load-Displacement Relationship

As summarized in Table 1, five of the load tests were performed to a displacement of less than 5% of diameter and hence a model should be used to best estimate the ultimate capacity of the piles at appropriate deflection. Vipulanandan et al., (2005) have used the non-dimensional hyperbolic relationship to predict the load-displacement behavior of ACIP piles in soils. The non-dimensional form of hyperbolic relationship is given by

$$\frac{Q}{Q_{ult}} = \frac{\rho/d}{\rho_{50}/d + \rho/d} \tag{4}$$

Where, ρ_{50}/d is the displacement to diameter ratio for Q/Q_{ult} ratio of 0.5. The ratio ρ_{50}/d for ten ACIP piles, except for one, varied from 0.3% to 2% as shown in Fig. 5. The ratio ρ_{50}/d for NGES-UH test pile was 0.36%. Earlier study showed that the ratio ρ_{50}/d varied from 0.35 to 1.5% (Vipulanandan et al, 2005).

CONCLUSIONS

Based on the NGES-UH load test and ten full-scale load tests in cohesive soils following can be concluded

1. For the ACIP pile in cohesive soil, most of the applied load was carried by the side friction. The contribution of the toe resistance increased near the failure load to about 10% of the side resistance. The unit side friction and unit end bearing were 69 kPa and 232 kPa respectively.
2. The load-displacement behavior of ACIP piles was represented by the non-dimensional hyperbolic relationship.
3. The ratio of ρ_{50}/d varied from 0.3% to 2% for most of the ACIP piles in cohesive soils.

ACKNOWLEDGEMENT

This study was supported by the Center for Innovative Grouting Materials and Technology (CIGMAT) with funding from the Texas Department of Transportation. The sponsor is not responsible for any of the conclusions made in this study.

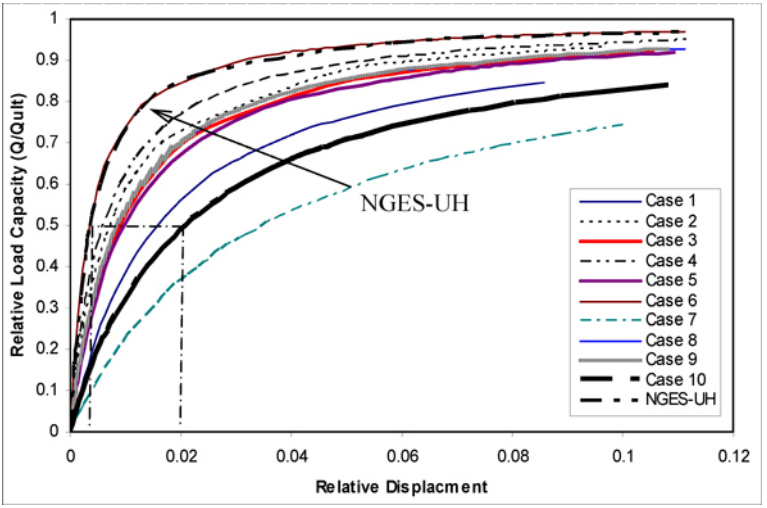

Figure 5 Variation of Relative Displacement and Relative Load Capacity of ACIP Piles

REFERENCES

ASTM D 1143-81 (1987), "Testing Piles Under Static Compressive Load," *ASTM International*, West Conshohocken, PA.

Davisson, MT (1972). "High Capacity Piles", *Proc., Lecture Series Innovations in Fndn. Construction*, ASCE Illinois Section, Chicago, 52 p.

Neate, JJ (1988). "Augered Cast-In-Place Piles", *Proc., 13th Annual Members' Conf., Deep Fndns. Inst.*, Atlanta, 167-175.

Neely, W. J. (1991). "Bearing Capacity of Auger-Cast Piles in Sand", *Jl. of Geotech. Engrg.*, ASCE 117(2), 331-345

O'Neill, M. W. (1994). "Review of Augered Pile Practice Outside the United States," *Transportation Research Record No. 1447*, TRB, Washington D. C, 3-9.

Vipulanandan, C., Tand, K. E. and Kaulgud, S. (2005) "Axial Load-Displacement Relationship and CPT Correlation for ACIP Piles in Texas Gulf Coast Soils", *Proc., Advances in Designing and Testing Deep Foundations, GSP 129*, ASCE Geo Institute, 290-308.

Copyrighted Materials
Copyright © 2009 American Society of Civil Engineers (ASCE)
Retrieved from www.knovel.com

Load Tests On Small Diameter Augered Cast-In-Place Piles Through Fill

W. Ken Beck, P.E., M.ASCE[1] and Patrick J. Harrison, P.E., M.ASCE[2]

Abstract: Due to the presence of a relatively thick layer of miscellaneous and rubble fill overlying low strength alluvial clay, augered cast-in-place (ACIP) piles were recommended for support of the Diamond Jo Casino and City of Dubuque parking ramp. During bidding, a deep foundation contractor proposed a significant cost savings if a reduction in the pile diameters would be considered. A test pile, with the smaller diameter proposed by the contractor, was installed at the Casino site and instrumented with strain gage sister bars to evaluate the side resistance support in the fill and underlying native soils. A similar pile load test program was later performed for the Ramp project. The pile load test results provided side resistance values greater than those used in the static design and allowed the use of the smaller diameter piles proposed by the contractor.

INTRODUCTION

In the late 1600's, the City of Dubuque Iowa became the first permanent European settlement west of the Mississippi River. The Diamond Jo Casino (Casino) and City of Dubuque parking ramp (Ramp) sites are located in previous low-lying areas along the banks of the Mississippi River known as The Port of Dubuque (The Port). Over the years, the low-lying areas were often filled with byproducts of adjacent industries. Fill materials commonly encountered beneath The Port include concrete, leather, metal, foundry sand, cinders, saw dust, wood and other miscellaneous materials.

In the Port, low strength alluvial clay is generally encountered beneath the fill underlain by loose to medium dense sand. Due to the combination of the fill and underlying low strength clay, deep foundations are often used for support of new structures. Since bedrock is about 60 meters (200 feet) below grade, deep foundations are primarily supported through side resistance in the native soils. Driven steel pipe piles, ACIP piles, pressure grouted ACIP piles and Stone Columns have been used for prior projects in The Port.

[1]Senior Principal, Terracon Consultants, Inc. 870 40th Avenue, Bettendorf, Iowa; PH (563) 355-0702, FAX (563) 355-4789; e-mail: wkbeck@terracon.con

[2]Senior Principal; Terracon Consultants, Inc., 135 Ambassador Drive, Naperville, IL 60540; PH (630) 717-4263; FAX (630) 357.9489; e-mail: pjharrison@terracon.com

PROJECT INFORMATION

The Diamond Jo Casino is a two-story (no lower level), steel-frame structure with a plan area of about 6,970 square meters (75,000 square feet). Maximum column and wall loads are on the order of 2,400 kN (540 kips) and 52 kN per linear meter (12 kips per linear foot), respectively.

The post-tensioned concrete Ramp has four stories above grade and shares three common property lines with the Casino (Fig. 1). Maximum column loads are in the range of 4450 to 6670 kN (1,000 to 1,500 kips).

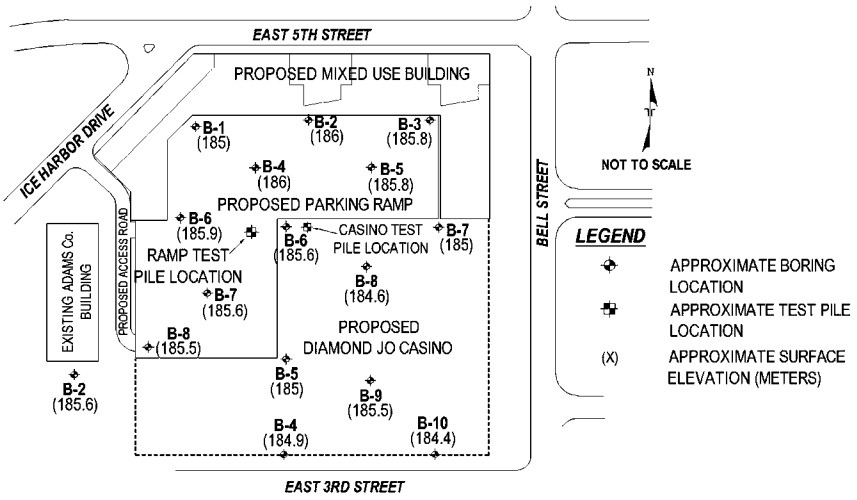

Fig. 1. Site Plan

The borings for the Casino site were performed in November 2006. Miscellaneous fill was present at the boring locations to depths ranging from about 3.6 to 6.1 meters (12 to 20 feet). A soft to stiff consistency alluvial clay layer, varying in thickness from approximately 0 to 6.1 meters (0 to 20 feet), was encountered beneath the fill. Primarily loose to medium dense sand was present beneath the alluvial clay to the termination depth of the borings ranging from about 16.8 to 29 meters (55 to 95 feet).

The field exploration for the Ramp was performed in March 2007. The subsurface conditions observed at the Ramp's boring locations were similar to the Casino site with miscellaneous fill to depths ranging from about 4.6 to 8.2 meters (15 to 27 feet). However, the alluvial clay layer was only present at Borings 1, 6, 7 and 8 located in the west and south ends of the site (Fig. 1). The clay layer at these boring locations extended to depths ranging from approximately 11.3 to 14.3 meters (37 to 47 feet) below grade. Loose to medium dense sand was also present beneath the fill and alluvial clay to the boring termination depths ranging from about 16.8 to 29 meters

(55 to 95 feet). No obvious rubble fill was observed at either the Casino or Ramp boring locations.

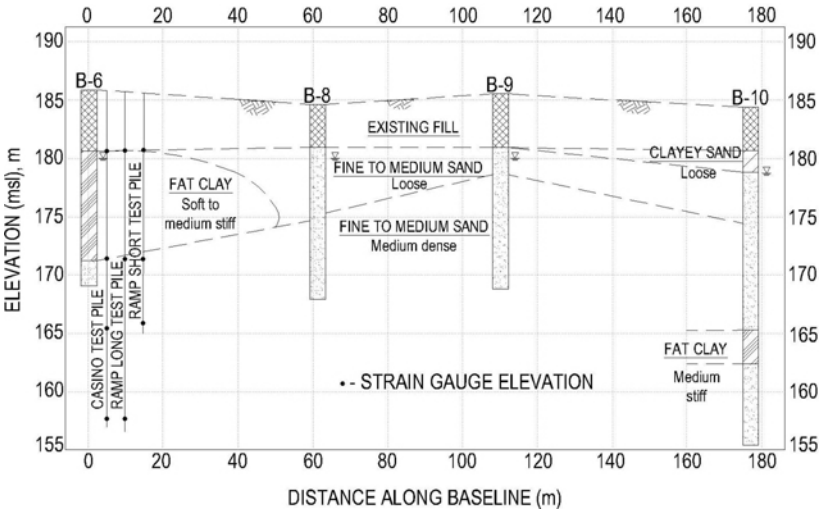

Fig. 2. Subsurface Cross-Section – Casino Site

STATIC PILE DESIGN

ACIP piles have been successfully used for support of previous buildings in The Port. For this reason, ACIP piles were recommended for both the Casino and Ramp projects. Due to the variable composition and thickness of the fill, pile support within the fill was ignored. The allowable soil design parameters provided in Table 1 were used for static pile design and are based on local experience and the methods presented by Reese and Wright (1977) for drilled shafts. The allowable side resistance and end bearing values include factors of safety of 2 and 3, respectively.

The structural engineer for the Casino specified two (2) pile design capacities; 245 and 476 kN (27.5 and 53.5 tons) for a 457-mm (18-inch) diameter ACIP pile. Based on the information in Table No. 1, respective design tip elevations of about 165 and 157 meters (542 and 517 feet) corresponding to lengths of approximately 20 and 27½ meters (65 and 90 feet) were estimated for the required capacities.

For the Ramp, three (3) pile capacities for a 457-mm (18-inch) diameter ACIP pile were specified by the structural engineer; 356, 600 and 712 kN (40, 67½, 80 tons). Using the values in Table No. 1, tip elevations of about 165, 160 and 157 meters (540 feet, 525 feet and 515 feet), corresponding to pile lengths of approximately 18.9, 23.5 and 26.5 meters (62, 77 and 87 feet) were respectively estimated by the structural engineer for the required static design capacities.

Table No. 1 Soil Design Parameters

Soil Description And Elevation	Allowable Side Resistance KPa (psf)		Allowable End Bearing KPa (psf)	
	Casino	Ramp	Casino	Ramp
All Fill	- - -	- - -	- - -	- - -
Clay and Sand Above Elevation 167 m (560 feet)	7 (150)	12 (250)	- - -	- - -
Sand Between Elevation of about 165 to 167 m (540 to 560 feet)	24 (500)	24 (500)	240 (5,000)	240 (5,000)
Sand Between Elevations of about162 to 165 m (530 to 540 feet)	12 (250)	12 (250)	- - -	- - -
Below Elevation of about 162 m (530 feet)	24 (500)	24 (500)	240 (5,000)	407 (8,500)

CASINO PILE LOAD TEST

A deep foundation contractor bidding on the Casino project had recent experience with a nearby project where 309-mm (12-inch) diameter, 27½ meter (90 feet) long ACIP piles were used. The pile load test for that project indicated that a 309-mm (12-inch) diameter should be able to support the Casino's 476 kN (53.5 ton) pile load providing cost savings to the owner. The design team agreed to load test a 309-meter (12-inch) diameter ACIP pile to observe if the 476 kN (53.5 ton) capacity could be supported solely within the native soils beneath the fill. For this reason, the load test had to be designed to measure the side resistance/capacities within the native soils. A total test load of 1334 kN (150 tons) was targeted to account for the required load to be supported within the native soils (two times the design load) and a load of 400 kN (45 tons) that was estimated to be supported by the fill.

When compared to the other borings, it appeared that the subsurface conditions at Boring 6 (Fig. 1) would provide a conservative test pile capacity. The test and reaction piles were installed by the contractor on June 15 and 16, 2007 near the location of Casino Boring 6. The test pile was installed to a depth of about 27½ meters (tip elevation 157 meter, 517 feet). Vibrating wire strain gage sister bars were installed at elevations of about 180.5, 171, 165.5 and 158.5 meters (592, 561, 541 and 520 feet) in the test pile (Fig. 2). The load test was completed on June 29, 2007 in general accordance with the "Quick Test" procedure provided in the "Standard Test Methods for Deep Foundations under Static Axial Compression Load" (ASTM 1143). Load on the pile was measured using a calibrated load cell.

The test pile was loaded to about 1334 kN (150 tons) and about 7.1 mm (0.28 inches) of movement was observed (Fig. 3). In an attempt to reach the ultimate pile capacity, the test load was increased to the capacity of the hydraulic jack and load cell at about 1735 kN (195 tons). At the higher load, 11.4 mm (0.45 inches) of movement was measured (Fig. 3). The strain gage readings (Fig. 4) indicated that the fill was supporting about 623 kN (70 tons), or about 1/3 of the total pile load. Side resistance values obtained for the fill, alluvial clay and sand soils from the strain gage readings

are provided in Table No. 2 and are substantially greater than those estimated for the static design (Table No. 1). Although the ultimate capacity of the test pile was not reached, the load test showed that the native soils could support the design load using the smaller diameter pile with a factor of safety of at least 2. Both the 245 and 476 kN (27.5 tons and 53.5 tons) piles were redesigned with 309-mm (12-inch) diameters.

PARKING RAMP PILE LOAD TEST

The structural engineer for the ramp project included three (3) test piles in the foundation specification package, corresponding to the previously discussed static design capacities. Prior to performing the load tests, the Casino deep foundation contractor proposed a cost savings for reducing the Ramp's ACIP pile diameters. The structural engineer agreed to reduce the 457-mm (18-inch) diameter piles to a 356-mm (14-inch) diameter pile. All three test piles were instrumented with strain gage sister bars at elevations of 181.5 and 171 meters (592 and 561 feet); additional gages were installed at lower pile elevations of 166, 161.5 and 158.5 meters (545, 530 and 520 feet) in the short, intermediate and long test piles, respectively.

Based on the load limitation observed for the Casino load test, a jack and load cell capacity of about 2667 kN (300 tons) was requested for the Ramp tests; however the contractor could only provide the 1735 kN (195 tons) previously used. The long test pile was loaded on September 7, 2007 to about 1646 kN (185 tons), and movement of about 7.6 mm (0.3 inches) was observed (Fig. 3). The side resistance values from the strain gage readings for this test pile are also in Table No. 2. Over 978 kN (110 tons) was supported within the fill. Although the side resistance value for the clay was greater than used for the static design, it was almost half of the value from the Casino pile load test. Similarly, the side resistance value for the underlying sand was significantly less than observed for the Casino test pile. Variations in subsurface conditions may have contributed to a portion of these differences; however, since the fill supported so much of the test load, the test pile did not likely move far enough to develop the magnitude of side resistance observed for the Casino test pile.

The short pile was also loaded on September 7, 2007 to about 756 kN (85 tons) with observed movement of approximately 2.3 mm (0.09 inches) (Fig. 3). This test pile was subsequently loaded to about 1600 kN (180 tons) and about 5.8 mm (0.23 inches) of deflection occurred prior to abrupt movement of the pile. The maximum sustainable load, after the pile's abrupt movement was approximately 1486 kN (167 tons). Prior to abrupt movement, the strain gage readings for this test pile indicated the side resistance values shown in Table No. 2, which were lower than those observed from the Casino load test, but greater than the values used for the static design. It is possible that the abrupt pile movement was due to structural failure of the pile or from the pile breaking away from extraneous grout "tentacles" that penetrated into voids, pipes, etc. within the fill. In either case, the limited movement of the short test pile after abrupt movement likely did not fully mobilize the side resistance within the sand and clay. However, prior to abrupt movement, the short pile supported about 845 kN (145 tons) within the native clay and sand layers (Fig.

4). Therefore the smaller diameter short pile appeared suitable to support the proposed 356 kN (40 ton) design load as well as the intermediate pile load of 600 kN (67½ tons) with a factor of safety of 2. For this reason, the intermediate pile load test was not performed. By using the side resistance value for the sand obtained from the short pile load test, the long pile appeared suitable to support the 712 kN (80 ton) load. The structural engineer redesigned the piles with the smaller diameter.

Table No. 2 Observed Side Resistance Values

Soil Layer	Observed Side Friction, KPa (psf)		
	Casino Pile	Ramp Long Pile	Ramp Short Pile
Fill	145 (3,000)	163 (3,300)	33 (685)
Clay	75 (1,600)	34 (730)	74 (1540)
Sand	90 (1,900)	20 (410)	31 (640)

CONCLUSIONS

Interpretation/evaluation of test piles extending through relatively thick layers of miscellaneous fill can be difficult. Based on our observations during construction, localized voids, buried pipes, large concrete rubble, etc. were present within the fill that were not observed at the boring locations. It is likely that the effective area/diameter of the test piles was greater within the random fill layer than the theoretical diameter. Due to the larger effective size, the fill layer supported a larger portion of the test load than expected and full mobilization of the pile within the underlying native soils could not be obtained to evaluate the ultimate side resistance and end bearing values with the jack and load cell capacity provided by the contractor. To reduce the uncertainty with the random fill layer on future load tests, the fill should be removed and replaced with loose sand at the test pile location. The use of a jack/load cell with a greater capacity would also help to reach full mobilization of future test piles.

Although test piles did not reach their ultimate capacities, the side resistance values from two of the tests were greater than those estimated for static design. Even with local experience and modifications, these pile load tests indicated that the Reese and Wright method for drilled shafts substantially underestimated the side resistance of the on-site low strength clays, and to a lesser extent, the native sands.

References

ASTM D1143-81 (1994), "Standard Test Methods for Deep Foundations under Static Axial Compression Load", American Society for Testing and Materials, Philadelphia, PA

Reese, L.C. and Wright, S.J. (1977), "Construction Procedures and Design for Axial Loading", Vol. 1, Drilled Shaft Manual, HDV-22, Implementation Package 77-21, Implementation Division, U.S. Department of Transportation, McLean, VA, 140 pp

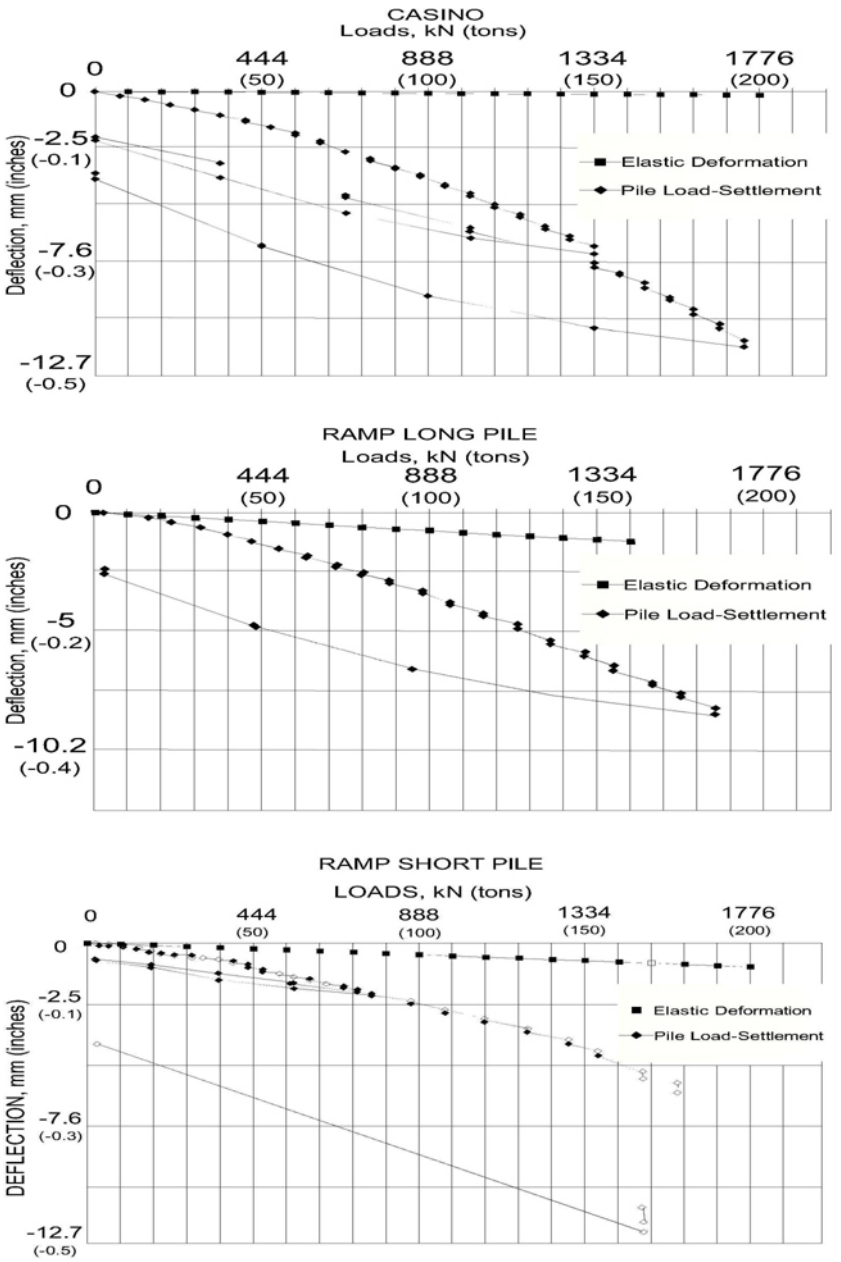

Fig. 3. Load Deflection

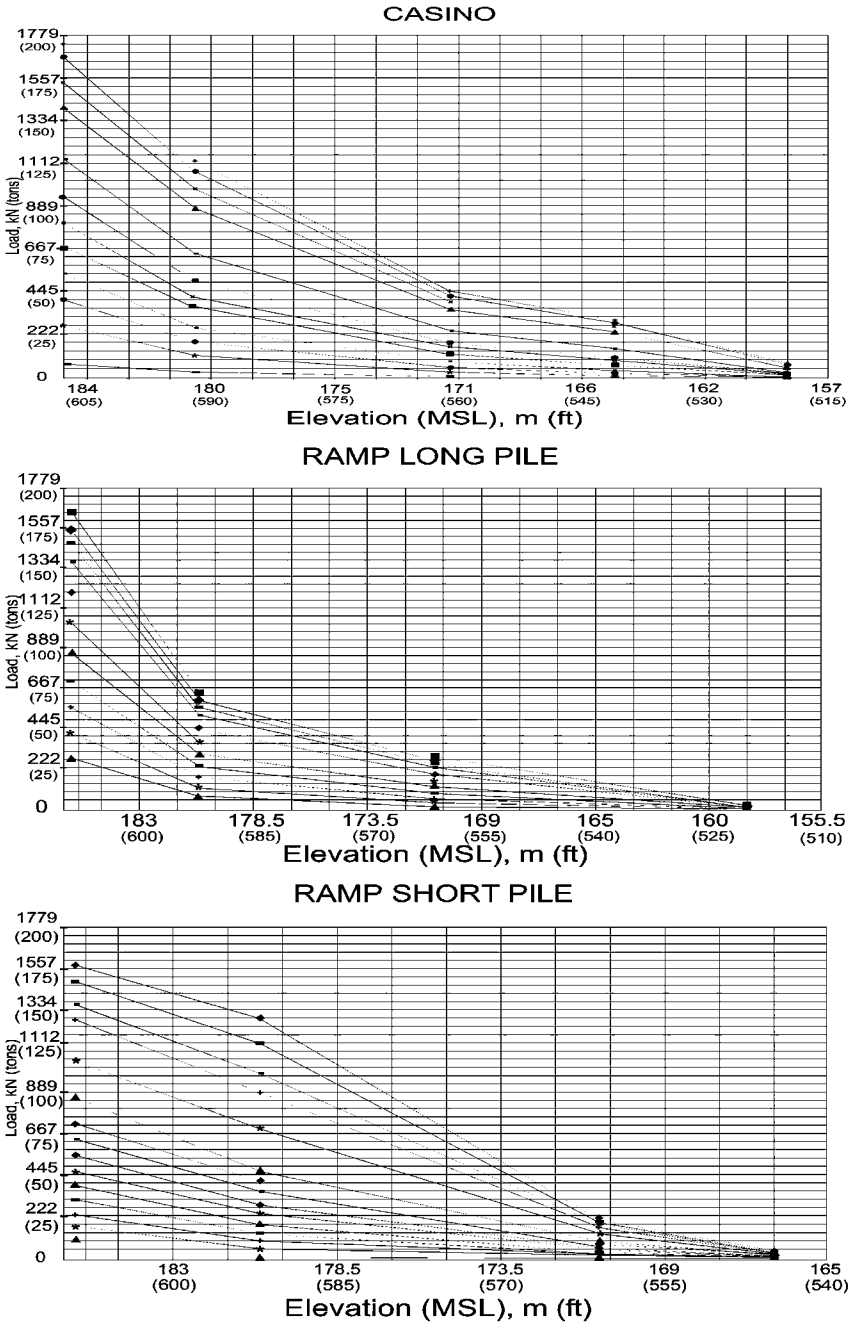

Fig. 4. Strain Gage Readings

Copyrighted Materials
Copyright © 2009 American Society of Civil Engineers (ASCE)
Retrieved from www.knovel.com

Practical Considerations for Design and Installation of Drilled Displacement Piles

W. Morgan NeSmith, PE[1] and J. Fox[2]

[1]Berkel & Company Contractors Inc., 834 Dekalb Avenue - Unit B, Atlanta GA 30307
PH (678) 528-1653, FAX (678) 528-8216; email: morgan_nesmith@comcast.net
[2]Berkel & Company Contractors, Inc., 3702 Rogers Industrial Park Road, Okahumpka FL 34762
PH (352) 365-4308, FAX (352) 365-4360; email: jfox@berkelapg.com

ABSTRACT

A design methodology for the capacity of Drilled Displacement (DD) piles was presented at the International Deep Foundation Congress in 2002. Advances in final design / installation developed since then were incorporated into a DD pile program for two large hotels in Orange County, Florida. The site consisted of granular soils to about 15-m (50-ft) depth underlain by inter-bedded coarse and fine-grained soils. The original design called for 457-mm (18-in) diameter by 29.3-m (96-ft) long conventional auger cast piles. It was estimated that 457-mm (18-in) DD piles installed in the granular materials within the upper 15 m (50 ft) would more efficiently support the proposed loads. The project team elected to utilize DD piles at a substantial cost savings. This paper focuses on one of the two hotel areas. The conditions and construction methods are applicable to both hotel sites.

PROJECT AND IN SITU DETAILS

The project consisted of two hotels with approximate design column loads of (1) Dead Load = 4450 kN (500 ton) to 6005 kN (675 ton) and (2) Live Load = 3115 kN (350 ton). Individual pile design compressive loads were estimated to be 1200 kN (135 ton). A factor of safety of 2 was applied to the design pile loads resulting in a required ultimate compressive load of 2400 kN (270 ton).

In-situ strength data consisted primarily of the results of Cone Penetration Tests (CPT) from a site characterization performed in January 2006. A composite plot of the CPT data in the example hotel area is shown on Figure 1.

DISPLACEMENT PILES – GENERAL METHOD

DD piles are constructed by advancing a displacement auger into the ground utilizing a track-mounted, fixed-mast, hydraulic drilling machine. As the required penetration is achieved, fluid grout is pressure injected through a grout pipe located centrally within the drill stem and out a port located at the tip of the displacement auger as the

displacement auger is slowly retracted. Once the displacement auger is fully retracted, reinforcing steel is inserted into the fluid grout column prior to initial set. The displacement tool and installation platform used for this project are shown in Figure 2. Further details regarding tooling and the installation method are available in NeSmith (2002).

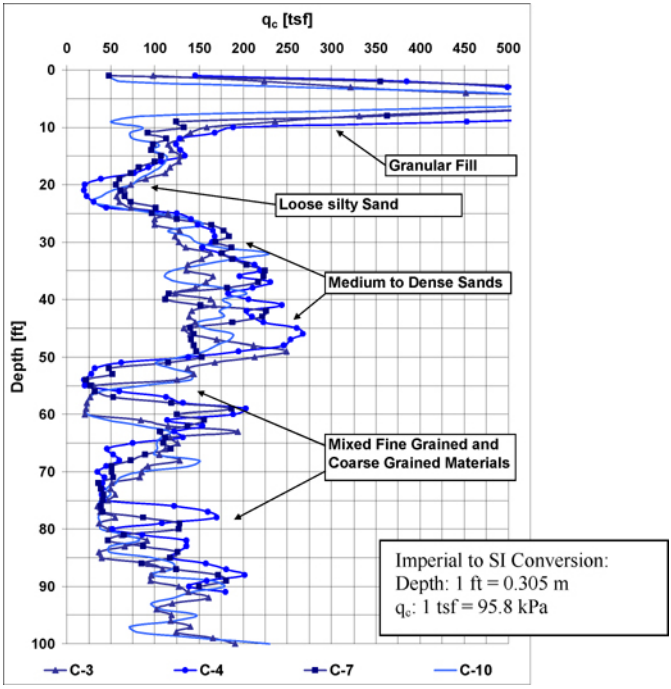

FIG. 1 – Composite CPT Results in Hotel Area

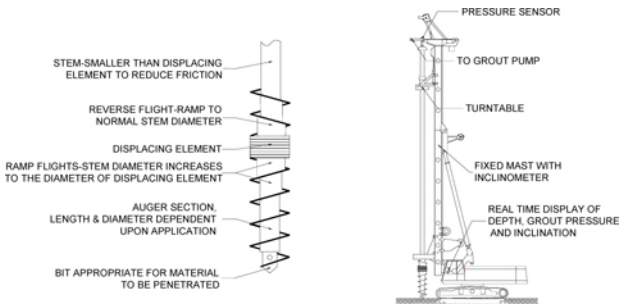

FIG. 2 – Schematic of DD Pile Tool and Installation Platform

ESTIMATION OF PILE RESISTANCE

The methodology for capacity of drilled displacement piles as installed by Berkel has been developed internally and is detailed in NeSmith (2002). Shaft and toe resistances were estimated from CPT tip resistance values with modifiers appropriate for the characteristics of the granular material penetrated. The calculation methodology is summarized in Tables 1 and 2.

Table 1: CPT-based Resistance Analysis Method

SHAFT RESISTANCE $f_{s,cpt} = 0.01 * q_c + w_s$	TOE RESISTANCE $q_{t,cp\,t} = 0.4 * q_{cm} + w_t$
$f_{s,cpt}$ = unit shaft resistance [tsf]; limited to 1.7 for rounded, uniform particles, fines>40%; limited to 2.2 for clean, angular, well-graded particles	$q_{t,cpt}$ = unit toe resistance [tsf]; limited to 75 for dirty, rounded, uniform particles; limited to 90 for clean, angular, well-graded particles
q_c = CPT tip resistance [tsf]; limited to $q_c \leq 200$ tsf	q_{cm} = CPT tip resistance [tsf] from 4 diameters above to 4 diameters below the pile toe; limited to $q_c \leq 200$ tsf
w_s = modifier for fines, angularity and uniformity	w_t = modifier for fines, angularity and uniformity
NOTE: 1 tsf = 95.8 kPa	

Table 2: Values for Resistance Modifiers

Soil Description	w_s	w_t
Rounded, ≥40% passing #200 sieve, Uniform coarse-grained particles	0.0 tsf	0 tsf
Increasingly cleaner, more angular and more well graded	interpolate	interpolate
Angular, ≤10% passing #200 sieve, Well Graded	0.5 tsf	15 tsf
NOTE: 1 tsf = 95.8 kPa		

The CPT results indicated that the predominantly sandy soils in the upper 15 m contained a range of fines quantities from ~ 30 percent to less than 5 percent. Capacity modifiers were selected based on these fines contents and considering the relative roundness and uniformity of the coarse grained materials in this area. Values used for analysis typically were 29 - 38 kPa (0.3 to 0.4 tsf) for the shaft modifier and 860 - 1150 kPa (9 to 12 tsf) for the toe modifier.

Analysis of the mixed fine- and coarse-grained material below 15-m (50-ft) depth indicated no group effects that would require a reduction in the allowable contribution of individual piles bearing in the sands in the upper 15 m (50 ft).

TEST PILE INSTALLATION DETAILS

Density variations in the sands in the upper 15 m (50 ft) indicated that installation of production piles to one elevation across the site would not be the most economical use of DD piles. A test program was established to evaluate the energy required to install piles to provide the required resistance. Minor drilling difficulty was incurred while installing test piles which raised concern regarding production pile spacing (1.2 m (4 ft) center-to-center). However, the owner and representatives were reluctant to re-design pile caps or consider smaller diameter piles at this phase of the program.

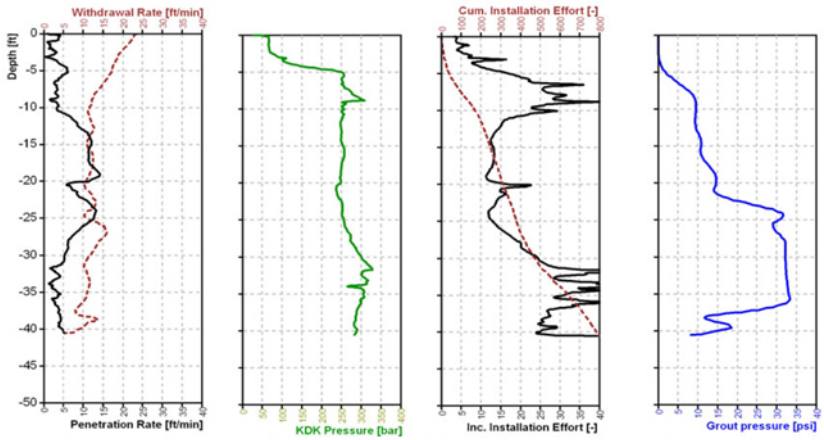

FIG. 3 – Installation Details of Test Pile CT-1

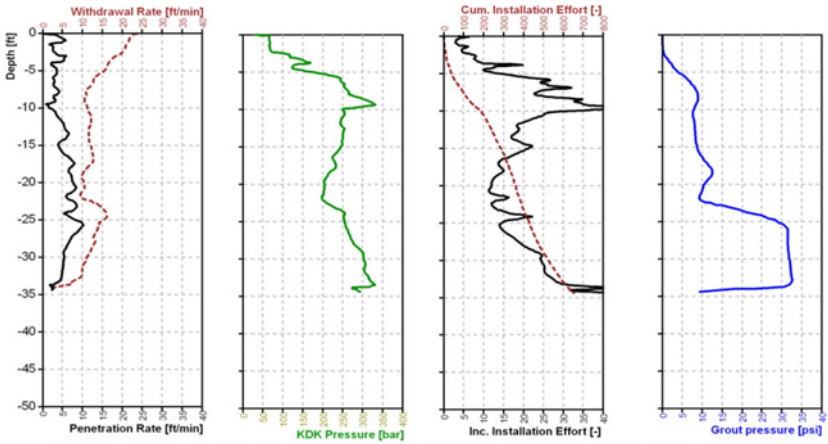

FIG. 4 – Installation Details of Test Pile CT-2

Two 457-mm (18-in) diameter test piles were installed for compression tests. Details recorded during these test pile installations are presented in Figures 3 and 4.

COMPRESSION LOAD TEST RESULTS AND ANALYSIS

Test piles were loaded in accordance with ASTM D1143 (Quick Test) in increments of 178 kN (20 ton) to a maximum load of 3380 kN (380 tons) and then fully unloaded. Plots of applied load versus pile head displacement are presented in Figures 5 and 6. Also presented in these plots are hyperbolic models of the load-displacement relationship.

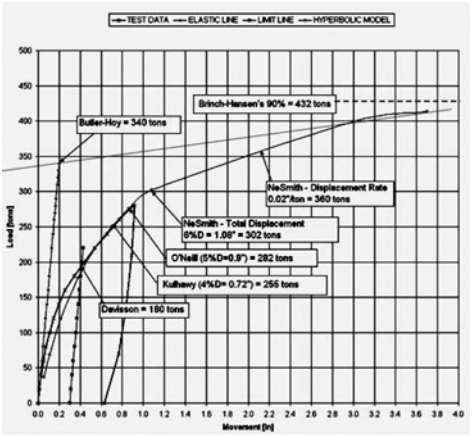

Conversion: 1 in = 25.4 mm; 1 ton = 8.9 kN

FIG. 5 – Pile CT-1 Load Test Results and Estimates of Ultimate Load

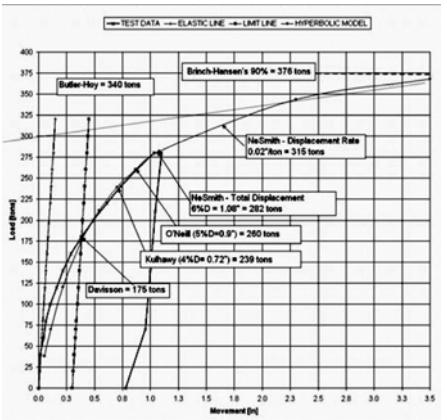

Conversion: 1 in = 25.4 mm; 1 ton = 8.9 kN

FIG. 6 – Pile CT-2 Load Test Results and Estimates of Ultimate Load

The above extrapolations were obtained by applying the method described by Chin (1970). Ultimate compressive resistance was defined as the lesser of the following two loads (NeSmith, 2002):

- The load at which the slope of the hyperbolic model of the pile head load-displacement relationship becomes 0.06 mm/kN (0.02 inches/ton)
- The load at which the pile head deflection is equal to 6 percent of the pile diameter

Applying the above criteria, and estimating shaft and toe components from the equations for the hyperbolic models, the ultimate resistances of the test piles was estimated to be as follows:

- CT-1 – Total: 2687 kN (302 tons) Shaft: 2224 kN (250 tons) Toe: 463 kN (52 tons)
- CT-2 – Total: 2509 kN (282 tons) Shaft: 2118 kN (238 tons) Toe: 391 kN (44 tons)

It is noted that while the Davisson Offset Limit method is listed as an acceptable method for evaluating ultimate load for pile foundations in IBC 2006, the method was originally developed for driven piles and is inappropriately conservative for cast-in-place foundations. Davisson (1993) recommends a modifier of between 2 and 6 when calculating the offset for evaluating a cast-in-place pile, as research has shown that toe deflections of 2 to 5 percent of the diameter are required to reach ultimate load, compared to less than 1 percent for driven piles.

PRODUCTION PILE SPECIFICATION AND INSTALLATION EFFORT

It was proposed to establish production toe elevations by electronically collecting pile installation data (as shown in Figures 3 and 4) and relating this, in real-time, to pile resistance. Pile installation parameters including time, tip depth, auger torque and auger rotations were recorded and displayed on the installation platform used in this project (NeSmith and NeSmith, 2006a). Berkel proposed to use the parameters recorded during test pile installation to set production installation requirements as per the methodology described in NeSmith and NeSmith (2006b). This was to include using KDK Pressure and Penetration Rate to estimate the rig energy expended during test pile installation (Installation Effort, IE) and comparing the total energy (Cumulative Installation Effort) with an internal database of IE and compressive resistance. The Cumulative IE for the two test piles (shown in Figures 3 and 4) was as follows:

- CT-1 – IE = 801, Ultimate Resistance = 2687 kN (302 tons)
- CT-2 – IE = 651, Ultimate Resistance = 2509 kN (282 tons)

The entire database and details from the project test pile program are shown on Figure 7. For an ultimate compressive resistance of 2400 kN (270) tons, the Cumulative Installation Effort required was 635 [-].

Due to the variation in local conditions across this project site, the project team was advised that it would be inefficient to set pre-determined pile lengths according to pile cut-off elevations or required effective pile lengths. It was anticipated that production

pile toe levels would vary by several feet across each of the features. However, initially the project team chose to adopt one effective pile length across each hotel, proposing to use the IE method as a check.

PRODUCTION INSTALLATION

Calibration of Installation Effort

Two drilling platforms were calibrated on site to address variations in their drilling parameters collected during installation. Calibration consisted of the rigs drilling ten probes simultaneously at closely spaced locations and plotting the calculated installation efforts for all of the probes from one rig against those from the other rig. It was determined that both platforms would calculate the same Installation Effort for a given soil condition.

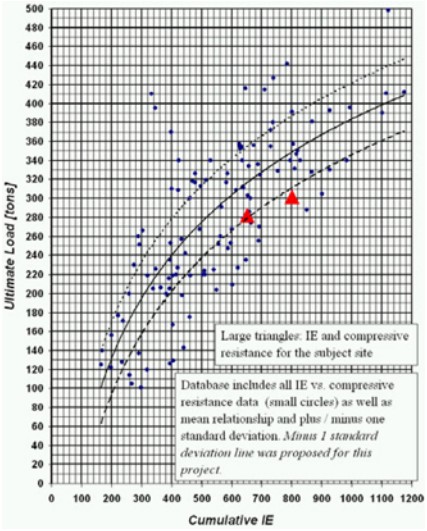

Conversion: 1 ton = 8.9 kN, IE is dimensionless

FIG. 7 – Database of Installation Effort vs. Compressive Resistance

Changes to Production Specifications

During production, the granular materials immediately adjacent to installed piles became significantly denser. Production times for adjacent piles increased by factors up greater than four. This was also reflected in an increase in the hydraulic fluid pressure required to advance and rotate the displacement tool (KDK Pressure) and the Installation Effort, an example of which is shown in Figure 8.

The increase in required effort and corresponding increase in heat generated by the drilling tool resulted in increased production time, difficulty placing reinforcing steel and unexpected equipment wear. Eventually, the pile termination criteria was changed to the data-acquisition method based described above, based on the increase in density and resulting increase in effort shown by the pile records such as in Figure 8.

SUMMARY AND CONCLUSIONS

In coarse-grained soils, Drilled Displacement piles can often provide significantly higher shaft resistance than conventional APG piles. However, DD piles are more susceptible to soil density than APG piles. Where significant variations in soil density exists across a site, it will typically not be most efficient to install DD piles to a uniform "effective length" or toe elevation across the entire site. Systems exist to measure and display pile installation parameters including estimations of the energy required to install the piles. These measurements provide a rational basis for determining the required installation level at a given pile location. They also demonstrate the density increase of subsurface materials through the DD pile production phase of a project.

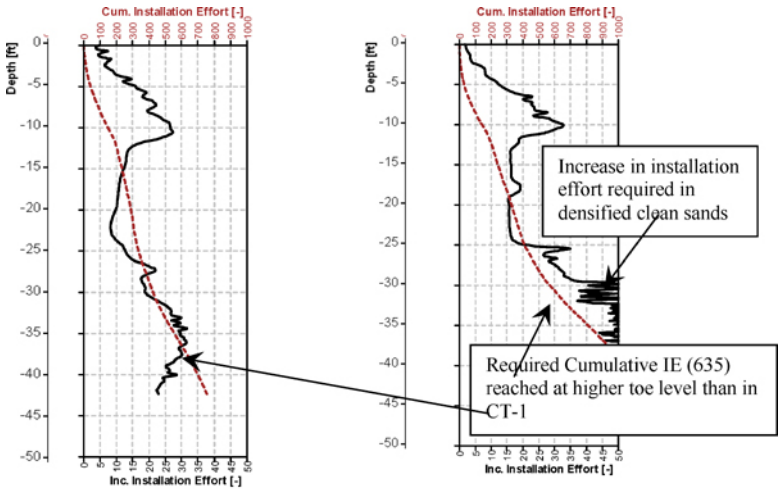

Dashed line – Cumulative IE; Solid Line – Incremental IE; 1 ft = 0.305 m

FIG. 8 – Comparison of IE of Test Pile CT-1 (left) and Production Pile (right)

REFERENCES

Chin, F.K., (1970), "Estimation of Ultimate Load of Piles not Carried to Failure", Proc. 2nd Southeast Asia Conference on Soil Engineering, 81-90.

Davisson, M.T. (1993). "Negative Shaft Resistance in Piles and Design Decisions". Proceedings of the Third International Conference on Case Histories in Geotechnical Engineering. St. Louis MO.

NeSmith, W.M. (2002), "Static Capacity Analysis of Augered, Pressure-Injected Displacement Piles", Proceedings of the International Deep Foundations Congress 2002, M. O'Neill and F. Towsend, eds., Geo-Institute, ASCE, 1179.

NeSmith, W.M. and NeSmith, W.M. (2006). Anatomy of a Data Acquisition System For Drilled Displacement Piles. *Geo-Congress 2006: Geotechnical Engineering in the Information Age*. Atlanta GA, USA. 27 February – 01 March 2006.

NeSmith, W.M. and NeSmith, W.M. (2006). Application of Data Acquired During Drilled Displacement Pile Installation. *Geo-Congress 2006: Geotechnical Engineering in the Information Age*. Atlanta GA, USA. 27 February – 01 March 2006.

Copyrighted Materials
Copyright © 2009 American Society of Civil Engineers (ASCE)
Retrieved from www.knovel.com

Advancements in Data Acquisition-Based Design for Drilled Displacement Piles

W. Morgan NeSmith[1] and Willie M. NeSmith, PE[2]

[1] Berkel & Company Contractors, Inc., 834 Dekalb Avenue - Unit B, Atlanta GA 30307; PH (678) 582-1653 FAX (404) 658-1063; email: morgan_nesmith@comcast.net
[2] Berkel & Company Contractors, Inc., 1503 Milner Crescent, Birmingham AL 35205; PH (205) 933-8900 FAX (205) 933-8979; email: wnesmith@bellsouth.net

ABSTRACT

The authors described the equipment and processes involved in the measurement of the effort expended by the drilling platform in the installation of Drilled Displacement (DD) piles (called Installation Effort or IE) in a paper presented at the 2006 ASCE GeoCongress (NeSmith and NeSmith, 2006a). The use of IE as an indicator of stratigraphy and DD pile capacity was addressed in a companion paper (NeSmith and NeSmith, 2006b). Recent advances in this area include improvements in the acquisition of data required to calculate IE; enhancements in the real time presentation of IE data during pile installation; modifications to the calculation of IE and Cumulative IE; and refinements in the relationship between Cumulative IE and pile capacity. These developments have facilitated the application of IE as a practical tool for DD pile design and for quality control of DD pile installation. The advances mentioned above are discussed herein and include comments on site characterization, an overview of design methodology, recommendations for test pile programs, and use of the database of Installation Effort vs. Capacity collected by the authors.

DESIGN METHODOLODY AND SITE CHARACTERIZATION

The methodology for capacity of drilled displacement piles as installed by Berkel has been developed internally and is detailed in NeSmith (2002). Shaft and toe resistances are estimated from either Cone Penetration Test (CPT) tip resistance values or Standard Penetration Test (SPT) N values with modifiers appropriate for the characteristics of the granular material penetrated. Since the referenced paper was published, hundreds of DD projects have been executed using the methodology described in the paper as the basis for design, and FHWA Geotechnical Engineering Circular No. 8 (2007) recommends the paper for estimating the axial resistance of DD piles.

Site Characterization and In Situ Testing

The authors' experience clearly indicates that axial resistance estimates based on CPT results are superior to those based on SPT data. DD piles are more susceptible than other cast-in-place systems to subtle variations in soil type and density across the site or within the stratigraphy at a particular location. The (essentially) continuous data

collected during a CPT as well as the shear number of CPTs that can be performed in a given time or monetary budget (compared to the number of borings and SPTs that could be performed in a similar budget) provide a significant advantage in the estimation of DD pile resistances.

It has also been the authors' experience that soil types estimated from CPT results provide a more accurate indication of the shaft and toe modifiers than do the visual-manual classifications or the results of laboratory tests provided in conjunction with most drilling and sampling operations. Thus, it is recommended that axial resistance estimates for DD piles be based on CPT results when possible.

Geologic Influences

A review of the database of load tests where Installation Effort (IE) was measured indicates additional considerations that should be included when evaluating axial resistance of DD piles. Figure 1 is the database of Ultimate Load vs. Cumulative IE collected by the authors. This database will be discussed in detail in a following section of the report. Figure 1 includes examples from two sites; one in central Florida and the other in southeastern North Dakota.

Both sites demonstrate the general relationship of IE and resistance on a given site. The sands in North Dakota were generally looser and had higher fines-contents than the sands at the Florida site. However, the 457-mm (18-in) diameter DD test piles installed in North Dakota provided greater resistances for similar or less effort than the similar piles installed in Florida. This difference in resistance is considered to be primarily due to the angularity of the sands at the North Dakota versus the rounded sands at the Florida site, and the densification of the sands under about the same penetration effort. Differences in the soil-grout bond strength from rounded to angular particles are also likely. Although not implicit in the design methodology at this time, geologic considerations such as age and depositional environment have been clearly demonstrated and should be considered in the design process.

UPDATED DATA ACQUISITION

At the time of the 2006 paper, the data acquisition system on the DD pile installation platforms had only recently changed from an analog system with a limited number of available signal inputs. Recording grout pressure for quality assurance during pile casting used one of the available inputs, leaving two remaining inputs for data recorded during penetration. These were used for recording of stem depth and KDK pressure (the hydraulic fluid pressure applied to the rotary head). Since then, this system has been replaced by the digital system described in NeSmith and NeSmith (2006a), which allows for greater flexibility in the number of inputs that can be acquired and recorded.

More importantly, the switch to the digital acquisition system increased the flexibility of the presentation of recorded data, allowing for remote real time display of data as well as real-time calculation and display of the Installation Effort described herein.

This in turn has improved the data display for both the drilling platform operator and the piling inspector. The results of these improvements to the data acquisition system are discussed in the following sections.

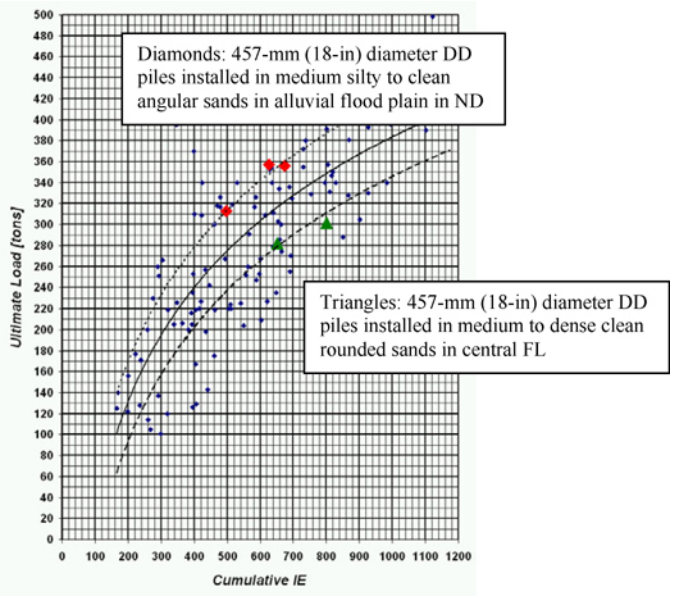

Conversion: 1 ton = 8.9 kN, IE is dimensionless

FIG. 1 - Examples of Installation Effort vs. Ultimate Load

REAL TIME DISPLAY OF INSTALLATION AND ENGINEERING DATA

The method of calculating Installation Effort as a function of drilling tool penetration rate and torque (as estimated from the KDK Pressure) was described in the previous paper. This calculation method is still in use. IE values are calculated at every 1-second recording interval based on the KDK Pressure and Penetration Rate recorded at that interval. Plots of IE vs. depth are produced in real-time in the field and continue to provide excellent agreement with stratigraphic representations from Cone Penetration Tests. This agreement has extended beyond the original database to a variety of geologic settings.

A dedicated monitor for the pile inspector was developed to increase the amount of data displayed during pile production (Figure 2). In addition, this remote monitor communicates with the computer on the drilling platform wirelessly, doing away with the need for the inspector to move the monitor with the drilling platform. More recently, the system has been modified so that the remote monitoring is available on a standard laptop computer rather than a dedicated monitor. Any laptop with wireless capability can become a monitor.

Figure 3 shows the main screen and engineering screen as viewed on the wireless monitor or laptop. The main screen includes general pile information such as date and time, pile number, current depth, etc. as well as graphical representations of KDK and grout pressures.

The engineering screen shows plots of KDK Pressure, Penetration Rate, Installation Effort and Cumulative Installation Effort vs. depth as drilling tool penetration occurs. This real-time display allows the inspector to observe the stratigraphy at the pile location and adjust the pile toe level as appropriate. It also allows the inspector to view Cumulative IE as it is developed to verify that the effort required for pile installation meets the specifications developed during the design and load test phases of the project.

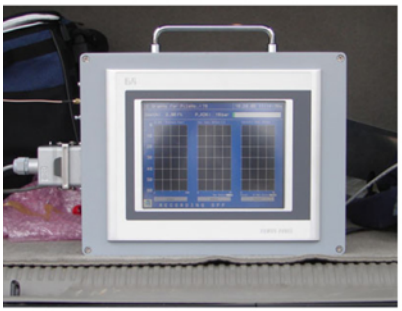

FIG. 2 - Wireless Remote Monitor

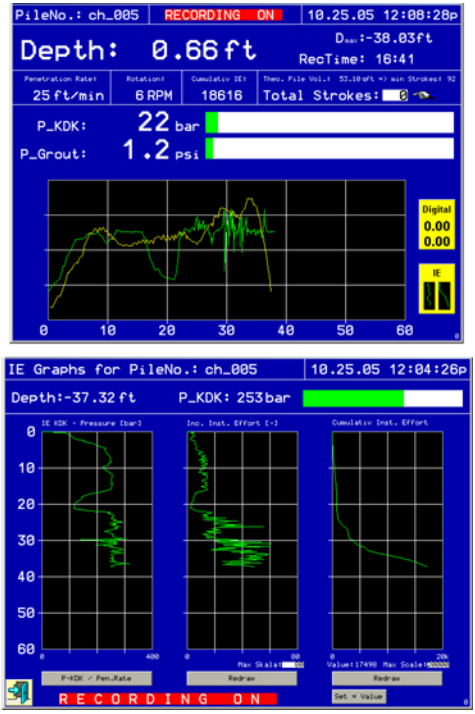

FIG. 3 - Main and Engineering Screen of Wireless Remote Monitor

UPDATED CALCULATION OF CUMULATIVE INSTALLATION EFFORT

In the 2006 paper, the term Cumulative IE was introduced. At that time, this was an estimate of the total Installation Effort as the sum of the IE values recorded at 1-second intervals during penetration of the drilling tool. The consistent relationship between

Cumulative IE and pile resistance was also demonstrated; however this relationship could not be extended to shaft capacity or toe capacity.

A study of the total IE developed during pile penetration (Cumulative IE vs. Depth) indicated that the Cumulative IE was heavily influenced by dense and hard layers and subsequently underestimated the contribution to capacity of loose or soft layers while severely overestimating the contribution to capacity of hard or dense layers. This also resulted in difficulty when trying to use IE to predict the capacity of variable pile lengths.

Drilling data is recorded and IE is calculated at 1-second intervals. When the drilling tool encounters a hard or dense layer, the Cumulative IE calculation is affected in two ways. First, the individual IE values calculated in that strata increase (as one would expect with an increase in density). Second, because drilling slows down in these layers and because these calculations are performed on a time interval, more IE values are recorded per unit length in these layers than in softer or looser layers. These additional recordings per unit length of penetration are what produce the exaggerated Cumulative IE in dense and hard materials. An example of this calculation from an IE vs. Capacity profile is shown in Figure 4.

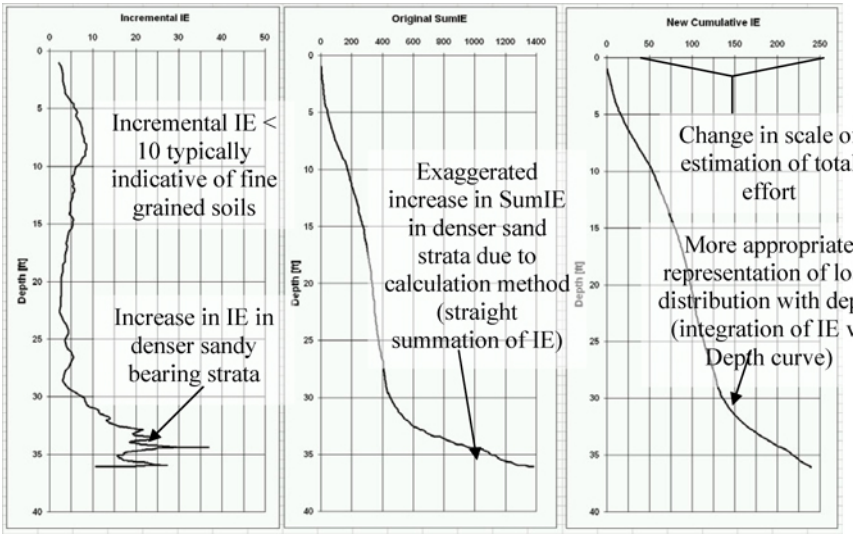

FIG. 4 - Example Incremental IE Profile with Calculated and Cumulative IE Profiles

The following adjustment was made to Cumulative IE calculation at about the time of publication of the 2006 paper. Instead of a straight summation of recorded Installation Effort values, each value is weighted according to the distance from the previous calculation depth; in effect an integration, rather than a summation, of the IE vs. Depth plot. The result is a smoother Cumulative IE vs. Depth plot which does not exaggerate

the influence of hard or dense layers (Fig. 4). Additionally, Cumulative IE shows a good correlation with shaft capacity, as one might expect considering that IE is calculated at 1-second intervals along the shaft of the pile.

CUMULATIVE IE DATABASE AND ITS USE IN FINAL DESIGN

As of the first publication in NeSmith (2003), Berkel's database of Installation Effort vs. Capacity consisted of 15 test piles from 9 project sites. The current database consists of over 110 load tests from over 50 project sites (Figure 5). The mean relationship and plus/minus one standard deviation are also shown.

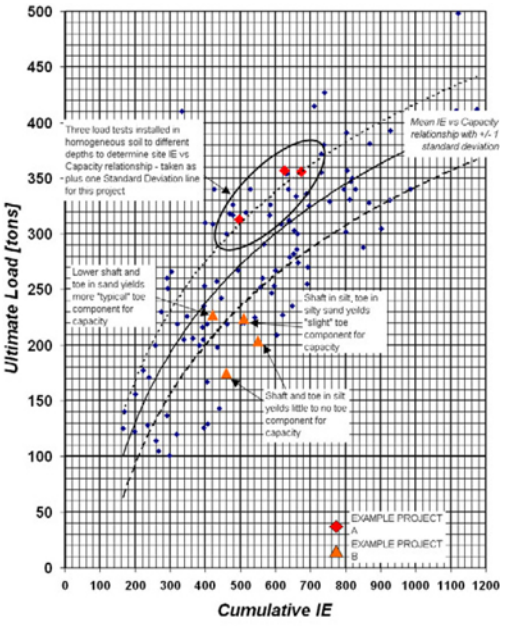

Conversion: 1 ton = 8.9 kN, IE is dimensionless

FIG. 5 - Database of Cumulative IE vs. Ultimate Load and Two Example Projects

Figure 5 also includes an example of load test results from two example projects, A and B. The resulting design Cumulative IE vs. Capacity line for Example A is also included. This is typical of the authors' current design process; the load test results from a project site are plotted on the entire database and the mean relationship is adjusted to fit the load test results for that particular site and to develop the relationship for use in final design of production piles on that project.

Typically, displacement piles in loose and medium dense sands have Cumulative IE and capacity relationships that fall within the plus/minus one standard deviation range of the database shown. Within a particular geologic setting, as fines contents increase

and density decreases, the relationship tends to move towards and then below the minus one standard deviation line. This is due to the decrease in shaft resistance developed in these materials for the same amount of effort expended by the drilling platform and the lower toe capacities developed by piles in these materials as well.

Example B on Figure 5 shows four load tests from a project site with two load tests with the entire shaft and toe in a sandy silt; one load test with the shaft in this silt and the toe in a slightly cleaner sand; and one load test with the bottom of the shaft as well as the toe in cleaner sandy material. The movement of the Cumulative IE – Capacity relationship from below the minus one standard deviation line to about the mean relationship as soil type and density change is illustrated in this example. Piles installed in denser and cleaner sands tend to have an IE – Capacity relationship that falls towards the plus one standard deviation line. Piles that fall well above this line have *typically* been installed with the pile toe in dense or cemented sands and/or gravels.

USE OF CUMULATIVE IE

Test Pile Programs for DD Piles

The development of the calculation of Cumulative IE vs. depth and the expansion of the IE – Pile Resistance database are significant tools in the design of DD piles. The database and the relationships developed from it are currently being used to set final test pile depths based on the Cumulative IE developed from probe and reaction piles installed prior to test pile installation, and production pile toe levels are being based on site specific Cumulative IE relationships

The authors recommend that for a given site, several load tests be performed on test piles that have been installed to a range of Cumulative IE values to evaluate the IE – Pile Resistance relationship. The number of load tests that are performed is a function of the number of piles to be installed, the variability of the subsurface conditions, and the extent to which the Cumulative IE approach can add value in terms of reduced pile footage and mitigation of difficult installation issues. The range of test pile IE values should be selected based on the pre-load test data base. The final Cumulative IE target (or targets) for production piles should be set based on the performance of the test piles. As discussed earlier, the IE profile as well as the Cumulative IE developed with depth may be monitored in real time during production by both the installation platform operator and third-party inspector.

Evaluation of Resistance of Pile Sections

In addition, Berkel often uses the new Cumulative IE vs. Depth curve (see Fig. 4) to evaluate the segmental capacity of pile shafts and to adjust production pile IE or depth requirements based on these segmental capacities. The most common application of this is on projects with deep excavations in some areas of the project site – for elevator pits or shear walls for example.

Typically, an adjusted pile capacity is developed considering the loss of Cumulative IE from the material that will be excavated and the final Cumulative IE required for these piles is adjusted if necessary. This process eliminates the need for production piles to be extended by a length equal to the depth of excavation, which is a common approach to the situation described. Instead, production piles are only extended to compensate for the IE developed in the material to be excavated. Production piles are often extended into materials that are denser than those nearer the surface and application of a Cumulative IE approach results in a more efficient use of the materials present at a given pile location.

Cumulative IE also provides a rational basis for setting production pile lengths since it is a reflection of the conditions at the pile location. It is noted that the installation of DD piles in granular soils increases the soil density in the vicinity of the pile and thus piles in a group that are installed later penetrate material that is more dense than the initial piles in the group. The result is that a target CIE would be reached at a shallower depth for the later piles in a group, and give rise to variation in pile length. The potential for variation in toe levels in a pile group should be considered in light of the overall subsurface conditions and the global performance of the pile group.

CONCLUDING REMARKS

As a result of improvements in supporting technology and refinements in computational processes, Installation Effort has evolved from a concept to a practical tool for the design and quality control of Drilled Displacement piles. A representation of the stratigraphy and parameters that can be correlated to compressive pile resistance can be viewed in real time on wireless enabled devices. The capability to assign a compressive capacity to each production pile, and to allot shaft resistance to pile segments provide a basis for making rational decision in non-standard or unanticipated situations.

It is noted that the authors are not suggesting that the ability to assess stratigraphy and capacity during drilling negates the need for a well planned and executed site characterization or a rational, analytical assessment of axial resistance. It is suggested, however, that the processes described constitute a viable adjunct, and are a valuable continuation of the design process.

9. REFERENCES

Brown, D.A., Dapp, S.D., Thompson, W.R., Lazarte, C.A. (2007). "Design and Construction of Continuous Flight Auger Piles". *FHWA Geotechnical Engineering Circular No. 8*. April 2007.

NeSmith, W.M., 2002. "Static Capacity Analysis of Augered, Pressure-Injected Displacement Piles", ASCE Geotechnical Special Publication No. 116, Proceedings from DEEP FOUNDATIONS 2002, Orlando, FL, pp. 1174-1186.

NeSmith, W.M. (2003). "Installation Effort as an Indicator of Displacement Screw Pile Capacity". Proceedings of the 4th International Conference on Bored and Augered Piles (BAP IV). Ghent, Belgium. June 2003.

NeSmith, W. M. and NeSmith, W.M. (2006). "Anatomy of a Data Acquisition System for Drilled Displacement Piles". Proceedings of the the American Society of Civil Engineers GeoCongress 2006. Atlanta GA USA. 26 February – 01 March 2006.

NeSmith, W.M. and NeSmith W.M. (2006). "Application of Data Acquired During Drilled Displacement Pile Installation." Proceedings of the American Society of Civil Engineers GeoCongress 2006. Atlanta GA USA. 26 February – 01 March 2006.

Copyrighted Materials
Copyright © 2009 American Society of Civil Engineers (ASCE)
Retrieved from www.knovel.com

Cylindrical Shear or Plate Bearing? – Uplift Behavior of Multi-Helix Screw Anchors in Clay

Alan J. Lutenegger
Department of Civil & Environmental Engineering
University of Massachusetts
Amherst, Ma.
lutenegg@ecs.umass.edu

ABSTRACT: The undrained ultimate uplift capacity of multi-helix screw pile anchors in clays depends on the failure mechanism developed between the anchor and the surrounding soil. The mechanism is in turn related to the specific geometry of the anchor, in particular the number of helices and the spacing of the helices along the shaft, which may be described by the spacing to diameter ratio, s/D. The load capacity of screw anchors can derive from individual plate bearing or soil shearing along a cylindrical failure surface between the plates. Results of vertical axial pullout field tests performed in clay are presented. The results are compared with estimated capacities using both design approaches and are used to illustrate the influence of spacing ratio on ultimate capacity.

INTRODUCTION

Helical anchors have been used to resist tension loading for a variety of structures such as transmission towers and cell phone towers, and resist uplift loading from bouyancy effects, such as in buried pipelines. Both single-helix and multi-helix screw anchors are in common use, and the selection for a particular design problem depends on a number of factors, including soil type, loading, availability, and installation equipment. The behavior of multi-helix screw anchors may also be dependent on the geometry used; (i.e., the number, diameter and spacing of the helices). In the past twenty years, work has been performed both in the laboratory and in the field to study the behavior of multi-helix screw anchors in a variety of soils. However, there have been few detailed studies performed on the behavior of multi-helix anchors in clays and no systematic field investigation of their behavior in natural soil deposits.

The behavior of multi-helix screw anchors depends on the relative helix spacing and the number of helices. Therefore the design approach must take into account the anchor geometry. Previous research studies (Rao et al. 1991; Rao and Prasad 1993) on small-scale laboratory model anchors in very soft remolded clay with undrained strengths from about 5 to 13 kPa have shown that for the helix spacing greater than about 1.5 times the helix diameter, the helices apparently acted independently and developed capacity individually. At helix spacing less than 1.5 the diameter it appears that there was not sufficient space between the helices for the soil to develop full plate bearing capacity for this soft clay. In this case, the soil between the plates acts together and failure takes place on the perimeter of the cylindrical surface between the plates (Fig. 1).

Worldwide, multi-helix anchors are generally available in two designs; those with constant diameter helical plates spaced at a uniform distance along the central shaft; and those in which the helical plate diameter progressively increases moving up the central shaft with the spacing between plates at some set ratio of the individual helix diameter. In the present study, anchors with constant diameter helical plates were tested.

A set of full-scale field load tests was performed on a series of screw anchors of varying geometry to determine when the transition from cylindrical shear to individual plate bearing occurs in the field. Tests were performed at the Geotechnical Experimentation Site at the University of Massachusetts in Amherst, where the clay deposit has been well characterized (e.g., Lutenegger 2000; Lutenegger and Dearth 2001). Multi-helix screw anchors with varying helix spacing were installed at the site and load tested to failure. Tests were performed in the upper stiff overconsolidated clay and the lower soft, near normally consolidated clay to investigate the behavior in both stiff and soft clay.

DESIGN OF MULTI-HELIX SCREW ANCHORS IN CLAY

There are two design approaches to determine the ultimate tension (uplift) capacity of multi-helix screw anchors based on soil mechanics that can be considered; 1) Individual Plate Method, and 2) Cylindrical Shear Method. Both methods require some simplifying assumptions in order to determine the ultimate capacity. Based on undrained bearing capacity theory the zone of the failure surface beneath a plate should be on the order of about one diameter, suggesting that if helices are spaced no closer than one diameter they should behave individually. However this does not appear to be the case.

Individual Plate Method - The individual plate method assumes that individual bearing failures occur simultaneously above each helix as shown in Figure 1. As a result, the uplift capacity of the anchors is simply equal to the sum of the resistance in uplift of each plate. For deep anchor installation (i.e., top helix greater than about 6 diameters below ground surface) the failure is similar to end bearing of deep foundations. The capacity of a multi-helix anchor plate in uniform clay with constant undrained strength is often expressed using Equation 1.

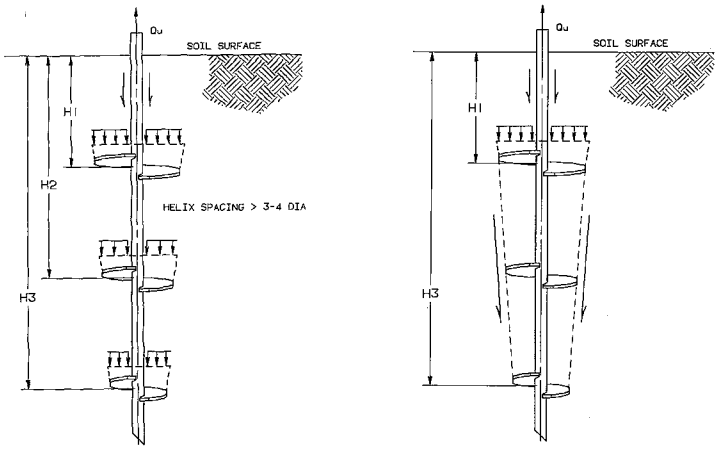

Figure 1. Comparison Between Individual Plate and Cylindrical Shear Behavior.

$$Q_u = nQ_e + W_s + W_a \quad [1]$$

$$Q_e = 9s_u A_e \quad [2]$$

where:
Q_u = Ultimate Uplift Capacity
Q_e = Ultimate Uplift of an Individual Helix
A_e = area of each helix
s_u = undrained shear strength
n = number of helices
W_s = weight of soil between helices
W_a = weight of anchor

Equation 1 does not include any component of uplift capacity from the anchor shaft. In the current study, square shaft anchors were used and since the square shaft produces a round cavity during rotation, no shaft contribution was included. For round shaft screw anchors, a component of capacity from the shaft between the helices and above the top helix may need to be included. Additionally, Equation 1 does not include any base suction below the bottom helix that may develop in undrained loading in saturated clays.

Cylindrical Shear Method - In the Cylindrical Shear Method of analysis, it is assumed that the soil in between the helices acts as a semi-rigid body and that a cylindrical failure zone develops along the perimeter section jointed between the helices as shown in Figure 1. In uplift, there would also be plate bearing resistance from the upper most plate, so in effect this method is actually a combination of cylindrical shear and plate bearing. The ultimate capacity in uplift may be taken as:

$$Q_u = Q_s + Q_e + W_s + W_a \quad [3]$$

where:
Q_s = cylindrical perimeter shear of soil prism between helices
Q_e = end bearing of top helix
W_s = weight of soil between helices
W_a = weight of steel

The contribution of the cylindrical shear zone between helices is obtained from:

$$Q_s = (\pi DL)\, s_{uave} \quad [4]$$

where:
D = diameter of the helices
L = length from bottom helix to top helix
s_{uave} = average undrained shear strength of soil between helices

As before, the bearing of the top helix is:

$$Q_e = 9 s_{ue} A_e \quad [2]$$

Both analyses rely on an accurate determination of the mobilized undrained shear strength in order to calculate the ultimate uplift capacity. For both single-helix and multi-helix anchors, the installation may have some influence on the soil as some remolding must take place simply to advance the anchor. The degree of disturbance is unknown and may be dependent on the skill of the equipment operator and other factors such as soil sensitivity. Initially, for the current study, the analyses were performed assuming no soil disturbance and used the undisturbed in situ undrained shear strength obtained from field vane tests. A detailed investigation of soil disturbance is beyond the scope of the current work but is part of other ongoing investigations at this and other sites.

INVESTIGATION

The current investigation included both an analytical parametric study and a field investigation to evaluate the behavior of mutli-helix screw anchors. The field investigation was limited to a single diameter production screw anchor simply because of the amount of time involved in installation, test set-up and load testing.

Parametric Analysis - A simple parametric analysis was initially performed to evaluate the sensitivity of Equations 1 and 2 for different anchor geometries using two different values of soil undrained shear strengths (31 kPa and 191 kPa) to represent both soft clay and stiff clay. The parametric analysis was performed to evaluate which design approach would control ultimate capacity for typical geometries of multi-helix anchors and to determine the influence of helix spacing on calculated capacity. In order to keep the analysis simple, a single diameter of helical anchor [(200 mm (8 in.)] was used and anchor geometries consisting of three helices with relative spacing of s/D = 0.75; 1.125; 1.5; 2.25; and 3 were evaluated. This is the same size and geometry of the anchors used in the field investigation. The relative helix spacings were also selected to be consistent with the actual spacing of helices on the field anchors, which was set as a multiple of the helix pitch so that each successive helix could track in the same path as the lead helix, in accordance with typical industry practice.

Figure 2 shows the variation in total uplift capacity as a function of helix spacing (s/D), for different three helix anchors as a function of the relative spacing obtained using both design approaches. The ultimate uplift capacity from the Individual Plate Method (Eq. 1) is of course constant for a fixed number of helices in the same soil and is independent of the helix spacing; (i.e., the calculated capacity depends only on the number of helices but would increase linearly with increasing number of helices).

The ultimate uplift capacity from the Cylindrical Shear Method (Eq. 3) depends on the specific anchor geometry and increases linearly as the helix spacing increases thereby increasing the cylindrical shear surface. The contribution of the top helix is a constant for all helix spacings. The anchor will fail under whichever of the mechanisms gives the lower calculated ultimate capacity for a given relative helix spacing. Figure 2 shows that up to a helix spacing of 2.25, Cylindrical Shear controls the anchor behavior but after s/D = 2.25 Individual Plate Capacity controls. The behavior is naturally independent of the undrained shear strength.

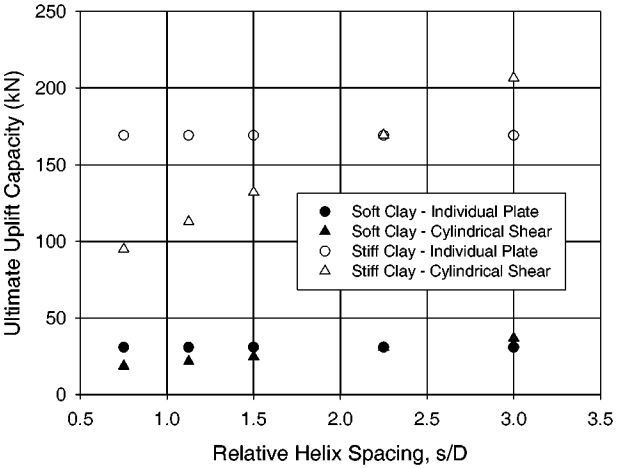

Figure 2. Parametric Comparison Between Individual Plate and Cylindrical Shear.

Field Load Tests - To verify the results of the parametric analysis, a full-scale field loading investigation was performed. Several multi-helix anchors were fabricated to provide a range in helix spacing. Multi-helix anchors consisted of three 100 mm (8 in.) diameter helices with a helix pitch of 76 mm (3 in.) and relative spacings of s/d = 0.75; 1.125; 1.5; 2.25; and 3. Anchors tests were performed at two depths, 3.0 m and 6.1 m. Tests were performed in Area B where the stratigraphy consists of about 2 m of stiff silty-clay fill overlying a thick deposit of lacustrine varved clay. Below the fill, the clay has a well-developed stiff overconsolidated crust which grades to near normally consolidated material. The site has been used previously for other field studies involving full-scale foundation behavior (e.g., Lutenegger and Dearth 2001). Field vane tests at depths of 3.05 m and 6.10 m give average values of undrained shear strength on the order of 200 kPa and 30 kPa, respectively. The sensitivity obtained from field vane tests indicate values of about 3 at a depth of 3.05 m and about 7 at a depth of 6.10 m.

Load Test Procedure - Tests were performed using the general procedures described in ASTM D3689 *Standard Test Method for Individual Piles Under Static Axial Tensile Load.* Load was applied by a single acting 250kN hydraulic jack placed on top of two reaction beams centered over the anchor and resting on wood cribbing. Load was transferred from the jack to the anchor using a threaded rod. The load was measured using a Geokon donut load cell placed over the threaded rod on top of the hydraulic jack and was read using an electronic digital indicator. Deformation measurements were made using two digital dial indicators attached to an independent reference beam and placed equidistant on opposite sides of the anchor. The dial indicators were referenced to a steel plate threaded to the top of the anchor. Loads were applied incrementally in the range of approximately 5 to 10% of the estimated ultimate capacity of each anchor. Each

increment of load was maintained for 15 minutes giving a time to reach a relative displacement of 20% of the helix diameter on the order of 4 to 4 ½ hours.

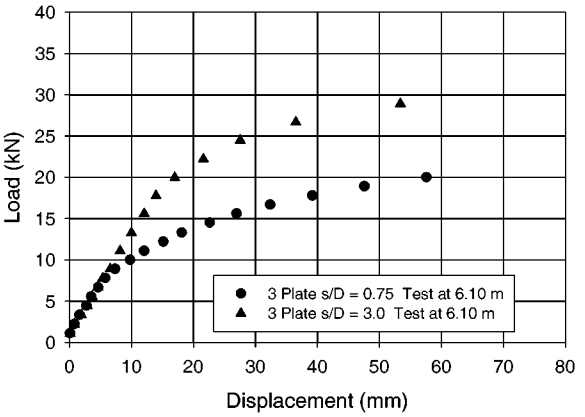

Figure 3. Typical Anchor Load Test Results.

RESULTS

Ultimate Capacity - Figure 3 shows a typical load-displacement curve for both a single-helix and multi-helix anchor of the same diameter. The ultimate capacity for all tests was taken as the load producing a relative displacement of 20% of the helix diameter. Figure 4 shows the measured ultimate capacity as a function of the relative helix spacing for tests performed at both depths. It can be seen that in both cases (i.e., stiff clay and soft clay), there is a linear increase in ultimate tension capacity, suggesting that at least up to a relative spacing of 3, the anchors all behave in Cylindrical Shear and there has been no transition to Individual Plate behavior. This is in contrast to the behavior predicted from the parametric analysis and previously reported for small-scale laboratory test on very soft clay.

However, the results obtained by Rao et al. (1991) were performed using remolded clay which is likely to have very low sensitivity and therefore may not be indicative of the behavior in natural soils in the field. Figure 4 indicates that the rate of increase in ultimate capacity is greater for tests in the stiff clay as compared to the soft clay which may be related to differences in soil disturbance and reduction of strength resulting from the installation. Another issue that may affect the behavior is the strain incompatibility between plate behavior and the cylindrical prism behavior. That is, it is likely that a cylindrical surface reaches peak shear at a different (smaller) displacement than the top plate does and which is likely to be different in stiff clay and soft clay.

The "efficiency" of the multi-helix anchors over a single anchor of the same diameter may also be considered. Figure 5 shows the ratio of measured ultimate capacity of the multi-helix anchors to the capacity of a single-helix anchor as a function of relative helix spacing (Efficiency Factor). For Individual Plate behavior the Efficiency Factor

would be equal to 3 (i.e., if each plate acts independently in plate bearing the Efficiency Factor is equal to the number of plates). At both depths the field results are lower than the predicted values and there again is no apparent transition to Individual Plate behavior. This is most likely a result of remolding of the soil during anchor installation which is unavoidable during actual construction. The soft clay has a higher sensitivity that the stiff clay which results in a larger loss of strength during installation. On the other hand, no consideration has been given to any possible thixotropic gain in strength with time after installation that may affect the results. These factors need further evaluation.

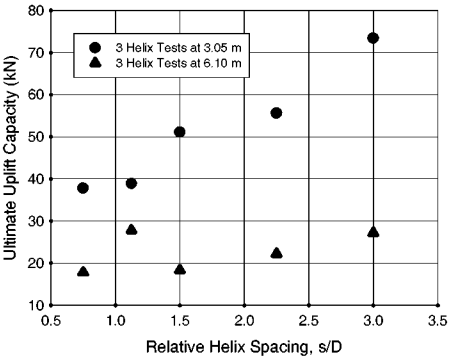

Figure 4. Measured Uplift Capacity as a Function of Relative Helix Spacing.

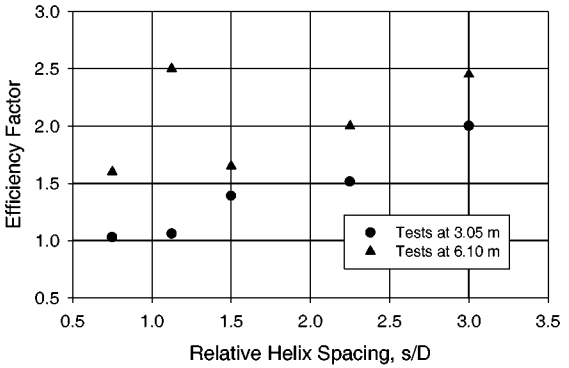

Figure 5. Efficiency Factor as a Function of Relative Helix Spacing.

Behavior at "Working Load" - The behavior of the anchors at "working load" levels may also be considered. One would suspect that at very small load levels (i.e., well below ultimate load) the behavior of all multi-helix anchors would be essentially independent of

the relative helix spacing since the full bearing capacity zone is not developed. Figure 5 shows the load at a relative displacement of 5% of the helix diameter for tests conducted at both depths. In this case, it can be seen that for the stiff clay the response becomes constant after a relative spacing of 1.5. For the soft clay there is a general increase in load response with relative spacing which may indicate installation disturbance in the softer more sensitive clay.

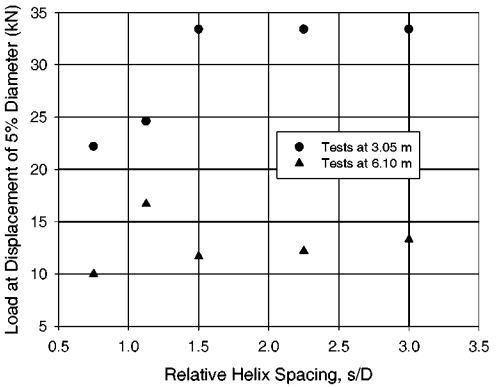

Figure 5. Load at 5% Displacement as a Function of Relative Helix Spacing.

CONCLUSIONS

Results of a field investigation on the behavior of multi-helix screw anchors in clay indicated that within a relative helix spacing (s/D) of 3 there is no distinct transition from Cylindrical Shear to Individual Plate behavior. This is in contrast to predicted behavior which suggests that in both stiff and soft clays this transition in capacity development should occur at a relative helix spacing of about 2.25. The difference may be related to disturbance during installation and the reduction of mobilized shear strength between the helices. However, at working loads well below ultimate capacity and displacements no greater than 5% of the helix diameter, the behavior in stiff clays appears to be entirely controlled by Individual Plate behavior above a relative spacing of 1.5.

REFERENCES

American Society for Testing and Materials, 2003. Standard Test Method D3689 *Standard Test Method for Individual Piles Under Static Axial Tensile Load.*

Lutenegger, A.J., 2000. National Geotechnical Experimentation Site - University of Massachusetts. National Geotechnical Experimentation Sites, ASCE, pp. 102-129.

Lutenegger, A.J. and Dearth, A., 2001. Scale Effects of Laterally Loaded Drilled Shafts in Clay. Foundations and Ground Improvement, ASCE, pp. 554-564.

Rao, S.N., Prasad, Y.V.S.N., and Shetty, M.D., 1991. The Behavior of Model Screw Piles in Cohesive Soils. Soils and Foundations, Vol. 31, No. 2, pp. 35-50.

Rao, S.N. and Prasad Y.V.S.N., 1993. Estimation of Uplift Capacity of Helical Anchors in Clays. Journal of Geotechnical Engineering, ASCE, Vol. 119, No. 2, pp. 352- 357.

Copyrighted Materials
Copyright © 2009 American Society of Civil Engineers (ASCE)
Retrieved from www.knovel.com

Lateral Resistance of Helical Piles in Oil Sands

Mohammed Sakr[1], P.Eng., Ph.D

[1]Lead Geotechnical Engineer, Almita Manufacturing Ltd, 6606 – 42nd Avenue, Ponoka, Alberta, Canada, T4J 1J8; PH: (800) 363-4868; FAX: (403) 783-2895; e-mail: mohammed.sakr@almita.com

ABSTRACT

Although there are several methods available for estimating the axial capacities of helical piles, there is little literature available on the lateral performance of helical piles. The results of a lateral pile load test program and field monitoring of helical piles with either single or double helixes installed in oil sand soil are presented in this paper. Soil stratifications and groundwater conditions are also summarized. The results of the load tests are compared to a theoretical model using LPILE Plus 5, a program widely used to estimate the lateral pile resistance based on the p-y curves. Based on the results of this study it was found that helical piles can develop considerable resistance to horizontal loads and their lateral resistance is almost exclusively controlled by the shaft diameter.

INTRODUCTION

Helical piles (or screw piles) are used extensively in Western Canada and USA to support residential, commercial and industrial facilities. Helical piles offer several advantages over cast-in-place concrete piles and driven steel piles such as high compressive and uplift capacities (three to five times that of driven steel piles with the same shaft diameter and length), the rapid speed of their installation (typical 10 m long pile can be installed in about three minutes), suitability for construction in very limited access conditions, installation in frozen or swampy soil conditions and their cost effectiveness. In addition to that, helical pile installation is a vibration-free process. Therefore, installation of helical piles in urban areas is very favourable in terms of reducing the level of noise and minimizing vibration to nearby structures.

There are several sources that contribute horizontal (or lateral) loading and moments onto piles, such as wind loading, axial thrust on pipelines, and load eccentricity. For helical piles lateral loads and moments is resisted utilizing the top part of pile shaft, similar to other deep foundation options, or through the use of battered piles in which the lateral forces is transformed into axial loads. Large lateral loads can be resisted using a group of battered helical piles.

The objectives of the present study are to evaluate the lateral resistance of helical piles in oil sands based on the results of full-scale pile load testing and to compare between the measured lateral resistances of helical piles and their estimated lateral resistances using p-y curves. In order to achieve these objectives four full scale lateral tests were carried out using helical piles with either a single or double helixes installed in oil sand. Summaries of the soil conditions, pile configurations, test setups and the results, are presented in the following sections.

SITE DESCRIPTION

The pile load test program was carried out at Cree Burn Lodge site located north of Fort McMurray, Alberta just west of highway 63 at the Albian Sand Junction and east of the Athabasca River. The site had been cleared and was originally covered with thick forest and brush. The topography of the site was relatively flat and was graded during the summer of 2007.

The load testing program consisted of four full-scale load tests carried out in two Phases at two different locations on the site. Each phase included two lateral load tests. Phase 1 of pile load tests was carried out in a location near the central part of the site while Phase 2 was carried out in the northwest corner of the site (due to inaccessibility of central part of the site at the time of testing). Phase 1 and 2 test locations were about 100 m apart.

SUBSURFACE SOIL CONDITIONS

The subsurface soil stratigraphy at the site consisted of fine to medium grained, compact to dense, moist to wet brown sand and contained traces of gravel, extending to varying depths between 1.1 m to 2 m. The sand was underlain by dense to very dense oil sand. Standard Penetration Test (SPT) results for sand layer were 11 to 22 blows per 300 mm of penetration indicating a compact sand state.

Oil sand was black, silty, fine to medium grained, moist and contained trace of gravel. SPT tests carried out at selected depths in the oil sand varied between 26 to over 100 blows per 300 mm of penetration indicating a dense to very dense state. The oil sand is typically composed of the following components (Scott and Kosar 1984): (1) fine to medium grained uniform quartz sand and (2) pore fluids consisting of bitumen, water and occasionally free gas. The sand grains were wet and the water formed a continuous phase throughout the oil and sand matrix. Bitumen occupied the remaining pore space. Dissolved gases were found within the liquid phases and some free gas was occasionally present depending on in situ temperatures and phases.

Groundwater level was relatively high and was measured at depths varying between 0.5 m to 2 m below existing ground. Wet and dry unit weight of sand was about 22 kN/m^3 and 19 kN/m^3 while for oil sand were 21.6 kN/m^3 and 18 kN/m^3. Results of triaxial compression tests on high quality cores in undisturbed oil sand samples

(Sharma et al.; 1986) indicated a peak frictional angle of 50° and a residual friction angle of 38°.

TEST PILE CONFIGURATIONS

Two pile configurations were considered for the study including a single and double helix pile as illustrated in Figure 1. The test piles were manufactured by Almita Manufacturing Ltd. of Ponoka, Alberta. Each pile is composed of a central cylindrical shaft with a diameter of 177.8 mm, 5.8 m long, with single and double helixes, 406 mm in diameter and 19.1 mm thick. Piles with double helixes were fabricated such that the spacing ratio (S/D) equaled 3 to reduce the interaction of the end bearing between the two helixes.

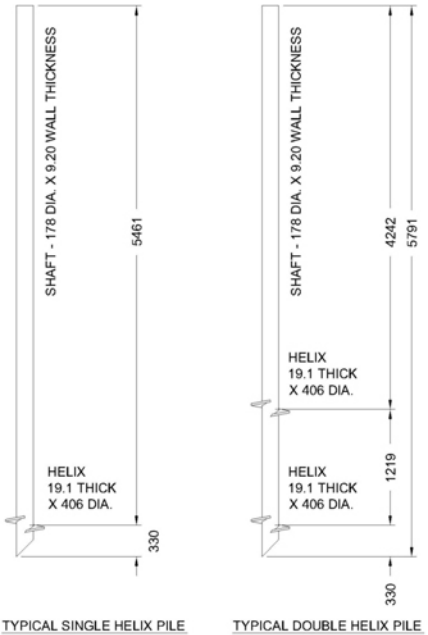

* All dimensions are in millimeters

Figure 1. Pile configurations for lateral load tests

PILE INSTALLATION

Helical piles were installed through the use of mechanical torque applied at the pile head. Applied torque was continuously measured and recorded throughout the entire installation. Final measured torque at the end of pile installation and total embedment depths are summarized in Table 1. It can be seen from Table 1, that in general, torque values for piles tested in Phase 1 were about 35% higher than those values recorded for piles tested in Phase 2. This can be attributed to the variability of oil sand depth

and soil strength as observed from torque chart records. Moreover, it can be noted from Table 1, that piles with double helixes required in general about 17% to 29% higher torque values compared to piles with a single helix.

Table 1. Testing schedule and installation summary

Pile No.	No. of Helixes	Date	Installation Torque kN.m (ft.lbs)	Embedment Depth, m
Phase 1 Pile Load Testing				
L1	Single	July 10, 2007	71.9 (53,000)	5.2
L2	Double	July 10, 2007	86.8 (64,000)	5.2
Phase 2 Pile Load Testing				
L3	Single	January 11, 2008	52.3 (38,600)	5.3
L4	Double	January 11, 2008	67.8 (50,000)	5.3

TEST SETUP

The lateral pile load test setup was conducted in general accordance with ASTM D3966, Standard Method of Testing Piles under Lateral Loads. A schematic sectional drawing of the lateral load test setup is shown in Figure 2. The lateral load test setup consisted of a test pile that was installed at about 3 m away from a reaction pile. The reaction pile was typically a helical pile with a shaft diameter of 324 mm and double, 610 mm diameter helixes and was installed to depth of about 5.2 m below ground surface. Loads were applied at distance of about 300 mm above ground level using a 800 kN hydraulic jack. The hydraulic ram acted directly against a steel strut placed between the base of hydraulic cylinder and the reaction pile.

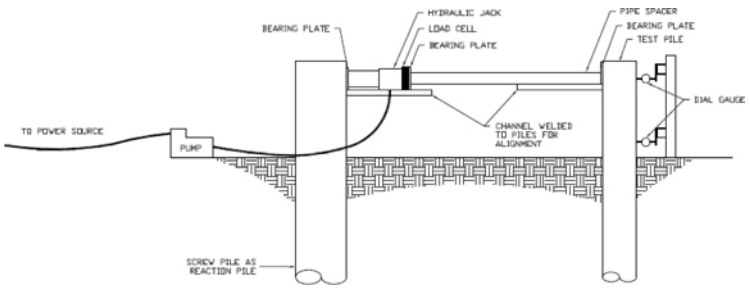

Figure 2. Lateral load test setup

Lateral movements were monitored at two points along the free length of the tested pile (at distances of 50 mm and 300 mm above ground surface) to measure lateral deflections and rotation at point of load application. The lateral deflections were measured using two independently-supported micrometer dial gauges with 0.025 mm subdivisions, and 50 mm travel. Lateral loads were applied in 2 kN increments @ 10 minutes time intervals.

TEST RESULTS

The horizontal deflections near the pile head (at about 300 mm above ground), y_o, versus the lateral loads for pile L1 with a single helix and pile L2 with double helixes are plotted in Fig. 3. It can be seen from Fig. 3 that the lateral responses of both piles were nonlinear. Piles L1 and L2 were loaded to maximum loads of about 43 kN and 42 kN, respectively which corresponded to maximum deflections of about 35 mm and 38 mm respectively. When piles rebounded to zero load, the net or permanent displacement were about 7 mm and 5 mm, for piles L1 and L2 respectively.

Comparing between the response of piles L1 and L2 indicate that pile L1 with a single helix showed slightly higher lateral resistance than pile L2 with double helixes. This observation suggests that the lateral resistance of helical piles is independent of the helix configuration and mainly governed by the shaft diameter. Therefore, the role of helixes in providing additional lateral resistance is minor given that the helixes are relatively deep (i.e. considered as long piles). Slight variations in the lateral resistances of piles L1 and L2 may be due to disturbance of soil during helical pile installation. Similar observations were reported by Puri *et al* (1984) during their lateral load tests of screw anchors using screw anchors.

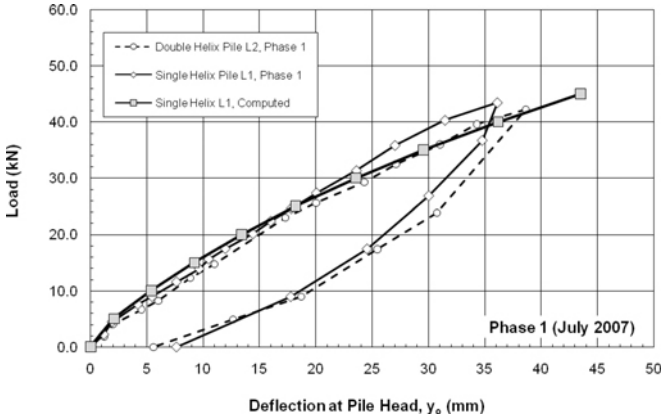

Figure 3. Lateral load-deflection curves for piles L1 and L2 (Phase 1)

Gaps were formed behind the piles during testing indicative of plastic deformation of the soil in front of the pile. Upon examination of each of the piles after the test, no noticable bending deformation of the shafts or other visible pile damage were noted, as would be indicative of a pile structural failure or development of plastic hinge during the test.

Lateral Resistance of Helical Piles in Frozen Soils

Cold temperatures in the northern climate result in freezing of the near surface ground during winter for several months. The depth of seasonal frost penetration ranges from

a minimal amount to several meters depending upon local climate, soil type, snow cover and traffic volume. Since the site was covered with snow, surface soils were dry and with no traffic to drive in the frost, the frost penetration depth at the pile load test location measured on January 12, 2008 was relatively shallow (about 300 mm). Two lateral load tests were carried out on January 12, 2008 to investigate the effect of frozen ground on the lateral performance of helical piles. The results are presented in Fig. 4 in terms of lateral deflections versus loads near the pile head. Both piles were loaded to maximum loads of about 85 kN and 60 kN respectively, which corresponded to maximum deflections of about 20 mm and 17 mm. When piles rebounded to zero loads from this point, the net or permanent displacement were about 1.5 mm and 2.5 mm for piles L3 and L4, respectively. It can be seen from Fig. 4 that the lateral response of both piles L3 and L4 were nonlinear. It can be seen from Fig. 4 that the lateral stiffness for both piles L3 and L4, defined as the ratio of lateral load to horizontal deflection at pile head, was relatively low at low deflection levels (up to about 7 mm) and increased with increasing lateral deflections. This can be explained as the installation process resulted in breaking the frozen ground near surface and therefore softer stiffness was observed at low deflection level. Pile L3 with a single helix showed slightly higher resistance compared to pile L4 with double helixes. As expected the lateral resistance of piles L3 and L4 (Fig. 4) were significantly higher than that of piles L1 and L2 (Fig. 3).

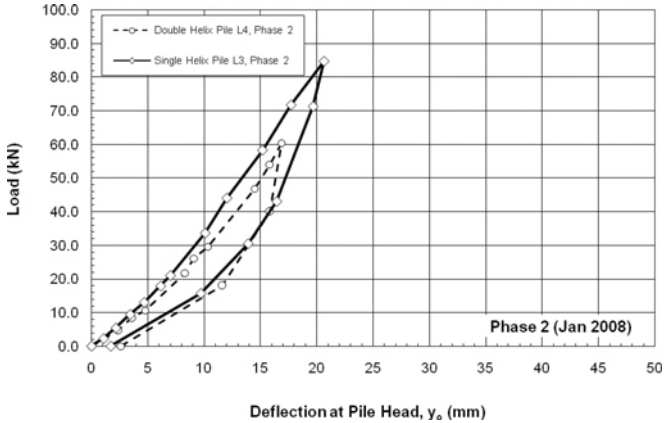

Figure 4. Lateral load-deflection curves for piles L3 and L4 (Phase 2)

Lateral Capacity of Tested Piles

The ultimate lateral load of piles is usually specified to satisfy a limiting lateral deflection criterion. This may result in specifying an "ultimate" lateral load that is much lower than the ultimate lateral capacity of the pile. For the helical piles considered in the present study with relatively short lengths, failure usually occurs by rotation of the pile within the soil. In this case, a large displacement is required to mobilize the passive resistance of the soil near the pile head and at the pile toe. Therefore, in the absence of a distinct failure criterion, the ultimate lateral load is

defined as the load that corresponds to a lateral deflection of 6.25 mm as suggested by Prakash and Sharma (1990). It should also be noted that lateral deflections in the order of 12.5 mm are often used for design of foundations supporting structures that are less sensitive to lateral movements such as power transmission lines and pipelines.

The lateral load capacities, Q_l, are presented in Table 2 at lateral deflections of 6.25 mm and 12.5 mm. Table 2 shows that the lateral resistances of piles with single helix (L1 and L3) were similar to that of piles with double helixes (L2 and L4) at low deflection level of about 6.25 mm. However at higher deflection levels (i.e. at deflection of 12.5 mm), pile L2 and L4 showed slightly lower resistance than piles L1 and L3. Comparing between piles tested in summer (Phase 1) and those tested in winter (Phase 2) showed that a significant increase in the lateral resistance was gained for piles tested in winter especially at high displacement levels. This behavior can be attributed to the increased lateral stiffness of frozen ground.

Table 2. Lateral load test results

Pile No.	No of helixes	Pile lateral resistance (Q_l) at 6.25 mm deflection, kN	Pile lateral resistance (Q_l) at 12.5 mm deflection, kN	Lateral resistance at end of test, kN	Lateral deflection at end of test, mm
L1	Single	10	18	43	35
L2	Double	9	16	42	38
L3	Single	18	45	85	20
L4	Double	16	39	65	17

Comparing between Measured and Estimated Lateral Resistances

The computer program LPILE Plus 5 (ENSOFT INC., 2000), based on the p-y curves developed by Reese et al. (1974), is widely used to predict the response of laterally loaded piles. For L-pile input, it has been assumed that soil layers consisted of compact sand, extending from the ground surface to a depth of 1.1 m over very dense oil sand that extended to beyond the bottom of piles. Groundwater level has been assigned at a depth of 1 m below ground level. Analyses were carried out for both piles L1 and L2 using free head condition. The results of load-deflection relationship were compared to the measured values as seen in Fig. 3. It can be seen from Fig. 3 that the measured and estimated values reasonably agree and that the interaction between the shaft and soil is the most significant element in resisting the lateral loads. The soil between the helixes played a minor role in the lateral resistance.

CONCLUSIONS

A full-scale pile load testing program was carried out using single and double helix piles to investigate their performance under lateral loads. The findings of this study can be summarized in the following conclusions:

1. Helical piles with a relatively small shaft and helix size were successfully installed into oil sand soil. The results of lateral load tests carried out in this study confirmed that helical piles can develop considerable resistance to lateral loads.
2. The lateral load versus deflection behavior of a helical pile is mostly controlled by the size of the shaft (i.e. diameter and thickness). The helixes have a minor effect on the lateral behavior of helical piles.
3. The use of multiple helixes may slightly reduce the lateral resistances of piles due to an additional soil disturbance. However, further investigation is required to confirm this point.
4. The lateral resistance of helical piles may be estimated analytically using the p-y curves approach. Measured and estimated lateral resistance of helical piles using LPILE Plus 5 plus program were in reasonable agreement.

ACKNOWLEDGEMENTS

The author would like to extend his gratitude to his employer and ATCO Frontec for the opportunity to carry out the load testing program at their site. The author would like to thank his coworkers and field staff for their patience, attention to details and careful installation and load testing methods for piles considered in this study. In particular the author would like to thank Messrs, Larry Kaumeyer, Richard Schmidt, Colin McCann, and Patrick Lentz.

REFERENCES

ASTM D 3966-90 (1990). "Standard Test for Piles Under Lateral Loads"; (Reapproved 1995). Annual Book of ASTM Standards, 1997, 04.08.

LPILE Plus 5. (2005). A program for the analysis of piles and drilled shafts under lateral loads, Ensoft Inc.

Prakash, S. and Sharma, H.D. (1990). "Pile Foundations in Engineering Practice". John Wiley and Sons, New York, N.Y.

Puri, V. K., Stephenson, R. W., and Goen, L. (1984). "Helical Anchor Piles Under Lateral Loading"; Laterally Loaded Deep Foundations: Analysis and Performance: ASTM STP 835, J. A. Langer, E. T. Mosley, and C. D. Thompson, Eds., American Society for Testing and Materials, 194-213.

Reese, L. C., Cox, W. R., and Koop, F. D. (1974). "Analysis of Laterally Loaded Piles in Sand". *In* Proceedings of the Offshore Technology Conference, Huoston, Texas, Paper OTC 2080, 473-483.

Scott, J. D., and Kosar, K. M. (1984). "Geotechnical Properties of Athabasca Oil Sands"; Presented at WRI-DOE Tar Sand Symposium Sponsored by Western Research Institute and U.S. Department of Energy, Vail, CO, 1-32.

Sharma, H. D., Haris, M. C., Scott, J. D. and McAllister, K. W. (1986). "Bearing Capacity of Bored Cast-in-Place Concrete Piles on Oil Sand"; Journal of the Geotechnical Engineering Division, ASCE, 112(12), 1101-1116.

Copyrighted Materials
Copyright © 2009 American Society of Civil Engineers (ASCE)
Retrieved from www.knovel.com

Load Transfer Behavior of Full-Scale Instrumented Screw Anchors

Kristen Tappenden[1], EIT, David Sego[2], PEng, and Peter Robertson[3], PEng

[1]Geotechnical Engineer, City of Edmonton Transportation Department, 11404-60 Avenue, Edmonton, Alberta, Canada, T6H 1J5; kristen.tappenden@edmonton.ca
[2]Professor, University of Alberta, Department of Civil & Environmental Engineering, 3-074 Markin/CNRL Natural Resources Engineering Facility, Edmonton, Alberta, Canada T6G 2W2; dave.sego@ualberta.ca
[3]Professor Emeritus,University of Alberta, Technical Director, Gregg Drilling & Testing Inc, 2726 Walnut Avenue, Signal Hill, CA 90755; probertson@greggdrilling.com

ABSTRACT: A research program was undertaken to study the load-transfer behavior of full-scale multi-helix screw anchors installed in natural soils. Four triple-helix screw anchors were instrumented with strain gauges at incremental distances along the inside of each anchor shaft. The test anchors were installed in glacio-lacustrine clay and aeolian sand deposits, and statically loaded in uplift and compression. Strain gauge readings collected during the load testing were used to delineate the stress transfer along the length of the test anchors to the surrounding soil. The resulting load distribution curves are compared to values predicted by the published "cylindrical shear" model, and discrepancies between the model and measured values are discussed. The results provide a context for the engineering design of screw anchors based on their interaction with the surrounding soil.

INTRODUCTION

This paper presents the results of a research program to study the load-transfer behavior of steel screw anchors installed in clay and sand soils. Screw anchors, also known as helical piles or screw piles, are deep foundations comprised of one or more circular helical plates affixed to a central shaft of smaller diameter. Screw anchors are embedded into the ground by applying a turning moment to the head of the anchor shaft, which causes the helix or helices to penetrate the soil in a "screwing" motion. For this research program, commercially manufactured triple-helix screw anchors were instrumented with strain gauges at incremental locations along the anchor shaft, and embedded into glacio-lacustrine clay and aeolian sand deposits. The instrumented test anchors were loaded to failure in axial compression and tension, and the strain gauge readings were recorded at various stages of applied loading. The load distributions along the length of the test anchors, as derived from the strain gauge readings during loading, are presented in this paper. These load distribution curves

delineate the transfer of applied axial load from the screw anchor to the surrounding soils.

FABRICATION OF TEST ANCHORS

Four steel screw anchors were fabricated for load testing as part of the research program. Each test anchor consisted of three 0.356 m diameter helices welded to a 0.219 m diameter circular hollow shaft. The three helices were vertically spaced along the screw anchor shaft at a distance equal to 1.5 times the helix diameter (0.533 m). The relative spacing of the helices along the anchor shaft, defined as the distance between adjacent helical plates divided by their average diameter, is termed the inter-helix spacing ratio. The pitch of the helices was 0.076 m, and the length of the test anchors was 5.18 m.

Each test anchor was instrumented with strain gauges installed at five levels along the inside of the anchor shaft. At each level, three axial strain gauges were installed 120 degrees apart around the circumference of the screw anchor shaft, so as to negate the effects of any bending or eccentric loading of the shaft. The strain gauge installations were protected by a silicon shell and fiberglass insulation to avoid extreme heating during assembly of the test anchors, and to prevent moisture damage during field testing. An electronic data logger system was used to monitor the real-time results and store the data collected (Zhang 1999). Fig 1 depicts the geometry of the test anchors and the locations of the strain gauge installations along the anchor shaft.

FIELD TESTING PROGRAM

Geology of Load Test Sites

The four instrumented test anchors were installed at two separate test sites in the vicinity of the city of Edmonton, Alberta, Canada. The two load test sites represented cohesive and cohesionless soils, respectively. The surficial sediments at the chosen test sites were glacio-lacustrine clay at the University of Alberta Experimental Farm in Edmonton, Alberta, Canada, and aeolian sand outside the town of Bruderheim, 60 km northeast of Edmonton. For characterization of the soil and groundwater conditions at the two test sites, a literature review of the regional geology was conducted, complemented by field and laboratory testing investigations.

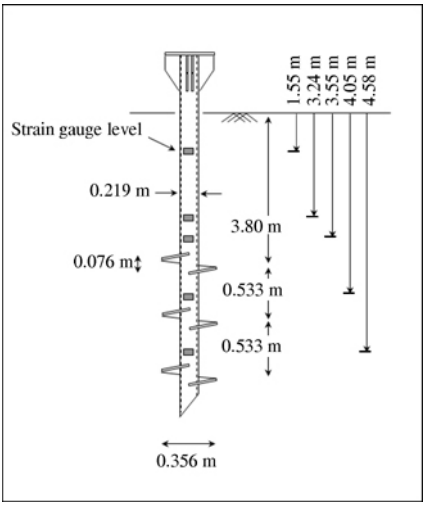

FIG 1. Geometry of Test Anchors and Strain Gauge Locations (Not to Scale)

The Edmonton test site is underlain by lacustrine sediments deposited by the proglacial Lake Edmonton, consisting of varved silts and clays typically becoming more silty and sandy with depth (Bayrock and Hughes 1962). Within the depth of the test anchor installations, the lacustrine soils generally consist of high plastic silty clay, with liquid limits of approximately 60 to 70 percent, and corresponding plasticity indices of 30 to 40 (Bhanot 1968). The stiff silty clay has an undrained shear strength of approximately 80 kPa within the depth of the test anchor installations, based on unconfined compressive strength, shear vane and Cone Penetration Tests (CPT). The groundwater level was at a depth of approximately 3 m. The surficial stratigraphy of the Bruderheim test site consists of fine- to medium- grained silty sand formed from dried wind-blown sediments originating from the proglacial Lake Edmonton (Zhang 1999). Within the depth of the test anchor installations, the silty sand was loose to compact, with corresponding friction angle of approximately 30 degrees based on CPT and Standard Penetration Test (SPT) N values (Bowles 1988). The groundwater level was at a depth of approximately 4.5 m.

Load Testing Program

Two instrumented screw anchors were installed at each of the two test sites. The dimensions of the test anchors, designated C1, C2, T1 and T2, are summarized in Table 1 below. At each test site, one anchor was loaded to failure in compression and one anchor was loaded to failure in tension, in accordance with the ASTM "quick test" procedures for static pile load testing (ASTM D 1143-81 and D 3689-90). Throughout the duration of load testing, strain measurements along the instrumented test anchor shaft were recorded and stored in an electronic data logger system (Zhang 1999).

Table 1. Geometry of Instrumented Test Anchors

Test Pile Designation (Tension, T or Compression, C)	Test Site	Anchor Length (m)	Embedment Depth of Uppermost Helix (m)	No. of Helices	Diameter of Helices (m)	Inter-Helix Spacing Ratio	Shaft Diameter (m)
C1	Edmonton	5.18	3.80	3	0.356	1.5	0.219
C2	Bruderheim	5.18	3.80	3	0.356	1.5	0.219
T1	Edmonton	5.18	3.80	3	0.356	1.5	0.219
T2	Bruderheim	5.18	3.80	3	0.356	1.5	0.219

Reactions for the axial compression and tension tests were developed from two triple-helix screw piles installed to a depth of 5.18 m on either side of the test pile. The reaction piles were connected to a horizontal test beam to form a reaction frame using high-strength steel bars. A calibrated 90 tonne hydraulic jack was used to apply compressive or tensile loading, as measured by an electronic load cell placed between the jack and the reaction frame. The vertical movement of the test anchor was monitored by two electronic displacement potentiometers diametrically positioned on

either side of the anchor. Vertical deflection of the reaction frame was measured manually by a dial gauge accurate to 0.01 mm (Zhang 1999).

For the purposes of this research program, the ultimate axial capacity of the test anchors was defined as the lesser of the applied load required to induce a displacement equal to 10% of the helix diameter (35 mm), or the applied load at the onset of plunging failure (i.e., continuous jacking required to maintain the test load).

MEASURED ANCHOR LOAD DISTRIBUTIONS

Fig 2 to Fig 5 present the load distribution curves for the instrumented test anchors, derived from the strain gauge measurements recorded at five levels along the screw anchor shafts. The multiple curves presented for each test anchor represent the measured load distribution at select loading increments up to the ultimate anchor capacity in tension or compression.

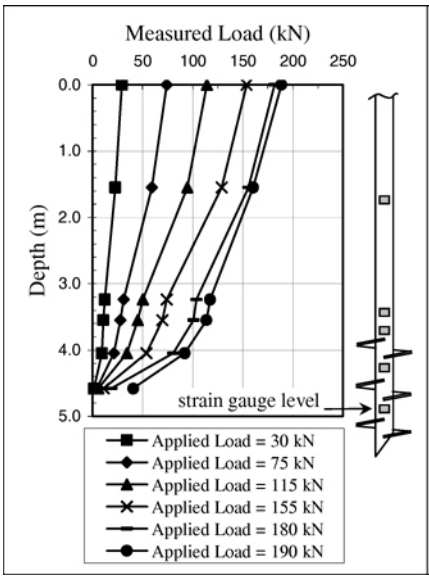

FIG 2. Load Distribution from Strain Gauge Readings during Compression Test: Anchor C1, Edmonton Site

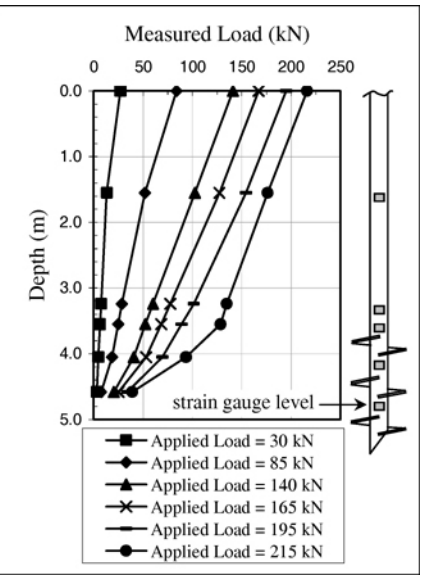

FIG 3. Load Distribution from Strain Gauge Reading during Tension Test: Anchor T1, Edmonton Site

The shape of the measured load distribution curves characterizes the mechanism of load transfer along the length of the test anchors to the surrounding soils. The right-most load distribution curve shown in Fig 2 to Fig 5 represents the distribution of applied load along the test anchor at the ultimate axial capacity. The change in measured load between two strain gauges represents the proportion of the applied load which is transferred to the soil by frictional and/or bearing contributions along the length of the test anchor between the two strain gauges.

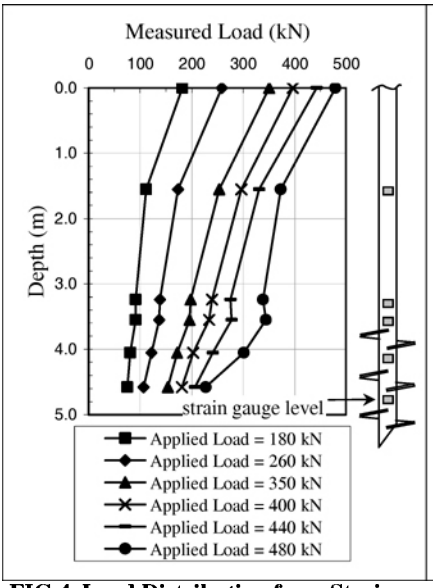

FIG 4. Load Distribution from Strain Gauge Readings during Compression Test: Anchor C2, Bruderheim Site

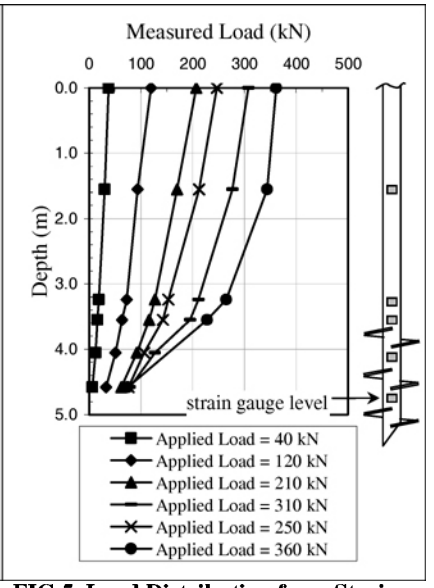

FIG 5. Load Distribution from Strain Gauge Readings during Tension Test: Anchor T2, Bruderheim Site

COMPARISON OF LOAD DISTRIBUTIONS TO CYLINDRICAL SHEAR MODEL

The screw anchors used in the current research study were each fabricated with three helices spaced along the anchor shaft at a distance of 1.5 times the helix diameter. The cylindrical shear model has been proposed in the literature to represent the behaviour of multi-helix screw piles under axial loading, where the helix spacing is less than twice the helix diameter. It is generally well accepted that the failure zone at the tip of a pile extends over a distance of almost twice the pile diameter (Zeevaert 1983). The cylindrical shear model assumes that interference between closely-spaced helical plates results in the formation of a failure surface along the cylinder of soil circumscribed between the upper and lowermost helices. The ultimate axial capacity of the screw anchor is then assumed to consist of frictional resistance along the cylindrical failure surface and along the upper portion of the anchor shaft, combined with bearing resistance above the top helix (in tension) or below the bottom helix (in compression). The cylindrical shear model has been primarily established on the basis of laboratory uplift tests performed on model screw anchors installed in sand, silt, and clay (Mitsch and Clemence 1985; Mooney et al. 1985; Narasimha Rao et al. 1993; Narasimha Rao et al. 1989), but has also been applied to laboratory compression tests performed on model screw anchors installed in clay (Narasimha Rao et al. 1991). The

components of the cylindrical shear model are depicted in Fig 6 for a multi-helix screw anchor under compressive and tensile loading conditions.

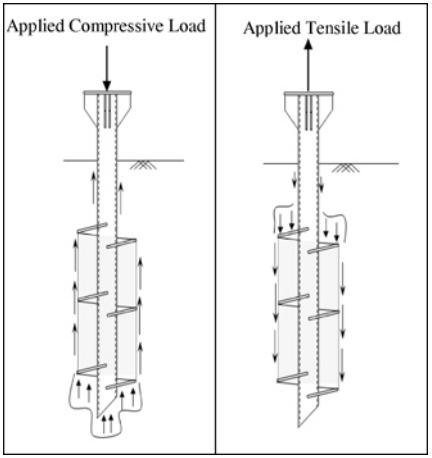

FIG 6. Cylindrical shear failure model for multi-helix screw anchor under (a) compressive load; and (b) tensile load

For comparison with the measured load distributions, the load distributions along the test anchors at failure were estimated using the cylindrical shear model. The components of shaft friction, cylindrical friction and plate bearing comprising the ultimate screw anchor capacities in tension and compression were calculated in accordance with published formulas, as compiled by Zhang (1999) and Tappenden and Sego (2007). Site-specific soil parameters estimated from the field and laboratory investigations were used in the calculations. The cumulative components of the calculated screw anchor capacities were plotted to correspond with the depth of the strain gauge installations. Fig 7 and Fig 8 show the load distributions calculated using the cylindrical shear model compared to the ultimate load distributions measured for the four test anchors.

Under applied compressive load, the ultimate capacity of the test anchors is closely estimated using the cylindrical shear model. However, the predicted distribution of compressive load along the length of the test anchors differs somewhat from the measured distribution. The cylindrical shear model appears to over-estimate the proportion of load carried in bearing by the lowermost helix in compression, while under-estimating the proportion of load distributed between the uppermost and lowermost helices (Fig 7 and Fig 8).

Under applied tensile loading, the predicted load distributions differ significantly from the measured load distributions at both test sites, and the ultimate capacity of the test anchors is significantly under-estimated using the cylindrical shear model (Fig 7 and Fig 8). In contrast to the assumptions of the cylindrical shear model (Fig 6(b)), the measured load distributions for anchors T1 and T2 show that the lowermost helix of both test anchors contributes significantly to the ultimate uplift capacity. Furthermore, any bearing above the uppermost helix on both anchors appears to contribute relatively little to the ultimate uplift capacity. However, the approximately linear decrease in load between the strain gauges above the uppermost and lowermost helices is captured by the cylindrical failure surface model. On the basis of the measured load distributions, it would appear that the behavior of the screw anchors in uplift would be better described by a failure model in which a bearing surface above the lowermost, rather than the uppermost helix, is considered to contribute substantially to the ultimate tensile capacity. The verification of such a model requires

additional research involving load testing of instrumented screw anchors in uplift.

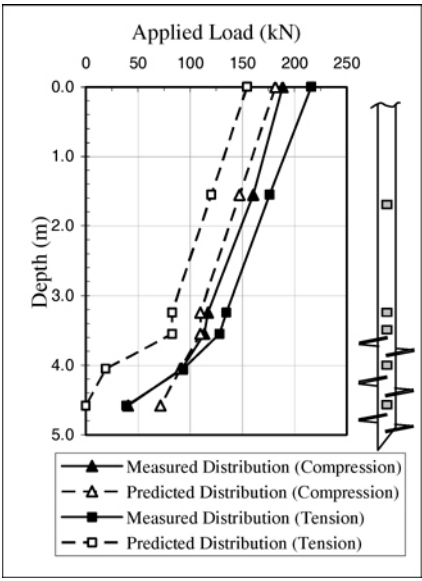

FIG 7. Measured and Predicted Ultimate Load Distributions, Edmonton Clay Site

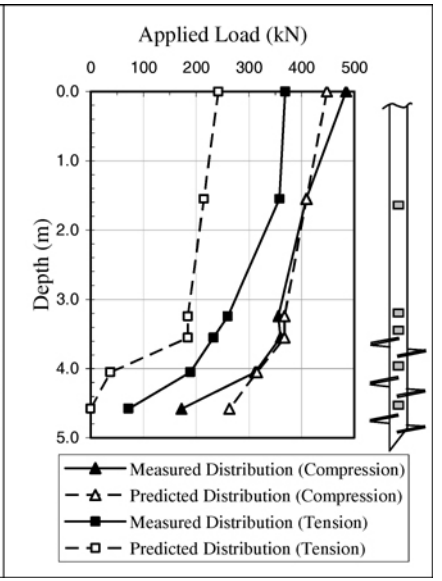

FIG 8. Measured and Predicted Ultimate Load Distributions, Bruderheim Sand Site

CONCLUSIONS

A load testing program of full-scale, instrumented screw anchors was undertaken to investigate the load transfer mechanism between multi-helix screw anchors and the surrounding soil during axial loading. Four steel screw anchors were instrumented with strain gauges at five levels along the length of the anchor shaft, and installed at two separate test sites comprising aeolian sand and glacio-lacustrine clay soils. At each test site, one screw anchor was loaded to failure in compression, and one loaded to failure in tension, in accordance with the ASTM "quick test" procedures for static pile load testing (ASTM D 1143-81 and D 3689-90). Measurements of axial strain at five locations along each test anchor shaft were collected using an electronic data logger system during incremental loading of the test anchors. The resulting load distribution curves determined at various stages of applied compressive or tensile load were presented for each of the four test anchors.

The measured load distributions at the ultimate compressive or tensile capacities were compared to the ultimate load distributions predicted by the cylindrical shear model. Reasonable agreement between the measured and predicted load distribution curves was obtained for the test anchors loaded in compression. For the test anchors loaded in tension, the predicted load distribution values differed significantly from the measured load distribution curves. In contradiction to the cylindrical shear model, the

lowermost helix of the test anchors loaded in tension contributed significantly to the ultimate axial capacity in uplift. The measured distributions support the notion of a modified failure model in which bearing above the lowermost, rather than the uppermost helix, should be considered to contribute to the ultimate tensile capacity of the anchor. Further research to investigate the behavior of full-scale instrumented screw anchors under tensile loading is required to substantiate this proposed modification to the cylindrical shear model.

ACKNOWLEDGEMENTS

The authors wish to acknowledge Diane Zhang and Gerry Cyre for their work in instrumenting the test anchors and conducting the anchor load tests documented in this paper. ConeTec Inc. and Almita Manufacturing Ltd. are thanked for their partnership and financial support of the research work presented herein.

REFERENCES

Bayrock, L.A. and Hughes, G.M. (1962). Surficial geology of the Edmonton district, Alberta. Research Council of Alberta, Preliminary Report 62-6, 40 p.

Bhanot, K.L. (1968). Behaviour of scaled and full-length cast-in-place concrete piles. *PhD Thesis*, Dept. of Civil and Environmental Engineering, University of Alberta, Edmonton, Alberta.

Bowles, J.E. (1988). Foundation analysis and design. 4th Edition, McGraw-Hill, New York, 1175 p.

Das, B.M. (1990). Earth anchors. Elsevier, New York, 241 p.

Mitsch, M.P. and Clemence, S.P. (1985). "The uplift capacity of helix anchors in sand." *Uplift Behaviour of Anchor Foundations in Soil*, ASCE, New York: 27-47.

Mooney, J.S., Adamczak, S. Jr. and Clemence, S.P. (1985). "Uplift capacity of helical anchors in clay and silt." *Uplift Behaviour of Anchor Foundations in Soil*, ASCE, New York: 49-72.

Narasimha Rao, S., Prasad, Y.V.S.N. and Veeresh, C. 1993. "Behaviour of embedded model screw anchors in soft clays." *Geotechnique* 43(4): 605-614.

Narasimha Rao, S., Prasad, Y.V.S.N. and Shetty, M.D. 1991. "The behaviour of model screw piles in cohesive soils." *Japanese Society of Soil Mechanics and Foundation Engineering* 31(2): 35-50.

Narasimha Rao, S., Prasad, Y.V.S.N., Shetty, M.D. and Joshi, V.V. 1989. "Uplift capacity of screw pile anchors." *Geotechnical Engineering* 20: 139-159.

Tappenden, K.M. and Sego, D.C. (2007). "Predicting the axial capacity of screw piles installed in Canadian soils." *Proc. 60th Canadian Geotechnical Conference,* Ottawa:1608-1615.

Zeevaert, L. (1983). Foundation engineering for difficult subsoil conditions. Van Nostrand Reinhold, New York, 2nd Edition, 652 p.

Zhang, D. (1999). Predicting capacity of helical screw piles in Alberta soils. *MSc Thesis*, Dept. of Civil and Environmental Engineering, University of Alberta, Edmonton, Alberta, 304 p.

Copyrighted Materials
Copyright © 2009 American Society of Civil Engineers (ASCE)
Retrieved from www.knovel.com

LRFD for Helical Anchors: An Overview

Donald Deardorff, P.E[1] and Ronaldo Luna, P.E., Ph.D[2].

[1] Senior Engineer, Chance Civil Construction, Division of Hubbell Power Systems, 210 North Allen Street, Centralia, MO 65240; ddeardorff@hps.hubbell.com
[2] Associate Professor, Missouri University of Science and Technology, Department of Civil, Architectural & Environmental Engineering, Rolla, MO 65409-0030; rluna@mst.edu

ABSTRACT

There is a trend for design of foundation elements using Load and Resistance Factor design (LRFD) in place of Allowable Stress Design (ASD). The ASD method accounts for design uncertainties in the form of a factor of safety, whereas the LRFD method assigns various factors to account for each uncertainty in the load and resistance. The 2004 NCHRP study on LRFD developed load and resistance factors for drilled and driven piles. The question is how does this methodology carry over to the design of helical anchors? The determination of regional load and resistance factors can be a daunting challenge for the practicing geotechnical engineer and is one of the reasons why the geotechnical industry fails to fully embrace LRFD. This paper presents a summary of what is required to develop resistance factors for helical anchors. Additionally, the First-Order Second Moment (FOSM) method is applied to a previous helical anchor study to determine resistance factors for an ultimate tension capacity strength limit state.

INTRODUCTION

The use of load and resistance factor design (LRFD) is well documented since the 1960's for structural applications when it was first adopted into the *American Concrete Institute Building Code* in 1963 and was established for geotechnical applications by the Danish Geotechnical Institute about the same time under the name of Limit State Design (LSD). The application of LRFD to foundation elements in the US has been a slow process for several reasons including:

- The LRFD method is more complex than Allowable Stress Design (ASD) and difficult to apply to geotechnical structures.
- The load and resistance factors provided in the American Association of State Highway Transportation Officials (AASHTO) LRFD bridge specifications are not applicable to all regional soils, thereby requiring regional calibration of resistance factors.
- The load factors and/or combination of load factors are not consistent between codes (i.e. AISC/ACI versus AASHTO).

- Practicing geotechnical engineers typically use local experience to supplement the amount of data available for a particular project which is not possible with the LRFD specifications.
- The methodology behind the LRFD specifications is not easily discernable regarding assumed design properties which affect the load and resistance factors.

Although the FHWA required all federally funded projects to use the LRFD method by 2007, many State Department of Transportations have yet to fully comply, primarily because of the geotechnical application problems discussed above. Due to this funding requirement, recent LRFD research has focused on common bridge foundations (i.e. driven or drilled shafts) resulting in good documentation for design using these methods. Unfortunately, it is not intuitive to the practicing geotechnical engineer how to create resistance factors for deep foundation systems that have design methodologies and installation techniques significantly different from driven or drilled shaft foundation systems.

Helical anchors typically use empirical methods for preliminary capacity design and a torque correlation methodology during installation to verify required capacity. This paper will attempt to create a roadmap for implementation of LRFD methodology for helical anchor design with particular attention paid to developing resistance factors. Additionally, the First-Order Second Moment (FOSM) method is applied to a previous helical anchor study (Hoyt and Clemence 1989) to determine resistance factors for an ultimate tension capacity strength limit state. The Hoyt and Clemence study included tension load test results of 91 multi-helix anchors at 24 different sites with varying soil conditions, embedment depths, shaft sizes, helix spacings and number of helices. As part of the study, the load test results are compared with three helical anchor capacity prediction methods to evaluate which method is the more precise indicator of anchor capacity. The results of the Hoyt and Clemence research provide the resistance bias statistics and probability density function distributions necessary for the FOSM analysis.

LRFD METHODOLOGY

The concept of the LRFD method is to establish factors for both the load and resistance which account for uncertainties using probability theory. The factors increase the nominal load and/or decrease the nominal resistance such that the probability of failure is an acceptable value. LRFD also accounts for the effects of load combinations (dead, live, seismic, wind, etc.) by determining the probability of the combined occurrence. The general form of the LRFD equation used by AASHTO is:

$$\sum_i \eta_i \gamma_i Q_{ni} \leq \varphi R_n \tag{1}$$

Where, γ_i = the load factor for i^{th} load component, Q_{ni} = the i^{th} nominal load component, η_i = modifiers applied to the load components to account for applicable factors such as ductility, pile redundancy and structure importance, $\sum \eta\ \gamma_i\ Q_{ni}$ = the total factored load for the load group, φ = the resistance factor, and, R_n = the nominal resistance (ultimate or service limit state).

Although the concept of LRFD is founded in probability theory, the development of resistance factors for geotechnical structures has mainly been determined by

correlation with ASD rather than analytical calibrations based on probabilistic analysis. With enough data for the load effect (Q) and the resistance (R) characteristics it is possible to model both as random variables and develop probability density functions as shown in Figures 1 and 2 (adapted from Withiam, et al. (1998) .

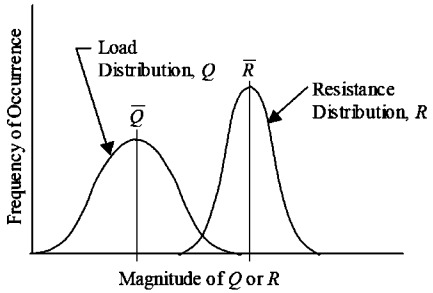

Figure 1: Probability density functions for the load and resistance

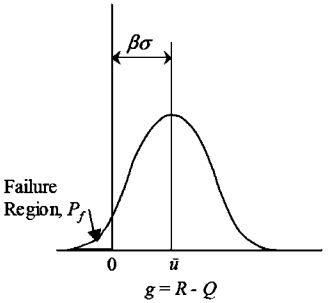

Figure 2: Combined probability density function for the limit state

When the normal distributions of the random variables associated with the limit state (g = R - Q) are plotted as shown in Figure 2, the probability of failure (P_f) is determined by the reliability index (β). The concept of LRFD is to use a reliability index appropriate to spread the distributions enough for an acceptable probability of failure.

CALIBRATION OF RESISTANCE FACTORS

Calibration by Fitting to ASD

One method of calibrating resistance factors (φ) is to fit the ASD factor of safety (FS) to a specific set of load factors (γ) thereby creating a similar margin of error. For two load sources, such as dead load (DL) and live load (LL), the resistance factor (φ) is a function of the DL to LL ratio as shown below:

$$\varphi = \frac{\gamma_{DL} \, DL/LL + \gamma_{LL}}{\left(DL/LL + 1\right) FS} \tag{2}$$

This method does not consider the bias or variability of the load factor sources or the relative magnitude of the loads and may be an appropriate method when limited statistical data is available for determination of resistance factors.

LRFD Resistance Factor Calibration Procedure

The steps required to perform the calibration are abbreviated below. For a more complete description see Allen, et al. (2005):

1. Obtain the statistical parameters of the random variables in the limit state function
2. Generate a cumulative distribution function (CDF) of the bias

3. Identify and remove outliers using caution and judgment
4. Use the CDF to determine the bias statistics
5. Scale the bias data to obtain the statistics for R and Q.
6. Determine the reliability index
7. Check the fit of the CDF function in the region near the design point
8. Plot the appropriate region of the CDF to obtain the required statistics including the mean, standard deviation and covariance of the bias

Previous research has used closed form solutions by assuming the load and resistance functions have similar distribution types and selecting a target reliability index (β_T), thereby eliminating steps 7 and 8 from above.

Determining the Target Reliability Index (β_T)

The selection of an appropriate reliability index is one of the most important steps in the calibration process. The reliability index is analogous to the ASD factor of safety where higher factors of safety reduce the risk of failure. The reliability index defines the acceptable probability of failure and the selection of a target value will vary depending upon several factors listed below:

- The reliability index associated with past design methods such as ASD may be a conservative starting point if the method has consistently provided safe results.
- The reliability index may be based on a predetermined acceptable probability of failure. Reliability indices used for design of bridge structures (researched by Paikowsky et al. (2004)) vary from 1.75 to 3.0 with a target reliability of 2.5 to 2.7 for relevant bridges.
- The consequences of failure and associated costs will control the selection of the reliability index.
- The redundancy of the system can control the selection of the reliability index. For geotechnical structures with no system redundancy (such as a single pile supporting a column) a reliability index of 3.5 is generally sufficient (Allen et al. 2005). Paikowsky (2004) recommends using β values of 2.33 for redundant piles (5 or more piles per pile cap) and 3.00 for non-redundant (less than 5 piles).

FOSM Closed Form Solution

Closed form solutions require load and resistance bias factor statistics where the bias factor is the ratio of the measured capacity over the predicted capacity (i.e. the ratio of the pile capacity from load tests to the capacity determined from a prediction model). The bias statistics include the mean bias of the load and resistance (λ_Q, λ_R) and the covariance of the load and resistance (COV_Q, COV_R). The resistance bias factor takes into account most of the uncertainty involved with the random variables associated with the resistance (i.e., random error, systematic error, spatial variability, model error, etc.). The quantity and quality of the data determine the amount of uncertainty covered by the bias. For higher confidence levels, larger databases of high quality data is needed.

A closed form solution of β is possible if sufficient data is available to characterize the load and resistance random variables. Closed form solution methods assume the

load and resistance limit state functions are either both normally distributed or both lognormally distributed and the limit state functions are linear. For lognormal distributions of the load and resistance, the reliability index (β) is:

$$\beta = \frac{\ln\left[(\bar{R}/\bar{Q})\sqrt{(1+COV_Q^2)/(1+COV_R^2)}\right]}{\sqrt{\ln\left[(1+COV_Q^2)(1+COV_R^2)\right]}} \tag{3}$$

AASHTO specifications currently use FOSM analysis developed by Barker et al. (1991) with the redundancy, ductility and operational importance factors set to 1.0 and lognormal distributions for the resistance. The basic form of the LRFD equation shown as Eq. (1) can be rewritten as:

$$\varphi = \frac{\sum \gamma_i Q_i}{R_n} \tag{4}$$

And since the nominal resistance (R_n) is equal to $\bar{R}/\lambda_R$:

$$\varphi = \frac{\lambda_R\left(\sum \lambda_i Q_i\right)}{\bar{R}} \tag{5}$$

From Eq. (3), $\bar{R}$ can be shown as:

$$\bar{R} = \frac{\bar{Q}\exp\left(\beta\sqrt{\ln\left[(1+COV_R^2)(1+COV_Q^2)\right]}\right)}{\sqrt{(1+COV_Q^2)/(1+COV_R^2)}} \tag{6}$$

And Eq. (5) can be rewritten as:

$$\varphi = \frac{\lambda_R\left(\sum \gamma_i Q_i\right)\sqrt{(1+COV_Q^2)/(1+COV_R^2)}}{\bar{Q}\exp\left\{\beta\sqrt{\ln\left[(1+COV_R^2)(1+COV_Q^2)\right]}\right\}} \tag{7}$$

By replacing the nominal load (Q_n) with $\bar{Q}/\lambda_Q$ and if only two load factors (i.e. DL and LL) are considered, Eq. (7) can be rewritten as:

$$\varphi = \frac{\lambda_R\left(\dfrac{\gamma_D Q_D}{Q_L} + \gamma_L\right)\sqrt{\dfrac{(1+COV_{Q_D}^2 + COV_{Q_L}^2)}{(1+COV_R^2)}}}{\left(\dfrac{\lambda_{Q_D} Q_D}{Q_L} + \lambda_{Q_L}\right)\exp\left\{\beta\sqrt{\ln\left[(1+COV_R^2)(1+COV_{Q_D}^2 + COV_{Q_L}^2)\right]}\right\}} \tag{8}$$

Where, λ_{QD}, λ_{QL} are the dead and live load bias factors, respectively

RESISTANCE FACTORS FOR HELICAL ANCHORS IN TENSION

There are three common capacity prediction methods used for helical anchor foundations outlined in Table 1.

Table 1 – Common Capacity Prediction Methods for Helical Pile Foundations

Individual bearing method (Klym et al. 1985)	**Conical shear method** (Mitsch and Clemence 1985)	**Torque correlation method**
$R_u = \sum_i^n A_{Hi}(c_i N_{ci}^* + q_i' N_{qi}^*)$	$R_u = \gamma' H_1 A_1 N_{qu} + \pi D_a s_u (H_3 - H_1) + A_1 s_u N_u + \frac{\pi}{2} D_a \gamma' (H_3^2 - H_1^2) K_u \tan(\phi_2')$	$R_u = K_t T$
R_u = ultimate uplift resistance A_{Hi} = Area of helix plate i i = helix identifier n = total number of helix plates c_i = cohesion at level of helix i q_i' = effective stress at the depth of helix i N_{ci}^* and N_{qi}^* are modified bearing capacity factors at the depth of helix i c_a = adhesion of the soil N_u = uplift bearing capacity factor for cohesive soils	R_u = ultimate uplift capacity γ' = effective soil unit weight K_u = uplift coefficient of lateral earth pressure (sand) ϕ_1 = soil friction angle above H_1 ϕ_2 = soil friction angle from H_1 to H_3 A_1 = area of the top helix N_{qu} = uplift capacity factor (sand) H_1 = depth to the top helix H_3 = depth to the bottom helix D_a = average helix diameter D_1 = diameter of the top helix P_s = perimeter of the anchor shaft W_s = soil weight above top helix s_u = undrained shear strength	R_u = ultimate uplift capacity K_t = empirical torque correlation factor T = average installation torque during final helical seating

Previous research by Hoyt and Clemence (1989) included statistical analysis of tension load test results of 91 multi-helix anchors at 24 sites with varying soil conditions, embedment depths, shaft sizes, helix spacings and number of helices. In this previous study, the load test results were compared with capacity prediction using the torque correlation method (TC), the individual bearing plate method (IB) and the cylindrical shear method (CS) a shown above. Table 2 presents the bias statistics from the Hoyt and Clemence study used herein to derive resistance factors for helical anchors in tension loading.

Table 2 – Hoyt and Clemence (1989) Bias Statistics

Prediction Method:	Mean (λ_R)	Std. Dev. of the bias	Covariance (COV_R)
Cylindrical Shear (CS)	1.50	1.18	0.79
Individual Bearing (IB)	1.56	1.28	0.82
Torque Correlation (TC)	1.49	0.88	0.59

In the absence of documented load factors for tension loaded helical anchors, the

researchers have assumed values that may be representative of a guy wire tiedown with a dead to live load ratio of 0.1. The load factors and bias statistics for the load effect are taken from Ellingwood et al. (1980) as $\gamma_D = 1.2$, $\gamma_W = 1.3$, $\lambda_{QD} = 1.05$, $\lambda_{QW} = 0.78$, $COV_{QD} = 0.10$ and $COV_{QW} = 0.37$.

Table 3 includes resistance factors calculated with the closed form solution (Eq. (8)) for two load effects, assumed lognormal load and resistance parameters, assumed linearity of the limit state function and the above assumed load bias statistics. The resistance factors are shown for each of the three prediction methods for various β values. The probability of failure associated with each β-value and the back calculated ASD FS from Eq. (2) are also shown in Table 3.

Table 3: Resistance Factors for Helical Anchors in Tension Loading

	Resistance Factors				ASD Fitted FS Values		
β	φ_{CS}	φ_{IB}	φ_{TC}	P_f	FS_{CS}	FS_{IB}	FS_{TC}
1.65	0.56	0.55	0.74	0.050	2.25	2.27	1.71
1.90	0.45	0.45	0.63	0.029	2.72	2.76	2.00
2.00	0.42	0.41	0.59	0.023	2.93	2.99	2.13
2.33	0.32	0.32	0.47	0.010	3.77	3.86	2.62
2.50	0.28	0.28	0.42	0.006	4.29	4.41	2.92
2.75	0.23	0.23	0.36	0.003	5.19	5.37	3.42
3.00	0.19	0.18	0.30	0.001	6.30	6.55	4.01

Discussion of Results

The torque correlation method for determining pile capacity allow higher resistance factors than the other prediction methods which is expected since the installation torque is a direct measurement of soil strength. Typical ASD FS used for helical anchor design are 2.0 which correlate to a reliability index of 1.9 for the given load and resistance bias statistics using the torque correlation prediction method. The probability of failure associated with this reliability index is about 3%. The resistance factors associated with the conical shear and individual bearing prediction methods indicate ASD FS of about 2.75 should be used to predict anchor capacity for a reliability index of 1.9.

The actual probability of failure for guy wire lines founded with helical anchors is unknown, however given that helical anchors have been in use for guy wire support for the past 40 years or so with limited significant failures due to the foundation elements, the reliability index of 1.9 (ASD FS=2) would seem appropriate for design until a more refined study can be performed.

CONCLUSIONS

Much of the recent research on LRFD application to geotechnical structures has focused on developing load and resistance factors for bridge foundations, primarily driven and drilled shaft deep foundations. Helical anchors are commonly used as tiedown support for many applications including power distribution and communication tower guy wire foundations. The FOSM calibration methodology is used to determine resistance factors based on bias statistics from a previous helical anchor study including 92 load tests at 24 sites. The results of the calibration for the

torque correlation method of capacity verification show general agreement with current ASD method safety factors.

Recommendations for further research include determination of more applicable load statistics and refinement of the statistical parameters from the Hoyt and Clemence study (λ_R, COV_R) including:

- Separating data based on soil type and strength
- Separating data based on shaft size and helix arrangement
- Separating data based on field torque determination methods
- Identify and remove possible outliers in the data
- Adding new bias statistics from additional load tests at the same limit state
- Use more robust reliability methods (i.e. advanced first-order second moment methods or Monte Carlo simulation) to confirm or modify the resistance factors

CITED REFERENCES

Allen, T. M., Nowak, A. S., and Bathurst, R. J. (2005). "Calibration to Determine Load and Resistance Factors for Geotechnical and Structural design." Transportation Research Board, Washington, DC.

Barker, R. M., Duncan, J. M., Rojiani, K., Ooi, P. l., Tan, C. K., and Kim, S. (1991). "NCHRP Report 343: Manuals for the Design of Bridge Foundations." TRB, National Research Council, Washington, D.C.

Ellingwood, B., Galambos, T. V., MacGregor, J. G., and Cornell, A. C. (1980). "Development of a Probability Based Load Criterion for American National Standard A58." National Bureau of Standards, Washington, D.C.

Hoyt, R. M., and Clemence, S. P. "Uplift Capacity of Helical Anchors in Soil." *12th International Conference on Soil Mechanics and Foundation Engineering*, Rio de Janeiro, Brazil, 1019-1022.

Klym, T. W., Radhakrishna, H. S., and Howard, K. (1985). "Helical Plate Anchors for Tower Foundations." *Symposium on Anchor Systems In Geotechnical Engineering*, 141-159.

Mitsch, M. P., and Clemence, S. P. "The Uplift Capacity of Helix Anchors in Sand." *Uplift Behavior of Anchor Foundations in Soil: Proceedings of a session sponsored by the Geotechnical Division of the American Society of Civil Engineers*, Detroit, Michigan, 26-47.

Paikowsky, S. G., Birgisson, B., McVay, M., Nguyen, T., Kuo, C., Baecher, G., Ayyub, B., Stenersen, K., O Malley, K., and Chernauskas, L. (2004). "Load and Resistance Factor Design (LRFD) for Deep Foundations." *0077-5614*, Transportation Research Board, Washington, D.C.

Withiam, J. L., Voytko, E. P., Barker, R. M., Duncan, J. M., Kelley, B. C., Musser, S. C., and Elias, V. (1998). "Load and Resistance Factor Design (LRFD) for Highway Bridge Structures." Federal Highway Administration, Washington, D.C.

Copyrighted Materials
Copyright © 2009 American Society of Civil Engineers (ASCE)
Retrieved from www.knovel.com

LOAD TEST RESULTS – LARGE DIAMETER HELICAL PIPE PILES

Kelly Hawkins[1], P.E., and Richard Thorsten[2], P.E.,

[1] Chance Civil Construction®/Division of Hubbell Power Systems, 210 N. Allen Street, Centralia, MO 65240; 573-682-8393, e-mail: kshawkin@hps.hubbell.com
[2] Chance Civil Construction®/Division of Hubbell Power Systems, 210 N. Allen Street, Centralia, MO 65240; 281-499-7901, e-mail: rethorst@hps.hubbell.com

This paper will review tests performed on large diameter (219 mm (8.625 in)) helical pipe piles with varying helical configurations (406 mm (16 in) to 762 mm (30 in)) at different locations. Included are descriptions of test pile, description of test procedure, installation procedure, soil profile, and a comparison of test results to theoretical capacities. The description of the test pile includes the helix configuration and characteristics. Different performance test acceptance criteria were evaluated relative to the ultimate capacity from the load test results. A torque correlation factor, Kt, was determined for each test pile. Both the theoretical bearing and friction capacity was calculated for each test pile.

INTRODUCTION

Seven load tests were performed at three sites, namely; four load tests in Lafayette, LA, two load tests in Philadelphia, PA, and one load test in Independence, MO. The following general designations will be used for the three sites:

LA – Lafayette, LA PA – Philadelphia, PA MO – Independence, MO

The piles consisted of 203 mm (8 in) nominal diameter pipe with varying helical configurations. Some of the test piles consisted of single 610 mm (24 in) diameter helices. Others consisted of multiple helices ranging in size from 203mm (8 in) to 762 mm (30 in) in diameter. Installation torques and load test results are presented. Ultimate compression capacities, as estimated from these load tests are compared to three theoretical methods in current use to estimate the ultimate compression capacities of the helical piles. Empirical torque factors (Kt), as estimated from the load tests and installation torques, are presented along with a comparison to Kt factors in current use for smaller diameter piles. Kt factors are also compared to normalized data using an estimated theoretical friction capacity/estimated total theoretical capacity ratio.

PILE DESCRIPTIONS

A detailed description of the piles as tested along with each pile referenced number as used throughout this paper is presented in Table 1. All test pile shaft material, except LA16x4A and LA24A was 219 mm (8.625 in) OD pipe with 6 mm (.25 in) wall. LA16x4A and LA24A shaft material was 219 mm (8.625 in) OD pipe with a 5 mm (.188 in) wall.

Table 1 Description of Test Piles

Pile Names	MO24	PA24	PA24-30	LA16x4A	LA24A	LA16x4B	LA24B
No. of Helices	1	1	2	5	2	4	1
Helix diameters (cm (in))	61 (24)	61 (24)	61-76 (24-30)	20-41-41-41-41 (8-16-16-16-16)	20-61 (8-24)	41-41-41-41 (16-16-16-16)	61 (24)
Tip Depth (m (ft))	14.9 (49)	9.7 (32)	9.7 (32)	7.4 (24)	5.5 (18)	12.8 (42)	11.6 (38)
Helix Thickness (mm (in))	19 (.75)	19 (.75)	19 (.75)	13 (.50)	19 (.75)	13 (.75)	19 (.75)

SITE SOIL DATA

The soil at the LA test site was clay to a depth of 11.3 m (37.0 ft). Sand was predominant below the 11.3 m (37.0 ft) depth. The helix (helices) of the two shorter piles as tested was positioned in clay with an Unconfined Compression Strength in the range of 12.5 kPa (0.13 tsf) to 174.3 kPa (1.82 tsf). The helix (helices) of the two longer piles as tested was positioned in clay with an Unconfined Compression Strength of 105.3 kPa (1.20 tsf), clay with an N-value (SPT value) of 16 or in sand with an N-value (SPT value) of 37.

The soil at the PA site was fill and clay to a depth of 6.9 m (22.5 ft). The soil between the 6.9 m (22.5 ft) and 9.1 m (30.0 ft) depth was defined as sand with clay or clay with sand. The soil at the 9.1 m (30.0 ft) depth was sand with an N-value (SPT-value) of 17. The helix (helices) of the two piles as tested was positioned in either clay with sand with an N-value of 5 or in sand with N-value (SPT value) of 17. There were no strength parameters given in the soil boring for the top 3.05m (10.0 ft) of fill. The boring was terminated at a depth of 9.2 m (30.0 ft). The effects of these factors on the calculated theoretical capacities will be addressed later in this paper.

The soil at the MO test site was predominantly clay to a depth of 19.8 m (65.0 ft) with traces of gravel at the 14.9 m (49.0 ft) and 18.0 m (59.0 ft) depths. The helix of the single pile as tested was positioned in clay with an N-value (SPT value) of 11.

PILE INSTALLATIONS

Typically square shaft helical piles and 114 mm (4.5 in) OD or less pipe shaft helical piles are installed using drive motors with output torque ranging from 3,390 N-m (2,500 ft-lb) to 27,112 N-m (20,000 ft-lb). Motors of these sizes can be mounted on light weight machines, such as, mini-excavators or rubber tire track-hoes. There is a difference in the drive motor output and machine size required when installing large diameter pipe piles verses square shaft or pipe shaft piles with a 114 mm (4.5 in) OD or less. The 219 mm (8.625 in) OD pipes require more torque and more crowd (down pressure). Test piles MO24, PA24, PA24-30, LA16x4B, and LA24B were installed with an Eskridge 1000 Series Digger. The motor weighed 9.6 kN (2,150 lb) and was

1.5 m (5 ft) long. The rated output torque was 113,000 N-m (83,000 ft-lb). The drive motor required a system operating pressure of 239.4 kN/m^2 (5,000 psi) at 340.7 L/min (90 gpm). At each test site the motor was mounted on a large track excavator. At the MO and PA test sites pressure gauges were used to monitor the installation torques of the piles. At the LA test site, a DPI (Delta Pressure Indicator), as manufactured by Energy Structures, Inc., was used to monitor the installation torques during the installation of the piles. The average installation torque (Ta) taken over the last 0.91 m (3 ft) of penetration into the bearing strata for each test pile is presented in Table 4.

LOAD TEST SET-UP AND TESTING PROCEDURES

Testing was conducted in accordance with ASTM D1143-81. Each load increment was held for 2 ½ minutes. Pile head displacements were measured using two dial gauges with a minimum of 50 mm (2 in) of travel. The maximum applied load for the LA24B and LA16x4B piles was 1334.4 kN (300,000 lbs). This was the maximum capacity of the loading apparatus.

LOAD TEST RESULTS

The maximum applied test loads along with the corresponding pile head displacements are shown in Table 2. Various methods to estimate the ultimate compression capacity of the piles from the load test results were considered. The method used to define the ultimate compression capacity will have a significant effect on the comparisons to the pile's calculated theoretical capacity and the torque capacity correlation factor, (Deardorff, 2007). Among these methods were the "Intersection of tangents", the Davisson Method, (Davisson, 1973), ultimate capacity based on "Full Mobilization of End bearing Method" (Terzaghi and Peck, 1948), and a defined limit on net settlement. The "Intersection of Tangents" is very subjective and was not used.

The method used to estimate the ultimate capacity of the tested piles was a combination of the Davisson Method, the "Full Mobilization of End bearing Method", and a defined limit on net settlement. The offset was defined as (4 + 0.06d) mm ((0.15 + 0.06d) inch), where d is the diameter of the largest helix in mm (inches). The defined limit of the offset was 25 mm (1 in). The estimated ultimate compression capacities (Uct) from the load verses displacement curves were based the point at which the 25.4 mm (1.0 in) offset + PL/AE line intersects the load vs. displacement curve. The offset was controlled by the defined limit of 25 mm (1 in) since the largest helix sizes range from 406 mm (16 in) to 762 mm (30 in) for these test piles. These values along with the gross pile head displacement at these estimated Uct are presented in Table 2. The values for the LA16x4B pile are estimated based on a linear extrapolation of the load verses displacement curve from 1,167 to 1,334 kN (262,500 to 300,00 lbs) since the maximum capacity of the test apparatus was limited to 1,334 kN (300,000 lb).

DISCUSSION OF LOAD TEST RESULTS

Comparison Theoretical Ultimate Capacities

Table 2 Maximum Applied Test Load and Gross Pile Head Displacement at Uct

Test Pile Number	Maximum Applied Test Load (kN (kips))	Pile Head Displacement (mm (in))
LA24A	467 (105)	47 (1.85)
LA16x4A	534 (120)	39 (1.55)
PA24	578 (130)	32 (1.26)
LA24B	1335 (300)	45 (1.79)
LA16x4B	1335 (300)	39 (1.55)
PA24-30	1223 (275)	77 (2.90)
MO24	832 (187)	66 (2.61)

The theoretical ultimate friction capacity (Ucfc) is based on the method presented by the US Navy (1974). The theoretical ultimate end bearing capacity (Ucbc) was investigated using the three methods in current use, namely, the "Individual Bearing Plate Method" (IPB Method), the "Cylindrical Shear Method" (CS Method), and the "Ultimate Capacity to Installation Torque Correlation Method" (CTC Method). The IBP Method assumes that the total theoretical end bearing capacity is equal to the summation of the theoretical end bearing capacities of each of the helices (Klym, Radhakrishna, et al, 1986 and Chance®, 2007). The CS Method assumes that the total theoretical end bearing capacity is equal to the summation of the ultimate friction resistance developed along a cylinder of soil formed between the bottom and top most helix plus the theoretical end bearing capacity of the bottom helix, if the loading is from compression (Clemence et al. 1985). The CTC Method assumes there is a correlation between the ultimate capacity of a helical pile and the torque applied during installation (Hoyt and Clemence, 1989 and Chance®, 2007). This correlation is defined by Ucc = Kt x Ta, where Kt is the empirical torque factor and Ta is the average installation torque. Ta is defined as the average installation torque taken over the last 0.91 m (3 ft) of penetration into the bearing strata (Chance®, 2007). Kt varies inversely with the pile shaft diameter. The default Kt values cited in the two references range from 33 m^{-1} (10 ft^{-1}) for all square shaft piles to 10 m^{-1} (3 ft^{-1}) for 219 mm (8.625 in) pipe shafts A compromised Kt of 13 m^{-1} (4 ft^{-1}) was used to calculate the total theoretical ultimate capacity for the test piles.

Table 3 Ratio of Ucc/Uct For Each Theoretical Capacity Method

Test Pile Number	Ucc/Uct		
	IBPM	CSM	CTCM
LA24A	0.67	0.67	0.87
LA16x4A	0.53	0.68	0.67
LA24B	0.77	0.77	0.71
LA16x4B	0.69	0.71	0.66
MO24	0.67	0.67	1.15
PA24	1.23	1.23	0.92
PA24-30	1.06	1.09	0.80
Averages	0.80	0.83	0.83

The Uct values from the load verses displacement curves are compared to the theoretical Ucc values from the three theoretical methods using the ratio of Ucc/Uct. The resulting ratios for each of the test piles using the IBP Method, the CS Method, and the CTC Method are shown in Table 3. All three theoretical methods on average under estimated the ultimate compression capacity. The IBP

Method under estimated the ultimate compression capacity by an average of 20%. The CS Method and CTC Method both under estimated the ultimate compression capacity by an average of 17%.

At the PA site, the IBP Method and the CS Method over estimated the ultimate compression capacity by averages of 15% and 16% respectively. The CTC Method under estimated the ultimate compression capacity by an average of 14% at this same site. This average under estimation of 14% is similar to the average under estimation of all the sites of 17%. Since the IBP Method and the CS Method rely on data from soil borings and the CTC Method relies on data taken during the installation of the test piles, the assumptions regarding the soil profile at this site used to calculate the ultimate compression capacity may be questionable. The soil below the 9.1 m (30.0 ft) may not continue as sand with an N-value of 17. Note that the soil boring was terminated at a depth of 9.1 m (30.0 ft) and the 610 mm (24 in) diameter helices are located at a bearing depth of 9.8 m (32.0 ft). Also, assumptions regarding the strength characteristics of the fill had to be made at this site.

At the MO site, the IBP Method and the CS Method under estimated the ultimate compression capacity by 33%. The CTC Method over estimated the ultimate compression capacity by an average of 15% at this same site. The Kt of 13.1 m^{-1} (4.0 ft^{-1}) used at this site appears to be high. This observation will be discussed in the next section.

Empirical Torque Correlation Factor (Kt)

The torque required for the installation of a helical pile and thus the resulting Kt factor is effected by a number of factors, such as, the shaft size, depth of embedment, helix diameter and thickness, pitch of helix, et al. An energy model used to estimate the ultimate capacity of a helical pile suggests that Kt is moderately affected by helical blade radius and strongly influenced by the shaft (hub) diameter and the helix thickness (Perko, 2000). Consideration of these factors is presented in the following section.

The Ta values from the installation of the piles along with the resulting Kt values are presented in Table 4. Five of the seven test piles had thick, large diameter helices. Two of the test piles, LA16x4A and LA16x4B, had thinner, smaller diameter helices.

Table 4 Average Installation Torque (Ta), Kt Factors, Theoretical Friction Capacities (Ucfc), and Theoretical Ultimate Total Compression Capacities (Ucc)

Test Pile Number	Ta (N-m (lbs-ft))	Kt (m-1 (ft-1))	Ucfc (kN (lbs))	Ucc (kN (lbs))
MO24	64,910 (47,875)	11.5 (3.5)	333.2 (74,900)	495.5 (111,400)
PA24	40,675 (30,000)	14.1 (4.3)	194.4 (43,700)	712.1 (160,100)
PA24-30	45,815 (33,791)	16.4 (5)	144.6 (32,500)	804.7 (180,900)
LA24A	27,674 (20,411)	15.1 (4.6)	93.4 (21,000)	279.8 (62,900)
LA16x4A	24,906 (18,370)	16.7 (5.1)	63.2 (14,200)	256.6 (57,700)
LA24B	69,316 (51,125)	18.4 (5.6)	222.4 (50,000)	988.4 (222,200)
LA16x4B	72,255 (53,292)	19 (5.8)	170.8 (38,400)	993.7 (223,400)

The Ta values and thus the Kt values for these two test piles were adjusted due to the efficiency of thin small diameter verses thicker large diameter helices. Kt is equal to Uct divided by Ta.

Also, shown in this table are the theoretical total Ucc values using the Individual Bearing Plate Method and the Ucfc values using the US Navy (1974) method. The Kt values are equal to or greater than the assumed Kt value of 13.1 m^{-1} (4.0 ft^{-1}) for six of the seven test sites. At the MO site, the Kt value is 11.5 m^{-1} (3.5 ft^{-1}). As previously stated, Kt varies inversely with the pile shaft diameter. Also, Kt is assumed to be constant for a given shaft size for shaft diameters less than 114.3 mm (4.5 in). It is assumed that the torque expended to install smaller diameter shafts is relatively small in relationship to the torque expended to install the helices. Therefore, Kt for smaller diameter shafts is assumed not to decrease as additional shaft material is installed. Kt for larger diameter piles consists of the energy, i.e., torque, to install the helices and the energy, torque, required to install larger diameter shafts. The torque expended to install larger diameter shafts could be relatively large in relationship to the torque expended to install the helices. As additional shaft material is installed, the surface area of the pile shaft in contact with the soil increases. This could require more energy for installation of the pile shaft. Therefore, it follows that Kt may vary inversely with the ultimate friction capacity of a pile. In other words, the higher the ultimate friction capacity, the more energy, (i.e., torque) must be expended to install the pile. To investigate if a possible relationship exists between Kt factors and the ultimate friction capacity of a pile, Kt factors from Table 4 were plotted as a function of the Ucfc/Ucc ratios. See Figure 1. It appears that if the Ucfc/Ucc ratio is less than 0.3, then a constant Kt value in the range of 14.8 m^{-1} (4.5 ft^{-1}) to 18. 0 m^{-1} (5.5 ft^{-1}) would provide a reasonable preliminary estimate of the pile's total theoretical ultimate compression capacity using the Ultimate Capacity to Installation Torque Correlation Method. For Ucfc/Ucc ratios greater than 0.3, Kt appears to vary inversely with the ultimate friction capacity of a pile. Kt factors of the magnitude of (6.0 – ((3.5 to 4.5) x (Ucfc/Ucc))) may be warranted.

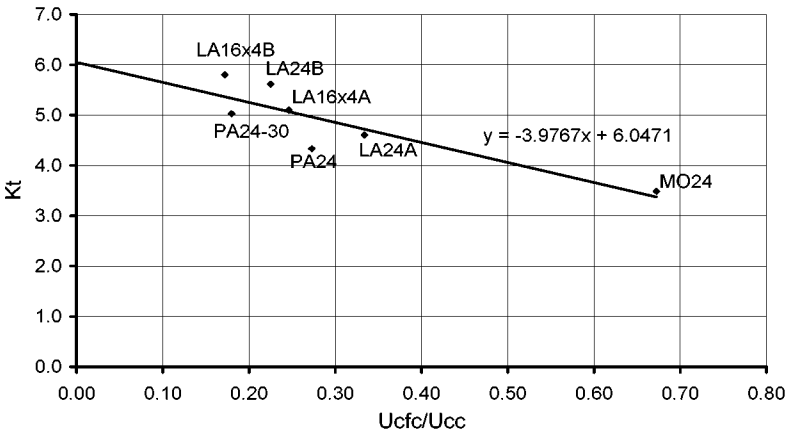

Figure 1 Kt Factors vs Ucfc/Ucc Ratios

CONCLUSIONS

The theoretical ultimate friction capacity method in conjunction with the theoretical ultimate end bearing capacity methods in current use, i.e., the "Individual Bearing Plate Method" and the "Cylindrical Shear Method" under estimated the total ultimate compression capacities as derived from the pile load tests on five of the seven test piles at two of the test sites. The average under estimation was 33% using the "Individual Bearing Plate Method" and 30% using the "Cylindrical Shear Method". At the other test site, both methods over estimated the total ultimate compression capacities 15% using the "Individual Bearing Plate Method" and 16% using the "Cylindrical Shear Method". These over estimations were probably the result of the assumptions that had to be made due the lack of soil strength parameters on the soil boring and the bearing depth of the helices relative to the termination depth of the soil boring. The "Ultimate Capacity to Installation Torque Correlation Method" using a Kt of 13 m^{-1} (4.0 ft^{-1}) under estimated the total ultimate compression capacities as derived from the pile load tests on six of the seven test piles at two of the test sites. The average under estimation was 23%. At the other test site, this method over estimated the total ultimate compression capacities by 15%. This over estimation was probably the result of the large amount of energy (torque) that was expended due to the high frictional capacity of the pile relative to its' total ultimate compression capacity. The empirical torque factor (Kt) varies inversely with the diameter of the pile shaft. Kt is also considered a constant for a given small diameter pile shaft. Kt may not be constant for a given large diameter pile shaft. Kt may vary inversely to the proportion of the theoretical ultimate friction capacity to the total ultimate compression capacity. The above conclusions are based on a very limited amount of load tests on large diameter helical pile shafts. Additional testing on both large diameter helical pipe shafts and large diameter helices is required to substantiate these conclusions.

ACKNOWLEDGEMENTS

At PA site, to DANBRO Distributors for their contribution of personnel, testing equipment, installation of the test piles, and the use of the land for the load tests.

At LA site, to Ark-La-Tex Helical Distributors, LLC for their contribution of personnel and testing equipment and to Helical Tower Foundations, LLC for their contribution of personnel, manufacturing and installation of the test piles, and the use of the land for the load tests.

REFERENCES

ASTM D1143-81(Reapproved 1994), Standard Test Method for Piles under Static Axial Compressive Load, American Society of Testing and Materials, Philadelphia, Pennsylvania

CHANCE® CIVIL CONSTRUCTION TECHNICAL DESIGN MANUAL, 2007, published by the Chance Division of Hubbell Power Systems, Inc. (Bulletin #01-0605), Centralia, MO.

CLEMENCE, S. P., Editor, Contributing Authors ADAMCZAK, Jr., S., CLEMENCE, S. P., DAS, B. M., FINN, M., HOWARD, R. E., KULHAWY, F. H., MITSCH, M. P., MOONEY, J. S., RAPOPORT, V., VALDES, J. A., YOUNG, A. G., 1985, Uplift Behavior of Anchor Foundations in Soil, American Society of Civil Engineers, New York City, New York.

DAVISSON, M. T., High Capacity Piles, 1973, Department of Civil Engineering, Illinois Institute of Technology, Chicago, Illinois.

DEARDORFF, D. A., 2007, "Torque Correlation Factors for Round Shaft Helical Piles", Proceeding of the Deep Foundation Institute 32nd Annual Conference on Deep Foundations, Colorado Springs, CO

HOYT, R. L. and CLEMENCE, S. P., 1989, Uplift Capacity of Helical Anchors in Soil, Proceedings of the 12th International Conference on Soil Mechanics and Foundation Engineering, Rio de Janeiro, Brazil.

KLYM, T. W., RADHAKRISHNA, H. S. et al, 1986, "Helical Plate Anchors for Tower Foundations", Symposium on Anchor Systems in Geotechnical Engineering, The Canadian Geotechnical Society, Toronto, Canada.

PERKO, H. A., 2000, "Energy Method for Predicting Installation Torque of Helical Foundations and Anchors", GeoDenver 2000, Denver, CO, ASCE Press, Reston, VA

TERZAGHI, K. and PECK, R. B., 1948, Soil Mechanics in Engineering Practice, John Wiley and Sons, New York City, New York

US NAVY DESIGN MANUAL DM7, NAVFAC, 1974, Foundations and Earth Structures, Government Printing Office, Washington, DC.

Copyrighted Materials
Copyright © 2009 American Society of Civil Engineers (ASCE)
Retrieved from www.knovel.com

Performance-based design for helical piles

Mamdouh Nasr, P.Eng, M. ASCE[1]

1. Managing director, M.N. Geotechnical Engineering, 11728 Wilshire Blvd, Los Angeles California, USA mamnasr@shaw.ca

ABSTRACT

Performance of a deep foundation under applied loading dictates the design. In all circumstances, performance is considered poor if significant settlement or deflection occurs. Although the physics around helical pile performance may be quite simple, it is often the most overlooked factor by practicing engineers using the current helical pile design methods. This paper shows the importance of understanding critical-state soils mechanics when designing helical piles and includes a case study, where a helical pile was installed in dense sand for which high energy torque was required for installation. Load tests from that test show affiliated dilation, and, ultimately, the helical piles poor-performance when evaluated under uplift loading. Finite element modeling is included that further validate these findings.

KEY WORDS

Helical pile, load test, sand, dilation, settlement, case history

INTRODUCTION

To understand the axial load-carrying capacity of multi-helix piles, Zhang (1999) conducted 18 pile load tests at a University of Alberta Farm site (cohesive soil) and at a Sand Pit site (cohesionless soil). Of these 13 use fully instrumented research piles and the remaining 5 s were carried out using regular, non-instrumented production piles. Various pile capacity formulas (e.g. Individual Plate Bearing Method Cylindrical Shear Method).

Most helical pile design engineers are familiar with equations for the Individual Plate-Bearing or Cylindrical Shear methods developed for helical piles installed in cohesive or cohesionless soils (Mooney 1985, Mitsch and Clemence 1985). These were derived taking into account pile geometry, pitch, number of helices, and inter-helix spacing, whereby two-dimensional stress-strain relationships are used to obtain ultimate stress and a safety factor is applied to produce an allowable stress under working loads.

Current design methods for helical piles do not predict pile settlement at working loads or take into consideration stress path, or altered stress paths during pile installation. As an example, the Cylindrical Shear method for cohesive soil utilizes undrained shear strength as the only stress path to the critical state. In the case of very dense, cohesionless soils, a high installation torque is required for installation. This alters the soil's state and ultimately brings the stress path to the critical state through dilate and loosening the soil from its in-situ state.

This paper shows the importance of critical state soils mechanics for designing helical piles and discusses the test results of a helical pile installed using very high torque in dense sand. The results of the load test shows how the high torque of installation led to sand dilation, and ultimately the helical piles poor-performance, when evaluated under uplift loading. Furthermore, current design formulas are shown to be deficient in both capacity prediction and cannot predict the pile settlement at any specific load. Finally, results from a finite element model are presented.

THESIS SUMMARY

Zhang (199) as part of a study on the behavior of single and multi-helices helical piles under compression and uplift forces suggested that if a helical pile has a shaft depth to helix diameter ratio (H/D) > 5, it can be considered as a deep helical pile. Zhang indentified a number of failure models for such piles when subjected to axial uplift forces. The Cylindrical Shear Method and Individual Bearing Method are most commonly used as indirect methods to predict uplift capacity.

Cylindrical Shear Method

The cylindrical shear method assumes a cylindrical shear failure surface connecting the uppermost and lowermost helices (fig. 1).

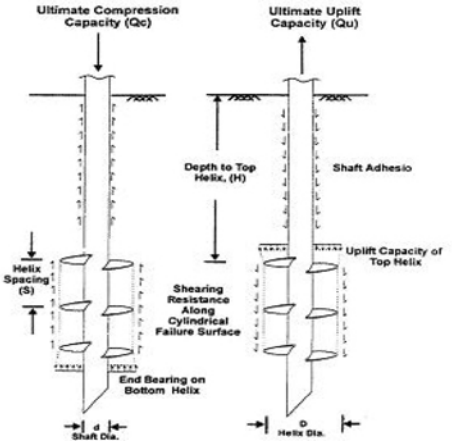

Figure 1. Screw Pile in Compression and Tension Loading (after Rao et al. 1991).

Uplift capacity is mainly derived from shear resistance along the cylindrical surface and bearing resistance above the top helix (eqn 1)

$$Q_t = Q_{Shaft} + Q_{helix} + Q_{Bearing} \quad \text{(eqn 1)}$$

where Q_t is the ultimate uplift capacity, Q_{Shaft} is the adhesion developed along the steel shaft, Q_{helix} is the shearing resistance mobilized along the cylindrical failure surface, and $Q_{Bearing}$ is the bearing capacity of the top helix.

Helical pile under uplift in sand

Zhang (1999) reports two distinct failure behavior patterns under uplift loading. Similar to what Meyerhof and Adam (1968) observed in the laboratory, failure could be approximated either as shallow or deep depending on the relative density (Dr) , the internal soil friction angle, φ, and the embedment ratio (H/D) of the sand. The maximum embedment ratio $(H/D)_{cr}$, where the failure mode changes from shallow to deep, increases with increased in Dr and φ. In laboratory tests on sand with relative densities ranging from 47% to 90%, a helical pile behaves as a shallow anchor with an embedment ratio (H/D) less than 5. For sand with the same Dr and H/D greater than 5, the helical pile is defined as a deep anchor where a failure zone develops directly above the top helix. The equation for estimating the shaft friction in homogeneous sand is provided by Meyerhof and Adam (1968). For deep anchors, the ultimate tensile capacity can be derived from eqn 2.

$$Q_t = \gamma' H_1 A_I N_q + \pi/2\, D_a \gamma' (H^2_3 - H^2_1) K_U \tan\varphi + P_s H_1 (\gamma' H_1/2) K_U \tan\varphi \quad \text{(eqn 2)}$$

where Q_t is the ultimate Helical pile uplift capacity, γ' is the effective unit weight of soil, K_U is the coefficient of lateral earth pressure in uplift for sands, A_I is the area of the top helix, N_q is the uplift capacity factor for cohesionless soils, H_1 is the depth to top helix, D_a is the average helix diameter, D_I is the diameter of the top helix, H_3 is the depth to the bottom helix, and P_S is the perimeter of the screw pile shaft

The major variable in the above equation is the lateral earth pressure coefficient in uplift (Ku). Zhang (1999) indicated that the lateral stress outside the cylindrical failure surface increases to a passive state due to the screw action during the installation process. The magnitude of the increase is dependent upon the amount of disturbance and the changes in stress level during the installation. Mitsch and Clemence (1985) provided values for Ku for screw piles (Table 1). The recommended values were based on the model and field tests, and are 30% to 40% lower than those provided by Meyerhof and Adam (1968), mainly as a result of installation disturbance

Helical pile under uplift in clay

Of note is that Zhang (1999) suggested the study of clay in undrained condition (φ=0). Research done on uplift anchor capacity by Ali (1968) and Kupfman (1971), Das(1980) and Narasimha Rao and Prasad (1989), indicate that the uplift bearing

capacity factor Nu increases with embedment depth/ helix diameter ratio (H/D) to a constant maximum value of 9.4 for H/D=4.0. Therefore, the uplift capacity equation is expressed as eqn 3.

$$Qt = A_l\ Cu\ Nu + \pi\ D_a\ Cu\ (H3 - Hl) + Ps\ H_1\ Ca \qquad \text{(eqn 3)}$$

Where Qt is the ultimate uplift capacity of the multi-helix screw pile, H1 is the depth to top helix, H3 is the depth to bottom helix, Da is the average helix diameter, Ps is the perimeter of anchor shaft, A_l is the area of top helix, Nu is the uplift bearing capacity factor for cohesive soils, Cu is the undrained shear strength of the clay, and Ca is the average cohesion of soil along the pile shaft.

Table 1. Recommended Uplift Coefficients, *Ku* for Helical Anchors (after Mitsch and Clemence 1985)

Soil Friction Angle (φ)	Meyerhof coefficient K_U	Mitsch and Clemence coefficient K_U
25	1.2	0.7
30	1.5	0.9
35	2.5	1.5
40	3.9	2.35
45	5.3	3.20

The Individual Plate Method assumes that bearing failure occurs above each individual helix (Zhang 1999), and the total uplift resistance is the sum of the individual capacities. A similar explanation of adhesion resistance along the pile shaft as discussed here is also applied (eqn 4).

$$Q_t = Q_{shaft} + \Sigma\ Q_{Bearing} \qquad \text{(eqn 4)}$$

where Qt is the ultimate uplift capacity, Q_{shaft} is the adhesion developed along the steel shaft and $\Sigma\ Q_{Bearing}$ is the sum of the bearing capacity of each individual helix.

At higher space to diameter ratio (S/D > 2), individual bearing method should provide better prediction of ultimate uplift capacity for screw piles. Adams and Klym (1971) state that at S/D > 2 each helix plate can be assumed to behave independently of the other. Rao et al. (1993) suggested that at higher S/D ratio, adhesion over a shaft length of 1.5D - 2.50 above each plate should be considered for multi-helix screw piles installed in cohesive soil.

HELICAL PILE INSTALLTION IN DENSE SAND- CASE STUDY

A helical pile design using 0.406 m shaft, 4.80 m deep with single 0.813 m helix was suggested for use as a foundation of transmission towers in Alberta Canada. A load test was performed to verify the pile capacity and to check the pile behavior under uplift forces. The soils investigation indicated a very dense sand layer with SPT > 50

at a depth of 3 m below ground level. Due to the expected high torque of installation, the sand from inside the pile was removed to minimize the friction and reduce the required torque of installation. The pile's final torque was around 190 kN.m.

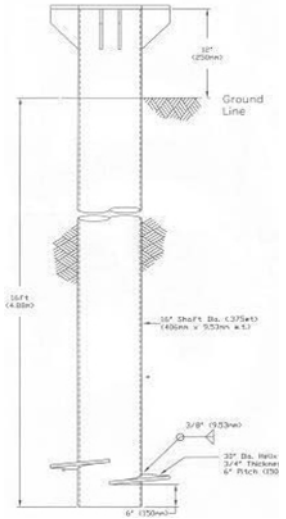

Figure 2. Schematic of tested helical pile (after Zhang 1999)

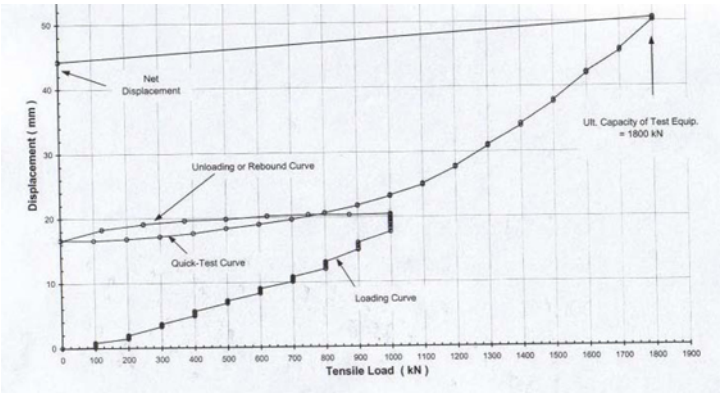

Figure 3. Displacement versus tensile load (after Zhang 1999)

The pile was load tested for uplift following ASTM-D3689 (Quick load testing method). The pile was loaded to 1000 kN with recorded total deflection of 20 mm. The pile was unloaded to zero load with recorded residual movement of 16 mm and reloaded to 1800 kN. The recorded deflection at 1000 kN was 24 mm and at maximum load of 1800 kN, 50 mm. Due to hydraulic jack limitation the load test stopped and pile was unloaded to zero load and the recorded deflection was 44 mm.

Using the suggested formulas for design of helical piles in dense sand (Zhang 1999) and a residual friction angle of 38 degrees (Sharma et al. 1986 indicated a peak frictional angle of 50° and residual one of 38° for oil sands), the pile shaft ultimate resistance was calculated at 830 kN and total ultimate uplift resistance as 3100 kN. Load test data agreed (assuming failure is defined as 10% of helix diameter).

Although test data confirmed ultimate capacity with the theory, behavior at a working load of 1000 kN (ultimate load /F.S. = 3) was not satisfactory as the pile moved 20 mm with 16 mm residual and 24 under reloading.

The high torque required to install the pile had dilated the very dense sand. During the load test, the sand had the opportunity to contract again. Under 1000 kN of load, sand contracted 14 mm, which has been shown as residual movement. When unloading and reloading additional contraction occurred (shown in the difference between the original movement at first load cycle and second load cycle). At higher loads and continuous pile movement, the dilated sand particles continued to contract leading to a pile residual movement of 44 mm.

In triaxial tests under low confinement pressures (100 kPa), dense sand shows dilation at relatively low strain levels (2-3 % axial strain). Guo and Su (2007) studied the behavior of round Ottawa sand and angular crushed limestone, in their study of shear strength, interparticle locking, and dilatancy. Their study included the stress-strain and volume change responses for both sands. The stress-strain response is presented as the principle stress ratio $R = \sigma'_1 / \sigma'_3$ against the axial strain. For Ottawa sand with Dr = 74%, following the initial volumetric compression at small axial strain, significant dilation occurs when the mobilized stress ratio approaches its maximum value. After the peak on the curve of stress ratio against axial strain, both the stress ratio and rate of volume dilation decrease quickly with continuous shearing until the critical state is reached. The peak stress ratio and the amount of volume dilation, which both tend to reduce with the increase of void ratio, vanish completely for a loose specimen with the initial void ratio $e_0 = 0.77$ (fig. 4).

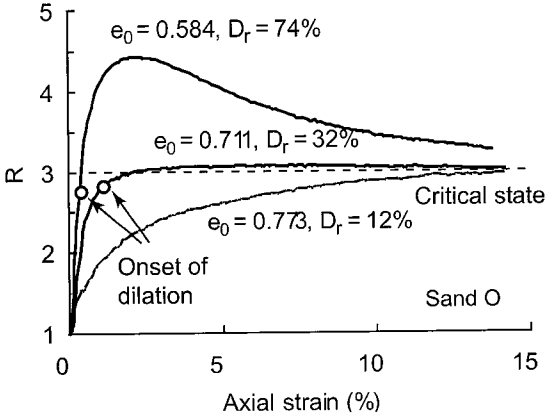

Figure 4. Principal stress ratio versus axial strain (after Guo and Su 2007)

Guo and Su (2007) concluded that Ottawa sand dilation starts at stress ratios smaller than at the critical state, indicating that the mobilized friction angle at the onset of dilation, φ_f, is smaller than the critical state friction angle φ_{cv}. Figure 4 shows the variation of φ_f and peak friction angle, φ_p, against the initial void ratio for Ottawa sand and shows that φ_f gradually approaches φ_{cv}, as void ratio increases.

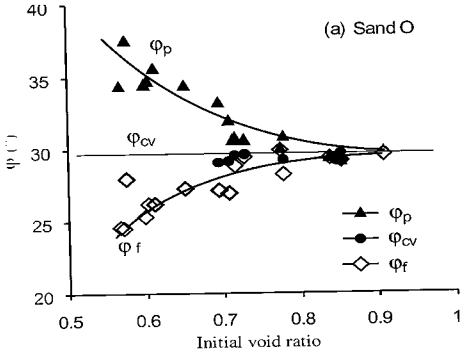

Figure 5. Friction angle changes with void ratio (after Guo and Su 2007)

An axisymmetry finite element analysis model in Plaxis V8 was used by the author to capture this behavior. The soil hardening constitutive model was used to represent the sand dilation. The dilated sand properties included in the input assumed peak angle of internal friction of 40 and dilation angle 34°. The output of the finite element model agreed with the test results showing a pile total deflection of 22 mm at 1000 kN, 17 mm when unloaded to zero, 23 mm after reloading to 1000 kN, 52 mm at 1800 kN and 43 mm when unloaded again to zero (fig. 6)

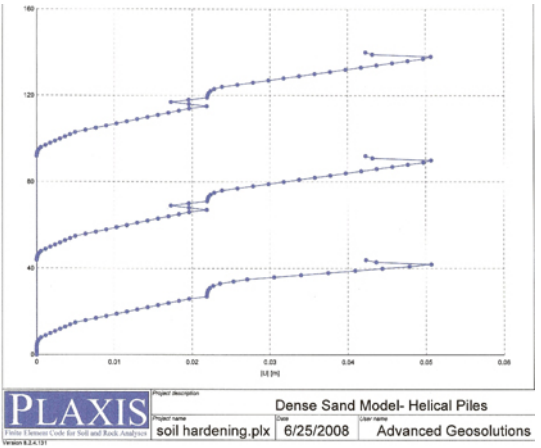

Figure 6. Finite Element Model output of pile displacement under loading

SUMMARY AND CONCLUSION

- Although the pile capacity calculated using the helical piles design formulas was verified from that load test (using the residual angle of friction of the dilated sand), the pile movement was not predicted and the pile movement at the allowable design load = 1000 kN (based on safety factor =3.0) was very high.
- Finite element methods should be used to model the helical piles, if the expected soil behavior indicates dilation (dense sand and over consolidated clays).
- The installation of helical piles has impact on the soil stress state and accordingly stress path. This effect should not be ignored in the design of helical piles.
- The author suggests a further study on the installation of helical piles in loose sand and normally consolidated clays.
- The author suggests a similar study to be done on the different types of deep foundation (driven and bored cast in place piles).

REFERENCES

Adams, J.I. and Klym, T.W., 1972. A Study of Anchors for Transmission Tower Foundations. Canadian Geotechnical Journal, Vol. 9, No. 1, pp. 89-104.

Guo, P. and Su, X., 2007. Shear strength, interparticle locking, and dilatancy of granular materials, Canadian Geotechnical Journal, 44(5): 579-591.

Meyerhof, G.G., and Adams, J.I., 1968. Ultimate Uplift Capacity of Foundations Canadian Geotechnical Journal, 5 (4): 225-244.

Mitsch, M.P. and Clemence, S.P., 1985. The Uplift Capacity of Helix Anchors in Sand. Uplift Behavior of Anchor Foundations in Soil, Proceedings of ASCE, New York, NY: 26-47.

Mooney, J., Adamczak, S. and Clements, S., 1985. Uplift Capacity of Helix Anchors in Clay and Silt, Proceedings of ASCE, New York, NY: 48-72.

Rao, S. and Prasad, Y.V.S.N., 1991. Estimation of Uplift Capacity of Helical Anchors in Clays, Journal of Geotechnical Engineering, 119 (2): 352-357.

Zhang, D.J.Y., 1999. Predicting Capacity of Helical Screw Piles in Alberta Soils, M.S. Thesis, Dept. of Civil and Environmental Engineering, University of Alberta.

Copyrighted Materials
Copyright © 2009 American Society of Civil Engineers (ASCE)
Retrieved from www.knovel.com

DESIGN AND CONSTRUCTION OF INTERMEDIATE FOUNDATION® SOLUTIONS FOR WIND TURBINES

Brendan FitzPatrick, P.E., M.ASCE[1], Richard Gernant, P.E., M.ASCE[2], Jeromy Miceli[3]

[1] Director of Engineering and Development – North America, Geopier Foundation Company, Inc., 150 Fairview Road, Suite 335, Mooresville, NC 28117, bfitzpatrick@geopier.com

[2] Principal Engineer, Geopier Foundation Company – Midwest, Inc., 4504 Ashley Park Drive, West Des Moines, IA 50265, dgernant@geopiermw.com

[3] Project Engineer, Iberdrola Renewables, 201 King of Prussia Road, Suite 500, Radnor, PA 19807, jmiceli@iberdrolausa.com

ABSTRACT: The demand for alternative energy sources has sparked significant growth in wind energy. Tower foundation designs consider static bearing and settlement like traditional buildings, but transient pressures from large overturning moments and the need for high foundation stiffness typically control the design. When soft or compressible soils encountered at tower sites do not provide adequate bearing capacity, fuel-intensive overexcavation and replacement, or resource-depleting deep foundations may be used. These solutions are environmentally insensitive. In addition, wind farms are typically located in remote areas, making equipment mobilization and material delivery a costly challenge.

This paper describes the use of Intermediate Foundation® solutions using Rammed Aggregate Pier® (RAP) systems to reinforce poor soils. The process involves constructing high density, stiff RAPs to control settlement and improve allowable bearing pressures and the rotational stiffness. Wind tower support using RAP systems started in Europe and is now more widespread in the United States. This paper details RAP design and construction for wind towers and discusses ancillary environmental benefits associated with this construction method.

1. INTRODUCTION

The demand for alternative energy sources in the United States has sparked significant growth in wind energy development. Wind farm construction continues to grow rapidly throughout the U.S. with a record breaking capacity of 5,249 megawatts constructed in 2007 for a total capacity of 16,824 megawatts (AWEA 2008).

Construction of an equal or greater generating capacity than in 2007 is expected by the end of 2008.

Tower designs mirror the wind industry growth with taller turbines capable of generating even greater energy capacity. The design of turbine foundations must incorporate traditional geotechnical engineering analyses for bearing capacity and settlement for static dead and live loading conditions much like conventional building foundation support. More importantly, though, the designs are often controlled by large transient pressures attributed to significant overturning moments from mean and critical wind characteristics. The design incorporates minimum requirements for foundation stiffness to provide adequate tower serviceability.

The wind industry is touted as a renewable, "green" industry. In addition to the engineering challenges to provide suitable foundation support, designers are often asked to provide sustainable solutions for projects.

FIG. 1: Gamesa G83 (2MW) Wind Tower

2. WIND TOWER DESIGN CONSIDERATIONS

Wind turbine foundation loading details are often related to the specific turbine manufacturer, make and model and may be a proprietary design detail. In general, tower heights have grown in recent years from early designs on the order of 60 meters (197 ft) to more than 90 meters (295 ft) in height and capable of generating more than 3MW of electricity. These tower heights are expected to grow with the wind industry; towers exceeding 125 meters (410 ft) and 6MW production capability are being unveiled in Europe by companies such as Enercon.

While the vertical loads resulting from dead and live loads for the 1.5 to 2MW towers typically range from only 3,100 to 4,500 kN (700 to 1,000 kips), large overturning moments from the horizontal wind pressures often range from 40,000 to 67,800 kN-m (30,000 to 50,000 ft-kips). The stiffness characteristics of the

foundation soils are critical for acceptable tower performance under the wind gust loading conditions. Most manufacturers require minimum horizontal and dynamic (rotational) stiffness criteria specific to the particular tower type be met.

3. FOUNDATION OPTIONS

While deep foundation or pile solutions are an historical option in poor soil conditions, the most cost-effective approach to wind tower foundation design often incorporates the use of a large mat foundation placed on competent soil. Mat foundation design becomes a balancing act tied to foundation sizes and overturning moments. In an effort to minimize the added complexity and cost associated with controlling uplift loads on the foundation, designers often look for the smallest foundation size possible that is yet large enough to preclude uplift pressure at the base. These foundation sizes often result in high foundation edge pressures that may overstress the underlying soil. In poor soil conditions, a low allowable bearing pressure may govern the foundation design unless alternative approaches are utilized.

Alternatives such as massive overexcavation of the poor soil and replacement with high strength backfill or Rammed Aggregate Pier® reinforcement may be used in these cases to support higher allowable bearing pressures and optimize the mat foundation size. Typical mat foundation designs for the 80 to 90 meter (260 to 295 ft) towers range in width (diameter) from 14 to 19 m (45 to 65 ft), resulting in bearing pressures from 144 to 215 kPa (3,000 to 4,500 psf) in many cases. The best solution must then reflect performance, cost-effectiveness and construction schedule.

4. PROJECT DESCRIPTION

Construction of the Winnebago 1 Wind Farm was distributed over 10 sites throughout Winnebago County, Iowa. The project incorporated 78 meter Gamesa® G83 2.0 MW wind turbines with static vertical loads of 2,936 kN (660 kips), horizontal base shear of 676 kN (152 kips) and overturning moments of 50,335 kN-m (37,120 ft-kips). A photograph of the turbines used is shown in Figure 1. Preliminary foundation designs involved "inverted tee" octagonal foundations with diameters ranging from 45 to 60 feet depending on the soil conditions. The foundations were designed to bear 2.75 m (9 ft) below grade.

5. SOIL CONDITIONS

The soil conditions across the ten different sites were explored by the project geotechnical engineer using a combination of Cone Penetration Tests (CPTs) and soil borings and Standard Penetration Tests (SPTs). Testing was performed up to depths of 50 feet at the tower locations. Additionally, shear wave velocity measurements were made at 4 turbine locations using a multi-channel geophone array.

The results of the explorations indicated the soils across the sites generally consisted of a mixture of clay, silt, sand and gravel representing glacial drift, alluvial

and colluvial soils extending to depths ranging from 4 to 15 m (13 to 50 ft). In many areas, these soils were underlain by glacial outwash sand and gravel. The upper soils consisted of soft to stiff silty clay with varying amounts of sand to depths of 4 to 5.5 m (13 to 18 ft) underlain by stiff to very stiff sandy lean clay. Groundwater was present at the site at depths of 1.8 to 7.3 m (6 to 24 ft) below existing grade. Moisture contents for the upper soils ranged from 14 to 41%. Undrained shear strengths from unconfined compression tests ranged from 42 to 135 kPa (870 to 2815 psf). Shear wave velocities at the sites increased with depth from approximately 183 to 229 mps (600 to 750 fps) near the bottom of footing elevation and extending to depths of about 7.5 m (25 ft) to 243 to 396 mps (800 to 1300 fps) at depths of 7.6 to 21 m (25 to 70 ft).

6. FOUNDATION RECOMMENDATIONS

As a result of the low shear strength material encountered near the bearing elevation, the allowable bearing pressure for these sites was limited to 120 kPa (2,500 psf) to control settlement and provide sufficient support As an alternate to over-sized foundations using 120 kPa bearing pressures, the design-build contractor utilized the Geopier® system (a type of Rammed Aggregate Pier® system) to improve the composite allowable bearing pressure, control settlement, improve the rotational stiffness all while providing cost savings by reducing the foundation sizes.

The wind tower contractor considered a variety of foundation sizes. The largest was designed to bear on native soils with a width of 20 m (65.5 ft), area of 330 m^2 (3554 ft^2) and resulting maximum bearing pressure of 120 kPa (2,500 psf). With the option of increasing the allowable bearing pressure to 215 kPa (4,500 psf), the contractor finalized plans to use a smaller 229 m^2 (2,460 ft^2) octagonal foundation with a maximum width of 16.6 m (54.5 ft). The design conditions and requirements for the specific foundation are shown in Table 1. The decision was related to cost savings in the concrete and steal for the foundations.

TABLE NO.1: Wind Tower Foundation Design Criteria

Design Parameter	Criteria
Total Settlement	50 mm (2 in)
Differential Settlement	3 mm/m (0.036 in/ft)
Rotational Stiffness	3 x 10^7 kN-m/rad (2.21 x 10^7 k-ft/rad)

7. GEOPIER® CONSTRUCTION

Construction of a Rammed Aggregate Pier (RAP) system using the *Geopier* approach is well-described in the literature (Lawton and Fox 1994, Wissmann et al. 2000). As depicted in Figure 2, RAP elements are installed by drilling 610 mm (24 inch) to 915 mm (36 inch) diameter holes to depths ranging between 2 m and 8 m (7 feet and 26 feet) below working grade elevations, placing controlled 0.3 m (1 ft) thick

lifts of stone within the cavities, and compacting the aggregate using a specially designed high-energy beveled impact tamper. During densification, the beveled shape of the tamper forces stone laterally into the sidewall of the excavated cavity. This action increases the lateral stress in the matrix soil thus providing additional stiffening and increased normal stress perpendicular to the perimeter shearing surface. RAP elements are installed to reinforce weak and compressible soils offering improvements in the composite shear strength and the composite compression characteristics of the reinforced deposit, thereby controlling settlement and improving bearing pressures.

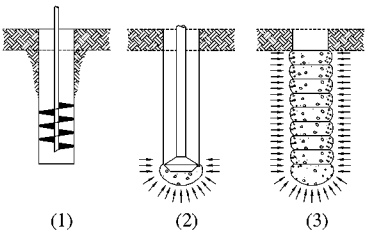

FIG 2: Rammed aggregate pier installation using the Geopier System

The Geopier system provides sustainable construction benefits in addition to increasing the foundation bearing capacity. The system uses locally-available natural aggregate or recycled concrete for construction of the piers. The volume of material utilized for Geopier elements beneath the foundation is typically only 10 to 20 percent of the material required for massive overexcavation and replacement. These factors limit excessive fossil fuel required for material delivery and disposal as compared to other solutions. Additionally, the equipment utilized for the pier installation consists of only 2 to 3 small excavators, thereby further limiting fossil fuel consumption and dramatically reducing the carbon footprint of the foundation construction activities.

8. GEOPIER DESIGN APPROACH

8.1 Settlement control and bearing capacity

In the case of the wind tower foundations, multiple loading scenarios are evaluated. These loading cases include the 1) static pressure only, 2) mean production pressure, and the 3) abnormal extreme pressure. The pier design is performed for the full range of pressures (Cases 1 – 3) to provide sufficient bearing capacity (strength) and maintain acceptable pier stress levels. Often, only the cases of static pressure and the mean production pressure are used for settlement estimates though. This is because the case of the abnormal extreme pressure is not anticipated to result in settlement particularly because of the short-term duration of loading. The pressures provided for a 215 kPa (4,500 psf) foundation are shown in Table 2.

TABLE NO.2: Wind Tower Foundation Design Pressures

Loading Condition	Maximum Edge Pressure
Static Pressure	71 kPa (1487 psf)
Mean Production Pressure	104 kPa (2180 psf)
Abnormal Extreme Pressure	199 kPa (4160 psf)

Allowable bearing pressures for RAP-supported foundations are developed based on classical limit equilibrium analyses and depend on the soil and pier characteristics. Allowable bearing pressures for RAP-supported foundations are often increased over unreinforced conditions by a factor of 2 or 3 because of the improved composite strength characteristics in the reinforced soil. Construction of the Rammed Aggregate Pier elements affords angles of internal friction on the order of 50 degrees which provides substantial improvement in the composite bearing support.

From a settlement perspective, the deflection of the RAP-reinforced zone supporting the foundation is estimated as the ratio of the top-of-pier stress (q_g) and the pier stiffness (k_g). The pier stiffness modulus is assumed as described in the literature (Lawton and Fox, 1994) based on known pier properties and the properties of the surrounding soil, and is then confirmed with a site specific modulus test. The top-of-pier stress is calculated as

$$q_g = q\left(\frac{R_s}{R_s R_a - R_a + 1}\right) \tag{1}$$

where q_g is the top-of-pier stress, R_s is the ratio of pier stiffness to matrix soil stiffness, R_a is the ratio of pier area to the total foundation area and q is the applied foundation stress. For support of transient loading conditions, it's important to evaluate the pier stress for both sustained static pressures as well as the dynamic maximum pressures to be sure the performance of the pier will be acceptable. Typical stiffness ratios for foundations supported by Geopier elements range from 6 to 40.

The settlement of the soils at depths below the reinforced zone is estimated using conventional consolidation or elastic geotechnical approaches. The change in pressure at the center of a compressible layer may be evaluated using a variety of different stress influence factors (i.e. Westergaard, Bousinesq, 2:1 distribution). Based on this estimated change in stress and the soil compressibility, the additional lower zone settlement is added to the reinforced-zone settlement to arrive at the total settlement.

8.2 Rotational Stiffness

Rotational stiffness calculations for wind tower foundations are evaluated using the following approach described in NAVFAC DM7.3 (1983):

$$k_{\varphi} = \frac{8Gr_o^3}{3(1-\nu)} \tag{2}$$

where G is the shear modulus value, υ is Poisson's ratio and r_o^3 is the foundation radius. For the Geopier-reinforced zone, the shear modulus value, which is proportional to shear wave velocity, may be evaluated using a composite approach as described by the following:

$$G_{comp} = G_g(R_a) + G_s(1-R_a) \tag{3}$$

where R_a is the Geopier element area ratio beneath the foundation, G_s is the shear modulus of the soil within the reinforced zone, and G_g is the shear modulus of the Geopier element (Miller et al. 2005). Research has shown that the shear modulus values of Rammed Aggregate Pier elements are on the order of 287 to 335 MPa (6,000 ksf to 7,000 ksf) (Sulieman et al. 2006). Depending on the levels of strain anticipated from the loading conditions (sustained or transient), degradation factors (G/G_{max}) may be applied to the values for the shear modulus of the soil and the pier. These degradation factors are determined based on soil type and strain level, which can be conservatively estimated based on deflection of the reinforced-zone.

9. PROJECT CONSTRUCTION AND TESTING

A total of 64 Geopier elements were installed prior to foundation excavation at each of the ten tower sites. Pier lengths extended 2.4 to 4.6 m (8 to 15 ft) below the bottom of the foundations. The piers were concentrated near the outer edges of the foundation to provide the improved bearing pressure where the overturning moments resulted in pressures exceeding the bearing capacity of the soil. Figure 3 shows a typical layout of the piers beneath one of the tower foundations. The piers were typically installed at each site within one to two days.

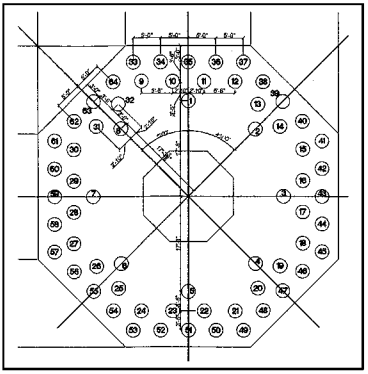

FIG. 3. Typical RAP Layout

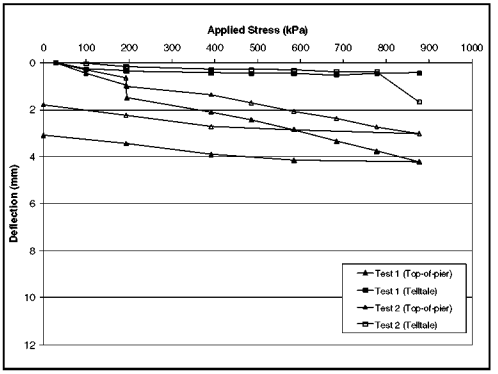

FIG. 4: RAP modulus test results

The performance of the system was evaluated at the project sites by performing modulus tests to evaluate the behavior of the pier under applied stress. The modulus test is performed in general accordance with a pile load test and is described in Shields et al. (2004). The results of two modulus tests are shown in Figure 4. The test results indicate a pier deflection of less than 4.3 mm (0.17 inches) at a stress level of 878 kPa (18.3 ksf) resulting in a pier stiffness of at least 204 MN/m^3 (750 pci). This value exceeded the design value of 48 MN/m^3 (175 pci) by a factor of 4.

10. CONCLUSIONS

This paper describes the use of Rammed Aggregate Pier® (RAP) solutions to reinforce soft to stiff clay soils at the site of ten towers. RAP reinforcement has been shown to be a cost-effective alternative to overexcavation and replacement or deep foundation for support of the towers. The Intermediate Foundation approach provides a more environmentally-conscious and sustainable solution for the wind industry. The RAP approach allows for a tailored solution to foundation support to provide improved allowable bearing pressures particularly where the applied pressures exceed the bearing capacity for the unreinforced soil. The piers also provide a significant improvement to settlement control and dynamic stiffness.

11. REFERENCES

American Wind Energy Association (2008). First Quarter 2008 Market Report. May 2008. www.awea.org

Naval Facilities Engineering Command. (1983). "Soil Dynamics, Deep Stabilization, and Special Geotechnical Construction: Design Manual 7.3". Alexandria, VA.

Miller, J., FitzPatrick, B.T., and Wissmann, K. (2005). "Seismic Site Classification Improvement using Geopier Soil Reinforcement." Geopier Foundation Company, Inc., Mooresville, NC.

Lawton, E. C. and Fox, N. S. (1994). "Settlement of Structures Supported on Marginal or Inadequate Soils Stiffened with Short Aggregate Piers." Proceedings, Vertical and Horizontal Deformations of Foundations and Embankments. College Station, TX. June 16-18

Shields, C., FitzPatrick, B. and Wissmann, K. (2004). "Modulus Load Test Results for Rammed Aggregate Piers in Granular Soils." *GeoSupport 2004*, GSP No. 124, ASCE, Reston, VA.

Suleiman, M. T., Pham, H. T. and White, D. J. (2003). "Field Determination of Shear Modulus for Geopier Foundations." Final Report. Iowa State University. November 2004.

Wissmann, K. J., White, D. J., and Lawton, E. (2007) "Load Test Comparisons for Rammed Aggregate Piers and Pier Groups." *GeoDenver 2007*. GSP No. 172, ASCE, Reston, VA

Copyrighted Materials
Copyright © 2009 American Society of Civil Engineers (ASCE)
Retrieved from www.knovel.com

Design of Monopile Foundations for Offshore Wind Energy Converters

Kerstin Lesny[1)], Peter Hinz[2)]

[1)] PD Dr.-Ing., Institute of Soil Mechanics and Foundation Engineering, University of Duisburg-Essen, Universitaetsstrasse 15, 45117 Essen, Germany, email: kerstin.lesny@uni-due.de
[2)] Dipl.-Ing., Institute of Soil Mechanics and Foundation Engineering, University of Duisburg-Essen, Universitaetsstrasse 15, 45117 Essen, Germany, email: peter.hinz@uni-due.de

ABSTRACT: Offshore wind energy converters in water depth up to 20-25 m are mostly built on monopile foundations. Although it is a simple structure the monopile behaviour under transient loading from wind, waves and currents is very complex. Consequently, monopiles are often designed for the relevant extreme load event in a quasi-static approach. However, the effect of cyclic loading on the monopile behaviour has to be analysed as well, but no general accepted procedure currently exists. In the present paper the general design strategy is introduced and a method is suggested to analyse the monopile behaviour under cyclic loading. This method includes a combination of laboratory element tests and an appropriate design method.

INTRODUCTION

Monopiles are the predominant foundation concept for offshore wind energy converters in moderate water depths up to 20-25 m. Steel pipe piles with diameters ranging from 2 m for the first small turbines in shallow waters up to 5 m for the latest more efficient turbines in greater water depths have been installed mainly by driving in various types of soil. Although a monopile is a very simple and straightforward design concept its behaviour is complex based on the load conditions which have to be considered. Monopile loading mainly results from environmental impact due to wind, waves and currents which cause very high lateral loads and bending moments especially during extreme storm events. On the other hand, in periods between extreme events moderate loads act on the foundation, but they recur millions of times within the entire service life of the structure.

In the following the general design procedure for monopiles is illustrated. After that, a procedure to predict the monopile behaviour under cyclic loading is suggested.

DESIGN PHILOSOPHY

Monopile foundations are highly laterally loaded structures which transfer the loading into the soil by subgrade reaction. This requires a sufficient bearing capacity of the upper soil layers over the whole service life of the structure which has to be ensured by a proper design.

Because of the complexity of the problem the design of monopiles usually follows a two-step procedure. In the first step, the piles are designed for the governing extreme load event, e. g. a 50-year extreme wave height which is assumed to act quasi-static. The basic dimensions of the monopile are defined and its stability and serviceability have to be verified according to the relevant design specifications for offshore wind turbines (see e. g. DNV, 2004; GL, 2005).

For the design of laterally loaded piles different methods are available, e. g. the well-known p-y method (see e. g. Reese and van Impe, 2001) or the Strain Wedge Model (SWM) developed by Norris (1986), Ashour and Norris (1998).

The monopile is usually designed as a flexible pile with a sufficient fixation in the soil to minimize the pile head deflections. In this case, the friction in the base of the monopile can be neglected as pile tip displacements are small. The effect of the large monopile diameter on the pile behaviour and the consequences for design are discussed e. g. in Lesny and Wiemann (2005), Lesny et al. (2007).

However, the design specifications for offshore wind turbines also ask for an analysis of the foundation behaviour under cyclic loading. This is a complex problem and research is still going on. Consequently, commonly accepted design methods how to perform such an analysis currently do not exist.

ANALYSIS OF MONOPILE BEHAVIOUR UNDER CYCLIC LOADING

Effects of cyclic loading and analysis strategy

Cyclic loading causes an accumulation of plastic strains in the vicinity of the pile (cyclic creep) which is often accompanied by either hardening (especially in normally consolidated clays or loose sands) or softening of the soil (especially in overconsolidated clays or dense sands). Additionally, excess pore water pressure may be accumulated around the pile depending on the drainage conditions (system geometry, permeability of the soil and load frequency). Cyclic creep especially depends on the cyclic stress ratio CSR which is defined as:

$$\mathrm{CSR} = \frac{(\sigma_1 - \sigma_3)_{\mathrm{cyc}}}{(\sigma_1 - \sigma_3)_{\mathrm{max,stat}}} \tag{1}$$

In equation (1) $(\sigma_1\text{-}\sigma_3)_{\mathrm{cyc}}$ is the cyclic deviator stress and $(\sigma_1\text{-}\sigma_3)_{\mathrm{max,stat}}$ is the deviator stress at failure under static conditions. Other influence parameters are e. g. the cyclic load amplitude, number of load cycles, load frequency and stress history.

For high CSR the strain increments increase and lead to progressive failure of a soil element after very few cycles. If the CSR can be maintained sufficiently small decreasing strain increments with increasing number of cycles lead to a stabilisation of the deformations and failure may occur only after a large number of cycles (see Figure 1). Especially in cohesive soils shakedown has been observed for very small CSR where the plastic increments reach zero after a certain number of cycles and the behaviour becomes purely elastic (see also Figure 1). However, Wichtmann (2005)

among others showed that in non-cohesive soils no shakedown and even no real stabilisation occur.

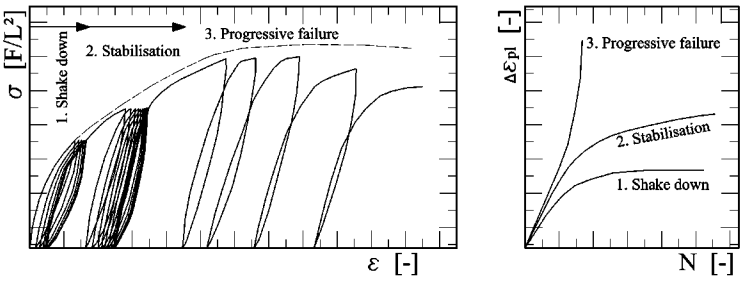

FIG. 1. Soil behaviour under cyclic lateral loading

The CSR of the soil elements in the vicinity of the pile corresponds to a resultant cyclic load ratio CLR of the whole pile-soil system which is the ratio of the cyclic load amplitude to the static bearing capacity of the pile. Hence, the aim of the analysis is to define the pile dimensions so that a critical CLR is not exceeded. With that, the accumulated plastic pile deformations during service life must be predicted and compared to serviceability criteria defined for the turbine operation.

P-y curves have been established also for cyclic loading, e. g. by Matlock (1970), Reese et al. (1974), but these methods include only a flat deterioration of the curves. Dunnavant and O´Neill (1989) as well as Long and Vanneste (1994) suggested methods in which the p-y curves deteriorate depending on the number of cycles. However, these methods are based on tests with only few cycles and effects like soil hardening or softening are not (explicitly) considered. The performance of finite element analyses is problematic as well. Techniques with implicit modelling of each load cycle are not suitable for large numbers of cycles as they require large computer capacities and produce accumulating numerical errors. On the other hand, explicit models which predict the accumulated plastic deformations by empirical equations (e. g. Wichtmann, 2005) are very complex for practical applications and especially the determination of model parameters is often difficult.

Method to predict monopile behaviour under cyclic loading

The method suggested in this paper is based on a combination of laboratory element testing and numerical calculations. Cyclic multistage triaxial tests are suitable to investigate the soil behaviour under cyclic loading with varying load intensity. The results from these tests are implemented into the SWM to calculate the pile behaviour after various load cycles. The SWM is especially capable to connect the behaviour of a soil element measured in the triaxial test to the behaviour of the whole pile-soil system (for details see Ashour and Norris, 1998).

The proposed method focuses on the prediction of plastic deformations. Pore water pressure generation must be investigated separately.

Cyclic multistage triaxial tests

The test apparatus for the multistage triaxial tests is depicted in Figure 2. Up to now, undrained, unconsolidated, stress controlled triaxial tests on saturated cohesive soils (model clay, natural high plasticity clay, low plasticity silt) have been conducted. During the tests the cell pressure σ_3 has been kept constant and the cyclic loading has been applied by alternating vertical stresses. With that, the deviator stress (σ_1-σ_3) varies between zero and the maximum value at the specific stress level CSR. The CSR to be investigated have been defined according to equation (1) with the shear strength measured in corresponding static triaxial tests. After at least 10,000 cycles the CSR has been increased until in the last stage progressive failure of the specimen occurred after very few cycles. Typical test results for high plasticity clay and low plasticity silt are shown in Figure 3.

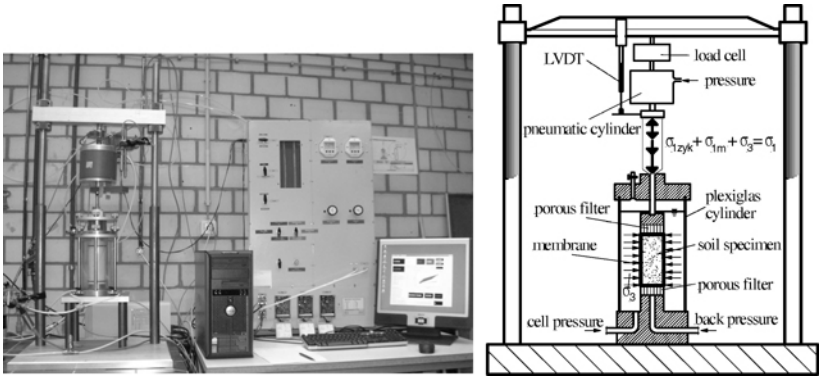

FIG. 2. Test apparatus for multistage triaxial testing

In design the CSR and the load frequency to be investigated must be defined in advance. Up to now especially the definition of the CSR is problematic as (i) the resultant cyclic loading on the pile from environmental impact is difficult to determine, and (ii) the corresponding stress level in the soil around the pile must be approximated by an appropriate method (see also Lesny and Hinz, 2007).

The load frequency should correspond to the particular conditions offshore. It has been shown that for typical sea state frequencies between 0.05 and 0.2 Hz the effect of the load frequency on the development of plastic deformations (but not on the excess pore water generation) is negligible (e. g. Wichtmann, 2005; Ansal and Erken, 1989). Hence, in the tests a constant frequency of 0.125 Hz has been adopted.

In the majority of the tests performed up to now a stabilization of the deformations has been observed at each CSR below the one which induces progressive failure. In this case the measured plastic strains accumulated at each CSR can be approximated by a power law that follows the degradation concept by Idriss et al. (1978):

$$\varepsilon_{pl}^{N} = \varepsilon_{pl}^{1} \cdot N^{\alpha} \qquad (2)$$

In equation (2) ε_{pl}^{N} are the accumulated plastic strains after N cycles and ε_{pl}^{1} is the plastic strain after the first cycle of the corresponding stress level which corresponds to the strain in a static test. The exponent α is the gradient of ε_{pl} vs. N in logarithmic scale and depends on the soil characteristics. Stress levels with different cyclic stress ratios can be considered within equation (2) by the well-known Miner's rule (for details of this procedure see Lesny and Hinz, 2007).

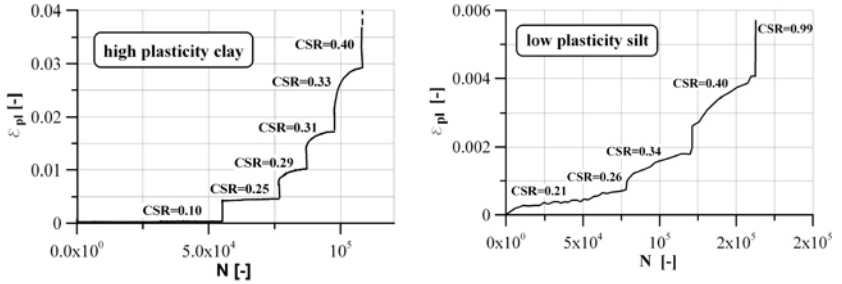

FIG. 3. Results from multistage triaxial tests on different soils

With that, the accumulated plastic deformations of the soil can be calculated for an arbitrary number of cycles for different stress levels if the plastic strain after the first cycle under the reference stress level and the degradation parameter α are determined from the element tests. However, in cases where no real stabilisation in the tests occurs the accumulation of plastic strain over N in logarithmic scale is no longer linear and α is not a constant. As an example the accumulated plastic strains of the silt at various CSR related to the strain after the last cycle of the preceding CSR are depicted in figure 4. This behaviour can be approximated by a bilinear function:

$$\varepsilon_{pl}^{N} = \begin{cases} \varepsilon_{pl}^{1} \cdot N^{\alpha} & N \le 10^{4} \\ \varepsilon_{pl}^{1} \cdot 10^{4(\alpha-\alpha')} \cdot N^{\alpha'} & N > 10^{4} \end{cases} \tag{3}$$

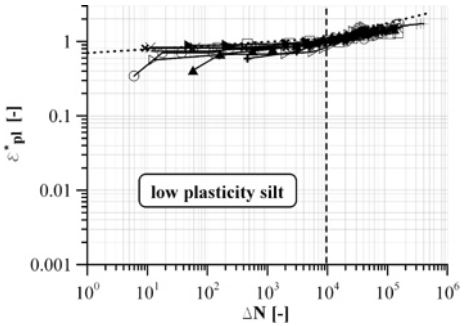

FIG. 4. Accumulation of normalised plastic strains ε_{pl}^{*} vs. ΔN for various CSR

Degradation parameters of $\alpha = 0.05$ for $0 \leq N \leq 10^4$ and $\alpha' = 0.2$ for $N \geq 10^4$ have been derived from the analysis of the test results shown in Figure 4.

If shakedown is observed in the test the measured strains can directly be extrapolated to greater numbers of cycles. In this case the accumulation according to equation (2) would lead to uneconomic results.

Numerical analysis with the SWM

According to Norris (1986), Ashour and Norris (1998) the SWM is based on the linearization of the pile deflection line in the upper soil layers. This area corresponds to the height of the earth pressure wedge mobilized by the current loading. The linearization leads to the assumption of a constant strain in the wedge. This strain is related to a reference strain ε_{50} which is derived from triaxial tests and corresponds to 50% of the deviator stress at failure. During the calculation the height of the earth pressure wedge is modified until equilibrium is reached between the outer loading of the pile and the soil reaction at the pile-soil interface.

In the proposed model it is assumed that the development of the strain ε_{50} in the mobilized wedge with increasing number of cycles corresponds to the degradation process defined in equation (2) or (3), respectively. Hence, after N cycles the reference strain ε_{50}^{N} to be used in the SWM calculations is:

$$\varepsilon_{50}^{N} = \varepsilon_{50}^{1} \cdot N^{\alpha} \tag{4}$$

The parameters ε_{50}^{1} and α have to be derived from multistage triaxial tests as proposed in section 3.2.1. With the corresponding reference strain according to (4) quasi-static SWM calculations can be performed for different numbers of cycles.

In the calculations the zone where the soil behaviour is affected by cyclic loading is limited to the upper soil layers up to a depth of approximately 1 to 2 x D for monopile diameters D between 4 and 8 m (see Lesny and Hinz, 2007). Using the multisublayer technique (see Ashour and Norris, 1998) ε_{50}^{N} is assigned to this area whereas in deeper areas the reference strain for static conditions is applied.

In Figure 5 the accumulated pile head deflections y_0/L (L: pile embedment length) calculated according to the proposed procedure are compared to results of model test on flexible steel pipe piles in soft clay under different CLR which have been performed by Mallikarjuna Rao (1992).

As no triaxial test results for the soft clay are available it has been assumed that the accumulation of the pile head deflections with N corresponds to the accumulation of plastic strain of a soil element level in the vicinity of the pile as defined in equation (2). Hence, the degradation parameter α and the reference strain after the first cycle ε_{50}^{1} have been derived from the model test results to $\alpha = 0.3$ and $\varepsilon_{50}^{1} = 0.0003$.

The comparison in Figure 5 shows that the measured pile behaviour can be predicted well at least for smaller CLR far away from progressive failure of the pile. However, more research is required on the verification of the proposed method especially on prototype measurements.

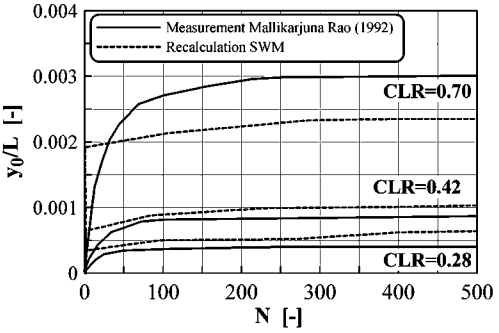

FIG. 5. Comparison of SWM results and measurements of accumulated pile head deflections from model tests performed by Mallikarjuna Rao (1992)

CONCLUSIONS

In the present paper a method has been proposed to analyse the behaviour of monopile foundations for offshore wind turbines under cyclic loading. The method is based on a combination of multistage triaxial testing and the well-known Strain Wedge Model. Multistage triaxial tests for different cohesive soils under various stress levels have been performed and a procedure to predict the accumulated plastic strains for an arbitrary number of cycles and various stress levels has been developed. In the procedure the reference strain required for the SWM calculations can be derived from the test results. With that, a quasi-static analysis of the pile behaviour after various numbers of load cycles can be performed.

It may be argued that multistage triaxial tests require sophisticated laboratory equipment. On the other hand, only a few parameters with a clear physical meaning have to be measured and with the SWM a numerical method is used which is especially suitable for application in the engineering practice.

However, the proposed method is based on several assumptions. Up to now, the development of a gap around the pile is difficult to predict and can only be considered roughly by assuming a reduced embedment length. Further on, the influence zone in which soil behaviour is affected by continuous cyclic loading and its development can only be estimated. Finally, the effect of different loading direction under offshore conditions is neglected within the procedure up to now.

ACKNOWLEDGEMENTS

The work presented in this paper has been conducted within the research project *Gigawindplus* sponsored by the German Federal Ministry for the Environment, Nature Conservation and Nuclear Safety and the research project *WindTide* sponsored by the German Federal Ministry of Economics and Technology. Their support is gratefully acknowledged.

REFERENCES

Ansal, A. M.; Erken, A. (1989): "Undrained Behavior of Clay under Cyclic Shear Stresses." *Journal of Geotechnical Engineering*, Vol. 115 (7), pp.968-983

Ashour, M., Norris, G. (1998). "Lateral Loading of a Pile in Layered Soil using the Strain Wedge Model." *Journal of Geotechnical and Geoenvironmental Engineering*, Vol. 124 (4), pp.303-315

DNV (2004). "Design of Offshore Wind Turbine Structures." *Offshore Standard DNV-OS-J101*, Det Norske Veritas Classification A/SDIN 1054

Dunnavant, T. W., O´Neill, M. W. (1989). "Experimental p-y Model for Submerged, Stiff Clay." *Journal of Geotechnical Engineering*, Vol. 115 (1), pp. 95-114

GL (2005). "Guideline for the Certification of Offshore Wind Turbines." *Rules and Guidelines – IV Industrial Services*, Germanischer Lloyd Windenergie, Hamburg, Germany

Idriss, I. M.; Dobry, R.; Singh, R. D. (1978): Nonlinear Behavior of Soft Clays During Cyclic Loading. *Journal of the Geotechnical Engineering Division*, ASCE, Vol. 104 (GT12), pp. 1427-1447

Lesny, K.. Wiemann, J. (2005). "Design Aspects of Monopiles in German Offshore Wind Farms." *Frontiers in Offshore Geotechnics*, edited by S. Gourvenec, M. Cassidy, Taylor & Francis Group, London, pp. 383-389

Lesny, K., Hinz, P. (2007). "Investigation of Monopile Behaviour under Cyclic Lateral Loading." *Proceedings of the 6th International Conference on Offshore Site Investigation and Geotechnics*, London, UK, pp. 383-390

Lesny, K., Paikowsky, S. G., Gurbuz, A. (2007). "Scale Effects in Lateral Load Response of Large Diameter Monopiles." *Proceedings of the ASCE Conference Geo Denver: New Peaks in Geotechnics*, February 18-21, Denver

Long, J. H., Vanneste, G. (1994). "Effects of Cyclic Lateral Loads on Piles in Sand." *Journal of Geotechnical Engineering*, Vol. 120 (1), pp. 225-244

Mallikarjuna Rao, K. (1992). "Behaviour of Vertical Piles Subjected to Static and Cyclic Lateral Loading." *PhD Thesis*, Ocean Engineering Centre, Indian Institute of Technology, Madras, India, 226 p.

Matlock, H. (1970). "Correlations for Design of Laterally Loaded Piles in Soft Clay." *Proceedings of the Offshore Technology Conference*, Paper No. OTC 1204, Houston, Texas,

Norris, G. (1986). "Theoretically Based BEF Laterally Loaded Pile Analysis." *3rd International Conference on Numerical Methods in Offshore Piling*, Nantes, France, pp. 361-386

Reese, L. C., van Impe, W. F. (2001). "Single Piles and Pile Groups under Lateral Loading." A. A. Balkema, Rotterdam

Reese, L. C., Cox, W. R., Koop, F. D. (1974). "Analysis of Laterally Loaded Piles in Sand." *Proceedings of the Offshore Technology Conference*, Paper No. OTC 2080, Houston, Texas

Wichtmann, T. (2005). "Explicit Accumulation Model for Non-Cohesive Soils under Cyclic Loading." *Schriftenreihe des Institutes Grundbau und Bodenmechanik*, Heft 38, edited by Prof. Dr.-Ing. T. Triantafyllidis, Ruhr-University Bochum

Copyrighted Materials
Copyright © 2009 American Society of Civil Engineers (ASCE)
Retrieved from www.knovel.com

Offshore Wind Energy in Germany compared to other European Areas - Challenges and Recent Developments -

Kerstin Lesny[1]

[1]PD Dr.-Ing., Institute of Soil Mechanics and Foundation Engineering, University of Duisburg-Essen, Universitaetsstrasse 15, 45117 Essen/Germany, kerstin.lesny@uni-due.de

ABSTRACT: Utilization of offshore wind energy in Europe is well in progress. A total capacity of about 1000 MW has already been installed. Eight wind farms with about 1300 MW are under construction and many more are planned. The existing wind farms are located relatively close to the shore in moderate water depths of up to 20 m. In contrast to this the site conditions in the planned wind farms in the German North and Baltic Sea are more demanding as these wind farms have to be built far off the shore. The present paper shows the current status of offshore wind energy in Europe and recent developments in Germany. Site conditions at various wind farm locations in the German North and Baltic Sea are illustrated and compared with the conditions in existing wind farms. Resulting consequences for foundation design and installation are discussed.

CURRENT STATUS OF OFFSHORE WIND ENERGY IN EUROPE

The development of renewable energies has top priority in many European countries. In 2004 European governments agreed to reach a 21% share of renewable electricity by 2010. This ambitious goal can only be achieved by a vast expansion of offshore wind energy. Today, offshore wind farms with a total capacity of 1,000 MW are already operating (see Table 1). About eight wind farms are currently under construction with a total capacity of 1,300 MW and more than 40 wind farms with a total capacity of roughly 23,000 MW are planned to be completed until 2018 (without Germany). Leading countries are especially Denmark, Great Britain, Sweden and the Netherlands. This is not only due to the availability of suitable locations near the coastline with moderate site conditions but also due to special governmental promotion of renewable energies which supports the cost-effectiveness of the projects. The increase of the total capacity may also be attributed to the development of more efficient wind turbines starting from the 0.5 MW in the early years up 3.6 MW nowadays. Turbines of the 5 MW class meanwhile passed prototype status and will be available for commercial production.

TABLE 1. Operating wind farms in Europe (current status August 2008)

wind farm/country/year	size	distance to shore (km)	water depth (m)	founda-tion
Vindeby/DK/1991	11 x 0.45 MW	1.5-3	2.5-5	GBF[a]
Lely/NL/1994	4 x 0.5 MW	0.8	4-5	monopile
Tunø Knob/DK/1995	10 x 0.5 MW	6	3-5	GBF[a]
Dronten/NL/1996	28 x 0.6 MW	0.3	1-2	monopile
Bockstigen/SWE/1998	5 x 0.55 MW	4	6	monopile
Blyth/GB/2000	2 x 2 MW	1	6	monopile
Middelgrunden/DK/2001	20 x 2 MW	2-3	2-6	GBF[a]
Utgrunden/SWE/2001	7 x 1.5 MW	12	7-10	monopile
Yttre Stengrund/SWE/2001	5 x 2 MW	5	8	monopile
Horns Rev/DK/2002	80 x 2 MW	14-20	6-14	monopile
Ronland-Jütland/DK/2003	8 x 2-2.3 MW	?	?	?
Samsø/DK/2003	10 x 2.3 MW	3.5	11-18	monopile
Frederikshaven/DK/2003	4 x 2.3-3 MW	0.5	1	monopile[b]
Rødsand/Nysted/DK/2003	72 x 2.3 MW	9	6-10	GBF[a]
Arklow Bank/IRL/2003	7 x 3.6 MW	7-12	5	monopile
North Hoyle/GB/2003	30 x 2.0	7-8	12	monopile
Kentish Flats/GB/2005	30 x 3.0 MW	8.5-10	5	monopile
Scroby Sands/GB/2004	30 x 2 MW	2.3	?	monopile
Barrow/GB/2006	30 x 3 MW	7	15-20	monopile
Beatrice/GB/2006	1 x 5 MW	25	45	jacket
OWEZ/NL/2006	36 x 3 MW	10-18	18	monopile
Bilbao Harbour/E/2006	5 x 20 MW	?	?	?
Burbo/GB/2007	25 x 3.6 MW	10	1-8	monopile
Lillgrund/SWE/2007	48 x 2.3 MW	7	4-8	GBF[a]
Q7-WP/NL/2008	60 x 2 MW	23	19-24	monopile

[a]: GBF = gravity based foundation, [b]: one turbine installed on a prototype suction bucket

The current German plans allow for an increase of the percentage of renewable energies on the gross electricity consumption from today 14.2 % up to 25-30 % in 2020 and also here these plans are only viable if an offshore wind energy industry is established. The development of renewable energies in Germany is supported by the renewable energy sources act (2004). According to this, the higher investments for offshore wind energy compared to onshore activities are accommodated by an increased price of 9.1 Euro cent/kWh to be paid over a period of 12 years for wind farms erected before 2010. For wind farms located in a distance to shore of more than 12 nm and in water depths above 20 m this time period will be extended depending on the distance to shore and the water depth. After this time period the basic price of 6.19 Euro cents/kWh will be paid. Beside the fixed prices, energy companies are obliged to provide the grid connection of the offshore wind farms on their own account.

Around 33 wind farms in the North Sea and the Baltic Sea are currently in planning. In later expansion stages many of these wind farms may consist of several

hundred windmills of up to 5 MW rated power each. Around 22 wind farms with a final capacity of 20,300 MW in the North Sea and 1,930 MW in the Baltic Sea have been approved, but only a few singular turbines have been built nearshore up to now.

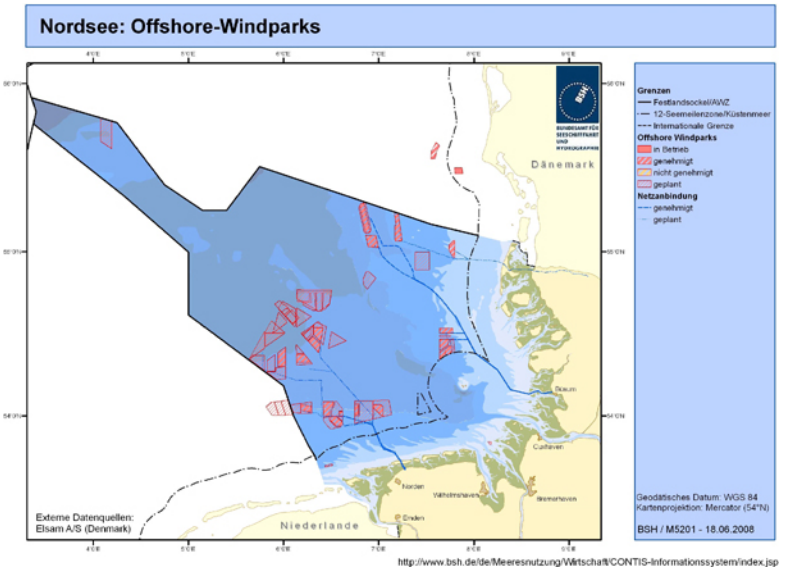

FIG. 1. Locations of offshore wind farms in the German North Sea (BSH, 2008)

The German wind farms are predominantly located far off the shore in the exclusive economic zone (EEZ) (see Figure 1 for the North Sea).

The EEZ is the area seaward of Germany's territorial sea, which is the 12-nm zone from the coastline, and is largely identical with the German continental shelf. Nearshore areas are mostly dedicated to environmental purposes (e. g. wadden sea, bird protection), shipping routes etc. where construction activity is not allowed. The site conditions at the offshore locations and little experience with such projects caused problems in risk assessment and the resulting financial situation. But also the grid connection and the approval of cable routes through highly sensitive areas like the wadden sea turned out to be difficult. These are the main reasons for the delay in realizing offshore wind energy projects in Germany.

Recently, the construction of the offshore test field Alpha Ventus has started. 12 wind energy converters with a rated power of approximately 5 MW are to be installed in water depths of 28-30 m 45 km north of the island Borkum. The first six turbines will be installed on tripod foundations, the foundation for the other six turbines is yet undecided. The first commercial wind farm to be erected will probably be *BARD Offshore I* in the North Sea with 80 turbines of 5 MW rated power in the first stage located in a distance to shore of 87 km in water depths of 39-41 m.

SITE CONDITIONS IN THE GERMAN NORTH AND BALTIC SEA

Only little reliable data about the environmental conditions in the southern North Sea and the Baltic Sea are available up to know (for details see Lesny, 2008 and also Lesny and Wiemann, 2005). In the North Sea high 50-year significant wave heights between 7.5 and 12 m may be expected with related wave periods between 10.8 and 15 s. Tidal currents of 0.5 to 1.5 m/s and subsurface currents of 0.1 to 0.6 m/s as well as the ice loading are moderate. In the Baltic Sea, however, ice loading is relevant for design as the sea freezes completely in rough winters, whereas the sea state is moderate with negligible currents and significant wave heights of 2.0 to 4.3 m.

According to Table 1 the wind farms in many European countries are located relatively close to shore at distances of about 15 - 25 km average. This corresponds to water depths between 5 m and 25 m. The demonstration project *Beatrice* in Great Britain is the first one realized in a challenging water depth of 45 m.

In contrast to this, the wind farms in the German EEZ have a distance to shore from 23 km minimum up to 120 km. The water depths in these areas range from 20 to 45 m with an average of 25 - 35 m.

The water depth is one of the most important issues for the design of wind energy turbines as it directly influences the resultant loading of the foundation. An offshore wind energy converter with a rated power of 5 MW has a hub-height of about 95 m above still-water-level and a rotor of 125 m diameter. It is a slender structure with a very small dead weight compared to the loading from environmental impact and the operating turbine. These conditions result in very high ratios of horizontal to vertical load of typically $H/V \approx 0.5$. An increasing water depth directly increases not only the lever arms of the hydrodynamic loading but also the lever arm of the aerodynamic loading. Consequently, water depths of 20-50 m, which are moderate in contrast to many offshore platform locations, cause extremely high load eccentricities (see Lesny, 2008).

The subsoil in the southern North Sea is characterized by non-cohesive soil layers of varying density. Holocene sediments of silty sands, sandy silt or tidal mud with low bearing capacity overlay Pleistocene sediments of medium dense to very dense fine to medium or coarse sands. Basin deposits of highly over-consolidated glacial till or clay can be found as well. Large boulders are located especially along the Pleistocene-Holocene boundary. Huge channel systems formed by large melt water streams during the warm intervals are a special feature of the southern North Sea. A typical soil profile is shown in Figure 2.

The subsoil conditions in the Baltic Sea are often more complex depending on the location. The upper Holocene layers mainly consist of mud (sandy, silty soils with organic contents, sapropelic mud) up to 20 m thickness with a very low bearing capacity. The Pleistocene soil layers include highly overconsolidated glacial till over cemented clays with stones and boulders. North of Ruegen, large chalk deposits are to be found below the glacial till. Typical soil profiles for the Bay of Mecklenburg and the Arcona Basin are depicted in Figure 2.

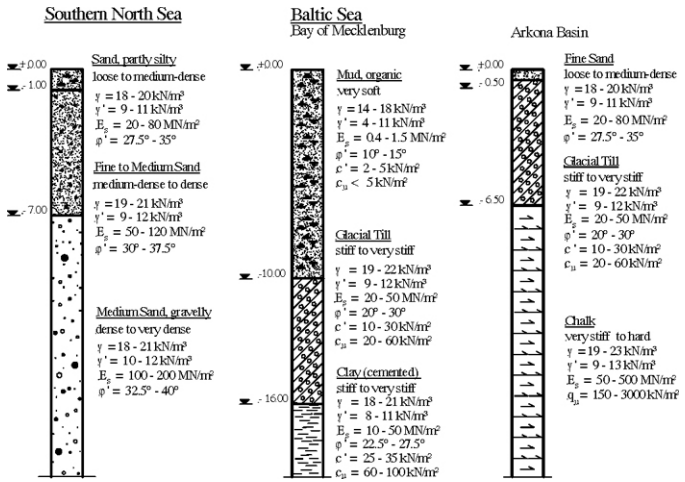

FIG. 2. Typical soil conditions at various German wind farm locations

FOUNDATIONS FOR OFFSHORE WIND ENERGY CONVERTERS

Foundation concepts

The site conditions described in chapter 2 and the great number of wind turbines to be installed in each offshore wind farm require economically and technically optimal solutions for foundation design, prefabrication, transport, installation and removal. Figure 3 shows common foundation concepts for offshore wind energy turbines which predominantly have been adopted from conventional offshore technology.

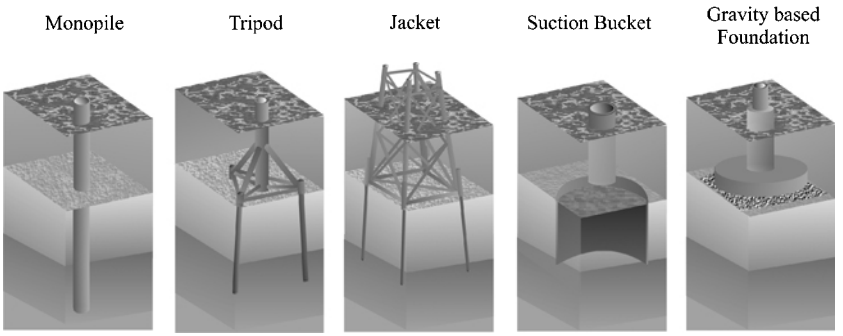

FIG. 3. Foundation concepts for offshore wind energy converters

Up to now, mainly monopile and gravity based foundations have been built (see Table 1). The monopile diameters range between 2 m for the first small turbines up to 4 to 5 m for today's larger turbines in various types of soil. Gravity foundations have been designed as concrete caissons except of one steel-concrete composite (wind farm *Middelgrunden*). A jacket foundations has been installed only for the two turbines of the demonstration project *Beatrice* up to now. One tripod foundation has been built for a Swedish turbine which is now out of operation. But more tripods are supposed to be installed in the German offshore test field *Alpha Ventus* (see chapter 2). A suction bucket has been successfully installed in a prototype test in Frederikshavn (Denmark). The installation of the suction bucket for a nearshore wind turbine in Wilhelmshaven (Germany) failed due to buckling.

However, fixed foundation structures are especially suitable in moderate water depths up to 20-30 m. In greater water depths floating structures may become more economic (see e. g. Butterfield et al., 2007). In Italy, a prototype of a floating 80 kW wind turbine comparable to a tension leg platform has been successfully installed in a water depth of 108 m.

Design considerations

The basic dimensions of the foundation are usually defined in a quasi-static analysis for the relevant extreme loading whereas the foundation behaviour under transient loading from wind, waves and currents has to be investigated separately (see Lesny, 2008).

The foundation design follows the procedures recommended in the design specifications of certification agencies such as Det Norske Veritas (DNV, 2004) or German Lloyd (GL, 2005) which widely refer to the methods proposed in API (2000). According to these recommendations the basic dimensions for a gravity based foundation and a monopile foundation have been determined for the site conditions in the German North Sea assuming a 50-year extreme wave height of 22.3 m and a wave period of 14.5 s and varying water depths t (see also Figure 2 and chapter 2). For the gravity based foundation the results are shown in Figure 4.

The effect of the water depth is obviously significant. Bearing capacity failure and overturning (which is substituted by the limitation of the load eccentricity) are the dominating failure modes. The site conditions require foundation diameters between 20 and 38 m with corresponding foundation heights between 5 and 35 m depending on the water depth. The bearing capacity is significantly affected by the friction angle of the soil. Hence, the lower limits of the soil parameters in Figure 3 require the largest diameters. In contrast to this the capacity against overturning is affected especially by the dead weight of the foundation requiring a sufficient combination of footing height and diameter.

A monopile foundation has been designed according to the p-y method recommended in API (2000) for mean values of the soil parameters in Figure 2. In the calculations the initial stiffness of the p-y curve has been modified to account for the effect of large monopile diameters on the pile behaviour (see Lesny and Wiemann, 2005).

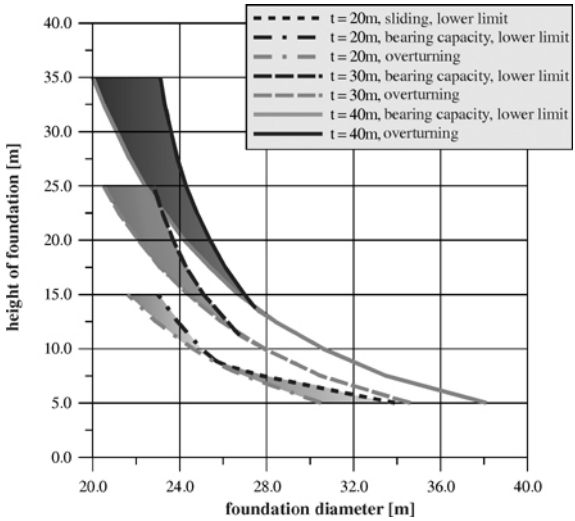

FIG. 4. Required footing dimensions for conditions in the German North Sea

The piles have been designed for (i) a vertical tangent at the deflection line near the pile tip and (ii) a maximum pile head rotation of 0.7°. The results in Figure 5 show that the water depth has no significant effect on the required embedment length.

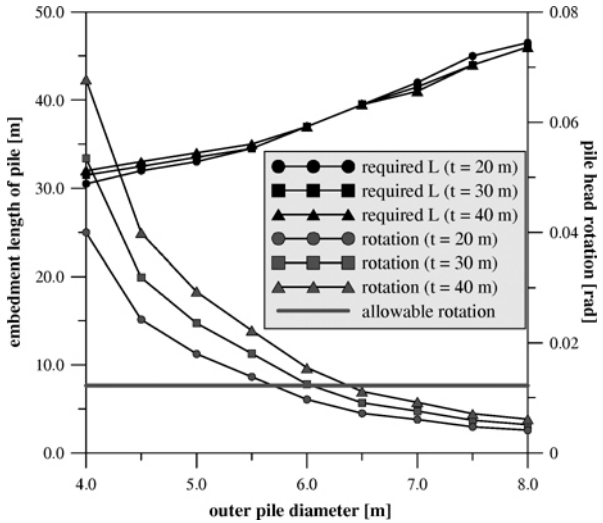

FIG. 5. Required monopile dimensions for conditions in the German North Sea

However, a significant influence of the water depth on the pile head rotation is visible especially for smaller pile diameters due to the smaller pile-soil stiffness of such piles. However, the allowable pile head rotation requires minimum diameters between 5.50 to 6.50 m which is greater than the diameters realised up to now. Furthermore, the driving equipment, which is available today, limits the diameter to 6.0 m, proper soil conditions provided. That means, for the conditions investigated here a monopile foundation is only feasible up to a water depth of about 30 m maximum.

CONCLUSIONS

The development and utilization of offshore wind energy in Europe is well under way and an extensive further expansion can be expected. However, design and construction of offshore wind farms is still a challenging task. Using the example of the German wind farm locations the different problems resulting from the specific site conditions have been illustrated. The resulting foundation dimensions are very large and require a sophisticated foundation design. In summary, it can be stated that foundations can be sufficiently designed today with the available design procedures. However, there are still many uncertainties involved not only in the design but also in the construction process. Hence, an optimization of the foundations is not yet possible.

REFERENCES

API (2000). "Recommended Practice for Planning, Designing and Constructing Fixed Offshore Platforms. Working Stress Design" *21st edition*, American Petroleum Institute, API Publishing Services, Washington D. C.

BSH (2008). "Uebersichtskarte Offshore Windparks.", *Bundesamt für Seeschifffahrt und Hydrographie*, www.bsh.de, Hamburg, Germany

Butterfield, S.; Musial, W.; Jonkman, J. (2007). "Engineering Challenges for Floating Offshore Wind Turbines." *Conference paper NREL/CP-500-38776*, National Renewable Energy Laboratory, Golden/Colorado, USA

DNV (2004). "Design of Offshore Wind Turbine Structures." *Offshore Standard DNV-OS-J101*, Det Norske Veritas Classification A/SDIN 1054

EEG (2004). „Erneuerbare Energien Gesetz." *Bundesgesetzblatt Jahrgang 2004*, Teil 1, Nr. 40. www.juris.de (in German)

GL (2005). "Guideline for the Certification of Offshore Wind Turbines." *Rules and Guidelines – IV Industrial Services*, Germanischer Lloyd Windenergie, Hamburg, Germany

Lesny, K. (2008). "Foundations for Offshore Wind Energy Converters – Tools for Planning and Design." *Habilitation thesis*, Faculty of Engineering, Department of Civil Engineering, University of Duisburg-Essen (to be published)

Lesny, K.; Wiemann, J. (2005). "Design Aspects of Monopiles in German Offshore Wind Farms." *Frontiers in Offshore Geotechnics*, edited by S. Gourvenec, M. Cassidy, Taylor & Francis Group, London: 383-389

Copyrighted Materials
Copyright © 2009 American Society of Civil Engineers (ASCE)
Retrieved from www.knovel.com

Analysis Collateral: Information needed for foundation integrity test data analysis

Bernard H. Hertlein, M.ASCE. Principal Scientist, NDE and Geophysics
AECOM, 750 Corporate Woods Parkway, Vernon Hills, IL 60061. bernie.hertlein@aecom.com

ABSTRACT

The term *Marketing Collateral* is well-established in the business development world as the collective name for the variety of media used to support the sales of a product or service. These sales aids are intended to make the sales effort easier and more effective. The author hereby suggests the term *Analysis Collateral* to define the additional information that makes analysis and interpretation of nondestructive deep foundation integrity test data easier and more effective.

This paper discusses the types of information that should be made available to, and be reviewed by, the analyst of deep foundation integrity test data, before coming to any conclusions about the data and the circumstances that generated it. Case histories are used to illustrate the results of failure to take notice of the available collateral information.

INTRODUCTION

When data from integrity tests on deep foundations indicate the presence of an anomaly, the analyst must go through a three-step process. First, the analyst must ascertain that the anomaly is not simply the result of faulty test equipment or improper testing procedure. Once it has been verified that the anomaly is, in fact, an irregularity in the foundation, its significance must be evaluated. This usually requires that the nature and physical extent of the irregularity be established. Finally, the design parameters of the shaft must be reviewed to assess the likely effect of the irregularity on the capacity and durability of the foundation.

Each of these steps will require more information than is available in the integrity test results. Hopefully the test operator performed more than one test to confirm equipment functionality and data repeatability. Additional testing, possibly using a different test method, may be necessary to establish the extent of the irregularity.

Determining the nature of the irregularity is important not only for evaluation of the existing foundation, but also to help the contractor revise or modify the construction procedure to prevent a similar irregularity occurring in the future. Determining the nature of the irregularity will likely require review of geotechnical exploration data for the site, the contractor's construction records, and the field inspector's notes.

INTEGRITY TESTS

There are three integrity tests that are commonly used to assess concrete piles and drilled shaft foundations – The impulse-echo test, the impulse response method, and cross-hole sonic logging (CSL). Gamma/gamma logging (GGL) is also available, but its use in the United States is typically restricted to the southwest, and only the California department of transportation CALTRANS uses the method regularly. All these methods have been extensively described elsewhere in the literature, most recently by the author and his mentor (Hertlein and Davis, 2006) so only a brief description is given here to aid in understanding the factors influencing the test results.

The impulse methods are similar in principal – both consist of striking the top of the shaft with a small hand-held hammer to generate a low-strain stress wave which propagates down the shaft. Where the stress-wave encounters a change in conditions, part or all of the energy will be reflected back to the surface, where it is detected by a motion transducer. The impulse-echo method uses an uninstrumented hammer, and an accelerometer connected to a data acquisition system to measure the shaft-head motion. The information recorded is a simple graph of acceleration over time, which can be used to calculate the depth of the reflector if a wave velocity for the concrete or grout is assumed. Conversely, if the depth is known, the wave velocity can be calculated. Since the velocity is a function of the modulus and density of both concrete and grout, it is a guide to material quality.

The impulse response method employs a hammer with a force transducer built-in, and a geophone velocity transducer to monitor pile-head motion. The force measurement allows a network analysis to be performed in which the data is converted from the time domain to the frequency domain by discrete Fourier transform and velocity is divided by force to standardize the result. The frequency-domain response curve contains information concerning:

- The depth of the reflector.
- The dynamic stiffness of the pile/soil complex.
- The shaft cross-sectional area.
- Concrete/grout quality.

CSL requires the placement of 38 mm or 50 mm (1.5 or 2.0 inch) internal diameter access tubes in the shaft prior to concrete placement. Typically one tube per 300 mm of shaft diameter is used, though this becomes excessive in shafts of more than two metres in diameter. The tubes are filled with water to provide acoustic coupling. An

ultra-sonic pulse transmitter is placed in one tube, and a receiving transducer in another tube. The transmitted pulse and the receiver signal are recorded electronically, and the time taken for the pulse to travel through the concrete from the transmitter is measured. A continuous series of pulses is emitted as the transducers are drawn up the access tubes, typically at a rate of about one pulse every 50 mm, thus recording a vertical profile of the material between the access tubes.

As with the stress wave velocity used in the impulse methods, CSL pulse velocity is a function of concrete modulus and density. If the distance between the access tubes is known, the velocity of the pulse can be calculated, and the concrete quality thus evaluated.

For gamma/gamma logging, a low-energy radiation source inserted in an access tube emits photons into the surrounding concrete. In a phenomenon known as Compton Scattering, the photons may be reflected, refracted, or absorbed by atoms in the various components of the concrete. Some of the reflected and/or refracted photons make their way to a scintillometer or radiation counter mounted a short distance above the source. Denser concrete will absorb more photons than less dense material, thus the number of particles detected by the counter in a given time is inversely proportional to concrete quality. Measurements are taken continuously as the gamma/gamma array is drawn up the access tube, building a vertical profile of variations in relative concrete density.

Whichever method is used to check the integrity of a foundation, the test output is essentially a line of data on a graph. For each of the methods discussed here, it is possible to generate a numerical model or computer simulation of the expected graph shape for the nominal foundation dimensions in the soil profile for that particular site.

Unfortunately, concrete quality and integrity are not the only factors that will affect the test results. The impulse methods are both sensitive to changes in shaft cross-section, and changes in soil properties. CSL and GGL are both sensitive to very local features such as access tube joints, reinforcing steel centralizers, and minor segregation caused by tie-wires or other devices used to fix the access tubes in place.

It requires a trained analyst to decide what the graph of test data represents. When disturbance of the expected graph shape occurs, the analyst needs additional information in order to determine the likely cause of the disturbance, and its potential significance to the capacity and durability of the foundation.

ANALYSIS COLLATERAL

People in the business development and marketing world understand the term *Marketing Collateral* to mean the wide variety of information, novelties and pictures that are used to make the sales effort easier for the seller and more enticing for the potential buyer. The author hereby suggests the phrase *Analysis Collateral*, to mean the additional information that makes the analysis, interpretation and evaluation of

deep foundation integrity test data easier and more reliable. For all foundation sites, this information may include:

- Geotechnical exploration report.
- Foundation design drawings and calculations.
- Contractor's construction records.
- Field Inspector's notes.

For drilled shafts and augered, cast-in-place (ACIP) piles, the contractor's construction records may include:

- Concrete or grout mix design.
- Reinforcing cage design.
- Concrete or grout delivery tickets.
- Superintendent's daily notes.
- Automated monitoring equipment (AME) data.

Where access tubes are installed for cross-hole sonic logging (CSL) or gamma/gamma logging (GGL), the author strongly recommends that the locations of any pipe joints, fixing points, and reinforcing cage spacers or centralizers are documented as part of the construction record or inspector's notes.

Often, the contractor wants to know the results of the integrity testing immediately, on site, because the next phase of construction is being held up, pending acceptance of the foundations. It is surprising how many of those same contractors withhold construction information from the tester, apparently with the intention of "seeing how good he is." Testing the tester by making it into a guessing game is likely to hinder the analysis process, and may result in inconclusive or ambiguous interpretation.

CASE HISTORY #1

The project that started the Author's train of thought regarding analysis collateral was not a deep foundation project, but did involve the use of impulse response testing, and clearly demonstrated the importance of reviewing all available information.

At a nuclear waste storage facility in the Pacific Northwest, 210 litre (55-gallon) drums of solidified nuclear waste were swelling. Scientists at the facility reviewed the possible causes of the swelling, and one possibility caused them great concern. They thought it possible that a chemical reaction was reversing the solidification process and generating cyanide gas, which was pressurizing the drums. They requested that the author's firm to develop a program of non-invasive testing to determine if the material in the drums had remained solidified, or was being converted back into a liquid/gas combination. The actual identities of the contents of the drums were considered classified, and the information was withheld from the author.

Using a combination of Impulse Response testing and rapid chilling of sample drums fitted with strain gages, the author determined that the material in the drums was still solid, and was in full contact with the walls of the drums, thus ruling out the cyanide gas theory. On completion of the analysis, the security personnel decided that the identities of contents were not, in fact, classified, and released that information to the author. On reviewing the manufacturer's cut sheet for the solidification agent, the author noticed that the material would expand by up to 25 percent if in contact with water. Part of the waste being solidified was radioactive water. Examination of the drum processing records showed that each drum had been completely filled, leaving no room for the expected expansion.

Apart from the obvious oversight by the original processors, had the manufacturer's information been made available to the author at the beginning of this project, the need for testing would probably have been avoided altogether.

CASE HISTORY #2

The author has been involved in several projects where CSL data showed apparent anomalies at the base of the shaft, but core-drilling the shaft showed no anomaly at the base of the concrete. In several of these cases it was possible to compare the lengths of the access tubes with accurate records of drilled shaft depth. The reinforcing cages did not extend to the full depth of the shaft, and the CSL tubes that extended beyond the bottom of the reinforcing cage were held in position by a few welded hoops of reinforcing steel. The accessible length of access tube below the top of concrete was greater than the concreted length of the shaft, indicating that the reinforcing cage had dropped somewhat during concrete placement or temporary casing removal, pushing the tips of the CSL tubes into the clay at the bottom of the excavation.

It is likely that the same had occurred in several other cases of anomalies that could not be confirmed by core samples, but the construction records were incomplete or insufficiently accurate to allow conclusive interpretation. The cost of the delays that these anomalies caused in the shaft acceptance process did serve to convince the contractors in each case that the benefits of accurate record keeping amply justified the cost involved when these situations arose.

CASE HISTORY #3

On a refinery site in Alberta, Canada, a large number of augered, cast-in-place (ACIP) piles had been constructed to support several new structures in close proximity to each other. The integrity of the piles was checked by the impulse-echo method. Several of the shafts produced anomalous results. The analyst interpreted the test results as indication of reductions in shaft cross-section, or 'neck-ins', and produced impedance logs that appeared to support that interpretation. Given the construction records, the contractor did not believe the interpretation, and contacted the author for peer review of the data, and some additional testing.

The author used the impulse response method on the questionable shafts, and ran some numerical models, or simulations, for comparison with the test data. The results of this testing and modeling strongly suggested oversized shaft sections, or bulges.

The geotechnical exploration for this site had included only one boring at the location of the ACIP pile project, and that showed relatively uniform clays and silts. Examination of the construction records, however, revealed that numerous pockets of loose or running sands had been encountered during the augering of the shafts.

The contractor subsequently excavated some of the shafts with the shallower anomalies for visual review. This revealed that the responses in the integrity test results were from zones where shaft diameter reduced from a bulge or oversized shaft cross-section down to nominal diameter. In each case shaft cross-section was either over-sized from the top, or increased gradually enough that the increase in cross-section was not immediately apparent in the test results.

CASE HISTORY #4

The author has been involved numerous projects where anomalies were reported in CSL or impulse test results that could not be explained by any of the occurrences noted in the construction records or the inspector's notes. When the tests were repeated a few days later, the anomalies had disappeared. In each, multiple admixtures had been used in the concrete. A typical admixture "cocktail" might include a high-range water reducer, a cement conditioner, an anti-washout agent, and a set retarder. The combined effect of this mixture is often much greater retardation of set than was expected – the author has been involved in projects where the concrete took several days to set, and is aware of other projects where the concrete took more than a week to set. Of more importance for the tester is the fact that the concrete often sets and gains strength unevenly, showing excellent CSL pulse velocities in some parts of the shaft, and very low velocities in other parts. When retested a few days later, the velocities are all within the normal range.

Where any admixtures are used in the concrete, the testing firm should receive a copy of the proposed mix design to consider when planning the test program, because premature testing is likely to produce anomalous results.

CASE HISTORY #5

A large number of ACIP piles hade been constructed for a new hospital project in Saskatchewan, Canada. The drilling rig used for the work was equipped with automated monitoring equipment (AME) which measured concrete pressure, auger lifting rate, auger torque, auger rotation rate, and drilling rate.

Impulse-echo testing was performed, and several questionable piles were identified. The worst anomaly was reported as a loss of the entire cross-section in the bottom two metres or so of the pile (Figure 1).

Since the AME report for the pile showed no indication of problems, the contractor asked the author to peer review the impulse-echo test data, and to perform additional testing. The author used the impulse response method, with computer simulation to assist in interpretation.

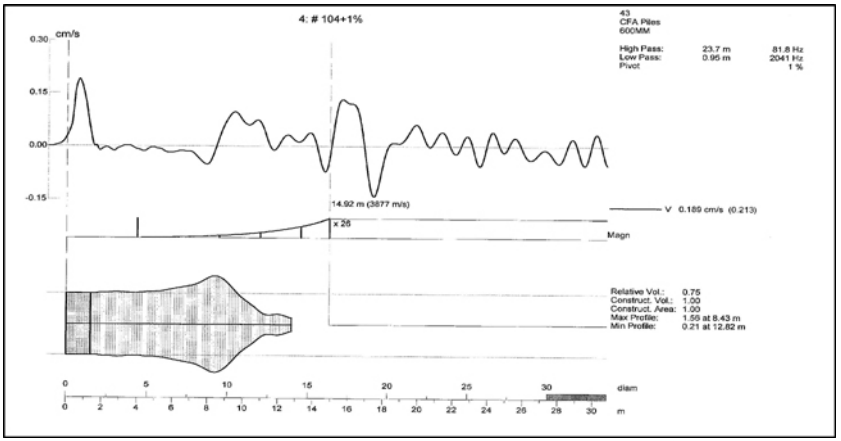

Fig. 1: Impulse-echo data and impedance log derived from it.

The best match between the test data and the simulation model showed a bulge in the pile at approximately the midpoint, but no other significant irregularities (Figure 2). In the author's experience, several documented trials on shafts with known shapes and defects have shown that this situation often causes artifacts in the test data that can mask the response from the base of the shaft (Davis, 1997).

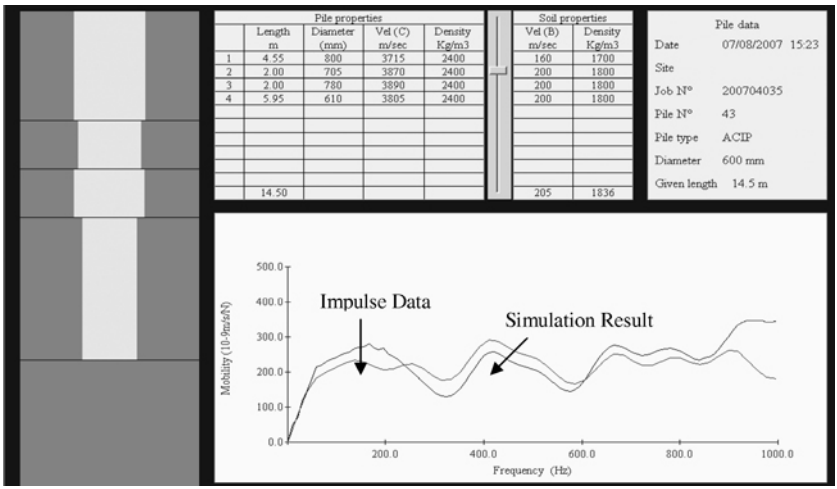

Fig. 2: Impulse response test data and simulation result

The analyst of the impulse-echo data on this project had access to the AME record, but apparently either did not request it, or chose to ignore it.

It is important for the analyst of Impulse-Echo and Impulse Response test data to be aware that the energy of the stress wave generated by the hammer impulse is damped progressively with depth by both the concrete of the shaft and the surrounding soils. It is therefore typical that the amount of wave energy reflected back to the surface by an anomaly in the upper portion of the shaft will be significantly greater than the amount of energy reflected by a similar sized anomaly in the lower portion of the shaft.

It is not unusual for a significant reduction in cross-section in the upper portion of the shaft to cause multiple responses as the wave energy is reflected to the surface and back down the shaft again. If this reflector is located close to the midpoint of the shaft, then the second reflection from it will coincide with the response from the base of the shaft. These two responses will combine, and, depending on their respective polarities, will either amplify or attenuate the net response at that point. In the time domain (Impulse-Echo test), the base response may be completely masked by the midpoint reflection, and in the frequency domain (Impulse Response test), the base response may distort the shape of the response from the midpoint of the shaft, leading to erroneous calculation of depth for both reflectors.

Thus it is of great importance that information regarding the depth of known or anticipated changes in cross-section, such as the bottom of temporary casing sections, documented caving of lateral soils, etc., is provided to the test analyst.

CONCLUSIONS

The entire foundation project team contributes to the data that is analysis collateral, though many are not aware of it. Hopefully a broader publication of the concept will help team members understand the importance of it, and the need for complete and accurate records of all aspects of the work. The analyst of nondestructive test data needs to take full advantage of the available information when interpreting the test data. The effectiveness and accuracy of deep foundation testing depend on it.

REFERENCES

Davis, A. G., 1997. "Nondestructive Evaluation Discussion 1" *Foundation Drilling.* March/April, 1997. pp. 2-3. ADSC-IAFD, Dallas, Texas.

Hertlein, B.H. and Davis, A.G. (2006) *Nondestructive Testing of Deep Foundations.* Pub. John Wiley & Sons, Chichester, UK. ISBN 0-470-84850-2.

Copyrighted Materials
Copyright © 2009 American Society of Civil Engineers (ASCE)
Retrieved from www.knovel.com

Capabilities and Limitations of Cross Hole Ultrasonic Testing of Piles

J.M. Amir F.ASCE [1] & E.I. Amir[2]

[1] Chairman, Piletest.com Ltd.
[2] President, Piletest.com Ltd.

ABSTRACT

This paper describes an attempt to quantify flaw detectability in cross hole ultrasonic testing of piles. To this end we constructed a bored pile with access tubes and three pre-fabricated flaws, and then tested it with the CHUM ultrasonic instrument. We analyzed the results and presented them in the conventional one-dimensional format, as well as in two- and three-dimensional tomographic images. We then compared the results with those of a finite element model which showed similar effect of the flaws. We concluded that a flaw is usually detectable by this method only if its size exceeds one-third of the access tube spacing. In addition, the use of advanced tomographic techniques may enhance flaw detectability.

INTRODUCTION

Cross hole ultrasonic testing technique is now well-known and has been standardized in several countries (Amir & Amir 2008). Still, there is still scant data regarding its performance in terms of flaw detectability. Sarhan et al. (2002) quoted a number of sources relating to this question, and concluded that flaws occupying up to 15% of the pile's cross section could remain undetected. Amir (2005) showed that flaw detectability is a function of its location in addition to its size.

In order to quantify the performance envelope of the cross hole ultrasonic test we constructed a test pile with three built-in flaws. The pile (or drilled shaft) was bored and cast in situ, with eight 50 mm. access tubes. We tested the pile several times with the Cross Hole Ultrasonic Monitor and then analyzed and presented the results in both one-dimensional presentation and tomography.

For comparison purposes, we modelled and analyzed the flaws by the dynamic module of Plaxis™ finite element program.

As the title of this paper implies, we limited ourselves to flaw detectability and did not address the influence of flaws on either capacity or durability of the piles. This important issue was dealt with by others (Sarhan et al. 2002, Iskander et al. 2003).

Description of the Pile

The 1200 mm dia. pile was bored through dry clayey sand to a depth of 5.50 m from the surface. The reinforcement cage was assembled with eight 50 mm access tubes evenly distributed on the inside. Four of the tubes were of steel (designated N, E, S and W) and the remaining four – of plastic (numbered 1 to 4). In addition, we installed three flaws at three levels. A general view of the setup is given in Figure 1 and details of the flaws are provided in Table 1

After lowering the cage into the hole, the pile was immediately cast with 30 MPa concrete.

FINITE ELEMENT SIMULATION

In order to obtain better understanding of the mechanism governing the cross hole method, we modeled the pile in the dynamic model of Plaxis® finite element program. The concrete parameters we assumed were as follows: Young's Modulus – $E = 3.6x109\ kN/m^2$, Poisson's Ratio - $\nu = 0.1$ and specific gravity - $\gamma = 23\ kN/m^3$. The resulting P-Wave speed was 4,001 m/sec. Due to software limitations we performed our analysis in two dimensions, assuming plane strain conditions (Figure 2). The pulse produced by the ultrasonic emitter in this simulation was represented by five stress cycles with a 50 kHz frequency.
We studied flaws No. 1 and No. 3 in three different profiles, each with a flaw present or absent, respectively (Table 2). Due to modeling difficulty (and triviality) we did not analyze flaw No. 2.

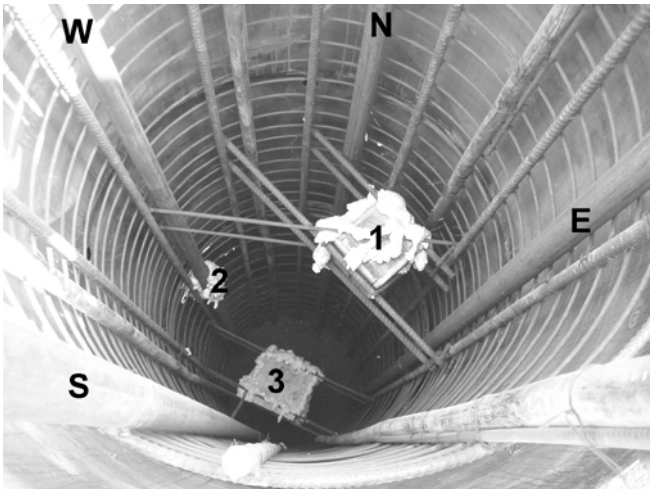

Figure 1: General view of the reinforcement cage, access tubes and flaws

Table 1: Details of Flaws

No	Mean depth (m)	Description	Size (mm)	% of tube spacing	% of cross-section
1	1.60	empty plywood box	200x200x200	32	3.5
2	2.60	bandage			
3	3.65	empty plywood box	300x300x300	32	8

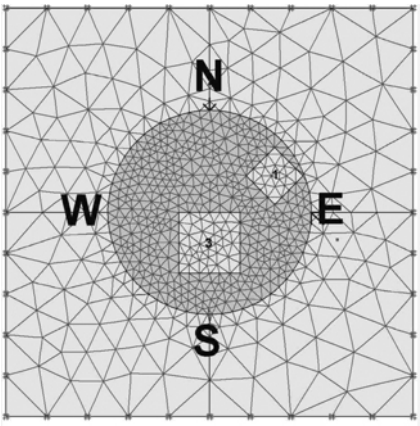

Figure 2 : Finite element simulation of pile with flaws

Table 2: Simulated Profiles

Run No.	Flaw No.	Profile	Spacing (mm)	Flaw
1	1	N-E	710	yes
2	1	N-E	710	no
3	3	N-S	1,000	yes
4	3	N-S	1,000	no
5	3	N-S	1,000	yes
6	3	N-S	1,000	no

Results of Finite Element Simulation

The results of all six runs were plotted in the form of particle velocity at the receiver as a function of elapsed time following the emitter triggering. An examination of a typical trace (Figure 3) shows the following properties:

1. The initial part of the trace is flat and featureless. At the First Arrival Time (FAT) a pulse consisting of periodic displacements is observed.
2. Although our input pulse consists of only five cycles, the particle velocity trace at the receiver consists of considerably more cycles. This proves that the pulse recorded is a superposition of numerous wave paths.

3. The pulse amplitude immediately following FAT is relatively small and it grows gradually with time, as more and more wave paths converge at the receiver.
4. The maximum amplitude is located at double to triple FAT value. It is caused by higher energy Rayleigh waves travelling at about half the P-Wave speed along the perimeter of the pile.
5. The existence of a flaw shows influence on both FAT and amplitude.

Table 3 summarizes the FEM simulation results.

Table 3: Simulation results

Flaw No.	Profile	FAT increase (%)	Attenuation increase
1	NE	11	Marked
3	NS	10	Considerable
3	EW	0	Negligible

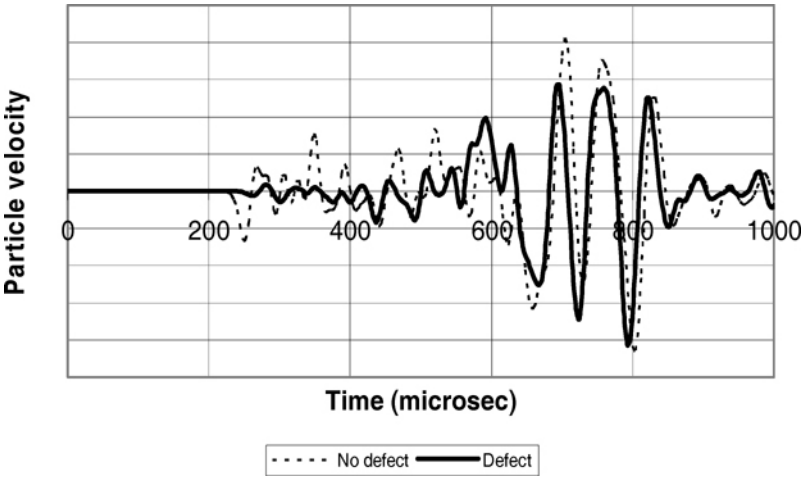

Figure 3: Profile N-S – influence of flaw No. 3

MODEL PILE TESTING

We performed the cross hole tests following ASTM Standard D6760-08 (ASTM 2008). We then analyzed the results and presented them using the following methods:

1. One-dimensional (1D) line plots of FAT and attenuation overlay on "waterfall" background.
2. Two-dimensional tomography (2DT) – fuzzy logic (Amir & Amir 1998)
3. Two-dimensional tomography - parametric (Amir & Amir 1998)
4. Three-dimensional tomography using straight-line wave propagation - 3DT (Haramy & and Mekic-Stall 2000)

Results of Model Pile Testing

The results are presented in Figures 4 to 7.

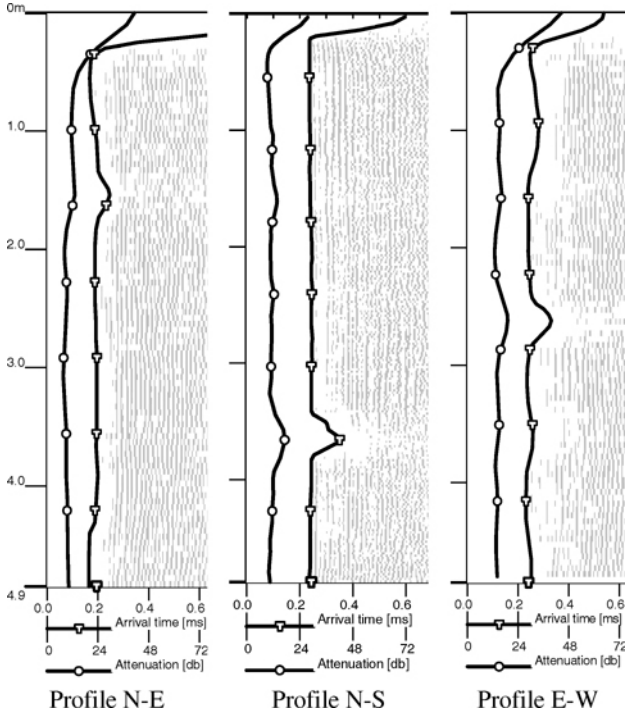

Figure 4: 1D results of cross hole logging

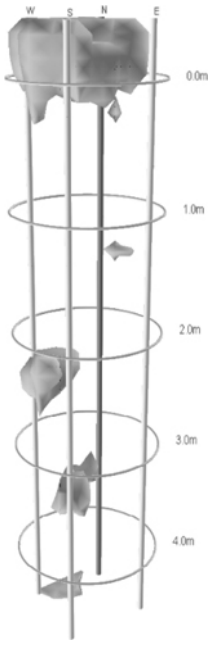

Figure 5: Results of attenuation-based 3DT

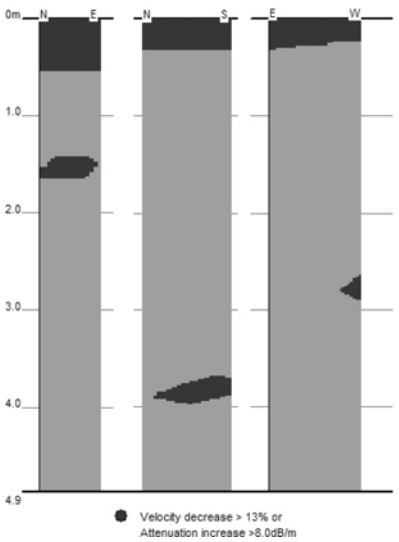

Figure 6: Results of fuzzy-logic 2DT

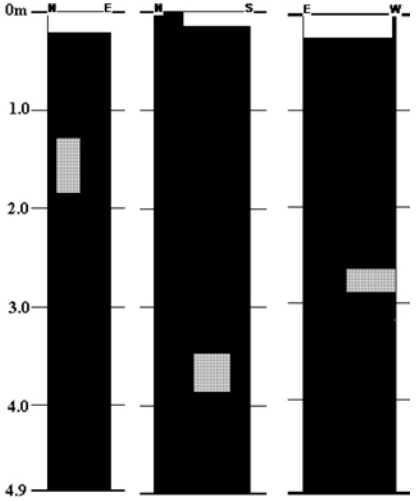

Figure 7 : Results of parametric 2DT

Discussion of the Results

One-dimensional presentation

The results of the one-dimensional presentation (Figure 4) were summarized in Table 4. Evidently, flaws No.1 and No. 3 hardly qualify for the Caltrans category of "significant anomalies" (severe signal distortion, much lower signal amplitude, FAT increase of more than 20%). In many real-life situations such flaws would escape detection altogether. Flaw No. 2, geometrically the smallest, made the strongest mark on the FAT, thus confirming that detectability is a function of location no less than of size.

Table 4: Summary of 1-D results

Flaw No.	Profile	FAT increase (%)	Attenuation increase (dB)
1	NE	20	6
2	EW	38	5
3	NS	20	6
3	EW	0	4

3DT

Although we took much care in collecting the data, regular FAT-based 3DT failed to reveal the flaws. At this point we decided to replace FAT with attenuation in the analysis. Apparently, the results we obtained (Figure 5) were quite good for flaws No. 1 and No. 3, while No. 2 again appeared much larger than its real size.

2DT

All three flaws show reasonably well in Fuzzy-logic tomography (Figure 6) and in parametric tomography (Figure 7). We managed to arrive at this result, however, only after some manipulation with the parameters. This means that while we were able to confirm the location (and to a certain degree the shape and size) of the flaw, we would probably fail to perform a class A prediction without prior knowledge.

CONCLUSIONS

The main conclusions we drew from this exercise are as follows:

1. The anomaly created by a flaw depends not only on the flaw's size, but also on its location. The closer a flaw is to an access tube the larger it appears in both 2DT and 3DT.
2. A flaw located half way between two access tubes is detectable only if its size exceeds about one third of tube spacing or about 10 percent of the pile's cross section.
3. Piles used for validation purposes should preferably be constructed with at least some of the flaws not smaller than 40 percent of the tube spacing.
4. Flaw detectability can be enhanced by using tomographic, and specifically 3DT techniques. Attenuation-based 3DT appears to be an especially effective technique and merits further investigation.
5. Plane strain finite element modelling is a useful tool for predicting the results of the cross hole ultrasonic test. Due, however, to modelling imperfections, the results are more qualitative than quantitative. The main discrepancies are the absence of the third dimension, the representation of the emitted pulse as unidirectional instead of radial and disregarding the access tubes and the water.

REFERENCES:

Amir, E.I & Amir J.M. (1998). "Recent advances in ultrasonic pile testing." *Proc. 3rd Intl Geotechnical Seminar on Deep Foundation On Bored and Auger Piles*, Ghent: 181-185

Amir, J.M. (2005). "Discussion on "Low Strain Integrity Testing of Piles: Three–Dimensional Effects" by Y.K. Chow, K.K. Phoon, W.F. Chow and K.Y. Wong, , *J. Geotechnical and Geoenvironmental Engrg.* 131 (2): 342-343

Amir, J.M. & Amir E.I. (2008). "Critical comparison of ultrasonic pile testing standards." *Proc. Intl. Conf on Application of Stress Wave Theory to Piling,* Lisbon (accepted for publication)

ASTM (2008). "Standard test Method for integrity testing of concrete deep foundations by ultrasonic crosshole testing, Designation D 6760-08," West Conshohocken PA: 3

Haramy, K.Y, and N. Mekic-Stall, 2000. "Evaluation of drilled shafts at Piney Creek Bridge using cross-hole sonic logging data and 3D tomographic imaging method." *Proc. 1st Intl. Conf. on the Application of Geophysical Methodologies & NDT to Transportation Facilities and Infrastructure*, St. Louis, MO:

Iskander, M., Roy, D., Kelley, S. and Ealy, C. 2003. "Drilled Shaft Defects: Detection, and Effects on Capacity in Varved Clay." J. Geotech. and Geoenvir. Engrg, Vol. 129, No. 12, pp. 1128-1137

Sarhan, H., Tabsh, S.W., O'Neill M., Ata, A. & Ealy, C. (2002): "Flexural behavior of drilled shafts with minor flaws, in Stiff Clay" Proc. Intl. Deep Foundations Congress, GSP No. 116, ASCE, Reston/VA: 1136-1150.

Copyrighted Materials
Copyright © 2009 American Society of Civil Engineers (ASCE)
Retrieved from www.knovel.com

Combined Parallel Seismic and Cone Penetrometer Testing of Existing Foundations for Foundation Length and Evaluation

Dennis A. Sack[1], Larry D. Olson[2], P.E.

[1]Vice President, Olson Engineering,12401 W. 49th Avenue, Wheat Ridge, CO 80033,
Ph – 303-423-1212,,Fx – 303-423-6071, dsack@olsonengineering.com
[2]President, Olson Engineering,12401 W. 49th Avenue, Wheat Ridge, CO 80033,
Ph – 303-423-1212,,Fx – 303-423-6071, ldolson@olsonengineering.com

ABSTRACT: The use of the Parallel Seismic (PS) test method has been well documented and has been shown to be effective for foundation length evaluation when used with a cased borehole adjacent to the foundation being evaluated. In addition, the use of the Cone Penetrometer Test (CPT) to evaluate soil properties without a borehole has also been well documented. Recent research, hardware development, and field testing have been conducted on a system which combines the two methods to allow fast and economical evaluation of both soil properties and foundation depth without requiring a drill rig. The combined system collects both PS and CPT data in one or two probe pushes into the soil. The combined system also uses a relatively low clearance rig which is self-propelled and designed for use on rough conditions. Thus, access is possible to bridge foundations that could not be tested with conventional means. The paper presents details of the principles and operations of the combined system, as well as field test data from driven pile bridge foundations as well as steel sheet piles under levee walls in New Orleans.

INTRODUCTION

Determining the true tip depth and foundation geometry for bridge foundations without documentation is becoming an increasingly important task for the nondestructive testing community. These unknown foundations are found under a wide variety of structures, ranging from bridges to antenna towers to buildings. For most of these foundations, the lack of any information is not a major concern if the structure has been performing adequately for a period of years. However, a variety of situations can arise which can suddenly make knowing the foundation depth and geometry be of prime importance. The most common situation that arises is a planned change in loading of the foundation element. For antenna towers, this situation occurs when new or heavier antenna elements must be added to the tower. For bridge foundations, this can be due to adding lanes to an existing bridge or reusing foundations for a totally new superstructure. The need for foundation information can also be driven by new scour analyses for bridges, to verify that the predicted or historic scour depths will not undermine the foundations during a major flood event.

Regardless of the actual reason for needing information on foundation depth and type, there is a clear requirement for reliable, fast, and cost-effective test techniques to allow this determination. There are several methods that can be used for unknown foundation evaluation, with the specific utility of each method usually dependent on the actual foundation to be tested. These methods include electromagnetic methods such as Ground Penetrating Radar and Induction Field, as well as various stress-wave based test methods such as surface Sonic Echo, Impulse Response, Ultraseismic (US) methods as well as the borehole-based and Parallel Seismic method. Previous research performed for the NCHRP by Olson Engineering (1,2) has shown that of the methods available, the Parallel Seismic (PS) test method is the most versatile and reliable. This method can be applied to a wide variety of foundation types and almost any foundation depth, and does not require direct physical access to the foundation being tested. The most significant limitation to wider application of the PS method is that it typically requires a cased borehole be placed in the ground next to the foundation in question using a truck-mounted drill rig.

As stated above, the biggest limitation to the wider application of the PS test method is the requirement for a cased borehole next to the foundation element. Recent research and development has resulted in a system that uses a cone probe system to simplify the borehole installation or eliminate it altogether. The newly developed system can be used to either install a small-diameter casing for PS testing, or can be used with an instrumented cone probe to allow collection of PS data without a borehole at all. For sites with stiffer soils, the cone probe rig can be used to install a cased borehole using hollow steel casing and a vibratory hammer. This casing can then be used to quickly perform a PS test using "conventional" methods, but still without requiring the use of a large truck-mounted drill rig. Sites with softer soil profiles can be tested with just an instrumented cone probe as the PS receiver. These two options are discussed below, after a brief summary of how the PS test method is used.

PARALLEL SEISMIC NDE METHOD

The Parallel Seismic (PS) test is normally performed by impacting an exposed foundation top or side, or impacting a part of the structure above the foundation (such as a pile cap or column). The impacts can be either vertical or horizontal, and are typically done with an instrumented impulse hammer to generate compressional waves. Testing can also be done with a non-instrumented hammer, using an accelerometer mounted nearby for the trigger source. These waves travel down the foundation and couple into the surrounding soil as shown in Figure 1. The coupled compressional waves are then picked up in the soil by a nearby hydrophone or geophone receiver. This receiver is typically suspended in a water-filled cased borehole, but can also be near the tip of an instrumented cone probe pushed into the ground. The impact data is collected at a series of multiple receiver depths and stored. This data is then used to create a plot of receiver signal arrival time versus depth, from which the analysis is performed.

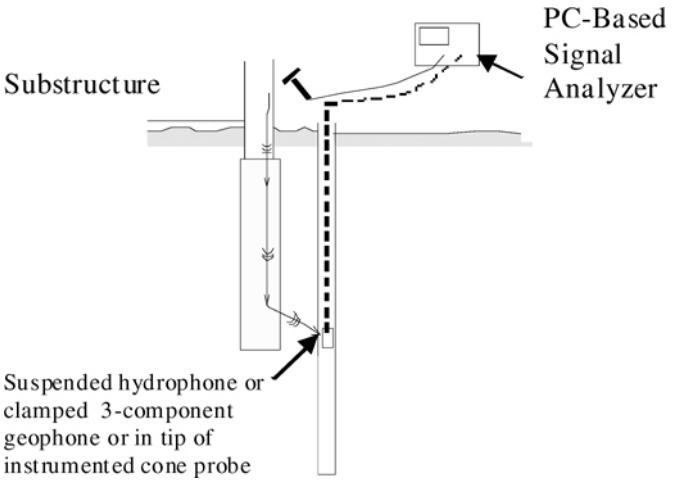

Figure 1 PS Test method

Regardless of the type of equipment used to collect the PS data, the tip depth of a foundation is typically indicated by an inflection point in the arrival time versus depth curve, along with a sharp drop in signal amplitude. Diffraction of wave energy from the foundation bottom has also been found to be indicative of foundation tip depth in PS tests as well. Other research at Northwestern University National Geotechnical Site (NGS) has also indicated that the PS method is effective in measuring foundation lengths of inaccessible piles (piles with no access to the pile sides or tops), although this research also pointed out that some care must be taken when using the method under certain soil/rock interface depth versus pile length conditions (4).

Typical Parallel Seismic Test Equipment

The PS test method required a relatively simple set of equipment to perform. A summary list is presented below:

1. PC based data acquisition system with a sampling rate of at least 100 kiloHertz (10 microseconds/12 bit digital data point) on at least 2 channels (4 channels needed for triaxial geophone) with at least 4096 data points per channel,
2. Signal amplifier(s) for receiver(s). Note: amplifiers can be built into the receivers in some cases.
3. Instrumented impulse hammer or non-instrumented hammer and an accelerometer. Hammers typically weigh 1.4 to 5.5 kg (3 to 12 lb) and must supply an accurate trigger time signal either through the built-in load cell or the nearby accelerometer.
4. Hydrophone or triaxial geophone receivers are required for borehole-based PS tests, while an instrumented cone probe is required for CPT-based tests.

Parallel Seismic Data Interpretation

The Parallel Seismic test is used primarily to determine the depth of unknown foundations, although information as to foundation type can usually be determined by an experienced testing firm based on the foundation velocity, inflection points, etc. The research done for NCHRP 21-5 and 21-5 (1,2) resulted in the establishment of several criteria for determining the foundation depths based on Parallel Seismic data as follows:

1. Breaks in the slope of the lines in a plot of depth versus recorded time,
2. Drop in energy amplitude below the bottom of the foundation, and
3. Diffraction of wave energy at the bottom of the foundation.

Example PS Test Data – Concrete Driven Pile Foundation

A PS test was performed on a 29 m (94 ft) deep foundation element supporting a bridge in Baton Rouge, Louisiana. The test was performed by using a CPT rig to install a hollow steel casing into the ground, into which a small diameter (2.5 cm, 1 in) PVC pipe with a slotted bottom was inserted. After insertion of the PVC, the steel casing was removed, leaving the PVC pipe behind. A PS test was then conducted on the foundation, with the impacts being supplied by a 1.4 kg (3 lb) instrumented hammer hitting the side of the bridge column above grade. The signals were received by a small diameter hydrophone suspended in the PVC casing. A typical PS test result from this testing is presented in Fig. 2 for a test done with the hydrophone moved at 1 foot intervals for the entire length of the casing. As seen, the arrival time versus depth plot starts with a velocity versus depth slope of about 3,658 m/s (12,000 ft/s). This is typical of the compression wave velocity of concrete. At a depth of about 29 m (94 ft) below grade, the slope of the arrival time plot changes abruptly to about 2011 m/s (6,600 f/s). This is the typical compression wave velocity of the saturated sands expected to be at and below the tip of the foundation. The foundation bottom depth is at the intersection point of the two lines (at the inflection depth).

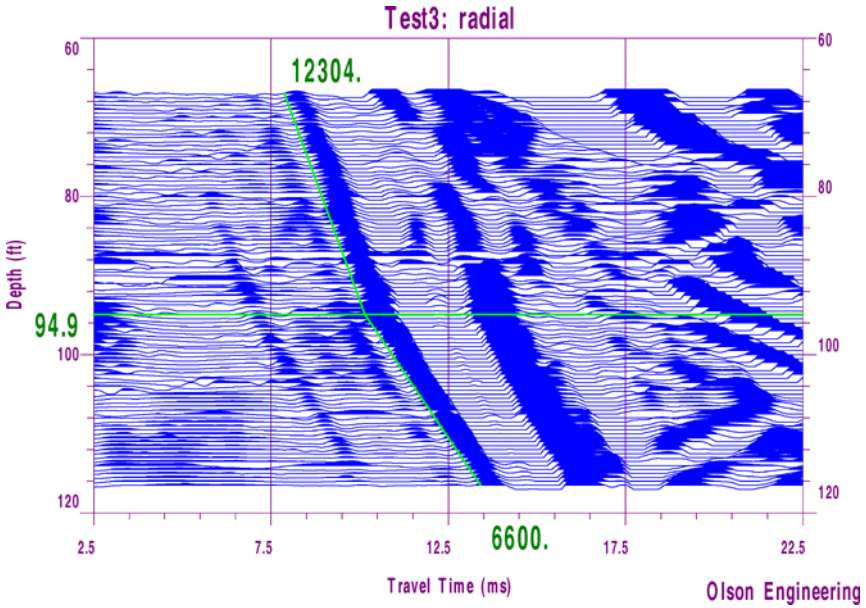

Figure 2 Sample PS Test Result

Example PS Test Data – Steel Sheet Pile Concrete Driven Pile Foundation

A series of tests were performed using the PS test method on sheet piles along the tops of levees in New Orleans, Louisiana. The levee walls in the area of the testing consisted of steel sheet piles driven into the levee soil, topped by a concrete wall which extended several feet into the soil of the levee with the tops of the steel sheet piles embedded into it. The PS data sets were collected using both the PS/CPT and conventional PS testing using boreholes and by a Geoprobe at selected locations near the levee walls.

The conventional PS data was collected for receiver depths from about 10 feet below the sheet pile tips up to just below grade. The impacts to the wall were done by impacting the concrete wall in both vertical and horizontal directions, as well as on the steel sheet pile itself at one location where a small excavation had been made to expose the top of the steel below the concrete.

An example of a PS test performed on a levee wall location is presented in Figure 3. This test was conducted using vertical impacts to the top of the concrete wall with a 1.4 kg (3 lb) instrumented impulse hammer, as shown in Figure 4. This location had a cased borehole installed using a CPT rig to install a small diameter PVC casing without a drill rig, as described in the previous section. Data was collected for receiver depths from 0.6 m (2 ft) to 9.1 m (30 ft) below grade using an Olson

Instruments Freedom Data PC for both signal conditioning and digitization/storage as shown in Figure 5. It should be noted that the borehole was located only about 0.76 m (2.5 ft) from the levee wall at this location, which provides for the best possible data. The data set showed clean data with a clear sheet pile tip depth. As seen in the figure, the steel sheet pile tip is apparent at a depth of 6.6 m (21.5 ft) below grade. The tip of the sheet pile acted as a point diffraction source, with much of the energy traveling in the pile coupling to the firmer sandy soil located only at or near the tip. Above the tip, the slope of the plot is negative, indicating that most of the energy picked up by the receivers at shallower depths was coming also from the pile tip and not from the sides of the pile. This unusual result is not uncommon with steel sheet piles, and still results in an easy to see pile tip depth indication.

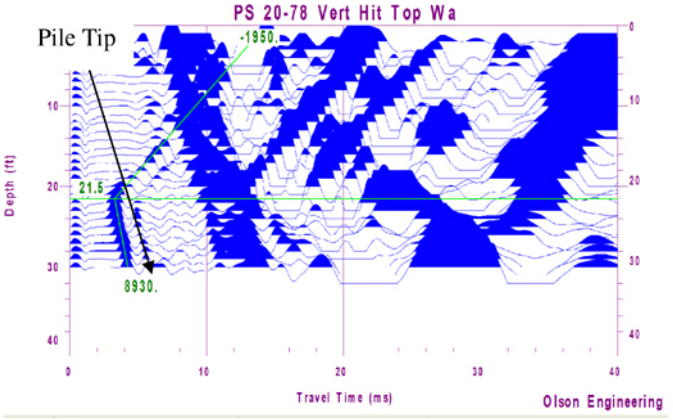

Figure 3 Sample PS Data on Concrete/Steel Levee Foundation

Figure 4 Impacting the Top of the Levee Wall

Figure 5 Data Collection System

PS Test Recommendations

For successful use of the PS method, regardless of whether data is collected with a PS/CPT system or a standard PS test setup, there are several considerations which must be taken into account at each proposed testing site.

1. The most effective PS testing is done when the transducer is located as close as possible to the foundation under test. Typically, the borehole to foundation distance should be 10 feet (3 m) or less for the highest quality and greatest foundation tip depth accuracy. This requirement is to reduce the effects of the velocity and attenuation of the surrounding soil, particularly at sites with unsaturated soil conditions. Where saturated soil conditions exist, PS tests have been successfully performed with larger horizontal offsets from foundation edges. The CPT rig used for the new PS/CPT tests allows the probe to be pushed into the soil at locations as close as 5-7 feet from the foundation edge, depending on access conditions

2. Ideally, the borehole (for traditional PS tests) or probe penetration depth (for PS/CPT tests) should extend at least 4.5 m (15 ft) below the minimum required foundation depth (from a capacity/scour perspective considering the subsurface geology) or suspected foundation depth, whichever is greater. This requirement is to ensure that data is collected to the depth of interest. If the borehole or probe is not at least somewhat deeper than the foundation bottom, one may only be able to determine that the foundation is at least as deep as the borehole or probe at the maximum depth (unless a foundation bottom diffraction event is recorded). We have seen a number of cases where the tip depth can be seen in the PS data at transducer depths above the tip depth based on diffractions from the pile tip. However, this type of analysis is not considered to be as reliable as collecting data to depths below the foundation tip and should only be used in cases where the borehole or probe is not or cannot be advanced to the required depth. It should be noted that when collecting data with a PS/CPT setup, it is possible to monitor the data from the PS tests as well as soil conditions from CPT data as the probe is gradually inserted deeper into the soil. Thus, the bottom depth of the foundation can be determined during the course of the testing along with the soil properties. This allows the early termination of testing if the foundation is found to be shallower than expected, or, conversely, allows the operator to continue testing until the bottom depth is seen if the foundation is deeper than expected.

3. For use of the PS/CPT system, site soil conditions must be suitable for testing with a CPT system. Thus, sites with shallow rock or boulders are not generally suited to this type of testing. In addition, the testing cannot be extended into the bedrock for sites with shallow bedrock or sites where the piles bear into bedrock. Thus, this system is most suited for testing driven piles or other foundations placed into relatively soft soils. Tests of sheet piles in a levee system are an ideal application for the PS/CPT system, since it can be driven along the levee top, and the soil conditions are ideal for pushing an instrumented cone probe to the depths required.

Based on experiences with PS testing of hundreds of unknown foundations as well as research tests conducted on known foundations, typical PS accuracies of 5% for bottom depth prediction are expected. If the data quality is poor, or the boreholes are located farther than 1.5 -2.1 m (5-7 ft) from the shaft being tested, accuracies of 10% may result. The accuracy of the method is greatest for sites with homogenous soil profiles, especially in the area around the shaft tip depth. Finally, the clearest and most reliable results are produced by using a relatively high frequency source such as a steel sledge or instrumented hammer with a hard tip to impact the foundation top or column/pile cap.

CONCLUSIONS

The PS test method has been found in previous research to be the most accurate and versatile method for unknown foundation length determination. One major drawback to this method has been the requirement for drilling a cased borehole at each test location. The combined PS/CPT system allows the collection of both soil data and PS foundation length data with the ease of a simple CPT test in locations where the soil profile allows direct pushing of the cone probe to depths below the pile tip depth. For sites with stiffer soils, the same cone probe rig can be used to install a cased borehole using hollow steel casing and a vibratory hammer. This casing can then be used to quickly perform a PS test using "conventional" methods, but still without requiring the use of a large truck-mounted drill rig. The flexibility and mobility of the new system should allow for easier and more cost effective collection of PS data on a wider variety of sites than was previously possible. In addition, the ability to determining soil conditions in parallel with PS data collection results in a more "complete package" of information for bridge owners, engineers, and designers who ultimately need both sets of data to estimate the actual capacity of the foundation element being tested.

REFERENCES

1. Olson, L.D., Jalinoos, F. and Aouad, M.F., Determination of Unknown Subsurface Bridge Foundations, NCHRP 21-5, Final Report, August, 1995.

2. Olson, L.D., and Aouad, M.F., Unknown Subsurface Bridge Foundation Testing, NCHRP 21-5 (2), Final Report, June, 2001.

3. Olson, L.D., Determination of Unknown Bridge Foundation Depths with NDE Methods, *Proceedings of 82nd Annual TRB Meeting* (CDROM), January 12-16, 2003, Paper No. 03-4039

4. Finno, R.J, Gassman, S.L, and Osborn, P.W., Non-Destructive Testing of a Deep Foundation Test Section at the Northwestern University National Geotechnical Experimentation Site, A Report Submitted to the Federal Highway Administration, June 1997

5. Schmertmann, J.H., "Guidelines for Cone Penetration Test Performance and Design", FHWA-TS-78-209, February, 1977

Copyrighted Materials
Copyright © 2009 American Society of Civil Engineers (ASCE)
Retrieved from www.knovel.com

A Case History Evaluation of CSL Access Tube Debonding

Joshua C. Adams[1], M. ASCE, Edward L. Hajduk[2], M.ASCE, D.Eng, PE,
Peo Halvarsson[3], and Al Neumann Jr.[4]

[1]Project Manager, WPC Inc., 1450 Fifth Street West, North Charleston, SC 29405; jadams@wpceng.com
[2]Assistant Professor, The Citadel, Department of Civil and Environmental Engineering, 171 Moultrie Street, Charleston, SC 29464; ed.hajduk@citadel.edu
[3]Project Engineer, Skanska Civil Southeast, 295 Bendix RD Suite 400, Virginia Beach, VA 23452; Peo.Halvarsson@skanska.com
[4]Vice President, Coastal Caisson Corp., 13203 Byrd Legg Drive, Odessa, FL 33556; aneumann@coastalcaisson.com

ABSTRACT: Crosshole Sonic Logging (CSL) testing has been shown to be an effective method to assess the quality of concrete within drilled shafts. CSL testing is conducted by placing ultrasonic transmitters and receivers in access tubes installed in the drilled shafts prior to concrete placement. When the bond between the concrete and access tubes is competent, the ultrasonic pulses are sent across the shaft and the pulse travel time and signal strength can be used to assess concrete quality. However, when the access tube/concrete bond is not competent, the ultrasonic signal can be significantly affected, leading to increased pulse travel time and signal strength. These changes in turn can lead the inability of the test to effectively evaluate the concrete condition and/or to the identification of false anomalies. The phenomenon of CSL testing loss of signal/signal interference due to access tube/concrete bonding issues is typically referred to as debonding.

For the new Turtle River Bridge along I-95 in Glynn County Georgia, CSL testing results repeatedly showed anomaly zones in the upper portions of the drilled shaft foundations. The suspected cause of these anomaly zones was debonding. A methodology of evaluating the concrete within the suspected debonding zones using drilled holes to provide CSL equipment access was developed to verify concrete condition. This subsequent testing showed that the CSL signal loss/erratic signals above the water line could be attributed to debonding and that the drilled shaft concrete in these zones was sound.

INTRODUCTION

A new bridge, founded on 428 drilled shafts, was constructed spanning the Turtle River on I-95 in Glynn County Georgia. Depending on the location within the bridge

structure, the drilled shafts for this bridge range in diameter from 1.37 m (4.5 ft) to 1.83 m (6 ft) with shaft lengths of up to 56.4 m (185 ft). The drilled shafts extend to heights of 5.8 m (19.2 ft) above mean sea level (MSL). The design of the bridge left little redundancy in the drilled shaft foundations. Therefore, integrity testing of the drilled shafts was of major importance to verify that these foundations were capable of supporting the bridge superstructure. Crosshole Sonic Logging (CSL) was selected as the primary testing method to evaluate drilled shaft integrity.

Crosshole Sonic Logging (CSL) testing evaluates deep foundation integrity by sending ultrasonic signals across the drilled shaft concrete via instrumentation lowered and raised in access tubes. These access tubes are attached to the drilled shaft steel reinforcement prior to concrete placement. As the ultrasonic transmitter and receiver are simultaneously raised, the ultrasonic signals are recorded. Concrete quality is assessed by examining the First Arrival Time (FAT) and relative energy of the signal along the shaft length. If the distance between the access tubes is known, an apparent signal velocity (i.e. wavespeed of the ultrasonic signal through the concrete) can be determined. Figure 1 presents a typical CSL testing setup while Figure 2 presents typical CSL testing results. CSL testing is described in detail by Chernauskas and Paikowsky (1999). CSL testing has been shown to be an effective method for evaluating drilled shaft integrity (e.g. Paikowsky et al., 2000, Branagan et al., 2000, Hajduk et al, 2004).

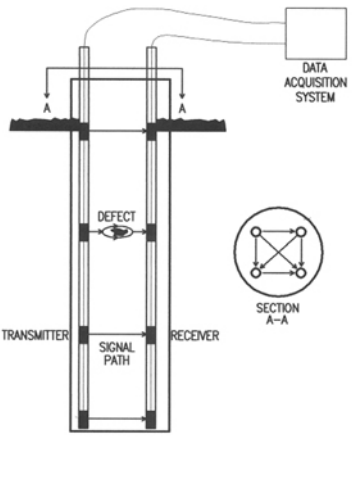

FIG. 1. Typical CSL Setup

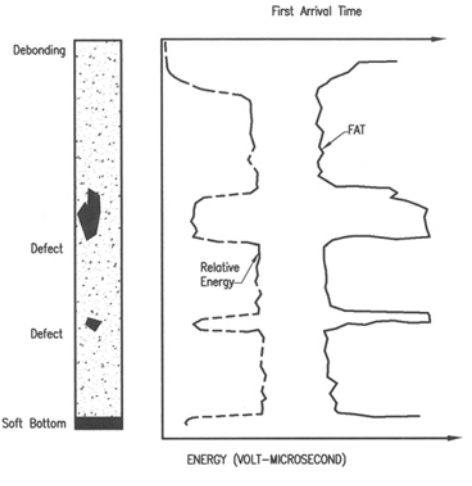

FIG. 2. Typical CSL Results.

(both figures after Chernauskas and Paikowsky, 1999)

During the initial CSL testing, anomaly zones were frequently detected within the upper portion of the drilled shaft foundations. These anomaly zones were generally located within the upper portion of the drilled shaft within the tidal zone (i.e. between the low and high tide marks), although these anomaly zones were sometimes

observed below the tidal zone. In general, the difference in high and low tides for this part of Turtle River was around 3 m (10 ft). Based on the observations of the drilled shaft inspectors, reviews of the drilled shaft installation records, the use of PVC access tubes, and previous experience with a similar CSL testing anomaly situation (Hajduk et al., 2004), it was suspected that these anomaly zones were caused by tube debonding. Based on the work of Hajduk et al. (2004), steel access tubes were added to the drilled shafts over the length of the observed anomaly zones (i.e. the upper 12 m (40 ft)) while PVC access tubes continued to be extend along the entire drilled shaft length. Even with the steel access tubes, CSL testing of drilled shafts in the river frequently showed loss of signal or signals indicative of anomalies in the shaft sections above the water line. Even when the addition of the steel access tubing failed to solve the problem, debonding remained the suspected cause of the upper drilled shaft CSL anomalies.

Access tube debonding is the separation of the access tube from the surrounding concrete and/or weakening of the interface between the two materials. Typically, access tube debonding occurs when polyvinyl chloride (PVC) pipe is used in place of steel, although debonding can occur when steel tubing is used. As the concrete cures, the heat of hydration causes increased temperatures with the drilled shafts. This increased temperature causes the access tubing to expand. As the concrete cools, the access tubes contract, cause separation between the two materials and/or weakening of the interface bond. If the material thermal expansion properties between the concrete and access tubing are substantially different, the potential for the interface (i.e. bond) between the two materials to be affected is greater. Disturbance of the interface or a separation between the two materials can cause increased FAT times, reduced relative energy of the signal, or both (Hajduk et al., 2004). Additional mechanisms that can cause access tube debonding include: contamination of the access tubes prior to concrete placement; external wrapping of joints with duct tape or similar material; mechanical stress when the concrete is still green, such as impact during clean-up or tightening or removing threaded couplers or pipe caps; and adding cold water to fill or top up tubes when the concrete still retains the heat of hydration (Hertlein, 2007). Most State DOT's specify that CSL tests be performed in 10 days or less after concrete placement for PVC tubes and in 45 days or less for steel tubes to avoid problems associated with tube debonding (Olson et al., 1998). By filling the access tubes immediately after casting the concrete, access tube debonding can be avoided, particularly for PVC tubes (Likins et al., 2004). These common mechanisms of access tube debonding were examined and it was determined that they did not cause the CSL anomalies. Given the non-redundant nature of the drilled shaft foundations, another method of evaluating the concrete within these CSL anomaly zones was required.

DRILLED ACCESS HOLE CSL TESTING

To evaluate the upper drilled shaft CSL anomaly zones, new access holes were drilled using percussion methods for CSL testing using 5.1 cm (2 inch) diameter concrete drill bits. Drilled access holes remove the possibility of access tube debonding as there is no tube to debond. The drilled holes generally extended 0.3 m

(1 ft) beyond the CSL anomaly zone, to depths between 1.5 m to 3.0 m (5 ft to 10 ft) below the top of the shaft depending on the extent of the anomaly zone encountered with the CSL testing. Due to limitations with the drilling equipment and site access issues, depths of 3.0 m (10 ft) could not be drilled. The holes were generally located near each of the PVC access tubes. In cases where the CSL anomaly was identified in only one or a two access tubes, the holes were drilled adjacent to those tubes and CSL testing combinations were performed between the drilled hole(s) and existing CSL access tubes. Typical PVC and drilled access hole CSL testing layouts are presented in Figure 3 in plan view.

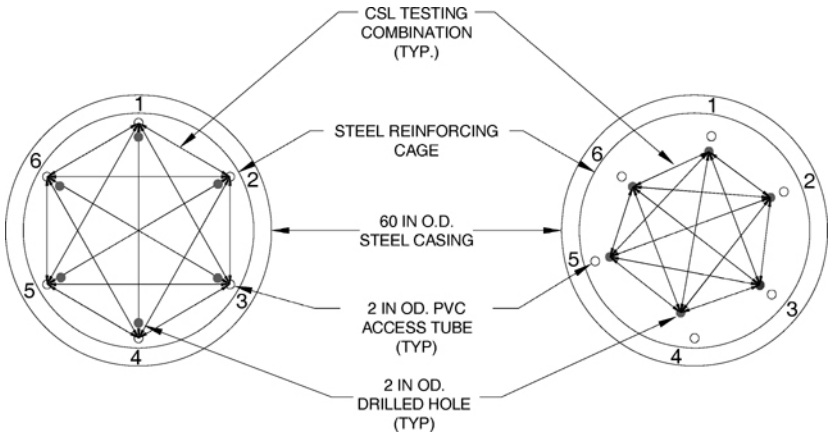

FIG. 3. Typical PVC and Drilled Access Hole CSL Testing Layouts.

Upon completion of drilling, the drilled access holes were cleaned of loose concrete debris and filled with water. PVC adapters were attached to the drilled holes so the CSL testing probes could extend above the top of the drilled shaft. A total of thirty (30) drilled shafts were further investigated with drilled hole CSL testing when access tube debonding was suspected as the cause of the upper shaft CSL anomaly zone. Table 1 provides a summary of the drilled shafts tested with drilled access holes. Table 1 shows the tested shaft identification numbers, drilled shaft diameter, the access tubes types tested, the depth of the initial CSL testing anomaly zone, the drilled hole depth, and if the drilled holes confirmed access tube debonding (i.e. if the drilled shaft was accepted for use within the bridge structure).

The assessment if the upper drilled shaft anomaly zones detected during initial CSL testing were comprised of sound concrete was based on the following:

1. Examination of the drilled shaft installation excavation and concrete placement records by the CSL testing engineer.
2. Examination of drilled shaft concrete compressive strength test records (if available).
3. Observations of the drilled access hole crews.

Table 1. Summary of Drilled Access Hole CSL Testing.

Drilled Shaft Number	Access Tube Material(s)[1]	Depth of Anomaly Zone[2] meters (ft)	Drilled Hole Depth meters (ft)	Drilled Shaft Accepted[3]
5.3.1B	P, DH	1.8 (6)	2.1 (7)	Y
5.3.4	P, DH	1.5 (5)	1.9 (6.3)	Y
6.3.4	P, S, DH	1.1 (3.6)	1.5 (5)	Y
7.1.4	P, DH	1.8 (6)	1.8 (6)	Y
7.3.4	P, DH	1.8 (6)	1.8 (6)	Y
8.1.1	P, DH	4.3 (14)	3.0 (9.9)	Y
8.1.3	P, DH	3.7 (12)	3.0 (9.9)	Y
8.1.4	P, S, DH	4.3 (14)	3.0 (9.9)	Y
9.1.1	P, DH	4.9 (16)	3.0 (9.9)	Y
9.1.2	P, S, DH	2.4 (8)	2.0 (6.5)	Y
9.1.3	P, DH	4.9 (16)	3.0 (9.9)	Y
9.1.4	P, DH	5.1 (16.7)	3.0 (9.9)	Y
9.2.2	P, DH	3.8 (12.6)	3.0 (10)	Y
9.2.3	P, DH	3.9 (12.8)	3.0 (10)	Y
10.1.1	P, DH	5.2 (17)	3.0 (9.9)	Y
10.1.2	P, DH	6.1 (20)	3.0 (9.9)	Y
10.1.3	P, DH	4.9 (16)	3.0 (9.9)	Y
10.1.4	P, DH	6.1 (20)	3.0 (9.9)	Y
10.2.2	P, DH	4.1 (13.5)	3.0 (9.9)	Y
10.2.3	P, S, DH	1.5 (4.8)	61.8 (6)	Y
10.3.2	P, S, DH	2.1 (7)	72.1 (7)	Y
10.3.3	P, S, DH	2.1 (7)	2.1 (7)	Y
10.3.4	P, S, DH	4.6 (15)	3.0 (9.9)	Y
11.1.4	P, DH	1.2 (4)	1.2 (4)	Y
11.3.4	P, S, DH	1.5 (5)	3.0 (9.9)	Y
16.2.3	P, DH	1.8 (6)	1.8 (6)	Y
23.2.2	P, DH	2.4 (8)	3.0 (10)	Y
26.3.1	P, DH	4.7 (15.5)	3.0 (10)	Y
30.2.2	P, DH	1.5 (5)	2.1 (7)	Y

NOTES:
1. P = PVC, S = Steel, DH = Drilled Holes.
2. As determined from initial CSL testing.
3. Drilled shaft accepted for use within the bridge structure.

4. Direct comparison of the drilled access hole and initial CSL testing results.
5. Evaluation of concrete apparent wavespeeds in the non-anomaly zones from the initial CSL testing and in the initial CSL testing anomaly zones using the drilled access hole CSL results.

A typical comparison of the initial and drilled access hole CSL test results are presented in Figure 4.

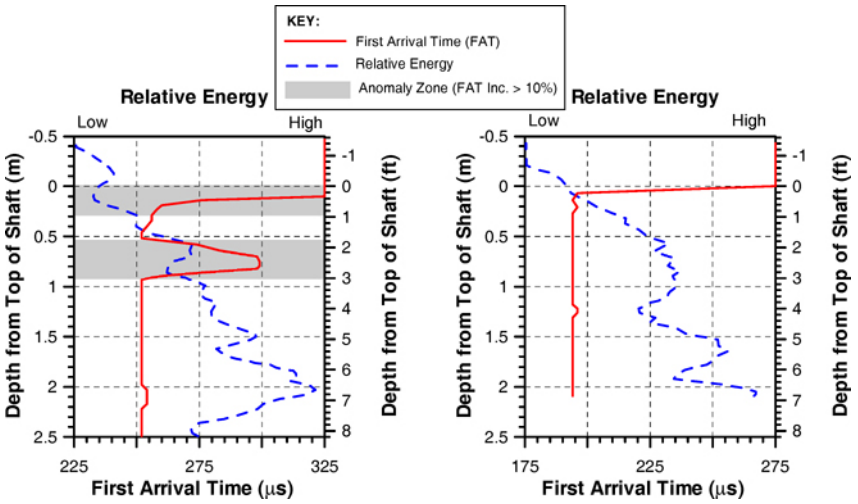

(a) Initial Testing (PVC) (b) Drilled Access Hole Testing

FIG. 4. Typical Initial and Drilled Access Hole CSL Testing Results (Drilled Shaft 30.2.2).

Concrete apparent wavespeeds (i.e. compressive wave velocities or ultrasonic pulse velocities) were calculated for each tested access tube combination using the FAT's and access tube distances at the TOS measured at the time of CSL testing and the procedure to account for access tube effects discussed by Amir et al. (2004). The evaluation of the apparent concrete wavespeeds was based on the following:

- A qualitative assessment of the differences in apparent wavespeeds using the Concrete Condition Rating Criteria (CCRC) (FHWA, 1996).
- A quantitative comparison of the calculated concrete apparent wavespeeds with several general guidelines for relating concrete quality with compression wave velocities (i.e. Malhotra (1976), Bungey (1980), Harrell and Stokoe (1984), Ferraro (2003), and DFI (2005).

Even under tight control, concrete properties will show a large scatter that will have a material influence on the results of the CSL testing (Amir et al., 2004). Therefore,

quantitative comparisons of concrete apparent wavespeeds with compressive strengths were used as a guide for evaluating concrete quality and not a sole means of acceptance or rejection of the drilled shaft.

For all thirty (30) drilled shafts tested with drilled access holes, the drilled access hole CSL testing results showed that the drilled shaft concrete within the initial CSL testing anomaly zones was similar to the concrete within the rest of the drilled shafts. When the drilled access hole CSL testing results were used in conjunction with other available drilled shaft records (e.g. installation records, compressive strength test results), the drilled shaft were determined to meet project specifications and were accepted for use within the bridge structure. Based on the results of the evaluation process detailed above using the drilled access hole CSL testing data, the initial CSL testing upper shaft anomalies were attributed to access tube debonding.

CONCLUSIONS

For thirty (30) drilled shafts for the new Turtle River bridge project along I-95 in Glynn County Georgia, upper shaft anomalies detected during initial CSL testing were evaluated using subsequent CSL testing in drilled access holes and detailed records evaluation. Based on the results of these tests and subsequent evaluations, the drilled shafts were approved for use in the bridge structure and the upper shaft anomalies in the initial CSL testing were attributed to access tube debonding.

The presented case history shows that CSL testing in drilled access holes, when used in conjunction with other quality control/assurance (QC/QA) documents such as installation records, can be used to effectively assess drilled shaft integrity when debonding of the installed access tubes occurs.

ACKOWLEDGEMENTS

The authors appreciate the efforts of the drilled shaft inspectors and project engineers from Skanska Civil Southeast, the drilled shaft installation crews from Coastal Caisson Corporation, and the CSL testing personnel (Mr. Craig Skiles and Mr. Cody Wisner) in collecting data for this paper. In addition, the support given by WPC Inc., Skanska Civil Southeast Inc., and Coastal Caisson Corporation is appreciated.

REFERENCES

Amir, J. M., Amir, E. I., and Felice, C. W. (2004). "Acceptance criteria for bored piles by ultrasonic testing." *Proc., 7th Int. Conf. on Application of Stress Wave Theory to Piling*, Kuala Lumpur.

Branagan, P., Vanderpool, W., Murvosh, H. amd Klein, M. (2000). "Crosshole Sonic Logging (CSL) Defines Cast-in-Drilled-Hole (CIDH) Defects; Coring Confirms Result", *New Technological and Design Developments in Deep Foundations*, GSP No. 100, ASCE, Reston, VA: 110-124.

Bungey, J.H. (1980). "Validity of Ultrasonic Pulse Velocity Testing of In-Place Concrete for Strength." *Nondestructive Testing International*, 13 (6).

Chernauskas, L.R. and Paikowsky, S.G. (1999). "Deep Foundations Integrity Testing: Techniques and Case Histories". *Civil Engineering Practice: J. Boston Society of Civil Engineers Section/ASCE*, 14 (1): 39-56

Paikowsky, S.G. and Paikowsky, S.G. (2000). "Defect Detection and Examination of Large Drilled Shafts Using a New Cross-Hole Sonic Logging System", *Performance Confirmation of Constructed Geotechnical Facilities,* GSP No. 94, ASCE, Reston, VA: 66-83

Deep Foundations Institute (2005). Manual for Non Destructive Testing and Evaluation of Drilled Shafts. Hawthorne, NJ.

Ferraro, C. (2003). "Advanced nondestructive monitoring and evaluation of damage in concrete materials". *Master of Civil Engineering Thesis*, University of Florida.

Federal Highway Administration (1996). Project Specification for Construction Requirements for Drilled Shafts and CSL Test Requirements, *FP-96,* Central Federal Lands Highway Division, Lakewood CO.

Hajduk, E.L., Tallent, M.R., Christopher, W.R., and Ledford, D.L. (2004). "Crosshole Sonic Logging Integrity Testing for the New Cooper River Bridge". *Proc. 5th Intern. Conf. on Case Histories in Geo. Engrg.,* New York, NY.

Haramy, K. Y. (2006). "Structural Capacity Evaluation of Drilled Shaft Foundations with Defects" Thesis University of Colorado at Denver

Harrell, S., and Stokoe, K.H. (1984). "Integrity Evaluation of Drilled Piers by Stress Waves". Research Report 2751F, Transportation Research Center, The University of Texas at Austin, 268 p.

Hertlein, B. (2007). "Application and Interpretation of CSL Testing: Some Common Errors", *Contemporary Issues in Deep Foundations,* GSP No. 158, ASCE, Reston, VA: 1-11.

Likins, G., Webster, S., and Saavedra, M. (2004). Evaluation of Defects and Tomography for CSL", *Proc., 7th Int. Conf. on Application of Stress Wave Theory to Piling*, Kuala Lumpur.

Malhotra, V. M. (1976). *Testing Hardened Concrete: Nondestructive Methods*, American Concrete Institute Monograph No. 9, ACI/Iowa State University Press, 204 pp.

Olson, L.D., Aouad, M.F., and Sack, D.A. (1998). "NDT Diagnosis of Drilled Shaft Foundations" *Proc. 77th Annual Meeting*, Transportation Research Board, Washington, D.C.

Copyrighted Materials
Copyright © 2009 American Society of Civil Engineers (ASCE)
Retrieved from www.knovel.com

The Use of Crosshole Tomography to Evaluate Drilled Shaft Repairs

Les R. Chernauskas[1], M. ASCE, P.E. and Edward L. Hajduk[2], M. ASCE, D.Eng, P.E.

[1]Principal, Geosciences Testing and Research Inc., 55 Middlesex Street, North Chelmsford, MA 01854, les@gtrinc.net
[1]Assistant Professor, The Citadel, Department of Civil and Environmental Engineering, 171 Moultrie Street, Charleston, SC 29464, ed.hajduk@citadel.edu

ABSTRACT: Occasionally, a drilled shaft contains a defect that will significantly affect its performance under design loading and therefore requires remediation. These defects are commonly identified via crosshole sonic logging (CSL) and crosshole tomography (CT) testing techniques and verified via coring. CSL and CT testing can also define the extent and location of the defective zone, which assists in the development of the remediation procedure. In addition to identifying and quantifying defective zones, CSL and CT testing can be used to evaluate the quality of the completed repair. When used in conjunction with repair documentation and materials testing, comparison of CSL and CT testing conducted before and after the repair allows for both qualitative and quantitative assessment of the remediation. The following paper presents several case histories in which CSL/CT testing was effectively used in evaluating drilled shaft defect repairs.

INTRODUCTION

Drilled shafts are becoming increasingly more common for supporting bridge and building foundations. Since drilled shaft foundations usually carry very high design loads, and often serve as non-redundant, single load-carrying units, there is a need for a high-level of quality assurance and control of the as-built unit. One such method is crosshole sonic logging (CSL) testing, in which ultrasonic signals sent across the drilled shaft concrete are used to assess concrete quality. Ultrasonic signals are sent and received across the drilled shaft from instrumentation lowered and raised in access tubes. These access tubes are attached to steel reinforcement prior to concrete placement. As the ultrasonic transmitter and receiver are simultaneously raised, the ultrasonic signals are recorded. Concrete quality is assessed by examining the First Arrival Time (FAT) and relative energy of the signal along the shaft length. If the distance between the access tubes is known, an apparent signal velocity (i.e. wavespeed of the ultrasonic signal through the concrete) can be determined. Figure 1 presents a typical CSL testing setup while Figure 2 presents typical CSL testing results. CSL testing is described in detail by Chernauskas and Paikowsky (1999).

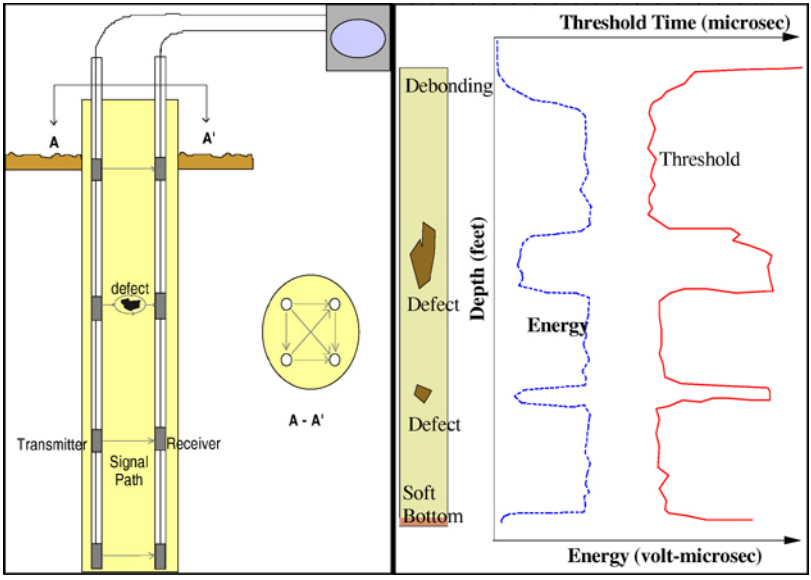

FIG. 1. Typical CSL Setup. **FIG. 2.** Typical CSL Results.
(both figures after Chernauskas and Paikowsky, 1999).

A variation on CSL testing is Crosshole Tomography (CT), which represents the condition of the concrete in a graphical manner. While CSL testing consists of simultaneous pulling the ultrasonic transmitter and receiver together through the access tubes, CT testing consists of raising and lowering the ultrasonic transducers so that data is collected at numerous angles through the anomalous zone. Figure 3 graphically presents the data collection procedure for CT testing. Two-dimensional (2D) or three-dimensional (3D) tomography can be performed. Tomographic analysis uses the cross-hole sonic logging (CSL) first arrival time (FAT) data that is converted to velocity based on the distance between the transducers. The signal energy (or attenuation) can also be used in tomography; however, most algorithms are based on velocity. Figure 4 presents typical 2D and 3D CT results. In Figure 4, lower velocities are represented by red and blue areas, while higher velocities are represented by green and gray areas. Simple tomographic techniques use linear wave propagation, while the more complex tomography techniques also use bent-ray and wave front analysis in an iterative approach. Further information on tomography is provided by Bowen and Dianguang (1992) and Piletest (2008).

The following paper examines two (2) drilled shaft case histories in which defects were detected and evaluated using CSL and CT testing, repairs were made, and the drilled shafts re-evaluated after the repair using CSL/CT testing.

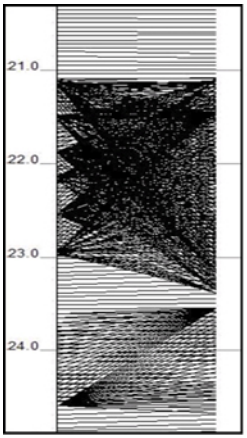

FIG. 3. Typical CT Test. (after Piletest.com, 2008)

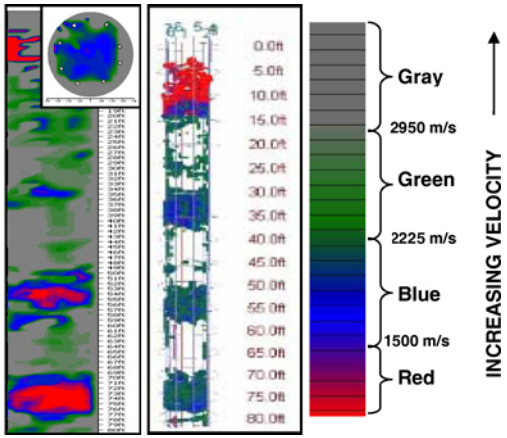

FIG. 4. Typical 2D & 3D CT Test Results. (key to the right represents velocity shading)

CASE HISTORIES

Case History 1 (Tremie Pipe Lost/Concrete Placement Problem)

A 2.4 m diameter shaft was constructed for a pier foundation for a bridge over a river crossing. The drilled shaft was constructed by advancing a permanent steel casing through the overburden soils and into rock to the bottom of the shaft. Concrete was delivered using a pump truck and placed using tremie procedures. During concrete placement, the lower 6m of the tremie pipe separated and was lost in the drilled shaft. After concrete placement was completed, excessive cement paste was noted at the top of the shaft.

The initial CSL and CT testing performed on the shaft indicated significant anomalies defined by increases in FATs typically greater than 100% and very weak energy levels. Three major anomalous zones, in the shape of "hockey pucks" around 0.9 to 1.8 meters thick, were detected in most tube profiles at approximately 9.8, 15.5, and 21.6 meters below the top of the steel casing. Figures 5a and 6a present the initial CSL testing results (FAT and relative energy) and 2D vertical CT results (apparent velocity), respectively, for a selected access tube combination across the drilled shaft. Figure 6a also presents the initial 2D horizontal (i.e. plan view) CT test results at the three major anomaly zones. As shown in Figure 6a, the upper zone does not appear to contain as much lower strength concrete, as represented by blue and green areas (velocities around 2,300 to 3,000 m/s) compared with the red and blue areas in the middle and lower zones (velocities around 1,500 to 2,300 m/sec).

Four 200 mm diameter core-holes (one in each quadrant of the shaft) were advanced through the anomalous zones to depths of around 24 to 26 meters below the top of the casing. Core samples were obtained and tested for compressive strength between depths of approximately 9 to 26 meters. The cores revealed weaker and segregated concrete in

three major zones at depths that correlated well with the anomalous zones identified by the CSL/CT testing. The results of the core testing indicated that the concrete compressive strengths typically ranged between approximately 4 and 18.6 MPa in the anomalous zones and between 31 to 44.9 MPa elsewhere.

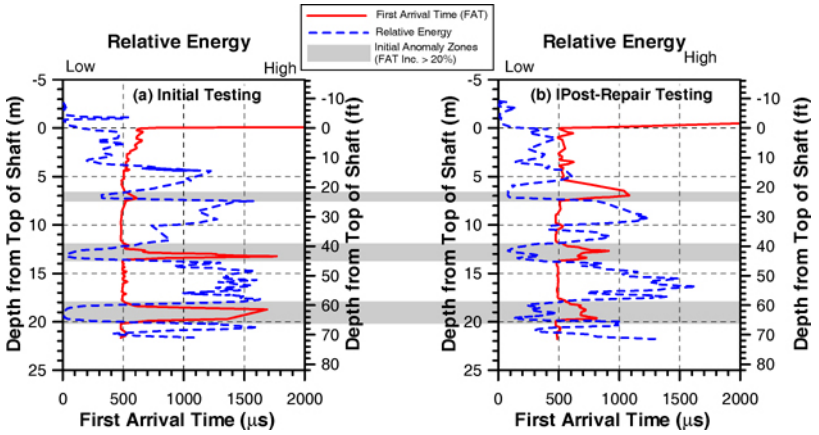

(a) Initial Testing (Profile 1-5) **(b) Testing after Repair (Profile 1-5)**

FIG. 5. CSL Testing Results with Depth for Case History 1.

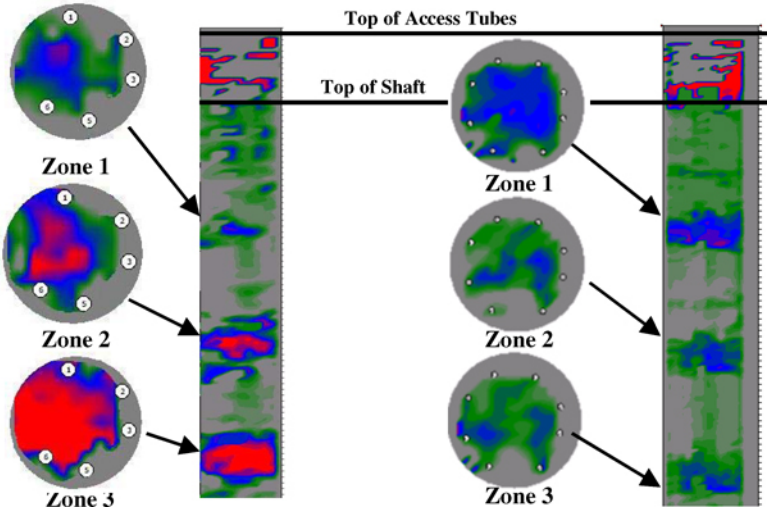

(a) Initial Testing (Profile 1-5) **(b) Testing after Repair (Profile 1-5)**

FIG. 6. 2D Vertical and Horizontal CT Results for Case History 1.
(use same velocity scale located in Figure 4)

The primary repair procedure involved using a high pressure head to blast out concrete in the three defective zones. Nozzle pressures upwards of 140 MPa were used to cut away and flush out the defective concrete. Remote inspection using a video camera was then performed after flushing and pumping of the zone to visually observe the repair process, which showed almost complete removal of the defective concrete. The zones were then filled with 40 MPa neat cement grout. This procedure was repeated for each zone starting from the lower zone to the upper zone.

CSL and CT testing was performed four (4) days after the completion of the repair of the last (i.e. upper) zone. The post-repair CSL and CT results are shown next to the initial testing results in Figures 5b and 6b, respectively. As shown in Figures 5 and 6, improvements (i.e. decreases in FAT, increases in apparent velocities and relative energy) were observed in the lower two anomaly zones. The velocities in the lower two anomaly zones typically increased to around 2,500 to 3,000 m/sec. The upper post-repair zone indicates a slightly thicker zone with lower velocities than those determined during the initial testing. The greater thickness of the upper zone is most likely a result of the high pressure cutting procedure used to remove the concrete, where additional "good quality" concrete may have been removed at the upper and lower boundaries. The higher FAT increases and lower velocities in the upper zone are most likely due to the shorter grout curing time of approximately 4 days as compared to several weeks for the lower zones. The compressive strengths determined from the post repair core samples indicated grout compressive strengths around 27.6 MPa after 7 to 10 days and over 34.5 MPa after 14 days. Based on the CSL/CT results in conjunction with QC/QA testing of the grout materials, the drilled shaft repair was considered to be successful.

Case History 2 (Temporary Casing Removal/Tremie Seal Concrete Problem)

A 1.98 m diameter shaft was constructed for a pier foundation for a viaduct. Temporary steel casing was advanced to the top of rock. A 1.3 m diameter rock auger was then used to excavate to the bottom of the rock socket (5.4 m in length). Concrete was then placed inside the shaft excavation to approximately ¼ of the way up the temporary casing using a tremie pipe. The temporary casing was then partially removed using a vibratory hammer. Concrete continued to be placed inside the temporary casing using the tremie pipe in the remaining portion of the excavation. During concrete placement, the tremie pipe became plugged, was pulled out of the concrete, and then reinserted within the concrete. The temporary casing was removed after placement of the concrete to approximately the ground surface elevation.

The initial CSL/CT testing indicated a significant anomalous zone approximately 9 to 10 meters below the top of tubes (4.9 to 5.9 m below top of concrete), defined by increases in FATs typically from 15% to 25% and associated reductions in relative energy. The FAT increases correlated to reductions in apparent velocity of ~20% or more from the nominal value in the non-anomaly zones. Increases in FATs from 40% to 50%, with associated large reductions in energy were observed in tube combinations within the southwestern portion of the socket (tube 1 is north). The FAT increases correlated to reductions in apparent velocity of ~30-35% or more from the nominal value in the non-anomaly zones. Figures 7a and 8a present the initial CSL and CT

testing with depth, respectively. Figure 8a also presents the horizontal tomographic slice through the anomaly zone.

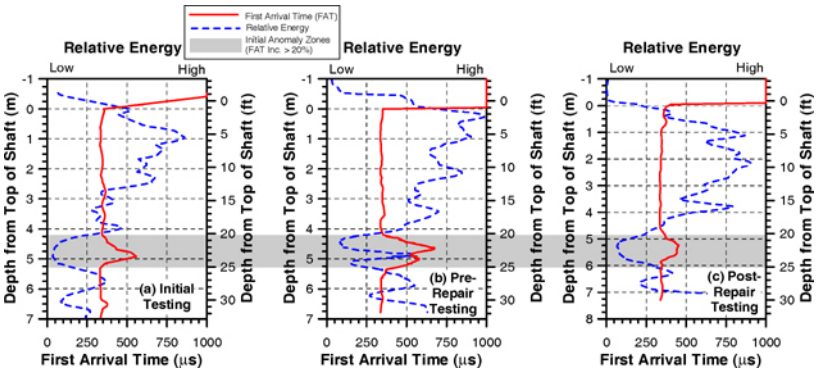

(a) Initial Testing **(b) after Flushing/Prior to Grout** **(c) After Repair**

FIG. 7. CSL Testing Results with Depth for Case History 2 (Profile 2-6).

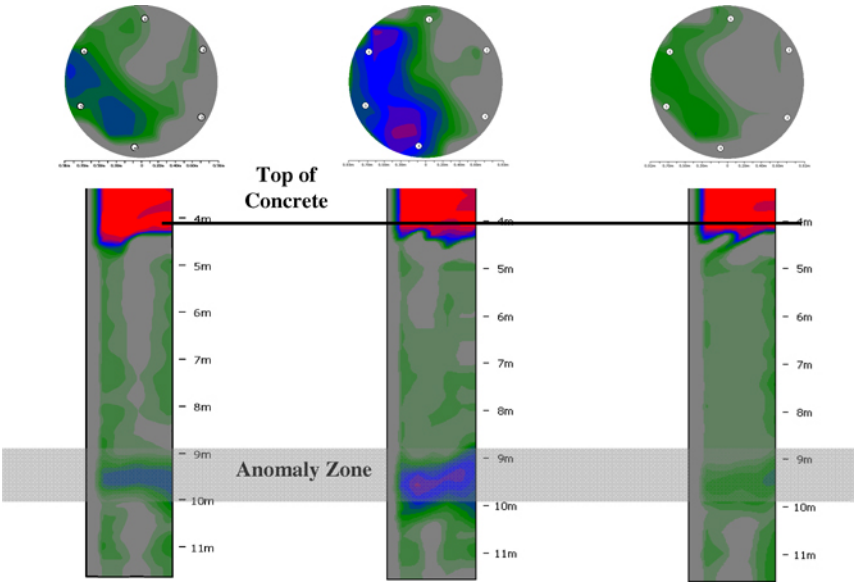

(a) Initial Testing **(b) after Flushing/Prior to Grout** **(c) After Repair**

FIG. 8. 2D Vertical and Horizontal CT Results for Case History 2 (Profile 2-6). (use same velocity scale located in Figure 4)

Three access core-holes were advanced to depths of around 5.2 to 5.7 meters below the top of the concrete. The locations of the holes were selected to provide access and adequate coverage for removal of the suspect concrete based on the CT results. The cores revealed weaker and segregated concrete in the anomalous zone. The concrete compressive strengths typically ranged from approximately 7 to 21 MPa between approximately 4.7 and 5.5 meters below the top of concrete and over 35 MPa above the defective zone. At around 5.5 meters, the material primarily consisted of weakly cemented segregated aggregate that prevented further advancement of the core holes and retrieval of core samples (i.e. the core barrel consistently jammed at this depth at the bottom of the defective zone).

The repair procedure involved using a high pressure nozzle to blast out concrete in the defective zone from the three access holes. Nozzle pressures upwards of 70 to 105 MPa were used to cut away the defective concrete at the top and below the suspect zone. Lower pressures were used to remove the sand/aggregate material in the middle to bottom of the defective zone. Remote inspection using a video camera was then performed after flushing and pumping of the zone to visually observe the repair process, showing that significant removal of the defective concrete was achieved leaving higher quality concrete in-place. After the flushing process was completed and prior to grouting, CSL/CT testing was performed again to characterize and define the water filled flushed out zone (see Figures 8b and 9b, respectively). The CSL/CT results at this stage indicated that the poor material was removed and the remaining void was filled primarily with water (wave speed around 1,500 to 2,000 m/s represented by the red and blue velocity areas).

The flushed out zone was then filled with 28 MPa neat cement grout. The grout was delivered under pressure using packers inserted and sealed off within two core holes. The grout was pumped until consistent return was observed flowing through the third open core hole. The 7-day grout compressive strengths ranged between 29 and 32 MPa. CSL/CT testing was performed three days after grouting for use as a comparison with the initial and pre-grouting CSL/CT test results. CSL and CT results for the post repair testing are presented in Figures 8c and 9c, respectively. As shown in Figures 8 and 9, improvements with respect to velocity and relative energy were observed in the repaired zone between initial and post-repair testing. The primary velocity in the post-repair grouted zone was around 3,000 m/sec compared to the typical value of 3,800 m/sec for the concrete above and below the repair zone. The 7-day grout compressive strengths were approximately 30 MPa. Based on the CSL/CT results in conjunction with QC/QA testing of the grout materials, the drilled shaft repair was considered to be successful.

CONCLUSIONS

CSL testing is a well established tool for identifying anomalous zones in drilled shaft concrete. CT testing can be used to further delineate these zones and aid in developing an investigation plan and repair procedure. As shown in the two (2) presented case histories, CSL and CT testing can also be successfully used to assess drilled shaft repairs compared with the surrounding "good" concrete signals and when considering various repair stages.

As shown in the case histories, apparent velocity ranges within the post repair grouted zones can be lower than the typical values of surrounding "sound" concrete, even when the repair grout 28-day compressive strength of the grout was approximately the same as the "sound" concrete. In addition to curing times, another primary reason for the lower grout velocities is due to the absence of large aggregate in the grout. As a result, under elastic loading conditions, the cement paste (grout) experiences higher strain for a given stress compared with concrete (Neville, 1996). Furthermore, there is no unique relationship between ultrasonic pulse velocity and compressive strength (Sturrup, et. al., 1984 and Popovics, 2001). For example, Sturrup et al. (1984) showed that the ultrasonic pulse velocity for mortar can be 15 to 20% lower than concrete and for cement paste can be 25 to 30% lower than concrete when the compressive strengths were determined to be the same. Therefore, velocities determined from CT testing for grouted repair zones can in some cases be expected to be somewhat lower than concrete of the same strength. In using CSL/CT testing to evaluate repairs, FAT decreases (i.e. velocity increases) and energy increases and their relative changes compared to surrounding "sound" concrete should be considered in the repair evaluation process more than matching apparent velocities alone.

ACKNOWLEDGEMENTS

The authors would like to thank Mr. Leo Hart and Dr. Samuel Paikowsky of GTR for their review and help with the above projects.

REFERENCES

Bowen, H. & Dianguang, W. (1992). "Application of Sonic Tomography in the Integrity Testing of Concrete Piles." *Proc. 4th Intl. Conference on Application of Stress Waves to Piles,* Rotterdam: 231-234.

Chernauskas, L.R. and Paikowsky, S.G. (1999). "Deep Foundations Integrity Testing: Techniques and Case Histories". *Civil Engineering Practice: J. Boston Society of Civil Engineers Section/ASCE*, 14 (1): 39-56

Neville, A. M. (1996). "Properties of Concrete", 4th Ed., John Wiley and Sons, Inc., New York, NY.

Piletest (2008). "Tomography." <http://www.piletest.com> (August 13, 2008).

Popovics, S. (2001). "Analysis of the Concrete versus Ultrasonic Pulse Velocity Relationship", *Materials Evaluation,* 59 (2): 123-130.

Sturrup, V. R., Vecchio F. J., and Caratin, H. (1984). "Pulse Velocity as a Measure of Concrete Compressive Strength", *ACI SP-82: In Situ/Non Destructive Testing of Concrete*, 201-27.

Copyrighted Materials
Copyright © 2009 American Society of Civil Engineers (ASCE)
Retrieved from www.knovel.com

Shortcomings of the Davisson Offset Limit Applied to Axial Compressive Load Tests on Cast-In-Place Piles

W. Morgan NeSmith, Member, Geo-Institute[1]
Timothy C. Siegel, P.E., Member, Geo-Institute[2]

[1] Berkel & Company Contractors, Inc., 834 Dekalb Avenue, Unit B, Atlanta, GA 30307, PH (865) 528-1653, email: morgan_nesmith@comcast.net
[2] Berkel & Company Contractors, Inc., 1808 Northshore Hills Boulevard, Knoxville, TN, 37922, PH (865) 357-1715, FAX (865) 357-1570, email: tcsiegel@knology.net

ABSTRACT

Since its introduction in 1973, the Davisson Offset Limit has been widely used in the United States for interpretation of axial compressive load tests on pile foundations and is one of three methods explicitly accepted by the 2006 International Building Code. An examination of the fundamental assumptions of the DOL shows that its application to cast-in-place piles lacks scientific basis and leads to over conservatism. Interestingly, these are the same reasons given by Davisson for its development. The results of the examination indicate that there are notable fallacies in the Davisson Offset Limit, including the assumptions that: (1) the cast-in-place pile behaves as a "fixed-base, free-standing column.", (2) an elastic line is a dependable reference line for interpretation of load tests on cast-in-place piles, and; (3) an offset of 3.8 mm + D (inches)/120 from the elastic line represents the movement necessary to mobilize toe resistance of cast-in-place piles. Considering these results, the authors present suggestions ranging from modifications to the Davison Offset Limit that recognizes the greater movement required to mobilize the toe resistance to codification of a more rational criterion better suited to interpret the axial compressive capacity of cast-in-place piles.

INTRODUCTION

The 2006 International Building Code explicitly accepts three interpretive methods for axial compressive load tests on piles. These three interpretative methods (by the names they are used in common vernacular): (1) Davisson Offset Limit (Davisson, 1972); (2) Brinch Hansen 90% Criterion (Brinch Hansen, 1963), and; (3) Butler-Hoy Criterion (Butler and Hoy, 1977). Generally speaking, the Davisson Offset Limit (DOL) is frequently used in the United States because it provides the lowest estimation of axial compressive capacity of the aforementioned methods. Also, it is most likely to provide an ultimate axial compressive pile capacity from the actual load-deflection curve. That is, the Brinch Hanson 90% Criterion and the Butler-Hoy Criterion often require extrapolation to extend the load-deflection curve in order to establish an ultimate axial compressive capacity. In the absence of established guidelines for extrapolation, there is a reluctance, and even opposition, to the extrapolation of load test results.

Its widespread application to all pile types in the US is sufficient justification for a critical examination of the appropriateness of the DOL, especially for the evaluation of load tests results for cast-in-place piles. The first part of this paper discusses the fundamentals that were involved in the formulation of the DOL and the fallacies associated with its application to load testing of cast-in-place piles. The second part of this paper presents examples of results from actual load tests that serve to illustrate the shortcomings of the DOL with respect to actual pile behavior and application to design. The third and final part of this paper presents suggestions for load test procedures and interpretation in light of the current understanding of geotechnical engineering.

FUNDAMENTALS OF THE DAVISSON OFFSET LIMIT

The Davisson Offset Limit (as it is currently referred to) was proposed by Davisson (1972) based on comparisons between the results of wave equation analyses of driven steel piles and static load tests. The DOL defined the ultimate pile load as the intersection of the pile load-deflection curve with an elastic line for a fixed-base, free-standing column offset by 3.8 mm (0.15 inches) plus the soil quake. Soil quake is the deformation (or pile movement) required to mobilize the strength of the soil below the pile tip. The soil quake is further simplified by the pile diameter (in inches) divided by 120. In his 1972 paper, Davisson is explicit that the criterion was developed for point bearing driven piles but goes on to state that it can also be applied to friction piles. Davisson explains his motivation in the paper's introduction:

> "There are many ways of interpreting a load test; almost all of them are unsatisfactory for high capacity piles. It appears that engineering practice is based primarily on experience, precedent, and perhaps prayer, even for low capacity piles. Because of the inadequate basis for practice, engineers tend toward over-conservatism in design; often this causes unnecessary problems. When the present day need for high capacity piles is considered in light of the state of practice with low capacity piles, it is obvious that engineers more than ever need a scientific basis for their engineering decisions."

FALLACIES OF THE DAVISSONS OFFSET LIMIT

Davisson was clearly aware of the challenges with load test interpretation and particularly, the tendency of the engineering community to accept over-conservatism in establishing the ultimate pile capacity. Ironically, the application (or misapplication) of the DOL to cast-in-place piles has not only led to greater conservatism but it fails as a rational, scientific criterion. The primary fallacies of the application of the DOL to cast-in-place piles are discussed in the following:

(1) **The assumption that the cast-in-place pile behaves as a "fixed-base, free-standing column."** Cast-in-place are generally designed using a combination of shaft and end resistances and the stress distribution in the pile element is unlike the "fixed-base, free-standing column" assumed by the DOL. This is especially true at test loads well below the ultimate capacity where the resistance is primarily developed along the shaft.

(2) **The assumption that an elastic line is a dependable reference line for interpretation of load tests on cast-in-place piles.** Kulhawy and Chen (2005) compared the estimated elastic shortening, based on the assumptions of the DOL, to the initial slope of the straight line portion of the load-deflection curve. Their study concluded that the DOL assumptions tended to overestimate the stiffness of short piles and underestimate the stiffness for longer piles.

(3) **The assumption that an offset of 3.8 mm + D (inches)/120 from the elastic line represents the movement necessary to mobilize toe resistance.** The soil quake proposed by Davisson is specifically for driven piles and is not appropriate where soil resistance beneath the pile toe has not been fully mobilized at the beginning of load testing. That is, Davisson study evaluated piles installed by driving where a compressed soil plug forms during placement. In contrast, cast-in-place piles and other types of drilled piles do not compress the soil beneath the pile toe during installation. Thus, a greater downward movement of the pile toe would be required to mobilize the end resistance for cast-in-place piles if all other conditions were equal. Analysis by Zheng *et al.* (2007) confirmed this based on results of load tests performed on displacement cast-in-place piles.

EXAMPLE LOAD TEST ANALYSES

Osceola, Arkansas Site

It is helpful to illustrate the shortcomings of the DOL using examples of actual load test results. For this purpose, we have selected test data from a load test performed by Berkel & Company Contractors, Inc. (Berkel) and published by Zheng *et al.* (2007). The data were collected during a quick load test (ASTM D1143) performed on a 457 mm (18 in) diameter displacement cast-in-place pile with a length of 12.8 m (42 ft). The load-deflection data are shown in Figure 1. Refer to the paper by Zheng *et al.* (2007) for details concerning the geotechnical conditions at the test site.

The DOL is illustrated by two lines in Figure 1. In this case, the elastic line was intentionally fit to the initial straight line portion of the load-deflection curve and corresponds to a slope of 37,200 MPa (5.4 x 10^6 psi). Intuitively, if the fundamental assumptions of the DOL are valid, then the combined modulus (*i.e.,* both grout and reinforcing steel) should closely correspond to the slope of the initial straight line portion of the load-deflection curve. In fact, strain gage measurements obtained in the upper portion of the cast-in-place pile indicate a combined modulus ranging from about 27,500 to 34,500 MPa (4 to 5 x 10^6 psi) which is significantly smaller than the slope of the straight line portion. This shows that not only does the DOL fail to appropriately represent a pile with substantial shaft resistance, but also suggests that selection of the appropriate modulus becomes problematic due to the stress-dependant non-linearity of the pile materials.

The DOL line was constructed by offsetting the elastic line by a distance of 3.8 mm (0.15 inches) plus the pile diameter in inches divided by 120. According to the DOL, the axial compressive capacity of the pile is 2200 kN (450 kips). However, it is clear

that the pile is capable of resisting additional compressive load up to 2850 kN (640 kips) at which point the test load was removed. It is recognized that Davisson (1993) proposed that the pile width (and thus the soil quake term) be multiplied by a factor of 2 to 6 for drilled piles in recognition of the greater pile movement that is required to mobilize the toe resistance. However, such a modification has yet to be formally established in those codes that specify the DOL, and as a result, incorporation of such a modification has not been widespread in engineering practice. Also, the different modifier values results in a wide range of pile capacity interpretations.

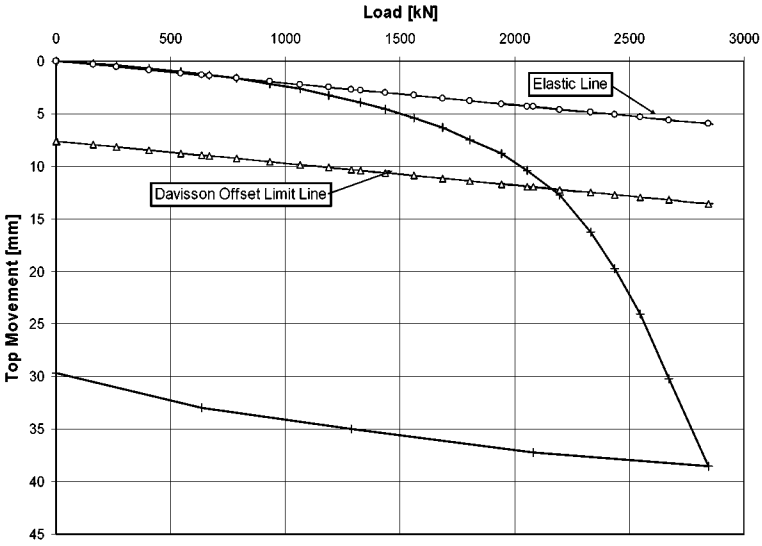

FIG 1. Load Versus Top Deflection Curve – Osceola AR Site (after Zheng *et al.*, 2007)

Des Moines, Iowa Site

A second example is from a load test performed by Berkel in Des Moines IA. The data were collected during a quick load test (ASTM D1143) performed on a 457 mm (18 in) diameter displacement pile with a length of 12.8 m (34.5 ft). The subsurface conditions at the pile location are characterized by a stiff fine-grained soil to about 6.1 m (20 ft) depth underlain by loose to dense clean sands. The load-deflection data are shown in Figure 2 along with a summary of ultimate load analysis methods. The methods include the three specifically listed in IBC 2006 as well as a method proposed by NeSmith (2002). This method was developed from a database of drilled, cast-in-place piles, and is based on defining ultimate load such that, applying a factor-of-safety of 2, the pile head deflection at the allowable load is no more than 6.4 mm (0.25 in).

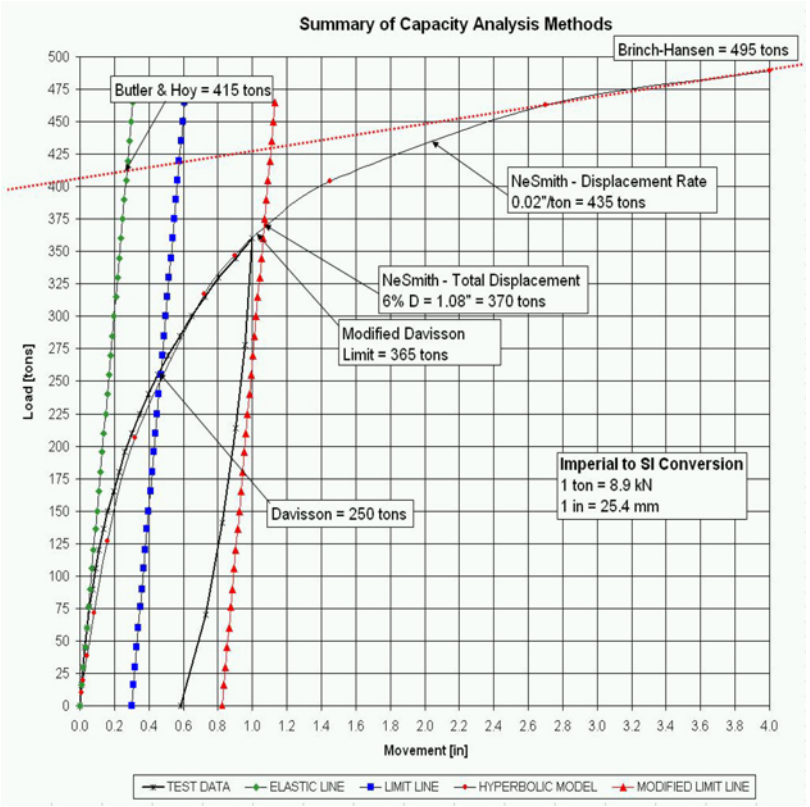

FIG 2. Applied Load vs. Pile Head Deflection and Ultimate Load Analysis

Again, it is clear that the pile is capable of resisting additional compressive load beyond the ultimate load defined by the DOL. For this project, a modifier of 4.5 was applied to the soil quake term in the DOL equation to obtain an ultimate load value in the range of the most conservative of the other three methods shown. A review of recent load tests available to the authors (performed from January 2007 to August 2008) indicates that offset modifiers of between 4 and 5 are typically required to obtain ultimate load values from the DOL that are in the range of those as calculated by the NeSmith (2002) method.

DISCUSSION AND SUGGESTIONS

An examination of the fundamental assumptions of the DOL shows that its application to cast-in-place piles lacks scientific basis and leads to over conservatism. Interestingly, these are the same reasons given by Davisson for its introduction in 1973. Because of its ease in application rather than its technical merit, the DOL continues to be widely used in the United States for the interpretation of load tests performed on all pile types. Due to its conservatism and, arguably, over-conservatism, the use of the DOL dramatically increases the likelihood of greater foundation costs.

The authors' experience is that the DOL is often applied indiscriminately with an end result of greater foundation costs unnecessarily. In light of this, the following suggestions are offered for the load test procedure and interpretation of cast-in-place piles:

- Ideally, load tests should be carried to a top deflection that allows the application of the Brinch Hanson 90% Criterion, Butler-Hoy Criterion, and/or other methods appropriate for cast-in-place piles. It is noted that most recent version of ASTM D1143 (2007) lists the Quick Load method as the standard compressive load test method with load to be applied in increments of about 5% of the estimated failure load and continuing until geotechnical failure.

- When the load tests are not carried to definitive geotechnical failure, the authors recommend the rational (and limited) extrapolation of the load-deflection curve to allow the application of either the Brinch Hanson 90% Criterion or the Butler-Hoy Criterion. A review of the load test data available to the authors indicates that at pile-head deflections of about 5% of the pile diameter, sufficient mobilization of the pile toe has occurred to allow for reasonable extrapolation according to the method described by Chin (1970)

- In the long term, a more rational criterion for establishing the cast-in-place pile capacity should be codified. Most notably, the L_1-L_2 method proposed by Hirany and Kulhawy (1989) recognizes aspects specific to cast-in-place piles. Furthermore, Kulhawy and Chen (2005) have combined the L_1-L_2 method with the slope tangent method to allow an empirical projection of axial compressive pile capacity.

- As a minimum (assuming none of the aforementioned changes have been implemented), the soil quake component should be modified as proposed by Davisson (1993) for cast-in-place piles when establishing the offset line for the DOL.

REFERENCES

ASTM (2007) "Standard test method for piles under static axial compressive load" *ASTM D 1143-07*.

Brinch Hansen, J. (1963): Discussion, "Hyperbolic stress-strain response. Cohesive soils", *Journal of Soil Mechanics and Foundations Division*, ASCE, 89(SM4), 241-242.

Butler, H.D. and Hoy, H.E. (1977) "User's manual for the Texas quick load method for foundation load testing" *FHWA-IP-77-8*, Federal Highway Administration, Office of Development, Washington, 59 pp.

Chin, F.K. (1970) "Estimation of ultimate load of piles not carried to failure" *Proceedings*, 2nd Southeast Asia Conference on Soil Engineering, 81-90.

Davisson, M.T. (1972) "High capacity piles" *Proceedings*, Lecture Series, Innovations in Foundation Construction, ASCE, Illinois Section, 52 pp.

Davisson, M.T. (1993) "Negative skin friction in piles and design decisions" *Proceedings*, Third International Conference on Case Histories in Geotechnical Engineering, St. Louis, 1793-1801.

Hirany, A. and Kulhawy, F.H. (1989) "Interpretation of load tests on drilled shafts – Pt. 1: Axial compression" *Fndn. Eng. Current Principles and Practices*, GSP 22, Ed. Fred Kulhawy, ASCE, New York, 1132-1149.

Kulhawy, F.H. and Chen, J-R. (2005) "Axial compression behavior of augered cast-in-place piles in cohesionless soils" *Advances in Deep Foundations*, GSP 132, ASCE.

NeSmith, W.M. (2002) "Design and installation of pressure-grouted, drilled displacement piles" *Proceedings*, Ninth International Conference on Piling and Deep Foundations, Nice, France.

Zheng, W., Hart, T.P., and Roldan, R.A. (2007) "Load test analysis on augered pressure grouted displacement piles" *Proceedings*, 32nd Annual Conference on Deep Foundations, Colorado Springs, Deep Foundations Institute, 25-36.

Copyrighted Materials
Copyright © 2009 American Society of Civil Engineers (ASCE)
Retrieved from www.knovel.com

Experimental investigation of the effect of shearing rate on the capacity of piles in soft silt

Paul Doherty[1] and Kenneth Gavin[2]

[1]PhD Candidate, Civil Eng Dept, School of Architecture, Landscape and Civil Engineering, University College Dublin, dohertyp@gmail.com
[2] Lecturer, Civil Eng Dept, School of Architecture, Landscape and Civil Engineering, University College Dublin

ABSTRACT

Recent improvements in effective stress design methods for the shaft capacity of displacement piles in clay require the inclusion of the interface friction angle at failure. This paper provides results from ring shear tests conducted on samples of Belfast soft sleech, which is a deposit of estuarine silty clay. The sleech has an upper (1-3 m thick) horizon with a high sand content, whilst the lower sleech has a high clay fraction. The stratification of the deposit is shown to be significant, with low residual friction angles being mobilised in the lower clayey sleech. The influence of shearing rate on the interface friction angle is examined using the ring shear apparatus and a positive rate effect is identified. In addition, results from field experiments conducted using the instrumented University College Dublin (UCD) model pile are presented. The pile axial resistance is shown to be a function of the test technique, with the peak capacity exhibiting strong rate dependence. Consideration of the porewater pressure response during loading revealed that during load application, the pore pressures measured at the pile-soil interface reduced temporarily after small pile head displacements. This pore pressure drop resulted in temporary increases in radial effective stress which were associated with the development of peak pile resistance values. This suggests that relatively high magnitude temporary loads (such as wind or wave loading) could be sustained for short periods whilst maintaining an adequate factor of safety on a pile.

INTRODUCTION

Intensive research over the past 30 years has led to the development of design methods for calculating the axial capacity of piles such as the Imperial College method (Jardine et al, 2005), which are based on a fundamental understanding of pile behaviour and, as such, have shown increased reliability (Chow, 1997). Evolution of design methods have tended toward effective stress approaches, which have generally been developed based on the results of instrumented pile tests. Predictions of average shaft shear stress (τ_{av}) from effective stress design methods adopt a mohr-coulomb failure criterion, as given by equation 1.

$$\tau_{av} = \beta \cdot \sigma'_{v0} = \sigma'_{rf} \tan \delta_f \quad (1)$$

Where $\beta = K_f \tan\delta_f$ and $K_f = \sigma'_{rf}/\sigma'_{v0}$. σ'_{rf} is the radial effective stress acting on the pile shaft at failure and σ'_{v0} is the in-situ vertical effective stress. The form of Eq. (1) demonstrates that an accurate assessment of the interface friction angle at failure, δ_f, is crucial to the prediction of the shaft resistance of a pile. This paper discusses results obtained from ring shear tests conducted on samples of Belfast 'sleech' when sheared against a steel interface in the Bromhead apparatus. The interface shear behaviour over a range of rates was established and is compared to the response observed at the pile-soil interface on instrumented model piles at the same site.

SITE CHARACTERISATION

The geotechnical test bed site is located just outside Belfast city in the North-East of Ireland. The geological properties of the underlying deposits, known locally as sleech, have been well documented by Bell (1977). The site stratification, shown in Figure 1, comprises four distinct soil layers. A metre of fill material, mainly consisting of building rubble and gravel, overlies a sandy silt layer approximately 2m thick, which in turn overlies 6m of soft silty clay "sleech". The soft estuarine deposits are underlain by a uniform fine to medium dense sand. Particle size distributions and Atterberg limits are shown in Figure 1. The sandy sleech, between 1m and 3m below ground level (bgl)., has proportions of sand to clay of 20 % and 10 % respectively, whilst below this level the proportions reverse with a maximum clay fraction of 38 %. X-Ray diffraction analysis establishes illite as the primary clay constituent with smaller quantities of chlorite present.

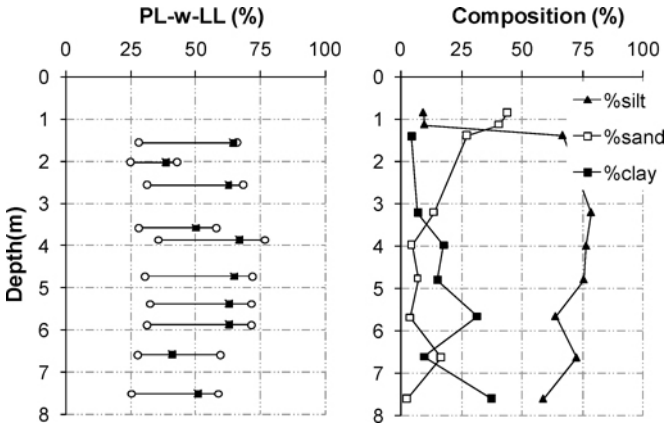

FIG. 1. Atterberg limits and particle size distribution with depth

RING SHEAR PROCEDURE

The peak and residual interface friction angles are measurable properties that are influenced by soil type, prior shearing history and the condition of the interface being tested, particularly the surface roughness. The interface friction angle at failure is assumed to lie between the peak and residual, with design typically assuming the conservative residual value. The process of pile installation and the subsequent equalisation modifies the in-situ soil state. An interface test that accommodates these changes is recommended by Jardine et. al (2005) and generally follows the procedure proposed by Ramsey et al (1998), who recommends simulation of the pile installation procedure involving periods of fast shearing "pulses" with stages of subsequent consolidation. These can be easily performed in the ring shear apparatus and lead to a shear surface/clay orientation similar to that developed at the pile-soil interface of a driven or jacked pile. Subsequent drained shearing allows the measurement of the interface friction angle. The total normal stress applied should be representative of the in-situ effective stresses with a consolidation period being applied prior to testing to allow the effective stress to be established. In the tests performed on the sleech, installation was simulated through application of a total displacement of at least 1m, provided via displacement increments of 200 mm at a rate of 500 mm/min and separated by pause periods of approximately 3 minutes. The excess pore pressure was allowed to dissipate fully, and a slow shearing stage was performed. All tests involved minimum displacements of 25mm to assure residual (failure) conditions were reached. Additional details pertaining to the apparatus and the factors influencing shear behaviour have been described by Tika (1989).

RING SHEAR RESULTS

McCabe (2002) reports triaxial test results on samples of sleech obtained at the test site. The constant volume friction angle (ϕ'_{cv}) of the sleech was found to be 33°, with no variation evident with depth. He noted that ϕ'_{cv} values measured using the simple shear apparatus were lower, ranging from 25°-30°. He also conducted ring shear tests to examine the soil-to-soil shearing behaviour. These tests covered a range of depths from 1.5m to 7m depth. The peak friction angles (ϕ'_p) measured in these tests (shown in Figure 2) were found to vary between 34°-23°, decreasing with depth as the clay fraction rises. The residual friction angle (ϕ_r) ranged from 33°-19°, typically showing a 1° degree post peak reduction from the peak values. The interface friction angle (δ) measured in soil-on-steel interface tests (and shown in Figure 2) reveal that interface friction angles are low, with the peak interface friction angle (δ_p) reducing from 16° in the sandy sleech to 10-11° in the clayey sleech. Values of the residual interface friction angle (δ_r) were typically 1° lower than peak values at any depth. The results agree well with a single interface shear test conducted against a steel interface by Von Lichschoten at Imperial College, shown as triangular symbols in Figure 2. Visual inspection of the annular

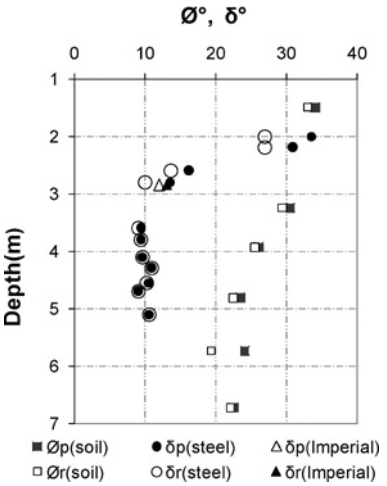

FIG.2. Soil and steel friction angles

sleech samples following shearing indicated a smooth polished surface on the soil sample, with failure occurring directly at the interface. The shear mode is consistent with a sliding failure, as described by Lupini et. al (1981), which contrasts with the turbulent behavior at shallow depths. It is interesting to consider the friction angle of the primary clay compound illite, which is approximately 10°. The measured interface friction angles exhibited a high degree of uniformity within the clayey sleech as clearly illustrated by the low variability of δ_r below 2.6m.

BEHAVIOUR IN FAST SHEAR

Following completion of the standard ring shear tests, described in the previous section, which were used to establish the interface friction response, a series of tests were performed to investigate the effect of shearing rate. Samples of the clayey sleech (from a depth between 3 to 5m) were consolidated under a normal stress of 50kPa, and then sheared at rates which varied from 0.0001 mm/sec to 20 mm/sec. It should be noted that as the standard ring shear apparatus does not measure pore pressure at the interface, at elevated rates the interface friction angle cannot be established. However these tests can be used to determine the approximate shear mode at higher rates and also quantify any changes in shear stress. Figure 3 plots the maximum shear stress normalised by the total consolidation stress prior to

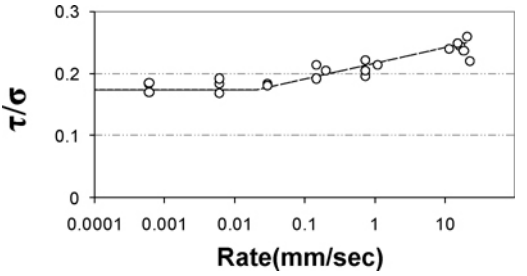

FIG.3. Shear behaviour at variable rates

shearing as a function of the rate. No noticeable change in shearing resistance was observed at the lower rates. For rates above approximately 0.1mm/sec a positive increase in stress occurred, possibly due to a change in shearing mode toward more turbulent behaviour. A 14% increase in stress per log cycle increase in rate can be established from this figure, which agrees well with the 12% rate effect observed by Lehane et al (2003) in triaxial compression tests on the sleech.

PILE TEST COMPARISON

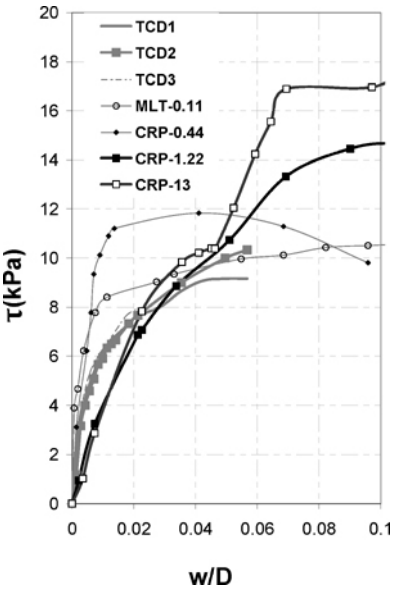

FIG. 4: Average shear stress during load tests

A series of load tests were conducted at the Kinnegar site using the UCD closed-ended instrumented pile. The pile is a 73 mm diameter steel tube capable of penetrations up to 7 m. The instrumentation measures effective stress changes through total stress and pore pressure sensors at three locations on the pile shaft. A number of maintained (incremental) load tests (MLT) and constant rate of penetration (CRP) tests were performed using the pile. These are described by the test type (MLT or CRP) and the displacement rate (mm/sec) in the test, e.g. CRP-0.44 refers to a constant rate of penetration test performed at a rate of 0.4 mm/sec. Mc Cabe (2002) describes MLT tests performed at the test site on three 250 mm square, 6m long, pre-cast concrete piles (referred to as TCD 1, TCD2 and TCD3). The MLT procedure involved applying the load incrementally, typically in 8-10 load lifts separated by pauses of approximately 30mins. As this paper is considering the peak capacity mobilised; the displacement rate for a MLT was defined as the maximum displacement rate during the load increment required to bring about failure (i.e. the final load lift). The constant rate of penetration tests involved continuous jacking, using an electronically controlled hydraulic cylinder.

The average shear stress values (τ_{av}) mobilised during the load tests are shown in Figure 4 as a function of the pile head displacement normalised by diameter, w/D. The τ_{av} values mobilised by the MLT test on the model steel pile and the full-scale concrete

piles (TCD 1-3) are comparable, reaching a maximum shear stress of approximately 10.5 kPa. Shortly after completion of the MLT test on the model steel pile, the pile was subject to a CRP test (CRP-0.44). The pile was seen to develop a peak load resistance at w/D of 0.04, after which the resistance reduced to levels similar to that measured in the MLT test on the pile. Further installations of the pile were performed to assess the effect of loading rate during first-time load tests. The CRP tests were performed at relatively high rates (CRP-1.22 and CRP-13). Their initial response up to displacement levels of 5% of the pile diameter, were very similar to the other piles test performed at the site. At this displacement level, the piles developed a distinct peak capacity and exhibited a brittle post-peak response. The highest peak capacity was developed on the pile with the highest loading rate.

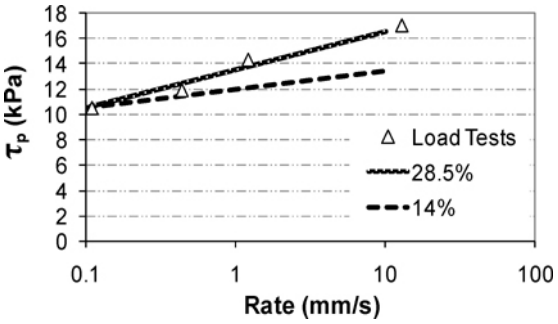

FIG. 5: Pile rate dependence

The variation of the peak shaft resistance (τ_p) developed during load tests on the model piles is shown in Figure 5 and is compared to the average rate dependence determined from the ring shear tests. Whilst a 14% increase in shear stress per log cycle increase in rate was noted in the ring shear tests, the increase noted in the pile tests was approximately double (at 28.5%). The physical mechanism governing this response can be understood by considering the undrained effective stress response at the pile-soil interface in Figure 6. The different initial values observed for the stress sensors in Figure 6 occur due to their relative location with respect to the pile tip, which is outside the scope of this paper. However, it is apparent that as the pile head displacement exceeded 3 mm, a reduction in porewater pressure (u) occurs, whilst radial total stresses (σ_r) increases (except at h/D=1.5). This results in enhanced radial effective stresses (σ'_r) at all levels on the pile shaft and an increase in the pile load resistance.

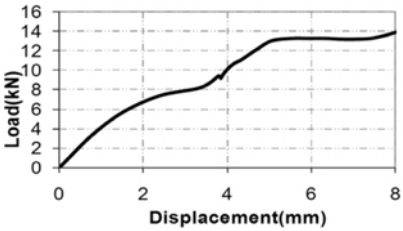

FIG. 6a: Load Test CRP-13

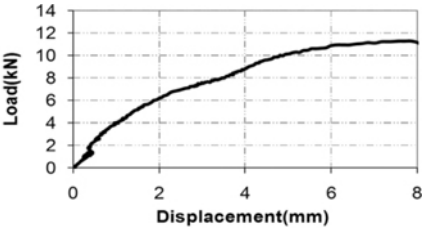

FIG 6e: Load Test CRP-1.22

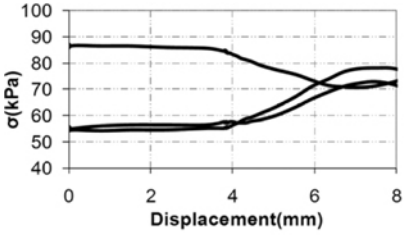

Fig 6b: Total Stresses CRP-13

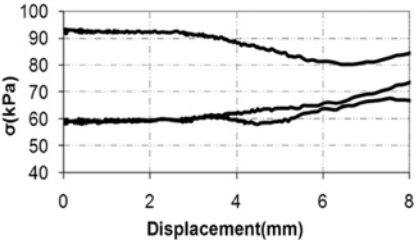

Fig 6f: Total Stresses CRP-1.22

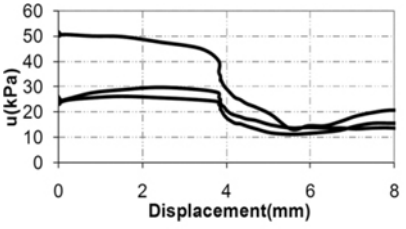

Fig 6c: Pore Pressures CRP-13

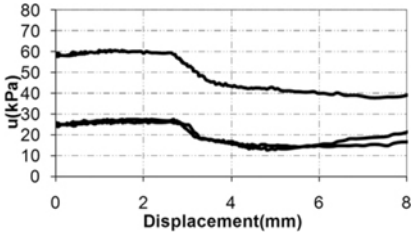

Fig 6g: Pore Pressures CRP-1.22

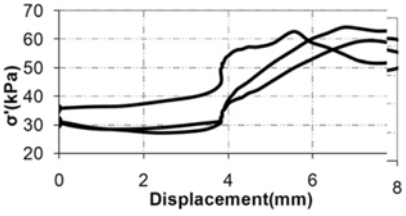

Fig 6d: Effective Stresses CRP-13

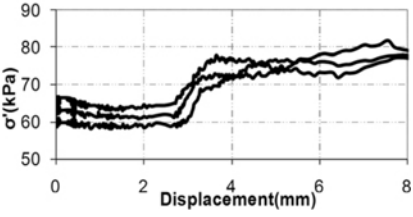

Fig 6h: Effective stresses CRP-1.22

CONCLUSION

This paper has described a series of interface ring shear tests to determine the shearing behaviour of Belfast sleech. The δ_r values were highly dependent on the clay fraction and decreased with depth to a steady value in the lower sleech of approximately 10°. The shearing mode was turbulent in the upper sleech dominated by the sand fraction with sliding shear prevailed in the lower material, occurring at the interface. Variable rate ring shear tests indicated a positive rate effect with a 14% increase in shearing resistance per log cycle increase in rate. Pile tests at the site also indicated a larger positive rate effect (approximately 28%) which was caused by elevated total stresses and depressed pore pressures during failure. This suggests that difficulty in recreating the boundary conditions applicable to the shear zone surrounding the pile may be responsible for the difference in rate effects observed in the laboratory and field.

ACKNOWLEDGMENTS

The first author would like to acknowledge the ongoing financial support of Sustainable Energy Ireland (SEI) in conducting this research. The authors would also like to thank Trinity College Dublin for use of the Bromhead apparatus.

REFERENCES

Bell, A. (1977). Laboratory Studies of the Belfast Estuarine Deposits. *PhD Thesis,* Queen's University of Belfast.

Chow, F. C.(1997). Investigations into the Behavior of Displacement Piles for Offshore Foundations, *Ph.D. Thesis*, Imperial College of Science, Technology and Medicine, University of London, London, United Kingdom.

Jardine, R., Chow, F., Overy, R and Standing, J. (2005) ICP design methods for driven piles in sands and clays, Thomas Telford

Lehane, B.M., Jardine, R.J. & McCabe, B.A. (2003). Pile group tension cyclic loading: field test programme at Kinnegar, Northern Ireland *HSE Research Report* RR101.

Lupini, J. F., Skinner, A. E. and Vaughan, P. R. (1981). "The drained residual strength of cohesive soils". *Géotechnique,*. 31 (2):181-213.

McCabe, B.A. (2002). Experimental investigations of pile group behaviour in soft silt. *PhD Thesis*, Univ. of Dublin (Trinity College Dublin)

Ramsey N., Jardine R.J., Lehane B.M. and Ridley A. (1998). "A review of soil-steel interfacetesting with the ring shear apparatus". *Proc. VI Conf. on Offshore site investigation and foundation behaviour*, SUT, London, 237-258.

Tika, T. M. (1989). The effect of fast shearing on the residual strength of soils. *Ph.D. Thesis*, University of London.

Copyrighted Materials
Copyright © 2009 American Society of Civil Engineers (ASCE)
Retrieved from www.knovel.com

Impedance Logs for Drilled Shafts at the Northwestern NGES

Sarah L. Gassman[1], P.E., Member, ASCE and Hongfen Li[2]

[1]Associate Professor, Department of Civil and Environmental Engineering, University of South Carolina, Columbia, SC 29208, gassman@engr.sc.edu
[2]Associate Engineer, Preconstruction Support Group, SCDOT, 955 Park Street, Columbia SC 29202, LiHF@dot.state.sc.us

ABSTRACT

The impulse response method is a nondestructive evaluation technique used to check the length and continuity of deep foundations. Uncertainty may exist when interpreting the results to quantify the size and location of the anomaly, if present. The analysis can be enhanced by developing a two-dimensional graphical image of the shaft using the impedance log technique. This paper describes the method used to develop impedance logs and shows results from drilled shafts at the Northwestern University National Geotechnical Experimentation Site. Two of the shafts were purposely constructed with anomalies representative of typical construction deficiencies. The ability to quantify the size and location of these anomalies using the impedance log technique is discussed.

INTRODUCTION

Nondestructive evaluation techniques have been used for a number of years to provide quality control of construction procedures for deep foundations such as drilled shafts and driven piles. In particular, the impulse response method has been used to check shaft length and continuity. When interpreting impulse response results, it may be difficult to quantify the size and location of an anomaly, and determine whether it is structurally detrimental to the shaft performance. One way to enhance the analysis is to develop a two-dimensional graphical image of the shaft using the impedance log technique: an interpretive extension of the impulse response method developed by Paquet (1968, 1991). It makes use of the simulated response of an ideal infinitely long shaft in soil and the experimental impulse response data of a real shaft to develop a two-dimensional image that can be used to visualize the shape of the shaft which is not visible from the ground surface (see Paquet (1991), Davis (1995), Rix (1993) and Baker et al (1993) for examples). The purpose of this paper is to describe the impedance log technique and show results from tests performed on

drilled shafts at the Northwestern University National Geotechnical Experimentation Site (NGES). The ability to quantify the size and location of anomalies is discussed.

IMPEDANCE LOG METHODOLOGY

Impedance logs were developed from data obtained from impulse response tests on drilled shafts constructed at the Northwestern University National Geotechnical Experimentation Site (Finno and Gassman, 1998). The site consists of five drilled shafts with diameters ranging from 610 to 910 mm and lengths varying from 12.2 to 27.4 m. Three of the shafts (Shafts 3, 4, 5) were constructed without pre-planned anomalies and two of the shafts were constructed purposely with defects: a reduced cross section (Shaft 2) and a thin, soil filled joint (Shaft 1). These defects represent typical construction deficiencies which can arise when a temporary casing is pulled as concrete is placed in a shaft. Details of the construction procedure were carefully documented for all shafts. The soils at the site are well characterized and, with increasing depth from the ground surface, consist of 0.6 m of top soil, 8.2 m of fine grained sand fill, 12.5 m of soft to medium clay and 6.1 m of hard silt and clay.

The impulse response method involves impacting the top of a deep foundation ("shaft" or "pile") with an instrumented impulse hammer that imparts transient vibrations to the shaft. Both the impact force and particle velocity on the impacted surface are measured in the time domain. These signals are digitally converted to the frequency domain using the fast Fourier transform (FFT). The resulting velocity spectrum is divided by the force spectrum to give the mobility as a function of frequency. Mobility curves for Shafts 1 and 3 are shown in Fig. 1 as examples.

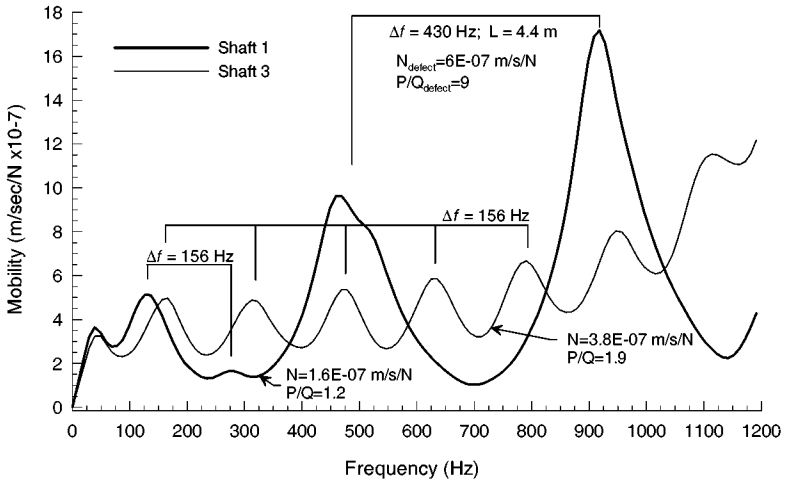

FIG 1. Mobility Curves for Shafts 1 and 3, both with D=0.61 m, L=12.2 m, and v_c=3810 m/s (after Gassman, 1997).

Quantitative information such as shaft length and impedance can be obtained from the mobility plot. By measuring the frequency change, Δf, between the resonant peaks, the length from the impacted surface to the source of the reflection is found by $L=v_c/2\Delta f$ where v_c is the bar wave velocity, or propagation velocity, in concrete. The shaft mobility, N, is found by taking the geometric mean of the height of the resonant peaks in the portion of the mobility curve where the shaft response is in resonance, and can also be defined theoretically as the inverse of pile impedance, Z. Thus, $N=1/Z=1/\rho_c v_c A$ (Davis and Robertson, 1975; Stain, 1982) where ρ_c is the density of concrete and A is the cross-sectional area of the shaft. If the actual N is greater than the theoretical value, it is likely that there is a defect in the shaft due to a smaller than anticipated cross-section (i.e. a neck) or poor concrete quality (low ρ_c or v_c).

Experimental data from an impulse response test is compared to the simulated response of an ideal infinitely long shaft buried in soil to obtain an impedance log that visually shows changes in impedance along the length of the experimental shaft. The program used herein to simulate the shaft response was coded in Labview and is based on work by Paquet (1968, 1991) and Davis (1994).

To develop an impedance log, the first step is to calculate the theoretical mechanical impedance, Z_c, and the mechanical admittance (mobility), N, of an infinitely long shaft buried in homogeneous soil as a function of frequency using $Z_c = \frac{A_c v_c}{r_0}\sqrt{r_0^2\rho_c^2 + \frac{2r_0\rho_c\rho_s v_s}{i\omega r_0} + \frac{\rho_c\rho_s v_s^2}{(i\omega)^2}}$, where A_c=shaft cross sectional area, r_0=shaft radius, ρ_c=concrete density, ρ_s=soil density, v_s=soil shear wave velocity and ω=frequency (after Paquet, 1968). At high frequencies (as $\omega\rightarrow\infty$), the characteristic impedance of the infinitely long shaft buried in soil is the same as that of the infinitely long free shaft ($Z=\rho_c v_c A$). At low frequencies, the impedance of an infinite long shaft buried in soil is a function of the damping and stiffness of the soil and the stiffness of the shaft. This can be observed in Fig. 2a which shows the result for an infinitely long shaft with D=610 mm, v_c=4050 m/s, ρ_c=2500 kg/m^3 and soil properties: ρ_s=1550 kg/m^3, v_s=125 m/s (model for Shaft 3).

Next, the impact force recorded from an impulse response test is used to calculate the theoretical shaft head velocity by transferring the experimental force time signal to the frequency domain by FFT, multiplying the resulting force and the simulated mobility in the frequency domain to obtain the velocity in the frequency domain (Z=V/F), and performing an inverse FFT on the velocity spectrum to deduce the simulated velocity in the time domain (see Fig. 2a inset). The simulated velocity has a single peak that represents the impact. For this case, the simulated contact time is equal to about 1 msec, corresponding to the experimental contact time. No reflections occur thereafter because the shaft is infinite and the soil is assumed to be homogeneous, thus there is no impedance change along the traveling path.

Several adjustments are made to the experimental velocity time signal. First the experimental velocity data is adjusted to suppress the impact peak (see Fig. 2b). Then, exponential amplification, $A_{mp}=e^{\tau n}$, is used to make the amplitude of reflections from depth comparable to the impact magnitude (Paquet, 1991; Rausche et al., 1992), where τ is determined by trial and error and ranges from -0.03 to -0.001 (Davis, 1994) and n is an index.

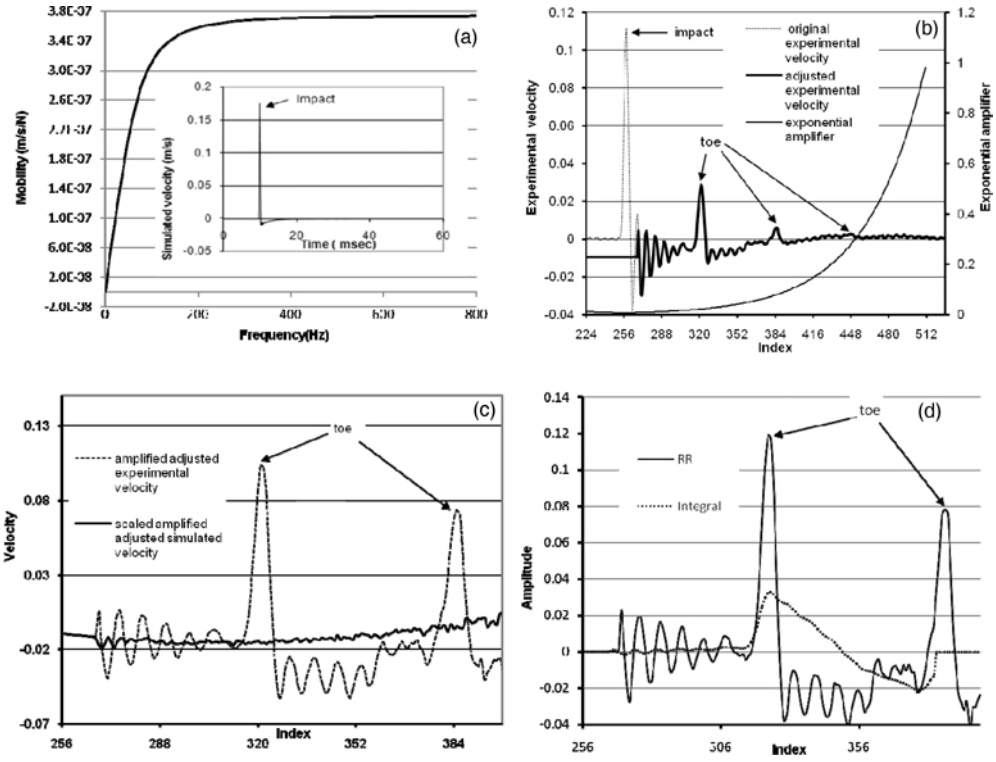

FIG 2. Steps: a) obtain the simulated velocity and mobility of an infinitely long shaft in soil; b) adjust the experimental velocity; c) apply an exponential amplifier; and d) obtain the relative reflectogram and integrate.

As shown in Fig. 2c, the amplitudes of the first and second toe reflections are comparable to each other after amplification. The third toe reflection was also seen (not shown) although not as clearly as the first two because it was masked by the rising waves from the soil resistance and surface boundary reflections. The simulated velocity (see Fig. 2c) is scaled so that the simulated impact magnitude matches that of the experimental impact magnitude, adjusted to suppress the impact, and amplified with the same factor used for the experimental result.

The relative reflectogram shown in Fig. 2d is found by taking the difference between the amplified adjusted tested velocity and the similarly modified simulated theoretical shaft velocity. A complete defect (zero impedance at a small distance from the shaft head) is equivalent to 100% reflection, while an infinitely long free shaft with no defects would give 0% reflection. Integrating the relative reflectogram yields the variation in impedance. In Fig. 2d, the impedance change associated with the shaft toe is clearly observed around index 320. Prior to this point, the amplitude of the integral oscillates slightly (due to rising soil waves and surface wave reflections) but is relatively insignificant compared to the impedance change at the toe. The graphical representation of the impedance log is obtained by plotting the integrated relative reflectogram vertically (twice, as offset mirror images) versus the traveling distance of the wave, and gives the variation in impedance along the shaft length.

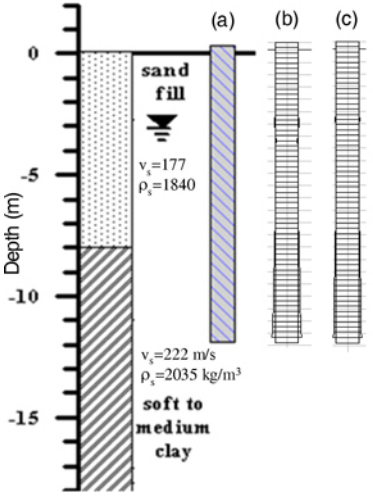

FIG 3. Shaft 3 (D=0.61, L=12.2 m): a) As-built Shaft, b) Best-Estimate Impedance Log and c) Best-Fit Impedance Log.

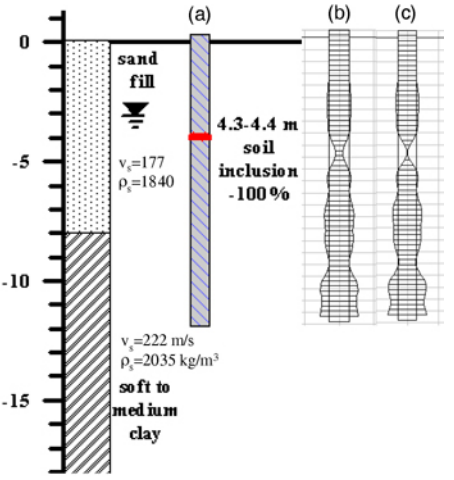

FIG 4. Shaft 1 (D=0.61, L=12.2 m): a) As-built Shaft, b) Best-Estimate Impedance Log and c) Best-Fit Impedance Log.

RESULTS FOR NORTHWESTERN NGES SHAFTS

Impedance logs were developed for the Northwestern University National Geotechnical Experimentation Site shafts using the following procedure. First, the infinitely long shafts were simulated using "best-estimate" parameters: the as-built shaft diameter, and the concrete properties (density and compressive wave velocity) and soil properties (density and shear wave velocity) determined from extensive site and laboratory investigations. Scaling factors and an exponential amplification factor were selected as described above. This resulted in the best-estimate impedance logs as seen in Figs. 3b, 4b and 5b, for Shafts 3, 1, and 2, respectively. Next, the parameter inputs were modified to more accurately match the impedance log to the as-built shape of the shaft. These are called "best-fit" impedance logs and are shown in Figs. 3c, 4c and 5c. Since the method requires modeling an infinite shaft in homogeneous soil (one-dimensional, axisymmetric conditions), and since the as-built shafts were constructed in layered soil profiles, the best-estimate trials were made using the weighted average of the properties from each soil layer surrounding the as-built shaft. Alternatively, the properties of the upper most layer were used to produce similar results. As will be shown, the soil parameters for the best-fit impedance logs correlate well with the best-fit soil parameters of the upper soil layer used to simulate the mobility response by Finno and Gassman (1998).

As shown in Fig. 3 the impedance log for Shaft 3 is indicative of a shaft with a relatively uniform cross-section carefully constructed in uniform soil having a moderate length to diameter ratio (L/D=20). The best-estimate parameters (v_s=195 m/s, ρ_s=1780 kg/m^3 and τ=-0.02) produced a relatively straight shaft with a slightly linearly increasing impedance with depth from 9 m downward (Fig. 3b). Adjusting the amplification factor to τ=-0.025 and increasing the index range over which the data was amplified resulted in an even straighter shaft in the lower portion (Fig. 3c).

The impedance log for Shaft 2 (L/D=23.3) shown in Fig. 5 indicates a clear reduction in impedance starting at a depth of 4 m for both the best-estimate and best-fit impedance logs. This corresponds well with the as-built neck at this depth that was constructed by tying sandbags to the reinforcing cage. The neck length was 0.71 m and the reduction in cross-sectional area was estimated to be -25% based on observations during construction. The best-estimate parameters (v_s=190 m/s, ρ_s=1965 kg/m^3 and τ=-0.02) produced a clear neck (-20%) followed by a linearly increasing impedance with depth (Fig. 5b). Adjusting the amplification factor to τ=-0.01 and reducing the magnitude of the soil parameters (v_s=115 m/s, ρ_s=1550 kg/m^3) resulted in a straighter shaft in the lower portion (Fig. 5c), yet exaggerated the reduction in impedance associated with the neck (-70%). In both cases, the necking defect appears to have a length of about 1 m. Thus, the impedance log was able to capture the vertical extent of the neck with good accuracy. The magnitude of the reduction in cross-sectional area of the as-built shaft was better shown in the best-estimate impedance log.

The impedance log for Shaft 1 (L/D=20) shown in Fig. 4 indicates a clear reduction in impedance starting at a depth of 4.4 m. This is associated with the soil-filled joint constructed at this depth in the as-built shaft. The soil-filled joint was constructed by placing concrete in the shaft up to a depth of 4.4 m, then placing pieces of soft clay

and sand to form a 10 cm layer of soil. The remaining concrete was placed the following day. In the impedance log, the soil-filled joint appears as a necking defect having a length of about 1 m, with a reduction in impedance between 50 and 90% from the best-estimate and best-fit logs, respectively. Thus, the impedance log was able to capture the significant reduction in impedance of the soil-filled joint, but not the vertical extent. There is also an impedance change at a depth of 10 m. This corresponds to the depth of the permanent liner (used to insure a uniform cross-section in the sand layer) and may also be a result of multiple reflections from the soil-filled joint.

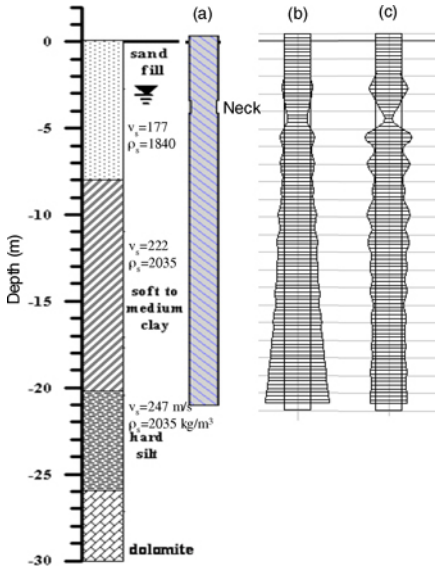

FIG 5. Shaft 2 (D=0.91 m, L=21.3 m): a) As-built Shaft, b) Best-Estimate Impedance Log and c) Best-Fit Impedance Log.

SUMMARY AND CONCLUSIONS

This paper presented the method used to develop two-dimensional graphical images of drilled shafts using the impedance log technique and showed results for three drilled shafts at the Northwestern University National Geotechnical Experimentation Site. One of the shafts was constructed without any preplanned anomalies and two of the shafts were purposely constructed with anomalies representative of typical construction deficiencies. The impedance log for Shaft 3 is indicative of a shaft with a relatively uniform cross-section carefully constructed in uniform soil having a moderate length to diameter ratio. The reduction in cross-sectional area from the neck in Shaft 2 was clearly observed in the impedance log. The vertical extent of the

neck was shown with good accuracy and the magnitude of the reduction in cross-sectional area was dependent upon the soil parameters used to model the surrounding soil. For Shaft 1, the impedance log was able to capture the significant reduction in impedance of the soil-filled joint, but not the vertical extent.

ACKNOWLEDGEMENTS

This material is based upon work supported by the NSF under Grant No. CMS 9875066. The support is gratefully acknowledged. The authors are indebted to the late Dr. Allen Davis for sharing his knowledge of the impedance log methodology.

REFERENCES

Baker, C.N., Parikh, G., Briaud, J.L., Drumright, E.E. and Mensah, F. (1993). "Drilled Shafts for Bridge Foundations," FHWA Publication No. FHWA-RD-92-004, Federal Highway Administration, McLean, Virginia, August.

Davis, A.G. (1994). "Impedance Log for the Length and Shape Measurements of Drilled Shafts from Mobility (TDR) Tests," a computer program, STS Consultants, Inc. March.

Davis, A.G. (1995). "Evaluation of Deep Foundations beneath Buildings Damaged During the 1994 Northridge Earthquake", *Proc. 31st Symp. Eng. Geol. & Geotech. Eng.*, Logan, UT, March, pp. 171-179.

Davis, A.G. and Robertson, S.A. (1975). "Vibration Testing of Piles," *Structural Engineering*, London, England, June, A7-A10.

Finno, R.J. & Gassman, S.L. (1998). "Impulse Response Testing of Drilled Shafts," *Journal of Geotechnical Engineering*, American Society of Civil Engineers, VOL. 124, NO. 10, October, pp. 965-975.

Gassman, S.L. (1997). "Impulse Response Evaluation of Inaccessible Foundations," a dissertation submitted to Northwestern University, Evanston, Illinois.

Paquet, J. (1968). "Étude Vibratoire des Pieux en Béton: Réponse Harmonique et Impulsionnelle Application au Contrôle" *Annales Inst. Tech. Batim.*, 21st year, No. 245, May. pp. 789-803 (French).

Paquet, J. (1991). "Une Nouvelle Orientation Dans Le Contrôle D'intégrité Des Pieux Par Solicitation Dynamique: Le Profil D'impédance "---A New Method for Testing Integrity of Piles by Dynamic Impulse: The Impedance Log. *Colloque International, Fondation Profondes*, Paris, pp. 1-10 (French).

Rausche, F., Likins, G.E., Ren-Kung, S. (1992). "Pile Integrity Testing and Analysis", *Proceedings of the Fourth International Conference on the Application of Stress-Wave Theory to Piles*, the Netherlands; pp. 613-617.

Rix, G.J., Jacobs, L.J., and Reichert, C.D. (1993). "Evaluation of Non Destructive Test Methods for Length, Diameter, and Stiffness Measurements on Drilled Shafts", *Transportation Research Record 1415*, Transportation Research Board, Washington, D.C., pp. 69-77.

Stain, R.T. (1982). "Integrity Testing," *Civil Engineering*, London, England, April and May, pp. 55-59 and 71-73.

Copyrighted Materials
Copyright © 2009 American Society of Civil Engineers (ASCE)
Retrieved from www.knovel.com

ADVANCES IN DYNAMIC FOUNDATION TESTING TECHNOLOGY

Garland Likins, P.E., MASCE [1] Ingemar Hermansson[2], Mike Kightley[3], Jon Cannon[4], and David Klingberg[5]

[1]President, Pile Dynamics, Inc., 4535 Renaissance Parkway, Cleveland OH 44128, USA; ph: 216-831-6131; fax: 216-831-0916; email: garland@pile.com
[2]Partner, Palanalys, August Barks Gata 13C, 421 32 Vastra, Frolunda, Sweden; ph: 46 31-45 43 07; fax: 46 31-45 99 80; email: ingemar@palanalys.se
[3]Managing Director, Testing and Analysis Ltd, Birchwood Way, Somercotes, Alfreton Derbyshire DE55 4QQ UK; ph: 44-1773-540880; fax: 44-1773-540760; email: mike.kightley@testal.co.uk
[4]Managing Director, Independent GeoSciences, 2 Letchworth Avenue, Brighton East, Victoria 3187, Australia; ph: 61 3 9553-8288; fax: 61 3 9553-8288; email: indgeo@optushome.com.au
[5]Piletest Manager, Wagstaff Piling, 1 Ashgrove Crescent, Brisbane, 4060 Queensland, Australia, ph: 61-7 3366 2555; fax: 61-7 3366 5608; email: d.klingberg@wagsttaffpiling.com.au

ABSTRACT

While dynamic pile testing is not new, and is included in many worldwide codes and specifications, dramatic changes from traditional testing methods and common practice have occurred in recent years. Traditionally, the sensors send their signals through a cable to the data acquisition equipment. Experience has shown that some poor data is caused by damage to these cables. New equipment now transmits sensor data from the pile wirelessly to receiving antennas on the data collection equipment. "Wireless" technology eliminates the cables and improves data quality. Sensors which remember their calibration sensitivity and transmit that information eliminate another common problem in data quality, namely having the wrong calibration assigned. Methods of protecting the sensors during installation allow attaching sensors prior to lifting the pile into the hammer leads, and hence speeding up the testing process, and promote safety. The most radical change in the data acquisition process is "remote" dynamic testing, which has revolutionized dynamic testing in some parts of the world. In remote testing, the data acquisition equipment is operated on site by an inspector or the pile crew, and sends the data over the internet to the test engineer in his office. Wireless and remote procedures are described and example experiences indicate the benefits, and areas of caution, of the new technology.

INTRODUCTION

Dynamic pile testing is not new. The original research began over 50 years ago at Case Western Reserve University (Eiber, 1958). Dynamic testing with the Pile

Driving Analyzer® (Analyzer) is included in many worldwide codes and specifications (Beim, 2008), so it is now routine standard practice. In fact, the Analyzer has become the most common measurement tool for assessing deep foundation performance.

For the first few decades, the routine dynamic test consisted of the engineer arriving on site with the test equipment, attaching the sensors to the pile and entering sensor calibrations and pile properties into the Analyzer. Upon hammer impact, the signals from the sensors were sent via a cable to the Analyzer. The engineer evaluated data on site blow by blow in real time by the Case Method. After field tests, critical data from end of drive or restrike was analyzed by CAPWAP® signal matching to obtain ultimate capacity, resistance distribution, and damping constants.

NEW POSSIBILITIES

Continual improvement in communication electronics has allowed alternate modes of operation that provide distinct advantages.

Data quality is of primary importance. Calibration of the sensors is obviously critical since the derived result is directly affected by signal sensitivity. There is an industry trend for the sensor to know and transmit its sensitivity to the parent data collection system using memory chips now installed in the sensors. Automatic detection of unusual signals further warns the engineer of suspect data quality.

Experience has shown that sometimes the cause of poor data is damage to or fatigue of the cables transmitting the signal from the pile to the Analyzer. The system can be equipped for "wireless" Bluetooth data transmission (Figure 1, 2), eliminating the main signal transmission cable entirely. A small battery powered transmitter transmits the data to the receiving Analyzer, located up to 100 meters from the pile.

FIG. 1. Wireless sensors and transmitter.

FIG.2. Wireless Analyzer in operation.

The sensors and transmitters can be protected by hard foam pads, allowing instrumentation to be attached to the pile on the ground prior to lifting the pile into the leads. For full length pile monitoring, this reduces testing time and improves safety because climbing the leads to attach the sensors is eliminated.

Wireless technology can send data from the jobsite to any worldwide destination using the internet. "Remote" testing was conceived and first enabled over 10 years ago through serial data transmission on TAPI cell phone systems (Gravare 2000).

In remote testing, the equipment is on site with the pile crew and a neutral observer to answer any questions from the test engineer. The sensors are attached to the pile by the pile crew, who already often attach the sensors even when the test engineer is on site. During remote testing, the test engineer may be anywhere in the world, but typically is in his office location, usually hours from the jobsite. Connection was made from the site equipment to the engineer's office computer. Data was then sent serially, although typically slow transmission rates resulted in a real time sample of about every sixth blow in continuous operation, or a short delay in time if a limited number of restrike blows were requested. Since every blow was captured by the Analyzer, all data could later be retrieved when requested.

Recently, the Analyzer has adapted to transmit data through cell phones equipped to access the internet. Through internet communications, the system is now able to achieve a significantly higher speed of data transfer; typically every second or third blow can be sent in real time, and perhaps every blow in the near future.

BENEFITS FROM CHANGE IN PRACTICE

Compared with having the test engineer on site, what real advantages are achieved with this "new technology"? Will the test produce the same quality measurements as with traditional on-site testing? Assuming all parties are willing to step out of their "comfort zone", how is the new technology best implemented?

Consider that if the engineer did not need travel time to return from the site to the office, the engineer could instead immediately begin data analysis (e.g. CAPWAP) and write the report sooner. Getting the results sooner can be vital to the project since this information is often on the project's critical path. The installation criterion can be established sooner and production piles then installed with confidence.

In traditional on-site testing, the test is scheduled conveniently for both contractor and tester. Often the test engineer is not available for last minute requests or "emergencies" (e.g. pile obtains a different blow count or vastly different penetration than expected). If the remote equipment is already on the site, a quick call to the test engineer is all that is needed to test and resolve the current crisis. Testing costs are known which allows more accurate budgeting.

Tests which involve installation testing followed by restrikes after several days wait time (or multiple tests) to observe the ultimate capacity with time, or to observe hammer consistency, can be easily scheduled at the contractor's convenience. For example, the engineer may test on-site for the initial installation, but leave the equipment on site for several days to allow for set-up and then perform a restrike test in a remote mode. The end result is a better design with more complete testing, thus reducing risk, and possible significant foundation savings.

Although the above justifications are often more compelling reasons to implement this new technology, traditional on-site testing generates significant travel time charges and travel time costs. Further, much of the engineer's time on site is actually spent waiting for something to happen. The direct engineering time of collecting data is often a small percentage of time billed, particularly for restrike tests. At some sites, extra training for safety required to enter the jobsite can be eliminated with remote testing. By eliminating all travel time and all travel costs, and eliminating all on-site non-testing time, the actual cost of the test is significantly reduced.

From the engineer's view, travel to site can be greatly reduced, and in many cases eliminated. Remote technology allows the test engineer to efficiently test piles from multiple jobsites, even from multiple countries, during the same day. Since there is an increasing concern for quality of testing (Seidel, 2000), access to the more experienced testers can be improved.

These reasons all help to keep the project on schedule and under budget. So how is remote technology best initially implemented? On larger projects, the tester might come to the site at the beginning (and train the crew to attach the sensors to the pile, if needed), but leave the equipment on site for later restrike tests. After developing sufficient confidence, future tests may be performed remotely. An independent on-site observer, usually already present to collect a driving record or assure the installation criterion has been met, can be the test engineer's eyes and ears. The test engineer in the office sees the same data, and can easily assess data quality from his office. If there is a problem with data quality, the test engineer simply instructs the site personnel to address the attachment of the problem sensor, and repeat the test. The engineer can transmit his findings instantaneously during the testing to the site, and even direct when the pile driving may be terminated.

Swedish Experience

High strain dynamic tests on driven piles have been routinely carried out in Sweden for approximately 30 years (Gravare 2004). Most pile tests are carried out during redriving to evaluate the bearing capacity including time-dependent set-up effects. The long distances in Sweden cause several hours of traveling for typically less than one hour of testing, such as testing three piles in a bridge abutment.

Since the first remote test 10 years ago in Sweden, the transition to remote testing has been fast and nowadays most tests in Sweden are remote tests. Altogether 13 remote units are currently operated in Sweden (Fig. 3). To receive data from up to 10 sites per day, a team of four consulting engineers operates a network of six computers connected to the remote units via modem or internet connection. The network allows quick movement between different sites in busy situations. Multiple engineers can immediately review difficult to interpret data and reach a fast judgment. The new remote unit with internet transmission allows monitoring during driving.

Properly attaching the transducers to the pile is essential for good data quality. Even though many Swedish piling crews are familiar with attaching sensors, it is still important to study data quality of each transducer individually. The force transducers particularly require correct attachment. The most common problem, incorrect spacing between the attachment holes, stretches the strain transducer beyond its balancing

range. The experienced site crew will notice field equipment then displays "Not Available" and drill new holes before starting testing. The balancing status can be viewed by the remote engineer, and adjustments made if required, prior to testing. For concrete piles, if attachment bolts are too long they bottom out on the anchors rather than bearing on the transducer. This is not always discovered on site as the crew experiences they have tightened the bolts as much as possible. This problem is easily detected in the office by the transmitted vibrating signal. Accelerometers not properly oriented parallel to the pile axis result in poor force-velocity proportionality.

FIG.3. Remote tests in Sweden

To prevent the same pile being tested over and over again (with different pile numbers sent to the engineer), the engineer can inspect the strain transducer balancing which should change when moved from pile to pile and, of course, look at the data itself to see if it is identical to the trace of that just previously tested. During many past years of remote testing this has not been a big problem.

As mentioned above, the remote testing saves travel time that can be used for evaluating and reporting. In a very urgent situation, remote testing, CAPWAP analysis and report writing were carried out simultaneously (by three engineers on three piles) and the client received the results shortly after the test was finished.

UK Experience

Dynamic pile testing has been carried out in the UK since 1979. Initially testing was carried out mainly on driven precast concrete piles with some testing of driven steel tubular and H-piles. As experience grew, dynamic load testing was carried out to cast in place piles and steel sheet piles. In the early years, reliable dynamic load testing required highly trained engineers to travel to site to carry out the testing and physically transport the test data to the office for CAPWAP analysis. This analysis and subsequent report would often be carried out some days after the site testing.

In the late 1990's the advent of the first remote Analyzer presented an opportunity for a step change in the method of working, while still ensuring the highest quality of

test data, essential to valid data analysis by CAPWAP. This remote equipment was quickly adopted in the UK as soon as it was available. The ability of the remote Analyzer to transmit data from site, during testing, and for an office based expert to assess the data and carry out immediate CAPWAP analysis has many advantages. Today the client can now expect almost immediate test results and same day reporting.

Quality is a key issue in any test and dynamic load testing by the remote system allows the expert control of all aspects of the test. The expert sends commands to the remote equipment to control its operation as if he were on site. The expert sees the data from each sensor to assess the data quality (and if anything is amiss, then can instruct the field crew to address and correct the problem prior to completing the test). This expert control of all testing is a key aspect of quality control.

The UK is a geographically small area. Remote pile testing equipment based with centrally and regionally based testing technicians can service sites in the UK more efficiently than moving the equipment from site to site by courier. The use of a dedicated trained technician rather than client supplied operatives ensures consistency of test data and rapid testing with no site delays. It is possible to test 10 piles per hour.

Today in the UK the use of the remote equipment allows clients to have UKAS accredited dynamic load testing carried out by locally based testing technicians supported real-time by office based expert engineers. This delivers a fast reliable service demanded in modern UK construction.

Australian Experience - Contractor View

High strain dynamic testing has become a routine part of the quality assurance process for foundations in Australia since 1983. Today, except for small projects, 5 to 10% of all driven piles are dynamically tested. Remote dynamic testing has been in regular use in Australia since 2001.

The introduction of the remote system has provided substantial cost savings for many projects located more than 1000 km from the nearest office of the testing engineer, requiring many hours of travel to and from the site. The reduction in testing costs have been substantial (by up to 75%) where intermittent testing has been required, with one of the most significant savings being associated with the reduction in "down time" by the site crews waiting for the engineer to arrive on site after a special or additional test has been required. In some isolated project sites, the down time waiting for a traditional on-site test has been almost 24 hours. Where remote testing can be utilized, this down time can be eliminated. Not only are there time savings, but the 'hidden' costs of the safety of the engineer traveling long distances to isolated project sites cannot be under estimated. Additional cost savings can also be associated with the elimination of on-site safety instructions for the testing engineer, which in some circumstances for mining sites can be more than one day.

The early remote systems relied on the mobile phone network with relatively slow data transfer. Monitoring of the pile driving during installation was less than ideal as every 7^{th} or 8^{th} blow would only be received by the remote computer in real time. Therefore, many driving tests required the testing engineer on site and only the

subsequent restrike tests were completed in remote mode (in restrike mode, every blow is sent sequentially). However, the recent introduction of the high speed internet broadband communications allows all blows to be received in real time, creating no disadvantage for remote testing during initial driving.

Many piling Supervisors are very familiar with the processes required for collecting dynamic test data. Sensor attachment, cable connections and data communications set-up are routine. However, the successful completion of the remote test requires clear communication between the field staff and the testing engineer in the office. Firstly, the testing engineer needs to be familiar with the remote testing equipment to problem-solve any issues that may arise, particularly for field personnel unfamiliar with the process. Secondly, the testing engineer must have sufficient experience with piling to ask appropriate questions of the field staff to gather all relevant information about the pile being tested.

With the remote testing engineer usually located in an office environment, other more experienced engineers are usually on hand to provide assistance and advice where required, providing quick assessments of piling test data on the critical path.

Australian Experience – Consultant View

Independent consulting using dynamic pile testing operated by Australians first began in Australia in 1984. Projects were conducted with the operator on-site all over Australia and in many South East Asia and Oceania countries. Independent testing in Australia is mostly in ports and bridges and other heavy civil infrastructure with most projects now funded by the booming mining sector of the economy.

Remote testing is a method particularly adapted to Australia's vast distances and low population density. Independent consulting jobs tend to be in remote locations far from home base. Remote systems were readily accepted owing to low mobilization cost, speed of response owing to low/no travel time, convenience of having the remote equipment available full-time on site for unscheduled use, and low cost to postpone tests while problems with the piling system are being resolved. The most common solution on large remote projects is to station the remote equipment on site for the duration of piling, often now required under the project specification. Having the operator on site is now unusual and only necessary if there is no phone system available.

Each Analyzer system is equipped with some minimum spare sensors. Multiple remote units can be serviced by one test engineer. Simultaneous testing is not common, but can be accomplished with multiple receiving stations at the test engineer's office. Data can be received during off hours by unattended computers. The number of remote units operated by the sole operator, currently 7 units by this consultant, is only limited by the available time to analyze data and timely report the results.

Although many piling contractors and deep foundation engineers know dynamic test methods, a step by step, button by button, guide is provided for field personnel unfamiliar with remote testing because there are still frequent new engineers in the Contractor's staff. When talking to people on site, it must be assumed they have very low knowledge of the Analyzer system. Patience and consideration are essential.

Data is received on a notebook computer. Thus even a sole operator can receive data at almost any time and location. The test engineer can be measuring data on one site while at the same time receiving separate data on the notebook from another location on the other side of the country. Frequently data is received in airport facilities, while in transit stopped by the side of the road, and even in a moving taxi.

New fast internet-based remote systems, in parallel with new advanced 3G mobile phones for non-internet based systems, provide very fast and relatively stable transfer of data, but they require some knowledge of windows-based pc's by the user and require stepping through more menus by the user.

SUMMARY

The new Analyzer technology can improve dynamic testing practices and result in even better quality assurance and lower risk for deep foundations. Wireless data transmission from the pile to the Analyzer improves data quality, and improves safety on site. When remote Analyzer equipment is already on site, piles can be immediately tested should problems arise. Data can be sent remotely using modern cell phones and the internet from the pile crew to the test engineer, typically in his office, allowing for better scheduling of testing, a more efficient use of engineer time, and considerably reduced testing costs and reduced scheduling difficulties. Good communication with the site and careful review of data are required to assure reliable results. Eliminating the travel time, analysis of the data can then proceed immediately, resulting in faster reporting of results, keeping installation of production piles on schedule. Different operational experience is observed in remote testing, depending on the geography and position of the tester.

REFERENCES

Beim, G., and Likins, G., (2008), « Worldwide dynamic foundation testing codes and standards", *Proc. Of the 8th Int'l Conf. on the Application of Stresswave Theory to Piles*, MillPress, Lisbon, Portugal

Eiber, R.J., (1958), "A Preliminary Laboratory Investigation of the Prediction of Static Pile Resistances in Sand", *Master's Thesis, Dept. of Civil Engineering, Case Institute of Technology*, Cleveland Ohio.

Gravare, C-J.,Hermansson, I., Gravare, M. (2004), "Swedish Practice for Verification of Pile Bearing Capacity", *Proc. Of the 7th Int'l Conf. on the Application of Stresswave Theory to Piles,* Geotechnical Division of Institution of Engineers Malaysia, Kuala Lumpur, Malaysia

Seidel, J. (2000), "The need for quality assurance in the dynamic pile testing industry", *Proc. Of the 6th Int'l Conf. on the Application of Stresswave Theory to Piles,* Balkema, Sao Paulo, Brazil

Copyrighted Materials
Copyright © 2009 American Society of Civil Engineers (ASCE)
Retrieved from www.knovel.com

Dynamic Pile Testing – Construction Control and Design Verification

Mr Benjamin Smith PE Civil (hons) BSc (geop) Advanced Foundation Solutions (AFS), Suite 106, 7-11 Clarke St Crows Nest NSW Australia 2065 ben@afsolutions.com.au

ABSTRACT

This paper gives an overview of pile testing, in particular dynamic pile testing. This paper explains why engineers should use pile testing for assessing pile construction methods and to verify their foundation designs. The paper also describes some testing methods available including Static Load, Osterberg Cell and Statnamic testing. The paper concludes with a case study that shows dynamic pile testing used for design verification and construction monitoring to ensure all piles installed were suitable to act as foundations for a piled raft. This case study is an example of where construction monitoring by dynamic pile testing has been used to ensure that piled foundations were built in accordance with a very prescriptive set of design installation criteria. A percentage of dynamic pile testing spread across the site as well as construction monitoring meant these piles were acceptable to the designers to act as the foundations for the piled raft.

INTRODUCTION

The current Australian Piling Code *AS2159-1995 Piling – Design and Installation* defines the following pile testing methods available: Static Load Testing, Dynamic Load Testing (High Strain), Integrity Testing (Low Strain): Sonic Impact Test (sonic echo test), Sonic Vibration Test (impulse response method) and Sonic Logging Test (cross hole sonic logging). Other test methods are allowed at the discretion of the designer some examples are Statnamic Testing and Osterberg Cell Testing. Pile testing methods provide confidence to the designer in the chosen pile construction method, prove pile capacity, predict pile load-deflection response as well as provide indications of pile integrity, quality and verification of foundation design.

SELECTION OF PILE TESTING METHOD

A systematic approach must be taken when selecting and applying pile testing methods. The type, location and quantity of pile testing are dependent on several factors including: geology, pile loads, geotechnical information, project budget and pile type. Further, an effective pile testing regime includes opportunity to improve the regime based on the results of the initial testing. Improving the pile testing regime can include the following: increasing or decreasing the number of tests, sampling a different geographical area, changing the type of test or changing the timing of testing.

Goble and Likins (1996) in their paper show how a combination of pile test methods can be used in a cost effective manner to ensure quality control of piling projects. Goble et al (1996) concluded that dynamic testing yielded good results in capacity prediction and could be used to replace static testing. Further, when

calibrated with a static load test, dynamic load testing could extend the static test result over the job site in a cost effective manner.

INTRODUCTION TO DYNAMIC PILE TESTING

Dynamic Pile Testing is a fast and effective method of assessing shaft friction capacity, end bearing capacity and integrity of piled foundations. Dynamic Pile Testing can also be used to assess the efficiency of a pile driving hammer and the driving conditions in different geology. The dynamic test involves instrumenting a pile with accelerometers and strain gauges, driving the pile with a pile driving hammer and analyzing data collected by the sensors. The dynamic test can be done on any driven pile, drilled shaft or other cast in place foundation on any material including concrete, steel and timber.

One set of gauges is made up of a strain transducer and an accelerometer; each set of gauges is located on opposite sides of the pile at 180 degrees. The gauges in perpendicular planes account for any bending effects and uneven hammer strikes. When the pile is hit by the pile driving hammer a stress wave travels down the pile, the force and velocity components of this stress wave are measured by the strain and accelerometer sensors respectively.

The dynamic test measures the total pile resistance when subject to a high velocity loading; so the measured soil resistance has both dynamic and static components. During the service life of the pile, it is subject to much slower or more static loading rates. In order to predict the pile load behavior under static conditions it is necessary to remove the velocity dependent forces measured during the test in the prediction of capacity. There are several methods used to predict the static pile capacity, these range from simplified single variable equations available to the field engineer to complex multi variable solutions that require post processing of the data, this is done using software, for example CAPWAP. Initially in the field an estimate based on one damping parameter can be made to predict the static capacity of the pile. This is known as the Case Method and relies on the damping parameter. This field prediction relies on the testing engineers experience and judgment.

Once the data has been collected in the field a more rigorous signal matching analysis can be performed, this can be done using various software programs. This analysis involves modeling the pile as a series of pile and soil segments where the static and dynamic soil resistance is modeled by a series of springs and dash pots. The measured data from the test is imported into the software and the analyst is able to adjust all of the various spring and dashpot parameters to produce a mathematical model that matches the collected field data. This process involves up to 16 parameters plus the ability to vary the shaft and base pile properties and soil resistance for the full length of the pile. Ultimately the software produces a model which is used to predict the static capacity with shaft and base distributions plus a predicted pile load deflection curve. The signal matching process is a more rigorous analysis than the initial Case Method or other prediction methods used in the field test.

Dynamic Pile Testing is used to prove pile capacity and integrity on projects throughout the world. Common examples include precast concrete piled foundations for bridges and tubular steel foundations used for wharves. Dynamic Pile Testing can also be used in conjunction with piling records and other pile testing methods to predict the dimensions, integrity and capacity of an existing unknown pile. An informed decision can be made to either use the pile as part of a new structure or to replace the pile. Further, the dynamic test has been used to verify pile performance and to confirm suitability of piles subject to negative skin friction effects.

WHY USE DYNAMIC PILE TESTING?

Geotechnical design is more nebulous when compared to structural design. Testing regimes for concrete and steel during both manufacture and construction are accepted and required. However, the material properties and behavior of steel and concrete under load are far better understood when compared to the properties of geology around a pile under load.

Geotechnical site investigation typically involves different types of sampling and testing techniques, including taking boreholes and Cone Penetration Test (CPT) data. This data is usually extrapolated across a site. The actual percentage of the ground sampled during the investigation is very small. In addition to the small sample volume the engineering properties of soil are difficult to model. This means geotechnical design and construction is a complex and risky procedure. The need for regular testing of structural components is widely accepted, yet the need for pile testing is greater because of these much larger uncertainties. Pile testing helps to fill the gaps across a site, and confirms the quality of the foundation construction technique.

Modern pile test methods enable the contractor to provide quantitative feedback to the designer, or alert the designer to potential problems in the design as they occur. When caught in time, the foundation design can be adjusted or optimised and failures prevented during the construction process. Pile testing gives the designer confidence that the piles are being installed and are behaving in the manner they were designed. Pile testing ensures quality assurance of pile construction. Finally, quantitative pile test results can be used to feed back into future designs, yielding greater efficiency.

ADVANTAGES AND DISDAVANTAGES OF DYNAMIC PILE TESTING

The most relevant advantage of dynamic pile testing is that any pile on a site can be selected by the verifier to test. No special preparation is required; hence the dynamic test can be used as a construction control method for quality assurance. Other advantages are its high speed and low cost. Further, dynamic pile testing provides an estimation of both skin friction distribution and end bearing capacity of the pile, as well as an assessment of pile integrity. The test provides a direct link between driving energy, pile set, pile temporary compression, pile static capacity and pile load deflection. It is both a foundation design verification test, and a construction control test.

Pile capacity can change with time. This is due to set-up or relaxation of the geology. Likins, Rausche, Thendean and Svinkin (1996) concluded that dynamic load testing with signal matching best predicted static load capacity of a pile when the dynamic test was conducted as long as possible after pile installation. Similarly, Likins, and Rausche (2004) concluded that long term service pile capacity estimations are improved by waiting at least 6 days after installation before dynamic restrike testing to allow for soil strength changes with time to stabilise.

The main disadvantage of the dynamic test is that it is an indirect test method that is dependent on high quality test data and also dependent on the experience and skill of the analyst. Middendorp, van Ginneken and van Foeken (2000) describe a key area where this is relevant is for dynamic testing on Continuous Flight Auger (CFA) piles and Bored Cast in Place piles; pile discontinuities for example neckings or bulbs introduce stress wave reflections which can be mistaken for soil properties. However, modern construction monitoring technology for CFA piles can measure soil resistance during drilling and pumped concrete volume during extraction of the auger. This information can assist the analyst as the monitoring creates a flow profile or "Pile Shape" of the pile casting process. This "Pile Shape" can be used for the pile model in signal matching software to hence enhancing the accuracy of the dynamic analysis. Similarly, the drilling resistance can be used to confirm the chosen soil model.

USING DYNAMIC PILE TESTING TO PREDICT PILE TENSION CAPACITY

Although the dynamic test provides a capacity distribution between end bearing and shaft friction care should be exercised when predicting pile tension capacity. Generally, pile tension capacity does not equal pile shaft friction capacity. Typically the overall pile compression capacity can be confidently predicted from the signal matching analysis. The exact distribution between shaft and base capacity is difficult to predict. As a result, additional reduction factors are used due to the lack of redundancy in the system. It is common practise to apply higher safety factors to dynamic test results when making estimates of pile tension capacity. Typically the 80% of the interpreted pile shaft friction is accepted as the tension capacity prediction. This site factor can be refined if dynamic and static tension tests are used in conjunction.

ALTERNATIVE TESTING METHODS

Static Load Testing

Static load testing is a universally accepted pile testing method. The static involves setting up a reaction frame with weight or calibrated jacks to load the pile in compression or tension. The pile top deflection is measured and plotted on a load/displacement curve. Previous to dynamic testing, static load testing was the principle method of measuring capacity of piled foundations.

The main advantage of the static test is that it is a direct test; load is applied and a displacement is measured. The test is easy to understand and gives engineers

confidence in the load deflection behavior of the pile. Generally, it is thought to require little or no interpretation.

The main disadvantages of the static test are that it is expensive and time consuming. Also, careful planning and special construction techniques are required to maximize information recorded in the static load test. After construction has begun, the exclusivity of the static test on site means the static load test is a verification test only and not a method of construction monitoring. However, the static load test can be used prior to production piling to define the pile capacity that is be used for the site. Finally, similar to borelogs and Cone Penetration Tests, the static test is statistically insignificant especially across large sites.

Osterberg Cell Testing

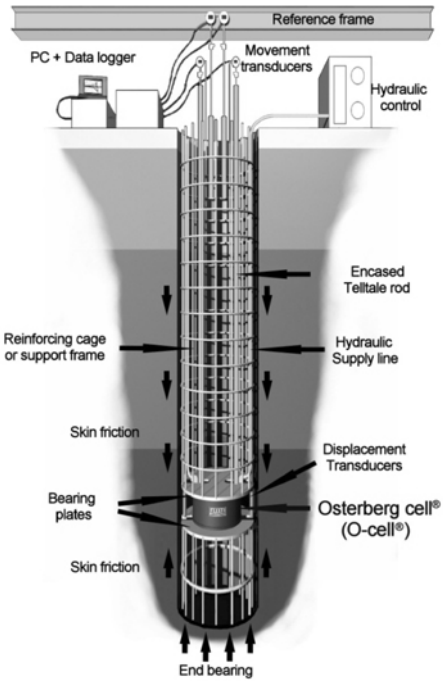

Figure 2 - Osterberg Cell Test Set Up

Bottom load testing or Osterberg Cell (O-Cell) testing is an alternative to static load testing. The method was patented in the US by Jorj Osterberg. As can be seen Figure 2, an Otserberg Cell Test involves a sacrificial load cell which is built into the pile toe. The load cell is built into the base of the pile, in order to separate the pile capacity into components for both skin friction and end bearing. Working in two directions, upward against the pile shaft friction and downward against pile end-bearing, the O-Cell test automatically isolates the two sources of pile capacity. Because it is installed in the foundation, the Osterberg Cell load does not require reaction systems or kentlage used in static testing. Instead, the O-Cell derives the reaction from the geology.

Pile end bearing capacity provides reaction for the skin friction portion of the O-Cell load test, and skin friction capacity and the weight of the pile provide the reaction for the end bearing portion of the test. O-Cell testing continues until one of three things occurs: ultimate skin friction capacity is reached, ultimate end bearing capacity is reached, or the maximum O-Cell capacity is reached.

The key advantage of O-Cell testing is that it generates a pile capacity distribution between pile shaft and pile end bearing capacity. Further, there is no external reaction system, so no heavy kentlage is required, also less stress applied to the pile during testing.

The key disadvantages of O-Cell testing are that the test is not a pure compression load test and the maximum applied load is limited by the three conditions mentioned above (shaft friction capacity, end bearing capacity or capacity of the O-Cell). Further, the O-Cell is sacrificial and needs to be specially fitted during pile installation. So, similar to static load testing, the careful planning and special construction techniques required to conduct an O-Cell test render this test a verification test only and not a construction control method.

Statnamic Testing

Statnamic rapid load testing was co-developed by The Netherlands Organisation (TNO) and Berminghammer Foundation Equipment Company of Ontario Canada. Statnamic testing is another form of pile testing and is a hybrid between static and dynamic testing. This method involves using a large reaction mass that is lifted off the test pile by means of a controlled explosion. Statnamic Testing utilises a calibrated load cell placed on the pile head. So, unlike dynamic testing, the measured load is not dependent on the pile properties Middendorp et al (2000). Relatively large forces can be applied to the pile without construction of a reaction frame. The applied load in a Statnamic test is slower than the load applied in a dynamic test, usually with reduced dynamic effects, so the direct predicted pile capacity is more similar to the static capcity. Middendorp et al (2000) concluded that Statnamic was preferable to dynamic testing for bored concrete piles, auger piles and caissons. Further Chang et al (2004) concluded that when compared with dynamic testing, Statnamic testing on bored piles mobilized larger displacement and higher capacity.

CASE STUDY: WOLLONGONG LINKS PROJECT – PILED RAFT FOUNDATION

Background

An example from a recent project where dynamic pile testing was used for both construction monitoring method and foundation design verification was the eight story Wollongong Links project in Australia in 2006. The geotechnical conditions of the site consisted of alluvial silts, sands and clays of variable strengths. The alluvium directly overlaid siltstone bedrock to depths of around 12-15m. The ground water table was 0.8 to 2.5m below the ground surface. The geotechnical report indicated the presence of acid sulphate soils. To carry the loads of this building the developers had two options:

1. Piles constructed down to rock: Large diameter continuous flight auger (CFA) piles 12-15m deep founding on rock, or
2. A piled raft foundation: Large numbers of short (9-12m deep) driven timber piles under a thickened concrete slab.

Piles constructed down to rock were more expensive, due to the cost of construction of the piles and the removal of the acid sulphate spoil generated by

the CFA piling process resulted in selection of the Piled-Raft foundation. The raft consisted of a thick concrete slab overlying approximately 650 driven timber piles.

Pile Design Criteria

Typically, a construction drawing nominates the ultimate structural pile load (S*) and the geotechnical strength reduction factor "ϕ-g" (phi-g). For dynamic testing with signal matching "ϕ-g" is defined by the Australian Piling Code between 0.65 and 0.85. The ultimate structural load (S*) is then increased by ϕ-g to yield the required ultimate geotechnical capacity (Rug). Dynamic testing is then used on a percentage of test piles across the site to establish the driving criterion, which is then used to ensure the remainder of the untested piles achieves capacity.

The structural design of the Piled Raft was conducted by designers Costin Roe. The pile installation criteria as noted on the drawing were as follows:
Criteria 1: Piles shall deflect between 3 and 6mm under a load of 500kN
Criteria 2: Piles are to be installed as friction piles with a minimum total capacity of 660kN of which no more than 40% to be carried as end bearing (pile toe) resistance
Criteria 3: Predicted movement at total resistance shall be 10mm minimum
Criteria 4: Dynamic testing and wave analysis (signal matching) is to be used to determine driving sets (driving criterion) and shall be carried out on 5% of all piles.
The reason for the prescriptive criteria set by the designers was to ensure the piles would settle along with the raft as a complete unit.

In order to determine the pile length and initial pile driveability analysis, a selection of test piles were installed on the sites of Cone Penetration Testing (CPT) conducted previously. The sites of the CPT and test piles where spread geographically across the site. Pile penetration, or length of pile embedment in the ground, is directly related to pile capacity and pile settlement. Dr Julian Seidel from FoundationQA used the results from the CPT and dynamic testing to produce a contour map overlaying each pile position. This contour map gave the penetration for each pile that would result in that pile behaving in accordance with the criteria set by the designers Costin Roe of the piled raft.

The drawing nominated 5% of all piles to be dynamically tested on the project. The results from the test piles were continually fed back into the model to check the design and monitor the construction process. This real time feedback loop ensured that the piles were satisfying the criteria set by the designers. As the project continued, the contour model was adjusted and updated to include the new test data. Driving energy, pile set and temporary compression were measured and recorded for every production pile to ensure that all piles were behaving similar to the test piles. A further 10% of piles were re-hit 24 hours later to confirm their behavior, as well as quantify potential soil set up or relaxation effects.

Summary of Test Pile Results

The results from the dynamic pile testing regime were as follows:

Criteria 1 - Piles shall deflect between 3 and 6mm under a load of 500kN

Only one pile out of the thirty three dynamic test piles performed marginally. The designers analyzed the effect of this result on the performance on the raft as negligible.

Criteria 2 - All piles are to be installed as friction piles with a minimum total capacity of 660kN of which no more than 40% is end resistance.

All thirty three test piles achieved total capacity in excess of this minimum target. Further, all piles satisfied the condition for friction piles.

Criteria 3 - Predicted movement at total resistance shall be 10mm minimum

All thirty three test piles achieved maximum settlements in excess of 10mm; hence the pile stiffness requirements for the raft were satisfied.

Conclusion

This project is an example of where dynamic pile testing was used in construction for design verification. The dynamic test results gave the designers confidence that the foundations were built and behaved in accordance with their design. A percentage of pile testing spread across the site as well as accurate installation monitoring of every pile meant these piles were acceptable to the designers to act as the foundations for the piled raft.

ACKNOWLEDGMENTS

The author would like to thank Phil Mackenzie and Peter Longstaff of Advanced Foundation Solutions, Dr Julian Seidel of FoundationQA, Wayne Costin of Costin Roe and Dr Melvin England of Loadtest for their assistance with this paper.

REFERENCES

Australian Standard *AS2159-1995 Piling – Design and Installation* (Piling Code), Standards Austrailia.

Chang, Y., Yang, H.W., Chang, F., and Lee, P. (2004). "Stanamic Loading Test on Instrumented Bored Piles". *The Seventh International Conference on the Application of Stresswave Theory to Piles 2004.* The Institution of Engineers Malaysia. Kuala Lumpur, Malaysia, 367-374

Goble, G. G., and Likins, G. E. (1996). "On the Application of PDA Dynamic Pile Testing". *Fifth International Conference on the Application of Stress-wave Theory to Piles* (STRESSWAVE '96): Orlando, FL; 263-273.

Likins, G. E., and Rausche, F. (2004). "Correlation of CAPWAP with Static Load Tests". *Proceedings of the Seventh International Conference on the Application of Stresswave Theory to Piles 2004*: Petaling Jaya, Selangor, Malaysia; 153-165.

Likins, G. E., Rausche, F., Thendean, G., and Svinkin, M. (1996). "CAPWAP Correlation Studies". *Fifth International Conference on the Application of Stress-wave Theory to Piles* (STRESSWAVE '96): Orlando, FL; 447-464.

Middendorp, P., van Ginneken, G.J.J., and van Foeken, R.J. (2000). "The advantages and disadvantages of dynamic load testing and statnamic load testing" *6th International Conference on the Application of Stress Wave Theory to Piles*, Sao Paolo, Brazil.

Copyrighted Materials
Copyright © 2009 American Society of Civil Engineers (ASCE)
Retrieved from www.knovel.com

Dynamic Pile Testing of Three Drilled Shafts on the Bridge over the Changuinola River in Panama.

Jorge W. Beim
Senior Engineer, Pile Dynamics, Inc. – 4535 Renaissance Parkway, Cleveland, OH, USA – jorge@pile.com

Cesar A. de Gracia G.
Quality Control/PDA Engineer, Constructora Urbana S.A. - Vía España Final y Calle 19, Rio Abajo Apartado 0816-06563, Zona 5 – Panamá, Panamá - cdegracia@grupocusa.com

ABSTRACT

The Changinola River project contemplates the construction of a bridge which will replace the existing one, which had been used for over one hundred years exclusively for railroad traffic. The new bridge is a double span concrete structure and will have two lanes for cars and a pedestrian pass. It will be supported by reinforced concrete piers, with a diameter of 1.3 m (51 inches) and depths varying from 18 m to 20 m (50 feet to 66 feet), including a 3.5 m (11.5 feet) socket perforated into sound rock, underlying predominantly clean gravel soil, characteristic of those tributaries. Three of those piers were tested, on three different abutments. One of the piles had previously been submitted to an Osterberg Cell load test, so the presence of the cell had to be taken into consideration when analyzing the dynamic test data. A comparison of the results of the Osterberg Cell and of the Dynamic Load test could also be made. The impact system used for the tests was carefully designed using wave equation analyses, and consisted of a 265 kN (59.5 kips) steel ram falling from a maximum height of 2.5 m (8.2 feet). A 250 mm (10 inches) thick plywood cushion was used between the ram and the top of the pile. Details of the wave equation analyses are also shown.

INTRODUCTION

The Changinola River project in the *Bocas del Toro* province in Panama contemplates the construction of a bridge which will replace the existing one, which had been used for more than one hundred years. The new bridge is a double span concrete structure and will have two lanes for cars and a pedestrian pass. The

foundation design calls for piers made of reinforced concrete with a nominal strength of at least 30 MPa (4.3 ksi), with a diameter of 1.3 m (51 inches) and depths varying from 18 m to 20 m (50 feet to 66 feet), including a 3.5 m (11.5 feet) socket drilled into sound rock, underlying predominantly clean gravel soil.

Three piles were selected for dynamic testing. Two of them were production piles which were later used in the structure (E-4-5 and E-3-14), and one was a test pile which had previously been subjected to an Osterberg Cell test (E-2-P).

The testing process consisted of four main phases:

1. Wave equation analyses were made using predicted and recommended soil parameters based on the available soil information. These analyses were made for determining the ram mass and drop height, so that a set of at least 2.5 mm (0.1 inch) was reached to insure full soil resistance mobilization, while making sure that the stresses along the pile were kept at a safe level. Since pile E-2-P had the Osterberg Cell installed approximately 3.5 m (11.5 feet) from the pile toe, a special wave equation analysis had to be made in this case, in order to take into account both the non-uniform pile characteristics and the reduced skin friction in the region of the cell.
2. A hammer system was specially constructed for the test, based on the results of the wave equation analyses.
3. The piles were cast with a specially reinforced extension to allow the installation of the gages. After the sensors were installed, a test sequence consisting of blows with increasing drop heights was applied.
4. The data from the blow corresponding to the maximum mobilized capacity was analyzed with the CAPWAP® program to confirm the results obtained in the field with the CASE method, and also to obtain the resistance distribution and other soil parameters. A non-uniform model was used for pile E-2-P, to take into account the presence of the Osterberg cell. The dynamic test results for this pile were compared with the results from the Osterberg cell.

A detailed explanation of each phase follows.

WAVE EQUATION ANALYSIS

Using wave equation analysis (Rausche et.al., 2004) it was possible to predict the pile set and stresses for blows of different ram weights using different drop heights. A simple drop hammer was simulated, with a ratio of kinetic to potential energy of 0.8. The driving system consisted only of a plywood cushion with the same cross-section area as the pile, placed between the ram and the top of the pile. The effect of changing the thickness of the plywood cushion was also investigated.

For piles E-4-5 and E-3-14, a simplified soil model was deemed sufficient. This model represented the soil as having two layers, the upper one with a triangular distribution, and the lower layer with constant resistance with a value 76% higher than the maximum resistance of the overlaying layer. Figure 1 below shows a diagram of the pile, hammer and soil model used.

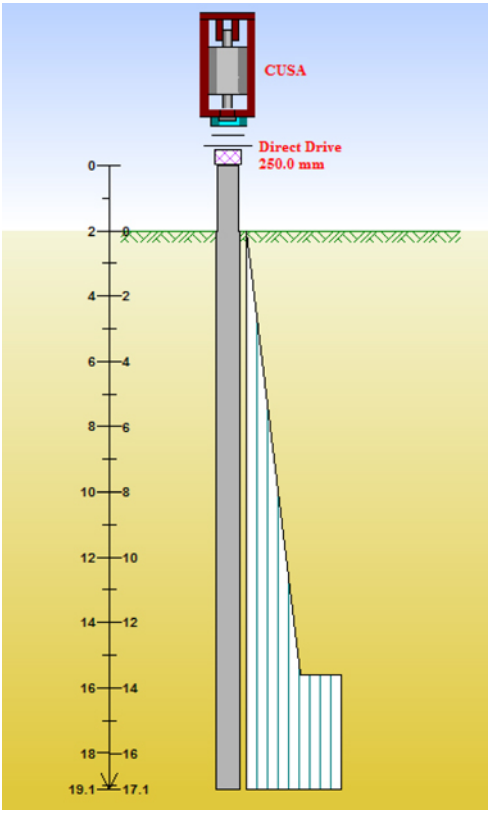

Figure 1: Pile, hammer and soil model for the uniform piles

An ultimate soil capacity of 14.7 MN (3300 kips) was used for the wave equation analyses. This is the specified capacity for pile E-3-14. The actual ultimate capacity for piles E-4-5 and E-2-P is 11.2 MN (2500 kips).

A non-uniform model was used for pile E-2-P, to take into account the presence of the 0.3 m (12 inches) thick, 0.4 m (16 inches) diameter Osterberg cell, with a top and bottom steel plate of 0.96 m (37.8 inches) diameter and 0.05 m (2 inches) thickness. A more elaborate soil model was used in this case, consisting of an upper poorly graded gravel layer, 12.5 m (41 feet) thick, with an average SPT N Value of 24, overlying a 3.5 m (11.5 feet) thick rock layer

with a unit skin friction of 294 kPa (6.1 ksf) and end bearing of 3285 kPa (68.6 ksf). Figure 2 below shows a diagram of the pile, hammer and soil model used.

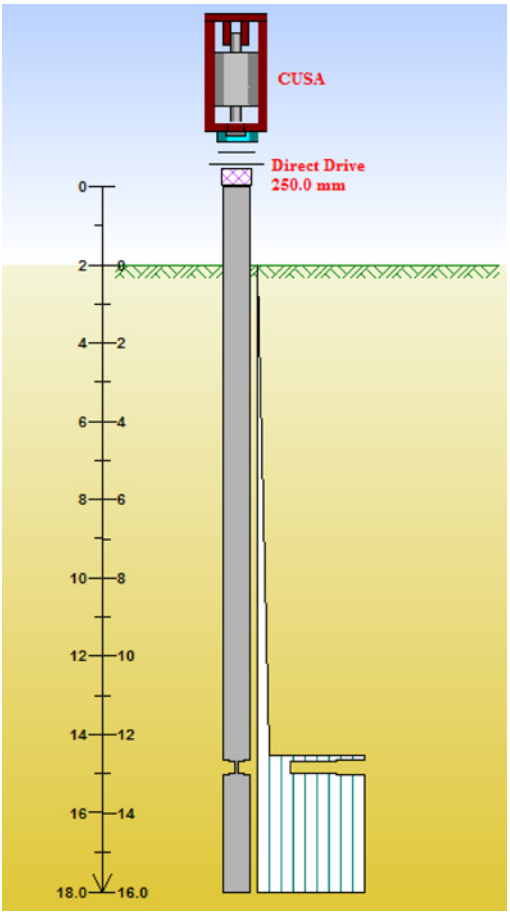

Figure 2: Pile, hammer and soil model for the non-uniform pile

Using the models described above it was possible to simulate several ram weight/hammer cushion thickness combinations, until a configuration was found that would work best in all cases. This consisted of a 265 kN (59.5 kips) ram with a wooden cushion 250 mm (10 inches) thick. The simulations indicated that a drop height of up to 2.5 m (8.2 feet) could be used without risking damaging the piles. For an ultimate load of 14.7 MN (3300 kips) the predicted compressive stresses were always below 19.4 MPa (2.8 ksi), and the tension stresses were below 4.6 MPa (0.7 ksi). For that load and drop height, the predicted set for the uniform piles was 10.7 mm (0.4 inches) and for the pile with the Osterberg cell the analysis

predicted a set of 7.5 mm (0.3 inches). Those sets were above the minimum necessary to guarantee full mobilization of the soil resistance.

TEST PROCEDURE

A driving system was constructed, with a ram consisting of A-36 steel plates held together by #11 grade 60 steel bars, which totaled the necessary weight. A 60 tonne (590 kN – 132 kips) crane was used to lift the ram, which was guided by a steel frame surrounding the pile. Figures 3a and 3b below show the driving system used.

Figure 3a and 3b: Driving systems used in the tests.

The piles were constructed by excavating using a casing oscillator and a mechanical grab. Concrete was then poured after insertion of the reinforcing cage, while the casing was extracted using the oscillator as the concreting process progressed. The test piles had an extension sticking out of the ground, with special reinforcement in order to withstand the hammer blows. The sensors were installed on the smooth surface resulting from the extraction of the casing.

DYNAMIC TEST RESULTS

The tests consisted of blows with increasing drop heights. The data from the sensors were sent to a Pile Driving Analyzer® (PDA), which processed and recorded the signals after each blow. The sets for each blow were measured by a laser beam placed a sufficient distance from the pile to reduce disturbance by soil vibrations. The signals from the blows corresponding to the maximum mobilized resistance (the last blows applied, in all three cases) were analyzed using the CAPWAP program (Likins et.al., 2000). This is a signal matching program (system identification analysis or reverse analysis), which allows the determination of the soil parameters from the inputs of the measured force and velocity signals and the geometry and stiffness of the pile.

Table 1 below summarizes the most important results.

Table 1: Dynamic test results

Pile	Length (m)	Blow nr	Drop height	set/blow (mm)	Max Transf'd Energy (kJ)	CAPWAP results (MN) Skin	Toe	Total
E-4-5	16.9	4	1.8	0.5	64.1	11.4	8.5	19.9
E-3-14	21.4	3	1.9	0.1	54.1	8.8	7.0	15.8
E-2-P	16.5	3	2.5	1.0	41.9	7.8	4.6	12.4

COMPARISON WITH OSTERBERG CELL RESULTS

Pile E-2-P had been previously tested using the Osterberg method. A detailed description of the Osterberg cell (O-cell) method (FHWA, 2006) is beyond the scope of this paper. In summary, the two O-cells were pressurized in 21 loading increments, holding each load increment constant for eight minutes, to 72.39 MPa (10,500 psi). This resulted in a bi-directional gross O-cell load of 13.10 MN (3000 kips). The loading was stopped after the 21st increment because the anticipated ultimate loads had already been exceeded and the nominal O-cell capacity had been reached. The maximum upward applied net load (gross O-cell load minus the buoyant weight of the pile above the cell) to the upper side shear was 12.71 MN (2800 kips). At this loading the upward movement of the O-cell assembly was 5.36 mm (0.2 inches). The maximum O-cell load applied to the combined end bearing and lower side shear was 13.10 MN (3000 kips). At this loading the average downward movement of the O-cell assembly was 11.71 mm (0.46 inch).

The results of an O-cell test can be used to estimate the top-loaded load-settlement curve. Based on this curve it was possible to estimate a settlement of 2.8 mm (0.11 inches) for a top loading of 7.4 MN (1660 kips - roughly equivalent to the maximum

service load of the piles). CAPWAP estimated about 3 mm (0.12 inches) for the same load (a difference of less than 7%).

For a top loading of 14.7 MN (3300 kips) the adjusted O-cell test data indicates a settlement of 6.4 mm (0.25 inches). The dynamic test of pile E-2-P did not reach this mobilized load. For the maximum mobilized capacity of about 12.4 MN (2800 kips) CAPWAP is indicating a settlement of 7.3 mm (0.29 inches), whereas the O-cell estimate is slightly more than 5 mm (0.2 inches) for this load. However, for pile E-3-14 the CAPWAP predicted settlements for 12.4 MN (2800 kips) and 14.7 MN (3300 kips) loads were respectively 4.7 mm (0.18 inches) and 6.0 mm (0.24 inches), therefore less than the O-cell predictions. The CAPWAP predicted settlements for pile E-4-5 were even smaller.

CONCLUSIONS

Three drilled shafts, 1.3 m (51 inches) in diameter and with lengths ranging from 16.5 m to 21.4 m (54.1 to 70.2 feet), including a 3.5 m (11.5 feet) rock socket, were dynamically tested. The driving system consisted of a 265 kN (59.5 kips) ram free falling from heights varying from 0.45 m (1.5 feet) to 2.5 m (8.2 feet). The driving system was designed using wave equation analyses so as to guarantee full soil resistance mobilization with safe stresses.

Total capacities between 12.4 MN (2800 kips) and 19.9 MN (4500 kips) were mobilized, with small permanent sets (0.1 mm to 1 mm – 0.004 inches to 0.04 inches), indicating that the actual ultimate resistances are still higher. The maximum mobilized capacities were satisfactory when compared to the required ultimate capacities.

One of the piles had previously been subjected to an Osterberg cell load test. The top-loaded load-settlement curve obtained from the Osterberg cell test data indicated a higher maximum mobilized load, and a stiffer pile-soil behavior at higher loads, when compared to the CAPWAP simulated load-settlement curve for this pile. However, for the two piles not tested with the O-cell the results of the top-loaded load-settlement curve derived from the Osterberg cell test data are showing a less stiff pile-soil behavior than the corresponding CAPWAP simulated load-settlement curves. The discrepancy in the results can therefore be attributed in part to the fact that the construction of the load-settlement curve from the Osterberg cell data does not take into consideration the reduction in pile stiffness caused by the cell itself, but instead assumes a uniform pile. It should be noted that the cell had not been grouted for the dynamic load test.

REFERENCES

Federal Highway Administration (FHWA) (April 2006). "Design and Construction of Driven Pile Foundations." *Publication No. FHWA NHI-05-043, Reference Manual* (Volume II): Chapter 19

Likins, G.E., Rausche, F. and Goble, G.G. (2000). "High strain dynamic pile testing, equipment and practice." *Proceedings, VI Conference on the Application of Stress Theory to Piles*, Niyama & Beim (eds), Balkema, Rotterdam: 327-333.

Rausche, F., Liang, L., Allin, R.C. and Rancman, D. (2004). "Applications and correlations of the wave equation analysis program GRLWEAP." *Proceedings, VII Conference on the Application of Stress Wave Theory to Piles*, The Institution of Engineers Malaysia, Petaling Jaya, Selangor, Malaysia: 107-123

Copyrighted Materials
Copyright © 2009 American Society of Civil Engineers (ASCE)
Retrieved from www.knovel.com

Evaluating Uplift Capacity of Driven Steel H-Piles, Comparing PDA and Load Test Results

Scott Newhouse, P.E., M.ASCE[1] Kenneth Bell, PhD., P.E., F.ASCE[2] John Davie, PhD., P.E., M.ASCE[3]

1 Senior Engineer
2 Chief Engineer
3 Senior Principal Engineer
Geotechnical Services
Bechtel Power Corporation
5275 Westview Drive
Frederick, MD 21703

ABSTRACT

Major power plant projects at two different Midwestern US sites entailed extensive foundation pile driving programs involving steel H-piles driven to bedrock. The sites are several hundred kilometers apart and thus the geology of each site is different, as well as the soils overlying the bedrock. Engineering efforts at each site included acquiring pile driving analyzer (PDA) data and performing pile static load tests – axial compression and uplift, and lateral. Refined analysis from PDA data (CAPWAP analysis) predicted the pile capacity components - skin friction (Qs) and tip resistance (Qp). The skin friction component of capacity should theoretically equal the pile's uplift capacity, allowing for the non-confining effects in uplift near the surface. The paper compares, at each site, the Qs capacity predicted by PDA data to the uplift capacity measured by load test. The comparison shows that PDA and load test results correlate closely at one of the sites, but not at the other. The paper presents analysis of the different soil conditions and resulting effects on correlation.

INTRODUCTION

Several thousand H-piles were driven to rock at each of two major power plants in the Midwestern portion of the USA. The skin friction (Qs) of the pile should theoretically equal the uplift capacity, allowing for the non-confining effects in uplift near the surface. Qs was calculated using Pile Driving Analyzer (PDA) and Case Pile Wave Analysis Program (CAPWAP) data and compared to static load test data. (Readers are referred to the Pile Dynamics, Inc. web-site for information on PDA testing and CAPWAP analysis, www.pile.com.) Capacity from static load test data was determined from tension test load-displacement plots using Davisson's method.

The comparison showed that PDA and load test results correlate closely at one of the sites, but not at the other. This paper presents analysis of the different soil conditions and resulting effects on correlation.

PDA and CAPWAP PDA testing measures acceleration and strain imparted to a pile during driving. These data are then used in CAPWAP to calculate pile capacity. The CAPWAP program runs a numerical simulation of load testing the pile. It compares calculated capacity to the acquired PDA data, iterating until it converges on the indicated pile capacity. Readers are referred to the Pile Dynamics, Inc. web-site for information on PDA testing and CAPWAP analysis, www.pile.com.

SITE AND SUBSURFACE CONDITIONS

One of the sites is in southern Illinois, in a primarily agricultural area while the other site is in Ohio along the Ohio River at the site of an existing power facility. Figures 1 and 2 illustrate the subsurface conditions at each site, and show that the main differences in the two subsurface profiles are:

- Presence of fill soil at the Ohio River site
- Illinois site is comprised entirely of clay, where Ohio River site has sand and gravel above bedrock
- Depth to rock is about 12- 15 m at the Illinois site, and 21- 27 m at the Ohio River site

The water table levels at both sites were about 6 to 9 m below grade.

LOAD TESTING DESCRIPTION

At the Illinois site several pile groups were driven for load testing purposes prior to production driving. This load test program included tension tests on three different HP shapes: HP 10 x 42, HP 12 x 63 and HP 12 x 74 sections, all Grade 50. Tension tests were run on a total of 4 piles, with two on the HP 12 x 74 sections and one on each of the other sections. PDA data were acquired on each of the test groups, allowing comparison with the tension load test results. Two load tests were run at one end of the site, and two on the other end. Design tension load was 445 kN for all piles, requiring a test load of 890 kN. HP 12 piles were driven with a Delmag D-46 hammer, and the HP 10 piles were driven with a Delmag D-30 hammer. Piles were driven to a refusal criterion to obtain the required axial compression capacity, but developed to limit stress on the pile to acceptable levels. The pile tip typically penetrated into rock from 6 to 15 cm.

At the Ohio River site, load tests were performed during production driving. Work at this site included 6 static tension load tests at 6 different locations around the site. The static tension load testing was performed in accordance with ASTM procedure D3689-07. PDA/CAPWAP data were acquired for these test piles, allowing comparison with load test results. Design tension load for piling on the Ohio River site varied from 267 to 800 kN. Pile driving through the sand and gravel layer shown on Figure 1 was not as difficult as was initially anticipated based on SPT N-values, which typically exceeded 50 blows per 300 mm. These high SPT N-values are likely

a result of the gravel in this layer. Piles at the Ohio site were driven to rock with a refusal criterion also developed to limit stresses to acceptable levels. Piles were driven with an ICE I-46 hammer or Pileco D30 hammer. Piles generally penetrated rock a distance of about 60 mm.

Increase in Qs Over Time

The increase in Qs with time is often referred to as soil setup or soil freeze. Setup will be most significant for piles driven into fine grained soil where driving can produce large pore pressures. The large pore pressures lower the effective stress in the soil surrounding the pile, resulting in a reduced pile capacity during and shortly after driving. After a sufficient time period beyond driving, soil pore pressure decreases (from drainage) and effective stress increases resulting in an increase in pile capacity. The pore pressure increase during driving is typically greater in displacement-type piles. In non-displacement piles such as the H-piles reported here, pore pressure build-up would be expected to be relatively small.

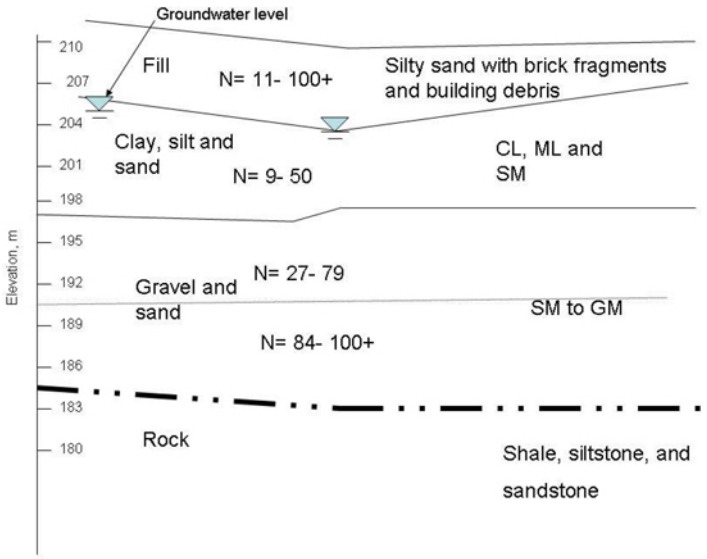

FIG. 1 Ohio River Site Subsurface Profile

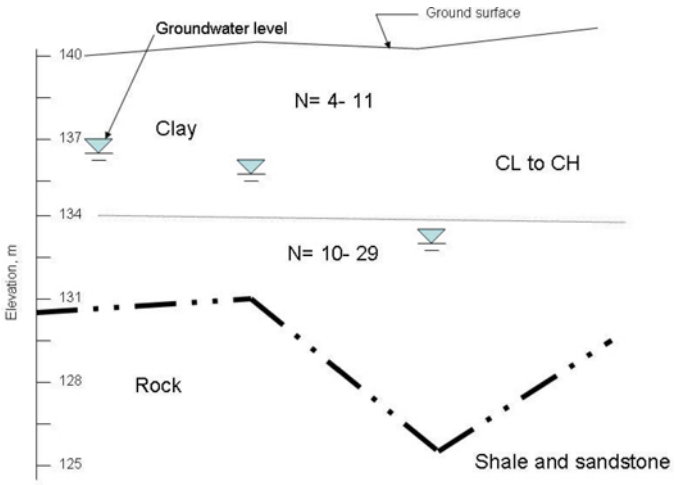

FIG. 2 Illinois Site Soil Profile

PDA-CAPWAP AND STATIC LOAD TEST RESULTS

Results of PDA-CAPWAP analysis and load tests at each site are tabulated below.

Illinois Site

Design tension load for the Illinois site was 445 kN. All piles tested in tension were loaded to twice the design load, i.e., a test load of 890 kN. All four of the static tension test piles showed capacity exceeding the test load, exhibiting only elastic deformation at the maximum test load of 890 kN.

TABLE 1. Qs CALCULATED AND MEASURED IN LOAD TEST- ILLINOIS SITE

Pile	PDA- CAPWAP Calculated Qs (kN)		Qs Measured in Load Test (kN)
	End of Initial Drive	Beginning of Re-strike	
HP 10 x 42	396	396	>890
HP 12 x 63	423	1308	>890
HP 12 x 74 (1)	609	672	>890
HP 12 x 74 (2)	378	520	>890

Ohio River Site

Design tension load for the Ohio River site varied from 267 kN on HP 12 x 63 to 800 kN on HP 14 x 73 piles. All piles tested in tension were loaded to twice the design load. Five of the 6 tension test piles on the site showed capacity exceeding the test load and exhibited only elastic deformation at the maximum test load. One of the HP 14 x 73 test piles failed at a test load less than twice its design load (refer to Table 2). Table 2 lists the range PDA-CAPWAP calculated capacity, as PDA data were acquired on 2 or more piles at each of the test locations.

TABLE 2. QS CALCULATED AND MEASURED IN LOAD TEST- OHIO RIVER SITE

Location + Pile	PDA-CAPWAP Calculated Qs (kN) End of Initial Drive	Qs Measured in Load Test (kN)
1- HP 14 x 73	1872 to 1957	>1601
2- HP 14 x 73	667 to 792	845
3- HP 12 x 63	467 to 605	>534
4- HP 14 x 73	1481 to 1610	>1334
5- HP 12 x 63	1014 to 1130	>534
6- HP 12 x 63	1090 to 1121	>534

DISCUSSION

Illinois Site

On the Illinois site, the PDA-CAPWAP data indicate that for 3 of the 4 piles tested in tension the test pile should have pulled from the ground prior to reaching maximum test load of 890 kN. The PDA-CAPWAP calculated capacity based on re-strike shows that ultimate Qs varies from 396 to 672 kN for all but one of the test piles. PDA-CAPWAP analysis under-predicted actual capacity in 3 of the 4 test piles. For the HP 12 x 63 test pile the PDA-CAPWAP calculated Qs was 1308 kN; only for this test pile did the calculated Qs exceed the test load of 890 kN. Thus, the 12 x 63 test pile was the only one of the 4 test piles for which PDA-CAPWAP analysis did not under-predict Qs for the Illinois site. Interestingly, this is the only test pile showing a significant gain in Qs between initial drive and re-strike. The 12 x 63 test pile showed increase in Qs from 423 kN at initial drive to 1308 kN at re-strike. Load testing demonstrates that the capacity at re-strike exceeds 890 kN. The remaining 3 test piles show increase in Qs of zero for the HP 10 x 42 to 142 kN for the HP 12 x 74(2) pile. The time lapse between initial drive and re-strike was typically 12 days for each of the 4 piles. Thus, none of the 4 piles had significantly more time to develop increased Qs than did the others.

The results show that PDA-CAPWAP data correlate better to measured Qs only when there is a significant increase in Qs over time.

Ohio River Site

At the Ohio River site the PDA-CAPWAP calculation indicates Qs greater than the maximum applied test load for 5 of the 6 load tested piles. For those 5 piles, load testing showed that PDA-CAPWAP capacity exceeded the applied test load. Accordingly, the CAPWAP prediction that capacity exceeds design load was accurate. However, although the maximum test load applied to these piles was twice the required design load, it was not equal to their ultimate capacity. Since the ultimate capacity is not known, we cannot conclude with certainty that CAPWAP Qs does not under-predict ultimate tension capacity. We can only conclude with certainty the accuracy of CAPWAP Qs if the ultimate tension capacity is known, as in the case of the HP 14 x 73 (Pile 2), discussed below. However, the data on HP 14 x 73 piles suggest a measure of accuracy of the CAPWAP calculation on this site, even if it is not conclusive. Two of the three HP 14 x 73 pile test loads are high, 1334 to 1601 kN. For these two piles, CAPWAP correctly predicted that the pile would hold those loads.

For HP 14 x 73 (Pile 2), the test load exceeded the calculated capacity. For this pile:

- Design Load = 667 kN
- CAPWAP Qs = 667 to 792 kN
- Load Test Measured Qs = 845 kN

The CAPWAP analysis indicates that this pile should have pulled from the ground prior to reaching a load of 845 kN. For this pile CAPWAP analysis under-predicted the capacity in tension, the same situation as the Illinois site results. However, the CAPWAP Qs for this pile, 729 kN average, differs by 116 kN from the load test measured Qs of 845 kN, or a difference of about 16%. At the Illinois site the difference between calculated and measured Qs typically exceeds 32%. Thus, for the one pile at the Ohio River site where PDA under-predicted capacity, it was much closer than at the Illinois site and was within 16% of the actual capacity.

CONCLUSIONS

Results show that for the site where Qs was developed primarily in sand and gravel, PDA appears to more reliably predict uplift capacity, although this conclusion is tentative since only one pile was tested to failure. For the site where Qs develops primarily in clay, the PDA significantly under-predicted uplift capacity for three out of the four piles. Data indicate that, Qs calculated from CAPWAP did not accurately account for increase in Qs with time for these three piles. The PDA data for the fourth pile showed significant increase in Qs between initial drive and re-strike.

Copyrighted Materials
Copyright © 2009 American Society of Civil Engineers (ASCE)
Retrieved from www.knovel.com

Driven Concrete Pile Foundation Monitoring With Embedded Data Collector System

Rodrigo Herrera[1], P.E., Lawrence E. Jones[2], P.E., Peter Lai[3], P.E.

[1]Florida Department of Transportation, Geotechnical Engineer. 605 Suwannee Street, MS 33, Tallahassee, Florida 32399-0450. Rodrigo.Herrera@dot.state.fl.us
[2]Florida Department of Transportation, Assistant State Structures Design Engineer and State Geotechnical Engineer. 605 Suwannee Street, MS 33, Tallahassee, Florida 32399-0450. Larry.Jones@dot.state.fl.us
[3]Florida Department of Transportation, Assistant State Geotechnical Engineer. 605 Suwannee Street, MS 33, Tallahassee, Florida 32399-0450. Peter.Lai@dot.state.fl.us

ABSTRACT

Florida Department of Transportation (FDOT) sponsored research performed at the University of Florida resulted in developing a wireless monitoring and real time static capacity estimate technology for driven piles. This new technology, Embedded Data Collector (EDC), uses two levels of instrumentation, embedded in the body of precast prestressed concrete piles near the head and tip. Strain and acceleration measurements obtained at these instrumentation levels during driving are sent wirelessly to a receiver in the field, and analyzed in real time to provide the operator with estimates of static capacity, stresses in the pile, transfer energy, damping factor, stroke height, and other relevant parameters used to evaluate the pile driving process and the driving system. The EDC system is currently undergoing phase one of a two phase field evaluation program planned by the FDOT to determine the level of reliability that can be anticipated by its use. The first phase consists of monitoring piles with EDC instrumentation and concurrently monitoring them with the Pile Driving Analyzer (PDA), given that there is ample data supporting the reliability of PDA. Measurements of strain and particle acceleration converted to force and velocity traces can then be compared between the two systems, along with the corresponding calculated magnitude of downward and upward traveling stress waves as they move along the pile at any point in time. Selected hammer blows recorded by PDA equipment are analyzed by means of signal matching software (CAPWAP) and the estimated static skin, end bearing, and total resistance obtained are compared against EDC static resistance predictions. The second phase of the evaluation will compare EDC estimates of static capacity against instrumented static load test results. The purpose of this paper, is only to present a summary of results obtained thus far in phase one, and compares EDC estimates of static capacity results with those from PDA and CAPWAP.

INTRODUCTION

The majority of State owned Bridges in Florida are supported on deep foundation systems comprised of precast prestressed concrete piles (PPC). In general, Florida's geology is amenable to this pile type because bearing layers often consist of soft carbonate rocks, dense sands, or over-consolidated clays, overlain by soil layers that in general do not pose major difficulties to pile driving operations. Driving stresses can usually be handled by PPC piles with proper pile cushion thickness and hammer stroke heights. Monitoring of test pile installation is of critical importance to ensure integrity of the pile and adequate resistance as well as to develop guidelines for production pile driving. Smith (1960) analyzed the problem by dividing the pile into unit lengths that underwent wave action under the blow of a hammer, and major advances have been made since through the use of computerized calculations. A reasonably comprehensive presentation of the history of wave mechanics applied to pile driving monitoring can be found in Hussein and Goble (2004). Currently, the most common method for dynamic load testing is to monitor driving with the PDA. The method has gained wide acceptance given the clear advantages in time and cost it offers when compared to static load testing techniques.

In recent years, work has been performed to provide alternate methods and equipment for dynamic load testing of deep foundations. As a result of research conducted at the University of Florida, a new procedure was developed for field monitoring as well as analyses through the use of two (or more) levels of instrumentation. This method is theoretically capable of calculating the damping factor between levels of instrumentation for each every hammer blow (McVay 2002). Therefore, real time static resistance can be theoretically estimated using computed damping values during pile driving, thus eliminating the need for signal matching to obtain improved damping values on selected hammer blow(s). This approach was implemented and later enhanced by Smart Structures, Inc., who holds a license to the patent and manufactures the instrumentation.

To evaluate the performance of the EDC system, FDOT is conducting a program of concurrently monitoring PPC test piles using PDA and EDC instrumentation for several projects during driving. The data gathered during these projects is then analyzed and compared. In addition, selected hammer blows from PDA data are being analyzed with Case Pile Wave Analysis Program (CAPWAP) signal matching software. The PDA and CAPWAP estimated static resistances are compared with the EDC estimated static resistance.

This paper is focused only on presenting the data gathered thus far on piles monitored with the EDC and PDA as well as comparing the EDC results with both PDA and CAPWAP estimates. The mathematical model used by the UF Method is based on McVay (2002). The manufacturer is in the process of developing a manual that will include a summary of the method's mathematical background.

Current Practice In Florida

Driven pile design and construction requirements for bridges are outlined in FDOT's Structures Design Guidelines, Soils and Foundations Handbook, Design

Standards, and the Standard Specifications for Road and Bridge Construction. The following is a brief description of the general procedure followed by the pile driving industry when performing dynamic load tests.

Typically dynamic load tests including PDA monitoring and signal matching with CAPWAP are used to set the criteria for driven pile installation. The PDA utilizes two accelerometers and two strain transducers connected diametrically on the pile at least one and one-half times the pile width or diameter from its head. Prior to driving, the PDA operator selects damping factors (J_c) that will be used for resistance estimates throughout the driving process in the PDA unit. This usually is based on previous experience with similar subsurface conditions. After driving, the engineer usually selects one blow per drive for CAPWAP analysis to obtain improved estimates of static resistance, as well as quake and damping factors. Using the calculated J_c and quake for skin and toe resistances, driving criteria for production piles (e.g., required number of blows per meter (foot) at prescribed stroke heights) is developed through the use of GRLWEAP software. Production piles are then driven to meet the driving criteria and embedment requirements for each pier or bent. However, quake and damping factors obtained through CAPWAP and the associated static resistance predictions are not unique solutions and different users may provide differing results depending on their level of expertise (Lai and Kuo 1994).

EMBEDDED DATA COLLECTOR

Because the PDA requires the user to assume a constant damping factor for static resistance estimates in the field, and CAPWAP analyses do not produce unique solutions, FDOT sought an alternate method to calculate static resistance from dynamic load test results. The EDC system was developed based on FDOT funded research project "Estimating Driven Pile Capacities during Construction", (McVay et al., 2002), at the University of Florida (UF). The research focused on the use of two levels of instrumentation consisting of one accelerometer and one strain transducer per level placed along the axis of the PPC piles prior to concreting. Currently, the top set of instruments is located two pile widths below the pile head, and the bottom set at one pile width above the pile tip. The bottom instrumentation is physically connected to the top level through insulated wiring. The top level includes a signal conditioner and connects to an antenna located at the face of the pile that transmits data from both levels of instruments to a receiver in the field. The receiver collects and analyzes the data in real time and provides the field inspector with estimates of static capacity, pile stresses and the energy transferred to the pile. These parameters allow the inspector to adequately assess the driving system and soil resistance is of major importance.

FDOT recognized the need to build a database of EDC records and to compare its results with the industry standard PDA-CAPWAP before it can be used as an alternate standard pile driving monitoring system. When enough data is collected, FDOT will eventually develop a resistance factor for Load Resistance Factor Design (LRFD).

EVALUATION OF EMBEDDED DATA COLLECTOR FIELD PERFORMANCE

FDOT has a two-phase field evaluation program planned to create a database and assess EDC performance. Phase I consists of comparing EDC predictions with PDA and CAPWAP results and is an ongoing effort. The field data for this phase were collected by Smart Structures, Inc., Applied Foundation Testing, Inc., Williams Earth Sciences, Inc., Foundation & Geotechnical Engineering, Inc., and Nodarse & Associates, Inc. As a future effort, Phase II is planned to compare EDC results with instrumented static load tests. PDA–EDC monitoring of test piles for Bridge structures has been an ongoing effort for approximately two years. However, project specific decisions during that time have been made based solely on PDA data. Some of the isolated issues encountered with the system during the evaluation period have included CPU overload of the field receiver, lost radio links resulting in missed blows during driving, and improper settings used in the field resulting in no data collection. Similarly, PDA problems were occasionally observed when EDC collected good data. FDOT considers that the evaluation phase has been of value to the development of the system and provided the manufacturer an opportunity to recognize and correct problems that have arisen in the field.

Comparison of EDC and PDA Predictions

Prior to the release of software that did not require user input for analysis other than the data gathered in the field, FDOT's evaluation of EDC was qualitative and compared field collected data between the systems. In May of 2008, the manufacturer provided software with a pre-determined set of calculation parameters that were to remain constant throughout the evaluation to eliminate any bias that could be attributed to user's input. This allowed a qualitative and quantitative evaluation of the previously collected and future data gathered by the EDC and PDA systems to begin.

All the information that has been gathered from EDC instrumented piles driven for State projects has been compiled into a database. The majority of those piles were concurrently monitored with PDA for comparison purposes, and current efforts are focused on evaluating the data when the PDA indicates a total resistance of 445 kN (50 tons) or more and providing statistical parameters for analysis since piles with such low resistance are of negligible value to FDOT. Table 1 includes a summary of concurrent data in the existing database.

Table 1. Summary of Database

File Type	Number of Concurrent Data Files
PDA (.W01)	122
EDC (.ssn)	122
CAPWAP (.cww or .pdf)	60

Of the four calculation methods currently implemented in the EDC software (i.e., Dynamic Case, Fixed Case, Paikowsky, and University of Florida), two were selected for evaluation; the Fixed-Case (Fixed) and the University of Florida (UF) methods.

The Fixed method was selected because the manufacturer implemented the same equations published in the PDA user manual (Pile Dynamics Inc., 2004). This method uses data collected only from the top EDC gages, and provides static capacity estimates based on a constant operator selected damping factor. The UF method uses EDC instrumentation located near the pile head and tip and provides estimates of static resistance based on a calculated damping factor for every hammer blow obtained from the measured stress wave characteristics.

A comparison of static resistance predictions by the two systems was accomplished by transferring PDA and EDC field collected data into an Excel spreadsheet and comparing the capacity predictions qualitatively and quantitatively for each drive. Of interest were the statistical characteristics of the EDC/PDA ratios (i.e., mean, standard deviation and coefficient of variation [COV]) to determine the level of consistency between predictions.

Analyses of the data revealed that during some drives the two systems did not always compute similar results (e.g., UF/PDA Method capacity > 1.9). To determine whether these large differences in predictions were common occurrences or outliers in the data, as suggested by qualitative inspection of the static capacity traces, two analytical methods were used. The first computed the mean +/- three standard deviations (μ +/- 3σ), and the second consisted in calculating a 95 percent confidence interval around the mean based on the standard deviation and the population size. The first method was selected because it includes a wider range of data.. Data outside the analysis range are not reported in Tables 2, 3 and Figures 1, 2.

Table 2. EDC/PDA Ratio of Static Capacity Predictions (n =116,048 blows from 68 piles)

Parameter	Fixed Method/PDA	UF Method/PDA
Percent of Total Population "n" within μ +/- 3σ	100	98.5
Mean (μ)	1.02	1.12
Median	0.97	1.07
Standard Deviation (σ)	0.25	0.24
COV	0.25	0.21

Table 3. EDC/PDA Stress, Energy, Integrity and Blow Count (n = 65,288 blows from 38 piles)

	CSX	CSB	TSX	EMX	BTA	B.C.
Mean	0.88	0.80	1.18	0.94	0.95	1.00
Median	0.92	0.85	1.24	0.96	0.98	1.00
Std. Dev.	0.10	0.30	0.46	0.29	0.09	0.18
COV	0.11	0.38	0.39	0.31	0.09	0.18

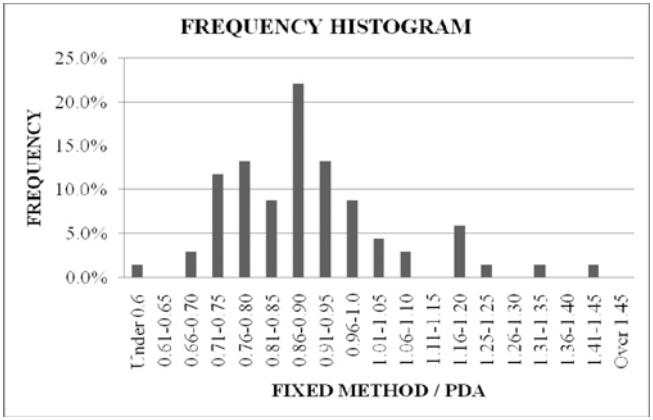

Figure 1. Fixed Method/PDA Static Capacity Frequency Histogram

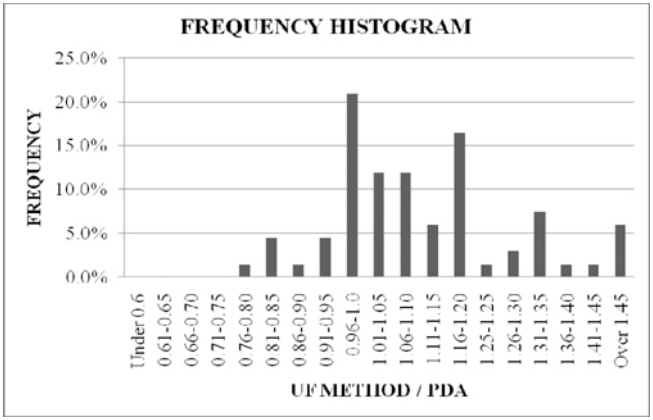

Figure 2. UF Method/PDA Static Capacity Frequency Histogram

In general, qualitative analysis of stress predictions between the two systems indicates, an acceptable correlation exists with the exception of compressive stress at the pile bottom, where significant discrepancies have been observed with EDC reporting noticeably smaller magnitudes of stress. FDOT funded research on force and velocity wave propagation currently being conducted at the UF is anticipated to shed light on actual stress levels after impact and provide additional data for comparison with both PDA and EDC predictions.

Comparison of CAPWAP and EDC Predictions

As with PDA-EDC data, only data points that fell within the range covered by three standard deviations from the mean was used in the analysis. The geotechnical engineers managing test pile programs during construction generally perform

CAPWAP analyses on high capacity blows near the end of drive. Additional CAPWAP analyses were subsequently performed on various blows from the drive by in-house or consultant engineers, to obtain a comparison that is not limited to high blow count conditions. Table 4 and Figures 2 and 3 summarize the findings.

Table 4. EDC/CAPWAP Ratio of Static Capacity (n = 60 blows from 40 piles)

Parameter	Total Resistance Fixed/CW	Total Resistance UF/CW	Skin Friction Fixed/CW	Skin Friction UF/CW	End Bearing Fixed/CW	End Bearing UF/CW
% n	98.3	98.3	98.3	96.7	98.3	100
Mean (μ)	0.98	1.08	0.63	1.55	1.20	1.04
Std. Deviation	0.22	0.18	0.63	1.14	0.54	0.37
COV	0.22	0.17	1.00	0.74	0.45	0.36

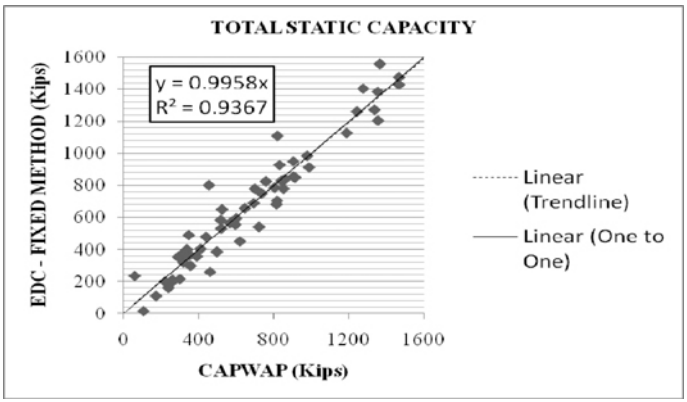

Figure 3. Fixed Method/CAPWAP Total Static Capacity Predictions

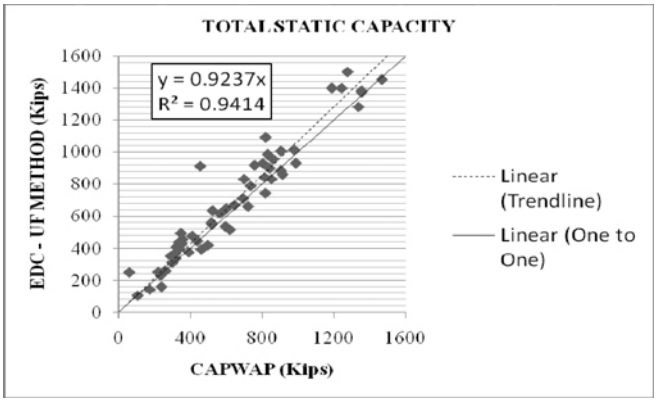

Figure 4. UF Method/CAPWAP Total Static Capacity Predictions

SUMMARY

The results obtained thus far in Phase I indicate that EDC provides total static resistance estimates that are comparable to PDA predictions, with COV values below 0.3 for the Fixed and UF methods. Comparisons to CAPWAP estimates also indicate total static resistance predictions by EDC are similar to CAPWAP with minor variation as indicated by COV values under 0.2. EDC distribution of resistance, namely end bearing and skin friction estimates for the methods investigated, are not always in close agreement with CAPWAP. The differences may be attributed to the proficiency of CAPWAP operators, the calculation approach used by the UF method or possibly due to differences in signal processing between PDA and EDC for the Fixed method, since the calculation method is reportedly the same. Discrepancies in reported stress levels during driving are still to be resolved. Current research efforts at UF are anticipated to provide further insight into the matter.

CONCLUSIONS

The evaluation program thus far has revealed that the EDC methods investigated provide results that are on average within 15 percent of PDA and CAPWAP estimates of total static resistance. An ongoing wave propagation research study will provide additional data points with which to gauge EDC's accuracy of predictions. EDC's theoretical ability to compute a new damping factor for every hammer blow and provide revised estimates of static resistance in real time, is considered a major potential advancement in dynamic load testing.

REFERENCES

Farlow, S.J. (1982). "Partial Differential Equations for Scientists and Engineers." Dover, ISBN 0-486-67620-X.

Hussein, M.H., Goble, G. G. (2004). "A Brief History of the Application of Stress-Wave Theory to Piles." *Current Practices and Future Trends in Deep Foundations, Geotechnical Special Publication No. 125, DiMaggio, J. A., and Hussein, M. H., Eds*, American Society of Civil Engineers: Reston, VA; 186-201.

Lai, P. and Kuo, C. L. (1994). "Validity of Predicting Pile Capacity by Pile Driving Analyzer" *Proceedings, International Conference on Design and Construction of Deep Foundations, Vol. 2*

McVay M.C., Alvarez, V.H., Zhang, L., Perez, A., Gibsen, A. (2002). "Estimating Driven Pile Capacities During Construction." *University of Florida. Final Report to FDOT.*

Pile Dynamics Inc. (2004) "PDA-W Manual of Operation For use with PDA models PAK and PAL"

Pile Dynamics Inc. (2000) "Case Pile Wave Analysis Program CAPWAP for Windows Manual"

Smith E.A.L. (1960). "Pile Driving Analysis by the Wave Equation." *Transactions.* American Society of Civil Engineers, 1962 Part I, Vol. 127, 1145-1171.

Copyrighted Materials
Copyright © 2009 American Society of Civil Engineers (ASCE)
Retrieved from www.knovel.com

IMPROVED METHODS FOR RAPID LOAD TESTS OF DEEP FOUNDATIONS

Takaaki Miyasaka, P.E.[1], Garland Likins, P.E., M.ASCE[2], Fumio Kuwabara[3], Frank Rausche, P.E., M.ASCE[4], Masayuki Hyodo[5]

[1]Director, Jibanshikenjo Co., Ltd., 4-29-5 Midori, Sumida-Ku Tokyo 130-0021, Japan; ph: 81-3-5600-2911; fax: 81-3-5600-2952; email: taka1010@jibanshikenjo.co.jp
[2]President, Pile Dynamics, Inc., 4535 Renaissance Parkway, Cleveland, Ohio 44128 USA; ph: 216-831-6131; fax: 216-831-0916; email: garland@pile.com
[3]Professor, Nippon Institute of Technology, Miyashiro-machi Saitama-ken 345, Japan; email: kuwabara@nit.ac.jp
[4]President, GRL Engineers, Inc., 4535 Renaissance Parkway, Cleveland, Ohio, USA,ph: 216-831-0916; fax: 216-831-0916; email: frausch@pile.com
[5]Professor, Yamaguchi University, Tokiwadai 2-16-1, Ube 755-8611, Japan; email: hyodo@yamaguchi-u.ac.jp

ABSTRACT

Rapid Load Tests have been promoted as an alternative for Static Pile Load Tests since the late 1980s. Rapid Load Tests create a relatively long duration force pulse in comparison with Dynamic Load Tests. However, a reliable prediction of pile static capacity with this test based on the so-called Unloading Point Method (UPM) has been subject to debate. Estimates of static capacity by UPM have overestimated static load test results when the applied force pulse produced too little axial movement. To resolve these issues, a drop mass Rapid Load Test called the Hybridnamic Test (HT) was developed with a ram mass up to 700 kN to reliably estimate the pile static ultimate bearing capacity up to a 35 MN. This paper discusses using a multi-cycle Hybridnamic Test in soil of mostly sand. A new interpretation method called Fully Mobilized UPM, with a required minimum net penetration per test cycle, was applied to this case study and comparison of estimated soil resistance was made between conventional UPM and Fully Mobilized UPM, and with signal matching of the dynamic force pulse data using CAPWAP. Finally a practical method to prepare a Static Load-Displacement Curve based on multi-cycle HT results is proposed.

INTRODUCTION

Rapid Load Tests (RLT) have been promoted as an alternative for Static Pile Load Tests since the late 1980s. Compared with Dynamic Load Tests, Rapid Load Tests create a relatively long duration force pulse by either a combustion process (i.e.

Statnamic Test, Bermingham & Janes, 1989) or an impact of a cushioned drop mass (i.e. Pseudo Static Test. Schellingerhout & Revoort, 1996). In 2002, "Method for Rapid Load Test of Single Piles," standardized by the Japanese Geotechnical Society, adopts the Unloading Point Method (UPM), which regards the test pile as a lump mass with a spring and a dashpot as shown in Figure 1. The force at the point when displacement is maximum (e.g. velocity is zero) is chosen to eliminate dynamic damping effects so the force at that time is then the ultimate static resistance. The UPM underestimates the static capacity compared to static load test results when the force pulse test has too little energy. On the other hand, estimates of static capacity usually significantly overestimate static load test results when the force pulse test has produced too little permanent axial movement, particularly in cohesive soil conditions due to the rate effect. Reliable prediction of static capacity with this test may be questionable because of the reasons below:

1. The UPM model lacks a slider element and therefore it is unable to separate the static resistance effect from the dynamic resistances, particularly in clay.
2. Longer piles cannot be considered a single lump mass for a short force pulse.
3. If end bearing is not fully mobilized, it is impossible to predict ultimate capacity.

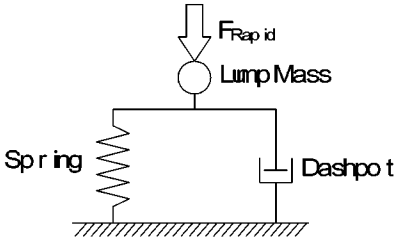

FIG.1. Model for UPM

FIG. 2. Single Hybridnamic cushion sheet

In addition, nonlinear soil properties increase the difficulty in estimating the ultimate soil resistance. Generally soil resistance assessable by UPM in one testing cycle is closely associated with the maximum applied force and energy transferred to the test pile during the force pulse and resulting net permanent movement. Therefore, a multi-cycle testing method may be necessary to assess ultimate soil resistance.

To resolve the above issues, a variation of the drop mass Rapid Load Test called the Hybridnamic Test (HT), developed in 2005, is equipped with a modular ram of up to 700 kN and a hybrid cushion with low resilience. HT is able to transfer sufficient energy to the test pile to totally activate and to estimate reliably the pile static ultimate bearing capacity up to 35 MN. The cushion block is assembled by stacking in parallel and/or in series single cushion sheets (primarily shaped rubber), as shown in Figure 2. The practical maximum force pulse duration is about 0.2 second.

A case study presents a multi-cycle Hybridnamic Test in soil consisting primarily of sand, with some thin layers of silt and stiff clay. A new interpretation method called Fully Mobilized UPM, in which a minimum net penetration per test cycle is required, was applied to this case study to estimate the ultimate soil resistance. Estimated soil resistances from conventional UPM and Fully Mobilized UPM were

compared with results of a static load test. Comparison is also made with signal matching of the dynamic force pulse data using the CAPWAP® software program.

CASE STUDY OF HYBRIDNAMIC TEST

In this case study, the testing frame and equipment shown in Figure 3 was used. This equipment consists of a ram with a mass of 70 kN, a stacked cushion with spring constant of 74.0 MN/m and with dimension of 0.72 x 0.72 x 0.15 m, and a 6.5 m high frame, which allows for a 2.0 m ram drop. Thus, this equipment can apply a force pulse with duration greater than 31.0 ms. This duration represents the time required for a stress-wave to travel more than six times upward and downward along the pile, exceeding the Japanese standard requirement (five round trip passages) for RLT.

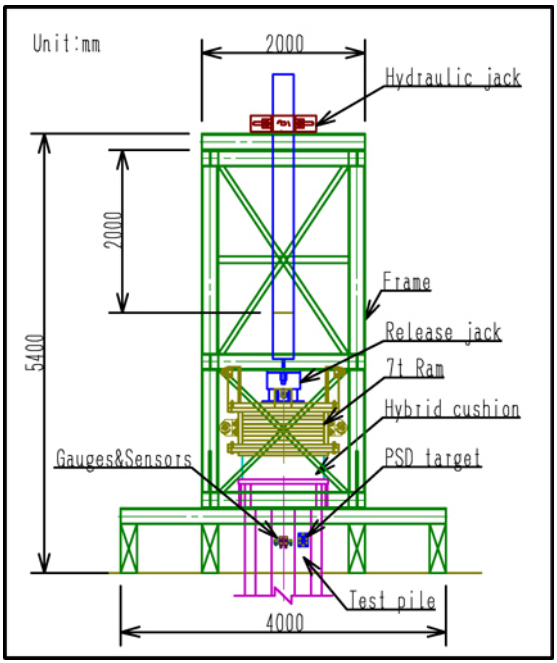

FIG. 3. Test frame and equipment (70 kN ram).

The test pile was a Type-10H steel sheet pile. This pile type has dimensions of 900 x 230 mm, a thickness of 9.2 to 10.8 mm, a perimeter of 2.3 m, pile length of 12.5 m, and has a cross-sectional area of 110 cm^2. The test pile was installed using a vibratory hammer.

Soils consist of a 2.9 m thick sand layer (N=10), followed by 2.7 m of silt (N=0), then 5.0 m coarse to gravelly sand N = 10 to 20), followed by a 1.2 m thick layer of stiff, gravelly clay, then dense fine sand beyond (N = 50+). Pile tip is located almost at the bottom of the stiff, gravelly clay layer with N value greater than 50.

Testing Procedures

A Static Load Test (SLT) conducted one month after installation, shown in Figure 4, indicates a yield point at 1.65 MN and ultimate load of 1.8 MN with a permanent pile top displacement of 99.3 mm. The summary of test results is shown in Table-1.

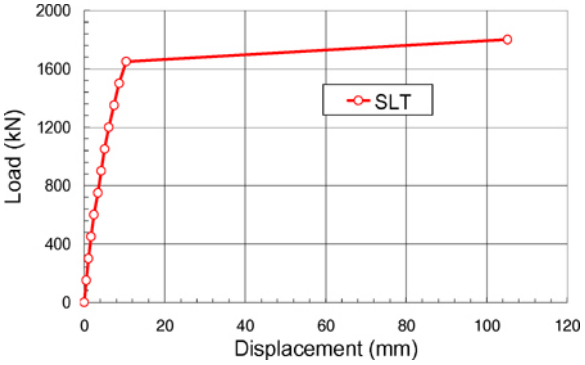

FIG. 4. Static load-displacement curve.

Table 1. Summary of Static Load Test Results

Yield Resistance			Ultimate Resistance		Pile-Soil Stiffness	
Load (kN)	Top Disp. (mm)	Tip Disp. (mm)	Load (kN)	Top Disp. (mm)	Tip Disp. (mm)	Ko (kN/mm)
1,650	11.7	4.8	1,800	106.5	99.3	140

Table 2. Summary of Hybridnamic Test

Drop Height	Pile Top Displacement (Total)	(Permanent)	Soil Resistance (Pile Top)
(m)	(mm)	(mm)	(kN)
0.20	4.8	1.0	1,064
0.60	10.4	2.0	1,994
1.00	15.7	4.0	2,578
1.50 (1)	25.8	16.0	1,762
1.50 (2)	28.6	19.0	1,821
1.50 (3)	29.4	19.0	1,927

The Hybridnamic Test was conducted 8 weeks after the Static Load Test. The ram was dropped from heights of 0.2 m, 0.6 m, and 1.0 m, and then was dropped three times from a height of 1.5 m. Measuring sensors consisted of two strain gages, two accelerometers, one optical displacement measuring device and one permanent displacement checking device. HT results are shown in Table 2.

The measured forces (F; also called the soil resistance Rsoil) and displacement (Δ), obtained from HT and SLT and shown in Figure 5, are normalized by the static ultimate soil resistance (Ru=1800 kN) and pile dimension (900 mm). Figure 5 reveals the following:

1. The curves of the 0.2m drop, 0.6m drop, and 1.0m drop are significantly different in general shape from the curves of the 1.5m drops.
2. When the applied force is less than the ultimate static resistance, the net permanent displacement will be near zero and the UPM underpredicts the ultimate capacity.
3. The soil resistance of the 0.2m drop has greatly underestimated the static soil resistance as compared with the SLT.
4. The soil resistances of the 0.6m drop and the 1.0m drop have overestimated the static soil resistance as compared with the SLT. The result from the 1.0 m drop (e.g. significant overprediction by factor of 1.43) is not necessarily the maximum that would be predicted from UPM if a slightly different drop height were selected.
5. The overprediction possibility can be even larger when the soil is cohesive.
6. The soil resistance of the 1.5m drops are close to the SLT static soil resistance.
7. The normalized maximum and net residual displacements for 1.5m drops of about 3% and 2% respectively are suggested minimum requirements for improved UPM

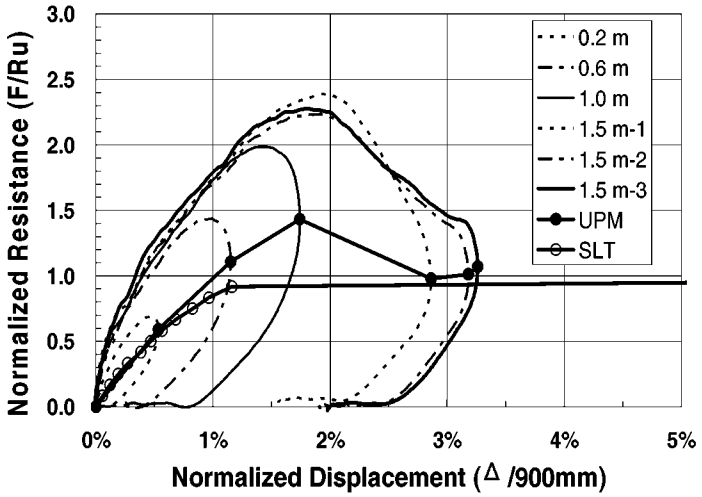

FIG. 5. Rsoil-displacement curve

INTERPRETATIONS

Because the static soil resistance obtained from drop heights under 1.5m (with low net permanent displacement) cannot be accurately extracted from the total response which includes dynamic damping effects, another evaluation method is required. The reason why the soil resistance values from the 1.5 m drop heights are close to that of SLT can be simply explained by the added slider element model shown in Figure 6, compared to the model shown in Figure 1. The Figure 6 model, named "Fully

Mobilized UPM," allows the lump mass to penetrate the bearing stratum and then retain significant permanent displacement. Subjected to significant permanent displacement and full soil resistance mobilization, the dynamic effect can be evaluated and the ultimate static resistance assessed more precisely. From Table 2, the net permanent displacement difference between the drop heights less than 1.5 m and that of 1.5 m is significant. The improved prediction reliability accompanying significant net permanent displacement is obvious from Figure 5.

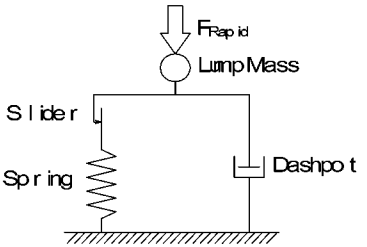

FIG. 6. Fully mobilized UPM model

To separate the dynamic component from the static component, signal-matching analysis of the measured data from various drop heights was also investigated by using CAPWAP (Rausche, 1972). Since full mobilization for a dynamic test requires only 2 mm net permanent set, data from even the 0.60 m drop should be useful. The load – displacement curves obtained from CAPWAP of the 0.60, 1.00 and 1.50 m drops are shown in Figure 7, with an average estimated capacity of 2150 kN. This result is 18 percent larger than the Full Mobilization UPM result. The CAPWAP solutions for low net permanent displacements avoid the large overpredictions of UPM (e.g. for the 1.0 m drop) and are therefore preferred when net displacements do not achieve "full mobilization" during a RLT. Since RLTs often have relatively low net penetration, signal matching may be useful.

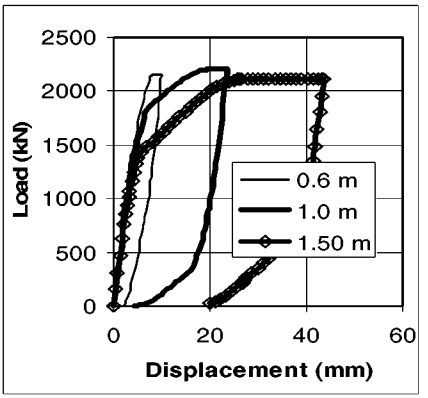

FIG. 7. CAPWAP Load–displacement curves

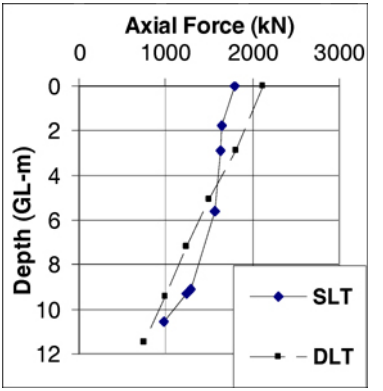

FIG. 8. Axial force distributions

The axial force distribution along the pile obtained from both SLT and signal matching for a 1.5m drop are shown in Figure 8. The two distributions are reasonably similar. Differences are attributed to the relatively long "rise time" in the HT force and velocity data that makes more exact distributions more difficult to obtain.

Preparation of Static Load-Displacement Relationship

A practical method to prepare a curve for static load-displacement from an HT test series is proposed in this study. The detailed procedures are described below:

1. Plot soil resistance versus the maximum displacement obtained from the first low height drop where supposedly the soil resistance remains in elastic domain.
2. Plot soil resistance at the Fully Mobilized UPM versus the displacement of D/10.
3. Complete the curve based on Weibull's Formula (NIST 2006).

The static load-displacement curve prepared using the above proposed method for this case history (Figure 9) matches well that obtained from the SLT.

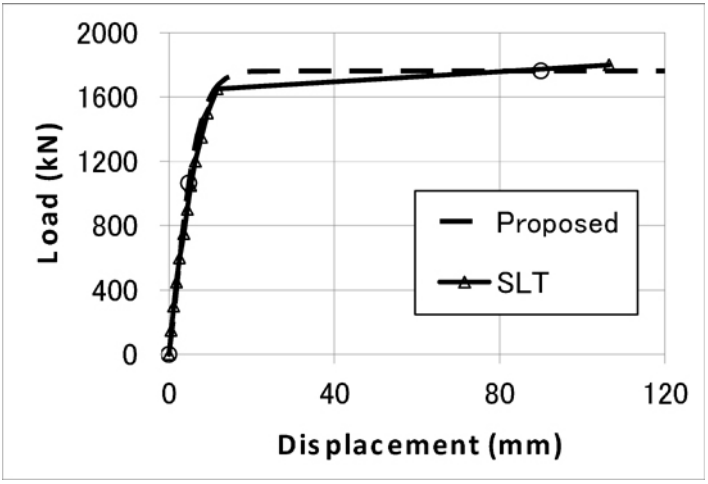

FIG. 9. Static load-displacement curve prepared based on proposed method.

CONCLUSIONS

An improved method for rapid load testing, called the "Hybridnamic Test" was introduced. A new interpretation method called Fully Mobilized UPM was applied to this multi-cycle Hybridnamic Test case study to estimate the ultimate soil resistance. The soil resistance from the Fully Mobilized UPM, requiring sufficiently large net permanent displacement, was compared to a conventional UPM. Comparison was

also made with signal matching of the dynamic force pulse data using CAPWAP. Finally a practical method to prepare a static load-displacement curve based on multi-cycle HT results was proposed. Through these studies, the following conclusions were reached:

1. Conventional UPM underestimates the ultimate static resistance from insufficient energy and applied maximum force less than the capacity (e.g. 0.2 m drop).
2. For applied force greater than the ultimate soil resistance, but with low net permanent displacement, the conventional UPM may greatly overestimate the ultimate static soil resistance due to rate effects, even in non-cohesive soils. At low net permanent displacement, even larger overpredictions are likely in cohesive soils.
3. Subjected to sufficient permanent displacement, the total soil resistance can be fully mobilized, and the ultimate static soil resistance can be assessed more accurately. This case history advocates a net permanent displacement of at least three percent of the pile diameter as the suggested minimum limit.
4. When the net permanent displacement is less than three percent of the pile diameter when Full Mobilization UPM does not apply, the most accurate method to determine ultimate soil resistance is to analyze the Rapid Load Test data (for the drop weight method of application) with signal matching such as CAPWAP.
5. The static load-displacement curve prepared based on the proposed method matches well that obtained from the Static Load Test.
6. Base on the authors' experience, it is recommended that the number of loading cycles should not exceed three cycles while the soil resistance remains in the elastic domain, and should not exceed two cycles after the soil resistance is fully mobilized and is in the plastic domain. The optimum number of loading cycles is suggested as three to five.

REFERENCES

Rausche, F., Moses, F., and Goble, G., (1972), "Soil resistance predictions from Pile Dynamics," *Journal of Soil Mechanics and Foundations*, ASCE, Vol. 98, No. SM9

Bermingham, P., Janes, M., (1989), "Innovative Approach to Load Testing of High Capacity Piles", *Proc. of the Int'l Conf. on Piling and Deep Foundations,* London,

Middendorp, P., Bermingham, P., Kuiper, B., (1992), "Statnamic load testing of foundation piles", *The 4th International Conference on the Application of Stress Wave Theory to Piles*, Balkema, Sao Paulo, Brazil

Schellingerhout, A.J.G., Revoort, E., (1996), "Pseudo Static Pile Load Tester", *Proc. of 5th Int'l Conf. on the Application of Stress Wave Theory to Piles,* Orlando

Japanese Geotechnical Society, (2002), "JGS Standards 1815", "Standards for Vertical Load Test of Piles, Method for Rapid Load Test of Single Piles"

NIST/SEMATECH, (2006), *e-Handbook of Statistical Methods,* Engineering Statistic Handbook, Chapter 1.3.6.6.8; Weibull Distribution

Copyrighted Materials
Copyright © 2009 American Society of Civil Engineers (ASCE)
Retrieved from www.knovel.com

Dynamic Verification of Static Load Testing of Pin-Piles in Seattle

G. Mann[1], P. E., M. ASCE, R. D. Holtz[2], PhD, PE, Dist. M. ASCE , and D. Maloney[3]

[1] President, Creative Engineering Options, Inc., 5418-159th Place N.E., Redmond, WA. 98052; engineeringgm@comcast.net
[2] Professor Emeritus, University of Washington; Dept of Civil & Environmental Engineering, Box 352700, Seattle, WA. 98195-2700; holtz@u.washington.edu
[3] Geotechnical Engineer, HWA Geosciences, 19730-64th Avenue West, Lynnwood, WA. 98036; david4_2@yahoo.com

ABSTRACT: In the Seattle area small diameter driven piles, known as pin-piles, are sometimes used to support small to moderate sized structures and for underpinning foundations. Seattle regulations impose a maximum allowable load of 18 kN on 60 mm diameter pipe driven with a 0.4 kN jack hammer, unless static load tests are performed. However, static load tests are often expensive due to difficulties providing site access and suitable reaction loads. Previous testing has shown that 60 mm piles develop axial capacities much greater than 18 kN with very small pile penetration or elastic shortening. We performed static and dynamic tests on three driven 60 mm steel pipe piles coupled with CAPWAP analysis. The results indicated that dynamic tests with a small drop weight and the PDA provide a reasonable correlation with static load test results. The results also indicate the dynamic testing is suitable for capacity verification of pin piles in the Seattle area, and that current overly conservative limits can probably be safely increased.

INTRODUCTION

For more than 25 years small diameter driven piles, known locally as pin-piles, have been used in the Seattle area to support small to moderate sized structures. The pile segments are spliced using internal couplings and are driven open or closed end with 0.35-0.4 kN pneumatic jack hammers for 60 mm diameter piles with a 5.5 mm wall thickness and steel area of 9.53 cm^2. Modified pavement breakers or hydraulic hammers are used in driving larger diameter piles. The smaller hammers typically

operate at 1,200 blows per minute. Data on typical piles and driving equipment are given by Haggard et al. (2001).

The original engineering for pin piles was developed by Dreubert and Yamane (1980) of Shannon & Wilson Inc. "for underpinning or supporting relatively light structures where access is restricted and a competent bearing layer is located at relatively shallow depth". A competent soil layer was defined as a soil with a SPT N-value >50 blows/300 mm. The suggested allowable load of 18 kN, corresponding to an axial stress of 18,665 kPa, was based on three static load tests, although only one plunged and that was during a reloading cycle. Consequently, no information was available on the real factor of safety. Also, to achieve an allowable load of 18 kN the pile had to be driven to a termination criterion defined as "less than one inch (25 mm) of pile penetration for one full minute of continuous driving with a 90 lb (0.4 kN) jack hammer". Since conventional pile driving formulae did not accurately determine pin pile capacity, more or less by default the Dreubert and Yamane termination criterion and the 18 kN maximum allowable axial load became the standard for pin pile use in the Seattle area.

Since 1980, the materials and equipment used for pin piles have developed considerably. Steel strength has increased and the jack hammers now being used are larger and are hitting the piles harder. Contractors report that pile heads are often severely damaged even with lighter weight driving hammers. Furthermore, experience has shown that an allowable load of 18 kN is quite conservative for the 60 mm schedule 80 black iron pipe piles presently in use. In spite of this experience, most local public agencies will only allow for an increase in the allowable load when verified by a static load test carried to at least twice the design load. This requirement is often very expensive and sometimes even impossible because, in many projects, access to the site is so difficult and providing sufficient reaction for the test load is impossible.

PREVIOUS STUDIES

In an effort to provide research data that would enable the safe use of a higher allowable pile capacities without the need for static load tests, the authors conducted a multi-phase research program. Phase I (Haggard et al., 2001) collected results from 55 load tests at 27 sites that demonstrated the overall reliability of small-diameter pipe piles in the Seattle area. Then load tests were performed on 50, 75, 100, and 150 mm diameter steel pipe piles driven with jack hammers or modified pavement breakers at two different sites. Lengths of the piles varied somewhat as did driving resistances, although almost all piles plunged when loaded. Haggard et al. (2001) concluded that pile driving formulas were not especially accurate predictors of ultimate loads. Rough estimates of the axial capacity could be obtained with a tangent-line interpretation method, similar to that proposed by Butler and Hoy (1977). The β-method (e.g., Fellenius, 2002) tended to over estimate the test load capacities, probably due to the use of conservative soil parameters and conservative estimates of failure loads from the results of the static tests.

Phase II involved the installation and load testing of four 50 mm diameter pin piles at a contractor's yard in Renton, a short distance southeast of Seattle. The piles were driven at different penetration rates through a profile of a medium dense silty sand and gravel fill over soft and compressible organic silt containing peat inclusions and

into a dense silty sand and gravel. Whilst the silty sand and gravel material was dense and competent, N-values in general were less than 50 blows per 300 mm. However, these pin-piles were driven to the above-described termination criterion within this dense granular soil which was considered to be a competent bearing material.

The results of the Phase I and II tests showed that the ultimate resistance of the pin piles ranged from approximately 95 kN up to about 175 kN, or more than four times the maximum current allowable axial load in the Seattle area for a 50 mm pile. This in spite of the fact that three of the four piles were driven with penetration rates far lower than the current termination criterion. We also noted that some piles could carry an axial load between about 15 and 30 kN before any significant deflection or penetration occurred. Westberg et al. (2005) concluded that a termination criterion of 50 to 100 mm per min would still yield satisfactory capacity. The allowable load without testing could also be increased significantly, although for very high loads, testing to verify the actual capacity and factor of safety are advisable. Higher capacities and reduced termination criterion would increase economy and reduce damage to driving equipment and piles. However, these conclusions were based on only four load tests, somewhat insufficient for a reliable assessment.

An alternative approach for assessing the ultimate pin pile capacity is dynamic tests. So for the next phase of our pin pile research we employed dynamic measurements (the Pile Driving Analyzer, PDA) to investigate whether a CAPWAP analysis of dynamic measurements on pin-piles driven with a small lightweight frame and drop weight system could determine static capacity with a reasonable degree of accuracy. By financial necessity this phase of testing was only possible with a three pile test program.

SITE DESCRIPTION AND TEST PILES

Our test site was in West Seattle in a contractor's yard in the Duwamish River floodplain. From the geology of the area, we knew that the site was underlain at shallow depth by Lawton Clay, a very stiff highly overconsolidated clayey silt (ML; natural water content about 28%; N-value ~ 33 at 6 m depth). Overlying soils were predominately loose alluvial sandy silts (ML; $5 < N < 11$). This soil profile was developed from an exploratory boring drilled in the immediate proximity of the test piles location. SPT blow count was about 33 at 6 m depths

To provide a reaction for the static load tests, three 150 mm diameter 9-m long drilled-in-place concrete anchor piles (with a central 29 mm steel rod) were installed in a roughly triangular pattern (Fig. 1). Then three 60 mm diameter schedule 80 strong black iron pipe test piles were driven between the anchor piles such that a horizontal steel reaction beam could be placed between any two reaction piles and centrally over a test pile (Fig. 1).

The test pin piles were driven open ended with a Collins 0.67 kN hammer, rather than a more common 0.4 kN jackhammer. The larger hammer helped to maintain vertical alignment of the piles since it did not require the operator to "lean" on the hammer during driving.

TABLE 1: Test Pile Data.

Pile number	Final resistance (mm/min)	Embedment depth (m)	Plug depth (m)
1	25	6.2	3.6
2	100	5.9	3.9
3	200	6.0	4.1

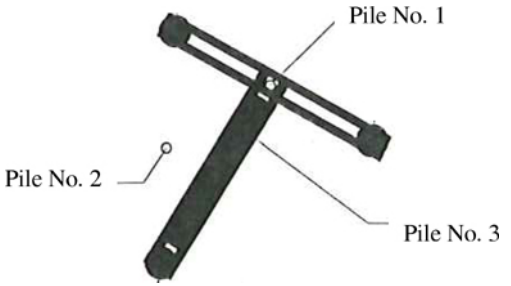

Fig. 1: Anchor and test pile location.

The three test piles were driven to different termination criteria [25, 100, and 200 mm per min] in an effort to determine if acceptable axial pile capacities could be achieved with a lesser degree of driving effort. A reduced termination criterion would reduce the potential for pile and hammer damage during driving. In our opinion a termination criterion of 75 mm per min would be an acceptable criterion without sacrificing pin pile load carrying capability, and should be expected to substantially decrease the damage to piles and driving hammers.

STATIC LOAD TESTS

Whilst it would have been advantageous to have been able to install and test a substantially larger number of piles because of the availability of suitable sites, the cost of performing these tests, and our reliance on voluntary contributions, we were only able to install and test three piles. Pile load tests generally followed the ASTM D 1143 (2000), Method A--Quick Load Test procedure, in which the applied load increments are an estimated 5% of the anticipated failure load. Since the failure loads were not known in advance, we estimated a maximum test load of about 9 kN based on our previous research. The test loads were applied to each pile in increments of approximately 0.45 kN until (1) the pile plunged, (2) maximum travel of the jack ram was reached, or (3) up to the maximum resistance provided by the anchor piles, whichever occurred first. All three test piles ultimately plunged as shown in Fig. 2. Maximum axial load capacities were between 42 kN and 63 kN. Unfortunately, we were unable retest the piles for "set up" because we were forced to abandon the test

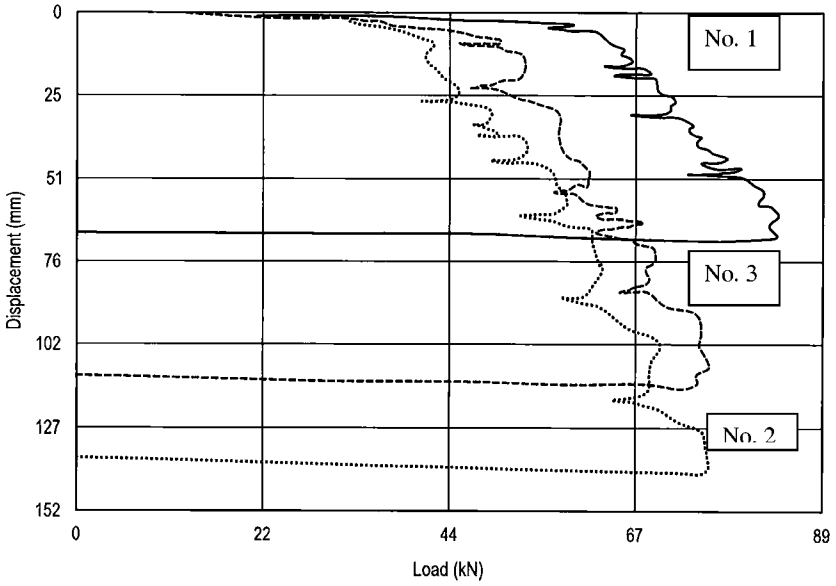

Fig. 2: Load-movement curves determined in the static tests for all three test piles.

site earlier than originally anticipated. Since these pin piles are used to support lightweight structures the authors believe that based on the research data it is not unreasonable to recommend an increase in allowable load from 18kN to 27 kN.

DYNAMIC LOAD TESTS

After the static axial testing was completed, the piles were left undisturbed for about three weeks and were then re-struck and dynamic measurements were obtained. The test data were then subjected to CAPWAP analysis to determine static pile capacity which was then compared to results of the static test on the same piles. Dynamic impacts were applied by a 1.27 kN steel weight drop hammer free-falling 762 mm. The weight was suspended by a block and tackle from a lightweight steel tripod after hoisting it with a hand winch. The weight was raised and dropped at least four, but as many as six, times on each test pile to generate adequate data for the PDA. For each drop of the weight an axial capacity was generated, and the results are shown in Table 2.

Note that dynamic tests were performed after the static load tests were completed, that is, after a period or roughly three weeks during which the static load tested piles had an opportunity to "set up" again. It is, therefore, reasonable to expect that the dynamic test loads recorded would be at least as high as, and potentially even higher

than, the maximum recorded static load test capacity as a result of the "re-setting" of the piles.

Table 2: Static and Dynamic Test Results.

Pile number	Static load test capacity (kN)	Minimum CAPWAP Capacity (kN)	Average CAPWAP capacity (kN)	Maximum CAPWAP capacity (kN)
1	63	43	117	171
2	42	68	104	140
3	50	27	84	141

A CAPWAP analysis was made for each blow recorded and the respective CAPWAP-determined static load-movement curves are shown in Fig. 3 for test pile No. 1. The PDA output also included a determination of the deflection of each pile under the applied (dynamic) load at various locations along the length of the pile. Predicted deflections at the pile head and toe are given in Table 3, and Fig. 3 is a detailed graphical representation of the dynamic head and toe deflections for pile number 1.

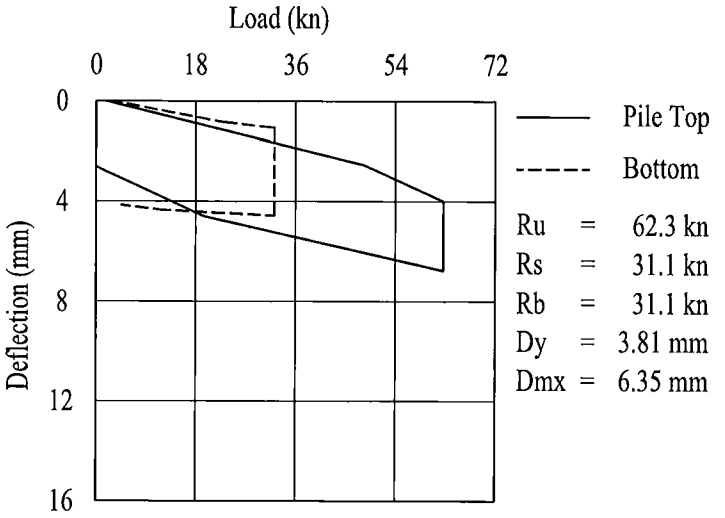

Fig. 3: CAPWAP-determined load-movement curves for test pile No. 1.

Table 3: Dynamic Deflections of the Test Piles.

Pile Number	Pile Head Deflection (mm)	Pile Toe Deflection (mm)
1	7	4.5
2	8	6.8
3	7.5	6.5

These PDA deflections are smaller than the magnitudes of pile deflection recorded on completion of the static load tests after removal of the test load (see Fig. 2). The pile head deflections recorded on completion of the static load test were 64, 109, and 135 mm, for piles 1, 2 and 3, respectively, but were "plunging" piles.

In summary, based on these limited PDA results, it is shown that the dynamic testing can provide an accurate determination of the axial capacity of pin piles. Thus, in our opinion, it is both feasible and acceptable to employ dynamic testing to verify in-situ pin-pile load capacities in lieu of more expensive and often difficult or impossible to perform static load tests.

After our test program was completed, we became aware of a similar dynamic testing on small diameter driven piles by Hajduk et al. (2005). Their results also showed good correlation between the dynamic PDA and the static load test data, and this gave us additional confidence in our test results.

CONCLUSIONS AND RECOMMENDATIONS

Our static load tests results indicate that 60 mm diameter piles are capable of developing significantly higher axial load capacities than are currently allowed by local public agencies without the need for load test verification. The static safety factor is at least two and may be as high as five when the piles are driven to the currently specified termination criterion. These results are consistent with our earlier pin pile research. The static load test data also show that in fine grained soils at least 32 kN and more granular soils at least 36 kN are required before the load vs. deflection curve begins to deviate from the initial straight line (elastic) portion of the load curve. The dynamic (PDA) load test results corroborate the static test results. Based on the limited test program, it appears that the PDA can be used to verify the ultimate axial capacity of pin piles with reasonable accuracy. Thus dynamic testing may be an economic substitute for load tests on pin piles.

Although our results agree reasonably well with research by Hadjuk et al. (2005), because of the limited number of test piles available for this research, additional PDA testing should be conducted on a number of local projects to confirm our conclusions.

Based on the static and dynamic load test results from the three phases of our research, we recommend that the allowable axial load for 60 mm diameter pin-piles be increased to at least 27 kN, provided that the piles are driven to the requisite termination criterion, without the need for a verification load test.

ACKNOWLEDGEMENTS

We are grateful for the assistance provided by several organizations and companies:

1. Seattle ASCE Geotechnical Group and the University of Washington for financial assistance.
2. Terra Firma, Inc. for installing the anchor and test piles at no cost.
3. Cemrock, Inc. for the use of their yard to perform the load test program.
4. Robert Miner Dynamic Testing, Inc. performed the dynamic testing and PDA analyses at no cost to the project.
5. The reviewers for their very helpful suggestions that greatly improved out paper.

These contributions are sincerely appreciated.

REFERENCES

Butler, H. D. and Hoy, H. E. (1977) *Texas Quick-Load Methods for Foundation Load Testing*, Users Manual, Federal Highway Administration, Report No. FHWA-IP-77-8, 59 pp.

Druebert, H. H and Yamane, G 1980. "Small Diameter Pipe Piles" presented at the ASCE Convention and Exposition, Portland, Ore. (convention preprint), 8 pp.

Fellenius, B. H. (2002) *Basics of Foundation Design*, Electronic Edition, website: www.fellenius.net; p. 7-2.

Hadjuk, E. L., Wright, W. B., Snow, W. L., and Adams, J. C. (2005) "A Drop Weight Hammer for Dynamically Testing Micropiles in Charleston, SC"; GEO3 Construction Quality Assurance/Quality Control Technical Conference; Irving, Texas; ADSC; November 6-9, 2005.

Haggard, K. K, Holtz, R.D. and Mann G. 2001. "Ultimate Bearing Capacity of Small Diameter Steel Pipe Piles". Proceedings, Specialty Conference *Foundation and Ground Improvement*, Blacksburg Va. 2001, GSP 113, ASCE, pp 380-394.

Vestberg, G., Mann, G., and Holtz, R. D. (2005). "Penetration Resistance and the Bearing Capacity of Small-diameter Steel Piles", *Proceedings, 16th International Conference on Soil Mechanics and Geotechncial Engineering*, Osaka, Japan, pp 2057-2060 (CD-ROM).

Mann, G., Vestberg, H. G., and Holtz, R. D. (2005) "Ultimate Bearing Capacity of Small-Diameter Pin-Piles and the Influence of Driving Penetration Resistance", *Proceedings,* 30th Annual Conference on Deep Foundations, Chicago, Ill., Deep Foundations Institute.

Copyrighted Materials
Copyright © 2009 American Society of Civil Engineers (ASCE)
Retrieved from www.knovel.com

AUTHOR INDEX

Index Terms	Links	
A		
Adams, Joshua C.	552	
Adeyefa, Ayoade	111	
Akili, Waddah	255	
Amir, E. I.	536	
Amir, J. M.	536	
Anundson, Wade	111	
Armour, Tom	398	
B		
Beck, W. Ken	430	
Beer, Ira	79	
Beim, Jorge W.	607	
Bell, Kenneth	247	615
Bodour, Wassel M. Al	103	
Bower, Kevin C.	351	
Brettmann, Tracy	422	
Brooks, Heather	263	
Brown, Dan	1	119
Byford, Brent	383	

This page has been reformatted by Knovel to provide easier navigation

Index Terms	Links	
C		
Cadden, Allen	143	
Cannon, Jon	591	
Capelli, Ralph	143	
Carpenter, Justin F.	239	
Castelli, Raymond J.	183	
Chang, Hsin-Wen	71	
Chatzigiannelis, Ioannis	215	
Chen, Jiun-Yih	239	
Chen, Yit-Jin	63	71
Chernauskas, Les R.	343	560
Chiu, Ting-Jui	71	
Choate, Loreen	191	
Chu, Tsu-Hung	63	
D		
Davie, John	615	
de Gracia G., Cesar A.	607	
Deardorff, Donald	480	
Demircan, Emrah	55	
Dobras, Thomas N.	295	
Doherty, Paul	575	
Dolezel, Vladimir	223	
Duan, Xinsheng	47	

This page has been reformatted by Knovel to provide easier navigation

Index Terms	Links			
E				
Elfass, Sherif	39			
Elsayed, Khaled	215			
F				
Falatok, David A.	351			
Fang, Yi-Chung	63			
Fernandez, Americo	31			
FitzPatrick, Brendan	504			
Fox, J.	438			
G				
Gassman, Sarah L.	583			
Gavin, Kenneth	575			
Gernant, Richard	504			
Gilbert, Robert B.	239			
Gray, Kathy	191			
Groneck, Paul B.	398			
H				
Hajduk, Edward L.	343	351	552	560
Halvarsson, Peo	552			
Hampton, Mark	383			

This page has been reformatted by Knovel to provide easier navigation

Index Terms	Links	
Harrison, David	335	
Harrison, Patrick J.	430	
Hartman, Jan J.	183	
Hawkins, Kelly	488	
Hermansson, Ingemar	591	
Herrera, Rodrigo	621	
Hertlein, Bernard H.	528	
Higgins, Karl A. III	271	
Hill, Jeffrey R.	207	
Hinz, Peter	512	
Hirany, Anwar	127	
Holman, Terence P.	359	
Holtz, R. D.	637	
Hori, Tomohito	135	319
Huang, Maosong	95	
Hussein, Mohamad H.	191	
Hyodo, Masayuki	629	

I

Isenhower, William M.	87	
Iskander, Magued G.	231	

J

Jones, Lawrence E.	621	
Justason, Michael D.	257	

This page has been reformatted by Knovel to provide easier navigation

Index Terms	Links	
K		
Kightley, Mike	591	
King, Phil	31	
Klingberg, David	591	
Krstic, Vedrana	167	
Kulhawy, Fred H.	47	127
Kuwabara, Fumio	629	
L		
Lacz, Stephen W.	414	
Lai, Peter	621	
Law, T. C. Michael	79	
Lesny, Kerstin	512	520
Li, Hongfen	583	
Liang, Robert Y.	103	159
Likins, Garland	591	629
Loehr, J. Erik	207	
Loukakis, Kostas	215	
Luna, Ronaldo	480	
Lutenegger, Alan J.	456	
M		
Mackiewicz, Scott M.	279	
Maloney, D.	637	

This page has been reformatted by Knovel to provide easier navigation

Index Terms	Links		
Mangogna, Robert	191		
Mankbadi, Raymond	167		
Mann, G.	637		
Martin, Paul D.	375		
Materek, Britain A.	239		
Mays, Timothy W.	351		
Miceli, Jeromy	504		
Miyasaka, Takaaki	629		
Moderie, Justin	327		
Mokwa, Robert L.	263		
Mu, Linlong	95		
Muchard, Mike	199		
N			
Nam, Moon S.	151		
Nasr, Mamdouh	496		
NeSmith, W. Morgan	447	568	438
NeSmith, Willie M.	447		
Neumann, Al, Jr.	552		
Newhouse, Scott	247	615	
Noorzad, Reza	406		
Norris, Gary	39		
O			
Olson, Larry D.	544		

This page has been reformatted by Knovel to provide easier navigation

Index Terms	Links	
Olson, Roy E.	231	
O'Neal, Jeff	247	
P		
Palmer, Rick	199	
Pando, Miguel A.	23	31
Pease, James B.	390	
Pegues, James C.	111	
Peltz, Asher	79	
Penn-Sanders, Elizabeth	343	
Perkins, Timothy S.	351	
Pooranampillai, Jeyasuthan	39	
Puskar, Frank J.	239	
Q		
Qian, H.	223	
R		
Rak, L.	223	
Ramakrishna, Aravinda	167	
Rao, B.	223	
Regan, John E.	271	
Rhyner, Frederick C.	79	

This page has been reformatted by Knovel to provide easier navigation

Index Terms	Links	
Rippe, Arlan H.	327	
Robertson, Peter	472	
Rodriguez, Javier	143	
Ruiz, Miguel E.	23	
S		
Sachin, P.	367	
Sack, Dennis A.	544	
Saghaee, G. Reza	406	
Sakr, Mohammed	464	
Schmidt, Frank	295	
Sego, David	472	
Shatnawi, Ehab S.	159	
Siegel, Timothy C.	568	
Simpson, Michael	199	
Smith, Benjamin	599	
Sritharan, Sri	303	
Suleiman, Muhannad	303	
T		
Tamate, Satoshi	135	319
Tappenden, Kristen	472	
Thompson, W. Robert III	119	207
Thorsten, Richard	488	

This page has been reformatted by Knovel to provide easier navigation

Index Terms	Links		
U			
Unnikrishnan, N.	367		
V			
van der Horst, Stephanie	343		
Vande Voort, Thomas	303		
Vanderpool, Walt	39		
Vembu, Kalaiarasi	422		
Vipulanandan, C.	422	151	55
W			
Walker, M. D. "Bo"	87		
Wells, Richard C.	414		
Wolosick, John R.	12		
X			
Xia, Ron	223		
Xu, Jinming	175		
Y			
Yamin, Mohammad	103		

This page has been reformatted by Knovel to provide easier navigation

Index Terms	Links
Z	
Zeilinger, Hermann	311
Zhang, Chenrong	95
Zhang, Lianyang	175

This page has been reformatted by Knovel to provide easier navigation

Copyrighted Materials
Copyright © 2009 American Society of Civil Engineers (ASCE)
Retrieved from www.knovel.com

SUBJECT INDEX

Index Terms	Links			
A				
Anchors	95	456	472	480
Anisotropy	159			
Arizona	398	406		
Automation	319			
Axial loads	175	231		
B				
Bearing capacity	367			
Bedrock	359			
Bonding	12	552		
Boreholes	87			
Bridge construction	167			
Bridge design	167			
Bridges	79	303	552	560
	607			
C				
Caissons	95			
Canada	223	464		

This page has been reformatted by Knovel to provide easier navigation

Index Terms	Links			
Case reports	31	135	207	335
	351	496	552	
Cast in place	430	568		
Catchments	398			
Cements	119	375		
Centrifuge models	319			
Chesapeake Bay	199			
China	47			
Clays	12	151	456	472
Cohesionless soils	231	239		
Cohesive soils	422	430		
Compaction	39			
Compression	63			
Concrete	55			
Concrete piles	271			
Cone penetration tests	544			
Construction	135	143	390	
Construction management	1	327	383	398
Costs	247			
Cylinders	199			

D

Data analysis	528			
Data collection	447	621		
Databases	351			
Deep foundations	1	111	271	343
	583	629		

This page has been reformatted by Knovel to provide easier navigation

Index Terms	Links			
Design	55	295		
Design/build	1			
Displacement	422	438	447	
District of Columbia	271			
Drainage	71			
Drilled shafts	23	31	39	47
	55	63	71	87
	103	119	127	151
	159	167	183	552
	560	583	607	
Drilling	87	135	143	438
	447			
Driven piles	255	263	257	303
	311	319	335	351
	621	637		

E

Europe	520
Experimentation	575

F

Facility expansion	375
Failures	127
Finite element method	95
Florida	191
Footings	367

This page has been reformatted by Knovel to provide easier navigation

Index Terms	Links			
Foundation design	223	504	520	528
	599			
Foundations	63	95	151	167
	183	215	295	375
	544	560	568	
G				
Geomaterials	263			
Great Lakes	383			
Grouting	23	31	39	47
	390			
H				
Health care facilities	390			
Holes	536	560		
Hurricanes	239			
I				
Illinois	383			
In situ tests	447			
Industrial plants	375			
Innovation	39	199	295	343
	438			
Iron	295			

This page has been reformatted by Knovel to provide easier navigation

Index Terms	Links			
L				
Laboratory tests	39			
Lateral loads	464			
Layered soils	71			
Limit states	480			
Load and resistance factor design	480			
Load tests	12	111	127	430
	488	496	568	615
	629	637		
Load transfer	23	472		
Loads	422			
Louisiana	544			
M				
Machinery	135	257		
Measurement	79			
Micro piles	12	359	367	375
	383	406	414	
Middle East	255			
Missouri	207			
Missouri River	207			
Model tests	319			
Monitoring	335	414	621	

This page has been reformatted by Knovel to provide easier navigation

Index Terms	Links			
N				
Nondestructive tests	583			
Numerical analysis	406			
O				
Offshore construction	215			
Offshore structures	215	239	512	
Optimization	111			
Oregon	327			
P				
Panama	607			
Pile foundations	223	255	359	512
	591	599	621	
Pile tests	591	599	607	
Piles	79	127	143	199
	207	215	231	239
	247	422	430	438
	447	464	496	536
	568	575		
Pipe piles	279	295	488	
Plates	456			
Powerplants	247			
Predictions	79	279		

This page has been reformatted by Knovel to provide easier navigation

Index Terms	Links			
R				
Raft foundations	223			
Rehabilitation	79	560		
Residual soils	414			
Risk management	1			
Rivers	183	271	607	
Rocks	103	119	151	159
	175	263	398	
S				
Sand	12	23	279	367
	464	472		
Seismic analysis	406			
Seismic effects	327	414		
Settlement	79	496		
Shafts	175	279		
Shale	151			
Silts	575			
Slope stability	103	207		
Slurries	47			
Soil conditions	191	311		
Soil properties	544			
Soils	263			
Static loads	637			
Steel piles	191	303	615	

This page has been reformatted by Knovel to provide easier navigation

Index Terms	Links			
T				
Technology	591			
Texas	31	239		
Turbines	504			
U				
Ultrasonic methods	536			
United States	119	615		
Uplift	456	615		
Urban areas	359			
Urban development	327			
V				
Vibration	311	327	335	343
	351			
Virginia	183			
W				
Washington	637			
Water temperature	79			
Waterfront structures	327			
Wind energy	504	512	520	

This page has been reformatted by Knovel to provide easier navigation